



Universidade Federal do Rio de Janeiro  
Escola Politécnica & Escola de Química  
Programa de Engenharia Ambiental

George Victor Brigagão

TECHNOLOGICAL ALTERNATIVES FOR CARBON  
ABATEMENT AND EXERGY EFFICIENCY: POWER  
GENERATION, PROCESSING OF CO<sub>2</sub>-RICH NATURAL  
GAS, AND BIOREFINERIES

Rio de Janeiro  
2019



UFRJ

George Victor Brigagão

TECHNOLOGICAL ALTERNATIVES FOR CARBON  
ABATEMENT AND EXERGY EFFICIENCY: POWER  
GENERATION, PROCESSING OF CO<sub>2</sub>-RICH NATURAL  
GAS, AND BIOREFINERIES

Tese de Doutorado apresentada ao Programa de Engenharia Ambiental, Escola Politécnica & Escola de Química, da Universidade Federal do Rio de Janeiro, como parte dos requisitos necessários à obtenção do título de Doutor em Engenharia Ambiental.

Orientadores: José Luiz de Medeiros, DSc.  
Ofélia de Queiroz F. Araújo, PhD.

Rio de Janeiro  
2019

Brigagão, George Victor.  
B854t Technological alternatives for carbon abatement and exergy efficiency: power generation, processing of CO<sub>2</sub>-rich natural gas, and biorefineries / George Victor Brigagão. – 2019.  
321 f.: il. 30 cm

Tese (doutorado) – Universidade Federal do Rio de Janeiro, Escola Politécnica e Escola de Química, Programa de Engenharia Ambiental, Rio de Janeiro, 2019.

Orientador: José Luiz de Medeiros.

Coorientadora: Ofélia de Queiroz Fernandes Araújo.

1. Captura de CO<sub>2</sub>. 2. Geração de eletricidade. 3. Gás natural. 4. Separação do ar. 5. Biorrefinaria. I. de Medeiros, José Luiz, orient. II. Araújo, Ofélia de Queiroz Fernandes, coorient. III. Universidade Federal do Rio de Janeiro. Escola Politécnica e Escola de Química. IV. Título.



UFRJ

# TECHNOLOGICAL ALTERNATIVES FOR CARBON ABATEMENT AND EXERGY EFFICIENCY: POWER GENERATION, PROCESSING OF CO<sub>2</sub>-RICH NATURAL GAS, AND BIOREFINERIES

George Victor Brigagão

Orientadores: José Luiz de Medeiros, DSc.

Ofélia de Queiroz F. Araújo, PhD.

Tese de Doutorado apresentada ao Programa de Engenharia Ambiental, Escola Politécnica & Escola de Química, da Universidade Federal do Rio de Janeiro, como parte dos requisitos necessários à obtenção do título de Doutor em Engenharia Ambiental.

Aprovada pela banca:

---

Prof. José Luiz de Medeiros, DSc, UFRJ (Orientador, Presidente)

---

Prof. Ofélia de Queiroz Fernandes Araújo, PhD, UFRJ (Orientadora)

---

Prof. Assed Naked Haddad, DSc, UFRJ

---

Prof. Bettina Susanne Hoffmann, DSc, UFRJ

---

Prof. Márcio José Estillac de Mello Cardoso, PhD, UFRJ

---

Prof. Carlos André Vaz Júnior, DSc, UFRJ

---

Fábio dos Santos Liporace, DSc, PETROBRAS

Rio de Janeiro  
2019

## AGRADECIMENTOS

Agradeço primeiramente aos meus amados familiares, que me deram todo o apoio para que eu pudesse realizar este trabalho com tranquilidade e conforto.

Ao Prof. José Luiz e à Prof.<sup>a</sup> Ofélia Araújo pela orientação, auxílio, dedicação, confiança, experiência e conhecimentos transmitidos.

Aos meus amigos e colegas de trabalho mais próximos Lara, Igor, Alexandre, Darley e Juliana, com quem tive a honra de participar em trabalhos de colaboração, e que além de terem me acompanhado durante todo este processo me dando importante motivação, diretamente contribuíram para o conteúdo desta tese.

Aos demais amigos e colegas de laboratório, que também me acompanharam de perto me auxiliando neste processo, em especial Israel, Ícaro, Guilherme e Matheus.

Aos demais amigos da UFRJ que me deram importante apoio para perseverar neste caminho, em especial Elisa, Cíntia e Andressa.

Aos queridos amigos fora da universidade, que exerceram também papel muito importante durante tão conturbada fase de minha vida, em especial Laiza, Júnior, Mara e Andréa.

À querida Aline, que desde o mestrado incentiva e dá força à minha formação acadêmica, e ao amigo Artur, que sem dúvidas foi responsável pelo *start* de minha carreira.

À Petrobras pelo suporte financeiro.

## RESUMO

BRIGAGÃO, G. V. **Alternativas Tecnológicas para Abatimento de Carbono e Eficiência Exergética: Geração Termelétrica, Processamento de Gás Natural Rico em CO<sub>2</sub> e Biorrefinarias**. Tese (Doutorado em Engenharia Ambiental), Programa de Engenharia Ambiental, Escola Politécnica & Escola de Química, Universidade Federal do Rio de Janeiro, 2019. Orientadores: José Luiz de Medeiros, Ofélia de Queiroz Fernandes Araújo

Em um cenário de longo prazo de aquecimento global, a implementação de alternativas tecnológicas para redução de emissões de CO<sub>2</sub> em termelétricas é importante para viabilizar metas de redução de carbono. Além disso, considerando a tendência provável para o crescimento no uso de gás natural nas próximas décadas, as atuais preocupações ambientais trazem particular atenção aos impactos ligados às atividades *upstream* de óleo e gás, especialmente em face das recentes descobertas de reservas contendo gás natural com alto teor de CO<sub>2</sub>. Neste contexto, este trabalho desenvolve e analisa tecnicamente, economicamente, ambientalmente e exergeticamente, alternativas tecnológicas que atendem aos desafios atuais ligados à redução de carbono na geração de eletricidade e na purificação de gás natural rico em CO<sub>2</sub>. Em primeiro lugar, foi desenvolvido um projeto inovador de separação criogênica do ar para produção de oxigênio em larga escala para suprir oxicombustão. Em seguida, é apresentado um conceito inovador de pré-purificação de ar para fracionamento criogênico utilizando separadores supersônicos como operação principal seguida por adsorção de acabamento, com desempenho econômico superior à rota convencional de pré-purificação de ar para plantas criogênicas de fornecimento de oxigênio. É mostrado que a pré-purificação de ar com separadores supersônicos apresenta também eficiência exergética superior à rota convencional. Em terceiro lugar, no processamento *offshore* de gás natural rico em CO<sub>2</sub>, para maior lucratividade, menores consumo de potência e impacto ambiental, abordam-se etapas sequenciais de separadores supersônicos – visando ao ajuste simultâneo de pontos de orvalho de água e hidrocarbonetos e à remoção de CO<sub>2</sub> – proporcionando aumento da produção de óleo e redução de investimento do processamento. Por fim, em áreas rurais analisou-se a produção de biogás e o processamento de sabugos de milho para gerar combustível de termelétricas, tendo em vista ambas viabilidades econômicas e impacto direto para redução de emissões de carbono no setor elétrico.

**Palavras-chave:** Captura de CO<sub>2</sub>; geração de potência; gás natural; separação do ar; eficiência exergética; biogás.

## ABSTRACT

BRIGAGÃO, G. V. **Technological Alternatives for Carbon Abatement and Exergy Efficiency: Power Generation, Processing of CO<sub>2</sub>-Rich Natural Gas, and Biorefineries.** DSc. Thesis (Doctorate in Environmental Engineering), Environmental Engineering Program, Escola Politécnica & Escola de Química, Federal University of Rio de Janeiro, 2019. Advisors: José Luiz de Medeiros, Ofélia de Queiroz Fernandes Araújo

In a scenario of long-term global warming, the implementation of technological alternatives for reducing CO<sub>2</sub> emissions of fuel-fired power plants is important to attain targets of carbon reduction. Moreover, considering the trend of growth of natural gas utilization in the next decades, sustainability concerns bring particular attention to environmental impacts associated with oil-gas upstream activities, especially in view of recent discoveries of natural gas reserves with high CO<sub>2</sub> content. In this context, this work develops and analyzes technically, economically, environmentally and exergetically technological alternatives to meet challenges of carbon reduction in electricity generation and processing of CO<sub>2</sub>-rich natural gas. Firstly, an innovative design was developed for cryogenic air separation units for large-scale supply of oxygen to oxy-combustion. Secondly, it is presented an innovative concept of air pre-purification unit for cryogenic air separation prescribing utilization of supersonic separators followed by a finishing adsorption step, with superior economic performance comparatively to the conventional route of air pre-purification for cryogenic oxygen supply plants. It is shown that air pre-purification with supersonic separators has also greater exergetic efficiency than the conventional route. Thirdly, for better profitability, lesser power consumption and environmental impact in offshore processing of CO<sub>2</sub>-rich natural gas, it is approached the utilization of sequential steps of supersonic separators – for simultaneous adjustment of water and hydrocarbon dew-points – allowing oil production increase and investment reduction. Finally, in rural areas, it was analyzed the production of biogas and the processing of corncobs for producing non-fossil fuels for power generation, in view of both proven economic viabilities and direct impacts for reducing carbon emissions in the electricity generation sector.

**Keywords:** CO<sub>2</sub> capture; power generation; natural gas; air separation; exergy efficiency; biogas.

# CONTENTS

1. INTRODUCTION _____	1
1.1. CO <sub>2</sub> Emissions _____	1
1.2. CO <sub>2</sub> Abatement Technologies _____	4
1.3. Techonological Gaps _____	7
1.4. Objectives _____	12
1.5. Justification _____	13
1.6. Outline of Thesis Structure _____	18
1.7. References for Chapter 1 _____	20
2. A Novel Cryogenic Vapor-Recompression Air Separation Unit Integrated to Oxyfuel Combined-Cycle Gas-To-Wire Plant with Carbon Dioxide Enhanced Oil Recovery: Energy and Economic Assessments _____	23
2.1. Introduction _____	25
2.2. Methods _____	31
2.3. Results and Discussion _____	35
2.4. Conclusions for Chapter 2 _____	49
2.5. References for Chapter 2 _____	50
3. A New Concept of Air Pre-Purification Unit for Cryogenic Separation: Low-Pressure Supersonic Separator Coupled to Finishing Adsorption _____	53
3.1. Introduction _____	55
3.2. Supersonic Separator _____	58
3.3. Methods _____	64
3.4. Results and Discussion _____	69
3.5. Conclusions for Chapter 3 _____	80
3.6. References for Chapter 3 _____	80
4. Improving Exergy Efficiency of Air Pre-Purification Unit for Cryogenic Fractionation: Low-Pressure Supersonic Separator Coupled to Finishing Adsorption	83
4.1. Introduction _____	85
4.2. PPU Design and Simulation _____	90
4.3. Exergy Analysis _____	95
4.4. Results _____	101
4.5. Discussion on Exergy Performance and RER Comparison _____	109
4.5. Conclusions for Chapter 4 _____	113
4.6. References for Chapter 4 _____	115

5. Carbon Capture and Supercritical Fluid Processing with Supersonic Separator: Cleaner Offshore Processing of Natural Gas with Ultra-High CO <sub>2</sub> Content _____	117
5.1. Introduction _____	119
5.2. Methods _____	124
5.3. Case Study 1: Conventional NG Processing vs. SS-SS Alternative _____	127
5.4. Case Study 2: SS-SS Alternative Consolidation _____	140
5.5. Conclusions for Chapter 5 _____	148
5.6. References for Chapter 5 _____	149
6. Carbon Dioxide Utilization in a Microalga-Based Biorefinery for Methanol Production: Economic Performance under Carbon Taxation _____	151
6.1. Introduction _____	152
6.2. Methods _____	155
6.3. Process Description _____	158
6.4. Results and Discussion _____	160
6.5. Conclusions for Chapter 6 _____	164
6.6. References for Chapter 6 _____	165
7. Upstream and Downstream Processing of Microalgal Biogas: Emissions, Energy and Economic Performances under Carbon Taxation _____	167
7.1. Introduction _____	169
7.2. Upstream Processing _____	171
7.3. Anaerobic Digestion Process _____	173
7.4. Downstream Biogas Processing _____	174
7.5. Simulation of Process Alternatives _____	178
7.6. Results and Discussion _____	181
7.7. Conclusions for Chapter 7 _____	192
7.8. References for Chapter 7 _____	193
8. A Techno-Economic Analysis of Thermochemical Pathways for Corncob-to-Energy: Fast Pyrolysis to Bio-Oil, Gasification to Methanol and Combustion to Electricity _	198
8.1. Introduction _____	199
8.2. Methods _____	203
8.3. Results and Discussion _____	215
8.4. Conclusions for Chapter 8 _____	225
8.5. References for Chapter 8 _____	226
9. CONCLUSIONS _____	230

APPENDIX A – Bibliographic production _____	235
APPENDIX B – Patent application on cryogenic air separation _____	242
APPENDIX C – Conference paper on cryogenic air separation – Proceedings of LA-SDEWES2018 _____	243
APPENDIX D – Scientific article on cryogenic air separation and Gas-To-Wire electricity generation with oxy-combustion CO <sub>2</sub> capture – Energy Conversion and Management _____	244
APPENDIX E – Patent application on air pre-purification for cryogenic separation plants _____	245
APPENDIX F – Conference paper on energy assessment of novel air pre-purification units for cryogenic air separation plants – Proceeding of the 4th Brazilian Congress on CO <sub>2</sub> in the Oil, Gas and Biofuels Industries _____	246
APPENDIX G – Scientific article on energy assessment of novel air pre-purification units for cryogenic air separation plants – Materials Science Forum _____	247
APPENDIX H – Scientific article on techno-economic assessment of novel air pre-purification units for cryogenic air separation plants – Separation and Purification Technology _____	248
APPENDIX I – Conference paper on exergy analysis of air pre-purification units for cryogenic air separation – Proceedings of SDEWES2018 _____	249
APPENDIX J – Conference paper on electricity generation in oxyfuel natural gas combined cycle power plant – Proceedings of Rio Oil & Gas 2016 _____	250
APPENDIX K – Register of softwares for calculation of multiphase and reactive equilibrium sound speed and simulation of supersonic separators _____	251
APPENDIX L – Conference paper on offshore CO <sub>2</sub> -rich natural gas processing with supersonic separators – Proceedings of LA-SDEWES2018 _____	252
APPENDIX M– Scientific article on offshore CO <sub>2</sub> -rich natural gas processing with supersonic separators – Journal of Natural Gas Science and Engineering _____	253
APPENDIX N – Scientific article on offshore CO <sub>2</sub> -rich natural gas processing with supersonic separators – Journal of Cleaner Production _____	254
APPENDIX O – Conference paper on CO <sub>2</sub> utilization in microalga-based biorefinery producing methanol – Proceedings of SDEWES2016 _____	255
APPENDIX P – Scientific article on CO <sub>2</sub> utilization in microalgae-based biorefinery producing methanol – Journal of Environmental Management _____	256
APPENDIX Q – Conference paper on sustainability analysis of biogas production from microalgae – Proceedings of LA-SDEWES2018 _____	257
APPENDIX R – Scientific article on techno-economic analysis of biogas production from microalgae – Renewable and Sustainable Energy Reviews _____	258

APPENDIX S – Scientific article on techno-economic analysis of thermochemical pathways of corncob conversion – Fuel Processing Technology _____	259
APPENDIX T – Scientific article on exergy-based sustainability analysis of CO <sub>2</sub> capture and storage or utilization to methanol production – Renewable and Sustainable Energy Reviews _____	260
APPENDIX U – Supplementary Material for Chapter 02 _____	261
APPENDIX V – Supplementary Material for Chapter 03 _____	265
APPENDIX W – Supplementary Material for Chapter 04 _____	275
APPENDIX X – Supplementary Material for Chapter 05 _____	283
APPENDIX Y – Supplementary Material for Chapter 06 _____	294
APPENDIX Z – Supplementary Material for Chapter 07 _____	305

# 1. INTRODUCTION

## 1.1. CO<sub>2</sub> Emissions

As the world energy matrix is still dominated by fossil fuels and few efforts are applied for carbon sequestration, CO<sub>2</sub> emissions continue to increase every year imposing a threat over humanity about the long-term consequences of global warming advancement. The IPCC (2014) have estimated that the major share ( $\approx 75\%$ ) of global warming impacts is assigned to CO<sub>2</sub> global emissions, so it is considered as the main greenhouse gas (GHG). In this sense, Fig. 1.1 illustrates the historical evolution of GHGs total emissions by component and origin in terms of CO<sub>2</sub>-equivalent (for accounting the actual global warming potential of each molecule). Details of CO<sub>2</sub> emissions parcel by use of fossil resources oil, gas and coal are presented in Fig. 1.2.

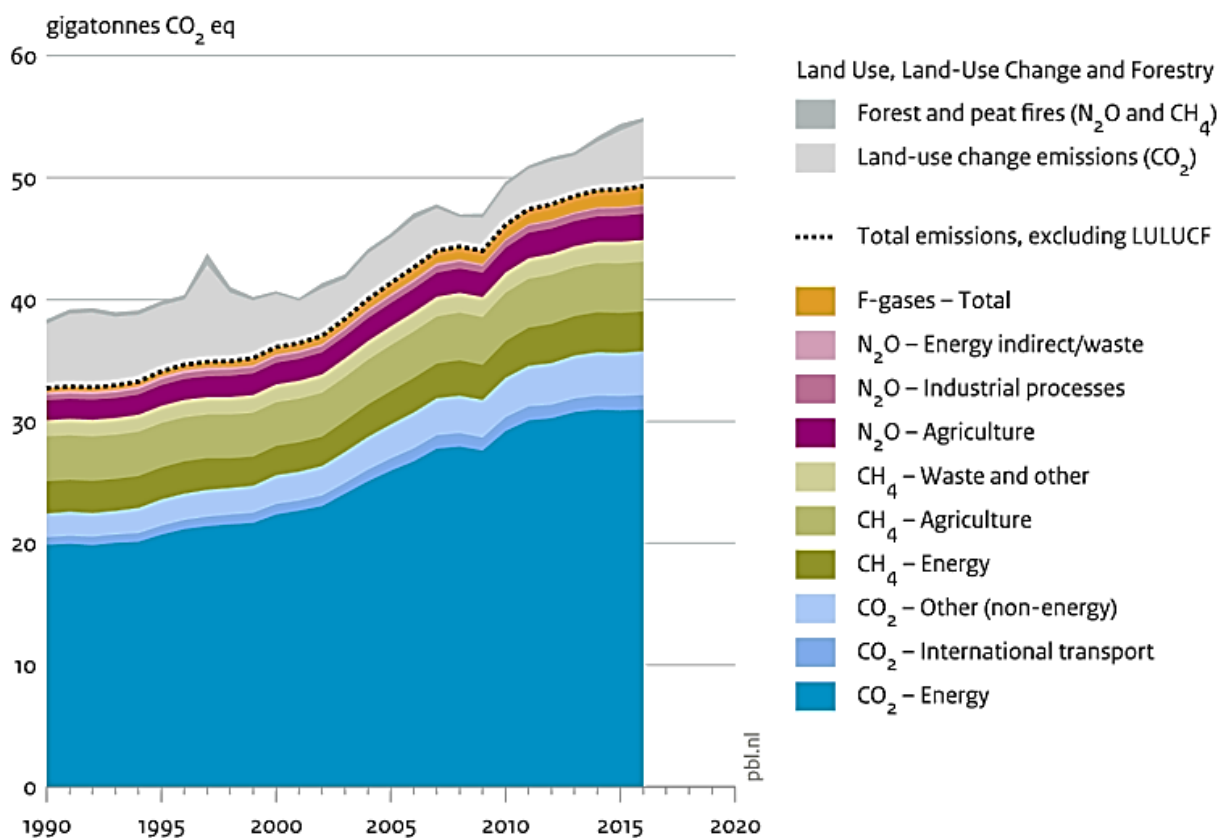


**Fig. 1.1.** Global emissions of greenhouse gases by component and origin (Olivier et al., 2017).

According to the IPCC (2013), it will be necessary to cut CO<sub>2</sub> emissions by 50% to limit the increase of average global temperature to 2°C by 2050. To impede global warming advancement, initiatives for carbon reduction in all economic sectors are made necessary,

while implementation of effective actions by private companies is usually driven by low-carbon policies imposed by governmental pressure, following determinations of international agreements in this regard. Among all human activities, electricity generation stands out as the most impactful economy sector in terms of carbon footprint. This is clearly demonstrated in Fig. 1.3, where historical evolutions of the footprints of several economy sectors are presented. Evidently, these emissions are derived from the operation of fossil fuel thermal power stations, which holds the largest share of world electricity generation. It can be understood, therefore, that implementation of technological alternatives for carbon reduction in this sector is critical for the achievement of Paris Agreement targets.

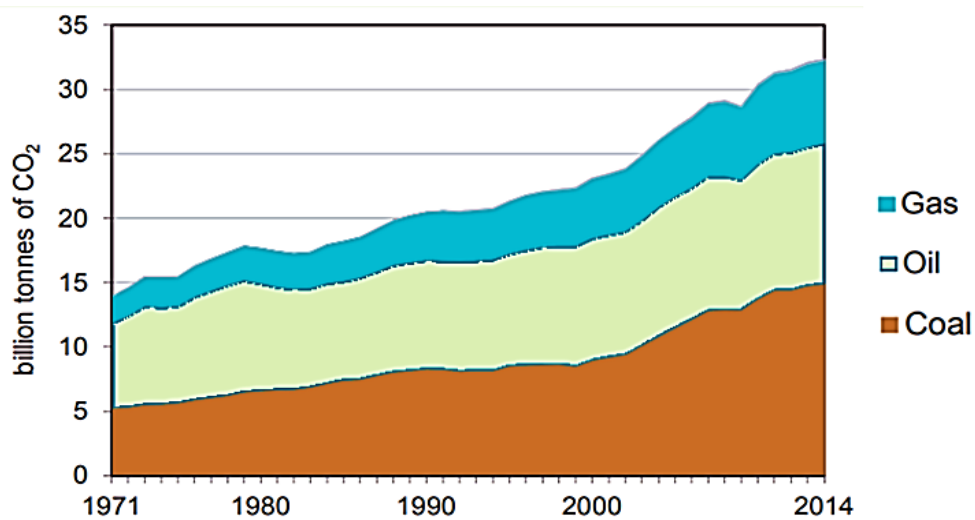


**Fig. 1.2.** Global emissions of CO<sub>2</sub> by fossil resources (IEA, 2016).

The world claims for less carbon emissions but also demands more energy supply, revealing a dual challenge for the current global energy system. The issue is addressed by gradual transition in world energy matrix, foreseeing a future with renewables playing central role in the place of fossil resources. Nevertheless, utilization of natural gas is also predicted to increase in the next few decades, acting as a bridge source into a renewable energy future. In this sense, Fig. 1.4 presents the prospects to 2035 on the use of principal energy sources as estimated by BP (2017), evincing natural gas gaining importance together with substantial advancement of renewable resources (Fig. 1.4b). Considering that there is a trend for growth in the use of natural gas, and that oil extraction will continue to be important in the near future (Fig. 1.4a), sustainability concerns bring particular attention to environmental impacts associated with oil-gas upstream activities.

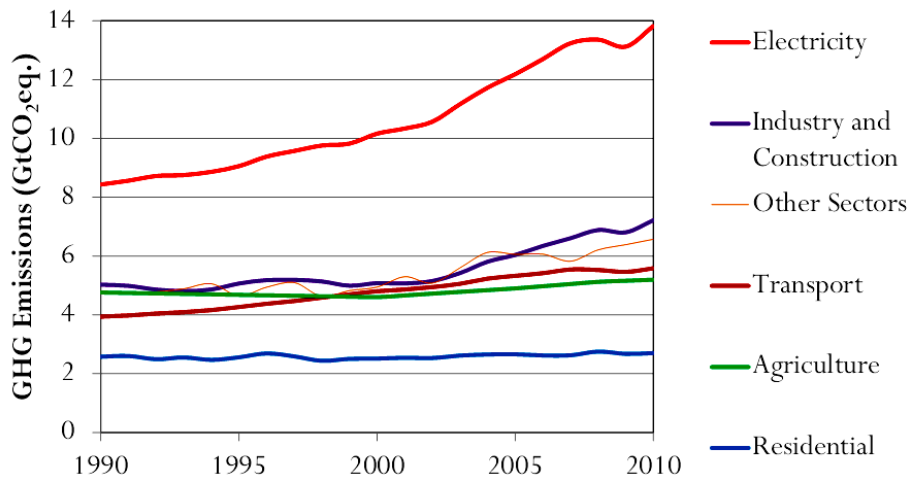


**Fig. 1.3.** Principal agents of CO<sub>2</sub> global emissions from 1970 to 2010. Own elaboration. Data sources: The Shift Project (2018) and World Bank (2018).

New oil-gas reserves often impose technological challenges for extraction and/or conditioning of products. In this regard, environmental impacts are expected to be worsened as more severe conditions are applied to upstream activities. Pre-salt fields of the Southeast Brazilian coast are inserted in such a context: among other issues, these fields are featured by huge flow rates of raw natural gas being associated to oil production and high/ultra-high CO<sub>2</sub> content in the gas, commonly exceeding 40%mol. Development of efficient and compact technological alternatives is required for such remote offshore scenario, solving challenges of CO<sub>2</sub> removal and fuel-gas use minimization, with reinjection to reservoir being the most suitable destination for the fossil CO<sub>2</sub>.

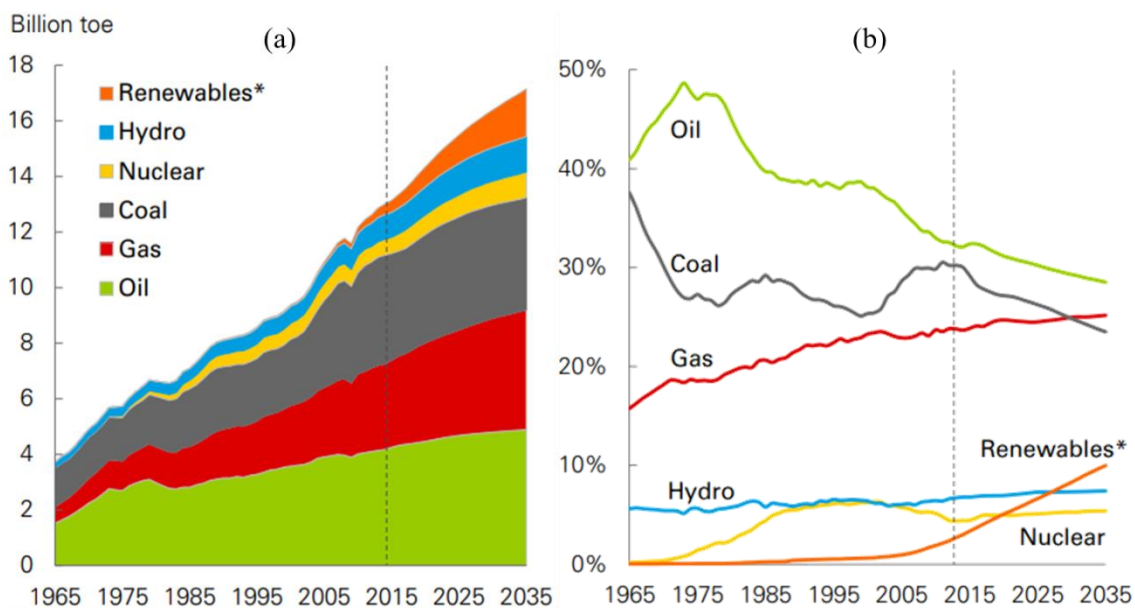


**Fig. 1.4.** World energy matrix by source. Historical evolution within 1965-2015 and projections to 2035: (a) primary energy consumption; and (b) shares of primary energy. \*Renewables includes wind, solar, geothermal, biomass, and biofuels (BP, 2017).

## 1.2. CO<sub>2</sub> Abatement Technologies

Carbon capture and storage (CCS) systems constitute important alternatives to substantially reduce CO<sub>2</sub> emissions from stationary sources while renewable energy sources are not widely – and intensively – applied. These CCS systems involve the following steps: CO<sub>2</sub> capture, compression, transportation, and final disposal in a geological reservoir, which is illustrated in Fig. 1.5 for a power plant with post-combustion CO<sub>2</sub> capture. In non-conventional capture routes (pre-combustion and oxy-combustion), power generation is part of the CCS scheme, as it is integrated with CO<sub>2</sub> capture implying substantial modifications in the original process. A major handicap is that all CCS steps are energy- and capital-intensive. Except when CO<sub>2</sub> injection is availed for enhanced oil recovery (EOR), CO<sub>2</sub> abatement solutions with geological storage vastly increase expenses without adding any revenues to the operating company. Therefore, to become economically feasible, CCS demands the intervention of governmental policies for reduction of GHGs emissions, such as the use of carbon taxation to charge CO<sub>2</sub> emissions, where avoidance of economic penalties becomes a driving-force for effective implementation of CCS routes. Moreover, another major issue is the need for long-distance transportation to geological reservoirs, which becomes critical in countries where the storage capacity is limited or only available and safe in remote offshore environments (Cuellar-Franca and Azapagic, 2015).

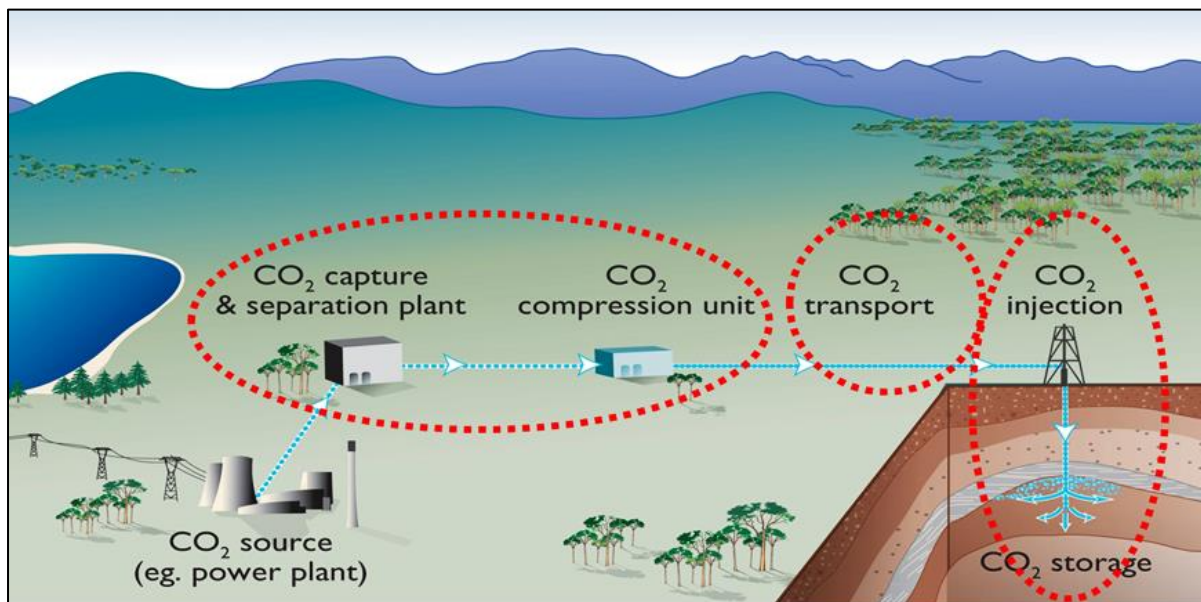


**Fig.1.5.** Conceptual steps of Carbon Capture and Storage (post-combustion capture illustration)

In the context of electricity generation in thermal power stations, CO<sub>2</sub> capture is generally conceived through one of the following conceptual routes: post-combustion, pre-combustion,

and oxy-combustion. A general scheme in this regard, also embracing processes not using combustion, is presented in Fig. 1.6 with inclusion of CO<sub>2</sub> industrial separation routes, depicting a wide view of main conceptual CO<sub>2</sub> capture pathways for industrial activities.

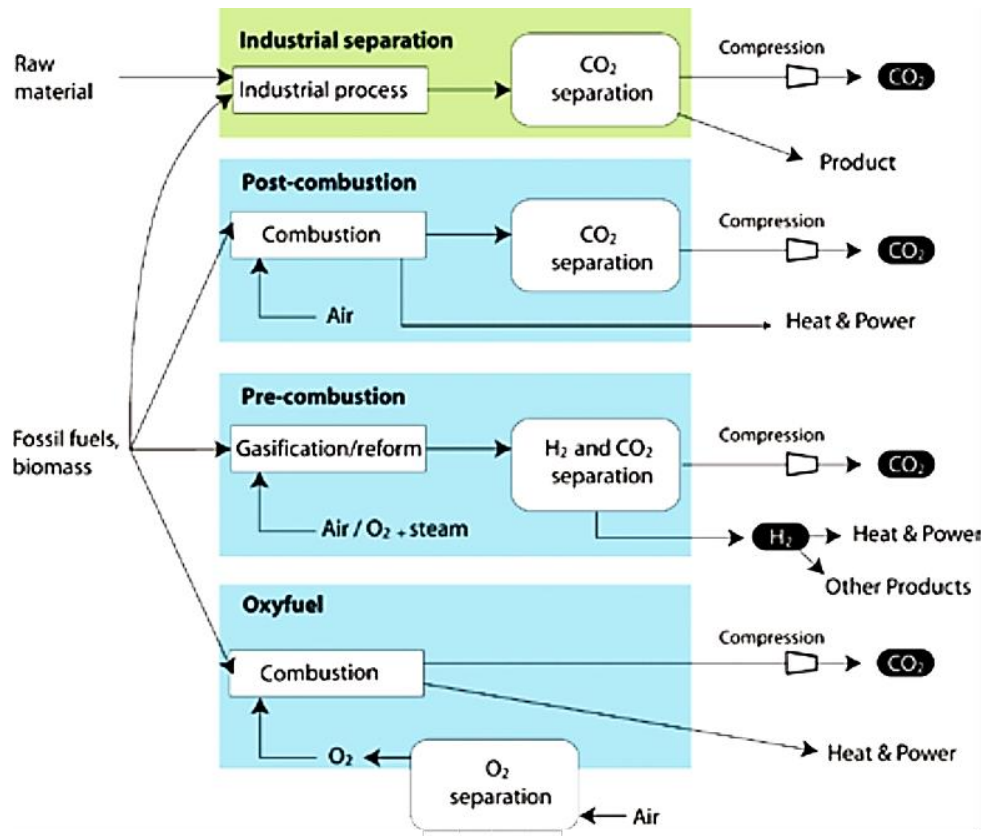


**Fig. 1.6.** CO<sub>2</sub> capture routes (IPCC, 2005).

Post-combustion route is characterized by CO<sub>2</sub> separation from flue gases, which is performed downstream to conventional air-fired combustion. All necessary structure for CO<sub>2</sub> capture can be simply attached to existent industrial plants in operation without any requirement to change the original process. Exhaust gases being processed are generally at nearly atmospheric pressure, presenting high N<sub>2</sub> content and low CO<sub>2</sub> content. As these streams have low CO<sub>2</sub> partial pressure, CO<sub>2</sub> removal is commonly performed via chemical absorption with amines, a mature technology. Post-combustion is by far the most usual method of CO<sub>2</sub> capture, mainly due to its advantage of implementation simplicity. However, compared to other capture routes, conventional post-combustion solutions usually entail higher operational costs and higher potential of other kind of environmental impacts (Kanniche et al., 2010; Cuéllar-Franca and Azapagic, 2015). Chemical absorption with amines has well-known issues of high heat duty involved in solvent regeneration and losses caused by solvent degradation, which motivate investigation of alternative technologies for CO<sub>2</sub> capture.

Pre-combustion CO<sub>2</sub> capture is based on fuel decarbonization prior to power generation, being characterized by CO<sub>2</sub> removal from H<sub>2</sub>-rich gas, for a clean combustion with H<sub>2</sub>. Firstly, synthesis gas (H<sub>2</sub>+CO+CO<sub>2</sub>) is produced by fuel gasification or reform – which is generally followed by shift reaction for CO conversion – and then CO<sub>2</sub> removal is executed. The lean gas, mostly comprising H<sub>2</sub>, is finally sent to power generation. Despite being usually the most expensive route in terms of capital investment, pre-combustion capture is featured by two particular advantages: (i) the conversion of solid fuels into high pressure gas allows the use of gas turbines, thus enabling to replace traditional Rankine cycles by more efficient combined-cycles (as in Integrated Gasification Combined-Cycle power plants); (ii) the operational cost of CO<sub>2</sub> separation step is substantially reduced compared to post-combustion CO<sub>2</sub> removal, since the synthesis gas has relatively high CO<sub>2</sub> content while being at much above atmospheric pressure, both aspects implying in high CO<sub>2</sub> partial pressure, thus favoring separation. In this sense, the elevated pressure of gas subjected to CO<sub>2</sub> capture in this route also allows utilization of physical absorption technology as an option to chemical absorption (Cuéllar-Franca and Azapagic, 2015).

Oxy-combustion CO<sub>2</sub> capture is based on practically pure oxygen replacing air in power generation, with requirement of partial recirculation of combustion products to abate flame temperature (water/steam, dry or humid exhaust gas). The particular advantage of this method consists in producing flue gas constituted mainly by CO<sub>2</sub> and H<sub>2</sub>O, so that CO<sub>2</sub> can be obtained after water condensation. Therefore, it is possible to replace a CO<sub>2</sub> removal step by an air separation unit (ASU) for oxygen production. Consequently, this is the only route allowing 100% capture (zero-emission power generation). Another characteristic is that generation of nitrogen oxides (NO<sub>x</sub>) is substantially reduced due to flue gas recirculation and avoidance of N<sub>2</sub> introduction to combustion chamber. The main disadvantage of this route is the requirement of exclusive ASU for permanent supply of gaseous oxygen (GOX), as ASUs are always expensive in terms of capital investment and manufacturing costs.

In relation to industrial processes not involving power generation, several technological alternatives are available for CO<sub>2</sub> capture (e.g. chemical absorption, physical absorption, membrane permeation, cryogenic distillation, adsorption, and – more recently – supersonic separation), and identification of most adequate options depends on working scenario and specific targets of the process. For instance, to meet demands of offshore raw natural gas processing, processes with reduced footprints and complexity are firstly taken into consideration, commonly implying in the election of membrane permeation technology.

### 1.3. Technological Gaps

#### 1.3.1. Oxygen production

The development of efficient technologies for air fractionation is a critical aspect for competitiveness of oxy-combustion systems due to its high oxygen demand. Naturally, the energy penalty for CO<sub>2</sub> capture in these systems is mostly concentrated in N<sub>2</sub>/O<sub>2</sub> fractionation, even if the CO<sub>2</sub> is posteriorly subjected to finishing purification. Currently, cryogenic separation is the only available option to produce GOX in the required scale of an oxyfuel power plant. Cryogenic ASUs are always energy- and capital-intensive, and the current technology, despite being mature in large-scale applications (up to 5000 tpd GOX), is much more power demanding than it could theoretically be. While the most efficient plants demand  $158 \text{ kWh/t O}_2$  (Higginbotham et al., 2011), the minimum consumption of a theoretical reversible process (calculated with the 2<sup>nd</sup> Law of Thermodynamics) is  $\approx 50 \text{ kWh/t O}_2$  for the same separation service (Fu and Gundersen, 2012). Since all of this excess power is wasted in irreversibilities in the process, there is clear evidence that the ASU power requirement can be substantially minimized by means of technological improvements in the process.

For instance, Fig. 1.7 illustrates (in yellow bars) the potential for reduction of energy penalty in air separation for a conventional ASU consuming  $240 \text{ kWh/t O}_2$  (typical consumption of GOX 99.5%mol production in modern ASUs) in the context of an oxy-coal power plant. The upper (light blue) portion of the bars represented in Fig. 1.7 is the contribution of a plausible downstream compression and purification unit (CPU) of CO<sub>2</sub> captured. In this example, while the CPU consumes slightly less than twice the theoretical minimum, the ASU strikingly demands 5-times the minimum (Fu and Gundersen, 2012), or 3-times at best using GOX 95%mol with  $158 \text{ kWh/t O}_2$  (Higginbotham et al., 2011).

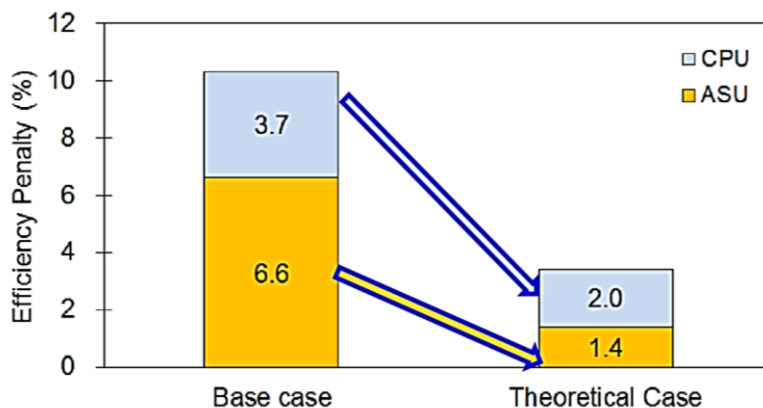


**Fig. 1.7.** Net efficiency loss (in %HHV) caused by ASU and CPU in an oxy-coal power station: conventional case and theoretical reversible processes (Fu and Gundersen, 2013a).

Another technological gap associated to cryogenic air fractionation is related with air pre-purification, where H<sub>2</sub>O, CO<sub>2</sub>, and further minor hazardous contaminants for cryogenic ASU operation are removed from air feed. Currently, these pre-purification units (PPUs) – most commonly regarded as part of the cryogenic ASUs – are totally based in separation by adsorption, comprising at least two alternating vessels with high amount of adsorbent material. As conventional PPU are usually designed with Temperature Swing Adsorption (TSA), significant consumption of heating utility is involved (e.g. low-pressure steam), with the required regeneration heat being dominated by removal of major contaminants H<sub>2</sub>O and CO<sub>2</sub>.

The most efficient processes for impure GOX production have their power demand minimized due to the reduction of required pressure in the main line of air supply to the cryogenic section of the ASU (Cold Box). Specifically, while the typical pressure of air supply for conventional Cold Boxes is in the range of 5-6 bar, efficient ASUs have a principal line at reduced pressure of  $\approx 3$  bar and a further one at  $\approx 5$  bar. Considering the plausible development of more efficient technologies for cryogenic separation, it will be possible to fractionate air supplying the Cold Box with a principal line at  $\approx 2$  bar (Fu and Gundersen, 2013b). Then in these processes where the Cold Box air feed pressure is minimized, the PPU service is substantially enlarged with H<sub>2</sub>O content increase. Moreover, the cooling capacity of air feed is also restricted, reducing water removal by condensation, thus also increasing adsorption service with higher regeneration duty. This issue is not addressed in most recent publications in air separation field, which usually only gives importance to ASU cryogenic section. These aspects evince the need for development of more efficient PPUs.

### *1.3.2. CO<sub>2</sub>-rich raw natural gas processing*

A current challenge associated with the relatively recent discoveries of giant Pre-Salt oil reserves nearby Brazilian Southeast (SE) coast is the offshore production of oil with high gas-to-oil ratio (GOR) and elevated CO<sub>2</sub> content in the gas. As burning raw gas in flares is ruled out demanding adequate processing, oil-gas upstream activities in such fields bears the following characteristics: (i) high power demand for processing the associated gas, for its conditioning to own utilization, exportation and reinjection; and (ii) equipment with much larger size than usual, a highly unwelcome aspect given the narrow availability of space and weight in floating platforms, with extremely high cost of occupied area. These circumstances

leverage the development of new technologies and imply in advances in the design of new FPSO rigs (Araújo et al., 2017).

In this context, raw natural gas (NG) processing involves dehydration – i.e. Water Dew Point Adjustment (WDPA) – to prevent hydrate formation, removal of heavy HCs – i.e. Hydrocarbon Dew Point Adjustment (HCDPA) – to prevent condensation in NG pipelines, and removal of acid gases – CO<sub>2</sub> and H<sub>2</sub>S – to increase gas heating value, reduce flow rate and avoid corrosion. Conventional processes solutionate these steps individually using large number of equipment and occupying large footprints. For CO<sub>2</sub> removal, membrane permeation offers a good alternative of compact size compared to conventional chemical absorption technology. However, membrane permeation has issues of low CH<sub>4</sub>/CO<sub>2</sub> selectivity entailing significant losses of CH<sub>4</sub> and high pressure drop in permeate side (CO<sub>2</sub>-rich gas) implying high compression power requirement. For gas dehydration, all conventional solutions – absorption with glycol and molecular-sieve (MS) adsorption – entail heavy units of large dimensions. For recovery of natural gas liquids (HCDPA), Joule-Thompson expansion with low-temperature condensate removal is generally applied, which presents drawback of intense depressurization implying high compression power demand.

All of the above aspects reveal clear demand for new compact technologies minimizing power demand in gas processing plant. In this regard, the recent technology of supersonic separation emerges as a promising method that is likely to be disseminated in the near future, as it is capable to perform all steps cited above – WDPA+HCDPA and CO<sub>2</sub> removal – fitting the platform needs in an economic and compact way (Machado et al., 2012; Arinelli et al., 2017). A visual comparison of footprints is presented in Fig. 1.9, where the alternative using conventional technologies – WDPA via absorption with triethylene-glycol and HCDPA via Joule-Thompson expansion – is compared to a plant using a single supersonic separator (SS) unit – comprising 2 SS nozzles solving simultaneous WDPA+HCDPA – for 1/3 of processing capacity, whereas full processing capacity would be attained with small increase of plant footprint. The SS technology is still poorly understood in current literature, with several misconcepted approaches to sound velocity calculation in multiphase systems and unappropriate modeling of SS performance, offering fruitful circumstance for the development of several original works of great scientific and technological contribution.

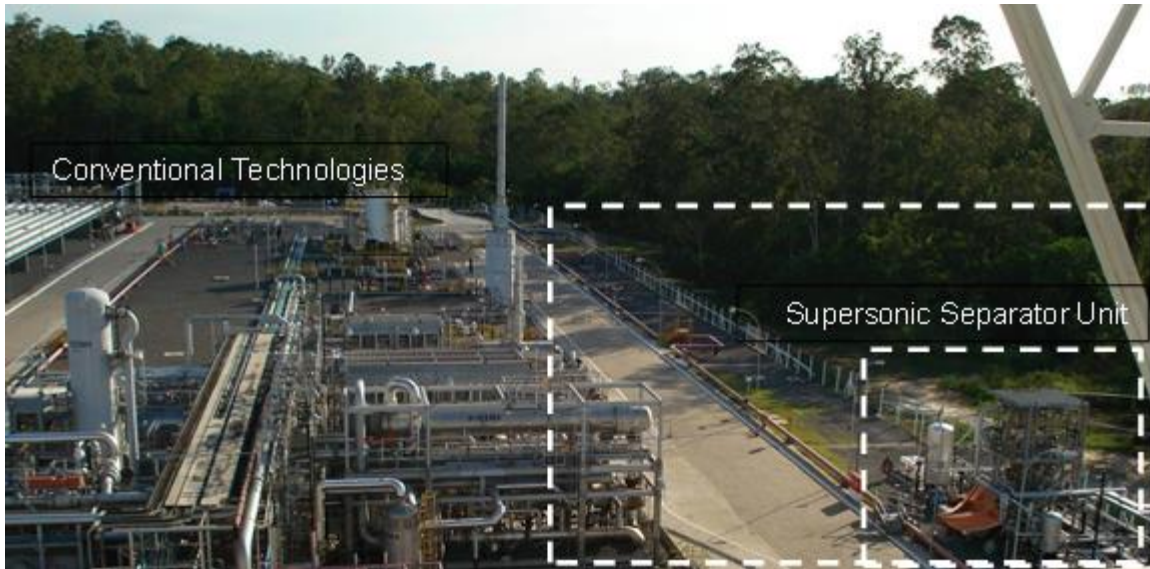


**Fig. 1.9.** Visual notion of required footprints for raw natural gas WDPA and HCDPA: conventional technologies against supersonic separator unit (de Melo, 2017).

### 1.3.3. *CO<sub>2</sub> utilization and biorefineries*

Alternatively to geological storage, CO<sub>2</sub> utilization (e.g. chemical conversion) is a generally preferred destination for the CO<sub>2</sub> captured, since it enables to aggregate revenues to the project (from the sale of valuable products) while avoids the need for long-distance transportation to reservoir. Far away from oil-gas fields, CO<sub>2</sub> utilization is usually conceived for application to large-scale production of fuels, solvents, chemical commodities and polymeric materials (e.g. polycarbonate). In this sense, carbon capture and utilization (CCU) alternatives constitute means for implementation of circular economy concept as prescribed by Industrial Ecology.

In the context of CO<sub>2</sub> utilization technologies, a plausible alternative is microalgae cultivation for biochemical CO<sub>2</sub> capture aiming the production of chemicals and biofuels. In this sense, Fig. 1.10 depicts several microalgae processing pathways, showing that a biorefinery fed with exhaust gas and mediated by microalgae production could offer a wide range of commercial products. However, such a concept for post-combustion CO<sub>2</sub> capture is rarely taken into account, maybe because the scale of such processes is supposed to entail prohibitively large photobioreactor area required for microalgae cultivation. Nevertheless, considering the possibility for vast land availability in areas of high solar irradiance, it is still reasonable to guess whether the revenues obtained from commercialization of biorefinery products is able to return capital invested on installation and replacement of photobioreactor modules.

While the majority of works in this regard reports experimental results, Process Engineering approaches including economic evaluation of alternatives are rarely found in the literature.

With the support of some experimental data, it is possible to implement these systems in a commercial process simulator. Considering that several CCU processes involving CO<sub>2</sub> biofixation in microalgal biomass were never analyzed before from technical and economic perspectives, this thesis explores gaps on methanol production via biomass gasification and biomethane production through anaerobic digestion.

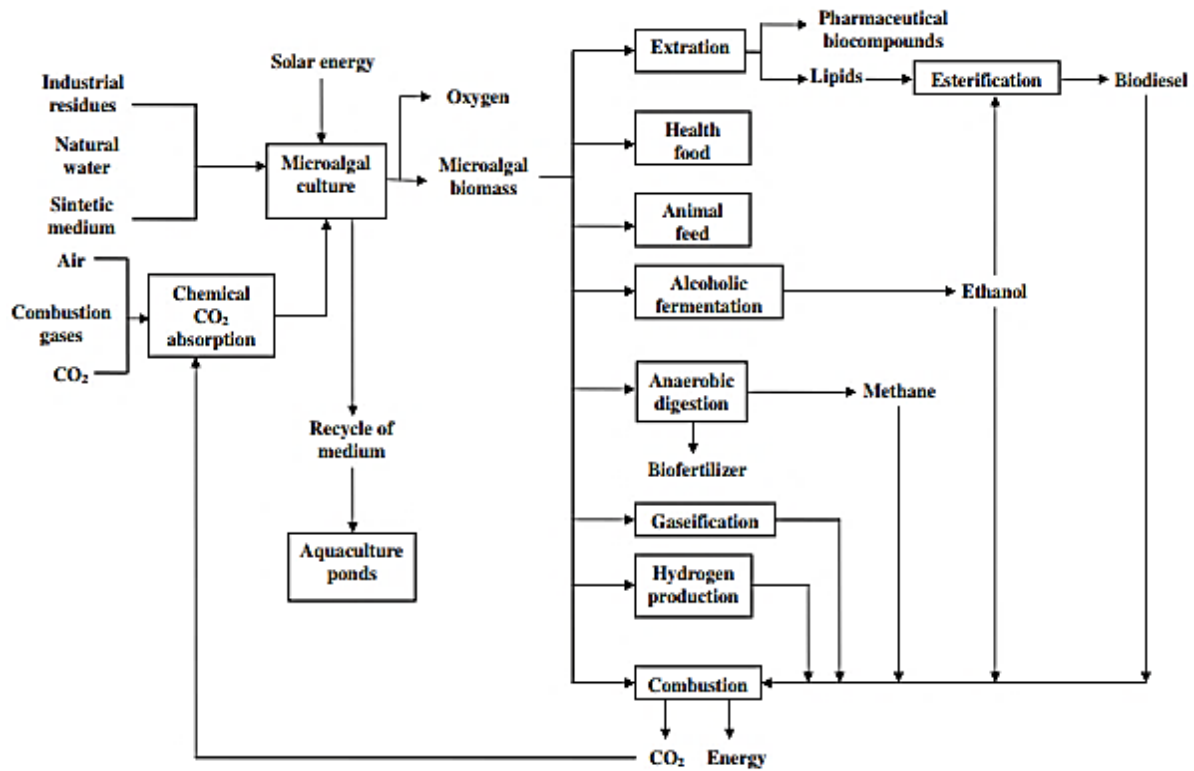


**Fig. 1.10.** Examples of microalgae processing technologies (Costa and Morais, 2011).

While CCU and CCS technologies are recommended to play an essential role in carbon reduction at electric and oil-gas sectors while world energy matrix moves towards renewable resources, efforts should be applied in the development and implementation of full biomass-based technologies. Biomass use for power generation has the advantage of being practically carbon-neutral, with CO<sub>2</sub> emissions being tolerable. However, biomass production for energy purposes endangers responsible land use, possibly entailing competition with food production. Moreover, biorefineries usually require high product prices for economic attractiveness, hampering competition with traditional processes based on fossil resources. Consequently, preferred resources for such applications are large-scale agricultural wastes (e.g. sugarcane bagasse and corncobs), which enables to simultaneously solve problems of waste management and carbon reduction in electricity generation and industrial activities. In this regard, this thesis explores a literature gap on comparative techno-economic analyses of corncob thermochemical conversion alternatives, including combustion to power generation.

## 1.4. Objectives

This thesis aims to develop and analyze technological alternatives that meet current challenges associated with carbon reduction in fuel-fired power plants and in raw CO<sub>2</sub>-rich natural gas processing, verifying technical, economic, environmental feasibility for practical implementation. Specifically, three lines of research are addressed, where there are clear technological gaps offering opportunity for the production of original technical material of great interest to scientific community: {R1} oxy-combustion CO<sub>2</sub> capture, with emphasis on oxygen production via cryogenic air separation from adequate air pre-purification; {R2} offshore CO<sub>2</sub>-rich NG processing; and {R3} chemical or biochemical CO<sub>2</sub> utilization and biorefineries, where two biomass sources are conceived: microalgae – due to its high photosynthesis efficiency – and corncobs – a large-scale agricultural residue.

Within the line {R1} of oxy-combustion, oxygen production and air pre-purification, the following cases are evaluated: (i) novel cryogenic ASU based on top vapor recompression distillation, for oxygen supply to a zero-emission NG combined-cycle power plant with oxy-combustion CO<sub>2</sub> capture to EOR (Brigagão et al., 2019a); and (ii) novel PPU for cryogenic ASU based on low-pressure supersonic separator (SS) followed by finishing adsorption (Brigagão et al. 2019b), which is assessed in terms of exergy efficiency (Chapter 4).

Within the line {R2} of offshore CO<sub>2</sub>-rich NG processing, application of SS technology is compared to conventional processes for performing the adjustment of water and hydrocarbon dew-points, and CO<sub>2</sub> removal. By comparison of several alternatives, the most attractive process is suggested for application in the topside of a large floating hub for gas processing (Arinelli et al., 2019; de Melo et al., 2019).

Within the line {R3} of CO<sub>2</sub> utilization and biorefineries, the following cases are evaluated: (i) thermochemical conversion of microalgae, cultivated for biofixation of CO<sub>2</sub> generated by a power plant, prescribing extraction of microalga oil and gasification for methanol production (Wiesberg et al., 2017); (ii) anaerobic digestion of microalgae biomass for the production of biomethane or electricity (Brigagão et al., 2019c); and (iii) thermochemical conversion of corncobs for the production of methanol, electricity or fast pyrolysis bio-oil (Brigagão et al., 2019d).

## 1.5. Justification

All technological alternatives investigated in this thesis are inserted in the context of plausible routes for carbon reduction, either by means of CO<sub>2</sub> capture, power consumption reduction lowering CO<sub>2</sub> emissions, CO<sub>2</sub> utilization or renewable resources utilization. Although not all considered processes share the same scope – not being directly connected (air separation, air pre-purification, raw NG processing, microalgae cultivation for gasification or anaerobic digestion, corncob thermochemical conversion) – there are several interface points worthing mention in addition to the main purpose of carbon reduction.

Although this work does not intend to compare the performance of all available technologies for CO<sub>2</sub> removal from gaseous streams to each working scenario, several alternatives for this purpose are addressed as most suitable choices accordingly to different applications: chemical absorption (applied to treat exhaust gas, biogas and low-pressure synthesis gas feeds) (Brigagão et al., 2019c; Brigagão et al., 2019d, Wiesberg et al., 2017), physical absorption (for high-pressure synthesis gas) (Wiesberg et al., 2017), adsorption (for atmospheric air) (Brigagão et al., 2019b), membrane permeation and supersonic separation (both for CO<sub>2</sub>-rich NG) (Arinelli et al., 2019; de Melo et al., 2019), besides biological CO<sub>2</sub> capture with microalgae cultivation (for exhaust gas) (Wiesberg et al., 2017). Supersonic separators and membranes are quite advantageous alternatives for bulk CO<sub>2</sub> removal applications (lean gas >20%mol CO<sub>2</sub>) in offshore processing of CO<sub>2</sub>-rich NG because of their compactness (Arinelli et al., 2017; Arinelli et al., 2019; de Melo et al., 2019). Adsorption is the ideal option for deep removal of trace compounds, which is the case of CO<sub>2</sub> removal from atmospheric air ( $\approx 400$  ppmv CO<sub>2</sub>) in a PPU for cryogenic air separation (Brigagão et al., 2019b). For biogas purification, chemical absorption is selected accounting for its technological maturity, since the plant relies on microorganisms' activity, which, in contrast, should inflict operational issues in large scale applications (Brigagão et al., 2019c). In high-pressure synthesis gas processing (obtained from microalgae gasification), physical absorption with refrigerated methanol (Rectisol Process) is considered more convenient, accounting for high-pressure operation, high CO<sub>2</sub> partial pressure, reasonable H<sub>2</sub>/CO<sub>2</sub> selectivity, and considering that methanol is the product of the evaluated system eliminating the need to purchase solvent to offset losses in the process (Wiesberg et al., 2017).

In raw NG processing, besides plausible SS application for CO<sub>2</sub> removal, SS technology is also availed for the simultaneous adjustment of water and hydrocarbon dew-points, as usually conceived for SS applications (Machado et al., 2012). Another common aspect in this work is

that SS performing dehydration is also proposed in this work for another context: in air pre-purification for cryogenic separation, where SS is suggested to play a central role performing bulk water removal. Since the SS alone is not capable to attain the required rigorous specification of air contaminants for admission to the Cold Box, a finishing purification step based on adsorption is necessary for removal of CO<sub>2</sub>, H<sub>2</sub>O traces and further minor contaminants (Brigagão et al., 2019b).

Microalgae cultivation executes CO<sub>2</sub> removal from atmospheric air or exhaust gas by means of photosynthesis simultaneously converting it into biomolecules of high molecular weight. Here, a closed photobioreactor system fed with exhaust gas is applied. Biological valorization of CO<sub>2</sub> generated by a power plant is attained from CO<sub>2</sub> biofixation in microalgae, enabling to have a wide range of valuable products with appropriate chemical processing of this biomass in a biorefinery. Considering that a major advantage of processes mediated by microalgae consists in elevated efficiency in the absorption and use of solar energy, this energy source avoids additional consumption of fossil fuels to perform CO<sub>2</sub> capture and utilization, which is widely known to generate other sorts of environmental impacts while mitigate global warming (i.e. life-cycle impacts related with increased fuels consumption) (Cuéllar-Franca and Azapagic, 2015).

Concerning CO<sub>2</sub> destination, EOR is applied in most alternatives (Arinelli et al., 2019; Brigagão et al., 2019a; Brigagão et al., 2019c; de Melo et al., 2019), while in the others chemical conversion or geological storage is also considered (Brigagão et al., 2019c; Wiesberg et al., 2017), with exception of corncob thermochemical processing, which is regarded as practically carbon-neutral, thus being acceptable for application without CO<sub>2</sub> capture (Brigagão et al., 2019d).

Among the considered chemical/biochemical CO<sub>2</sub> conversion routes, the principal products being suggested are methanol (Wiesberg et al., 2017) and biomethane (Brigagão et al., 2019c), which are substances commonly derived from fossil NG. Synthesis gas used in methanol production can be produced from biomass instead of natural gas, but with the penalty of CO<sub>2</sub> capture being required to adjust the H/C proportion. Biogas mainly consists of CH<sub>4</sub> and CO<sub>2</sub>, also requiring contaminants removal for dispatch at suitable conditions like CO<sub>2</sub>-rich raw NG, with CO<sub>2</sub> capture being the major penalty. Compared to fossil NG, the main difference is that biogas is practically free of HCs C<sub>2</sub>+, thus biogas purification mainly consists of acid gas (CO<sub>2</sub>, H<sub>2</sub>S) removal and biomethane dehydration.

An overview of main covered topics showing other connections between the proposed process alternatives and their working scenarios is presented in Table A3.1 at Appendix A3. Specific discussion on originality aspects of each process alternative being addressed in research lines {R1}, {R2} and {R3} is presented in Secs. 1.5.1, 1.5.2, and 1.5.3, respectively.

#### *1.5.1. Oxygen production via cryogenic air separation*

This thesis presents an innovative technology for large-scale oxygen production, exhibiting less power demand than any process ever reported in technical literature, which is already registered as patent application BR102016022807-7 (Brigagão et al., 2016). This process is based on cryogenic top vapor recompression distillation, which basically comprises a single distillation column operating at nearly atmospheric pressure, contrasting with the usual method based on separation in two or more columns operated at different pressure levels. Although both methods require preliminary step of air compression, to provide a minimum viable delta temperature in the condenser-reboiler of the distillation column, the vapor recompression alternative avoids unnecessary compression of O<sub>2</sub> contained in air feed (Fu and Gundersen, 2013b). Moreover, it further enhances separation performance by reducing the required reflux ratio by feeding the column with liquified air, in addition to the increase in N<sub>2</sub>/O<sub>2</sub> relative volatility due to elimination of high-pressure fractionation column. These aspects are then translated into substantial savings in terms of separation power demand. The main innovation of this process consists in the operation of a cold (cryogenic) compressor allowing nitrogen condensation through heat exchange with vaporization of liquid oxygen or liquid from an intermediate portion of the fractionation column, this being associated with the fact that in addition to the nitrogen reflux, the column is fed with liquefied air in its upper portion causing reduction of nitrogen reflux demanded at the top. The new cryogenic ASU is compared to several other process configurations and applied to supply gaseous oxygen to an oxy-combustion power plant operating nearby an oil-gas field for implementation of Gas-To-Wire concept (where NG transportation is replaced by electricity transmission requiring *in situ* power generation), with the CO<sub>2</sub> captured being availed for EOR (Brigagão et al., 2019a).

Another innovative point of this thesis is the development of a novel concept of air pre-purification for cryogenic separation, with supersonic separator (SS) performing dehydration. Although SS use is an already known unit operation in the current state-of-the-art of high-pressure raw NG processing to recover condensable compounds (H<sub>2</sub>O+HCs or CO<sub>2</sub>+HCs), such application substantially differs from raw NG processing. Air pre-purification is

characterized by strict specification of contaminants, with raw air feed showing few parts per million in volume (*ppmv*) of HCs and  $\approx 400$  *ppmv*  $CO_2$ , while being typically at  $<10$  bar. Therefore, unlike NG processing, there is no possibility of recovering valuable products with this SS application. The use of SS performing air dehydration in the context of a cryogenic ASU has never been proposed before in the literature. The present proposal was therefore registered as patent application BR102017027727-5 (Brigagão et al., 2017), comprising a pre-purification unit (PPU) constituted by a battery of supersonic separators, which removes the great majority of  $H_2O$ , followed by a finishing adsorption step for the removal of  $CO_2$ , residual  $H_2O$ , and further trace contaminants (e.g. HCs). The adsorption unit (e.g. TSA) is needed to complement SS bulk purification, because the SS alone is not capable to perform deep purification to allow cryogenic air processing. The economic viability of this alternative is demonstrated by comparison with a conventional unit, fully based in TSA, for application to a Cold-Box with reduced air feed pressure of  $\approx 3$  bar (Brigagão et al., 2019b). This Cold-Box assumes the use of a typical efficient ASU for producing  $GOX$  95%*mol*, as recommended for oxy-combustion  $CO_2$  capture in power generation, to minimize the capture penalty making it economically competitive – and even more advantageous in environmental terms – in relation to other  $CO_2$  capture conceptual routes.

#### *1.5.2. $CO_2$ -rich natural gas processing with supersonic separators*

While there are some recent studies in the literature dealing with NG processing with SS, works considering rigorous thermodynamic calculations are extremely rare given the multiphase-equilibrium conditions that characterize the SS interior. Moreover, the possibility of  $CO_2$  freeze-out is also often not taken into account in most works regarding large-scale SS application for  $CO_2$  capture. Contrasting with these aspects, the present work applies rigorous thermodynamic approach with appropriate calculation of sound speed in multiphase systems, according to the methods of Arinelli et al. (2017), de Medeiros et al. (2017) and de Medeiros et al. (2019). The several process alternatives being investigated are contextualized for installation in a large-scale gas-hub receiving high-pressure multiphase fluid from risers, aiming the recovery of the oil and the reinjection of the  $CO_2$ -rich gas for EOR, designating a small fraction of processed NG to serve as fuel gas to the platform, meeting its power demand. The proposal of a gas-hub with giant capacity for NG processing, although hypothetical, is perfectly compatible with the actual challenge of operating remote offshore oil fields with high gas-to-oil ratio (GOR) and high  $CO_2$  content in the associated gas (Arinelli et al., 2019; de Melo et al., 2019).

### 1.5.3. CO<sub>2</sub> utilization and biorefineries

Biological CO<sub>2</sub> capture and valorization is challenged by economic aspects, and sustainability analyses of biofuel-driven biorefineries must regard this perspective to improve attractiveness of such alternatives (Chea et al., 2016). However, studies addressing economic analysis of process alternatives conceiving microalgae cultivation for CCU are rarely found in the literature. Even considering that technological advancements are needed to allow effective large-scale implementation of microalgae biorefineries for abatement of CO<sub>2</sub> emissions from a power plant, this work contributes with a process engineering approach to identify potential barriers for such a concept, with economic performances leveraged by CO<sub>2</sub> taxation policy.

Performance comparison between the new proposed biorefinery for methanol production and conventional chemical absorption for CCS is first time presented in the literature. The biorefinery consists of a CCU route using exhaust gas from a power plant, with CO<sub>2</sub> capture being performed by *Chlorella pyrenoidosa*, which biomass is subsequently availed for microalga oil extraction and methanol production through gasification (Wiesberg et al., 2017). One aspect of great relevance, still often neglected in the literature, is the inclusion of carbon taxation in the assumptions of economic assessments. This work defines a break-even taxation point determining feasibility for such biorefinery alternative.

Furthermore, although anaerobic digestion of microalgae has been intensively studied in the literature (but essentially limited to experimental works), economic performance of such a process – embracing all processing stages from the reception of the microalgal biomass to biomethane commercialization – is first time presented in the literature. Two biogas monetization alternatives are evaluated, with and without CO<sub>2</sub> capture: biomethane production and bioelectricity generation,. Performances are evaluated under diverse economic scenarios, considering revenues from biogas products and CO<sub>2</sub> sale allied to taxes and cap & trade mechanism, a new approach that has never been addressed to analyze such a concept (Brigagão et al., 2019c).

Finally, in connection with the world demand for transition into a renewable energy future, for replacement of fossil resources with effective carbon reduction without the need to perform CO<sub>2</sub> capture, performance evaluation of three biorefinery concepts using a large-scale agricultural waste is presented. In this regard, this thesis investigates the application of corncobs, filling a literature gap on techno-economic comparison of corncob thermochemical processing alternatives for the production of electricity, methanol and fast pyrolysis bio-oil (Brigagão et al., 2019d).

## 1.6. Outline of Thesis Structure

This thesis is structured as a collection of published articles (Chapters 2, 3, 7, 8), new research (Chapter 4), and shortened versions of co-authorship works (Chapters 5, 6). The research lines {R1}-{R3} are represented by the following distribution given in Table 1.1 (Chapters 2, 3, 7 and 8 fully reproduce their reference scientific articles).

**Table 1.1.** Scientific articles associated with chapters contents.

<b>Research Line</b>	<b>Chapters</b>	<b>Articles References</b>
{R1} Oxy-combustion CO <sub>2</sub> capture	02	Brigagão et al. (2019a)
	03	Brigagão et al. (2019b)
	04	–
{R2} Offshore CO <sub>2</sub> - rich NG processing	05	Arinelli et al. (2019) de Melo et al. (2019)
	06	Wiesberg et al. (2017)
{R3} CO <sub>2</sub> utilization and biorefineries	07	Brigagão et al. (2019c)
	08	Brigagão et al. (2019d)

Chapter 2 (Brigagão et al., 2019a) proposes an alternative cryogenic distillation process for large-scale gaseous oxygen supply, which is based on cryogenic top vapor recompression distillation in a single column operated at nearly atmospheric pressure. Results from simulation and optimization of several processes for low-pressure gaseous oxygen supply are presented. The study applies the new air separation unit to a natural gas combined cycle Gas-To-Wire plant with oxy-combustion CO<sub>2</sub> capture, assuming CO<sub>2</sub> destination to EOR. The overall system is evaluated by means of economic assessment and compared to conventional air-fed combined cycle.

Chapter 3 (Brigagão et al., 2019b) proposes a new concept of air pre-purification unit for cryogenic fractionation prescribing a supersonic separator upstream to a finishing adsorption unit. Processes adopting this concept with or without compression heat recovery are compared to a conventional pre-purification unit totally based on temperature swing adsorption. Results from economic analysis of process alternatives are presented.

Chapter 4 conducts exergy analyses of process alternatives described in Chapter 3 to compare thermodynamic performances and indicate improvements for better resources utilization. This is the only chapter bearing contents that are not published yet.

Chapter 5 (Arinelli et al., 2019; de Melo et al., 2019) proposes adopting supersonic separators for dew-point adjustments and CO<sub>2</sub> capture for processing raw NG with ultra-high CO<sub>2</sub> content in a high-capacity floating-hub. Case Study 1 (de Melo et al., 2019), in Sec. 5.3,

economically compares one alternative adopting conventional technologies to a SS-SS alternative featured by one SS unit for WDPA+HCDPA and another one for CO<sub>2</sub> removal. Case Study 2 (Arinelli et al., 2019), in Sec. 5.4, starts with the same SS-SS alternative and investigates structural changes in the process, maintaining SS use for WDPA+HCDPA. Alternatives are compared in terms of power demand, profitability and CO<sub>2</sub> emissions. This chapter embraces contents of two co-authored scientific publications (Arinelli et al., 2019; de Melo et al., 2019) giving emphasis on comparison of suitable process alternatives.

Chapter 6 (Wiesberg et al., 2017) evaluates a biorefinery route prescribing post-combustion CO<sub>2</sub> biofixation in microalgae, extraction of microalgae oil and microalgal biomass gasification for methanol production, which is economically compared to conventional carbon capture and storage route adopting CO<sub>2</sub> capture via chemical absorption with amine. This chapter is a shortened version of a co-authored scientific publication (Wiesberg et al., 2017) giving emphasis on economic performance of proposed microalga-based biorefinery.

Chapter 7 (Brigagão et al., 2019c) evaluates alternative biorefinery arrangements processing microalgal biomass via anaerobic digestion. Biomass low-cost pretreatment strategies, application of pressurized digester and downstream biogas processing alternatives – for power generation or biomethane production – are compared in terms of energy, economic and carbon footprint performances.

Chapter 8 (Brigagão et al., 2019d) evaluates three pathways for thermochemical conversion of a specific agricultural waste – corncobs – as a renewable resource with plausible large-scale implementation to a biorefinery: combustion for power generation, gasification for methanol production, and fast pyrolysis for bio-oil recovery. Comparison of techno-economic performances is presented.

Chapter 9 then finally encloses all studies with an overall conclusion addressing combined discussion of specific results, highlighting the main specific findings of all works.

Appendix A presents a summary of all products derived from this research – including published scientific articles, conference papers, and pending patents – and further discusses personal contributions on co-authorship works (Chapters 5 and 6).

Appendices B-S unveil front pages and complete bibliographic data of all publications.

Appendices T-Z are supplementary materials for Chapters 2, 3, 4, 5, 6 and 7.

## 1.7. References for Chapter 1

Araújo, O. Q. F.; Reis, A. C.; de Medeiros, J. L.; Nascimento, J. F.; Grava, W. M.; Musse, A. P. S. Comparative analysis of separation technologies for processing carbon dioxide rich natural gas in ultra-deepwater oil fields. *Journal of Cleaner Production*, 155, 12–22, 2017. <https://doi.org/10.1016/j.jclepro.2016.06.073>

Arinelli L. O.; Trotta T. A. F.; Teixeira, A. M.; De Medeiros, J. L.; Araújo O. Q. F. Offshore Processing of CO<sub>2</sub> Rich Natural Gas with Supersonic Separator versus Conventional Routes. *Journal of Natural Gas Science and Engineering*, 46, 199–221, 2017. <https://doi.org/10.1016/j.jngse.2017.07.010>

Arinelli, L. O.; de Medeiros, J. L.; de Melo, D. C.; Teixeira, A. M.; Brigagão, G. V.; Passarelli, F.; Grava, W. M.; Araújo, O. Q. F. Carbon capture and high-capacity supercritical fluid processing with supersonic separator: natural gas with ultra-high CO<sub>2</sub> content. *Journal of Natural Gas Science and Engineering*, 66, 265-283, 2019. <https://doi.org/10.1016/j.jngse.2019.04.004>

BP. BP energy outlook, 2017 edition, 2017.

Brigagão, G. V., de Medeiros, J. L., Araújo, O. Q. F., inventors; Universidade Federal do Rio de Janeiro, applicant. Processo de destilação criogênica para separação do ar para produção de oxigênio gasoso. BR Patent application 102016022807-7. Filed in September 30th, 2016.

Brigagão, G. V., Arinelli, L. O., de Medeiros, J. L., Araújo, O. Q. F., inventors; Universidade Federal do Rio de Janeiro, applicant. Purificação do ar para fracionamento criogênico com separador supersônico de baixa pressão. BR Patent Application 102017027727-5. Filed in December 21st, 2017.

Brigagão, G. V.; de Medeiros, J. L.; Araújo, O. Q. F. A novel cryogenic vapor-recompression air separation unit integrated to oxyfuel combined-cycle gas-to-wire plant with carbon dioxide enhanced oil recovery: energy and economic assessments. *Energy Conversion and Management*, 189, 202-214, 2019a. <https://doi.org/10.1016/j.enconman.2019.03.088>

Brigagão, G. V., Arinelli, L. O., de Medeiros, J. L., Araújo, O. Q. F. A new concept of air pre-purification unit for cryogenic separation: low-pressure supersonic separator coupled to finishing adsorption. *Separation and Purification Technology*, 215, 173-189, 2019b. <https://doi.org/10.1016/j.seppur.2019.01.015>

Brigagão, G. V.; Wiesberg, I. L.; Pinto, J. L.; Araújo, O. Q. F.; de Medeiros, J. L. Upstream and downstream processing of microalgal biogas: emissions, energy and economic performances under carbon taxation. *Renewable and Sustainable Energy Reviews*, 112, 508-520, 2019c. <https://doi.org/10.1016/j.rser.2019.06.009>

Brigagão, G. V.; Araújo, O. Q. F.; de Medeiros, J. L.; Mikulcic, H.; Duic, N. A techno-economic analysis of thermochemical pathways for corncob-to-energy: fast pyrolysis to bio-oil, gasification to methanol and combustion to electricity. *Fuel Processing Technology*, 193, 102-113, 2019d. <https://doi.org/10.1016/j.fuproc.2019.05.011>

Cheah, W. Y.; Ling, T. C.; Juan, J. C.; Lee, D. J.; Chang, J. S.; Show, P. L. Biorefineries of carbon dioxide: from carbon capture and storage (CCS) to bioenergies production. *Bioresource Technology*, 215, 346–356, 2016. <https://doi.org/10.1016/j.biortech.2016.04.019>.

Costa, J. A. V.; Morais, M. G. The role of biochemical engineering in the production of biofuels from microalgae. *Bioresource Technology*, 102, 2–9, 2011. <https://doi.org/10.1016/j.biortech.2010.06.014>

Cuellar-Franca, R. M.; Azapagic, A. Carbon capture, storage and utilisation technologies: a critical analysis and comparison of their life cycle environmental impacts. *Journal of CO<sub>2</sub> Utilization*, 9, 82-102, 2015. <https://doi.org/10.1016/j.jcou.2014.12.001>

Darde, A.; Prabhakar, R.; Tranier, J. P.; Perrin, N. Air separation and flue gas compression and purification units for oxy-coal combustion systems. *Energy Procedia*, 1, 527-534, 2009. <https://doi.org/10.1016/j.egypro.2009.01.070>

de Medeiros, J. L.; Arinelli, L. O.; Araújo, O. Q. F. Speed of sound of multiphase and multi-reactive equilibrium streams: a numerical approach for natural gas applications. *Journal of Natural Gas Science and Engineering*, 46, 222-241, 2017. <https://doi.org/10.1016/j.jngse.2017.08.006>

de Medeiros, J.L., Arinelli, L.O., Teixeira, A.M., Araújo, O.Q.F. Offshore processing of CO<sub>2</sub>-rich natural gas with supersonic separator: multiphase sound speed, CO<sub>2</sub> freeze-out and HYSYS implementation, 1st ed., Springer International Publishing, Springer Nature Switzerland AG, 2019. <https://doi.org/10.1007/978-3-030-04006-2>. ISBN:978-3-030-04006-2(e-Book)/978-3-030-04005-5(Hardcover).

de Melo, D. C. Tratamento offshore de gás natural rico em CO<sub>2</sub>: análise da viabilidade técnica e econômica para o desenvolvimento da produção de óleo e gás do pólo Pré-Sal. DSc Qualifying Examination Document (Doctorate in Chemical and Biochemical Process Technology), Escola de Química, Federal University of Rio de Janeiro, 2017.

de Melo, D. C.; Arinelli, L. O.; de Medeiros, J. L.; Teixeira, A. M.; Brigagão, G. V.; Passarelli, F.; Grava, W. M.; Araújo, O. Q. F. Supersonic separator for cleaner offshore processing of supercritical fluid with ultra-high carbon dioxide content: economic and environmental evaluation. *Journal of Cleaner Production*, 234, 1385-1398, 2019. <https://doi.org/10.1016/j.jclepro.2019.06.304>

Fu, C.; Gundersen, T. Using exergy analysis to reduce power consumption in air separation units for oxy-combustion processes. *Energy*, 44, 60-68, 2012. <https://doi.org/10.1016/j.energy.2012.01.065>

Fu, C.; Gundersen, T. Optimal integration of compression heat within oxy-coal power plants. AICHE Annual Meeting, San Francisco, 2013a.

Fu, C.; Gundersen, T. Recuperative vapor recompression heat pumps in cryogenic air separation processes. *Energy*, 59, 708-718, 2013b. <https://doi.org/10.1016/j.energy.2013.06.055>

Higginbotham, P.; White, V.; Fogash, K.; Guvelioglu, G. Oxygen supply for oxyfuel CO<sub>2</sub> capture. *International Journal of Greenhouse Gas Control*, 5, S194–S203, 2011. <https://doi.org/10.1016/j.ijggc.2011.03.007>

IEA. CO<sub>2</sub> emissions from fuel combustion: highlights. 2016.

IPCC. IPCC Special Report on Carbon Dioxide Capture and Storage. Prepared by Working Group III of the Intergovernmental Panel on Climate Change. Metz, B.; Davidson, O.; Coninck, H. C.; Loos, M.; Meyer, L. A. (Eds.). Cambridge University Press, Cambridge, 2005.

IPCC. Climate Change 2013: The Physical Science Basis, Intergovernmental Panel on Climate Change, 2013. Available at <https://www.ipcc.ch/report/ar5/wg1/>.

IPCC. Climate change 2014: synthesis report. Contribution of Working Groups I, II and III to the Fifth Assessment Report of the Intergovernmental Panel on Climate Change. Core Writing Team, Pachauri, R. K.; Meyer, L. A. (eds.). IPCC, Geneva, Switzerland, 151 pp, 2014.

Kanniche, M., Gros-Bonnivard, R., Jaud, P., Valle-Marcos, J., Amann, J.M., Bouallou, C. Pre-combustion, post-combustion and oxy-combustion in thermal power plant for CO<sub>2</sub> capture. *Applied Thermal Engineering*, 30, 53-62, 2010. <https://doi.org/10.1016/j.applthermaleng.2009.05.005>

Machado, P. B.; Monteiro, J. G. M.; de Medeiros, J. L.; Epsom, H. D.; Araujo, O. Q. F. Supersonic separation in onshore natural gas dew point plant. *Journal of Natural Gas Science and Engineering*, 6, 43-49, 2012. <https://doi.org/10.1016/j.jngse.2012.03.001>

Olivier, J. G. J.; Schure, K. M.; Peters, J. A. H. W. Trends in global CO<sub>2</sub> and total greenhouse gas emissions: summary of the 2017 report. PBL Netherlands Environmental Assessment Agency, The Hague, 2017.

The Shift Project. Historical GHG emissions – breakdown by sector. Available at <http://www.tsp-data-portal.org/Historical-GHG-emissions-by-Sector>. Accessed in Jan. 20<sup>th</sup>, 2018.

Wiesberg, I. L.; Brigagão, G. V.; de Medeiros, J. L.; Araújo, O. Q. F. Carbon dioxide utilization in a microalga-based biorefinery: efficiency of carbon removal and economic performance under carbon taxation. *Journal of Environmental Management*, 203, 988-988, 2017. <https://doi.org/10.1016/j.jenvman.2017.03.005>

World Bank. Carbon emissions by sector. World Development Indicators. Available in <http://wdi.worldbank.org/table>. Accessed in Jan. 20<sup>th</sup>, 2018.

## 2. A Novel Cryogenic Vapor-Recompression Air Separation Unit Integrated to Oxyfuel Combined-Cycle Gas-To-Wire Plant with Carbon Dioxide Enhanced Oil Recovery: Energy and Economic Assessments

*This chapter is published as an article in Energy Conversion and Management.*

BRIGAGÃO, G. V.; DE MEDEIROS, J. L.; ARAÚJO, O. Q. F. A novel cryogenic vapor-recompression air separation unit integrated to oxyfuel combined-cycle gas-to-wire plant with carbon dioxide enhanced oil recovery: energy and economic assessments. *Energy Conversion and Management*, 189, p. 202-214, 2019.

### **Abstract**

Oxyfuel carbon capture is both power and capital intensive due to oxygen demand. Consequently, oxyfuel requires the development of more efficient air separation units. This work proposes an alternative cryogenic distillation process for large-scale gaseous oxygen supply. Instead of using different pressure columns, the new air separation unit couples top vapor recompression to a single atmospheric cryogenic air distillation double-reboiler column, whose nitrogen-rich top vapor is compressed to heat the intermediate column reboiler, while the bottom reboiler is heated with compressed saturated air. Several processes for low-pressure oxygen gas supply were simulated and optimized. The power requirement of the new air separation unit producing atmospheric oxygen at 95% mol attained the best value of 139.0 kWh/t (oxygen basis). A sensitivity analysis for oxygen purity was performed showing that, even for higher purities, the new developed process achieves the lowest specific power for low-pressure gaseous oxygen production. The economic leverage of the new air separation unit is proven via successful supply of low-pressure oxygen to oxyfuel natural gas combined-cycle Gas-To-Wire plant. Assuming carbon dioxide destination to enhanced oil recovery, even with an investment about 100% higher than the counterpart of a conventional air-fed combined-cycle Gas-To-Wire plant and despite net efficiency penalty of 6.88%, the oxyfuel combined-cycle Gas-To-Wire solution coupled to the new air separation unit was capable of achieving comparatively superior profitability under carbon taxation above 13.5 USD/t.

**Keywords:** Air separation; vapor-recompression cryogenic distillation; oxy-combustion; CO<sub>2</sub> capture; Gas-To-Wire; natural gas.

### **Supplementary Materials**

Supplementary Materials for this chapter are found in Appendices U1, U2 and U3 and U4.

## Nomenclature

### Abbreviations

1REB	: Single-Reboiler
2REB	: Dual-Reboiler;
2COL	: Double-Column;
3COL	: Triple-Column;
ASU	: Air Separation Unit;
BAC	: Booster Air Compressor;
CONV	: Conventional;
CW	: Cooling-Water;
EOR	: Enhanced Oil Recovery;
GAN	: Gaseous Nitrogen;
GOX	: Gaseous Oxygen;
GT	: Gas-Turbine;
HRSG	: Heat-Recovery-Steam-Generation;
HP	: High-Pressure;
LAIR	: Liquefied Air;
LCOE	: Levelized Cost of Electricity;
LHV	: Lower Heating Value;
LOX	: Liquid Oxygen;
LIN	: Liquid Nitrogen;
LP	: Low-Pressure;
MAC	: Main Air Compressor;
MHX	: Main Heat Exchanger;
MP	: Medium-Pressure;
NG	: Natural Gas;
NGCC	: Natural Gas Combined-Cycle Power Plant;
O <sub>x</sub> -NGCC-EOR	: Oxyfuel NGCC with EOR;
PCC	: Post-Combustion CO <sub>2</sub> Capture;
RVRC	: Recuperative Vapor Recompression;
ST	: Steam-Turbine;
TEG	: Triethylene-Glycol
TVR	: Top Vapor Recompression Distillation;
USD	: US Dollar.

### Variables

<i>AP</i>	: Annual profit (USD/y)
<i>COM</i>	: Cost of manufacturing (USD/y)
<i>CUT</i>	: Cost of utilities (USD/y)
<i>E<sub>sep</sub></i>	: Specific separation power demand (kWh/tO <sub>2</sub> )
<i>F</i>	: Molar flow rate (kmol/h)
<i>FCI</i>	: Fixed capital investment (USD)
<i>GAP</i>	: Gross annual profit (USD/y)
<i>ITR</i>	: Income tax rate (%)
<i>NPV</i>	: Net present value (USD)
<i>P</i>	: Pressure (bar)
<i>REV</i>	: Revenues (USD/y)
<i>RR</i>	: Reflux ratio ( $F_{LIN}/F_{GAN}$ )
<i>T</i>	: Temperature (°C)
<i>W</i>	: Mechanical power (kW)
<i>z</i>	: Molar fraction

## 2.1. Introduction

The electricity generation sector is a major agent of global carbon dioxide (CO<sub>2</sub>) emissions, where implementation of carbon capture, storage and utilization (CCSU) offers an alternative to limit global warming advance while new energy sources are not widely established. Besides the driving forces of government regulation and international protocols – now converging into charging power companies with carbon taxation – attractiveness of CCSU requires reasonable economic feasibility to assure that CO<sub>2</sub> mitigation would not severely impact the electricity generation cost and sales price. The development of efficient methods to capture CO<sub>2</sub> is then mandatory to reduce the associated mitigation penalty [1].

### 2.1.1. Oxy-Combustion

Although post-combustion has been the standard solution for CO<sub>2</sub> capture as presents the most well-developed technology, that is easy to implement in comparison with pre-combustion and oxy-combustion routes, it is not necessarily the most energy efficient choice, nor even possibly the most economical one. Moreover, the oxy-combustion route, i.e. combustion with oxygen (O<sub>2</sub>) replacing air, necessarily offers the best environmental performance, especially when comparing these routes for a fixed power penalty if considering a life-cycle point of view, as it is remarkably the only option enabling zero-emission power generation [2].

The economic competitiveness of oxy-combustion CO<sub>2</sub> capture is heavily dependent on cost-effective large-scale gaseous oxygen (GOX) supply from air separation units (ASU). Such a demand profile is most properly supplied with onsite production from cryogenic air fractionation. Alternatively, ceramic ion transport membranes has recently been suggested as a promising technology for GOX production particularly for this application, due to high selectivity above 800°C through oxygen-ion (O<sup>2-</sup>) species permeation [3], thus producing high-purity GOX and also enabling integration with power generation processes [2]. However, considering that the maximum demonstrated capacity is 100 t/d [4], the current available scale is too far from commercial power plant requirements, while the current market positioning is on small-scale high-purity GOX production (>99.5%O<sub>2</sub>) [3]. Therefore, cryogenic separation will certainly be applied for at least the first generation of commercial oxyfuel power plants [5].

### 2.1.2. Cryogenic Air Separation

The major portion of power penalty for CO<sub>2</sub> capture in the oxy-combustion systems is consumed by GOX production. According to Darde et al. [6], the specific power requirement ( $E_{sep}$ ) of a conventional ASU to produce low-purity 95%mol GOX at 1 atm is 200 kWh/tO<sub>2</sub>, while the counterpart of state-of-the-art ASU can be as low as 160 kWh/tO<sub>2</sub>. Power demand typically increases moderately from 90%mol to nearly 97%mol thanks to nitrogen (N<sub>2</sub>) removal from O<sub>2</sub> plus argon (Ar) mixture, the N<sub>2</sub>/(Ar+O<sub>2</sub>) fractionation. Thereafter, the power demand increases sharply at higher purities due to Ar/O<sub>2</sub> fractionation, which are components that have very close boiling points. Production of high-purity 99.5%mol GOX is then much more power consuming, about 245 kWh/tO<sub>2</sub> [7]. Soundararajan et al. [8] found that the optimum purity for oxyfuel application is usually about 97%mol, leading to the conclusion that removing Ar from flue gas is more preferable than removing Ar from GOX. Most works thus adopt 95%mol as nominal purity to oxy-combustion CO<sub>2</sub> capture systems when GOX is produced cryogenically [9].

Higginbotham et al. [5] compared the power demand of several ASUs for low-purity GOX supply and presented the lowest power demand for GOX production ever reported in the literature. Without heat integration, the most efficient flowsheet ( $E_{sep}$ =158 kWh/tO<sub>2</sub>) had three fractionation columns operating at distinct pressure levels, two of them designed for gaseous nitrogen (GAN) generation. They further investigated the benefit of: (i) transferring compression heat to a N<sub>2</sub>-Brayton cycle by discounting N<sub>2</sub> expander power generation from the ASU separation index  $E_{sep}$ ; or (ii) exporting pressurized GAN (p-GAN) for industrial customers by discounting the compression power that is avoided from  $E_{sep}$ . Heat integration to generate hot p-GAN for expansion, without using external heating, saves only 1 kWh/tO<sub>2</sub> ( $E_{sep}^{Disc}$ =157 kWh/tO<sub>2</sub>), while compression power avoidance for p-GAN supply at 2.5 bar would be more effective saving 20 kWh/tO<sub>2</sub> ( $E_{sep}^{Disc}$ =138 kWh/tO<sub>2</sub>). The best configuration for co-production of p-GAN, however, was rather found to be a double-column scheme with two reboilers in the lower pressure column – operated substantially above atmospheric pressure in this case – resulting in a discounted index of  $E_{sep}^{Disc}$ =128 kWh/tO<sub>2</sub> with p-GAN exportation at 4 bar. In addition to the undesirable higher-complexity control of highly integrated processes, the major drawbacks of these specific solutions are the following: (i) the N<sub>2</sub>-Brayton cycle would not be cost-effective – also requiring additional superheating for better yield, consequently involving gas-gas waste heat recovery at gas-turbine discharge, and; (ii)

unlikely existence of industrial clients with onsite permanent demand for p-GAN nearby oxy-combustion power plants (otherwise such an advantage for oxy-combustion is restricted to specific industrial areas).

Fu et al. [10] investigated the optimal configuration for compression heat recovery from a conventional double-column ASU for pre-heating boiler feed water in an oxy-coal power plant. Steam extractions were minimized via mixed-integer nonlinear programming taking into account feasibility constraints for heat exchanger network designs. The maximum improvement on power generation net efficiency was found to be 0.6% of fuel lower heating value (LHV), and adiabatic air compression was shown to give better results than intercooled compression at the ASU.

Recently, hybrid ASUs based on polymeric membranes followed by cryogenic fractionation of O<sub>2</sub>-enriched air have also been suggested for best energy efficiency. Polymeric membrane-permeation is a well-known technology for N<sub>2</sub> recovery and such a concept could be applied to any cryogenic ASU with an upstream unit featuring additional compression stages for the feed and the permeate streams. Skorek-Osikowska et al. [11] compared conventional and hybrid ASU schemes for implementation to an oxy-coal power plant and pointed better efficiency (+1.1%LHV) to membrane-cryogenic combination, though requiring extremely large permeation area. Burdyny and Struchtrup [12] investigated several arrangements of such a system and compared conventional cryogenic separation in terms of power consumption, concluding that it is possible to achieve a small advantage over cryogenic fractionation in oxy-combustion applications. Such hybrid units, however, would be best suited to GOX production from small to medium scales, in the order of few hundred tons per day [12]. Janusz-Szymanka and Dryjanska [13] similarly analyzed a lignite oxy-combustion plant integrated to hybrid membrane-cryogenic ASU with state-of-the-art polymeric membrane technology for N<sub>2</sub> removal, showing increased overall efficiency of 1.62%LHV due to electricity demand reduction from 226 kWh<sub>e</sub>/tO<sub>2</sub> to 179 kWh<sub>e</sub>/tO<sub>2</sub>. Compression heat recovery was also investigated by [13] to pre-heat boiler feed water, increasing power plant net efficiency by 0.5%LHV.

Remaining as the most practical and realistic choice for GOX supply in oxy-combustion systems, full standalone cryogenic air fractionation offers a palette of field-proven process configurations for ready implementation. Most of the existing plants follow a core concept depending on two heat integrated fractionation columns: one operated at higher pressure for

p-GAN production as top distillate and the other operated at nearly atmospheric pressure for O<sub>2</sub> recovery. Several modifications on process flowsheet have been introduced to reduce ASU power consumption but without changing the general concept of having a higher pressure column for p-GAN generation.

Instead of using the conventional integrated double (or multiple) column design, the ASU may alternatively comprise only a single top vapor recompression (TVR) column operated at nearly atmospheric pressure. In this case, a portion of top vapor is compressed – at above ambient temperature [14] or cryogenically [15] – subsequently condensed by latent heat exchange in the column reboiler and returned to the column as liquid nitrogen (LIN) for reflux. The application of TVR distillation to ASUs has been explored since the development of most early cryogenic ASUs [14], but its performance has been considered inferior to the double-column design, which was consolidated as a standard for cryogenic plants [16]. However, apparently with low industrial interest, many inventions dealing with TVR distillations were developed [17], while most of them follows a particular system, named as recuperative vapor recompression (RVRC) distillation [18]. RVRC distillation avoids a cryogenic GAN compressor replacing it by a standard compressor operated at above ambient temperature [19]. RVRC systems extract part of the cryogenic top N<sub>2</sub> vapor to the exterior of the Cold-Box, which is heated via heat exchange with Cold-Box air feed at ambient temperature, then compressed, cooled with water, and returned to the Cold-Box to be cooled and liquefied against O<sub>2</sub> vaporization, thus finally serving as top liquid reflux to the column.

Standard compression (RVRC distillation) has been regarded to be more convenient than cryogenic compression for plant simplicity and flexibility, as it enables the use of ordinary cooling towers to dissipate compression heat, while cold compression requires extra refrigeration effort for the plant [18]. On the other hand, the compression power is drastically reduced at such cryogenic temperatures, and in the case of air separation, it also avoids the irreversibilities associated with unnecessary heat transfer and head-loss introduced by returning p-GAN at ambient temperature to the Cold-Box [20]. This study was capable of proving that, to produce GOX, vapor recompression distillation does not need to be recuperative, as cryogenic vapor recompression can be much more efficient with appropriate flowsheet design.

For many decades, the use of cryogenic compressors were not technically or economically feasible. However, most advanced cryogenic materials and machinery currently allow to

operate compressors at temperatures as low as 4.2 K (-269 °C), such as those used in helium refrigeration cycles [21]. Many recent developments suggest commercially feasible installation of cryogenic compressors in ASUs [22], most notably in combination with integrated regasification of cryogenic liquids [23], which compensates compression power input to the Cold-Box with the benefit of improving the efficiency of energy management in a peak/off-peak scenario with liquid oxygen (LOX) storage [24]. Cryogenic compressors are also generally implemented when liquefied natural gas is injected into the ASU for efficient regasification. In this sense, a recent study [25] applied such an integration into an originally RVRC-based ASU and added cryogenic compression stages to minimize overall power consumption.

### **2.1.3. Gas-To-Wire**

Gas-to-Wire consists of generating electricity nearby oil-gas fields [26], so that a gas-turbine converts natural gas chemical energy into electricity for dispatch in high-voltage cables thus simplifying energy transportation and also relaxing specifications for raw gas processing. It also has the advantage of avoiding the rather higher losses associated with gas transportation in comparison with the transmission lines. Furthermore, in the case of carbon capture and storage (CCS) implementation, CO<sub>2</sub> transportation is avoided, as the CO<sub>2</sub> contained in exhaust gas – derived from both combustion reactions and raw gas – can be captured and readily injected underground for enhanced oil recovery (EOR) or storage in depleted fields, thus abating transportation costs and eliminating plausible problems with public acceptance – the Not-In-My-Backyard reactions [26]. In this sense, Andrei and Sammarco [26] discussed such an integrated Gas-To-Wire CCS scheme with post-combustion CO<sub>2</sub> capture (PCC) for a gas producing field and performed an economic analysis to determine the levelized cost of electricity (LCOE) and the CO<sub>2</sub> captured cost for different transmission distances, natural gas price and flow rate. Since EOR was not considered – which limits CCS revenues – and there was not any environmental constraint or penalty for CO<sub>2</sub> emission, the CCS alternatives were all shown to give higher LCOE though still being competitive for some electricity markets.

### **2.1.4. The Present Work**

The present study develops a novel technology for large-scale GOX production exhibiting the lowest separation power requirement ever reported. The proposed technology is based on cryogenic TVR distillation, which basically comprises a single nearly atmospheric column, contrasting with the standard method based on thermally coupled double or multiple columns

at distinct pressures. The TVR solution avoids unnecessary compression of O<sub>2</sub> from the air, and takes advantage of the higher N<sub>2</sub>/O<sub>2</sub> relative volatility at low-pressure, lowering the required reflux ratio, thus leading to substantial energy savings [18]. Low-pressure GOX supply to an oxy-combustion natural gas combined cycle (Ox-NGCC) power plant was exploited and its performance was reported for the basis of ≈4500 t/d GOX production at 95% mol. The Ox-NGCC and the ASU are considered to operate independently. Since full heat integration is not investigated in this work, the overall efficiency of power generation could be still somewhat improved.

Secondly, Andrei and Sammarco [26] in their Gas-To-Wire analysis with a conventional NGCC burning NG with air followed by PCC – but without an EOR destination capable to monetize CO<sub>2</sub> – did not implement a deep technical assessment neither contemplated CO<sub>2</sub> taxation, only considering cost aspects finding a high LCOE. The present work has various differences from Andrei and Sammarco [26] besides a much greater scope of analysis; namely: (i) an oxy-combustion NGCC is considered entailing simple and immediate CO<sub>2</sub> capture from exhausts deprived of troublesome N<sub>2</sub>, while [26] adopted PCC with its well-known energy-penalty and large column drawbacks, particularly critical for large-capacity Gas-To-Wire; (ii) the high performance of a totally new, up-to-date TVR ASU technology was rigorously simulated and compared with other up-to-date ASU technologies, proving to have the best  $E_{sep}$  and saving power for exportation; (iii) a plausible carbon taxation scenario in the near-future is considered, which rises the competitiveness of the present Ox-NGCC-EOR solution compared to conventional NGCC (despite also benefiting the Gas-To-Wire PCC from [26]); and (iv) CO<sub>2</sub> monetization is contemplated through EOR, creating a powerful new revenue raising the competitiveness of Ox-NGCC-EOR, making it highly profitable and benefiting the nearby oil production. The above aspects configure a literature gap explored for the first time in the present work.

Ox-NGCC-EOR is suited to remote oil-gas fields and is implemented as an oxy-fuel Gas-To-Wire solution, conveniently transporting gas energy as electricity thus avoiding gas pipelines, natural gas liquefaction, or any other expensive method for long-distance gas transportation. The proposed Ox-NGCC-EOR Gas-To-Wire concept offers potentially greater profitability while being much more environmentally adequate than conventional NGCC. To the authors' best knowledge, energy and economic assessments of Ox-NGCC-EOR including operation of high-performance new cryogenic ASU, besides Gas-To-Wire revenues from CO<sub>2</sub> EOR, never appeared in the literature before.

## 2.2. Methods

Assumptions for operation, simulation, design and economic analysis of process alternatives are presented: (i) in Sec. 2.2.1, concerning the technical assessment of GOX production in ASU alternatives and methods for development of the new proposed TVR cryogenic air separation unit, so-called TVR-2REB ASU; (ii) in Sec. 2.2.2, for technical analysis of oxyfuel natural gas combined-cycle power plant with EOR – Ox-NGCC-EOR – and its conventional NGCC counterpart; and finally (iii) in Sec. 2.2.3, for economic assessment of the new Ox-NGCC-EOR Gas-To-Wire solution using TVR-2REB ASU against conventional NGCC.

### 2.2.1. Air Separation Unit

The working hypothesis is that TVR atmospheric distillation could be more efficient for ASU than conventional double-column or multi-column distillations. Process development was carried out by introducing modifications in the ASU of Kapitza [15]. Several flowsheet configurations for low-pressure GOX production were tested and optimized, considering LIN reflux and liquefied air (LAIR) as variable rates. The optimization procedure followed a pattern search method. Ar recovery was not considered here, but could optionally be adapted to TVR distillation with some modifications [27].

The considered processes were ranked by their specific power requirement ( $E_{sep}$ ). As defined by Darde et al. [6], the  $E_{sep}$  of an ASU is expressed as the required mechanical power to produce 1 metric ton of O<sub>2</sub> contained in GOX stream at 1 atm for a given purity, considering ISO conditions for the atmospheric air feed (1 atm, 15°C, 60% relative humidity) and for cooling-water supply (15°C), neglecting losses in electric motors and generators, without considering the power demand for molecular sieve regeneration and cooling-water system operation.  $E_{sep}$  is calculated in Eq. (2.1), where  $W_j^{comp}$  represents the power input of compressor  $j$ ,  $W_j^{turb}$  is the power output of turbo-expander  $j$  (both in kW),  $F_{GOX}$  is the molar flow rate of GOX product (kmol/h),  $z_{O_2}$  is the O<sub>2</sub> molar fraction in GOX and  $MW_{O_2}$  is O<sub>2</sub> molar mass (kg/kmol).

$$E_{sep} = (\sum_{j=1}^{n_{wc}} W_j^{comp} - \sum_{j=1}^{n_{wt}} W_j^{turb}) / (F_{GOX} z_{O_2} MW_{O_2}) \quad (2.1)$$

Besides the cryogenic TVR distillation alternatives, a state-of-the-art ASU with low-pressure triple-column design [5] and three RVRC distillation processes [18] were also simulated.

Technical evaluation of all processes was conducted through steady-state HYSYS simulation. The flowsheet with the lowest  $E_{sep}$  was selected as the final configuration and described in detail. The configuration was analyzed in terms of the heat exchange profile at optimum conditions and its sensitivity to liquid inlet flow rates to the column. Another sensitivity analysis investigates the effect of GOX purity on  $E_{sep}$ .

The main operation-simulation assumptions used for the new proposed TVR ASU and other ASUs being compared (if applicable) are presented in Table 2.1, while detailed process conditions of TVR-2REB are found in Appendix U1 (Supplementary Materials).

**Table 2.1.** Operation-simulation assumptions for GOX production.

Item	Assumption
{A1}	Thermodynamic Modeling: Peng-Robinson Equation-of-State [28]
{A2}	Air intake: 32131 kmol/h ( $\approx 720,000$ Nm <sup>3</sup> /h) at 1 atm, 15°C, 60% relative humidity (1.01% water) [6] Dry-Basis (% mol): 78.08%N <sub>2</sub> , 20.95%O <sub>2</sub> , 0.934%Ar, 360 ppm-mol CO <sub>2</sub>
{A3}	Main Air Compressor Adiabatic Efficiency: $\eta=88\%$ [5]
{A4}	Adiabatic Efficiency of other ASU Compressors: $\eta=84\%$ [29]
{A5}	Adiabatic Efficiency of Expanders: $\eta=90\%$ [7]
{A6}	Direct-Contact After-Cooling: $T=12^\circ\text{C}$
{A7}	Cooling-Water (CW) Heat Exchangers: $\Delta T^{APPROACH}=15^\circ\text{C}$ , $\Delta P/P=3\%$
{A8}	Air Pre-Purification: $\Delta P=10$ kPa [30]
{A9}	Main Heat Exchanger (MHX): $\Delta P^{AIR}=10$ kPa, $\Delta P^{GAN}=10$ kPa $\Delta P^{GOX}=10$ kPa [13]
{A10}	Distillation Columns: Structured-Packing, $\Delta P^{STAGE}=0.07$ kPa [7], $P^{TOP}=1.2$ bar [5]
{A11}	Sub-Cooler: $\Delta P=1$ kPa
{A12}	Cryogenic Latent Heat Exchange: $\Delta T^{APPROACH}=1^\circ\text{C}$ [31]
{A13}	Cryogenic Liquid/Gas and Liquid/Liquid Heat Exchanges: $\Delta T^{APPROACH}=2^\circ\text{C}$
{A14}	MHX Gas/Gas Heat Exchanges: $\Delta T^{APPROACH}=2.78^\circ\text{C}$ [32]
{A15}	Cryogenic Liquids Withdrawal: No
{A16}	Heat Exchange with External Environment: No
{A17}	$E_{sep}$ for 1 atm GOX production (pressure excess discounts equivalent GOX compression power)
{A18}	GOX Purity: 95% mol

### 2.2.2. Oxyfuel Combustion Power Plant

Considering that a zero-emission oxyfuel natural gas combined-cycle power plant with total CO<sub>2</sub> injection to EOR – Ox-NGCC-EOR – can be more profitable than the conventional NGCC without capture in a scenario of carbon taxation, it is desired to estimate the necessary minimum CO<sub>2</sub> tax level to make the net present value (*NPV*) of the Ox-NGCC-EOR superior to the corresponding *NPV* of conventional NGCC by the end of a project lifetime of 30 years.

Technical evaluation of alternatives was conducted through steady-state HYSYS simulation. The main operational-simulation assumptions used for the newly proposed Ox-NGCC-EOR and conventional NGCC being compared (if applicable) are presented in Table 2.2, while detailed process conditions of Ox-NGCC-EOR are found in Appendix U2 (Supplementary Materials).

**Table 2.2.** Operation-simulation assumptions for power generation.

Item	Assumption
{B1}	Thermodynamic Modeling: Peng-Robinson Equation-of-State (in general) [28]; Glycol-Package (CO <sub>2</sub> Dehydration); ASME-Table (Steam-Cycle)
{B2}	NG (% mol): 2650 kmol/h (1.53 MMSm <sup>3</sup> /d), $T=25^{\circ}\text{C}$ , $P=40$ bar, 89% methane, 7% ethane, 1% propane, 0.1% n-butane, 0.01% n-pentane, 2.5% CO <sub>2</sub> , 0.38% N <sub>2</sub> , 0.01% water (H <sub>2</sub> O)
{B3}	Stoichiometric GOX (% mol): 5809 kmol/h (4474 t/d), $T=15^{\circ}\text{C}$ , $P=1$ atm, 95% O <sub>2</sub> , 2.39% Ar, 2.61% N <sub>2</sub>
{B4}	NGCC Configuration: 1:1 (Gas:Steam turbines)
{B5}	Expanders Adiabatic Efficiency: $\eta=90\%$
{B6}	Compressors Adiabatic Efficiency: $\eta=84\%$
{B7}	Pumps Adiabatic Efficiency: $\eta=75\%$
{B8}	Gas-Turbine (GT) Expander Inlet: $1300^{\circ}\text{C}@39.5$ bar
{B9}	Steam-Turbine (ST) Inlet (outlet quality $\geq 90\%$ ): $560^{\circ}\text{C}@56$ bar (Ox-NGCC-EOR); $430^{\circ}\text{C}@22$ bar (conventional NGCC, $T^{GT-EXHAUST}=476^{\circ}\text{C}$ )
{B10}	Vacuum-Condenser: $T^{OUTLET}=35^{\circ}\text{C}$ , $\Delta P=1$ kPa
{B11}	Heat-Recovery Steam Generator (HRSG): $\Delta T^{APPROACH} \geq 15^{\circ}\text{C}$ , $\Delta P^{GAS}=2$ kPa, $\Delta P^{H2O}=50$ kPa
{B12}	Flue-Gas Direct-Contact Column: Structured-packing, Stages=3 (theoretical), $25^{\circ}\text{C}$ recycled-water, $P^{TOP}=1$ atm, $\Delta P=2$ kPa
{B13}	Intercoolers: $T^{GAS}=30^{\circ}\text{C}$ , $T^{CW-INLET}=15^{\circ}\text{C}$ , $T^{CW-OUTLET}=25^{\circ}\text{C}$ , $\Delta P=3\%P \leq 50$ kPa
{B14}	Compressor Stage Discharges: $T^{CO2}=120^{\circ}\text{C}$ , $T^{GOX}=133^{\circ}\text{C}$ , $T^{GOX-Last-Stage}=140^{\circ}\text{C}$
{B15}	CO <sub>2</sub> Dehydration (TEG-Absorption): Triethylene-glycol (TEG) 98.5% w/w, $30^{\circ}\text{C}@50$ bar
{B16}	TEG Absorber: Pall Rings 1", Stages=10 (theoretical), $P^{BOTTOM}=50.5$ bar
{B17}	TEG Regenerator: Pall Rings 1", Stages=4 (theoretical), $P^{TOP}=1$ atm
{B18}	CO <sub>2</sub> Liquefaction: $30^{\circ}\text{C}@130$ bar
{B19}	EOR Fluid: $P=350$ bar

### 2.2.3. Economic Analysis of Gas-To-Wire Alternatives

Gas-To-Wire alternatives were economically assessed using the methods of Turton et al. [33] with fixed capital investment (*FCI*) estimated from equipment sizes, dimensioned in accordance with Campbell [34]. Different carbon taxation scenarios – 0, 20, 40 and 60 USD/tCO<sub>2</sub> – were considered to investigate the economic feasibility of the proposed Ox-NGCC-EOR Gas-To-Wire solution versus conventional Gas-To-Wire NGCC.

The revenues (*REV*) components: (i) electricity exportation; and (ii) CO<sub>2</sub> to EOR rated at 74 USD/t. The oil yield has been estimated in the range of 0.6-2.6 bbl/tCO<sub>2</sub> for mature fields in Texas, US [35], thus a conservative yield of 1 bbl/tCO<sub>2</sub> is assumed giving 74 USD/t as underrated EOR fluid value. The major assumptions for economic analysis are presented in Table 2.3 (formulas are found in Appendix U3 of Supplementary Materials).

**Table 2.3.** Assumptions for economic analysis.

Item	Assumption
{C1}	Prices (USA June/2018): Electricity=0.1087 USD/kWh, NG=3.43 USD/MMBTU, Oil=74 USD/bbl.
{C2}	CO <sub>2</sub> to EOR: 74USD/t
{C3}	Cost of Utilities ( <i>CUT</i> ): <i>CW</i> =0.016 USD/t
{C4}	Equipment <i>FCI</i> : extrapolated with 0.6 exponent if exceeds Turton et al. [33] correlations ranges
{C5}	ASU <i>FCI</i> : extrapolated with 0.5 exponent from <i>FCI</i> =141 MMUSD for 52 kg/s GOX [36]
{C6}	<i>FCI</i> Inflation Factor: <i>CEPCI</i> =567.5
{C7}	Construction: three years with 20%, 30% and 50% investment allocations
{C8}	Operation: 8000 h/y
{C9}	Income Tax Rate: <i>ITR</i> =34%
{C10}	Annual Depreciation: 10% <i>FCI</i>
{C11}	Horizon: 30 years
{C12}	Annual Interest Rate: <i>i</i> =10%

## 2.3. Results and Discussion

The new breakthrough TVR ASU is developed in Sec. 2.3.1 jointly with its direct antecessors and several up-to-date competing configurations. Sec. 2.3.2 presents the benchmarking of the new ASU and Appendix U1 describes its operation. Sec. 2.3.3 conducts specific analyses of its performance. Finally, a techno-economic analysis of conventional and oxy-combustion NGCC systems including consolidated best ASU flowsheet is addressed in Sec. 2.3.4.

### 2.3.1. The Development of Breakthrough Cryogenic Air Separation Unit

Many decades after the first ASU patent with RVRC distillation process [14], the most simple ASU configuration with cryogenic TVR distillation was reported in a patent of Kapitza [15] still in the first half of the 20<sup>th</sup> century. It had a single pressurized air stream feeding the main heat exchanger (MHX) of a Cold-Box that is thereafter sent to a turbo-expander before feeding the single fractionation column. Part of the GAN flowing from the top of the column is directly sent to a cryogenic compressor, which discharges p-GAN for condensation in the bottom reboiler, in order to provide top reflux for the column. The column can optionally have intermediate reboilers, which would involve a side extraction of N<sub>2</sub>-rich vapor from somewhere along the column to send to another cold compression stage allowing condensation in the intermediate reboiler. The process idea of Kapitza [15] was here updated and simulated in accordance with the current knowledge and available technology for cryogenic air fractionation. Fig. 2.1 presents the updated version – hereafter named as TVR-1REB – with corresponding process conditions at optimum LIN reflux rate for minimum separation power requirement, equivalent to  $E_{sep}=189.7$  kWh/tO<sub>2</sub> for GOX production at 95% mol.

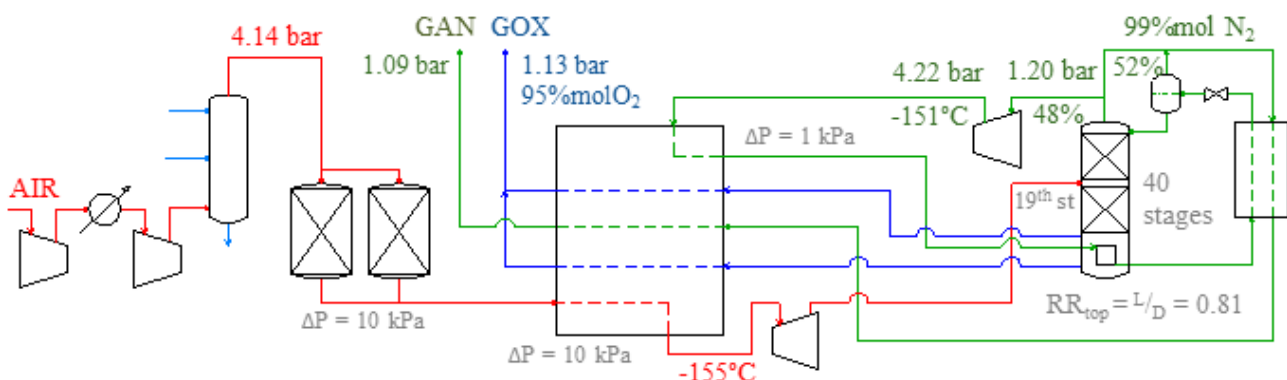


**Fig. 2.1.** Base configuration of cryogenic TVR distillation of air (TVR-1REB).

Looking to enhance ASU performance, the same principle that features a LOXBOIL process can then be applied to TVR-1REB distillation. The LOXBOIL concept is a remarkable

improvement made in standard low-pressure double-column design (CONV-2COL) that consists of using a separate vaporizer for the O<sub>2</sub> product stream which liquefies a portion of the air feed. Better efficiency is achieved as a consequence of feeding the first fractionation column with LAIR, enhancing separation performance and reducing top reflux requirements. The O<sub>2</sub> is extracted as a saturated liquid instead of as vapor, which is beneficial to process safety, also requiring much less LOX drain from the main reboiler thus saving significant amount of energy [16], though this effect is not generally accounted. Furthermore, static head slightly increases the pressure of O<sub>2</sub> product. Higginbotham et al. [5], reported a power coefficient of  $E_{sep}=187$  kWh/tO<sub>2</sub> for the double-column design using O<sub>2</sub> vaporizer to produce GOX 95%mol. The process flowsheet of such adaptation into TVR distillation (TVR-LOXBOIL) is presented in Fig. 2.2 with operational conditions at optimum LIN reflux rate, for minimum power demand for GOX 95%mol production, where  $E_{sep}=174.7$  kWh/tO<sub>2</sub>.

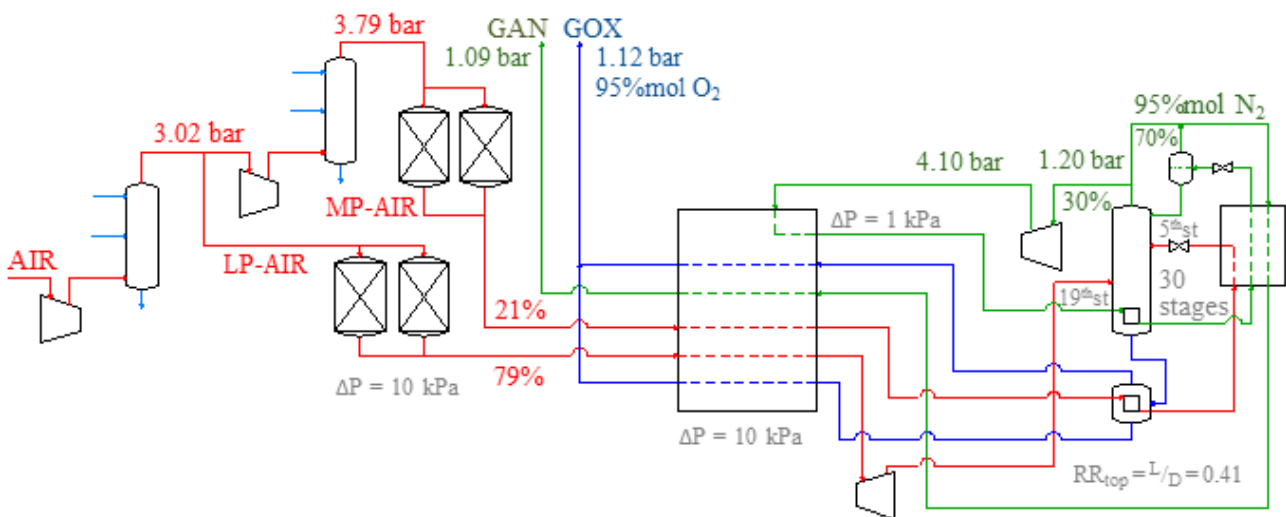


**Fig.2.2.** Air TVR distillation with separate O<sub>2</sub> vaporizer/ air condenser (TVR-LOXBOIL).

Another improvement that can be made to enhance TVR distillation performance is to add an intermediate column reboiler. The strategy of using an additional reboiler in the main fractionating column (low-pressure column) is well-known in the current state-of-the-art. As this exchanger boils a fluid with lower boiling temperature than bottom liquid, it is possible to condense p-GAN at a respective lower temperature, so that the operating pressure at the high-pressure column can be lowered, enabling to reduce the discharge pressure of the main air compressor (MAC). Moreover, the intermediate reboiler improves the exergy efficiency of a distillation column, thus it can operate closer to equilibrium (mass transfer pinch) despite of increasing the column height [30]. In this sense, Fu and Gundersen [30] have already

performed an exergy analysis that evaluates the effect of including an additional reboiler to a double-column ASU. According to Higginbotham et al. [5], the separation power requirement of typical dual-reboiler double-column ASU (LP-2COL-2REB) is 167 kWh/tO<sub>2</sub>. In terms of RVRC distillation, intermediate reboiler has already been applied by Fu and Gundersen [18] operating GAN condensation within the bottom or even the both intermediate and bottom reboilers at different pressures. There is no mention, however, about a plausible advantage of condensing air in the bottom reboiler instead of GAN. What is here suggested is to implement the dual-reboiler concept into an ASU with cryogenic TVR using air liquefaction at bottoms. The resulting process flowsheet is remarkably not an obvious modification of the idea of Kapitza [15] for a dual-reboiler column. Instead of using a side extraction of N<sub>2</sub>-rich vapor to compress it cryogenically to generate secondary refluxes (which would require extra cold compression stages), it provides liquefaction of an air stream (previously compressed outside the Cold-Box) to partially feed the column with liquid. Fig. 2.3 presents the flowsheet of such a process – hereafter named TVR-2REB – at optimal operational conditions, with corresponding minimum separation power requirement of  $E_{sep}=139.0$  kWh/tO<sub>2</sub> for GOX production at 95%mol. In cryogenic TVR distillation of air, condensing GAN in the intermediate reboiler proved to be crucial for significant power savings, which made it possible to achieve better energy performance for low-pressure GOX production in comparison with the processes of Higginbotham et al. [5] and Fu and Gundersen [18]. The process was therefore registered as a preferred embodiment of the patent application BR102016022807-7 [27]. Further TVR-2REB description is left to Appendix U1.

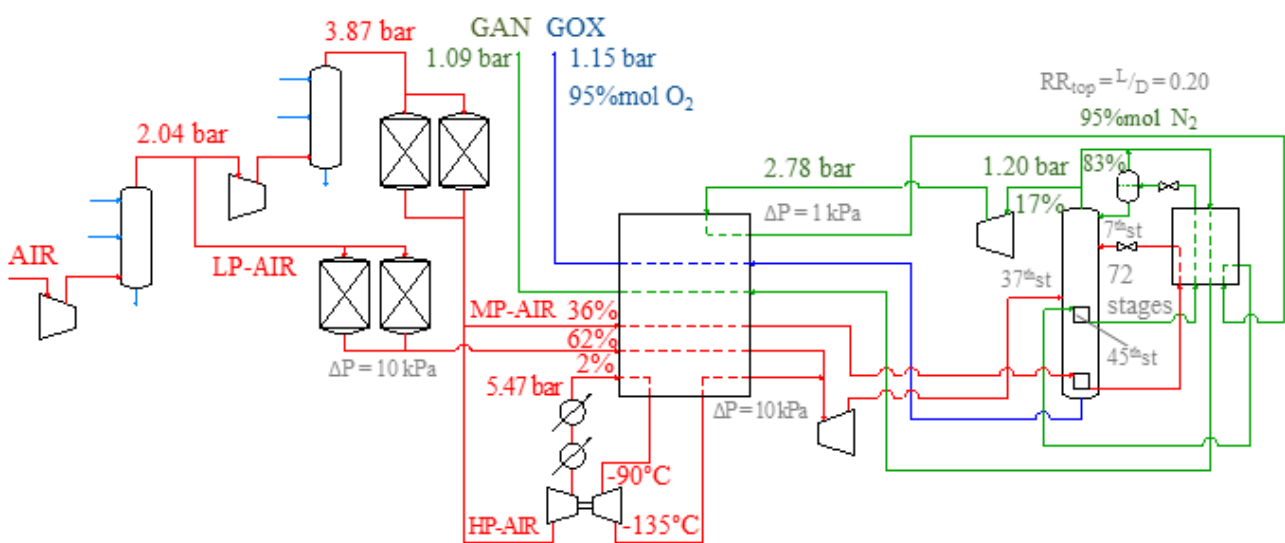


**Fig. 2.3.** Air TVR distillation in dual-reboiler single-column novel design, with GAN condensation at the intermediate reboiler – selected configuration for low-pressure GOX supply (TVR-2REB).

In order to evaluate the potential benefit of using so-called power-saving cold compressors instead of standard machines for GAN compression, recuperative vapor recompression processes were also simulated following the same assumptions. For this purpose, two processes were selected from the literature and another one was proposed as a RVRC variant for the present TVR-2REB flowsheet. The selected processes were based on the most efficient RVRC designs (Cycles 5 and 6) of Fu and Gundersen [18] with limited changes for adequate comparison ( $N_2$  turbo-expander must be placed within the Cold-Box of Cycle 5 [18] to suit the assumed temperature approaches. In Cycle 6 [18] reversing heat exchanger is abolished thus requiring another pre-purification unit). Figs. 2.4 and 2.5 present such adaptations – hereafter named RVRC-2REB-2LIN and RVRC-2REB-1LIN, respectively – with optimized results for corresponding minimum  $E_{sep}$  for GOX 95%mol production of 185.3 kWh/tO<sub>2</sub> and 167.2 kWh/tO<sub>2</sub>.

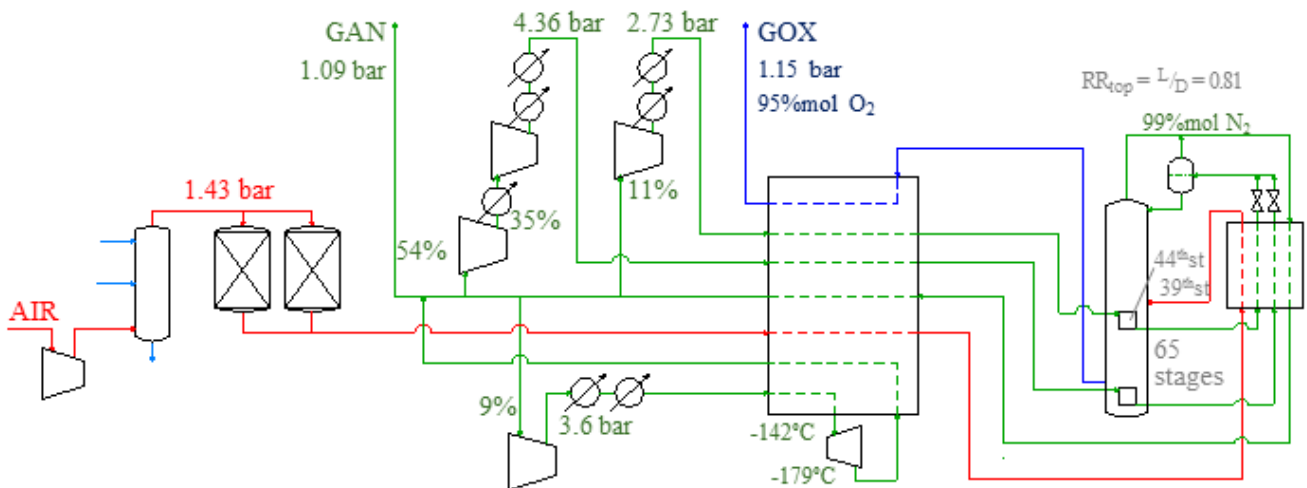


**Fig. 2.4.** Recuperative vapor recompression distillation process using dual-reboiler single-column, two pressure levels of condensing GAN, and p-GAN turbo-expander (RVRC-2REB-2LIN).

Besides enabling the comparison of the effect of using a cryogenic compressor, the RVRC variant of TVR-2REB – shown in Fig. 2.6 and named as RVRC-2REB-LAIR – also evaluates the advantage of condensing air instead of GAN in the column bottom reboiler by comparison with RVRC-2REB-1LIN results. The minimum power demand of  $E_{sep}=148.1$  kWh/tO<sub>2</sub> for production of GOX 95%mol can be achieved with optimized process conditions (Fig. 2.6), which is above TVR-2REB consumption but still lower than triple-column ASU requirement.

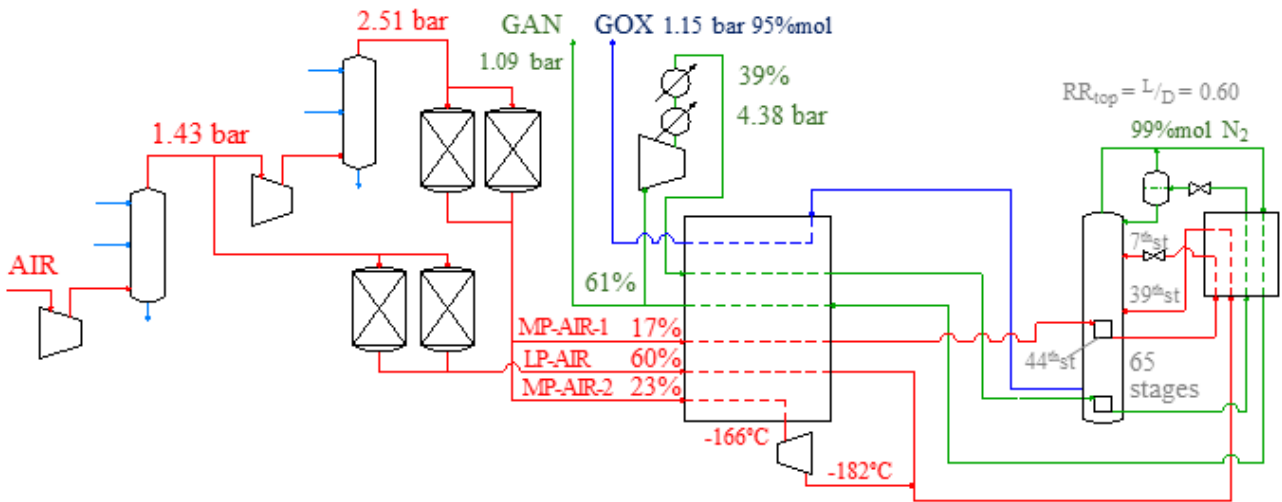


**Fig. 2.5.** Recuperative vapor recompression distillation process using dual-reboiler single-column, GAN condensation at bottom reboiler, and air turbo-expander (RVRC-2REB-1LIN).

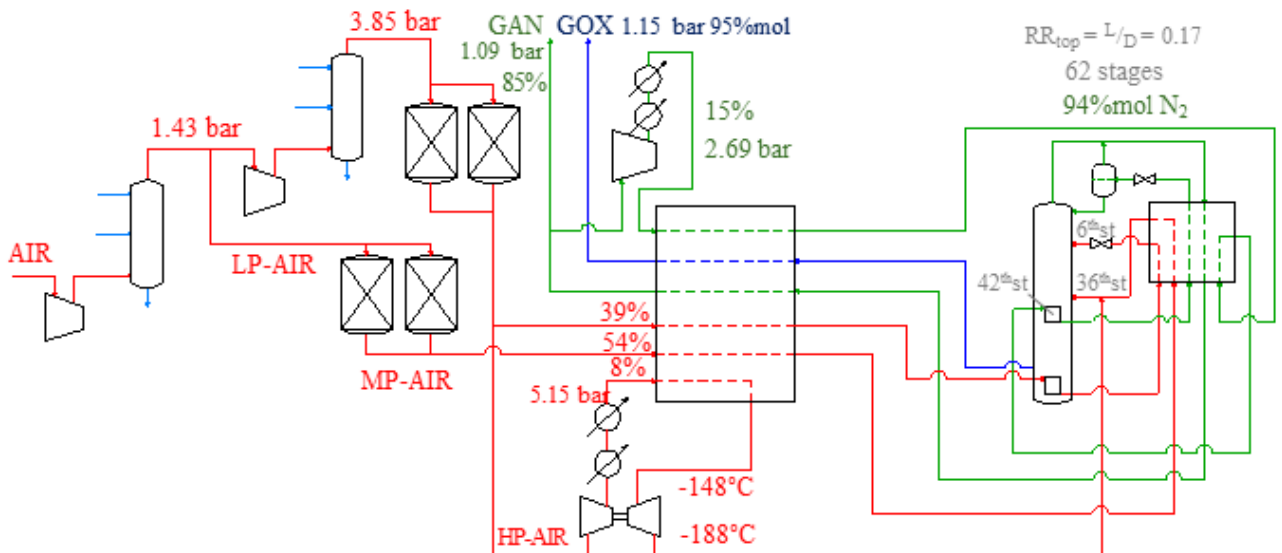


**Fig. 2.6.** Recuperative vapor recompression distillation process using dual-reboiler single-column, GAN condensation at intermediate reboiler, and air compander (RVRC-2REB-LAIR).

A low-pressure triple-column ASU design – as a state-of-the-art reference process, henceforth denominated LP-3COL-2REB – was then simulated to validate assumptions and produce comparable results to evaluate the supposed benefit of TVR distillation.

The LP-3COL-2REB flowsheet presented in Fig. 2.7 is similar to Dillon et al. [9], whose configuration was utilized by Higginbotham et al. [5] to update the corresponding power demand coefficient for current available technology (158 kWh/tO<sub>2</sub>). Fig. 2.7 also presents the operating conditions for minimum power demand for GOX production at 95%mol, estimated as  $E_{sep}=157.8$  kWh/tO<sub>2</sub>.

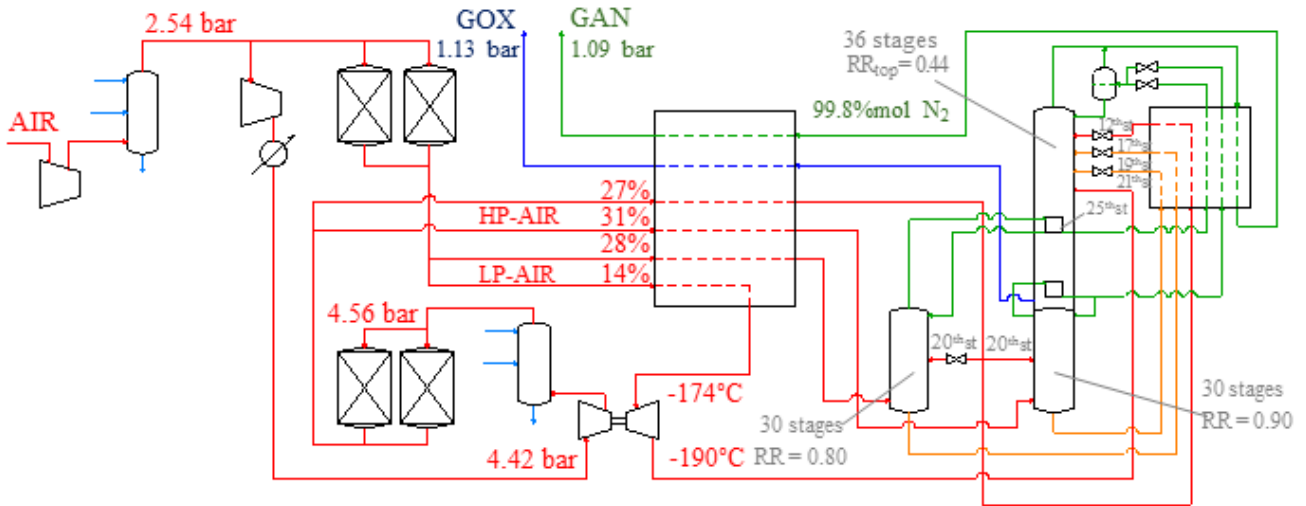


**Fig. 2.7.** Low-pressure triple-column for impure GOX production (LP-3COL-2REB).

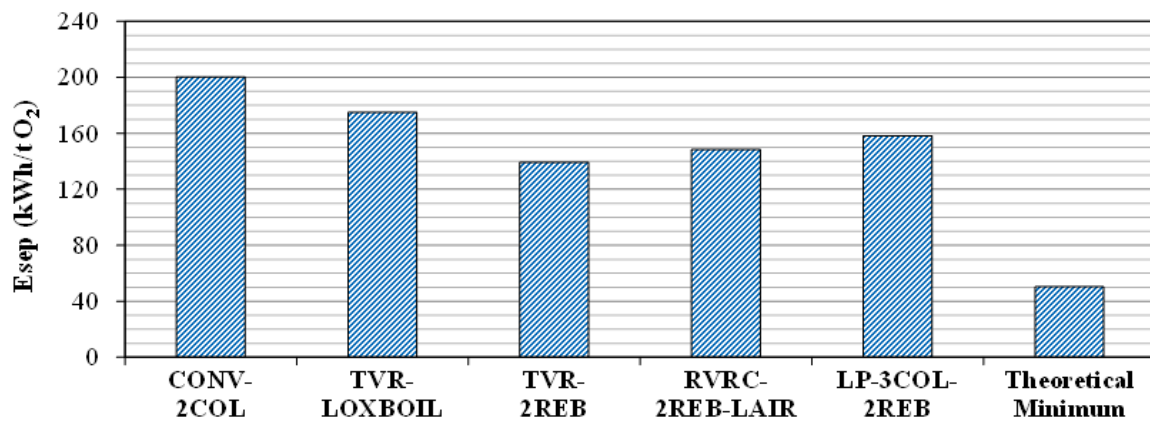
### 2.3.2. Benchmarking of the Novel Air Separation Unit

Separation power coefficients of flowsheets presented in Figs. 2.1-2.7 for low-pressure GOX production at 95% mol are summarized in Table 2.4 with process operational data. The TVR-2REB configuration outperformed all cases in terms of power requirement, followed by the recuperative variant RVRC-2REB-LAIR. Although process performance has been significantly improved, it is noteworthy to demonstrate that it is still far away from the theoretical minimum separation requirement of 50 kWh/tO<sub>2</sub> for a reversible process [30], which still indicates a large opportunity for further enhancements in ASU performance from the thermodynamic point of view. Fig. 2.8 thus illustrates the power demand of some of these processes with a conventional double-column ASU [6] and the theoretical minimum power.

Table 2.4 unveils most TVR ASUs requiring lower air feed pressures than LP-3COL-2REB, with the only exception of TVR-1REB, indicating less power consumption in air supply to the Cold-Box. However, as their performances are critically influenced by N<sub>2</sub> compression, only TVR-2REB and RVRC-2REB-LAIR outperformed LP-3COL-2REB (Fig. 2.8). TVR-2REB presents slightly higher air feed pressures than RVRC-2REB-LAIR, consuming ≈15% more electricity in air supply (while ≈25% less than LP-3COL-2REB) but showing considerably lower  $E_{sep}$  (Fig. 2.8). This is largely explained by drastically lower (≈71%) power demand to compress N<sub>2</sub>, despite similar pressures (Table 2.4), besides having an extra turbo-expander producing power (Fig. 2.3). Therefore, this pre-screening of ASU flowsheets, portrayed by comparison of optimum  $E_{sep}$  in Fig. 2.8, elects the novel TVR-2REB alternative to be analyzed in-depth and to be employed in the proposed Ox-NGCC-EOR Gas-To-Wire plant.

**Table 2.4.** Technical performance of simulated processes for GOX 95%mol production.

	TVR-1REB	TVR-LOXBOIL	TVR-2REB	RVRC-2REB-2LIN	RVRC-2REB-1LIN	RVRC-2REB-LAIR	LP-3COL-2REB
Flowsheet	Fig. 2.1	Fig. 2.2	Fig. 2.3	Fig. 2.4	Fig. 2.5	Fig. 2.6	Fig. 2.7
Top Vapor Recompression	Cold	Cold	Cold	Hot	Hot	Hot	-
Air Condenser Location	N/A	Product Vaporizer	Bottom Reboiler	N/A	Secondary Reboiler	Bottom Reboiler	MHX
Air Supply Feed Ratio (LP, MP, HP)	100% LP	79% LP/ 21% MP	62% LP/ 36% MP/ 2% HP	100% LP	60% LP/ 40% MP	54% LP/ 39% MP/ 8% HP	42% LP/ 58% HP
Air Supply Pressure (bar)	4.14	3.02 / 3.79	2.04 / 3.87 / 5.47	1.43	1.43 / 2.51	1.43 / 3.85 / 5.15	2.54 / 4.56
N <sub>2</sub> Compressor Discharge (bar)	4.22	4.10	2.78	2.73 / 4.36	4.38	2.69	N/A
O <sub>2</sub> Recovery	97.5%	84.2%	82.9%	98.2%	98.4%	80.1%	99.8%
$E_{sep}$ , GOX 95% molO <sub>2</sub> (kWh/tO <sub>2</sub> )	189.7	174.7	139.0	185.3	167.2	148.1	157.8

**Fig. 2.8.** Power demand coefficients for low-pressure GOX production at 95% mol.

### 2.3.3. Technical Analysis of Novel Air Separation Unit

The sub-ambient MHX+Subcooler heat transfer profile is unveiled in Fig. 2.9 to demonstrate conformity with assumptions {A12}-{A14} (Table 2.1). The selected criteria of minimum temperature difference for heat transfer can be examined in the curve shown in Fig. 2.9a, where the first local maximum from the hot end of the MHX corresponds to the output of HP-AIR that feed the secondary turbine (compander), while the first local minimum corresponds to the return of the stream from the turbine back to the MHX. Fig. 2.9b is the respective temperature-heat duty diagram that generates Fig. 2.9a. Fig. 2.9c illustrates the magnification of the coldest portion of the diagram, where the left of the plateau (LOX vaporization) represents the heat exchange in the sub-cooler, while the other part represents

the MHX at its cold end, where minimum  $\Delta T$  occurs due to latent heat exchange between LOX and medium-pressure air (MP-AIR) (Fig. 2.3). Condensation of MP-AIR is completed at bottom reboiler. Fig. 2.9c also demonstrates that, in this process, a small portion of LOX needs to be vaporized by cooling air in gaseous phase, which is more clearly revealed by the global maximum  $\Delta T$  of Fig. 2.9a.

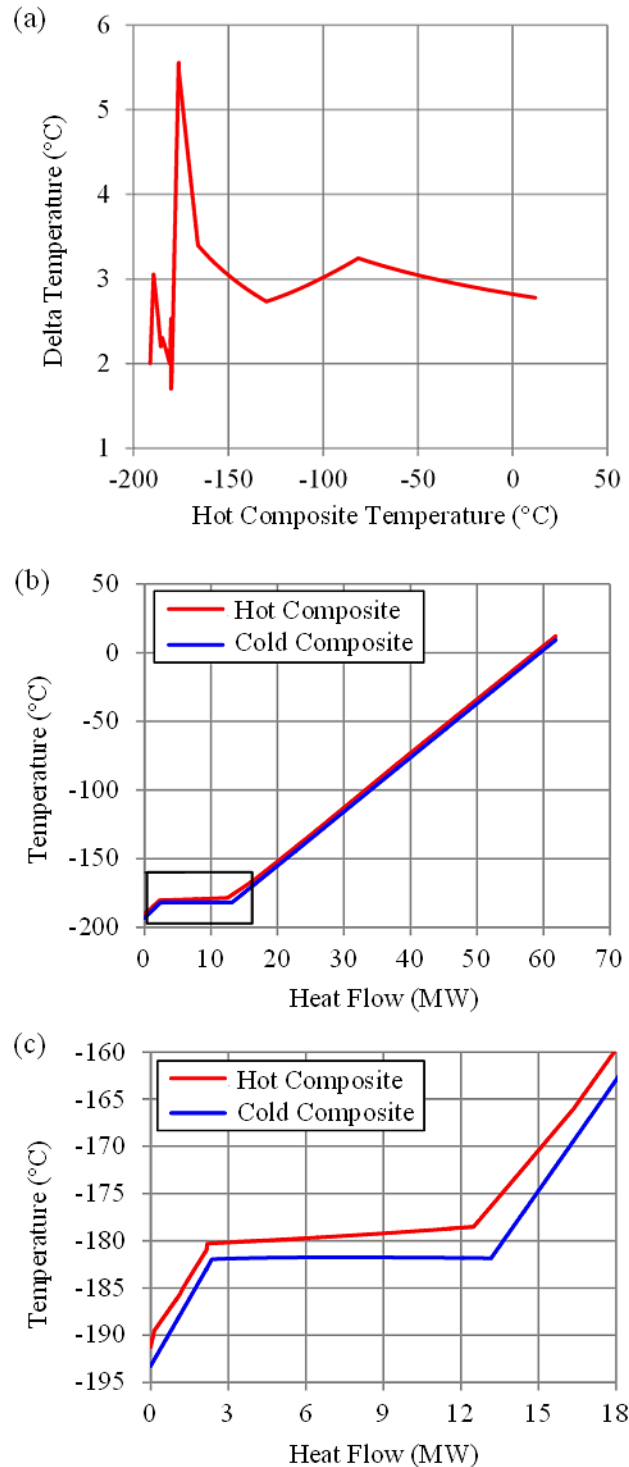


**Fig. 2.9.** Sub-ambient heat transfer profile in TVR-2REB (MHX+Subcooler): a) hot composite temperature versus  $\Delta T$ ; b) temperature-heat duty diagram; c) temperature-heat duty diagram below -160  $^{\circ}\text{C}$ .

Process optimization here mainly involves defining the flow rate of GAN being recompressed and the proportion of air intake to each line of Cold-Box feed, with pressure degrees of freedom being determined by feasibility for heat transfer matching the referred thermal approaches. The TVR-2REB process has two key variable flow rates to be optimized for best energy performance: the flow rates of MP-AIR and GAN for recompression (Fig. 2.3), which means optimizing the liquid feeds to the column (LIN and LAIR). The proportion between LP-AIR and HP-AIR is then determined by refrigeration needs. The region of minimum separation power demand  $E_{sep}=139$  kWh/tO<sub>2</sub> is presented in Fig. 2.10 as a function of ratios of recompressed GAN and MP-AIR by total molar flow rate of purified air sent to the Cold-Box, indicating 0.17 for p-GAN and 0.36 for MP-AIR. This means respectively 5400 kmol/h and 11438 kmol/h for producing 4475 t/d GOX 95% mol (31796 kmol/h pure air feed).

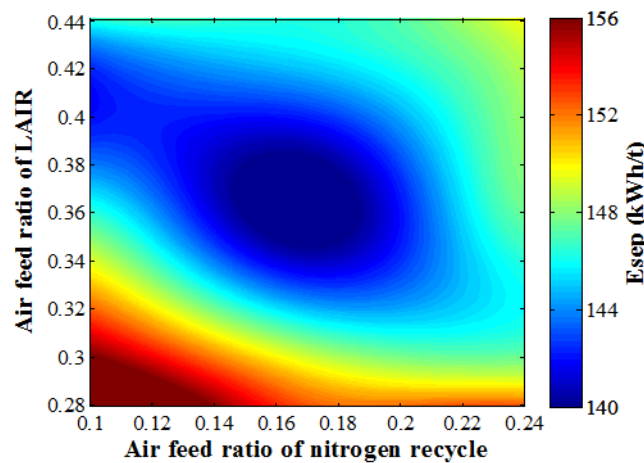


**Fig. 2.10.** Specific separation power demand ( $E_{sep}$ ) as a function of GAN for recompression (column recycle) and LAIR flow rates.

Fig. 2.10 expresses the trade-off between O<sub>2</sub> recovery and ASU power consumption, as both streams affect compression duties. On the one hand, higher MP-AIR flow rate loads more power to the booster air compressor (BAC), and on the other, the flow rate of GAN recompression increases cryogenic compressor power, which needs to be dissipated by correspondingly higher turbo-expansion output, loading refrigeration effort by requiring extra air compression, influencing the proportion between LP-AIR and HP-AIR besides the inlet pressures for turbo-expanders.

The minimization of  $E_{sep}$  was obtained for a relatively low O<sub>2</sub> recovery of 83%, contrasting with most ASUs, where it is above 98% though being less efficient in energy terms (Table 2.4). The low O<sub>2</sub> recovery occurs due to O<sub>2</sub> loss in the top product – waste GAN with impurities, 95% mol N<sub>2</sub> – due to limited LIN reflux. In face of usual high-purity specifications

for GAN, TVR-2REB is not capable of simultaneously delivering pure  $N_2$  while producing GOX with high energy efficiency. For this purpose, it is preferable to use a cycle characterized by higher LIN reflux, which is the case of the classic TVR-1REB configuration. On the contrary, as disclosed in Brigagão et al. [27], Ar recovery would be easily performed by introducing few optional process modifications on TVR-2REB. With the same flowsheet but adapting the column specifications, a sensitivity analysis of ASU minimum power demand was performed varying the GOX purity, with results in Fig. 2.11. While GOX 95%mol production at 1 atm requires 139.0 kWh/tO<sub>2</sub>, for a near complete N<sub>2</sub>-removal, with 0.01%mol N<sub>2</sub> in GOX ( $\approx 97.32\%$ mol O<sub>2</sub>), the minimum  $E_{sep}$  would be 143.5 kWh/tO<sub>2</sub>. Ar removal causes drastic  $E_{sep}$  increase at higher purities (Fig. 2.11), so that at 99.5%mol O<sub>2</sub>, the  $E_{sep}$  is 185 kWh/tO<sub>2</sub>, a remarkable value relative to conventional pure GOX plants, with usual  $E_{sep} \approx 245$  kWh/tO<sub>2</sub> [7].

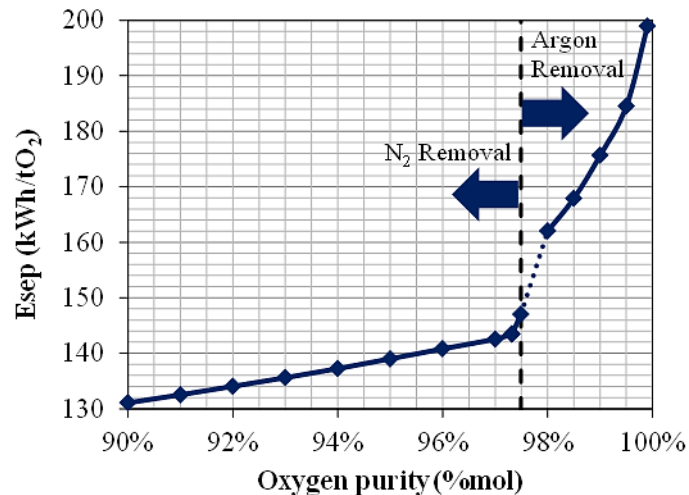


**Fig. 2.11.** Sensitivity analysis of TVR-2REB power requirement varying GOX purity.

### 2.3.4. Techno-Economic Analysis of Oxy-Combustion Power Generation Systems

The process flow diagram of the Ox-NGCC-EOR plant is presented in Fig. 2.12 with its main process conditions. The numerical results of Ox-NGCC-EOR streams are shown in Table 2.5. The process begins with low-pressure GOX from TVR-2REB ASU being compressed to 40 bar before entering the gas-turbine (GT) combustion chamber (at 39.5 bar) in stoichiometric proportion to high-pressure NG. The expander inlet temperature is set to 1300°C, resulting in a high-temperature discharge of 680°C, despite of high expansion ratio of 37.5, due to the high specific heat capacity of CO<sub>2</sub>-rich oxy-combustion exhaust gas compared to N<sub>2</sub>-rich gas of conventional NGCC, where GT discharge is only at 476°C.

**Table 2.5.** Main streams of power plant alternatives.

	<i>Conventional NGCC</i>				<i>Ox-NGCC-EOR</i>							
	<i>Air Intake</i>	<i>GT Outlet</i>	<i>Stack</i>	<i>ST Inlet</i>	<i>GOX Feed</i>	<i>GT Outlet</i>	<i>Flue Gas from DCC</i>	<i>ST Inlet</i>	<i>Water Purge</i>	<i>CO<sub>2</sub> to ABS</i>	<i>CO<sub>2</sub> from ABS</i>	<i>CO<sub>2</sub> to EOR</i>
<i>T (°C)</i>	15	476	150	430	15	680	30	560	25	30	32.5	72.8
<i>P (bar)</i>	1.013	1.033	1.013	22	1.013	1.053	1.013	56	1.10	50.5	50	350
<i>F (kmol/h)</i>	81373	84147	84147	15250	5809	47020	41762	19964	5259	3192	3150	3150
<i>CO<sub>2</sub></i>	0.0004	0.0347	0.0347			0.7708	0.8678		0.0002	0.9038	0.9045	0.9045
<i>H<sub>2</sub>O</i>	0.0101	0.0739	0.0739	1.0000		0.1489	0.0418	1.0000	0.9998	0.0020	138ppm	138ppm
<i>O<sub>2</sub></i>	0.2074	0.1350	0.1350		0.9500	0.0000	0.0000		0.0000	0.0000	0.0000	0.0000
<i>Ar</i>	0.0092	0.0089	0.0089		0.0239	0.0371	0.0417		0.0000	0.0435	0.0440	0.0440
<i>N<sub>2</sub></i>	0.7729	0.7476	0.7476		0.0261	0.0432	0.0487		0.0000	0.0507	0.0513	0.0513

Hot GT exhaust gas enters the heat recovery steam generation (HRSG) section to produce high-pressure superheated steam at 560°C/56 bar for the Rankine cycle and low-pressure steam for the triethylene-glycol (TEG) reboiler. The exhaust gas leaves the HRSG at 89°C to be cooled down to 30°C in the direct-contact column (DCC) with water at 25°C. This exhaust has ≈87%mol CO<sub>2</sub> and ≈92% of it is recycled to the oxy-combustion to attenuate flame temperature. The CO<sub>2</sub>-rich recycle is compressed in the GT adiabatic axial compressor, while the remaining ≈8% of the exhaust (≈90%mol CO<sub>2</sub>) is sent to multistage intercooled-compression to 50.5 bar. At this point, the exhaust is dehydrated via counter-current contact with lean TEG 98.5%w/w at 30°C, to lower the water (H<sub>2</sub>O) content to 138 ppm mol. Dehydrated CO<sub>2</sub>-rich gas then goes to the last compression stage before being totally liquefied at 130 bar/30°C, so that it finally can be pumped to dispatch pressure of 350 bar for EOR purpose.

The conventional NGCC was simulated for the same NG feed, stoichiometric air and expander inlet at 1300°C/39.5 bar to be compared with Ox-NGCC-EOR. Stream results for both plants are shown in Table 2.5 with molar fraction compositions, except when indicated otherwise. Conditions of high-pressure superheated steam are different for NGCC and Ox-NGCC-EOR: 430°C/22 bar for conventional NGCC and 560°C/56 bar for Ox-NGCC-EOR. This is a consequence of the different GT expander outlet temperatures, which affect heat transfer limits differently and the steam pressure taking into account assumption {B9} (Table 2.2) which stipulates minimum 90% of expanded steam quality at steam-turbine (ST) outlet. Stack emissions at conventional NGCC attains 128.5 t/h CO<sub>2</sub>, while Ox-NGCC-EOR has no CO<sub>2</sub> emissions, producing 3150 kmol/h of EOR-fluid with 90.45%mol CO<sub>2</sub>, 5.13%mol N<sub>2</sub>

and 4.40% mol Ar. Certain amount of N<sub>2</sub> is carried to the EOR-fluid from GOX at the nominal purity of 95% mol – 2.61% mol N<sub>2</sub> in the case of TVR-2REB – but an optimized GOX purity within 95% mol-98% mol could optionally be applied for the best overall efficiency. In this case, in exchange for slightly higher  $E_{sep}$  (Fig. 2.11), less N<sub>2</sub> can reduce the compression power of EOR-fluid.

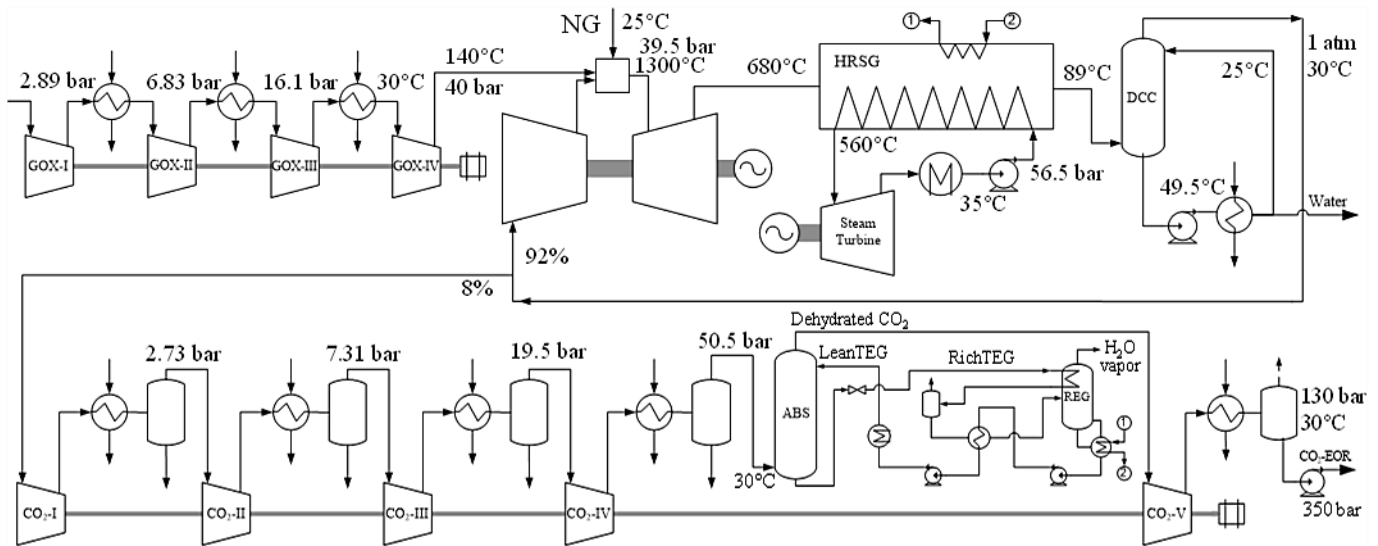


**Fig. 2.12.** Flowsheet of Ox-NGCC-EOR Gas-To-Wire plant.

Positive and negative power contributions for overall power plant efficiency are presented in Table 2.6, showing that the conventional NGCC evidently has greater power output. Electricity generation is reduced by 6.88%LHV from conventional NGCC to Ox-NGCC-EOR. Total power output of combined GT+ST is  $\approx$ 3%LHV higher in Ox-NGCC-EOR, but GOX production and compression consume 3.98%LHV and 3.33%LHV, respectively, with CO<sub>2</sub> compression and pumping demanding further 2.52%LHV.

**Table 2.6.** Contributing power production/consumption items of alternatives.

Power/Item	Conventional NGCC		Ox-NGCC-EOR + TVR-2REB ASU	
	MW	%LHV	MW	%LHV
ASU TVR-2REB	-	-	-24.55	-3.98%
GOX Compressor	-	-	-20.56	-3.33%
Gas-Turbine	278.72	45.19%	249.10	40.38%
Steam-Turbine	74.79	12.12%	123.25	19.98%
CO <sub>2</sub> Compressors & Pump	-	-	-15.55	-2.52%
Auxiliary Equipment	-0.23	-0.04%	-0.85	-0.14%
<b>Net Output</b>	<b>353.28</b>	<b>57.27%</b>	<b>310.84</b>	<b>50.39%</b>

Fixed capital investment (*FCI*) of conventional NGCC and Ox-NGCC-EOR coupled to TVR-2REB ASU are presented in Fig. 2.13, which shows that *FCI* of ASU and GOX compression would be comparable to the *FCI* of conventional GT with bottoming ST of equivalent capacity, so that total *FCI* practically duplicate in Ox-NGCC-EOR with TVR-2REB ASU – from 187.62 to 358.20 MMUSD – since further items have little effect over total *FCI*. Despite of much higher capital investment, it is evident that in a scenario with monetization of CO<sub>2</sub> recovery for EOR and incidence of carbon taxation, economic performance of zero-emission Ox-NGCC-EOR with TVR-2REB ASU could overcome the large-scale CO<sub>2</sub> emitting conventional NGCC.

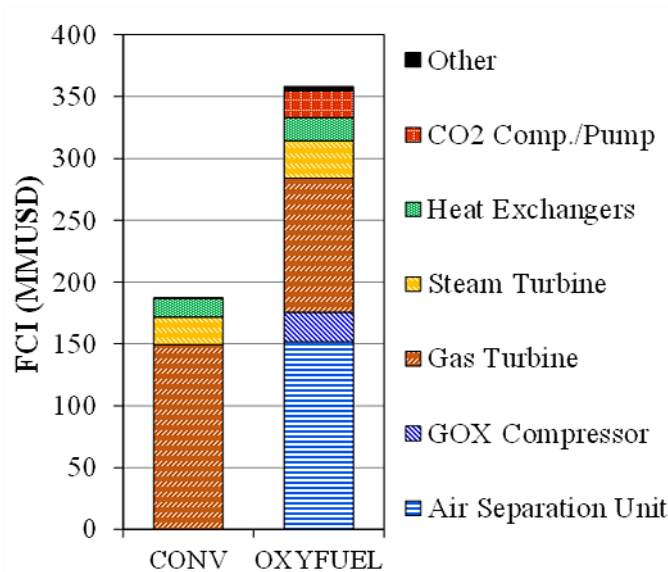


**Fig. 2.13.** *FCI* of alternatives.

Without carbon taxes, Table 2.7 demonstrates economic performance of process alternatives, considering the same electricity price, showing profitability of Ox-NGCC-EOR + TVR-2REB ASU with positive net present value (*NPV*) for 30 years of operation:  $NPV(30y)=765$  MMUSD. Greater annual profit (*AP*) is obtained for Ox-NGCC-EOR + TVR-2REB ASU – 150.63 MMUSD/y against 137.82 MMUSD/y – as a consequence of 14.1% higher revenue due to CO<sub>2</sub>-EOR in spite of 6.88% LHV of net efficiency penalty (Table 2.6). More exactly, 135.5 t/h of EOR-fluid is assumed to be capable of producing 135.5 bbl/h of crude oil, thus giving a revenue of  $\approx 80$  MMUSD/y for the considered price of 74 USD/bbl (operating-hours 8000 h/y). The revenue from electricity is  $\approx 270$  MMUSD/y, for  $\approx 311$  MW priced at 0.1087 USD/kWh from assumption {C1} (Table 2.3). Therefore, Ox-NGCC-EOR + TVR-2REB ASU totalizes  $REV \approx 350$  MMUSD/y, contrasting with  $REV \approx 307$  MMUSD/y from  $\approx 353$  MW electricity sale of conventional NGCC (Table 2.6).

However, Ox-NGCC-EOR with TVR-2REB ASU is still not capable of overcoming conventional NGCC  $NPV(30y)=818.33$  MMUSD (Table 2.7) because of the much higher (+90.9%) *FCI* of the former, so that the advantage of the annual profit of Ox-NGCC-EOR with TVR-2REB ASU should be even higher, which is only attained with carbon taxation. ASU and GOX compressor are major contributors for the increase of the total cost of manufacturing (*COM*), as total *FCI* not only negatively impacts cash flows in construction years, but also indirectly increase the *COM*. The cost of raw materials (*CRM*) is almost the same but slightly higher in Ox-NGCC-EOR with TVR-2REB ASU due to TEG reposition, while the cost of utilities (*CUT*) increases significantly (+60.6%) – but with little influence – due to higher cooling-water duty to dissipate compression heat, and to condense water and CO<sub>2</sub>. At this point, although not considered here, implementation of heat integration would rise overall efficiency, as electricity exportation would increase with simultaneous reduction on CW utilization, thus improving total annual profit (*AP*).

**Table 2.7.** Economic performance of alternatives.

<b>Power Plant</b>	<b>Conventional NGCC</b>	<b>Oxy-NGCC-EOR + TVR-2REB ASU</b>
<i>FCI</i> (MMUSD)	187.62	358.20
<i>COM</i> (MMUSD/y)	108.06	140.72
<i>REV</i> (MMUSD/y)	307.21	350.49
<i>CRM</i> (MMUSD/y)	57.75	57.76
<i>CUT</i> (MMUSD/y)	2.41	3.87
<i>GAP</i> (MMUSD/y)	199.15	209.77
<i>AP</i> (MMUSD/y)	137.82	150.63
<i>NPV-30years</i> (MMUSD)	818.33	765.67

Fig. 2.14 depicts the influence of different scenarios of CO<sub>2</sub> taxation – 0, 20, 40, 60 USD/t – in the *NPV* of conventional NGCC against the zero-emission Ox-NGCC-EOR with TVR-2REB ASU along the 33 years of the project (30 operational years). The initial sequences of bars express the construction years, where Ox-NGCC-EOR + TVR-2REB ASU stands out with the lowest *NPV* levels due to higher *FCI*. Supported by greater revenue due to CO<sub>2</sub>-EOR and profit reduction of competitor CO<sub>2</sub>-emitting NGCC from carbon taxation, superiority of zero-emission Ox-NGCC-EOR+TVR-2REB ASU along the operational years appears with *NPV* advancing over progressively lower CO<sub>2</sub> taxes. By the 9<sup>th</sup> year (6<sup>th</sup> of operation), it first overcomes the *NPV* of NGCC at 60 USD/t, while for the scenario of 40 USD/t it takes just further two years. For the level of 20 USD/t, the advantage appears after 20 years from

construction, and break-even taxation for the end of the project horizon is quoted as 13.5 USD/t CO<sub>2</sub>. In other words, it means that even presenting zero CO<sub>2</sub> emission, Ox-NGCC-EOR with TVR-2REB ASU is more profitable than conventional NGCC if current carbon taxation policy is above 13.5-20.0 USD/t CO<sub>2</sub> depending on the project lifetime – which is already a reality for some European countries – especially considering that progressive taxes are expected over the future.

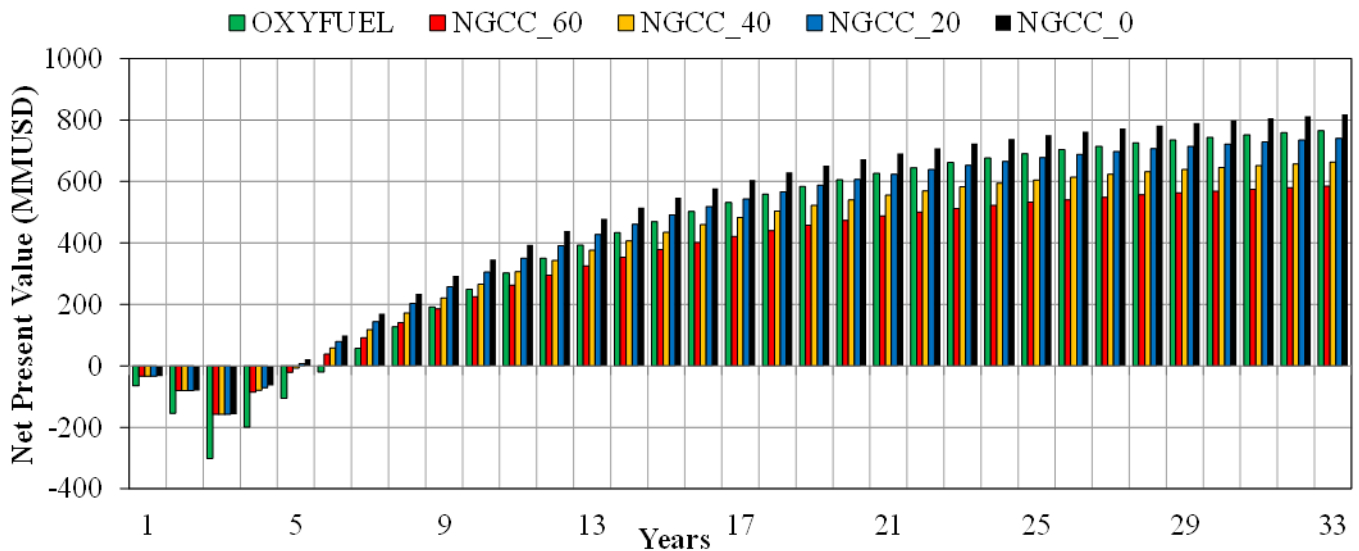


**Fig. 2.14.** Profile of net present value of Ox-NGCC-EOR with TVR-2REB ASU and conventional NGCC at distinct carbon taxation scenarios (USD/tCO<sub>2</sub>).

## 2.4. Conclusions for Chapter 2

In this work, a new cryogenic TVR distillation column was developed as a new ASU concept, the so-called TVR-2REB. The technical evaluation of GOX production of TVR-2REB ASU was performed by process simulation and compared with several ASU concepts including state-of-the-art ASU, with the conclusion that TVR-2REB ASU achieves best specific separation power consumption  $E_{sep}=139$  kWh/tO<sub>2</sub> for GOX production with 95% mol O<sub>2</sub>.

The process configuration of TVR-2REB ASU involves a single atmospheric cryogenic top vapor recompression distillation column with two reboilers: an intermediate reboiler and the habitual bottom reboiler. The intermediate reboiler is heated with compressed GAN from the column top, while saturated compressed air feed heats the bottom reboiler. The mentioned p-GAN is a fraction of the atmospheric column top vapor, which is pressurized via cryogenic compression. The cryogenic distillation column is fed with LAIR, produced by latent heat exchange with boiling O<sub>2</sub> in the column bottom reboiler.

The power requirement for the production of both low-purity (95%mol) and high-purity (99.5%mol) GOX by TVR-2REB ASU is significantly lower than current state-of-the-art ASU. Differently from the standard ASU, there is no need for additional higher pressure columns to generate LIN to reflux the main low-pressure column. It was also demonstrated that compressing GAN cryogenically entails less power consumption than compressing it at ambient temperature, despite increasing refrigeration effort.

In the second part of this work, the new proposed TVR-2REB ASU is coupled to a zero-emission oxyfuel NGCC with CO<sub>2</sub> EOR – Ox-NGCC-EOR – in the context of Gas-To-Wire plants, which was investigated considering different economic scenarios of carbon taxation. Ox-NGCC-EOR with TVR-2REB ASU achieves superior profitability compared to conventional CO<sub>2</sub>-emitting air-fed NGCC, in spite of the ≈100% higher investment of the former relative to the investment of the latter. It was demonstrated that for a project lifetime of 30 years of operation, any carbon tax above 13.5 USD/tCO<sub>2</sub> would guarantee economic superiority of the proposed Ox-NGCC-EOR with TVR-2REB ASU due to increased oil revenues from EOR and zero emission taxation costs.

## 2.5. References for Chapter 2

- [1] Araújo OQF, de Medeiros JL. Carbon capture and storage technologies: present scenario and drivers of innovation. *Curr Opin Chem Eng* 2017; 17:22–34. <http://doi.org/10.1016/j.coche.2017.05.004>
- [2] Foy K, Yantovski E. History and state-of-the-art of fuel fired zero emissions power cycles. *Int J Thermodyn* 2006; 9(2):37–63.
- [3] Geffroy PM, Blond E, Richet N, Chartier T. Understanding and identifying the oxygen transport mechanisms through a mixed-conductor membrane. *Chem Eng Sci* 2017; 162:245–61. <https://doi.org/10.1016/j.ces.2017.01.006>
- [4] Anderson LL, Armstrong PA, Broekhuis RR, Carolan MF, Chen J, Hutcheon MD, et al. Advances in ion transport membrane technology for oxygen and syngas production. *Solid State Ion* 2016; 288:331–7. <https://doi.org/10.1016/j.ssi.2015.11.010>
- [5] Higginbotham P, White V, Fogash K, Guvelioglu G. Oxygen supply for oxyfuel CO<sub>2</sub> capture. *Int J Greenh Gas Control* 2011; 5S:S194–03. <https://doi.org/10.1016/j.ijggc.2011.03.007>
- [6] Darde A, Prabhakar R, Tranier JP, Perrin N. Air separation and flue gas compression and purification units for oxy-coal combustion systems. *Energy Proc* 2009; 1:527–34. <https://doi.org/10.1016/j.egypro.2009.01.070>
- [7] Schwenk D. Recovery of nitrogen, oxygen and argon. In: Häring HW, editor. *Industrial gases processing*, Weinheim: WILEY-VCH Verlag GmbH & Co. KGaA; 2008, p. 13–58. <https://doi.org/10.1002/9783527621248.ch2>
- [8] Soundararajan R, Gundersen T, Ditaranto M. Oxy-combustion coal based power plants: study of operating pressure, oxygen purity and downstream purification parameters. *Chem Eng Trans* 2014; 39:229–34. <https://doi.org/10.3303/cet1439039>

- [9] Dillon DJ, White V, Allam RJ, Wall RA, Gibbins J. IEA Greenhouse Gas R&D Programme: Oxy-combustion processes for CO<sub>2</sub> capture from power plant. Engineering Investigation Report, 2005.
- [10] Fu C, Anantharaman R, Gundersen T. Optimal integration of compression heat with regenerative steam Rankine cycles in oxy-combustion coal based power plants. *Energy* 2015; 84:612–22. <https://doi.org/10.1016/j.energy.2015.03.023>
- [11] Skorek-Osikowska A, Bartela L, Kotowicz, J. A comparative thermodynamic, economic and risk analysis concerning implementation of oxy-combustion power plants integrated with cryogenic and hybrid air separation units. *Energy Convers Manag* 2015; 92:421–30. <https://doi.org/10.1016/j.enconman.2014.12.079>
- [12] Burdyny T, Struchtrup H. Hybrid membrane/cryogenic separation of oxygen from air for use in the oxyfuel process. *Energy* 2010; 35:1884–97. <https://doi.org/10.1016/j.energy.2009.12.033>
- [13] Janusz-Szymanka K, Dryjanska A. Possibilities for improving the thermodynamic and economic characteristics of an oxy-type power plant with a cryogenic air separation unit. *Energy* 2015; 85:45–61. <https://doi.org/10.1016/j.energy.2015.03.049>
- [14] Linde C, inventor and applicant. Apparatus for producing pure nitrogen and pure oxygen. US Patent 795,525. Filed in Oct. 22<sup>nd</sup>, 1903. Patented in July 25<sup>th</sup>, 1905.
- [15] Kapitza PL, inventor and applicant. Method and means for rectification and distillation of liquids with low temperature boiling points. GB Patent 625,107. Filed in Apr. 8<sup>th</sup>, 1946. Patented in June 22<sup>nd</sup>, 1949.
- [16] Kerry FG. Industrial gas handbook: gas separation and purification. Boca Raton: CRC Press; 2006.
- [17] Benedict M, inventor; Hydrocarbon Research Inc., applicant. Rectification of gaseous mixtures. US Patent 2,627,731. Filed in June 18<sup>th</sup>, 1949. Patented in Feb. 10<sup>th</sup>, 1953.
- [18] Fu C, Gundersen T. Recuperative vapor recompression heat pumps in cryogenic air separation processes. *Energy* 2013; 59:708–18. <https://doi.org/10.1016/j.energy.2013.06.055>
- [19] Gundersen T, Fu C, Eimer D, inventors; Norwegian University of Sci. & Tech. (NTNU), applicant. Air separation. Patent Application WO2013/014252. Filed in July 26<sup>th</sup>, 2012.
- [20] Brigagão GV. Technical evaluation of oxygen production by cryogenic vapor recompression distillation (*in Portuguese*). MSc Thesis, Fed.Univ. of Rio de Janeiro, 2016.
- [21] Van Sciver SW. Advances in helium cryogenics. In: Timmerhaus KD, Reed RP., editors. *Cryogenic engineering: fifty years of progress*. New York: Springer; 2007, p. 161–178. [https://doi.org/10.1007/0-387-46896-X\\_9](https://doi.org/10.1007/0-387-46896-X_9)
- [22] Agrawal R, Herron DM, Zhang Y, inventors; Air Products and Chemicals Inc., applicant. Single expander and a cold compressor process to produce oxygen. US Patent 5,901,576. Filed in Jan. 22<sup>nd</sup>, 1998. Patented in May 11<sup>th</sup>, 1999.
- [23] Brugerolle JR, Ha B, inventors; Air Liquide SA, applicant. Low temperature air separation process for producing pressurized gaseous product. US Patent 8,769,985. PCT Filed in July 12<sup>th</sup>, 2005. Patented in July 8<sup>th</sup>, 2014.
- [24] Goloubev D, Alekseev A. Integration of ASU in process of power generation. 3<sup>rd</sup> Oxyfuel Combustion Conference, Ponferrada, Spain, 2013.
- [25] Kim D, Giametta REH, Gundersen T. Optimal use of liquefied natural gas (LNG) cold energy in air separation units. *Ind Eng Chem Res* 2018; 57:5914–23. <https://doi.org/10.1021/acs.iecr.7b04282>
- [26] Andrei M, Sammarco, G. Gas to wire with carbon capture and storage: a sustainable way for onsite power generation by produced gas. SPE Abu Dhabi Int. Petroleum Exhibition & Conference. Society of Petroleum Engineers, 2017. <https://doi.org/10.2118/188845-MS>
- [27] Brigagão GV, de Medeiros JL, Araújo OQF, inventors; Federal University of Rio de Janeiro, applicant. Processo de destilação criogênica para separação do ar para produção de oxigênio gasoso. BR Patent Application 102016022807-7. Filed in Sep. 30<sup>th</sup>, 2016.

- [28] Chen CC, Mathias PM. Applied thermodynamics for process modeling. *AIChE J* 2002; 48(2):194–200. <https://doi.org/10.1002/aic.690480202>
- [29] Tonziello J, Vellini M. Oxygen production technologies for IGCC power plants. *Energy Proc* 2011; 4:637–44. <https://doi.org/10.1016/j.egypro.2011.01.099>
- [30] Fu C, Gundersen T. Using exergy analysis to reduce power consumption in air separation units for oxy-combustion processes. *Energy* 2012; 44:60–8. <https://doi.org/10.1016/j.energy.2012.01.065>
- [31] Schmidt W. ASU reboiler/condenser safety. European Industrial Gas Association, Production Safety Seminar, 2006.
- [32] McGuinness RM, Kleinberg WT. Oxygen production. In: Baukal CE, editor. Oxygen-enhanced combustion. 2<sup>nd</sup> ed. Boca Raton: CRC Press; 2013.
- [33] Turton R, Bailie RC, Whiting WB, Shaeiwitz JA, Bhattacharya D. Analysis, synthesis, and design of chemical processes. 4<sup>th</sup> ed. New Jersey: Prentice Hall; 2012.
- [34] Campbell JM. Gas conditioning and processing, v. 2: the equipment modules. 7th ed. Norman/Oklahoma: Campbell Petroleum Series; 1984.
- [35] McCoy ST. The economics of CO<sub>2</sub> transport by pipeline and storage in saline aquifers and oil reservoirs. PhD Thesis, Carnegie Mellon University, USA, 2008.
- [36] Clausen LR, Elmegaard B, Houbak N. Technoeconomic analysis of a low CO<sub>2</sub> emission dimethyl ether (DME) plant based on gasification of torrefied biomass. *Energy* 2010; 35(12):4831–42. <https://doi.org/10.1016/j.energy.2010.09.004>

### 3. A New Concept of Air Pre-Purification Unit for Cryogenic Separation: Low-Pressure Supersonic Separator Coupled to Finishing Adsorption

*This chapter is published as an article in Separation and Purification Technology.*

BRIGAGÃO, G. V., ARINELLI, L. O., DE MEDEIROS, J. L., ARAÚJO, O. Q. F. A new concept of air pre-purification unit for cryogenic separation: low-pressure supersonic separator coupled to finishing adsorption. *Separation and Purification Technology*, 215, 173-189, 2019.

#### **Abstract**

In commercial cryogenic manufacturing of oxygen, air to the Cold-Box must pass through a Pre-Purification Unit (PPU) to remove water, CO<sub>2</sub> and other impurities. The conventional PPU – FULL-TSA – comprises compression, cooling pre-dehydration and temperature-swing adsorption (TSA) for dehydration and CO<sub>2</sub> removal, supplying treated air at 3.1 bar. This work discloses a new PPU concept – SS-TSA – prescribing a supersonic separator (SS) upstream to TSA handling 98.5% of dehydration, greatly lowering TSA costs. SS-TSA comprises compression, cooling pre-dehydration, SS dehydration and a smaller TSA for finishing dehydration and CO<sub>2</sub> removal. A SS-TSA variant – TSA-HI – additionally recovers compression heat lowering heating costs. SS-TSA, FULL-TSA and SS-SS-TSA-HI were analyzed. Flowsheets were simulated in HYSYS with full thermodynamic SS modeling via a new HYSYS Unit Operation Extension – SS-UOE – rigorously calculating the multiphase sound speed. SS was designed for only 3.5% of head-loss, recovering 98.5% of water as super-cooled liquid, lowering make-up and chilled-water costs, while shrinking the TSA service to 10% of the FULL-TSA counterpart. For commercial-scale PPU considering 20 years of operation at 10% interest rate, the purified 3.1 bar air breakeven prices reached 5.28, 5.19, and 5.18 US\$/kNm<sup>3</sup>, respectively for FULL-TSA, SS-TSA and SS-TSA-HI, establishing superiority of SS alternatives over the conventional FULL-TSA.

**Keywords:** air pre-purification; air dehydration; supersonic separator; multiphase supersonic flow; multiphase sound speed.

#### **Supplementary Materials**

Supplementary Materials for this chapter are found in Appendices V1, V2 and V3 and V4.

#### **Abbreviations**

1D One-Dimensional; AA Activated Alumina; ASU Air Separation Unit; BAC Booster Air Compressor; C3+ Propane and Heavier HCs; ChW Chilled-Water; CW Cooling Water; DCA Direct Contact Aftercooler; EOS Equation of State; EWC Evaporative Water Cooler; FULL-

TSA Conventional TSA PPU; HC Hydrocarbon; HCDPA Hydrocarbon Dew-Point Adjustment; LP Low-Pressure; MAC Main Air Compressor; MMSm<sup>3</sup>/d Millions Standard m<sup>3</sup> per Day; MS Molecular Sieve; MS-TSA Smaller TSA of SS PPU; MMUSD/y Millions USD/y; NG Natural Gas; PPU Pre-Purification Unit; PR-EOS Peng-Robinson EOS; PSA Pressure-Swing Adsorption; REVEX Reversing Heat Exchanger; RH Relative Humidity; SS Supersonic Separator; SS-TSA New SS+TSA PPU; SS-TSA-HI New SS+TSA Heat-Integrated PPU; TSA Temperature-swing Adsorption; VLE Vapor-Liquid Equilibrium; VLWE Vapor-Liquid-Water Equilibrium; UOE Unit Operation Extension; USD US Dollar; WDP Water Dew-Point; WDPA Water Dew-Point Adjustment. WW Warm Water.

## Nomenclature

- $A(x)$  : Flow section area at axial position  $x$  (m<sup>2</sup>)  
 $c(T, P, \underline{Z})$  : Sound speed property of multiphase equilibrium fluid at  $(T, P, \underline{Z})$  (m/s)  
 $COM, CUT$  : Costs of manufacturing and of utilities (USD/y)  
 $\bar{C}_p \equiv \left( \frac{\partial \bar{H}}{\partial T} \right)_{P, \underline{Z}}$  : Molar isobaric heat capacity of multiphase fluid (J/kg.K)  
 $D, D_b, D_T, D_O$  : Diameter and SS internal diameters at inlet, throat and outlet (m)  
 $F$  : Feed flow rate (kmol/h)  
 $FCI$  : Fixed capital investment (USD)  
 $\bar{H}$  : Molar enthalpy of multiphase fluid (J/K.mol)  
 $L, L_C, L_D$  : SS lengths: total, converging section and diverging section (m)  
 $L^{Laval}, L^{Shock}$  : Laval nozzle length and SS axial position where  $Ma=Ma^{Shock}$  ( $=L^{LAVAL}$ ) (m)  
 $Ma=v/c$  : Mach Number  
 $Ma^{Shock}$  : Maximum supersonic  $Ma$   
 $M_M$  : Molar mass (kg/mol)  
 $nc$  : Number of components  
 $NPV$  : Net present value (USD)  
 $P$  : Absolute pressure (bar) or (Pa)  
 $REC\%H_2O$  : Percent recovery of H<sub>2</sub>O as SS condensate  
 $REV$  : Revenues (USD/y)  
 $\bar{S}$  : Molar entropy of multiphase fluid (J/K.mol)  
 $T$  : Absolute temperature (K)  
 $v$  : Axial velocity of multiphase fluid (m/s)  
 $x$  : SS axial position (m)  
 $\underline{Z}$  : Vector ( $nc \times 1$ ) of mol fractions of multiphase fluid  
**Greek Symbols**  
 $\alpha, \theta$  : Converging and diverging angles (deg) of SS with linear diameter profiles  
 $\eta^{EXP}\%, \eta^{CMP}\%$  : SS adiabatic expansion and compression efficiencies (%)  
 $\psi$  : Molar vapor fraction of multiphase fluid  
 $\rho$  : Multiphase fluid density (kg/m<sup>3</sup>)  
 $\bar{E}_p \equiv \left( \frac{\partial \rho}{\partial P} \right)_{T, \underline{Z}}$  : Derivative of  $\rho$  with  $P$  at const.  $T, \underline{Z}$  for multiphase fluid (kg/Pa.m<sup>3</sup>)

$$\mathcal{E}_T \equiv \left( \frac{\partial \rho}{\partial T} \right)_{P, Z} : \text{Derivative of } \rho \text{ with } T \text{ at const. } P, Z \text{ for multiphase fluid (kg/K.m}^3\text{)}$$

*Superscripts*

*Inlet, Outlet* : SS inlet and SS outlet

*Shock* : Just before normal shock and before condensate withdrawal

*Subscripts*

*AS* : Just after shock

*BS* : Just before shock and after condensate withdrawal

### 3.1. Introduction

Cryogenic air separation units (ASU) configure the most suitable technology for large-scale air fractionation, currently widespread applied for oxygen supply to steelworks and coal gasification [1]. The uprising of oxy-combustion CO<sub>2</sub> capture in thermoelectric plants signalizes a probable increase of the global demand for oxygen gas in next decades requiring large-scale efficient ASUs. Large-scale ASU comprises two processes with very distinct characteristics, namely: (i) air compression, pre-cooling and purification hereinafter referred to as Pre-Purification Unit (PPU); and (ii) cryogenic fractionation or Cold-Box. PPU supplies purified pressurized air to Cold-Box, both owned by the same company according to current practices. However, it is conceivable, particularly in large-scale ASUs, to have outsourced PPU for best overall profitability. As the Cold-Box is highly capital intensive, the development of more efficient large-scale PPU is interest of oxy-combustion.

PPU compresses and treats air preventing entrance of ice-forming contaminants (H<sub>2</sub>O and CO<sub>2</sub>) and traces of flammable hydrocarbons (HCs) in the Cold-Box. Freezing-out components plug the main Cold-Box heat exchanger, representing operational and safety hazards, besides economic loss associated to defrosting shut-downs, while HCs concentrate in the oxygen sump of the main column thanks to higher boiling points than oxygen, leading to dangerous auto-ignition mixtures [2].

Currently, the most common PPU concept – so-called FULL-TSA PPU – is based on temperature-swing adsorption (TSA) over an activated alumina (AA) bed followed by a molecular sieve (MS) bed, the former for removing water and the latter for CO<sub>2</sub> and HCs removal [3,4]. TSA adopts periodic bed regeneration combining heating with depressurization via heated decontaminated 1 atm nitrogen from Cold-Box. As purging water from AA bed is harder than purging CO<sub>2</sub>+HCs from MS bed, TSA requires hot purging nitrogen above 120°C for complete desorption. FULL-TSA PPU also involves pre-cooled air

feed for reducing moisture, thus lowering TSA costs and adsorbent load and/or extending TSA cycles, typically of 4-8h [3,4]. Large-scale FULL-TSA PPU features large TSA vessels, high heat demand for bed regeneration, besides adsorbent replacement owing to breakage by thermal-mechanical stress from cycling [5].

Pressure-Swing Adsorption (PSA) is an alternative to TSA with some advantages by eliminating regeneration nitrogen and pre-cooled air. However, due to lower loadings, PSA demands short cycles ( $\approx 20$  min) with several drawbacks, such as high maintenance costs of switching valves, larger adsorbent inventories, higher mechanical stress on beds and air losses by frequent depressurization [6,7]. Furthermore, PSA loses competitiveness as the air feed design pressure decreases, a trend for reducing power consumption, a major ASU cost. Current impure oxygen gas production requires  $\approx 3$  bar air feed [8], contrasting with conventional  $\approx 5.5$  bar Cold-Boxes [9]. Thus, in low-pressure ASUs, FULL-TSA PPU is dominant [10]. Low-pressure ASU is approached with vapor recompression cryogenic distillation requiring main air feed at 1.5 bar and adopting former reversing heat exchangers (REVEX) pre-purification claiming 5% less power consumption than conventional ASU [11]. On the other hand, REVEX is an obsolete technology, characterized by sending raw pressurized air to Cold-Box without purification, so that as it gradually cools down in the main heat exchanger, contaminants freeze out and are retained [2,7]. The superiority of FULL-TSA PPU over REVEX is consequence [2] of REVEX cycles of only 4-10 min, where raw air alternates with nitrogen from Cold-Box allowing resilient traces of frozen HCs to partially evaporate into the feed air, accumulating in the distillation system. Comparatively to REVEX, FULL-TSA PPU offers safer ASU operation, consequently REVEX is no longer used [2,7].

Works on FULL-TSA PPU mostly focus on experimentation and modeling aiming at to address adsorbent performance as in [12] for H<sub>2</sub>O, CO<sub>2</sub> and HCs with several adsorbents; in [13,14] for TSA of H<sub>2</sub>O on F-200 AA including H<sub>2</sub>O-CO<sub>2</sub> competition and capillary H<sub>2</sub>O condensation; and in [10] for H<sub>2</sub>O/CO<sub>2</sub> TSA on F-200 AA. Other experiments demonstrated superior CO<sub>2</sub>/CH<sub>4</sub> loadings on Li-LSX zeolite MS comparatively to conventional 13X zeolite MS [15]; and TSA on AA composites with 13X zeolite MS, giving higher HC loadings than conventional 13X zeolite MS [16]. Kawai and Nakamura [17] disclosed a FULL-TSA PPU with larger MS bed and higher air velocity to limit CO<sub>2</sub> competition against N<sub>2</sub>O and HCs, while Nakamura et al. [18] discussed FULL-TSA PPU with AA and MS beds using two simultaneous desorption gases: Cold-Box nitrogen at 100-250°C and 60-250°C raw air.

This survey proves the preponderance of FULL-TSA PPU in large-scale ASUs, but it is evident that ponderable capital and operational costs are inherent to TSA. Research on ASU mostly quests for low-pressure Cold-Boxes [8,11], particularly for oxy-combustion oxygen, while typical PPU papers in the literature explore 5.5-7.0 bar FULL-TSA PPUs, ignoring cases below 4 bar.

Counterpointing this trend, the present work addresses a new PPU concept at lower air pressure, radically lowering the size of costly TSA by adopting a upstream low-pressure supersonic separator (SS) handling  $\approx 98.5\%$  of the dehydration load of pre-cooled  $10^\circ\text{C}$  raw air ( $\approx 3886 \text{ ppmH}_2\text{O}$ ). With SS, TSA must now finish only  $\approx 1.5\%$  of dehydration load and remove  $\approx 370 \text{ ppmCO}_2$  and minor HC contaminants totaling  $\approx 10\%$  of the entire dehydration load. Hence the AA bed is unnecessary and only a MS bed is required approximately  $\approx 15\%$  larger than its previous size in FULL-TSA for same cycle-time. This new PPU concept is called SS-TSA so as to emphasize SS and TSA collaboration for air pre-purification. A heat-integrated SS-TSA variant – SS-TSA-HI – is also demonstrated for improved profitability by avoiding heating costs of MS regeneration. Both SS-TSA and SS-TSA-HI regenerate the MS bed with hot 1 atm dry nitrogen from Cold-Box, the difference being the heating source: low-pressure (LP) steam in SS-TSA and warm water from compression heat recovery in SS-TSA-HI.

The advantages of SS-TSA and SS-TSA-HI over FULL-TSA were unveiled via technical and economic analyses after simulating the respective flowsheets with HYSYS 8.8. In SS-TSA and SS-TSA-HI the SS unit was rigorously thermodynamically modeled via a HYSYS Unit Operation Extension (UOE) SS-UOE previously developed [19], whose algorithm is disclosed in Appendix V1. SS-UOE handles multiphase equilibrium supersonic flow and phase-split, calculating the correct multiphase equilibrium sound speed ( $c$ ) with PEC-UOE, another UOE from previous work [20]. SS-UOE is validated in Appendix V2 with SS data from the literature.

Scientific and patent literatures never considered before such PPU concept using SS combined with smaller finishing MS-TSA for large-scale ASU. Therefore SS-TSA and SS-TSA-HI are original and novel frameworks using breakthrough SS separation technology, both more profitable than the conventional FULL-TSA PPU. SS-TSA and SS-TSA-HI configure embodiments of pending patent No. BR102017027727-5 registered in Brazilian Patent and Trademark Office [21].



attained in the supersonic section, supersonic flow becomes metastable as it expands against a higher downstream  $P^{Outlet}$ . This meta-stability increases with  $P^{Outlet} - P$ , such that somewhere in the diverging section a normal shock front occurs (Fig. 3.1). Normal shock is an irreversible transition that suddenly turns the flow back to subsonic ( $Ma < 1$ ), accompanied by sharp, practically discontinuous, increase of  $P$ ,  $T$  and molar entropy ( $\bar{s}$ ). The after-shock diverging section is a diffuser where the subsonic flow gradually recompresses, heats up and decelerates towards the SS outlet at  $P = P^{Outlet}$ . Compressible flow is practically isentropic upstream and downstream the shock, so that the shock is the unique great source of irreversibility along the SS flow path, which explains why  $P^{Outlet} < P^{Inlet}$ . In other words, there must be some head-loss from inlet to outlet, increasing with shock intensity, which rises with  $Ma$  just before shock or  $Ma_{BS}$ . The isentropic character of expansion and compression SS paths can be relaxed by specifying respective adiabatic efficiencies  $\eta^{EXP}\%$ ,  $\eta^{CMP}\%$  [19]. The location of collecting vanes is specified with  $Ma^{Shock}$ , the maximum supersonic  $Ma$  before shock. At  $Ma = Ma^{Shock}$  condensate is withdrawn, leaving dry gas at  $Ma_{BS}$ , ready for shock ( $1 \leq Ma_{BS} \leq Ma^{Shock}$ ).  $Ma^{Shock}$  determines the Laval Nozzle, i.e. the converging-diverging nozzle extending from inlet to pre-shock (Fig. 3.1). In SS operation with raw NG, water and C3+ (propane and heavier HCs) condensate should be withdrawn at the Laval's end, just before shock, centrifugally pushed towards the collecting vanes. Any non-collected liquid is re-vaporized through the shock destroying separation [19].

SS research has evolved in last decade via thermodynamic approaches [19,23,24,25] and computational fluid dynamic (CFD) approaches [26,27]. As proven elsewhere [19], despite easily implemented and dominating SS literature, CFD SS approaches lack completeness as CFD cannot handle complex multicomponent phase behavior and phase-change – VLE (vapor-liquid equilibrium) or VLWE (vapor-liquid-water equilibrium) transitions – neither the multiphase sound speed ( $c$ ), both essential SS features with condensing feeds (e.g. raw NG or raw air). For example, Yang et al. [26] and Wen et al. [27] are two recent CFD representative SS works with raw NG. The former studied the impact of expansion ratios and pre-shock  $Ma$  on pressure recovery, while the latter compared diffuser geometries regarding pressure recovery. Despite apparently different, these works share two fundamental aspects: both model SS flow path with CFD software and use raw NG with condensable C3+ and water. Such choices lead evidently to SS profiles with some error as CFD cannot generate phase-change effects on SS flow path, a feature inherent to raw NG feeds. Several other limitations found in these and similar CFD works are: (i) the multiphase sound speed ( $c$ ) is

not correctly calculated as phase-change is ignored, a critical factor in SS with raw NG; (ii) too cold and wrong pre-shock  $T$  profiles result from ignoring phase-change in SS path; and (iii) inclined linear trends on  $P$ ,  $T$ ,  $Ma$  profiles across normal shock, besides improper oscillating anomalies just upstream and downstream the front. Therefore, there is a need for rigorous thermodynamic formalisms to handle SS with condensing feeds. The truth is that CFD is insufficient for SS engineering and design with such feeds. Recently, Shooshtari and Shahsavand [28] considered SS with raw NG for better pressure recovery given the degree of dehydration via condensation-nucleation theory and droplet growth. Despite not using CFD, this work also explored a limited SS model considering single-phase compressible flow with PR-EOS, which was used only for calculating single-phase density and isothermal compressibility, and not for full phase-equilibrium and multiphase  $c$ ; i.e., the phase-equilibrium on SS flow path and multiphase  $c$  property were not taken rigorously. There were other limitations: (i) normal shock via ideal gas with constant heat capacities ratio; (ii) Raoult's Law for high-pressure water VLE; (iii) sound speed for ideal gas with constant heat capacities ratio.

On the other hand, thermodynamic SS approaches handle phase transitions and multiphase  $c$ , but demand full thermodynamic equilibrium, perhaps not fully attainable in the SS lapse of milliseconds. Nevertheless, thermodynamic SS approaches are more valuable for condensing feeds as they can represent limiting SS behaviors under strict observance of the Second Law of Thermodynamics, while ordinary CFD SS approaches with condensing feeds violate the 2<sup>nd</sup> Law as CFD predicts unrealistic too cold pre-shock temperatures implying adiabatic destruction of entropy, a forbidden outcome [19]. In other words, it may be possible that a real SS departs somewhat from the predictions of thermodynamic equilibrium SS modeling, but such equilibrium modeling cannot be viewed as wrong because all thermodynamic laws are respected, especially the 2<sup>nd</sup> Law.

A rigorous thermodynamic SS modeling was presented by Arinelli et al. [19] who developed SS-UOE, a HYSYS 8.8 UOE appropriate for SS design and simulation. SS-UOE models multiphase 1D compressible flow in SS path matching SS design with throat sonic flow, besides executing condensate separation, normal shock and diffuser recompression. SS-UOE requires the phase-equilibrium sound speed ( $c$ ) property, which is calculated by PEC-UOE, another HYSYS UOE for rigorous determination of  $c$  under single-phase (gas), two-phase (gas and liquid C3+ or gas and water) or three-phase (gas, liquid C3+ and water) compressible flows as disclosed in de Medeiros et al. [20]. SS-UOE and PEC-UOE can

efficiently handle SS with raw NG feeds producing two immiscible condensates – C3+ and water – as occurs in WDPA+HCDPA applications [19,25], while other thermodynamic SS models cannot handle water and are restricted to HC condensate only [23,24]. Arinelli et al. [19] also demonstrated SS for CO<sub>2</sub> removal from CO<sub>2</sub>-rich NG feeds previously WDPA+HCDPA treated to allow exclusive CO<sub>2</sub> condensation in SS. However, SS path must be designed choosing  $Ma^{Shock}$  lesser than a certain  $Ma^{Freeze-Out}$  to prevent excessive temperature drop possibly crossing the CO<sub>2</sub> freeze-out border, this way avoiding dry-ice precipitation potentially plugging the SS.

SS is specified in SS-UOE via following parameters: (i) inlet flow rate, temperature, pressure and component mole fractions ( $F^{Inlet}$ ,  $T^{Inlet}$ ,  $P^{Inlet}$ ,  $\underline{z}^{Inlet}$ ); (ii) SS expansion/compression adiabatic efficiencies ( $\eta^{EXP}\%$ ,  $\eta^{CMP}\%$ ); (iii) converging/diverging wall angles ( $\alpha$ ,  $\beta$ ) and inlet/outlet diameters ( $D_I$ ,  $D_O$ ) (Fig. 3.1); and (iv) maximum attained supersonic  $Ma$  ( $Ma^{Shock}$ ). SS-UOE automatically retrieves feed inlet parameters from HYSYS flowsheet and, reciprocally, exports the calculated SS product streams to it. In each simulation the SS design is obtained by SS-UOE via determination of lengths  $L_C$ ,  $L_D$ ,  $L^{Shock}$ ,  $L^{Diffuser}$  and throat diameter  $D_T$  (Fig. 3.1), simultaneously with outlet conditions of gas and condensate, besides the SS head-loss.

SS utilization for condensable separation from pressurized gas is evolving rapidly beyond NG applications WDPA, HCDPA and CO<sub>2</sub> removal. Recently, Teixeira et al. [25] presented an “out of the box” SS recovery of hydroxylated thermodynamic hydrate inhibitors – methanol, ethanol and ethylene-glycol – from a pressurized raw NG stream previously contacted with inhibitors in pipelines, obtaining remarkable results. By treating such raw NG in a SS with small water injection it is possible to recover the inhibitor trapped in aqueous condensate, besides producing saleable LPG and conditioned NG in terms of WDPA+HCDPA. In [25], SS operated with supersonic three-phase flow comprising gas, liquid C3+ and water-inhibitor condensate, requiring determination of the three-phase equilibrium sound speed property ( $c$ ). SS results of [25] were generated by simulating HYSYS 8.8 flowsheets for treating raw NG with anti-hydrate inhibitors using HYSYS UOEs SS-UOE [19] and PEC-UOE [20], where all multiphase-equilibrium separations and properties were calculated with the Cubic-Plus-Association Equation-of-State (CPA-EOS) which can handle associating three-phase VLWE (vapor-liquid-water equilibrium) systems including hydroxylated anti-hydrate inhibitors [29].

The present work extends once more the applicability of SS by defining, for the first time in the literature, new PPU's SS-TSA and SS-TSA-HI where  $\approx 98.5\%$  of the water content of raw air was abated by low-pressure SS with  $Ma^{Shock}$  carefully chosen to give SS pressure recovery

of  $\approx 96.5\%$  saving compressor power and complying with state-of-the-art Cold-Boxes using purified air at  $3.1 \text{ bar}$ . SS was also simulated with SS-UOE and PEC-UOE, whose mathematical models and theory are not discussed in the text and should be found elsewhere [19,20]. Nevertheless, in order to give a clear convincing presentation of the thermodynamic SS modeling used in the calculations and also to validate it, the algorithm of SS-UOE is disclosed in Appendix V1 for SS nozzles with linear diameter profiles (Fig. 3.1). Additionally, the validation of SS-UOE was conducted in Appendix V2 by comparing its results with Arina's data presented by Yang et al. [26], which refers to a SS application with non-linear diameter profiles for low-pressure dry air. The concordance of SS-UOE results with Arina's data is unquestionable.

At last, it is advisable to address the adaptability of SS to variable load of ASUs. Despite the fact that the conceptual scenario of this work should correspond to very large-scale ASUs for large-scale oxy-fuel power plants – whose operation should be stable beforehand – indeed smaller conventional ASUs are subject to sudden load changes. Analogously to centrifugal compressors, there are some SS particularities that should be observed for adequate performance. Let a SS design in Fig. 3.1. For successful operation, it is necessary and sufficient that sonic flow ( $Ma=1$ ) exists at the throat. Consequently, other things constant, the sonic throat is lost if the inlet flow rate decreases or if the inlet pressure increases, since both occurrences lower the inlet speed displacing the new sonic point downstream the throat, which results in unattainable sonic flow because the diverging section recompresses the subsonic flow slowing it down. At first, one would blame such effects as SS issues. But this is an unfair interpretation. Similar phenomenon also happens with centrifugal compressors, whose operation can be disrupted by surge effects from sudden falls of flow rate or suction pressure. Thus, in both centrifugal compressors and SS, control schemes must protect the operation against disruptions.

The truth is that a given SS is designed for a given inlet Mach ( $Ma^{in}$ ), not for a given inlet pressure or inlet flow rate. Thus, if the inlet flow rate falls occasionally, a control scheme should throttle the feed to lower its pressure increasing inlet speed and restoring the design  $Ma^{in}$ . Analogously, if inlet pressure falls, control should reduce inlet flow rate decreasing inlet speed to restore  $Ma^{in}$ . An inverse reasoning also works replacing “falls” by “increases”, “lower” by “rises” and “throttling” by “compressing”.

This behavior is easily demonstrated for a SS expanding ideal gas with constant heat capacity ratio ( $k \equiv \bar{C}_p / \bar{C}_v \cong const.$ ) for which it is easily shown the applicability of Eqs. (3.1a), (3.1b) and (3.1c) correctly describing 1D isentropic compressible flow in a converging-diverging nozzle, where inlet is referred by  $^{in}$ , flow area section is represented by  $A$  and Eq. (3.1d) is obtained from Eq. (3.1a) by inserting  $Ma=1$  and  $A=A^{Throat}$ . Thus, given a SS with geometry  $A^{in}$ ,  $A^{out}$ ,  $A^{Throat}$ ,  $L$ , etc, and inlet temperature  $T^{in}$ , Eq. (3.1d) stipulates a unique  $Ma^{in}$  for the design  $A^{Throat}/A^{in}$  in order to achieve sonic throat flow. Therefore Eqs (3.1a) and (3.1b) show that  $Ma$  and  $T$  profiles will match the design objectives (i.e. supersonic  $Ma>1$  in the diverging section causing low temperature  $T \ll T^{in}$ ) if the inlet  $Ma$  is kept at the correct  $Ma^{in}$  stipulated by Eq. (3.1d), not importing if  $P^{in}$  is manipulated away from its design value to secure  $Ma^{in}$  constant under fluctuations of inlet flow rate. That is,  $P^{in}$  is adjusted to accommodate different inlet flow rates (and vice-versa) for a given nozzle design properly working with sonic throat. Another strategy to protect SS operation for air processing – which can be complemented by the previous  $Ma^{in}$  compensation schemes – is to install an arrangement of smaller parallel SS nozzles that are individually deactivated (or activated) by the control scheme according to the total inlet flow rate, guaranteeing each nozzle always fed with its design  $Ma^{in}$ .

$$\frac{A}{A^{in}} = \frac{Ma^{in}}{Ma} \left\{ \frac{1 + \left(\frac{k-1}{2}\right) \cdot (Ma)^2}{1 + \left(\frac{k-1}{2}\right) \cdot (Ma^{in})^2} \right\}^{\frac{k+1}{2(k-1)}} \quad (3.1a)$$

$$\frac{T}{T^{in}} = \left\{ \frac{1 + \left(\frac{k-1}{2}\right) \cdot (Ma^{in})^2}{1 + \left(\frac{k-1}{2}\right) \cdot (Ma)^2} \right\} \quad (3.1b)$$

$$\frac{P}{P^{in}} = \left\{ \frac{1 + \left(\frac{k-1}{2}\right) \cdot (Ma^{in})^2}{1 + \left(\frac{k-1}{2}\right) \cdot (Ma)^2} \right\}^{\frac{k}{k-1}} \quad (3.1c)$$

$$\frac{A^{Throat}}{A^{in}} = Ma^{in} \left\{ \frac{1 + \left(\frac{k-1}{2}\right)}{1 + \left(\frac{k-1}{2}\right) \cdot (Ma^{in})^2} \right\}^{\frac{k+1}{2(k-1)}} \quad (3.1d)$$

### 3.3. Methods

New PPU's SS-TSA and SS-TSA-HI prescribe SS to abate  $\approx 98.5\%$  of the dehydration load of raw air, reducing TSA service to less than  $500 \text{ ppm}$  of contaminants, where  $\approx 370 \text{ ppmCO}_2$  is the main load. Thus, SS becomes the main PPU step complemented by a finishing TSA step executed by a MS bed – 13X zeolite MS – hereinafter called MS-TSA, whose service is  $\approx 15\%$  greater than the MS service in conventional FULL-TSA PPU. MS-TSA differs considerably from the big TSA unit of FULL-TSA PPU of same capacity, because: (i) heat consumption for bed regeneration is significantly reduced owing to smaller adsorbate purge; (ii) adsorbent inventory is reduced and/or TSA cycle-time is extended for the same reason, allowing less MS vessels and lower adsorbent thermo-mechanical stress, lowering fragmentation and replacement costs; (iii) temperature of  $1 \text{ atm}$  nitrogen for bed regeneration is lowered to  $80^\circ\text{C}$  due to weak  $\text{CO}_2$ -MS interaction, lower  $\text{H}_2\text{O}$  content and weaker  $\text{H}_2\text{O}$ -MS interaction relatively to  $\text{H}_2\text{O}$ -AA interaction.

FULL-TSA, SS-TSA and SS-TSA-HI were simulated in HYSYS 8.8 for mass and energy balances. Simulation results were used in equipment sizing and costing via Turton et al. [30] method for economic analysis. Fig. 3.2a presents a methodology overview, while Fig. 3.2b details the determination of equipment design and utilities consumption.

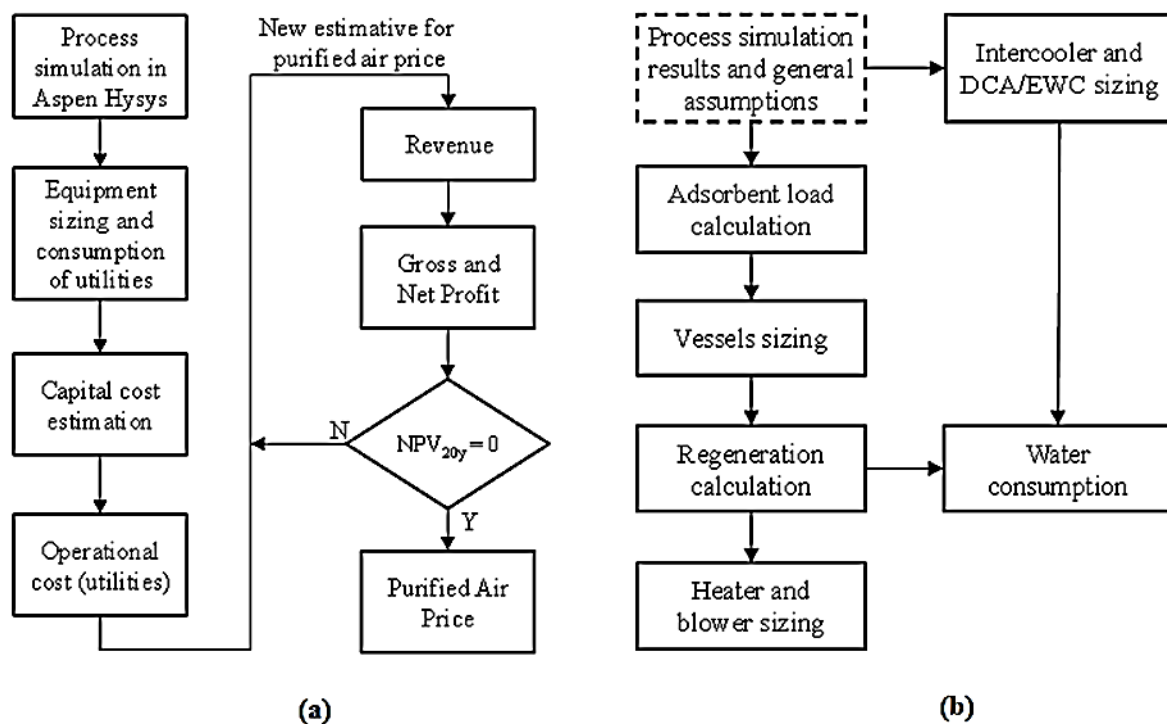


**Fig. 3.2.** Methods: (a) overview; (b) equipment sizing and utility consumption.

### 3.3.1. PPU Simulation

Block diagrams of conventional PPU FULL-TSA and alternative SS-TSA and SS-TSA-HI are respectively depicted in Figs. 3.3, 3.4 and 3.5. All flowsheets initiate at the two-stage main air compressor (MAC), whose hot effluent air (stream #2) at  $3.18 \text{ bar}$  (FULL-TSA) or  $3.292 \text{ bar}$  (SS-TSA and SS-TSA-HI) feeds the direct contact aftercooler (DCA), where bottom hot air firstly contacts cooling water (CW) at  $30^\circ\text{C}$ , then enters the upper DCA section to contact chilled-water (ChW) at  $\approx 9^\circ\text{C}$  produced in the evaporative water cooler (EWC) via evaporative direct contact of CW with dry nitrogen at  $\approx 14^\circ\text{C}$  (FULL-TSA) or  $12^\circ\text{C}$  (SS-TSA and SS-TSA-HI) from Cold-Box. The water-saturated nitrogen from EWC (stream #6) is liberated in the atmosphere at  $\approx 27^\circ\text{C}$ . In all diagrams water-saturated ( $100\% \text{ RH}$ ) cold air (stream #3) leaves the DCA at  $10^\circ\text{C}$ . From this point onwards, differences among FULL-TSA, SS-TSA and SS-TSA-HI become significant. In FULL-TSA (Fig. 3.3) stream #3 ( $T=10^\circ\text{C}$ ,  $P=3.12 \text{ bar}$ ) feeds a bulky TSA unit with an AA bed for water removal and a MS bed (13X zeolite) for  $\text{CO}_2/\text{HCs}$  removal. Beds are regenerated with  $1 \text{ atm}$  dry  $\text{N}_2$  from Cold-Box heated up to  $133^\circ\text{C}$  (stream #9) with LP steam. Purified air stream #7 from TSA ( $T\approx 17^\circ\text{C}$ ,  $P=3.1 \text{ bar}$ ) feeds the Cold-Box exchanger to heat dry  $\text{N}_2$  from Cold-Box to  $\approx 14^\circ\text{C}$ .

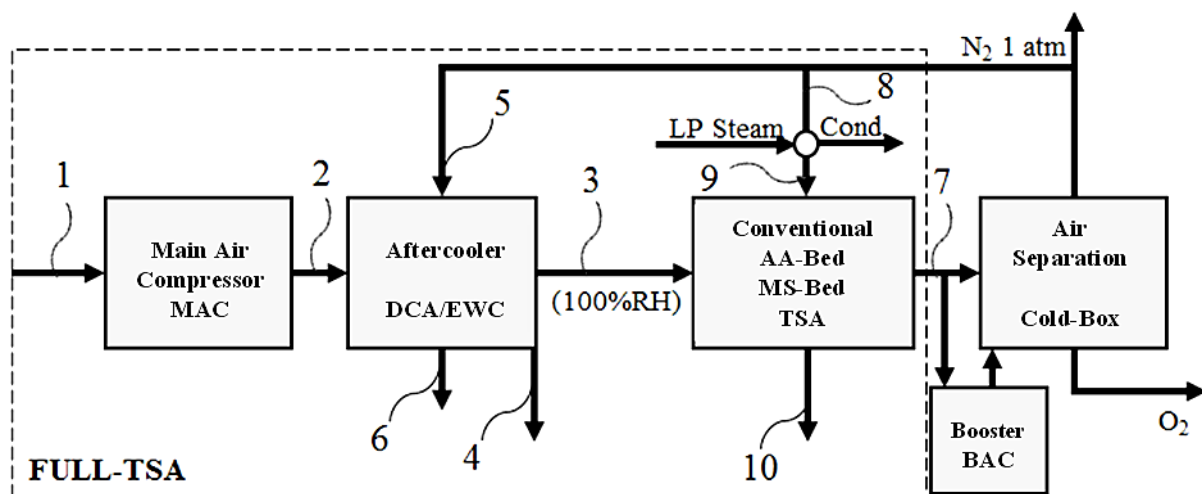


**Fig. 3.3.** Conventional FULL-TSA PPU for purified air supply to Cold-Box.

In SS-TSA and SS-TSA-HI stream #3 ( $T=10^\circ\text{C}$ ,  $P=3.25 \text{ bar}$ ) feeds a SS designed to capture  $\approx 98.5\%$  of the water of stream #3 with  $\approx 96.5\%$  of pressure recovery. The slight higher pressure of stream #3 (relatively to FULL-TSA) accounts for the SS head-loss of  $\approx 3.5\%$ . The SS effluent air stream #11 ( $T\approx 15^\circ\text{C}$ ,  $P=3.12 \text{ bar}$ ) with only  $\approx 1.5\%$  of its initial humidity feeds MS-TSA with a MS bed (13X zeolite) for finishing water removal besides  $\text{CO}_2$  and HCs removal. The other SS effluent is stream #12 super-cooled liquid water ( $T\approx 48^\circ\text{C}$ ,

$P=3.12 \text{ bar}$ ) which is recycled to ChW pool lowering CW make-up and EWC demand of cold  $N_2$  from Cold-Box. MS beds of SS-TSA and SS-TSA-HI are regenerated with  $1 \text{ atm}$  dry  $N_2$  from Cold-Box heated up to  $80^\circ\text{C}$  with LP steam in SS-TSA and with warm water (WW) at  $90^\circ\text{C}$  in SS-TSA-HI (stream #13), where WW is generated via heat recovery from hot MAC air. Purified air (stream #7) leaves MS-TSA at  $\approx 15^\circ\text{C}$  and  $3.1 \text{ bar}$  thanks to lower adsorption load with SS. Stream #7 feeds the Cold-Box leading its dry  $N_2$  outlet to  $12^\circ\text{C}$  ( $2^\circ\text{C}$  less than in FULL-TSA).

Simulation flowsheets of FULL-TSA, SS-TSA and SS-TSA-HI PPUs are respectively shown in Figs. 3.6a, 3.6b and 3.6c where TSA vessels on-adsorption and on-regeneration are represented as “TSA/OP” and “TSA/REG” respectively.

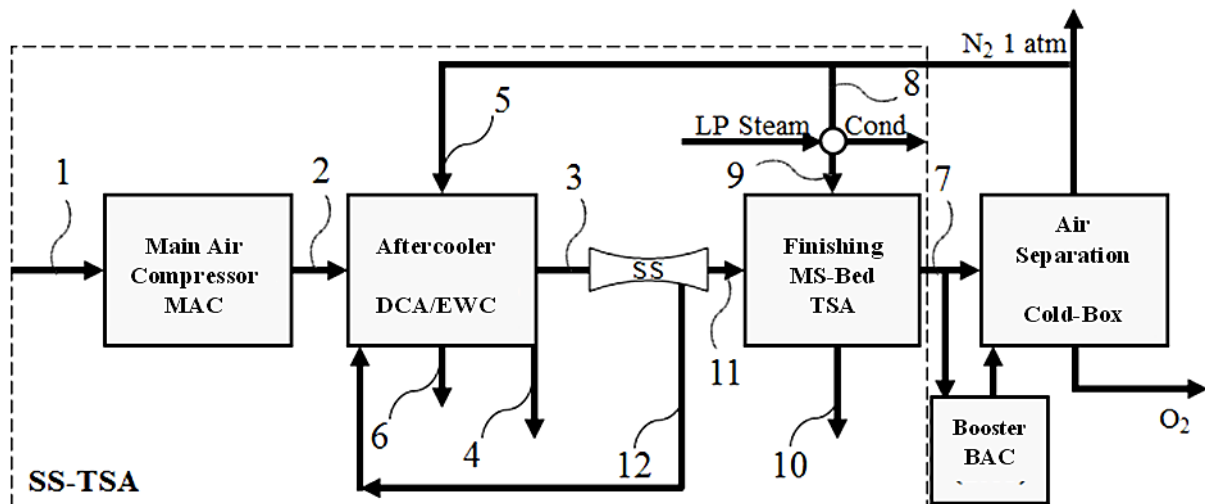


Fig. 3.4. SS-TSA PPU for purified air supply to Cold-Box.

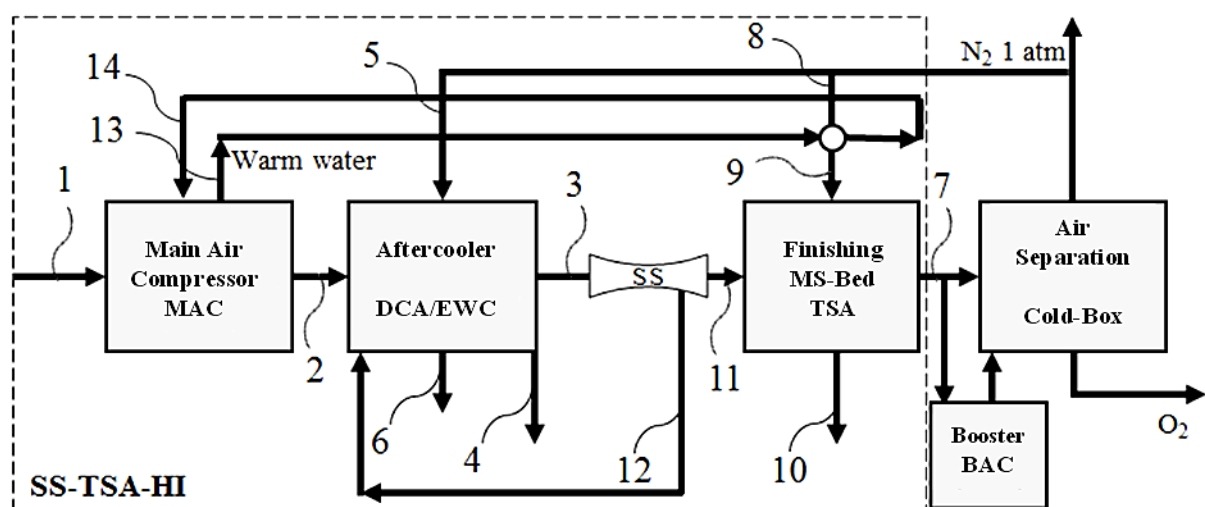
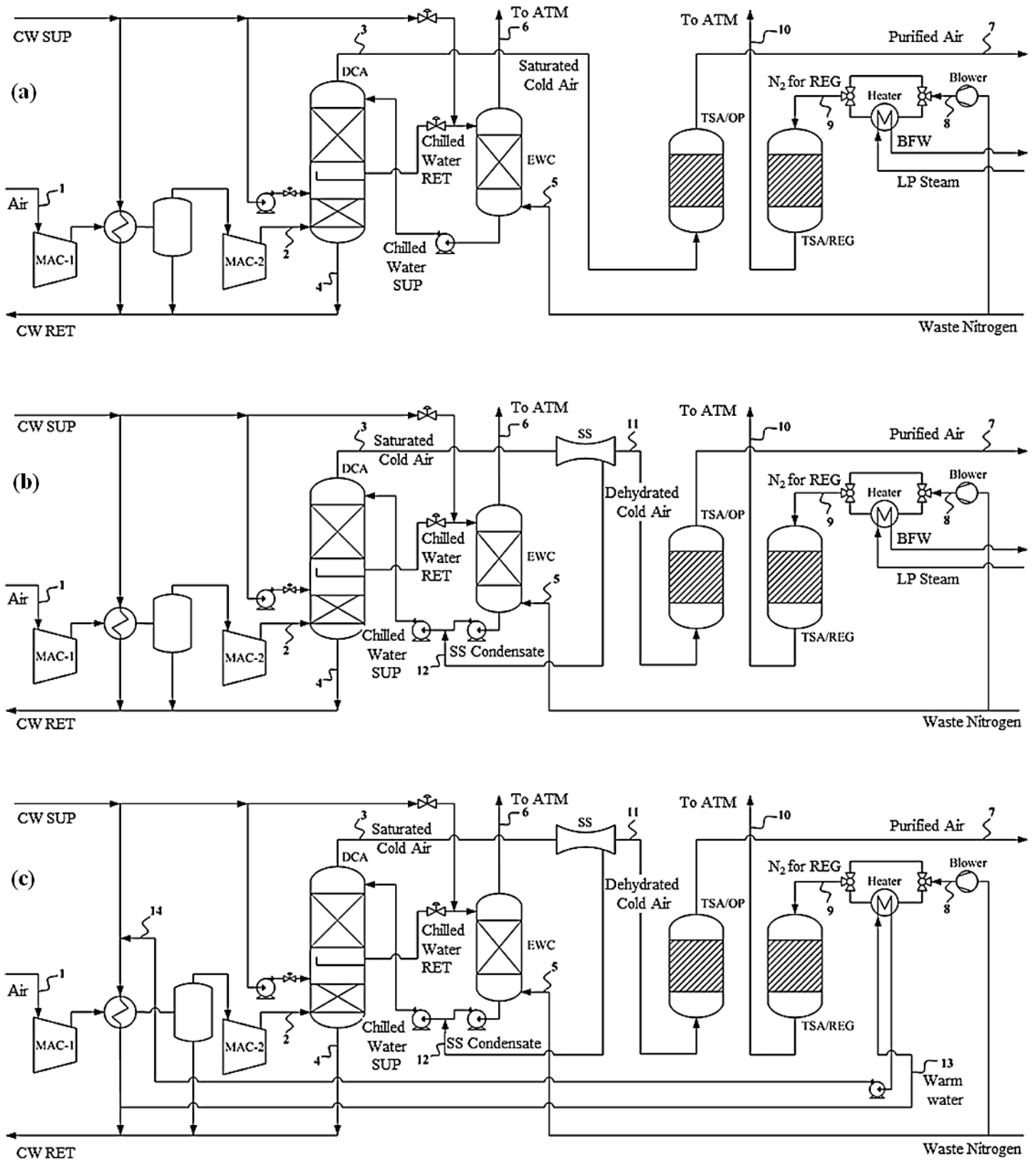


Fig. 3.5. SS-TSA-HI PPU for purified air supply to Cold-Box adopting compression heat recovery.



**Fig. 3.6.** PPU Simulation flowsheets: (a) conventional FULL-TSA; (b) SS-TSA; (c) SS-TSA-HI (REG=Regeneration, RET=Return, SUP=Supply).

### 3.3.1.1. Simulation Assumptions

HYSYS 8.8 simulation of FULL-TSA, SS-TSA and SS-TSA-HI adopted the following assumptions. {S1} Simulation of SS unit in SS-TSA and SS-TSA-HI: Using SS-UOE [19] with phase-equilibrium sound speed from PEC-UOE [20]. {S2} Thermodynamic modeling: Peng-Robinson Equation-of-State (PR-EOS). {S3} Raw air:  $13580 \text{ kmol/h}$ ,  $25^\circ\text{C}$ ,  $1.013 \text{ bar}$ ,  $60\% \text{ RH}$ , composition (molar basis)  $N_2=76.61\%$ ,  $O_2=20.55\%$ ,  $Ar=0.91\%$ ,  $H_2O=1.89\%$ ,  $363 \text{ ppmCO}_2$  (neglecting species  $\leq 10 \text{ ppm}$ ). {S4} Air filters: MAC suction and TSA outlet, each with  $\Delta P=1 \text{ kPa}$ . {S5} Cold-Box air feed:  $3.10 \text{ bar}$  complying with triple-column ASU [31]. {S6} Intercoolers:  $40^\circ\text{C}$  outlet air,  $\Delta P=10 \text{ kPa}$ . {S7} DCA: bottom structured-packing with  $03$  theoretical stages,  $\Delta P=2 \text{ kPa}$ , CW fed at the top; top structured-packing with  $10$  theoretical stages,  $\Delta P=4 \text{ kPa}$ , ChW fed at the top, exiting air at  $10^\circ\text{C}$ . {S8} CW:  $30^\circ\text{C}$  at cooling-tower outlet. {S9} LP steam: saturated,  $4 \text{ bar}$ . {S10} Machine adiabatic efficiencies: MAC  $85\%$ ; nitrogen blower  $75\%$ . {S11} Heat transfer coefficients:  $170 \text{ W/m}^2\text{K}$  for air intercoolers and nitrogen heater. {S12} SS in SS-TSA and SS-TSA-HI: single SS,  $T^{\text{Inlet}}=10^\circ\text{C}$ ,  $P^{\text{Inlet}}=3.25 \text{ bar}$ ,  $D_I=0.87 \text{ m}$ ,  $D_O=0.69 \text{ m}$ ,  $\alpha=12.67^\circ$ ,  $\beta=2.66^\circ$ ,  $\eta^{\text{EXP}}=\eta^{\text{CMP}}=100\%$ ,  $Ma^{\text{Shock}}=1.2$ . {S13} MS-TSA in SS-TSA and SS-TSA-HI:  $03$  vertical vessels (two adsorbing, one desorbing) with  $13\text{X}$  zeolite MS,  $\frac{1}{4}''$  particles, axial reversible flow,  $12\text{h}$  cycle-time,  $4\text{h}$  regeneration-time,  $\Delta P=1 \text{ kPa}$ . {S14} TSA unit in FULL-TSA:  $08$  vertical vessels (four adsorbing, four desorbing) with AA and  $13\text{X}$  zeolite MS beds,  $\frac{1}{4}''$  particles, axial reversible flow,  $8\text{h}$  cycle-time,  $4\text{h}$  regeneration-time,  $\Delta P=1 \text{ kPa}$ . {S15} Bed saturation:  $95\%$  of capacity. {S16} Bed capacity: via loading versus partial pressure experimental isotherms [12] corrected to  $15^\circ\text{C}$ , the design adsorption temperature. {S17} AA and MS inventories in FULL-TSA: sized respectively from water and  $\text{CO}_2$  loadings and Table 3.1. {S18} MS inventory in SS-TSA and SS-TSA-HI: sized from  $\text{CO}_2$  and residual water loadings and Table 3.1. {S19} Adsorbent lifespan:  $20 \text{ years}$  for  $13\text{X}$  zeolite MS in SS-TSA and SS-TSA-HI, against  $5 \text{ years}$  of AA and  $15 \text{ years}$  of MS in FULL-TSA [6] due to larger SS-TSA cycle-time with less adsorbent thermo-mechanical stress and fragmentation. {S20} Equipment design equations: from [32]. {S21} Regeneration heat load: from [6]. {S22} WW temperature in SS-TSA-HI:  $90^\circ\text{C}$ .

**Table 3.1.** Adsorbent data for TSA design.

<i>PPU</i>	<i>Adsorbent</i>	<i>Adsorbate</i>	<i>Bulk Density</i> ( <i>kg/m<sup>3</sup></i> )	<i>Cost</i> ( <i>USD/kg</i> )	<i>Specific Heat</i> ( <i>kJ / kg.K</i> )	<i>Lifetime</i> ( <i>years</i> )	<i>Adsorption Heat<sup>e</sup></i> ( <i>kcal/mol</i> )	<i>Capacity<sup>f</sup></i> ( <i>g/kg</i> )
<i>FULL-TSA</i>	<i>AA</i>	<i>H<sub>2</sub>O</i>	769 <sup>a</sup>	1.32 <sup>a</sup>	1.00 <sup>c</sup>	5 <sup>d</sup>	11.6 ( <i>H<sub>2</sub>O</i> )	64
	<i>13X zeolite MS</i>	<i>CO<sub>2</sub></i>	640 <sup>b</sup>	1.5 <sup>b</sup>	0.92 <sup>c</sup>	15 <sup>d</sup>	8.2 ( <i>CO<sub>2</sub></i> )	51
<i>SS-TSA</i>	<i>13X zeolite MS</i>	<i>H<sub>2</sub>O</i>	640 <sup>b</sup>	1.5 <sup>b</sup>	0.92 <sup>c</sup>	20	12.3 ( <i>H<sub>2</sub>O</i> )	83
<i>SS-TSA-HI</i>		<i>CO<sub>2</sub></i>					8.2 ( <i>CO<sub>2</sub></i> )	51

<sup>a</sup> BASF, BASF F-200 Activated alumina for liquid and gas drying, 2009; <sup>b</sup> Alibaba, Jiuzhou 13X molecular sieve: purification of air and nitrogen, 2017; <sup>c</sup> Hahne, E. "Heat storage media". In: Ullmann's Encyclopedia of Industrial Chemistry, 2005; <sup>d</sup> Kerry [6]; <sup>e</sup> Rege et al. [12]; <sup>f</sup>  $T_{ADS}=15^{\circ}C$  (Design T)

### 3.3.1.2. Economic Analysis Assumptions

The following parameters were assumed. {E1} Operational year: 8000 h. {E2} Horizon: 30 years. {E3} Fixed Capital Investment (*FCI*, USD) of installed equipment: from [30]. {E4} Scale-up exponent: 0.6 [30]. {E5} Chemical Engineering Plant Cost Index: 550.3 (Sept-2015) from Chemical Engineering Magazine Nov-2016. {E6} PPU construction: one year. {E7} Annual interest rate: 10%. {E8} Income tax rate: 34%. {E9} Depreciation rate: 10%. {E10} SS *FCI* (USD): extrapolated from SS processing 6  $MMSm^3/d$  of NG [22] including pressure deflation to low-pressure air operation at 3.25 bar. {E11} Adsorbent costs: Table 3.1. {E12} Electricity, LP steam and CW make-up costs: 71 USD/MWh, 26.85 USD/MWh and 0.793 USD/m<sup>3</sup>. {E13} Cost of Utilities (*CUT*, MMUSD/y): sum of electricity, LP steam and CW make-up annual costs; {E14} Revenues (*REV*, MMUSD/y): purified pressurized air to Cold-Box with unitary breakeven price for 20 years operation. {E15} Cost of Manufacturing (*COM*, MMUSD/y): *CUT* added to annual bed replacement costs.

## 3.4. Results and Discussion

There are three categories of results: (i) technical comparisons of processes; (ii) operational aspects of SS for air dehydration; and (iii) economic comparison of processes. The following sub-sections approach them.

### 3.4.1. Technical Comparison of FULL-TSA, SS-TSA and SS-TSA-HI

Utility consumptions of PPU are shown in Table 3.2. Table 3.3 shows design and operational conditions of SS for SS-TSA and SS-TSA-HI. Table 3.4 details process streams of all PPU according to Figs. 3.3 to 3.6. In SS-TSA and SS-TSA-HI SS is fed with 10°C water saturated (3886 ppmH<sub>2</sub>O) pressurized air (stream #3) for dehydration. Air leaves SS with 56.4 ppmH<sub>2</sub>O in stream #11, which feeds MS-TSA for finishing water removal and CO<sub>2</sub> removal. MS-TSA of SS-TSA and SS-TSA-HI remove the same CO<sub>2</sub> load as conventional FULL-TSA, since SS recovery of CO<sub>2</sub> is negligible at these conditions; but, thanks to SS, instead of water, CO<sub>2</sub>

becomes the biggest MS-TSA service (Fig. 3.7), also highlighting MS-TSA with much less loading than FULL-TSA. Therefore, with molar loading reduced by a factor of 8-10, MS-TSA is substantially less energy and capital intensive than TSA of FULL-TSA.

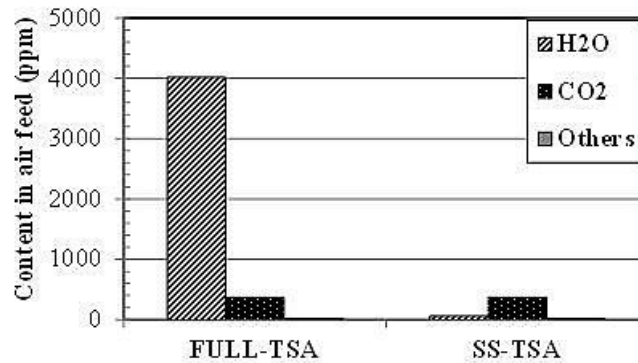


**Fig. 3.7.** Adsorption services of FULL-TSA and SS-TSA.

In Table 3.2 utility consumptions of SS-TSA comprise 15,315 kW of electricity (15,248 kW in MAC and 68 kW in N<sub>2</sub> blower), 161 kW of LP steam and ≈5.37 kg/s of CW make-up. Compared to FULL-TSA, SS-TSA consumes ≈88.3% less LP steam, ≈3.1% less CW make-up, despite ≈2.2% higher electricity consumption, a consequence of ≈3.5% SS head-loss. SS-TSA-HI, besides no consumption of steam, exhibits the lowest CW make-up of ≈5.29 kg/s and the lowest heat duty in CW tower, thanks to lowest CW tower circulation due to moving compression heat via WW for MS-TSA regeneration. The lower CW make-ups of SS-TSA and SS-TSA-HI are consequence of recycling SS super-cooled water to ChW pool; i.e., the combined actions of DCA and SS retain more than 98.5% of air humidity as liquid water, while in FULL-TSA the entire water in DCA effluent air was lost in the atmosphere during TSA regeneration. The proof is in Table 3.4: 4019 ppmH<sub>2</sub>O were lost in FULL-TSA (stream #3), whereas SS-TSA and SS-TSA-HI discarded only 56.4 ppmH<sub>2</sub>O (stream #11). Table 3.3 reports 96.54% of SS pressure recovery ( $\Delta P=0.11$  bar), an excellent value that was decisive to make SS-TSA and SS-TSA-HI more profitable than FULL-TSA with its TSA-based dehydration. The underlying fact is SS specification  $Ma^{Shock}=1.2$ , inferior to usual  $Ma^{Shock} \cong 1.5$  for treating raw NG with SS. Another difference to raw NG, is the huge inlet diameter of this air SS (34.2") relatively to typical NG SS's (≈6") for similar molar flow rates, consequence of the low-pressure PPU scenario vis-à-vis typical high-pressure NG applications. In SS-TSA and SS-TSA-HI, thanks to low SS head-loss, only a small increase in MAC power is noticed in Table 3.2 (+≈0.46 MW), partially offset by a small decrease of N<sub>2</sub> blower power (-0.12 MW), also consequence of lower N<sub>2</sub> flow rate to regenerate MS bed of SS-TSA and SS-TSA-HI.

**Table 3.2.** PPU utility consumption.

<i>Item</i>	<i>FULL-TSA</i>	<i>SS-TSA</i>	<i>SS-TSA-HI</i>
Power MAC (MW)	14.79	15.25	15.25
Power N <sub>2</sub> Blower (MW)	0.188	0.068	0.068
LP Steam N <sub>2</sub> Heater (MW)	1.370	0.161	---
CW Make-up (kg/s)	5.536	5.366	5.295

**Table 3.3.** SS design and conditions in SS-TSA and SS-TSA-HI.

<i>Specified Items</i>		<i>Calculated by SS-UOE</i>	
<i>No. of SS's</i>	1	$D_T(m)$	0.4198
$D_I(m)$	0.8679	$L_C(m)$	0.9965
$D_O(m)$	0.6943	$L_D(m)$	2.955
$\alpha$	12.67°	$L(m)$	3.952
$\beta$	2.66°	$L^{Shock}(m)$	1.067
$Ma^{Shock}$	1.20	$L^{Diff}(m)$	2.885
$\eta^{EXP}\%$	100	$P_{BS}(bar)$	1.342
$\eta^{CMP}\%$	100	$T_{BS}(^{\circ}C)$	-48.21
$P^{Inlet}(bar)$	3.23	$Ma_{BS}$	1.195
$T^{Inlet}(^{\circ}C)$	10.0	$P^{Outlet}(bar)$	3.12
$MMSm^3/d$	7.72	$T^{Outlet}(^{\circ}C)$	14.56
$ppmH_2O^{Inlet}$	3881	$REC\%H_2O$	98.56%
$ppmCO_2^{Inlet}$	366	$\%P Recovery$	96.54%

\* After condensate withdrawal

Additionally, SS-TSA and SS-TSA-HI minimize *FCI* of TSA step and maximize TSA cycle-time, allowing extended adsorption time and milder desorption temperatures (80°C), entailing less thermo-mechanical stress, extending adsorbent lifetime and reducing bed replacement costs. As shown in Table 3.4, the flow rate of regeneration nitrogen is reduced in SS-TSA and SS-TSA-HI, thanks to lower regeneration duty, allowing availability of 1980 kmol/h of decontaminated dry nitrogen as sale gas or refrigeration utility. Alternatively, EWC can be designed with higher capacity allowing exportation of ≈9°C ChW. Furthermore, dry N<sub>2</sub> from Cold-Box is ≈2°C colder in SS-TSA and SS-TSA-HI, improving cooling capacity, a consequence of TSA increase of air temperature in FULL-TSA of 7°C, while in SS-TSA and SS-TSA-HI only 0.5°C of increase occurred in MS-TSA due to lower loading.

**Table 3.4.** Main streams of FULL-TSA, SS-TSA and SS-TSA-HI PPU (stream numbers as in Figs. 3.3 to 3.6).

<i>Stream #</i>	<i>1</i>			<i>2</i>			<i>3</i>			<i>4</i>			<i>5</i>		
<i>PPU</i>	<i>FULL TSA</i>	<i>SS TSA</i>	<i>SS TSA HI</i>	<i>FULL TSA</i>	<i>SS TSA</i>	<i>SS TSA HI</i>	<i>FULL TSA</i>	<i>SS TSA</i>	<i>SS TSA HI</i>	<i>FULL TSA</i>	<i>SS TSA</i>	<i>SS TSA HI</i>	<i>FULL TSA</i>	<i>SS TSA</i>	<i>SS TSA HI</i>
<i>T (°C)</i>	25.0	25.0	25.0	98.4	101.3	101.3	10.0	10.0	10.0	36.0	36.3	36.3	14.1	12.0	12.0
<i>P (bar)</i>	1.013	1.013	1.013	3.180	3.292	3.292	3.120	3.232	3.232	3.180	3.292	3.292	1.053	1.053	1.053
<i>F (kmol/h)</i>	13,584	13,584	13,584	13,584	13,584	13,584	13,379	13,377	13,377	65,071	65,077	65,077	7315	6621	6621
<i>%mol N<sub>2</sub></i>	76.61	76.61	76.61	76.61	76.61	76.61	77.77	77.78	77.78	-	-	-	99.04	99.04	99.04
<i>%mol O<sub>2</sub></i>	20.55	20.55	20.55	20.55	20.55	20.55	20.87	20.87	20.87	-	-	-	0.61	0.61	0.61
<i>%mol Ar</i>	0.91	0.91	0.91	0.91	0.91	0.91	0.93	0.93	0.93	-	-	-	0.35	0.35	0.35
<i>ppmCO<sub>2</sub></i>	363	363	363	363	363	363	366	366	366	-	-	-	-	-	-
<i>ppmH<sub>2</sub>O</i>	18,892	18,892	18,892	18,892	18,892	18,892	4019	3886	3886	100%	100%	100%	-	-	-
<i>Stream #</i>	<i>6</i>			<i>7</i>			<i>8</i>			<i>9a (heating phase)</i>			<i>9b (cooling phase)</i>		
<i>PPU</i>	<i>FULL TSA</i>	<i>SS TSA</i>	<i>SS TSA HI</i>	<i>FULL TSA</i>	<i>SS TSA</i>	<i>SS TSA HI</i>	<i>FULL TSA</i>	<i>SS TSA</i>	<i>SS TSA HI</i>	<i>FULL TSA</i>	<i>SS TSA</i>	<i>SS TSA HI</i>	<i>FULL TSA</i>	<i>SS TSA</i>	<i>SS TSA HI</i>
<i>T (°C)</i>	27.2	26.8	26.8	17.2	15.1	15.1	14.1	12.0	12.0	133	80.0	80.0	14.1	12.0	12.0
<i>P (bar)</i>	1.013	1.013	1.013	3.100	3.100	3.100	1.053	1.053	1.053	1.023	1.023	1.023	1.053	1.053	1.053
<i>F (kmol/h)</i>	6470	6796	6796	13,320	13,320	13,320	3084	1108	1108	3084	1108	1108	3084	1108	1108
<i>%mol N<sub>2</sub></i>	95.52	95.60	95.60	78.12	78.12	78.12	99.04	99.04	99.04	99.04	99.04	99.04	99.04	99.04	99.04
<i>%mol O<sub>2</sub></i>	0.59	0.59	0.59	20.95	20.95	20.95	0.61	0.61	0.61	0.61	0.61	0.61	0.61	0.61	0.61
<i>%mol Ar</i>	0.34	0.34	0.34	0.93	0.93	0.93	0.35	0.35	0.35	0.35	0.35	0.35	0.35	0.35	0.35
<i>ppmCO<sub>2</sub></i>	-	-	-	-	-	-	-	-	-	-	-	-	-	-	-
<i>ppmH<sub>2</sub>O</i>	35,506	34,694	34,694	-	-	-	-	-	-	-	-	-	-	-	-
<i>Stream #</i>	<i>10 (cooling phase)</i>			<i>11</i>			<i>12</i>			<i>13</i>			<i>14</i>		
<i>PPU</i>	<i>FULL TSA</i>	<i>SS TSA</i>	<i>SS TSA HI</i>	<i>FULL TSA</i>	<i>SS TSA</i>	<i>SS TSA HI</i>	<i>FULL TSA</i>	<i>SS TSA</i>	<i>SS TSA HI</i>	<i>FULL TSA</i>	<i>SS TSA</i>	<i>SS TSA HI</i>	<i>FULL TSA</i>	<i>SS TSA</i>	<i>SS TSA HI</i>
<i>T (°C)</i>	-	-	-	-	14.6	14.6	-	-48.2	-48.2	-	-	90.0	-	-	30.0
<i>P (bar)</i>	1.013	1.013	1.013	-	3.120	3.120	-	3.120	3.120	-	-	3.00	-	-	2.50
<i>F (kmol/h)</i>	3084	1108	1108	-	13,326	13,326	-	51.2	51.2	-	-	494	-	-	494
<i>%mol N<sub>2</sub></i>	99.04	99.04	99.04	-	78.07	78.07	-	-	-	-	-	-	-	-	-
<i>%mol O<sub>2</sub></i>	0.61	0.61	0.61	-	20.95	20.95	-	-	-	-	-	-	-	-	-
<i>%mol Ar</i>	0.35	0.35	0.35	-	0.93	0.93	-	-	-	-	-	-	-	-	-
<i>ppmCO<sub>2</sub></i>	-	-	-	-	368	368	-	-	-	-	-	-	-	-	-
<i>ppmH<sub>2</sub>O</i>	-	-	-	-	56.4	56.4	-	100%	100%	--	-	100%	-	-	100%

### 3.4.2. SS Operational Aspects in SS-TSA and SS-TSA-HI

The SS unit in SS-TSA and SS-TSA-HI accomplishes air dehydration with a single “big mouth” SS (Table 3.3) with length  $L=3.952\text{ m}$ , inlet diameter  $D_I=87\text{ cm}$ , throat diameter  $D_T=41.98\text{ cm}$  at axial position  $L_C=0.9965\text{ m}$ ,  $Ma^{Shock}=1.2$  at axial position  $L^{Shock}=1.067\text{ m}$ , and  $Ma$  after condensate withdrawal and before normal shock of  $Ma_{BS}=1.1952$ . SS recovers 96.54% of pressure and captures 98.56% of water as super-cooled liquid at  $T_{BS}=-48.21^\circ\text{C}$ .

SS operation is explained via Figs. 3.8a to 3.8f portraying several conspicuous “SS signatures” – Eqs. (3.2a) and (3.2b) – which are rigorous graphical features of SS profiles at sonic throat discussed in Appendix V2. SS signatures were proved elsewhere [20] for SS nozzles with  $(dA/dx)^{Throat} \neq 0$  (Fig. 3.1), where  $x$ ,  $A$ ,  $v$ ,  $c$ ,  $\psi$  respectively represent SS axial position, flow section area, flow velocity, multiphase sound speed and molar vapor fraction. SS signatures occur at sonic throats with  $(dA/dx)^{Throat} \neq 0$  independently if the flow is single-phase or multiphase, non-reactive or multi-reactive [20], but the  $dc/dx$  singularity changes sign whether flow is gas-dominated – Eq. (3.2a),  $\psi \approx 1$  – or liquid-dominated – Eq. (3.2b),  $\psi < \approx 0.5$  (Appendix V2).

$$\frac{dT}{dx} = -\infty, \quad \frac{dP}{dx} = -\infty, \quad \frac{dv}{dx} = +\infty, \quad \frac{dc}{dx} = -\infty, \quad \frac{dMa}{dx} = +\infty \quad (Ma^{Throat} \rightarrow I^-, \psi \approx 1) \quad (3.2a)$$

$$\frac{dT}{dx} = -\infty, \quad \frac{dP}{dx} = -\infty, \quad \frac{dv}{dx} = +\infty, \quad \frac{dc}{dx} = +\infty, \quad \frac{dMa}{dx} = +\infty \quad (Ma^{Throat} \rightarrow I^-, \psi < \approx 0.5) \quad (3.2b)$$

Fig. 3.8a depicts SS axial profiles of diameter and molar vapor fraction ( $\psi$ ) showing inlet air 100% vapor ( $\psi=1$ ) at  $T=10^\circ\text{C}$  and  $P=3.23\text{ bar}$ , while at pre-shock ( $x=L^{Shock}=1.067\text{ m}$ ,  $Ma=Ma^{Shock}=1.2$ )  $\approx 3800\text{ ppmH}_2\text{O}$  condenses giving  $\psi=99.62\%$ . Condensed water is removed at  $x=L^{Shock}$ , with  $\psi$  increasing back to  $\psi=1$ , simultaneously reducing  $Ma$  of dry air at constant  $T$  and  $P$  to  $Ma_{BS}=1.195$ . At this point, normal shock occurs, turning the air flow back to subsonic at higher  $T$  and  $P$ . From this point on, dry air (100% vapor,  $\psi=1$ ) flows subsonically through the diffuser, decelerating and recovering  $T$  and  $P$ .

Fig. 3.8b presents  $P$  and  $Ma$  axial profiles with perfect SS signatures  $dP/dx=-\infty$ ,  $dMa/dx=+\infty$  at the throat ( $Ma \rightarrow I^-$ ), showing minimum SS pressure  $P_{BS}=1.34\text{ bar}$  at pre-shock where  $Ma=Ma^{Shock}=1.2$  and reporting outlet pressure  $P^{Outlet}=3.12\text{ bar}$ . Condensate removal does not

affect  $T$  and  $P$ , but promotes a small  $Ma$  drop from  $Ma^{Shock}=1.2$  to  $Ma_{BS}=1.195$ , which subsequently suddenly drops vertically at normal shock to  $Ma_{AS}=0.8454$ .

Fig. 3.8c depicts  $T$  and  $c$  axial profiles, also with SS signatures of vapor-dominated flow Eq. (3.2a)  $dT/dx=-\infty$ ,  $dc/dx=-\infty$  at the throat ( $Ma \rightarrow 1^-$ ), showing minimum SS temperature of  $T=T_{BS}=-48.21^\circ C$ , where  $Ma=Ma^{Shock}=1.2$ , and reporting outlet temperature  $T^{Outlet}=14.57^\circ C$ . Besides the SS signature in Eq. (3.2a), an abrupt change of inclination is seen in  $c$  profile at  $x \cong 0.15m$  without any similar disturbances in  $T$  and  $P$  profiles. This occurred because  $c$  is a multiphase equilibrium property inversely influenced by density ( $\rho$ ) and isothermal compressibility  $\Xi_p=(\partial\rho/\partial P)_{T,Z}$  as seen in Eqs. (3.3a) and (3.3b) [20]. In Fig. 3.8c both  $\rho$  and  $\Xi_p$  suddenly increase at  $x \cong 0^+m$  – specially  $\Xi_p$  – due to appearance of micro-droplets of liquid as the WDP curve of the water saturated air feed is crossed by SS path at  $x \cong 0^+m$  (Fig. 3.8f) forcing  $c$  to fall linearly from  $340 m/s$  to  $320 m/s$  while the first 1% of water condenses (Fig. 3.8d), increasing  $\Xi_p$  as air changes from an almost ideal gas to a mist, a very different condition in terms of compressibility. This mist is established at  $x \cong 0.15m$  so that further condensation does not appreciably increase  $\Xi_p$ , with the consequence that  $c$  falls slowly from  $x \cong 0.15m$  until near the throat, where almost  $\approx 98.5\%$  of water condensed (Fig. 3.8d) and  $c$  now starts to fall rapidly due to proximity of its sonic signature Eq. (3.2a). Downstream the respective SS signatures Eq. (3.2a) at the throat,  $T$  and  $c$  profiles fall with finite rate until the pre-shock at  $x=1.067 m$ , the point of minimum  $T=T_{BS}=-48.21^\circ C$ , minimum  $P=P_{BS}=1.34 bar$  and maximum  $Ma=Ma^{Shock}=1.20$  (Fig. 3.8b). Here, water condensation is expressive, while  $CO_2$  and other air species only have trace condensations, respectively reaching (Fig. 3.8d) 98.56%, 0.0047% and 0.00005%. Water condensate is withdrawn under constant  $T$  and  $P$  causing  $Ma$  to fall to  $Ma_{BS}=1.195$  due to mist removal under constant flow section. Normal shock then theoretically occurs just after liquid withdrawn, producing sudden increase of  $T$ ,  $P$  and  $c$  accompanied by sudden decrease of  $Ma=Ma_{BS}$  to  $Ma_{AS}=0.8454$ . From this point on, the flow is sub-sonic with  $T$ ,  $P$  and  $c$  monotonously increasing (the latter because  $T$  directly influences  $c$  of gases [20]) through the SS ending diffuser, while  $Ma$  smoothly decreases as  $v$  falls under compression. Condensation profiles (Fig. 3.4d) end at  $x=1.067 m$  as condensation is only meaningful upstream the pre-shock collecting point.

$$c = \frac{1}{\sqrt{\Xi_p - (M_M T / \rho^2) \Xi_T^2 / \bar{C}_p}} \quad (3.3a)$$

$$\Xi_P \equiv \left( \frac{\partial \rho}{\partial P} \right)_{T,Z}, \quad \Xi_T \equiv \left( \frac{\partial \rho}{\partial T} \right)_{P,Z}, \quad \bar{C}_P \equiv \left( \frac{\partial \bar{H}}{\partial T} \right)_{P,Z} \quad (3.3b)$$

Fig. 3.8e depicts the influence of  $Ma^{Shock}$  on pre-shock vapor fraction ( $\psi$ ), CO<sub>2</sub> content in final air and  $Ma$  just after withdrawal  $Ma_{BS}$ . It confirms that this SS application is not capable of any significant CO<sub>2</sub> recovery even for high  $Ma^{Shock}$ . Similarly, the minimum vapor fraction at pre-shock ( $\psi=99.62\%$ ) could not be decreased appreciably by imposing higher  $Ma^{Shock}$ ; i.e. a higher  $Ma^{Shock}$  would only rise shock intensity, increasing SS head-loss without perceptible increase of air dehydration. Since water condensation cannot be appreciably increased beyond the already attained  $\approx 98.5\%$ ,  $Ma_{BS}$  responds quasi-linearly to  $Ma^{Shock}$ , being always lesser than  $Ma^{Shock}$ .

Fig. 3.8f portrays the SS path on plane  $P \times T$  also containing WDP curves of the SS air feed (stream #3, Table 3.4) for several water contents: saturated feed ( $3886 \text{ ppmH}_2\text{O}$ ), SS outlet dry air ( $56.4 \text{ ppmH}_2\text{O}$ ) and intermediate dehydration levels ( $1000 \text{ ppmH}_2\text{O}$  and  $300 \text{ ppmH}_2\text{O}$ ). Fig. 3.8f and Fig. 3.8d show that immediately after feed admission in SS, condensation starts as stream #3 is saturated, with most intense condensation (Figs. 3.8b/3.8d) near and after the throat at  $x=L_C=0.9965 \text{ m}$  associated to colder sonic and supersonic temperatures. As shown in Figs. 3.8d/3.8e there is no expressive precipitation of liquid or solid CO<sub>2</sub> as CO<sub>2</sub> partial pressure is too small in air flow. Even so, CO<sub>2</sub> freeze-out could happen if SS temperature reaches ultra-cold levels  $\approx 134^\circ\text{C}$  and extremely low-pressures in the supersonic regime, entailing anti-economic low outlet pressures and proving the inadequacy of such SS application for CO<sub>2</sub> removal. Lastly, it is didactical to observe in Fig. 3.8f the succession of classic SS thermodynamic transitions: (i) SS path traces a smooth descending expansion arc towards the lowest  $(T,P)$  on the  $56.4 \text{ ppmH}_2\text{O}$  WDP locus; (ii) at this point liquid is collected without changing  $(T,P)$ ; (iii) normal shock occurs at  $Ma_{BS}=1.195$ , depicted as a rectilinear jump back to higher after-shock  $(T,P)$  at  $T_{AS}\approx 252 \text{ K}$ ,  $P_{AS}\approx 2 \text{ bar}$  (Figs. 3.8b/3.8c); and (iv) dry air flows sub-sonically through the diffuser regaining  $(T,P)$  and losing velocity and  $Ma$  towards SS outlet at  $P^{Outlet}=3.12 \text{ bar}$ ,  $T^{Outlet}=14.56^\circ\text{C}$ .

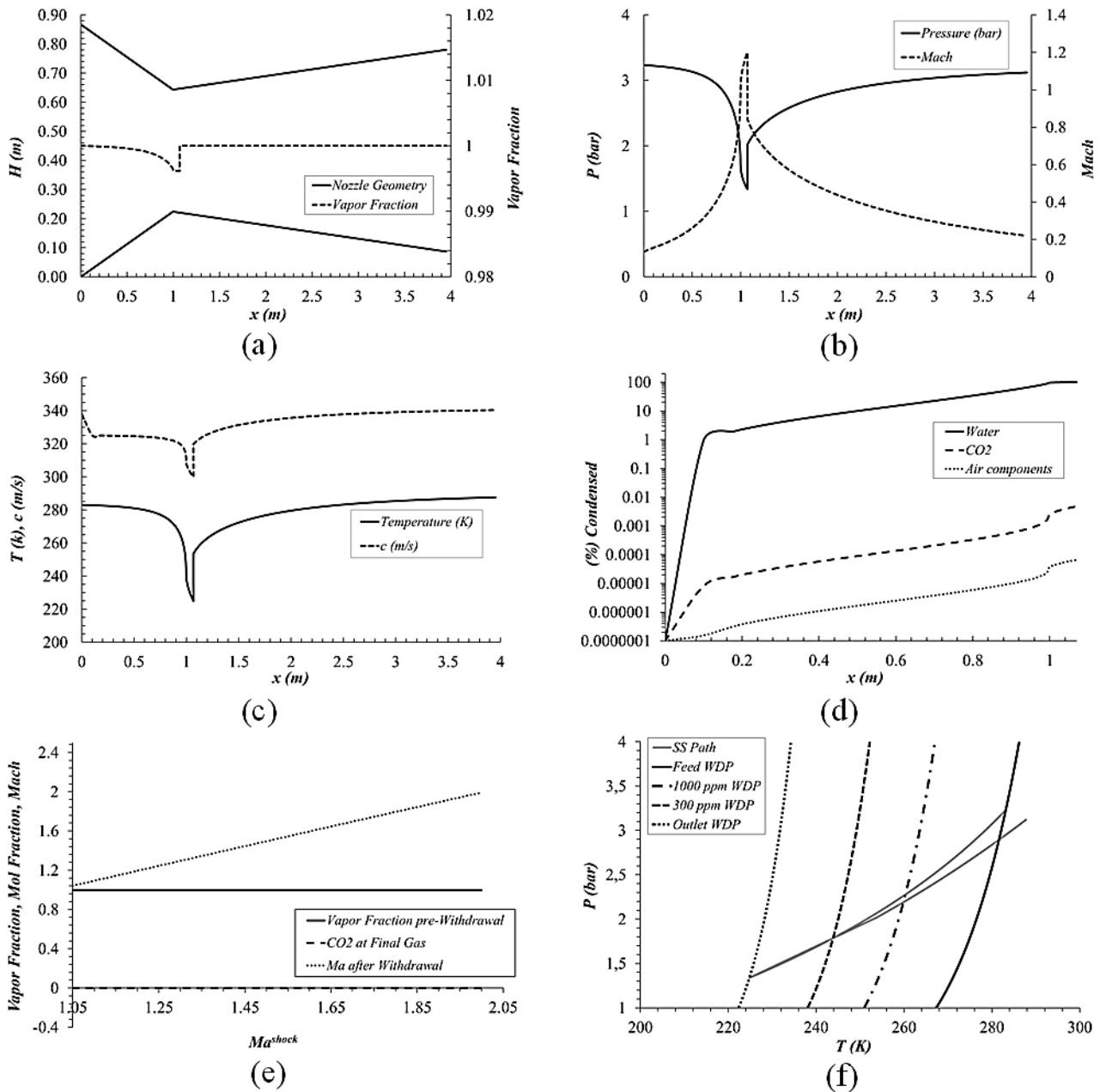


**Fig. 3.8.** SS air drying: (a) SS diameter & mol vapor fraction vs  $x(m)$ ; (b)  $P(\text{bar})$ ,  $Ma$  vs  $x(m)$ ; (c)  $T(K)$ ,  $c(m/s)$  vs  $x(m)$ ; (d) %Condensed  $H_2O$ ,  $CO_2$  & air species vs  $x(m)$ ; (e) pre-shock values (mol vapor fraction,  $CO_2$  mol fraction,  $Ma_{BS}$ ) vs  $Ma^{Shock}$ ; (f) SS path on plane  $P \times T$  and WDP loci (3886 ppm $H_2O$  fed air, 56.4 ppm $H_2O$  dry air, 300 ppm $H_2O$  air, 1000 ppm $H_2O$  air).

Fig. 3.9a and its magnification Fig. 3.9b depict SS path on  $T \times \bar{S}$  plane. As SS operates adiabatically,  $T \times \bar{S}$  diagrams can certificate 2<sup>nd</sup> Law obedience of SS simulations. SS path starts at the WDP locus of the water-saturated SS feed. It extends isentropically downwards (A→B, Figs. 3.9a/3.9b) to a point slightly beneath the WDP locus of dry air (56.4 ppm $H_2O$ ) due to vapor-liquid coexistence at  $\psi=99.62\%$ . This is the coldest SS point ( $Ma=Ma^{Shock}$ ) at pre-shock. As low-entropy condensate is withdrawn, SS path moves isothermally to the right

(B→C) towards the greater molar entropy of dry air at WDP. This dry air is still supersonic with  $Ma_{BS}=1.195$ , hence normal shock happens (C→D). Shock C→D is the only entropy creating step in SS path as expansion and after-shock compression are isentropic by Assumption {S12} (SS-UOE can have non-isentropic expansion/compression if the adiabatic efficiencies are chosen  $\eta^{EXP}\%<100\%$  and/or  $\eta^{CMP}\%<100\%$ ). As the shock is crossed, sudden heating, recompression and entropy creation take place, seen in Fig. 3.9b as an inclined linear path C→D ( $\Delta T > 0$ ,  $\Delta \bar{S} > 0$ ). The after-shock SS path moves isentropically upwards (D→E) continuously recompressing and heating dry air through the diffuser towards the SS outlet.

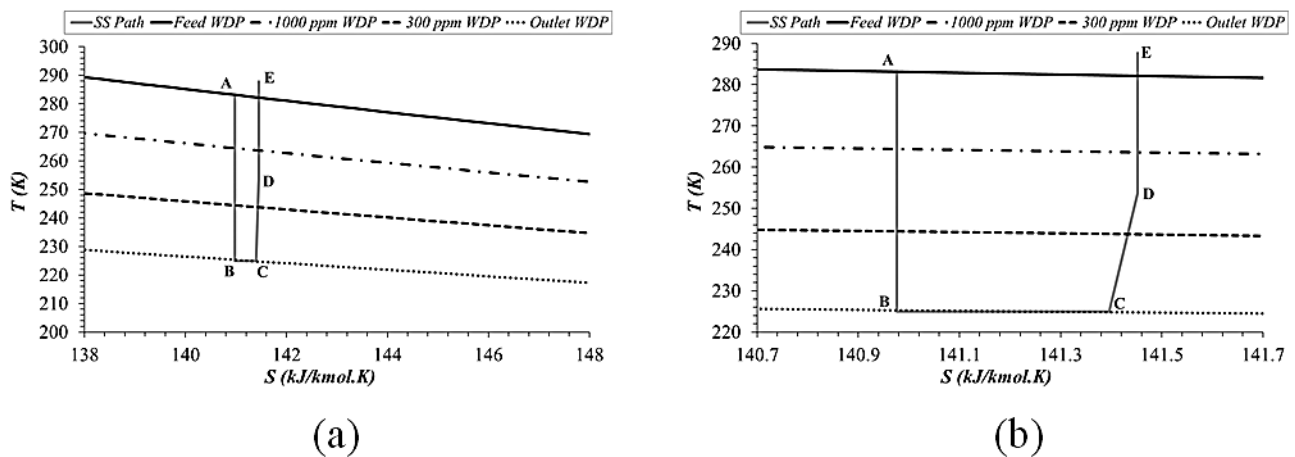


**Fig. 3.9.** SS air dehydration on plane  $T \times \bar{S}$ : (a) SS path with WDP loci of inlet 3886 ppmH<sub>2</sub>O air, 1000 ppmH<sub>2</sub>O air, 300 ppmH<sub>2</sub>O air and outlet 56.4 ppmH<sub>2</sub>O dry air; (b) magnification of (a).

### 3.4.3. Economic Comparisons

Figs. 3.10 and 3.11 respectively depict components of *COM* and *FCI* of PPU, while Table 3.5 summarizes PPU economic performances. In comparison with SS-TSA and SS-TSA-HI, the conventional FULL-TSA exhibits higher *FCI* and *COM*: 28.80 *MMUSD* and 8.97 *MMUSD/y* against 27.91 *MMUSD* and 8.86 *MMUSD/y* for SS-TSA, and 28.04 *MMUSD* and 8.82 *MMUSD/y* for SS-TSA-HI, where it is seen that MAC dominates *COM* and *FCI* in all PPU. In SS-TSA and SS-TSA-HI, despite its “big mouth” (resembling an aircraft engine) the low-pressure SS is not too expensive with *FCI* of 4.42 *MMUSD* (Fig. 3.11), contributing decisively to reduce operational costs via lower LP steam costs (-0.26 *MMUSD/y*), which offsets its slightly higher MAC electricity demand (+0.19 *MMUSD/y*). SS also contributes (Fig. 3.10) to decrease adsorbent replacement costs (-0.75 *MMUSD* in 20 years, or  $\approx -0.04$  *MMUSD/y*).

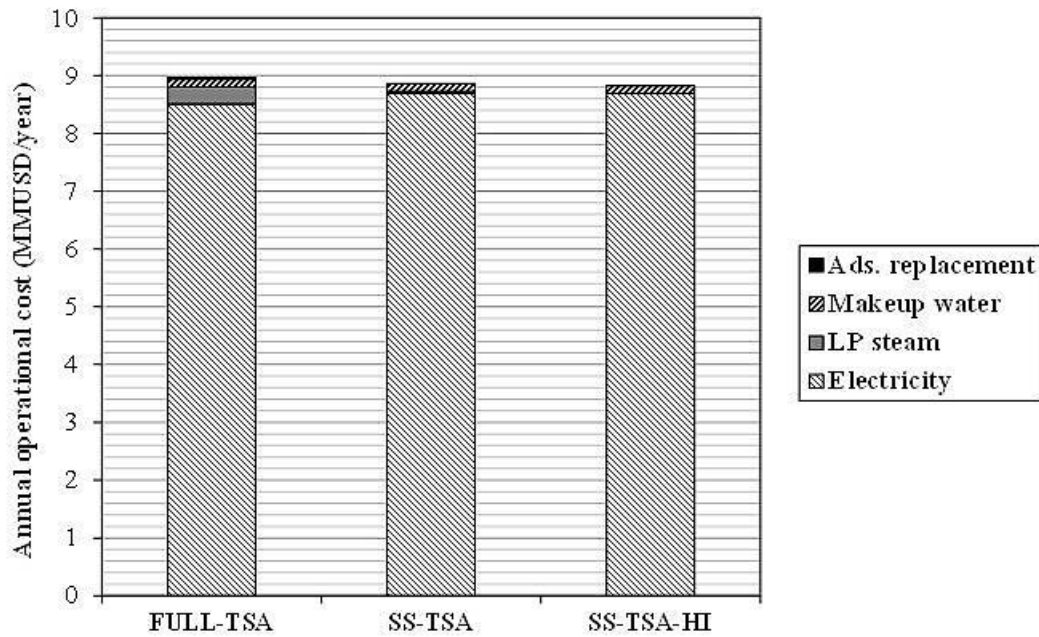


**Fig. 3.10.** Annual operational costs of FULL-TSA, SS-TSA and SS-TSA-HI.

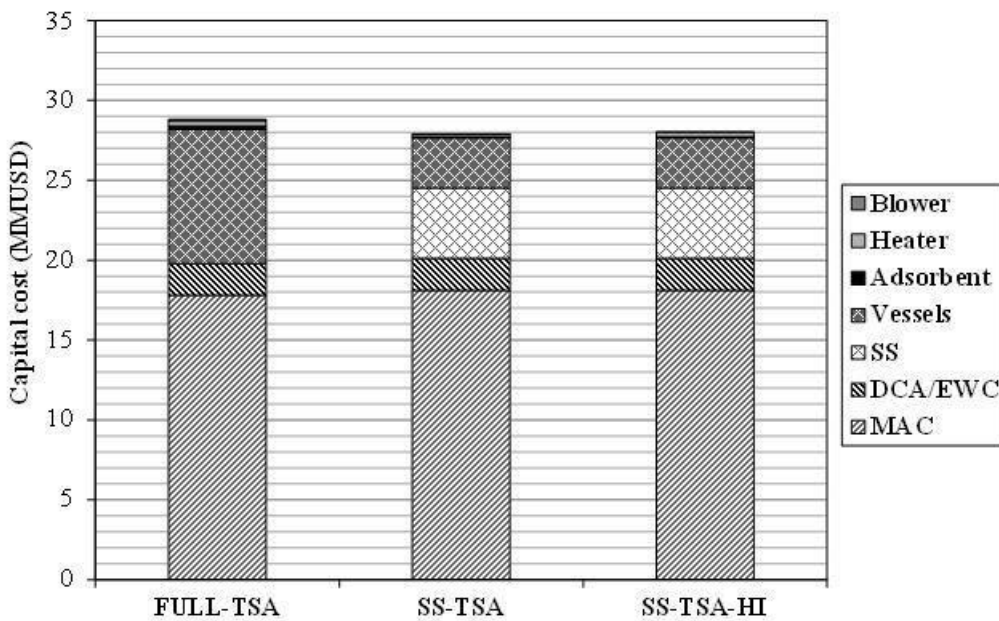


**Fig. 3.11.** Components of fixed capital investment (*FCI*) of PPU.

For a minimum acceptable 10% rate of return, Table 3.5 shows purified air breakeven prices necessary to yield zero Net Present Value (*NPV*) with 20 years: 5.28 USD/kNm<sup>3</sup> for FULL-TSA, 5.19 USD/kNm<sup>3</sup> for SS-TSA and 5.18 USD/kNm<sup>3</sup> for SS-TSA-HI. Fig. 3.12 presents *NPV* profiles of FULL-TSA, SS-TSA and SS-TSA-HI for 30 years of horizon assigning same purified air unitary price of 5.28 USD/kNm<sup>3</sup> to all PPU. Fig. 3.12 also demonstrates that the payback of the *FCI* increment in SS-TSA-HI for compression heat recovery to MS-TSA regeneration occurs after 6 years of operation, when SS-TSA-HI surpasses SS-TSA in profitability.

**Table 3.5.** Economic performance of PPU with purified air at breakeven prices.

<i>PPU</i>	<i>FULL-TSA</i>	<i>SS-TSA</i>	<i>SS-TSA-HI</i>
<i>FCI</i> (MMUSD)	28.80	27.91	28.04
<i>COM</i> (MMUSD/y)	8.97	8.86	8.82
Purified air breakeven price (USD/kNm <sup>3</sup> )	5.28	5.19	5.18
Revenues (MMUSD/y)	12.61	12.39	12.37
20 years NPV (MMUSD)	0.00	0.00	0.00

New SS-TSA and SS-TSA-HI demonstrate that SS reduces drastically the water content (98.5%) of air sent to the smaller finishing MS-TSA step, allowing significant economic advantages and lowering the cost of pressurized air supply to Cold-Box, since: (i) MS-TSA demands less bed regeneration heat; (ii) MS-TSA operates with reduced adsorption load, as well as smaller TSA vessels and less adsorbent inventory; and (iii) MS-TSA generates less adsorbent replacement costs, thanks to increased lifetime from lower thermo-mechanical stress from less frequent switches. Another advantage of new SS-TSA is its lower MS-TSA regeneration temperature, allowing creation of another new PPU SS-TSA-HI where waste heat from MAC intercooler heated regeneration nitrogen. New SS-TSA and SS-TSA-HI also minimize CW make-up due to water retained from air dehydration and reduced evaporative heat duty in CW tower. Furthermore, despite not included in the economic analysis, another comparative advantage of SS-TSA and SS-TSA-HI has to do with their lower flow rate of regeneration nitrogen, allowing availability of dry decontaminated nitrogen for commercialization.

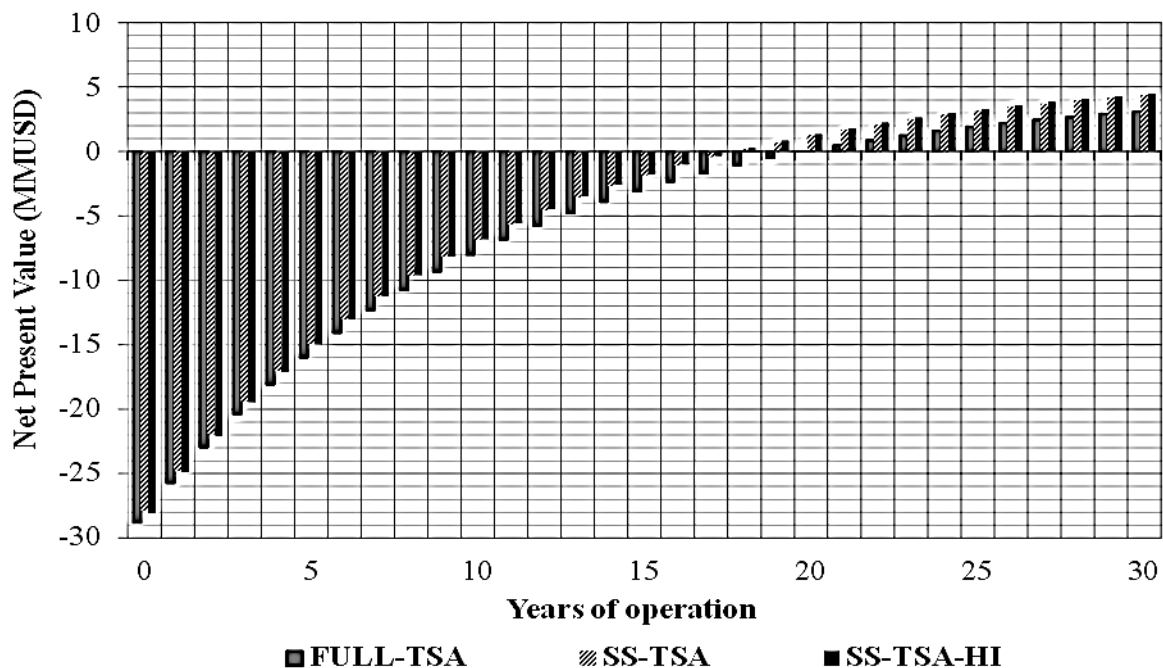


**Fig. 3.12.** NPV of FULL-TSA, SS-TSA and SS-TSA-HI (purified air at 5.28 USD/kNm<sup>3</sup>).

### 3.5. Conclusions for Chapter 3

Three concepts of air pre-purification unit (PPU) were technically and economically compared: the conventional TSA-based FULL-TSA PPU and two new PPUs adopting air dehydration with supersonic separator (SS), namely, SS-TSA and SS-TSA-HI, the latter a SS-TSA variant lowering heating costs via compression heat recovery. Both new PPUs outperformed FULL-TSA for supplying air to Cold-Box thanks to drastic reduction of air humidity via SS, leaving only a small dehydration load to be executed by new finishing smaller MS-TSA units prescribed in SS-TSA and SS-TSA-HI. While FULL-TSA removes  $\approx 4000 \text{ ppmH}_2\text{O}$  and  $\approx 363 \text{ ppmCO}_2$  with dual bed AA+MS TSA, the smaller single-bed MS-TSA of SS-TSA and SS-TSA-HI removes only  $56.4 \text{ ppmH}_2\text{O}$  and  $\approx 363 \text{ ppmCO}_2$  implying substantial reduction of bed size and regeneration heat consumption (-88.3%). Besides MS-TSA lower bed size, its cycle-time can be extended giving higher lifespan of adsorbent and switching valves.

SS-TSA and SS-TSA-HI also present lower *COM*, as well as lower plant *FCI* thanks to high SS pressure recovery with only 3.46% head-loss, demanding a slightly larger air compressor (MAC) relatively to conventional FULL-TSA. The breakeven (20 years) unitary prices of 3.10 bar purified air from FULL-TSA, SS-TSA and SS-TSA-HI reach, respectively, 5.28, 5.19, and 5.18 USD/kNm<sup>3</sup>. Adoption of the highest breakeven price (5.28 USD/kNm<sup>3</sup>) by all PPUs lead to clear advantage of SS-TSA and SS-TSA-HI over FULL-TSA in terms of 30 years NPV, with best performance by SS-TSA-HI seconded by SS-TSA.

Finally, it only was possible to explore such two new SS-based PPU concepts because a thermodynamically rigorous, equilibrium-based, SS multiphase simulation model and multiphase sound speed determination tool were developed as reliable and efficient HYSYS Unit Operation Extensions – SS-UOE [19] and PEC-UOE [20] – to be inserted in HYSYS 8.8 flowsheets allowing to compute phase-change effects and multiphase sound speed in SS units for any kind of process.

### 3.6. References for Chapter 3

- [1] Suresh B, Schlag S, Yokose K, Ping Y. Air separation gases: CEH marketing research report. The Chemical Economics Handbook - SRI Consulting, 2011.
- [2] Schmidt W. ASU reboiler/condenser safety. European Industrial Gas Association, Production Safety Seminar, 2006.

- [3] Tian Q, He G, Wang Z, Cai D, Chen L. A novel radial adsorber with parallel layered beds for prepurification of large-scale air separation units. *Industrial & Engineering Chemistry Research*, 54(30), 7502–7515, 2015. <https://doi.org/10.1021/acs.iecr.5b00555>.
- [4] Acharya DR, Jain R. Recent advances in molecular sieve unit design for air separation plants. *Separation Science and Technology*, 30, 3489-3507, 1995. <https://doi.org/10.1080/01496399508015131>
- [5] Golden TC, Taylor FW, Johnson LM, Malik NH, Raiswell CJ, inventors; Air Products and Chemicals, Inc., applicant. Purification of air. US Patent 6,106,593. Filed in October 8, 1998. Patented in August 22, 2000.
- [6] Kerry FG. *Industrial gas handbook: gas separation and purification*. CRC Press, 2006.
- [7] Dawson B, Kalbassi M, Siegmund S, Thayer M. Optimizing oxygen plant performance: improving production and reliability of existing plants while reducing costs. ALTA Conference, Perth, Australia, 2010.
- [8] Higginbotham P, White V, Fogash K, Guvelioglu G. Oxygen supply for oxycoal CO<sub>2</sub> capture. *Energy Procedia*, 4, 884-891, 2011. <https://doi.org/10.1016/j.egypro.2011.01.133>
- [9] Goloubev D. Oxygen production for oxyfuel power plants: status of development. Workshop on Oxyfuel-FBC Technology, 2012.
- [10] Shi YF, Liu XJ, Guo Y, Kalbassi MA, Liu YS. Desorption characteristics of H<sub>2</sub>O and CO<sub>2</sub> from alumina F200 under different feed/purge pressure ratios and regeneration temperatures. *Adsorption*, 23, 999-1011, 2017. <https://doi.org/10.1007/s10450-017-9907-0>
- [11] Fu C, Gundersen T. Recuperative vapor recompression heat pumps in cryogenic air separation processes. *Energy*, 59, 708-718, 2013. <https://doi.org/10.1016/j.energy.2013.06.055>
- [12] Rege SU, Yang RT, Buzanowski MA. Sorbents for air pre-purification in air separation. *Chemical Engineering Science*, 55, 4827-4838, 2000. [https://doi.org/10.1016/S0009-2509\(00\)00122-6](https://doi.org/10.1016/S0009-2509(00)00122-6)
- [13] Liu XJ, Shi YF, Kalbassi MA, Underwood R, Liu YS. Water vapor adsorption isotherm expressions based on capillary condensation. *Separation and Purification Technology*, 116, 95-100, 2013. <https://doi.org/10.1016/j.seppur.2013.05.020>
- [14] Liu XJ, Shi YF, Kalbassi MA, Underwood R, Liu YS. A comprehensive description of water vapor equilibriums on alumina F-200: adsorption, desorption, and H<sub>2</sub>O/CO<sub>2</sub> binary adsorption. *Separation and Purification Technology*, 133, 276-281, 2014. <https://doi.org/10.1016/j.seppur.2013.05.020>
- [15] Epiepang FE, Li J, Liu Y, Yang RT. Low-pressure performance evaluation of CO<sub>2</sub>, H<sub>2</sub>O and CH<sub>4</sub> on Li-LSX as a superior adsorbent for air prepurification. *Chemical Engineering Science*, 147, 100-108, 2016. <https://doi.org/10.1016/j.ces.2016.03.022>
- [16] Mulgundmath VP, Kunkel M, Tezel FH, Golden TC, Mogan J, Morin B. Adsorption equilibrium parameters of trace impurities. *Separation Science and Technology*, 44, 874–893, 2009. <https://doi.org/10.1080/01496390802697064>
- [17] Kawai M, Nakamura M, inventors; Taiyo Nippon Sanso Corporation, applicant. Purification method and purification apparatus for feed air in cryogenic air separation. US Patent 9,651,302. Filed in December 12, 2006. Patented in May 16, 2017.
- [18] Nakamura M, Kawai M, Takei H, inventors; Taiyo Nippon Sanso Corporation, applicant. Method of purifying air. US Patent 8,690,990. Filed in February 25, 2010. Patented in April 8, 2014.

- [19] Arinelli LO, Trotta TAF, Teixeira AM, de Medeiros JL, Araújo OQF. Offshore Processing of CO<sub>2</sub> Rich Natural Gas with Supersonic Separator versus Conventional Routes. *Journal of Natural Gas Science and Engineering*, 46, 199-221, 2017. <https://doi.org/10.1016/j.jngse.2017.07.010>
- [20] de Medeiros JL, Arinelli LO, Araújo OQF. Speed of sound of multiphase and multi-reactive equilibrium streams: a numerical approach for natural gas applications. *Journal of Natural Gas Science and Engineering*, 46, 222-241, 2017. <https://doi.org/10.1016/j.jngse.2017.08.006>
- [21] Brigagão GV, Arinelli LO, de Medeiros JL, Araújo OQF, inventors; Universidade Federal do Rio de Janeiro, applicant. Processo de preparo e purificação do ar para fracionamento criogênico utilizando separador supersônico de baixa pressão. BR patent application 102017027727-5, Filed in December 21, 2017.
- [22] Machado PB, Monteiro JGM, de Medeiros JL, Epsom HD, Araújo OQF. Supersonic separation in onshore natural gas dew point plant. *Journal of Natural Gas Science and Engineering*, 6, 43-49, 2012. <https://doi.org/10.1016/j.jngse.2012.03.001>
- [23] Castier M. Effect of side streams on supersonic gas separations. *Journal of Natural Gas Science and Engineering*, 35, 299-308, 2016. <https://doi.org/10.1016/j.jngse.2016.08.065>
- [24] Secchi R, Innocenti G, Fiaschi D. Supersonic Swirling Separator for natural gas heavy fractions extraction: 1D model with real gas EOS for preliminary design. *Journal of Natural Gas Science and Engineering* 34, 197-215, 2016. <https://doi.org/10.1016/j.jngse.2016.06.061>
- [25] Teixeira AM, Arinelli LO, de Medeiros JL, Araújo OQF. Recovery of thermodynamic hydrate inhibitors methanol, ethanol and MEG with supersonic separators in offshore natural gas processing. *Journal of Natural Gas Science and Engineering*, 52, 166-186, 2018. <https://doi.org/10.1016/j.jngse.2018.01.038>
- [26] Yang Y, Wen C, Wang S, Feng Y. Theoretical and numerical analysis on pressure recovery of supersonic separators for natural gas dehydration. *Applied Energy* 2014, 132, 248-253. <https://doi.org/10.1016/j.apenergy.2014.07.018>
- [27] Wen C, Cao X, Yang Y, Li W. Numerical simulation of natural gas flows in diffusers for supersonic separators. *Energy* 2012, 37, 195-200. <https://doi.org/10.1016/j.energy.2011.11.047>
- [28] Shooshtari SHR, Shahsavand A. Maximization of energy recovery inside supersonic separator in the presence of condensation and normal shock wave. *Energy* 2017, 120, 153-163. <https://doi.org/10.1016/j.energy.2016.12.060>
- [29] Karakatsani E.K., Kontogeorgis G.M. Thermodynamic Modeling of Natural Gas Systems Containing Water. *Ind. Eng. Chem. Res.* 2013, 52, 3499–3513. <https://doi.org/10.1021/ie302916h>
- [30] Turton R, Bailie RC, Whiting WB, Shaeiwitz JA. Analysis, synthesis, and design of chemical processes. Prentice Hall International Series in the Physical and Chemical Engineering Sciences, 3<sup>rd</sup> ed., 2009.
- [31] Dillon DJ, White V, Allam RJ, Wall RA, Gibbins J. IEA Greenhouse Gas R&D Programme: Oxy-combustion processes for CO<sub>2</sub> capture from power plant. Engineering Investigation Report, 2005.
- [32] Campbell JM. Gas conditioning and processing, v. 2: the equipment modules. Campbell Petroleum Series, 7<sup>th</sup> ed., 1984.

## 4. Improving Exergy Efficiency of Air Pre-Purification Unit for Cryogenic Fractionation: Low-Pressure Supersonic Separator Coupled to Finishing Adsorption

*The contents of this chapter have not been published yet.*

### Abstract

Cryogenic air separation requires a Pre-Purification Unit (PPU) for air compression and removal of H<sub>2</sub>O, CO<sub>2</sub> and trace-species for Cold-Box operation. The conventional PPU – FULL-TSA – adopts temperature swing adsorption (TSA) with an activated-alumina bed for H<sub>2</sub>O adsorption and a molecular-sieve bed for CO<sub>2</sub> and trace-species removal. A novel alternative – SS-TSA – prescribes a Supersonic Separator (SS) abating ≈98.5% of H<sub>2</sub>O followed by a small single-bed molecular-sieve TSA removing remaining impurities. SS-TSA-HI is a SS-TSA variant using compression heat for molecular-sieve regeneration. This work conducts exergy analyses of FULL-TSA, SS-TSA and SS-TSA-HI to compare thermodynamic performances and indicate improvements for better resources utilization. Exergy analyses are supported by HYSYS simulation using unit operation extensions for SS simulation and phase-equilibrium sound speed calculation. Since exergy rates depend on Reference Environmental Reservoir (RER), two RER formalisms are employed at *1 atm* and 25°C. RER#1 adopts air with 60% relative humidity (the same condition of raw air feed), while RER#2 prescribes air in equilibrium with liquid water. RER#1 is shown to be appropriate for overall system analysis, while RER#2 is appropriate for sub-systems analysis as it dramatically lowers exergy flows of cooling-water. SS-TSA has 61% less exergy losses than FULL-TSA in contaminant-removal step as SS accomplishes bulk purification drastically reducing steam and N<sub>2</sub> consumptions for TSA regeneration. RER#1 exergy efficiencies of FULL-TSA, SS-TSA and SS-TSA-HI attained 57.9%, 60.0%, and 60.3%, respectively.

**Keywords:** exergy analysis; air pre-purification; air dehydration; supersonic separator; multiphase sound speed; cryogenic air separation.

### Supplementary Materials

Supplementary Materials for this chapter are found in Appendix W.

### Abbreviations

1D One-Dimensional; AA Activated-Alumina; ASU Air Separation Unit; ChW Chilled-Water; CW Cooling-Water; DCA Direct-Contact Aftercooler; EWC Evaporative Water-Cooler; LPS Low-Pressure Steam; MAC Main-Air-Compressor; MMSm<sup>3</sup>/d Millions Standard m<sup>3</sup> per Day; MS Molecular-Sieve; MS-TSA Molecular-Sieve TSA; NG Natural

Gas; PPU Pre-Purification Unit; PR-EOS Peng-Robinson Equation-of-State; PSA Pressure-Swing Adsorption; RER Reference Environmental Reservoir; RH Relative Humidity; SS Supersonic Separator; TSA Temperature-Swing Adsorption; UOE Unit Operation Extension; VLE Vapor-Liquid Equilibrium; WW Warm-Water.

## Nomenclature

$c$	: Sound speed property of multiphase-equilibrium fluid (m/s)
$D_I, D_T, D_O$	: SS inlet, throat and outlet internal diameters (m)
$\dot{E}$	: Exergy flow rate (kW)
$F_j$	: $j^{\text{th}}$ feed flow rate (kmol/h)
$\bar{H}$	: Molar enthalpy (kJ/kmol)
$K_j$	: $j^{\text{th}}$ product flow rate (kmol/h)
$L, L_C, L_D$	: SS lengths: total, converging section and diverging section (m)
$L^{\text{Laval}}$	: SS Laval nozzle length (m)
$L^{\text{Shock}} = L^{\text{LAVAL}}$	: SS axial position just before normal shock and condensate withdrawal (m)
$Ma = v/c$	: Mach Number
$Ma^{\text{Shock}} = Ma_{\text{BS}}$	: $Ma$ just before normal shock and condensate withdrawal
$nc$	: Number of components
$nfs, nps$	: Numbers of feed and of product streams
$nwps$	: Number of waste product streams
$nwe, nwi$	: Numbers of power-streams exported and imported by the system
$P, T$	: Pressure (bar) and Temperature (K)
$\dot{Q}_0$	: Heat transfer from heat reservoir to system (kW)
$R_H, R_k$	: Heat and species $k$ reservoirs
$\bar{S}$	: Molar entropy (kJ/kmol.K)
$\dot{U}$	: Internal energy rate (kW)
$v$	: Axial velocity (m/s)
$\dot{W}$	: Work rate (kW)
$x$	: axial position (m)
$Y_k$	: Species $k$ mole fraction
<b>Greek Symbols</b>	
$\alpha, \beta$	: Converging and diverging angles of SS with linear diameter profiles( $^\circ$ )
$\beta^{\text{Shock}}$	: Pre-Shock molar vapor-fraction
$\varepsilon$	: Exergy efficiency(%)
$\mu_k$	: Chemical potential of species $k$ (kJ/kmol)
$\eta^{\text{CMP}}, \eta^{\text{EXP}}$	: SS compression/expansion adiabatic efficiencies(%)
$\eta^{\text{DRIVE}}$	: Driver mechanical efficiency(%)
$\eta^{\text{MAC}}$	: MAC adiabatic efficiency(%)
$\dot{\Xi}_k$	: Energy transfer rate from species $k$ reservoir to system (kW)
$\psi$	: Rational exergy efficiency(%)
$\dot{\Omega}_S, \dot{\Omega}_k$	: Creation rates of entropy (kW/K) and species $k$ (mol/s) in Universe
<b>Superscripts</b>	
$_{\text{DESTR, IN, OUT, Sys}}$	: Destruction, inlet, outlet and system
$_{\text{Shock}}$	: Just before normal shock and condensate withdrawal
<b>Subscripts</b>	
$_{\text{BS}}$	: Just before normal shock and after condensate withdrawal

## 4.1. Introduction

Air separation is central for oxy-combustion CO<sub>2</sub> capture as it demands large-scale oxygen gas production. Thus, beyond commercialization of O<sub>2</sub>/N<sub>2</sub>, advances in air separation are of interest vis-à-vis global warming. In the context of large-scale power generation, onsite oxygen supply should come from large-scale cryogenic Air Separation Units (Cryo-ASU). Although ceramic ion-transport membranes have been considered promising for oxygen production in synergy with power generation, its current scale is sub-commercial, so Cryo-ASUs are suitable for at least the first oxy-combustion plants [1]. Cryo-ASUs are divided into two sections, namely: (i) Pre-Purification Unit (PPU) for air compression and purification; and (ii) Cold-Box for cryogenic fractionation.

### 4.1.1. Pre-Purification Unit (PPU)

The PPU is placed upstream the Cold-Box for air compression and removal of freezable (H<sub>2</sub>O/CO<sub>2</sub>) and flammable (hydrocarbons) contaminants. Current PPUs are based on adsorption, most commonly Temperature-Swing Adsorption (TSA) operating with cycle-times of 4-8 h, having an Activated-Alumina (AA) bed for removing H<sub>2</sub>O and a 13X zeolite molecular-sieve (MS) bed for removing CO<sub>2</sub> and trace-species [2]. Double-bed TSA firstly dehydrates air, a recommendation for best CO<sub>2</sub> removal [3].

TSA-PPU variants merely change bed composition and desorption method. For instance, Pressure-Swing Adsorption (PSA) exhibits less operational costs than TSA, but with drawbacks from its minute  $\approx 20\text{min}$  cycle-times such as larger adsorbent inventories, lower adsorbent durability, higher maintenance costs, and air loss from depressurizations [4]. Therefore, combining temperature and pressure desorption effects is the most cost-effective air pre-purification [5]. However, given the trend to reduce power consumption, PSA loses effectiveness as Cold-Box pressure decreases [6]. In this sense, triple-column Cold-Boxes have been proposed for oxygen supply from  $\approx 3\text{ bar}$  air [1, 7], contrasting with common  $\approx 5.5\text{ bar}$  double-column Cold-Boxes. Consequently, TSA-based PPUs are dominant for low-pressure Cold-Boxes. However, Zhou et al. [8] pointed out disadvantages of TSA-based PPUs when vapor-recompression distillation is employed with single low-pressure column, reducing adsorbent capacity and shrinking cycle-times.

Brigagão et al. [9] presented an alternative PPU concept based on supersonic separator (SS). In SS-based PPUs the SS performs the lion-share of the purification service removing  $\approx 99\%$

of H<sub>2</sub>O from the compressed raw air feed, requiring only a small finishing MS-TSA unit to remove the remaining H<sub>2</sub>O, CO<sub>2</sub> and trace-species. Such SS-based PPU comprising air compression, air cooling, SS and MS-TSA is hereinafter referred as SS-TSA, while the conventional TSA-based PPU is referred as FULL-TSA. A heat-integrated SS-TSA variant – SS-TSA-HI – can also be devised replacing low-pressure steam (LPS) by warm water (WW) from compressor intercooler to heat nitrogen for TSA regeneration. SS-TSA and SS-TSA-HI are embodiments of the pending patent No. BR102017027727-5 registered in the Brazilian Patent and Trademark Office [10].

Energy and economic assessments of SS-TSA, SS-TSA-HI and FULL-TSA, were object of a previous work [9]. SS-TSA-HI seconded by SS-TSA economically outperformed FULL-TSA, achieving lower purified air break-even prices, due to drastic reduction in LPS for heating regeneration nitrogen, despite a tiny increase in compression power accounting for SS head-loss. In the present work SS-TSA, SS-TSA-HI and FULL-TSA are analyzed from the perspective of exergy preservation.

#### 4.1.2. Supersonic Separator

Supersonic separators (SS) are commonly applied under high-pressure in offshore natural gas (NG) conditioning for removal of condensable hydrocarbons with minimum head-loss [11]. SS is also utilized for simultaneous water dew-point adjustment and hydrocarbon dew-point adjustment of high-pressure NG [12]. Moreover, Arinelli et al. [12] also demonstrated SS utilization for CO<sub>2</sub> removal from dry CO<sub>2</sub>-rich NG. Fig. 4.1 portrays SS geometry with linear diameter profiles restricted to essential one-dimensional (1D) axial flow characteristics of SS modeling including swirling and collecting vanes. SS phenomenology was fairly explained in Arinelli et al. [12] and Brigagão et al. [9].

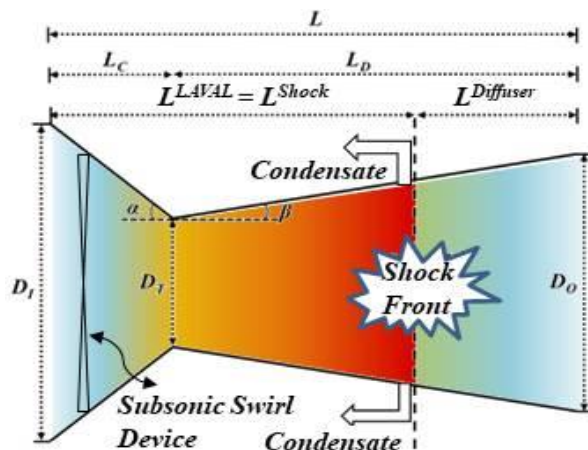


**Fig. 4.1.** SS Sketch with linear diameter profiles depicting velocity gradient.

SS operation is regulated by kinetic energy conversion affecting conditions and properties of the fluid. A critical aspect for SS modeling is the correct determination of the multiphase equilibrium sound speed ( $c$ ) property for estimation of the Mach number ( $Ma = v/c$ ) on SS path. A rigorous thermodynamic model for sound speed ( $c$ ) evaluation was provided in de Medeiros et al. [13] including the development of a HYSYS unit operation extension (UOE) for determination of the phase-equilibrium  $c$ , named PEC-UOE. For SS design and simulation in HYSYS, Arinelli et al. [12] developed a SS unit operation extension – SS-UOE – capable to handle multiphase supersonic flow, condensate removal and normal shock transition. SS-UOE uses PEC-UOE for multiphase  $c$  and sizes SS nozzles with linear diameter profiles determining (Fig. 4.1) converging ( $L_C$ ), diverging ( $L_D$ ) and total ( $L$ ) lengths and throat diameter ( $D_T$ ) so that sonic flow ( $Ma=1$ ) occurs at the throat. SS-UOE obtains SS stream products at stagnation – treated gas and condensate – demanding the following inputs (Fig. 4.1): feed stream at stagnation, inlet/outlet diameters ( $D_I, D_O$ ), converging-diverging wall angles ( $\alpha, \beta$ ), compression/expansion adiabatic efficiencies ( $\eta^{CMP}, \eta^{EXP}$ ), and maximum attained supersonic  $Ma$  ( $Ma^{Shock}$ ). While other SS thermodynamic models are generally limited to simple vapor-liquid equilibrium (VLE) [14], SS-UOE and PEC-UOE efficiently simulates SS processing of raw NG with three-phase flow of immiscible water and hydrocarbon liquid phases in equilibrium with gas. SS-UOE automatically retrieves the feed stream from the HYSYS flowsheet and inserts the solved SS product streams in the flowsheet. SS feed and product streams are all at stagnation conditions to comply with other process streams, where external energy balance of each unit operation is only enthalpy-dependent. Therefore, there is no contribution of kinetic energy to exergy of streams in the flowsheet.

#### 4.1.3. Exergy Analysis and Reference Environmental Reservoirs

Exergy analysis evaluates exergy preservation/destruction relatively to a reference environmental reservoir (RER) conceived to assess chemical and power plants [15]. By determining the exergy content of streams, exergy analysis detects thermodynamic imperfections in the process, identifying and locating entropy sources (irreversibilities), and also enabling waste minimizations and optimum resource utilization [16].

Exergy of streams is context sensitive and has no meaning without a RER [17], as streams must have zero exergy when attaining chemical and thermo-mechanical equilibrium with RER. For some systems with working fluids in closed-circuits, changes of chemical exergy are neglected limiting exergy analysis to thermo-mechanical transformations [18]. However,

most applications require complete RER framework, with two considered routes: (i) choose suitable RER to the problem [19]; or (ii) use a generalized universal RER, such as the equilibrium-based model [20] and the reference-substance model [21]. Considering that RERs can be arbitrarily chosen to best fit the analyzed system and its surroundings, a good practice is to perform exergy analysis using at least two different RERs to avoid RER inconsistencies and blind spots. An adequate RER avoids overrated exergy values preventing hidden irreversibilities from inflated exergy efficiencies ( $\varepsilon$ ) [20]. To bypass exergy overrating, some exergy works have focused on exergy variation instead on its absolute value, replacing efficiency  $\varepsilon$  by rational exergy efficiencies  $\psi$  defined for each unit [7]. Ghannadzadeh et al. [22] demonstrated in their study on NG processing with the RER of Szargut et al. [21], that  $\psi$  displays thermodynamic performance of equipment revealing irreversibilities, while  $\varepsilon$  hides them due to values above 99.4%.

In spite of this, it is possible to deflate exergy values by merely choosing RER adequately to have better description of thermodynamic performances with unambiguous  $\varepsilon$ . In this work exergy analysis is performed by means of two RER approaches and exclusively using traditional exergy efficiencies ( $\varepsilon$ ).

#### **4.1.4. Exergy Analysis of PPU for Cryogenic Fractionation**

Several recent works address exergy analysis of ASUs but very few presented analysis of PPU. Additionally, cooling-water (CW) systems have been neglected in overall process performance despite the considerable exergy flows associated to evaporative CW-cooling, CW pumping and air exhaustion. Furthermore, all these works performed exergy analysis exclusively using standardized RERs with fixed tabular composition and chemical exergy factors.

Cornelissen and Hirs [23] carried out exergy analysis of a low-pressure double-column Cryo-ASU producing gas and liquid products coupled to a N<sub>2</sub> liquefaction unit. The liquefaction unit uses N<sub>2</sub> compression above 30 bar, being identified as the major exergy sink overcoming ASU losses. Within the ASU, the PPU with air compression and TSA represented the main source of irreversibilities. Raw air was compressed to 6.2 bar with 70% of polytropic efficiency and sent to a Direct-Contact Aftercooler (DCA) fed with CW and 7°C chilled-water (ChW) from a freon chiller. TSA used superheated steam (11 bar, 210°C) for heating N<sub>2</sub> to 170°C. For exergy evaluation authors used a commercial extension for Aspen-Plus [24] working with the RER of Szargut et al. [21]. Increasing the polytropic efficiency of compressors to 85% the PPU efficiency reached  $\varepsilon \approx 59\%$ . Excluding chiller losses  $\varepsilon$  reached  $\approx 61\%$ .

Fu and Gundersen [25] presented exergy analysis of a conventional Cryo-ASU producing low-pressure  $95\%mol$  oxygen. The PPU comprises main air compressor (MAC), air cooling and TSA. MAC and air cooling represented the largest exergy losses, accounting for  $38.4\%$  of total losses of base-case, with MAC adiabatic efficiency  $\eta^{MAC}=82\%$  and driver efficiency  $\eta^{DRIVER}=97\%$ . The TSA generated  $12.6\%$  of exergy losses. With available data one can estimate the PPU efficiency ( $\varepsilon$ ) within  $50-60\%$ .

More recently, Fu and Gundersen [26] performed exergy assessment of an oxy-combustion coal-fired power plant, which besides the Cryo-ASU and power generation also included  $CO_2$  conditioning for storage. In both works RER choice follows Szargut et al. [21]. The same previous ASU was evaluated with slightly different conditions. While the exergy losses of the oxy-combustion system were dominated by combustion reactions, the largest exergy loss related with  $CO_2$  capture occurred in MAC and air cooling in the PPU. A high  $\varepsilon\approx 88\%$  was presented in MAC and air cooling ( $\eta^{MAC}=82\%$ ,  $\eta^{DRIVER}=97\%$ ), a reflex of high exergy values of CW streams, contrasting with  $75\%$  less exergy destruction in TSA, despite its lower  $\varepsilon\approx 81\%$ . Considering as waste exergy the exergy increase of CW streams leaving the PPU, the overall PPU efficiency reached  $\varepsilon\approx 60\%$ .

Van der Ham and Kjelstrup [7] performed exergy analysis of two Cryo-ASUs: a double-column and a triple-column, with focus on the Cold-Box, assuming both ASUs fed with  $5\text{ bar}$  purified air. Thus, the PPU was not assessed. Exergy destruction in the triple-column ASU was found to be  $\approx 12\%$  lower than in the double-column, but such advantage was underrated as the triple-column actually requires air at only  $3\text{ bar}$ . In later work, Van der Ham [27] investigated overall exergy efficiency of an integrated-gasification-combined-cycle gasifying coal with oxygen from a heat-integrated distillation Cold-Box without PPU.

Querol et al. [28] developed an applicative for exergy and thermo-economic analyses of processes implemented in Aspen-Plus and applied it to a Cryo-ASU without PPU as it was assumed  $6.6\text{ bar}$  contaminant-free air intake. However, from the furnished data one can estimate an analogous PPU efficiency of  $\varepsilon\approx 71.6\%$  with  $\eta^{MAC}\approx 75\%$ . The same ASU was later investigated by Ebrahimi et al. [29], which performed energy, exergy and economic analyses. From the data, a PPU efficiency of  $\varepsilon\approx 74\%$  is estimated assuming  $\eta^{MAC}=80\%$  in the 1<sup>st</sup> MAC stage and  $\eta^{MAC}=76\%$  in the 2<sup>nd</sup> stage.

Zhou et al. [8] carried out exergy analyses of vapor-recompression distillation ASUs and compared their performance to a double-column ASU. This work also privileged Cold-Box

exergy analysis. The PPU was not considered, as a single valve replaced the TSA unit, therefore being limited to head-loss, besides neglecting H<sub>2</sub>O in air feed, which explains a high PPU efficiency of  $\approx 73\%$  for 4.3 atm air with  $\eta^{MAC}=80\%$ .

#### 4.1.5. The Present Work

The PPU relevance for Cryo-ASU exergy performance has been frequently neglected in the literature and those works including it in the exergy analysis address only FULL-TSA PPUs with air feed pressure above 4 bar without considering the CW-System. Counterpointing these trends, the present work explores a new SS-based PPU concept for low-pressure  $\approx 3$  bar ASUs, addressing exergy analysis of SS-TSA and SS-TSA-HI SS-based PPUs comparing them with conventional FULL-TSA PPU. The SS abates  $\approx 99\%$  of the water drastically lowering the TSA load which now requires only a small TSA unit to remove water-traces and CO<sub>2</sub>. PPU improvements are also pinpointed to reduce utility consumption and exergy destruction. Additionally, RER choices are quantitatively discussed for efficient PPU exergy analysis. The literature does not have similar exergy assessment of SS-based air purification.

#### 4.2. PPU Design and Simulation

Simulation and design of FULL-TSA, SS-TSA and SS-TSA-HI were performed in HYSYS 8.8. From these results operating conditions, compositions and thermodynamic properties ( $\bar{H}, \bar{S}$ ) of material streams were extracted for exergy analysis. HYSYS was also used for calculating RER chemical potentials of species. A TSA routine was integrated to simulation for sizing and for estimating regeneration heat duties.

FULL-TSA, SS-TSA and SS-TSA-HI are respectively depicted in Figs. 4.2a-4.2c, with TSA vessels on-adsorption tagged as "TSA/OP" and those on-regeneration as "TSA/REG". FULL-TSA, SS-TSA and SS-TSA-HI are briefly described. Complete descriptions are found in the Supplementary Materials and in Brigagão et al. [9]. Exergy analysis was applied to overall flowsheets as well as to sub-flowsheets in shaded boxes of Figs. 4.3a-4.3c. Only streams crossing boundaries were taken into account. Tables W1.1 and W1.2 of Appendix W1 list material and energy streams crossing boundaries of each sub-system and inform the origin, destination and description of streams according to Figs. 4.2a-4.2c and 4.3a-4.3c.

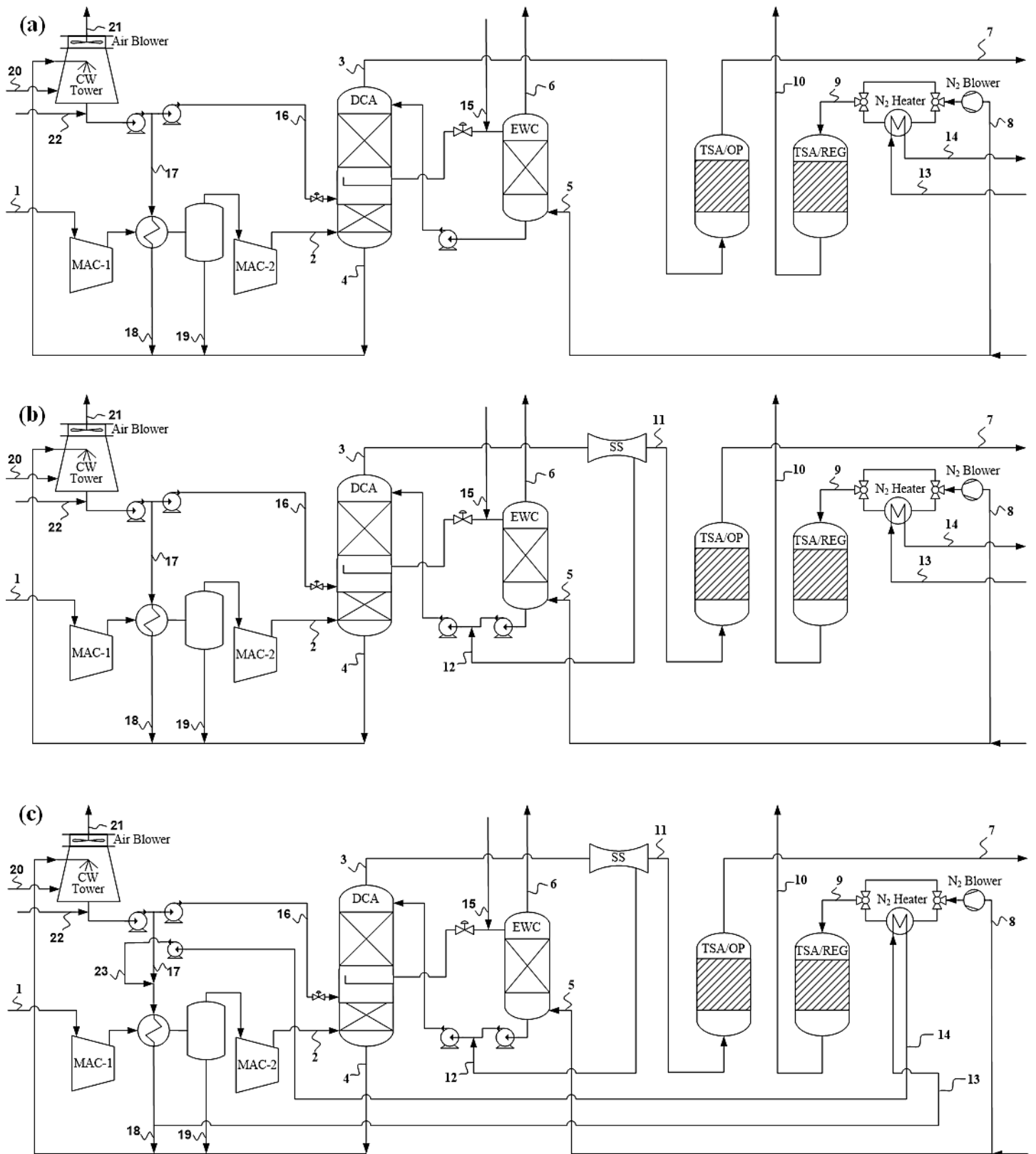


**Fig. 4.2.** (a) FULL-TSA; (b) SS-TSA; (c) SS-TSA-HI  
(TSA/OP=on-adsorption; TSA/REG=on-regeneration).

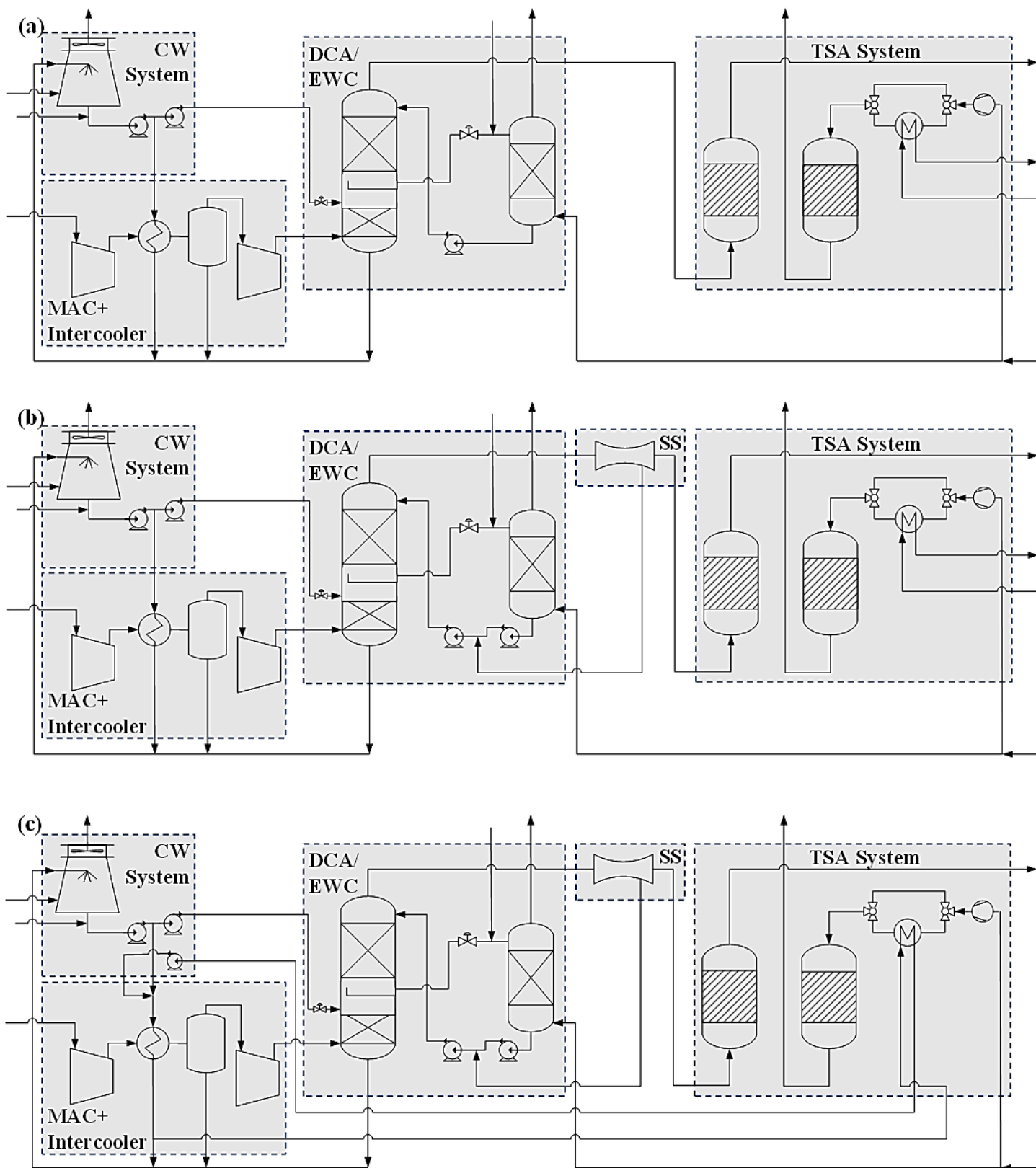


**Fig. 4.3.** Sub-systems boundaries: (a) FULL-TSA; (b) SS-TSA; (c) SS-TSA-HI (MAC/Intercooler; DCA/EWC; SS; TSA-System (AA/MS-TSA or MS-TSA); CW-System (Cooling-Tower/Pumps)).

PPUs initiate with atmospheric air stream#1 ( $P=1 \text{ atm}$ ,  $T=25^\circ\text{C}$ ,  $RH=60\%$ ) feeding the two-staged intercooled Main Air Compressor (MAC) sub-flowsheet. A condensate drum (stream#19) follows the intercooler, but no liquid is formed at  $T=40^\circ\text{C}$ ,  $P=1.9 \text{ bar}$ . MAC discharges air (stream#2) at  $P=3.180 \text{ bar}$  in FULL-TSA (Fig. 4.2a), and at  $P=3.225 \text{ bar}$  in SS-TSA/SS-TSA-HI (Fig. 4.2b-4.2c) to handle the SS head-loss targeting the same purified air pressure ( $3.10 \text{ bar}$ ) leaving the PPU (stream#7). The compressed air (stream#2) goes to Direct-Contact Aftercooler and Evaporative Water-Cooling (DCA/EWC) (Figs. 4.3a-4.3c) being cooled to  $10^\circ\text{C}$  (stream#3) before purification.

In SS-TSA/SS-TSA-HI compressed air at  $10^\circ\text{C}$  (stream#3) goes to SS (Figs. 4.3b-4.3c), whereas in FULL-TSA it is sent to TSA. In SS-TSA/SS-TSA-HI, SS plays a central role abating 98.65% of  $\text{H}_2\text{O}$  from compressed air at  $10^\circ\text{C}$  (stream#3), producing dry air at  $3.165 \text{ bar}$  (stream#11) with less than  $500 \text{ ppm}$  of contaminants to be removed by the finishing MS-TSA. The SS super-cooled condensate (stream#12) is injected into the ChW from EWC reducing water losses (Figs. 4.2b-4.2c).

The finishing MS-TSA of SS-TSA/SS-TSA-HI differs from conventional TSA of FULL-TSA PPU as the big activated-alumina (AA) bed is eliminated considerably reducing adsorbent inventory and equipment size. Purified air leaves TSA (or MS-TSA) and passes through a particulate filter (not shown) and goes to the Cold-Box (stream#7). Exhaust  $\text{N}_2$  from TSA regeneration is released to the atmosphere (stream#10).

There are two differences between SS-TSA and SS-TSA-HI: (i)  $\text{N}_2$  for MS-TSA regeneration is heated with LPS in SS-TSA and with warm-water (WW) in SS-TSA-HI (stream#13); and (ii) CW leaves the MAC intercooler at  $45^\circ\text{C}$  in SS-TSA, while WW leaves the MAC intercooler at  $90^\circ\text{C}$  in SS-TSA-HI. In this work, the CW-System is included in the exergy analysis for evaluation of the effect of compression heat dissipation instead of considering CW as external input/output streams, so that heat exchange with CW is internalized avoiding large transit of exergy through PPU boundaries.

#### 4.2.1. Assumptions for PPU Simulation and Design

- [A1] Thermodynamic model: Peng-Robinson Equation-of-State (PR-EOS).
- [A2] SS design/simulation via HYSYS SS-UOE [12] and PEC-UOE for phase-equilibrium sound speed calculation [13].
- [A3] Air intake:  $13580 \text{ kmol/h}$ ,  $P=1 \text{ atm}$ ,  $T=25^\circ\text{C}$ ,  $RH=60\%$ ,  $N_2=76.61\%\text{mol}$ ,  $O_2=20.55\%\text{mol}$ ,  $Ar=0.91\%\text{mol}$ ,  $H_2O=1.89\%\text{mol}$ ,  $CO_2=363 \text{ ppm-mol}$ .
- [A4] Filters: MAC inlet and TSA outlet,  $\Delta P=1 \text{ kPa}$  each [4].
- [A5] Triple-Column Cold-Box purified air:  $P=3.10 \text{ bar}$  [30].
- [A6] Booster Air Compressor: absent.
- [A7] Intercooler air-outlet:  $T=40^\circ\text{C}$ ,  $\Delta P=10 \text{ kPa}$ .
- [A8] Direct-Contact Aftercooler (DCA): bottom-structured-packing fed with CW, 03 theoretical stages,  $\Delta P=2 \text{ kPa}$ ; top-structured-packing fed with ChW, 10 theoretical stages,  $\Delta P=4 \text{ kPa}$ ,  $T^{\text{Top-Air}}=10^\circ\text{C}$ .
- [A9] CW:  $[30^\circ\text{C}, 45^\circ\text{C}]$ , 3 bar,  $\Delta P=50 \text{ kPa}$ .
- [A10] WW/CW (SS-TSA-HI MAC-Intercooler):  $[30^\circ\text{C}, 90^\circ\text{C}]$ , 3 bar,  $\Delta P=50 \text{ kPa}$ .
- [A11] LPS: saturated-steam, 4 bar,  $143.6^\circ\text{C}$ , leaving as saturated-liquid.
- [A12] Adiabatic efficiencies:  $\eta^{\text{MAC}}=85\%$ ;  $\eta^{\text{BLOWERS}}=75\%$ ;  $\eta^{\text{FAN}}=75\%$ ;  $\eta^{\text{PUMPS}}=75\%$ .
- [A13] Driver efficiency: 100%.
- [A14] SS specifications (Fig. 4.1): single SS nozzle,  $D_I=0.87\text{m}$ ,  $D_O=0.69\text{m}$ ,  $\alpha=12.67^\circ$ ,  $\beta=2.66^\circ$ ,  $\eta^{\text{EXP}}=\eta^{\text{CMP}}=100\%$ ,  $Ma^{\text{Shock}}=1.2$ .
- [A15] MS-TSA (SS-TSA/SS-TSA-HI): 03 vertical vessels, flow-reversal, 02 vessels adsorbing, 01 desorbing,  $\frac{1}{4}$ " 13X zeolite, cycle-time=12h, regeneration-time=4h,  $\Delta P=1 \text{ kPa}$ .
- [A16] TSA (FULL-TSA): 08 vertical vessels, flow-reversal, 04 vessels adsorbing, 04 desorbing,  $\frac{1}{4}$ " AA,  $\frac{1}{8}$ " 13X zeolite, cycle-time=8h, regeneration-time=4h,  $\Delta P=1 \text{ kPa}$ .
- [A17] Regeneration heat duty: uniformly distributed along TSA cycle-time.
- [A18] TSA/MS-TSA bed saturation: 95%.
- [A19] TSA/MS-TSA capacity: from experimental isotherms and adsorbate partial-pressure [31] corrected to design feed temperature of  $15^\circ\text{C}$  (Table 4.1).
- [A20] FULL-TSA: AA sized for  $H_2O$  removal; MS sized for  $CO_2$  removal; regeneration  $T^{\text{N}_2}=133^\circ\text{C}$ .
- [A21] SS-TSA/SS-TSA-HI: MS sized for  $H_2O$ -trace/ $CO_2$  removal; regeneration  $T^{\text{N}_2}=80^\circ\text{C}$ .
- [A22] CW cooling-tower: 03 theoretical stages,  $Head^{\text{FAN}}=1.325 \text{ kPa}$ ,  $P^{\text{Outlet-Air}}=1 \text{ atm}$ .
- [A23] TSA design: from Campbell [32]; regeneration equations from Kerry [4].
- [A24] Cold-Box pure  $N_2$ :  $P=1 \text{ atm}$ ,  $T=14^\circ\text{C}$ .

**Table 4.1.** Adsorbent parameters for TSA routine.

PPU	Adsorbent/ Adsorbate	Bulk Density (kg/m <sup>3</sup> )	Specific Heat <sup>c</sup> (kJ/kg.K)	Ads. Heat <sup>d</sup> (kJ/mol)	Ads. Capacity <sup>e</sup> (g/kg)
FULL-TSA	AA/H <sub>2</sub> O	769 <sup>a</sup>	1.00	48.6	64
	MS/CO <sub>2</sub>	640 <sup>b</sup>	0.92	34.3	51
SS-TSA /	MS/H <sub>2</sub> O	640 <sup>b</sup>	0.92	51.5	83
SS-TSA-HI	MS/CO <sub>2</sub>			34.3	51

<sup>a</sup> BASF, F-200 Activated-Alumina for liquid/gas drying, 2009; <sup>b</sup> Alibaba, Jiu Zhou 13X Molecular Sieve: air purification, 2017; <sup>c</sup> Hahne, E. "Heat storage media". In: Ullmann's Encyclopedia of Industrial Chemistry, 2005; <sup>d</sup> Rege et al. [31]; <sup>e</sup>  $T_{ADs}=15^{\circ}C$  (Design T).

### 4.3. Exergy Analysis

The exergy flow rate of a material stream represents the maximum rate of work obtainable when the stream reaches equilibrium with RER. Power streams represent pure exergy streams, while the exergy equivalent of a heat stream corresponds to equivalent power produced by a Carnot machine fed with the heat stream and connected to the RER. In this sense, the exergy analysis of a system involves evaluating the exergy flow rate of all input/output material and energy streams using the RER definition.

#### 4.3.1. Theoretical Aspects

Fig. 4.4 depicts a finite steady-state open system and its interactions (curly arrows) with reservoirs with indefinite contours. Reservoirs are infinite and in perfect internal equilibrium. They have selective boundaries allowing bidirectional flow only of their specific exchangeable quantities. Each reservoir is characterized by one or more intensive constant parameters that determine the exchange of its specific quantities like heat and species mass. Reservoirs are infinitely larger than the system, so their characteristic intensive parameters are invariant [19].

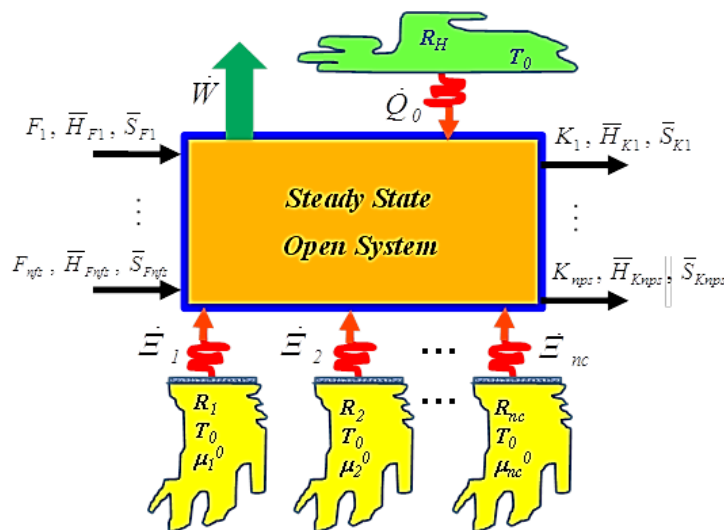


**Fig. 4.4.** Steady-state open system coupled to heat and species reservoirs.

The system of Fig. 4.4 has several feed flow rates ( $F_1, F_2, \dots, F_{nfs}$ ) and product flow rates ( $K_1, K_2, \dots, K_{nps}$ ) expressed in mol/s, where the numbers of feed/product streams are  $nfs$  and  $nps$ . The system interacts with a heat reservoir ( $R_H$ ) of constant volume and temperature  $T_0$  and with reservoirs of each species  $k$  ( $R_1, R_2, \dots, R_{nc}$ ) with constant volume at constant  $T_0$  and  $k$  chemical potential  $\mu_k^0$  ( $k=1 \dots nc$ ). The  $R_k$  reservoir interacts with the system transferring only species  $k$  with rate  $\dot{N}_k^{(R_k)}$  accompanied by energy exchange rate  $\dot{\Xi}_k$ . The heat transfer  $\dot{Q}_0$  represents the system- $R_H$  interaction. Fig. 4.4 depicts all system-reservoirs interactions, not necessarily implying system-reservoirs equilibrium. Energy, mass and work effects ( $\dot{Q}_0, \dot{\Xi}_k, \dot{N}_k^{(R_k)}, \dot{W}$ ) follow the usual 1<sup>st</sup> Law signal-convention:  $\dot{W} > 0$  when system exports;  $\dot{Q}_0 > 0, \dot{\Xi}_k > 0, \dot{N}_k^{(R_k)} > 0$  when system imports.

Relationships for exergy analysis result from the First and Second Laws of Thermodynamics. The 1<sup>st</sup> Law is written in Eq. (4.1) for the system with all streams assumed at stagnation conditions (no kinetic energy). Eqs. (4.2a) and (4.2b) represent Fundamental Relationships for reservoirs  $R_H$  and  $R_k$  from the internal equilibrium premise. Then, Eq. (4.3) results from Eq. (4.1) by applying Eqs. (4.2a) and (4.2b). Additionally, net creation rates of entropy ( $\dot{\Omega}_s$ ) and of species  $k$  ( $\dot{\Omega}_k$ ) in the Universe are written in Eqs. (4.4) and (4.5), where <sup>sys</sup> refers to the system.

$$\sum_j^{nps} K_j \bar{H}_{K_j} = \sum_j^{nfs} F_j \bar{H}_{F_j} + \sum_{k=1}^{nc} \dot{\Xi}_k + \dot{Q}_0 - \dot{W} \quad (4.1)$$

$$\dot{U}^{(R_H)} = T_0 \dot{S}^{(R_H)} = -\dot{Q}_0 \quad (4.2a)$$

$$\dot{U}^{(R_k)} = T_0 \dot{S}^{(R_k)} + \mu_k^0 \dot{N}_k^{(R_k)} = -\dot{\Xi}_k \quad (k=1 \dots nc) \quad (4.2b)$$

$$\sum_j^{nps} K_j \bar{H}_{K_j} - \sum_j^{nfs} F_j \bar{H}_{F_j} + T_0 \left( \dot{S}^{(R_H)} + \sum_{k=1}^{nc} \dot{S}^{(R_k)} \right) + \sum_{k=1}^{nc} \mu_k^0 \dot{N}_k^{(R_k)} = -\dot{W} \quad (4.3)$$

$$\dot{\Omega}_s = \dot{S}^{Sys} + \dot{S}^{(R_H)} + \sum_{k=1}^{nc} \dot{S}^{(R_k)} + \sum_j^{nps} K_j \bar{S}_{K_j} - \sum_j^{nfs} F_j \bar{S}_{F_j} \quad (4.4)$$

$$\dot{\Omega}_k = \dot{N}_k^{Sys} + \dot{N}_k^{(R_k)} + \sum_j^{nps} K_j Y_{k_{K_j}} - \sum_j^{nfs} F_j Y_{k_{F_j}} \quad (4.5)$$

Without chemical reactions species creation rates are zero ( $\dot{\Omega}_k = 0$ ). However, even with chemical reactions in the system,  $\dot{\Omega}_k = 0$  is valid provided species reservoirs are in mutual chemical equilibrium, so that molecules can be reversibly interconverted between these reservoirs without changing thermodynamic conditions of the Universe.

Since the system is at steady-state, one has  $\dot{S}^{Sys} = 0$ ,  $\dot{N}_k^{Sys} = 0$  in Eqs. (4.4) and (4.5). Substituting Eqs. (4.4) and (4.5) in Eq. (4.3), the rate of work produced by the system is written as shown in Eq. (4.6a). The maximum production of work in Eq. (4.6b) results from Eq. (4.6a) at reversible conditions with null entropy creation in the Universe ( $\dot{\Omega}_s = 0$ ). Finally, subtracting Eq. (4.6a) from (4.6b) one gets the rate of lost work ( $\dot{W}^{LOST}$ ) in Eq. (4.7). With  $\dot{\Omega}_s$  from Eq. (4.4), the lost work in Eq. (4.7) can be used to cross-check the consistency of exergy destruction rates.

$$-\dot{W} = \sum_j^{nps} K_j \left( \bar{H}_{K_j} - T_0 \bar{S}_{K_j} - \sum_{k=l}^{nc} \mu_k^0 Y_{k_{K_j}} \right) - \sum_j^{nfs} F_j \left( \bar{H}_{F_j} - T_0 \bar{S}_{F_j} - \sum_{k=l}^{nc} \mu_k^0 Y_{k_{F_j}} \right) + T_0 \dot{\Omega}_s \quad (4.6a)$$

$$-\dot{W}^{MAX} = \sum_j^{nps} K_j \left( \bar{H}_{K_j} - T_0 \bar{S}_{K_j} - \sum_{k=l}^{nc} \mu_k^0 Y_{k_{K_j}} \right) - \sum_j^{nfs} F_j \left( \bar{H}_{F_j} - T_0 \bar{S}_{F_j} - \sum_{k=l}^{nc} \mu_k^0 Y_{k_{F_j}} \right) \quad (4.6b)$$

$$\dot{W}^{LOST} = \dot{W}^{MAX} - \dot{W} = T_0 \dot{\Omega}_s \quad (4.7)$$

From Eq. (4.6b) the exergy flow rates ( $\dot{E}$ ) of feed and product streams are defined in Eqs. (4.8a) and (4.8b), so that the maximum rate of work is just given by the difference of flow rates of entering and exiting exergy in Eq. (4.8c). Returning to Eq. (4.6a), the actual overall rate of work ( $\dot{W}$ ) can be expressed as the sum of all exported rates of work minus the sum of all imported rates of work as in Eq. (4.8d) using absolute values, where  $nwe$  and  $nwi$  are the numbers of exported and imported rates of work. Analogously to Eq. (4.8c),  $\dot{W}^{LOST}$  corresponds to the rate of destroyed exergy  $\dot{E}^{DESTR}$  in Eq. (4.8e). Eqs. (4.8a), (4.8b), (4.8d), (4.8e) and (4.7) are then used to rewrite Eq. (4.6a) – which represents the actual system behavior – as Eq. (4.8f). Redefining terms in Eq. (4.8f) as shown in Eq. (4.8g), Eq. (4.8f) is finally rewritten as Eq. (4.8h). It must be noticed that exergy flow rates ( $\dot{E}$ ) are relative to the Reference Environmental Reservoir (RER), which corresponds to the union of reservoirs  $R_H, R_1, R_2, \dots, R_{nc}$  (Fig. 4.4).

$$\dot{E}_{F_j} \equiv F_j \left( \bar{H}_{F_j} - T_0 \bar{S}_{F_j} - \sum_{k=1}^{nc} \mu_k^0 Y_{k_{F_j}} \right) \quad (4.8a)$$

$$\dot{E}_{K_j} \equiv K_j \left( \bar{H}_{K_j} - T_0 \bar{S}_{K_j} - \sum_{k=1}^{nc} \mu_k^0 Y_{k_{K_j}} \right) \quad (4.8b)$$

$$\dot{W}^{MAX} = \sum_j^{nfs} \dot{E}_{F_j} - \sum_j^{nps} \dot{E}_{K_j} \quad (4.8c)$$

$$\dot{W} \equiv \sum_j^{nwe} |\dot{W}_j^{Exported}| - \sum_{j=1}^{nwi} |\dot{W}_j^{Imported}| \quad (4.8d)$$

$$\dot{W}^{LOST} = T_0 \dot{\Omega}_S \equiv \dot{E}^{DESTR} \quad (4.8e)$$

$$\sum_j^{nfs} \dot{E}_{F_j} + \sum_j^{nwi} |\dot{W}_j^{Imported}| = \sum_j^{nps} \dot{E}_{K_j} + \sum_j^{nwe} |\dot{W}_j^{Exported}| + \dot{E}^{DESTR} \quad (4.8f)$$

$$\dot{E}^{IN} \equiv \sum_j^{nfs} \dot{E}_{F_j} + \sum_j^{nwi} |\dot{W}_j^{Imported}| \quad ; \quad \dot{E}^{OUT} \equiv \sum_j^{nps} \dot{E}_{K_j} + \sum_j^{nwe} |\dot{W}_j^{Exported}| \quad (4.8g)$$

$$\dot{E}^{IN} = \dot{E}^{OUT} + \dot{E}^{DESTR} \quad (4.8h)$$

In the second part of Eq. (4.8g) there is a wasted exergy term associated to product streams discarded in the environment. This term is isolated in Eq. (4.9a), where “ $Wr$ ” represents the  $r^{th}$  waste-product stream and  $nwps$  is the number of waste-product streams. In Eq. (4.8h) one always have  $\dot{E}^{IN} \geq \dot{E}^{OUT}$  and  $\dot{E}^{DESTR} \geq 0$ , which allows to define the exergy efficiency in Eq. (4.9b) using Eq. (4.9a).

$$\dot{E}_{WASTE}^{OUT} = \sum_r^{nwps} \dot{E}_{W_r} \quad (4.9a)$$

$$\varepsilon = \frac{\dot{E}^{OUT} - \dot{E}_{WASTE}^{OUT}}{\dot{E}^{IN}} = \frac{\dot{E}^{IN} - \dot{E}^{DESTR} - \dot{E}_{WASTE}^{OUT}}{\dot{E}^{IN}} \quad (4.9b)$$

All terms in exergy formulas Eqs. (4.8a), (4.8b) and (4.8g) are retrieved from process simulations. The only exceptions are RER parameters  $T_0, \mu_k^0$ , which do not belong to process streams and depend on the RER definition. In this work two RER definitions are used – RER#1 and RER#2 – which are discussed in next subsections.

### 4.3.2. RER#1

RER#1 consists of atmospheric air at  $T_0=25^\circ\text{C}$  and  $P_0=1\text{ atm}$  with  $RH=60\%$  and molar composition  $N_2=76.61\%$ ,  $O_2=20.55\%$ ,  $Ar=0.91\%$ ,  $H_2O=1.89\%$ , and  $CO_2=363\text{ppm-mol}$ . The conditions of RER#1 are the same of the PPU air feed (Sec. 4.2.1).  $\mu_k^0$  represents the chemical potential of species  $k$  in RER#1 with molar fraction  $Y_k^0$ . As HYSYS do not export chemical potentials,  $\mu_k^0$  is calculated using the fact that RER#1 represents an ideal gas mixture. Thus pure component streams are created in HYSYS for  $N_2$ ,  $O_2$ ,  $Ar$  and  $CO_2$  at  $(T_0, P_0)$  – which are also ideal gases – with the respective chemical potentials calculated from the molar enthalpy and entropy exported by HYSYS in Eq. (4.10a).  $\mu_k^0$  follows via an isothermal and isobaric ideal gas transition to RER#1 composition in Eq. (4.10b).

$$\mu_k(T_0, P_0, \text{pure } k) = \bar{H}(T_0, P_0, \text{pure } k) - T_0 \bar{S}(T_0, P_0, \text{pure } k) \quad \{k \neq H_2O\} \quad (4.10a)$$

$$\mu_k^0 = \mu_k(T_0, P_0, \text{pure } k) + RT_0 \ln Y_k^0 \quad (4.10b)$$

As pure  $H_2O$  is a liquid at  $(T_0, P_0)$ , a stream of pure water is created in HYSYS at  $T_0$  and at sufficient low pressure  $P^*=0.01\text{ atm}$  such that an ideal gas state is valid. At  $(T_0, P^*)$  the chemical potential of  $H_2O$  is calculated with the molar enthalpy and entropy exported by HYSYS in Eq. (4.10c).  $\mu_{H_2O}^0$  follows via an isothermal ideal gas transition to RER#1 composition and pressure in Eq. (4.10d).

$$\mu_{H_2O}(T_0, P^*, \text{pure } H_2O) = \bar{H}(T_0, P^*, \text{pure } H_2O) - T_0 \bar{S}(T_0, P^*, \text{pure } H_2O) \quad (4.10c)$$

$$\mu_{H_2O}^0 = \mu_{H_2O}(T_0, P^*, \text{pure } H_2O) + RT_0 \ln \left( \frac{P_0 Y_{H_2O}^0}{P^*} \right) \quad (4.10d)$$

### 4.3.3. RER#2

RER#2 is chosen as a two-phase environment at  $T_0=25^\circ\text{C}$  and  $P_0=1\text{ atm}$  containing the same dry-basis atmospheric air as before, but with excess of water so that an infinite body of liquid water coexists in equilibrium. The air phase is now saturated in water, with molar composition  $N_2=75.65\%$ ,  $O_2=20.30\%$ ,  $Ar=0.90\%$ ,  $H_2O=3.11\%$  and  $CO_2=358\text{ppm-mol}$ .

For all species  $k \neq H_2O$ , the RER#2 chemical potentials ( $\mu_k^0$ ) are calculated as in RER#1 using Eqs. (4.10a) and (4.10b) with new molar fractions  $Y_{N_2}^0 = 0.7565$ ,  $Y_{O_2}^0 = 0.2030$ ,  $Y_{Ar}^0 = 0.0090$

and  $Y_{CO_2}^0 = 0.000358$ . For water, since it is in VLE with air, the  $\mu_{H_2O}^0$  in RER#2 is obtained by creating in HYSYS a stream of pure liquid water at  $(T_0, P_0)$  whose exported molar enthalpy and entropy are used as shown in Eq. (4.11).

$$\mu_{H_2O}^0 = \bar{H}_L(T_0, P_0, \text{pure } H_2O) - T_0 \bar{S}_L(T_0, P_0, \text{pure } H_2O) \quad (4.11)$$

#### 4.3.4. RER#1 versus RER#2

Table 4.2 lists chemical potentials of species in RER#1 and RER#2 for exergy analysis of PPU's using HYSYS 8.8 with PR-EOS.

$\mu_{H_2O}^0$  increases from RER#1 to RER#2 due to higher water content in air, while  $\mu_k^0$   $k \neq H_2O$  behave oppositely. Consequently, CW and ChW streams should present lower exergy flow rate with RER#2 formalism relatively to RER#1 formalism, while the exergy flow rate of dry air is higher with RER#2 formalism.

**Table 4.2.** RER#1 and RER#2 chemical potentials of species.

<i>Species</i>	$\mu_k^0$ (kJ/mol)	
	<i>RER#1</i>	<i>RER#2</i>
<b>N<sub>2</sub></b>	-44.81345	-44.84447
<b>O<sub>2</sub></b>	-47.16142	-47.19244
<b>Ar</b>	-47.40285	-47.43387
<b>CO<sub>2</sub></b>	-464.8654	-464.8965
<b>H<sub>2</sub>O</b>	-303.4369	-302.2325

Figs. 4.5a-4.5c depict the respective exergy flow rates of 1 kmol/h of pure water, dry air, and saturated-air at  $P=P_0$  and for several temperatures in the vicinity of  $T_0$  according to RER#1 and RER#2 formalisms. Calculations were done with HYSYS 8.8 using PR-EOS. In the saturated-air case (Fig. 4.5c), the temperature range actually expresses water dew-point range with varying H<sub>2</sub>O content according to the dew-point. A characteristic of Figs. 4.5a-4.5c is that the exergy flow rate must pass through zero at  $T=T_0$  for streams in equilibrium with RER. This occurs in Fig. 4.5a for pure water at  $T=T_0=25^\circ C$  with RER#2 and in Fig. 4.5c for saturated-air at  $T=T_0=25^\circ C$  with RER#2. In Fig. 4.5a, RER#1 prescribes positive exergy flow rates everywhere so that in terms of exergy ratio, the contrast between RER#1 and RER#2 deepens in the vicinity of  $T=T_0=25^\circ C$ . On the other hand, Fig. 4.5b shows an inverted scenario for dry air, with greater RER#2 exergy flow rate relatively to RER#1, which is reasonable since dry air is thermodynamically more distant from  $RH=100\%$  air (RER#2) than from  $RH=60\%$  air (RER#1).

Contrarily to Figs. 4.5a-4.5b, with fixed composition so that exergy flow rate relies only on physical exergy contribution, in Fig. 4.5c RER#1 exergy flow rate decreases when approaching RER#1 composition, so the minimum RER#1 exergy flow rate is situated between  $T_0$  and the dew-point of RER#1 composition ( $\approx 17^\circ\text{C}$ ). Therefore, Fig. 4.5c presents for saturated-air minimum zero RER#2 exergy flow rate at  $T=T_0=25^\circ\text{C}$  and minimum RER#1 exergy flow rate at  $T\approx 20^\circ\text{C}$ . The chemical exergy contribution of  $\text{H}_2\text{O}$  is also clearly revealed on the right side of both RER#1 and RER#2 exergy flow rate curves associated to rapid increase of water content in saturated-air as temperature increases.

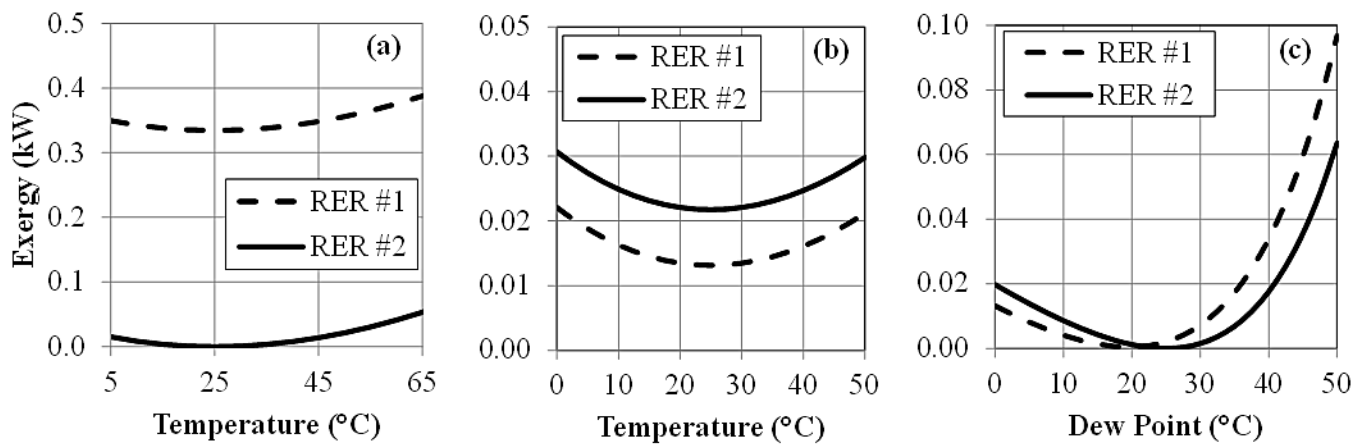


**Fig. 4.5.** Exergy flow rate of 1 kmol/h streams at  $P=P_0=1 \text{ atm}$  for RER#1 and RER#2: (a) pure water; (b) dry air; (c) saturated-air.

## 4.4. Results

Results are presented for PPU's FULL-TSA, SS-TSA and SS-TSA-HI in terms of power and heat consumptions and exergy analysis considering RER#1 and RER#2 formalisms.

### 4.4.1. Power/Heat Consumptions and SS Performance

The utility consumptions of FULL-TSA, SS-TSA and SS-TSA-HI are presented in Table 4.3, while Table 4.4 shows the respective power consumptions discriminating contributions from MAC, blowers and pumps. Table 4.5 presents SS design and performance data in SS-TSA and SS-TSA-HI from simulation results and specifications (assumption [A14]).

Tables 4.4-4.5 show that high SS pressure-recovery slightly increases MAC power in SS-TSA and SS-TSA-HI, but such increase is partially offset by power savings in other units. In both SS-TSA/SS-TSA-HI  $\text{N}_2$  flow rate for TSA regeneration is 64% lower relatively to FULL-TSA, entailing proportional power savings in  $\text{N}_2$  blower (Table 4.4). SS-TSA-HI has lower CW circulation thanks to the WW closed-loop through MAC intercooler leaving at

90°C (assumption [A10]) and subsequently cooled down to 30°C after heating regeneration N<sub>2</sub> from Cold-Box; consequently lowering cooling-tower load and power consumption in CW-System (CW pumps and cooling-tower fans, Table 4.4).

**Table 4.3.** Utilities consumption.

	<i>FULL-TSA</i>	<i>SS-TSA</i>	<i>SS-TSA-HI</i>
<i>Power(MW)</i>	15.42	15.49	15.44
<i>LPS(MW)</i>	1.370	0.161	---
<i>CW(kg/s)</i>	5.590	5.364	5.267

**Table 4.4.** Power consumption.

	<i>FULL-TSA</i>	<i>SS-TSA</i>	<i>SS-TSA-HI</i>
<i>MAC(MW)</i>	14.79	14.98	14.98
<i>N<sub>2</sub> Blower(MW)</i>	0.18	0.06	0.06
<i>CW Air Fan(MW)</i>	0.13	0.13	0.11
<i>CW Pumps(MW)</i>	0.31	0.31	0.28
<i>ChW Pumps(MW)</i>	0.01	0.01	0.01

Among several SS benefits, the main advantage of SS-TSA/SS-TSA-HI over FULL-TSA relies on reduced LPS consumption (Table 4.3), saving 88% ( $\approx 1.2$  MW) in SS-TSA, since SS performs  $\approx 98.65\%$  water removal (Table 4.5), leaving only  $\approx 56$  ppmH<sub>2</sub>O, drastically reducing TSA load. Consequently, SS-TSA/SS-TSA-HI only require a small single-bed MS-TSA as CO<sub>2</sub> becomes the main adsorbate since SS CO<sub>2</sub> capture is negligible. Another SS benefit is lower water make-up in CW-System due to water recovery from air, injected as super-cooled stagnated liquid ( $-34.17^\circ\text{C}$ , Table 4.5) into ChW stream, saving  $\approx 0.226$  kg/s in SS-TSA/SS-TSA-HI. Additionally, no LPS consumption occurs in SS-TSA-HI because closed-loop WW heats MS-TSA regeneration N<sub>2</sub>, entailing even lower water make-up by reducing CW circulation and cooling-tower evaporation. These aspects positively influence the exergy efficiency of SS-TSA/SS-TSA-HI over FULL-TSA, despite their slightly higher power consumption.

The keystone of SS is its 98.59% pressure-recovery for 98.65% water removal, consequence of choosing low maximum supersonic  $Ma$  ( $Ma^{Shock}=1.20$ ). SS pressure-recovery is also sensitive to the withdrawn condensate-fraction, so the low 0.38% condensate-fraction ( $\beta^{Shock}\%=99.62\%$ , Table 4.5) contributes to high pressure-recovery. SS-TSA/SS-TSA-HI superiority relies on low SS head-loss, otherwise LPS savings would be eclipsed by high MAC power demand. Thermodynamic transitions in SS operation for air dehydration are briefly graphically discussed as follows. Further details of SS performance in SS-TSA and SS-TSA-HI are found in [9].

**Table 4.5.** SS design and performance in SS-TSA and SS-TSA-HI.

Specified items		Calculated by SS-UOE	
No. of SS's	1	$D_T(m)$	0.4267
$D_I(m)$	0.8679	$L_C(m)$	0.9813
$D_O(m)$	0.6943	$L_D(m)$	2.878
$\alpha$	12.67°	$L(m)$	3.859
$\beta$	2.66°	$L^{Shock}(m)$	1.051
$Ma^{Shock}$	1.20	$L^{Diffuser}(m)$	2.808
$\eta^{EXP}\%$	100	$P_{BS}(bar)$	1.299 <sup>#</sup>
$\eta^{CMP}\%$	100	$T_{BS}(^{\circ}C)$	-48.86 <sup>#</sup>
$P^{Inlet}(bar)$	3.165	$Ma_{BS}$	1.195 <sup>#</sup>
$T^{Inlet}(^{\circ}C)$	10.0	$\beta^{Shock}\%$	99.62% <sup>&amp;</sup>
$MMsm^3/d$	7.72	$P^{Outlet}(bar)$	3.12
$ppmH_2O^{Inlet}$	3965	$T^{Outlet}(^{\circ}C)$	16.48*
$ppmCO_2^{Inlet}$	367	%H <sub>2</sub> O Recovery	98.65%
		%P Recovery	98.59%
		$T^{Condensate}(^{\circ}C)$	-34.17*

\*Stagnation ( $P=3.12$  bar). <sup>&</sup> $\beta^{Shock}$ : pre-shock molar vapor-fraction.

<sup>#</sup><sub>BS</sub>: before shock, after liquid withdrawal.

Figs. 4.6a/4.6b/4.6c depict SS path on  $P \times T$  and  $T \times \bar{S}$  planes with several water dew-point (WDP) loci traced (3886ppmH<sub>2</sub>O inlet air, 1000ppmH<sub>2</sub>O air, 300ppmH<sub>2</sub>O air and 56.4ppmH<sub>2</sub>O outlet dry-air), where Fig. 4.6c magnifies Fig. 4.6b. SS path is marked with points A/B/C/D/E correspondingly plotted on  $P \times T$  and  $T \times \bar{S}$  planes. The importance of  $T \times \bar{S}$  plane derives from the adiabatic character of SS operation, which validates  $T \times \bar{S}$  plots as instances of certification of 2<sup>nd</sup> Law obedience of SS simulations. SS path starts at “A” on the WDP locus of the water-saturated air feed. It expands isentropically downwards (A→B, Figs. 4.6b/4.6c/4.6a) to point “B” slightly beneath the  $T \times \bar{S}$  WDP locus (56.4ppmH<sub>2</sub>O air) in equilibrium with 0.38% of liquid ( $\beta\%^{Shock}=99.62\%$ ). “B” and “C” ( $T_B=T_C=T_{BS}=-48.86^{\circ}C$ ) are the coldest SS points ( $Ma=Ma^{Shock}=1.20$ ) at pre-shock. Withdrawing low-entropy condensate, SS path moves isothermally to the right (B→C, Figs. 4.6b/4.6c) towards the higher molar entropy of WDP dry-air. “B” and “C” have same ( $P, T$ ) coordinates ( $P \times T$ , Fig. 4.6a). “C” dry-air is still supersonic with  $Ma_{BS}=1.195$  after condensate withdrawal, leading to normal shock (C→D). Shock C→D is the unique entropy-creator step in SS path as expansion and after-shock compression are isentropic (assumption [A14], but SS-UOE can handle non-isentropic expansion/compression if  $\eta^{EXP}\%<100\%$  and/or  $\eta^{CMP}\%<100\%$ ). Across the shock sudden heating, recompression and entropy-creation occur as an inclined linear path C→D ( $\Delta T > 0$ ,  $\Delta \bar{S} > 0$ ) on Figs. 4.6a/4.6b/4.6c. The after-shock SS path is again isentropic, extending upwardly (D→E, Figs. 4.6a/4.6b/4.6c) recompressing and heating dry-air in the diffuser towards the SS outlet, and beyond, until stagnation.

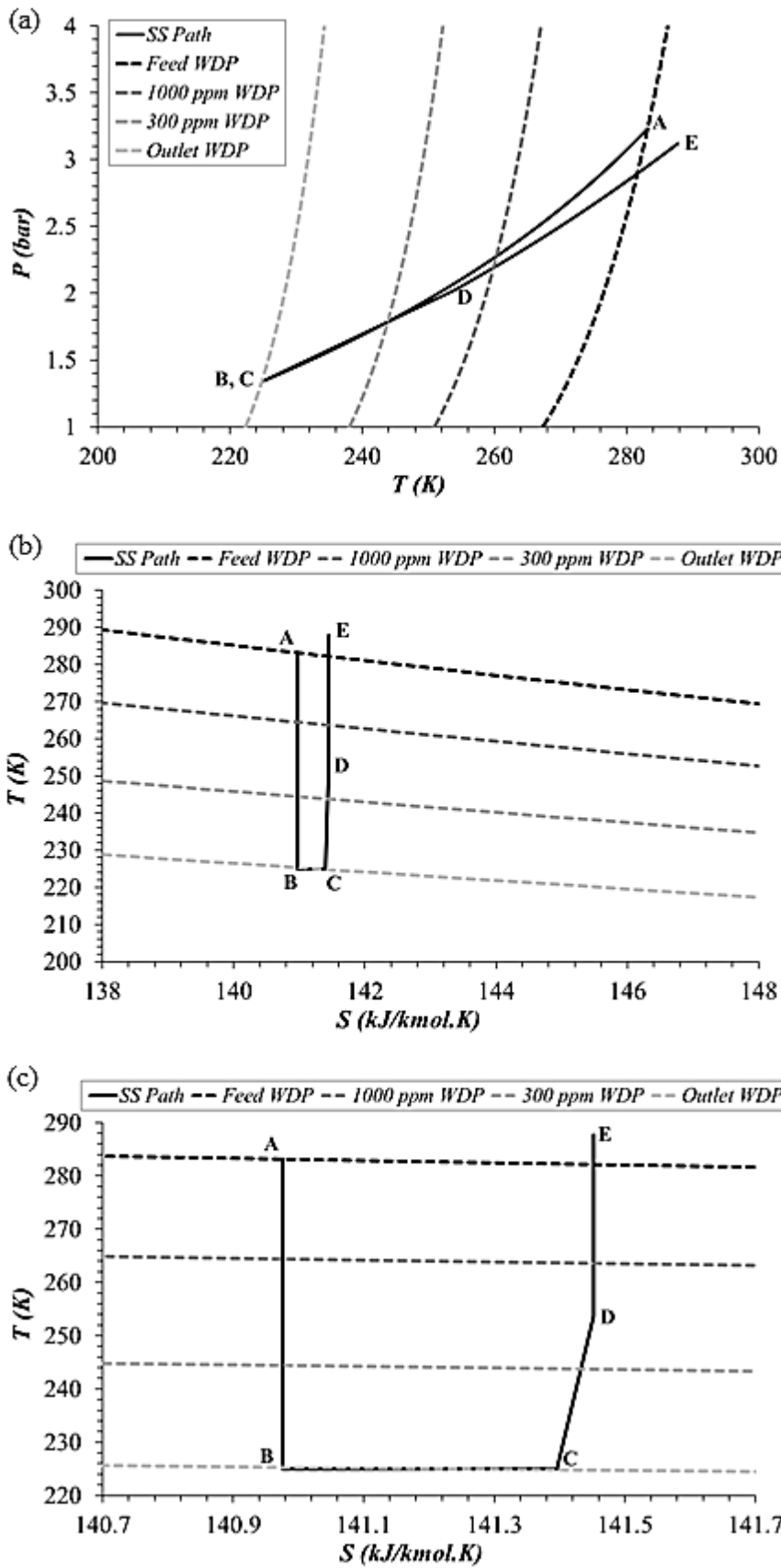


**Fig. 4.6.** Air dehydration SS path with WDP loci of 3886 ppmH<sub>2</sub>O inlet-air, 1000 ppmH<sub>2</sub>O air, 300 ppmH<sub>2</sub>O air and 56.4 ppmH<sub>2</sub>O outlet dry-air: (a) plane  $P \times T$ ; (b) plane  $T \times \bar{S}$ ; (c) magnification of (b).

#### 4.4.2. Exergy Analysis

Table 4.6 exhibits results of exergy analysis using RER#1 and RER#2 formalisms for all flowsheets and sub-flowsheets, including exergy inlet flow rates, exergy destruction rates, waste exergy flow rates and exergy efficiency ( $\epsilon$ ). All exergy flow rates are positive as they should be.

With RER#1, all sub-flowsheets efficiencies are greater than 84.6%, with CW-System attaining 93.5%, giving the wrong impression that these processes operate relatively close to thermodynamic reversibility. On the other hand, RER#2 produces lower efficiencies, the most remarkable contrast being the CW-System, with efficiency of 16.4%, a realistic estimative. The higher efficiencies obtained with RER#1 are directly connected to large exergy flows of CW, boosting efficiencies of some sub-flowsheets. RER#2 caused a clear reduction in the inlet exergy flow rates of the same sub-flowsheets, particularly in CW-System, from 30.11 to 1.15 MW (Table 4.6). RER#2 naturally reduces the exergy flow rate of liquid water as illustrated in Fig. 4.5a, lowering the exergy flows of CW-System as it operates nearby  $T_0$  (assumptions [A9-A10]).

Exergy Sankey diagrams for SS-TSA-HI overall system are shown in Figs. 4.7a-4.7b, with no CW streams crossing the system boundaries, excepting a CW make-up stream with small exergy flow rate. The same situation occurs in FULL-TSA and SS-TSA (Table 4.6).

Figs. 4.8a-4.8j present exergy Sankey diagrams for sub-systems of SS-TSA-HI (Figs. 4.8a-4.8e for RER#1 and Figs. 4.8f-4.8j for RER#2) with colors: yellow for power streams; blue for material streams with useable exergy, and red for exergy destruction or material wasted exergy. Comparison of results for RER#1 and RER#2 shows drastic shrinkage of CW/WW exergy flow rates with RER#2. Appendices W2 and W3 respectively present analogues of Figs. 4.7 and 4.8 for PPU's FULL-TSA and SS-TSA.

In Figs. 4.8a-4.8j all inlet and outlet exergy flow rates are disclosed, showing small enlargement of exergy flow rates of raw air in RER#2. Since no condensation occurs in MAC intercooler, the compressed air discharge has the same composition of air intake, which is equal to RER#1 composition, so that exergy flow rates are expected to be smaller with RER#1 formalism. Moreover, DCA cold air outlet (SS feed) is water-saturated but has much lower H<sub>2</sub>O content than saturated-air at  $(T_0, P_0)$ , therefore its exergy flow rate with RER#2 is closer to the analogous value with RER#1. Fig. 4.5c shows that even at atmospheric pressure, the exergy of saturated air at  $T=10^\circ\text{C}$  is smaller in RER#1 and similarly in Fig. 4.5b for dry air. Thus, the dry compressed air leaving the TSA system must also have smaller exergy flow rate with RER#1. All these aspects are exhibited by the present results of exergy analysis.

#### 4.4.3. Validation of Exergy Analysis via Cross-Check of Consistency

Table 4.7 presents comparison between exergy destruction rate in Eq. (4.8f) and the lost work rate from  $T_0 \dot{\Omega}_s$  in Eqs. (4.7) and (4.5).

Exergy destruction rate and lost work rate must have the same value, but are calculated through completely different ways. From the outset, Eqs. (4.5) does not depend on RER#1/RER#2 properties and demand only the determination of molar entropy values of feed/product streams crossing the system boundaries because the following terms in Eq. (4.5) are identically zero:  $\dot{S}^{Sys} = 0$  (steady-state),  $\dot{S}^{(R_H)} = 0$  (no heat exchange across process boundaries) and  $\sum_{k=1}^{nc} \dot{S}^{(R_k)} = 0$  (no species exchange across process boundaries).

On the other hand, Eq. (4.8f) demands exergy flow rates of power streams and of feed/product streams crossing the system boundaries, where the material exergy flow rates depend on properties of RER#1 or RER#2. Despite the presence of RER properties in the exergy flow rates of feed/product streams, actually the exergy destruction rate depends on certain RER parameters ( $T_0$ ) but not on the differences between RER#1 and RER#2 as can be seen in Table 4.6. Thus, as occur in several other similar validations of consistency in Thermodynamics (e.g. Gibbs-Duhem consistency test), the concordance of these two determinations of the lost work rate should attest the consistency of the whole procedure of exergy analysis. These comparisons are done in Table 4.7 for all sub-systems and the overall system of FULL-TSA, SS-TSA and SS-TSA-HI with RER#1 and RER#2. Results show very low discrepancies below 0.25%, indicating consistency of the present exergy analyses of PPU.

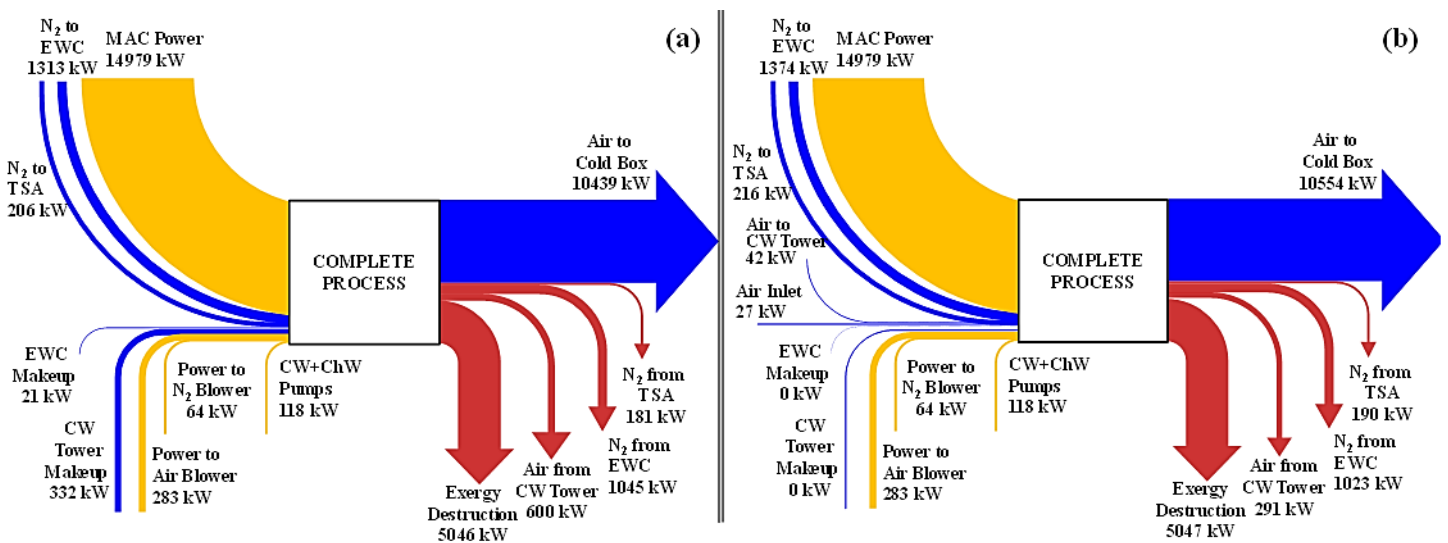
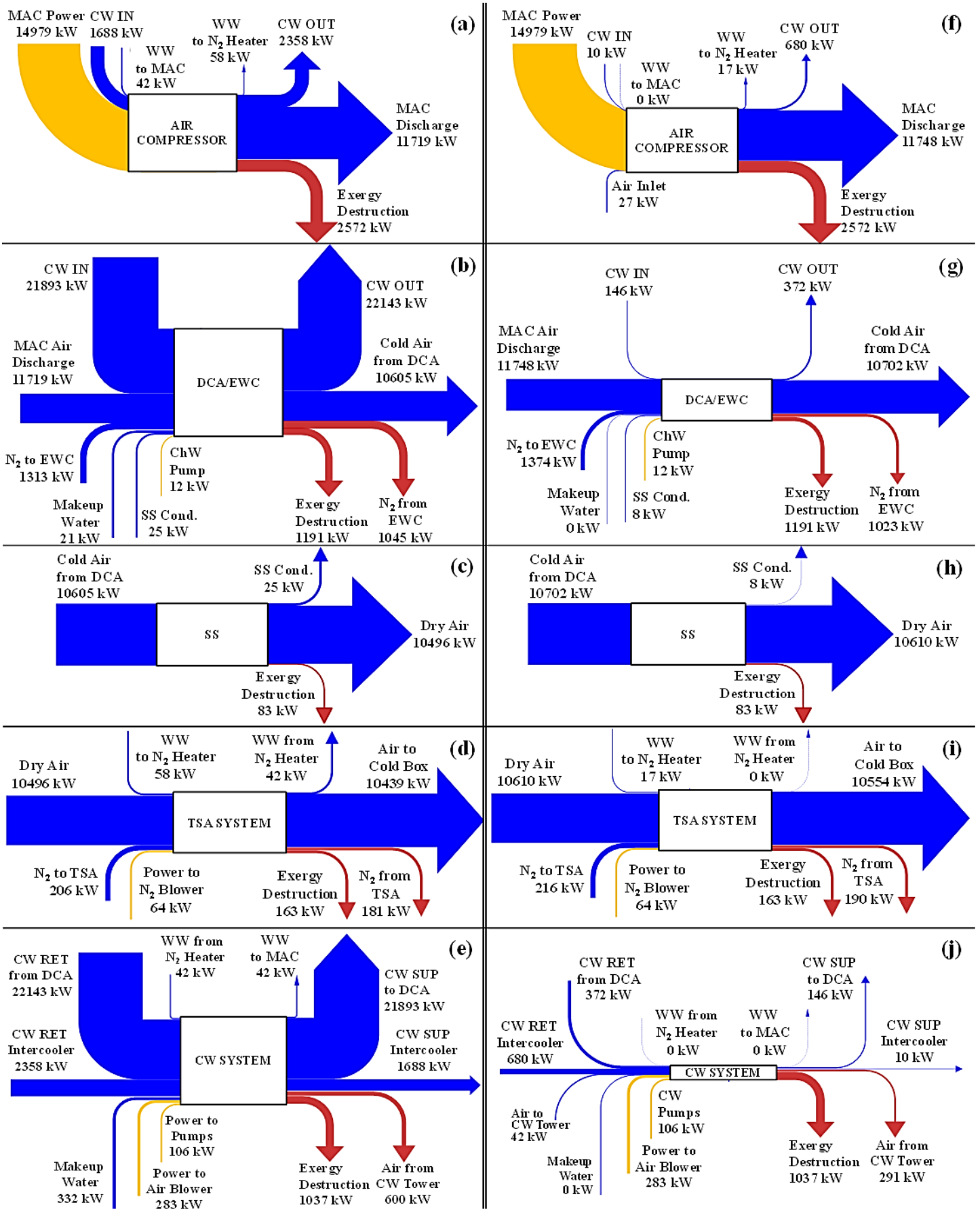


Fig. 4.7. SS-TSA-HI overall exergy Sankey diagram: (a) RER#1; (b) RER#2.



**Fig. 4.8.** SS-TSA-HI exergy Sankey diagrams: (a)-(e) RER#1, (f)-(j) RER#2 (RET=return, SUP=supply, REG=regeneration).

**Table 4.6.** Exergy Analysis of FULL-TSA, SS-TSA and SS-TSA-HI with RER#1 and RER#2. Sub-systems and overall system.

RER	System	Inlet Exergy(MW)			Exergy Destruction (MW)			Waste Exergy (MW)			Exergy Efficiency (%)		
		FULL TSA	SS TSA	SS TSA HI	FULL TSA	SS TSA	SS TSA HI	FULL TSA	SS TSA	SS TSA HI	FULL TSA	SS TSA	SS TSA HI
RER#1	MAC+Intercooler	21.74	21.93	16.71	2.98	3.00	2.57	0.00	0.00	0.00	86.3	86.3	84.6
	DCA/EWC	34.86	34.98	34.98	1.17	1.19	1.19	1.08	1.05	1.05	93.5	93.6	93.6
	SS	-	10.60	10.60	-	0.08	0.08	-	0.00	0.00	-	99.2	99.2
	TSA-System	11.71	10.82	10.82	0.70	0.19	0.16	0.47	0.18	0.18	90.0	96.6	96.8
	CW-System	30.11	30.13	25.26	0.70	0.71	1.04	0.56	0.57	0.60	95.8	95.7	93.5
	Overall System	18.20	17.42	17.31	5.55	5.17	5.05	2.12	1.80	1.83	57.9	60.0	60.3
RER#2	MAC+Intercooler	14.86	15.05	15.02	2.98	3.00	2.57	-	0.00	0.00	80.0	80.1	82.9
	DCA/EWC	13.16	13.29	13.29	1.17	1.19	1.19	1.06	1.02	1.02	83.1	83.3	83.3
	SS	-	10.70	10.70	-	0.08	0.08	-	0.00	0.00	-	99.2	99.2
	TSA-System	11.79	10.94	10.91	0.70	0.19	0.16	0.48	0.19	0.19	90.0	96.5	96.8
	CW-System	1.15	1.16	1.48	0.70	0.71	1.04	0.26	0.26	0.29	16.4	16.2	10.5
	Overall System	17.95	17.21	17.10	5.55	5.17	5.05	1.80	1.48	1.50	59.1	61.4	61.7

**Table 4.7.** Exergy analysis cross-check: exergy destruction rate versus lost work rate ( $T_0\dot{Q}_s$ ).

RER	System	Lost Work Rate $T_0\dot{Q}_s$ (MW)			Exergy Destruction Rate (MW)			Discrepancy (%)		
		FULL TSA	SS-TSA	SS-TSA HI	FULL TSA	SS-TSA	SS-TSA HI	FULL TSA	SS-TSA	SS-TSA HI
RER#1	MAC+Intercooler	2.98	3.00	2.57	2.98	3.00	2.57	0.00	0.00	0.00
	DCA/EWC	1.17	1.19	1.19	1.17	1.19	1.19	0.24	0.11	0.02
	SS	-	0.08	0.08	-	0.08	0.08	-	-0.08	-0.08
	TSA-System	0.70	0.19	0.16	0.70	0.19	0.16	0.00	0.01	0.05
	CW-System	0.70	0.71	1.04	0.70	0.71	1.04	0.00	0.00	0.09
	Overall System	0.70	0.19	0.16	5.55	5.17	5.05	0.05	0.03	0.02
RER#2	MAC+Intercooler	2.98	3.00	2.57	2.98	3.00	2.57	0.00	0.00	0.00
	DCA/EWC	1.17	1.19	1.19	1.17	1.19	1.19	0.24	0.11	0.02
	SS	-	0.08	0.08	-	0.08	0.08	-	-0.08	-0.08
	TSA-System	0.70	0.19	0.16	0.70	0.19	0.16	0.00	0.01	0.05
	CW-System	0.70	0.71	1.04	0.70	0.71	1.04	0.00	0.00	0.10
	Overall System	0.70	0.19	0.16	5.55	5.17	5.05	0.05	0.03	0.02

## 4.5. Discussion on Exergy Performance and RER Comparison

Discussion is sub-system/system oriented with support of Table 4.6 and Figs. 4.8a-4.8j.

### 4.5.1. MAC+Intercooler

Exergy destruction is slightly higher in SS-TSA ( $\dot{E}^{DESTR} = 3MW$ ) relatively to FULL-TSA ( $\dot{E}^{DESTR} = 2.98MW$ ) due to small increase of MAC power – from  $14.79 MW$  to  $14.98 MW$  – caused by SS head-loss ( $4.5 kPa$ ). The greater exergy destruction in this case is consequence of two slightly greater irreversibilities: MAC higher compression-ratio with  $\eta^{MAC} = 85\%$  (assumption [A12]) and greater temperature difference in MAC intercooler. Since shaft-work exergy is not RER dependent, exergy inlet flow rate is  $0.19 MW$  higher in SS-TSA with both RER#1/RER#2. However, the best MAC+Intercooler performance belongs to SS-TSA-HI ( $\dot{E}^{DESTR} = 2.57MW$ ) due to less irreversible heat exchange in MAC intercooler thanks to lower temperature difference:  $90^\circ C$  WW+CW outlet (assumption [A10]), contrasting to  $45^\circ C$  CW outlet (assumption [A9]) in FULL-TSA/SS-TSA. Additionally, CW+WW flow rate through MAC intercooler is  $75\%$  lower relatively to FULL-TSA/SS-TSA, entailing significant lower inlet exergy flow rate with RER#1 –  $16.71MW$  vs  $21.74MW / 21.93MW$  for FULL-TSA/SS-TSA – while with RER#2 the corresponding values are  $15.02MW$  vs  $14.86MW / 15.05MW$  for FULL-TSA/SS-TSA.

Comparison of MAC+Intercooler of FULL-TSA, SS-TSA and SS-TSA-HI, reveals an illusory worst efficiency of SS-TSA-HI with RER#1. This results from apparent efficiency increase of FULL-TSA/SS-TSA due to relative eclipsing of their greater exergy destruction rates by large exergy inlet flow rates, indicating RER#1 as a bad RER choice for MAC+Intercooler. Meanwhile, RER#2 unveils the best performance of SS-TSA-HI:  $82.9\%$  efficiency against  $80.0\%$  in FULL-TSA and  $80.1\%$  in SS-TSA. Figs. 4.8a/4.8f show MAC+Intercooler inlet/outlet exergy flow rates of SS-TSA-HI, respectively with RER#1 and RER#2, evidencing clearer predominance of power exergy with RER#2.

### 4.5.2. DCA/EWC

Minor exergy flow differences are found among FULL-TSA, SS-TSA and SS-TSA-HI. With RER#1 SS-TSA/SS-TSA-HI performed identically with slightly greater exergy destruction relatively to FULL-TSA –  $\dot{E}^{DESTR} = 1.19MW$  vs  $\dot{E}_{FULL-TSA}^{DESTR} = 1.17MW$  – which is offset by SS-TSA/SS-TSA-HI lower waste exergy –  $\dot{E}_{WASTE}^{OUT} = 1.05MW$  vs  $\dot{E}_{WASTE, FULL-TSA}^{OUT} = 1.08MW$ . Due

to slightly higher MAC discharge pressure in SS-TSA/SS-TSA-HI relatively to FULL-TSA ( $3.165\text{ bar}$  vs  $3.12\text{ bar}$ ) air at higher temperature ( $100^\circ\text{C}$  vs  $98^\circ\text{C}$ ) feeds DCA/EWV for the same  $10^\circ\text{C}$  target (assumption [A8]), explaining SS-TSA/SS-TSA-HI higher inlet exergy flow rate with RER#2 –  $\dot{E}^{IN} = 13.29\text{ MW}$  vs  $\dot{E}_{FULL-TSA}^{IN} = 13.16\text{ MW}$ . On the other hand, SS injection of super-cooled condensate into ChW to DCA/EWC lowers EWC heat duty, reducing  $\approx 3.6\%$  of  $\text{N}_2$  feed and water evaporation, lowering wet  $\text{N}_2$  from EWC and its waste exergy flow rate. The high CW flow rate leads to high CW inlet exergy flow rate with RER#1 – almost twice the compressed air exergy flow rate – shown in Fig. 4.8b for SS-TSA/SS-TSA-HI, inflating efficiency to  $\approx 93.5\%$ , while with RER#2 CW exergy flow rate shrinks making hot compressed air the major exergy inlet flow rate, downing efficiencies to  $83.1\text{-}83.3\%$ .

#### 4.5.3. SS

Figs. 4.8c/4.8h depict exergy flows across SS sub-system of SS-TSA/SS-TSA-HI, as SS has identical operating conditions in SS-TSA/SS-TSA-HI. SS presents minute  $\dot{E}^{DESTR} = 0.08\text{ MW}$  and high  $\varepsilon = 99.2\%$ , as entropy is only created at normal shock, since isentropic flow is assumed through SS converging-diverging sections from  $\eta^{CMP} = \eta^{EXP} = 100\%$  (assumption [A14]), making the shock the only reason of SS head-loss. Such low exergy destruction rate reflects SS high pressure-recovery of  $98.59\%$  an outcome perfectly in accordance with the 2<sup>nd</sup> Law and with the consistency cross-check via  $T_0\dot{Q}_s$  in Table 4.7.

#### 4.5.4. TSA-System

The most prominent exergy flow differences among FULL-TSA, SS-TSA and SS-TSA-HI are found in this sub-system. Here, SS benefits become clear as SS-TSA/SS-TSA-HI attain considerably less  $\dot{E}^{DESTR}$  and  $\dot{E}_{WASTE}^{OUT}$  relatively to FULL-TSA. TSA-System exergy destruction lowers from  $\dot{E}^{DESTR} = 0.7\text{ MW}$  in FULL-TSA to  $\dot{E}^{DESTR} = 0.19\text{ MW}$  in SS-TSA due to much lower LPS consumption (Table 4.3), which is related to large temperature difference at the colder end of  $\text{N}_2$  heater, where saturated-water ( $T = 143.6^\circ\text{C}$ , assumption [A11]) contacts Cold-Box  $\text{N}_2$  ( $T = 14^\circ\text{C}$ ). Reduced temperature difference due to  $90^\circ\text{C}$  WW utilization further lowers exergy destruction in SS-TSA-HI – from  $\dot{E}_{SS-TSA}^{DESTR} = 0.19\text{ MW}$  to  $\dot{E}^{DESTR} = 0.16\text{ MW}$ . In terms of exergy waste rate,  $\approx 0.29\text{ MW}$  is saved in SS-TSA/SS-TSA-HI, owing to substantially lower wet  $\text{N}_2$  release to atmosphere, where SS-TSA/SS-TSA-HI performed similarly due to same wet  $\text{N}_2$  exhausts as  $\text{N}_2$  is equally heated to  $T = 80^\circ\text{C}$  despite the different heating media (assumption [A21]). RER#1 and RER#2 cause small differences

in exergy flow rates (Figs. 4.8d/4.8i) explaining the similar exergy efficiencies. Uniting SS with TSA-System, air purification exergy destruction reduces 61% from FULL-TSA to SS-TSA.

#### 4.5.5. CW-System

The exergy destruction increases from  $\dot{E}^{DESTR} = 0.70MW$  in FULL-TSA to  $\dot{E}^{DESTR} = 0.71MW$  in SS-TSA due to slightly higher cooling-tower load connected to higher SS-TSA MAC discharge pressure. Similarly, the exergy inlet flow rate raises in SS-TSA-HI with RER#2 as MAC intercooler produces 90°C CW above the WW demand of regeneration N<sub>2</sub>, entailing redirecting 90°C CW to the cooling-tower with higher  $\dot{E}^{DESTR} = 1.04MW$ . In terms of waste exergy, SS-TSA-HI wastes  $\approx 0.03MW$  more exergy than SS-TSA due to higher wet air temperature from the cooling-tower – 37.8°C vs 36.7°C – despite reduced heat load and fan flow rate. With RER#2, wet air waste exergy is  $\approx 0.3MW$  lower for all PPUs than with RER#1 (Figs. 4.8e/4.8j). In terms of inlet exergy flow rates, FULL-TSA and SS-TSA are more sensitive to RER change due to higher CW consumption. Moreover, while exergy inlet flow rate to SS-TSA-HI with RER#1 is the smallest, accounting for lower CW flow rate, with RER#2 it becomes the highest due to highest cooling-tower inlet CW temperature (90°C).

Changing from RER#1 to RER#2 produces bold shrinkage of all CW exergy flow rates (Figs. 4.8e/4.8j) with CW inlet exergy flow rate for SS-TSA-HI totaling 24.50MW with RER#1 and 1.05MW with RER#2. This entails expressive efficiency reduction, suggesting opposite exergy preservation performance of all CW-Systems – from 93.5% to 10.5% in SS-TSA-HI.

#### 4.5.6. Overall Systems

Exergy analyses of overall systems show that SS-TSA-HI achieved the best performance among PPU alternatives seconded by SS-TSA, with FULL-TSA presenting highest rates of exergy destruction, waste exergy, and inlet exergy. Fig. 4.9 depicts the contributions of sub-subsystems to overall exergy losses of FULL-TSA, SS-TSA and SS-TSA-HI with RER#1; where TSA-System savings reflect the main leverage of SS utilization. Given inlet exergy flow rates with RER#1, exergy losses entail 57.9%, 60.0% and 60.3% respective overall efficiencies of FULL-TSA, SS-TSA and SS-TSA-HI. While exergy efficiencies of sub-subsystems with large CW transit are highly sensitive to RER change, variations of overall exergy efficiencies with RER#2 in place of RER#1 attain only 1.2-1.4 percent points.

Therefore Fig. 4.9 still reasonably portraits exergy losses with RER#2, excepting the case of CW-System bars, which shorten  $\approx 0.3MW$  in waste exergy terms.

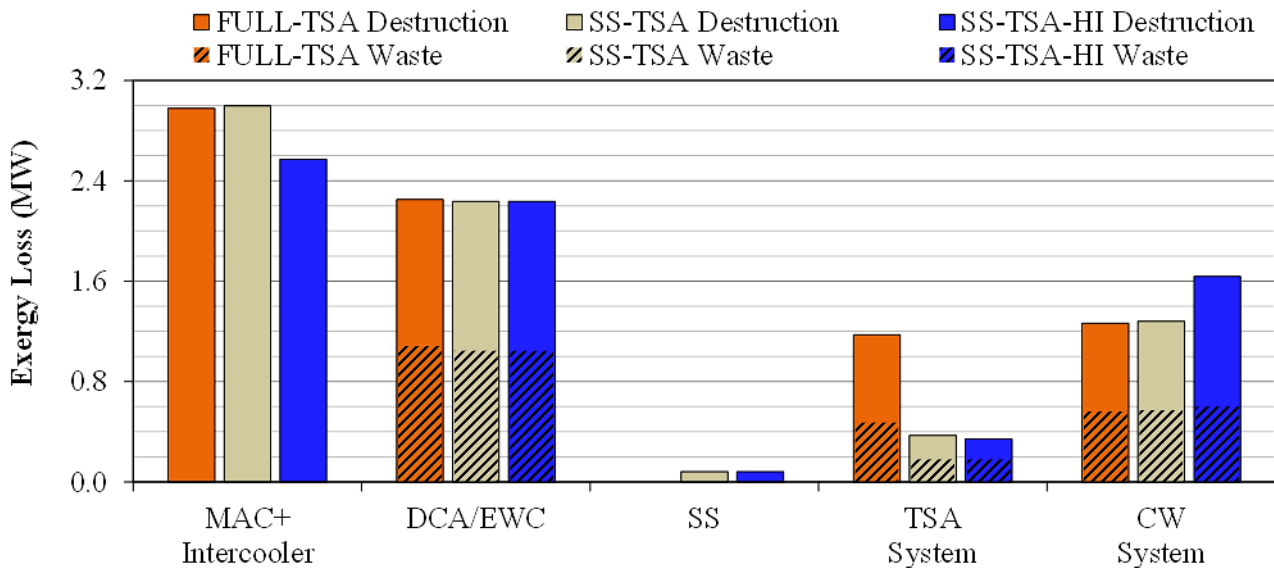


**Fig. 4.9.** FULL-TSA, SS-TSA and SS-TSA-HI exergy losses with RER#1: exergy destruction (clean) vs waste-exergy (hachured).

FULL-TSA efficiency of 57.9% is found in reasonable agreement with values from Cornelissen and Hirs [23] and from Fu and Gundersen [26], with differences reaching  $\approx 5$  percent points due to different assumptions:  $\eta^{MAC}=85\%$  is higher; air purification occurs at lower pressure  $\approx 3$  bar, and CW-System is included in the analysis increasing power consumption, exergy destruction and waste exergy (wet air and  $N_2$  exhausts).

Removing CW-System and attaching CW inlet/outlet to the PPU, the overall FULL-TSA efficiency with RER#1 would also reach 62%. Despite relevance of TSA in FULL-TSA exergy destruction, Fig. 4.9 portrays air compression and cooling as major contributors to overall exergy destruction.

#### 4.5.7. SS Interference on TSA-System

CW-System considerably impacts exergy analysis presenting exergy destruction rate of same order of TSA-System in FULL-TSA. Counterpointing this, SS in SS-TSA/SS-TSA-HI presents a tiny exergy destruction rate despite its important role in air pre-purification, lowering about 10X the TSA load of TSA-System, as well as abating  $\approx 70\%$  of the respective exergy losses (destruction plus waste) with both RER#1/RER#2. The underlying reason is that SS promotes drastic savings of LPS and regeneration  $N_2$ , besides recovering liquid water consequently lowering water release in TSA regeneration.

#### 4.5.8. Other Aspects

Figs. 4.7a-4.7b present exergy Sankey diagrams of SS-TSA-HI and convey some notion of exergy inlet/outlet flow rates in FULL-TSA/SS-TSA (whose analogous Sankey diagrams are presented in Appendices W2/W3), excepting the absence of LPS inlet and saturated-water outlet. Now, observing exergy inlet flow rates in Fig. 4.7b with RER#2, a problematic interpretation arises with RER#2. As revealed in Table 4.6 and Figs. 4.8a-4.8j, RER#1 is problematic in most PPU sub-systems due to inflated CW exergy flow rates, raising efficiencies and hiding irreversibilities; an evanescent issue regarding overall system analysis (Fig. 4.7a). Concerning material exergy inlet flow rates to FULL-TSA, SS-TSA and SS-TSA-HI overall systems, the problem is related to water make-up inlets depicted with negligible exergy flow rates in Figs. 4.7b/4.8g/4.8j with RER#2, contrasting with analogous Figs. 4.7a/4.8b/4.8e with RER#1. In fact, this configures a RER#2 blind spot, because with RER#2 it is impossible to recognize exergy savings associated to water make-up, since water streams have null exergy flow rates at  $(T_0, P_0)$  with RER#2. This wrongly suggests that water is not a valuable resource under exergy viewpoint. Actually, water consumption is a concern that must be taken into account. Such outcome emphasizes the importance of comparing different RER approaches for exergy analysis.

Finally, with whichever RER#1 or RER#2, novel SS-TSA and SS-TSA-HI PPUs exhibited higher exergy efficiencies than conventional FULL-TSA. The underlying fact is that SS performs the lion-share of the purification load removing 98.65% H<sub>2</sub>O with low exergy destruction due to high 98.59% pressure-recovery, lowering about 10X the TSA load and downing  $\approx 70\%$  of its exergy losses mainly from 88% less regeneration duty and 64% less regeneration N<sub>2</sub> in MS-TSA (Table 4.3). Moreover, SS-TSA/SS-TSA-HI entail  $\approx 4\%$  less water make-up and such benefits only cause minor increase of power consumption. With air pre-purification exergy losses downed in SS-TSA and SS-TSA-HI, further PPU improvements should focus on MAC and air-cooling steps.

#### 4.5. Conclusions for Chapter 4

Two novel PPU concepts prescribing SS coupled to finishing TSA for supplying purified air to cryogenic fractionation – SS-TSA and SS-TSA-HI – were compared to conventional FULL-TSA via power/heat consumptions and exergy analyses considering low-pressure Cold-Box feed (3.1 bar).

SS produces great water removal (98.65%) from raw air with 98.59% pressure-recovery, entailing low exergy destruction rate, lowering 10X the TSA load and abating  $\approx 70\%$  of the exergy loss of TSA-System. Insertion of SS significantly reduces utilities consumption, particularly LPS demand and regeneration  $N_2$  flow rate. These points ballast SS-TSA/SS-TSA-HI superiority from power consumption and exergy preservation points of view.

A discussion on exergy flow rate sensitivity to RER is provided, and for this purpose two RER approaches are chosen to evaluate exergy flow rates across FULL-TSA, SS-TSA and SS-TSA-HI overall systems and their sub-systems: (i) RER#1 as atmospheric air at same conditions of PPU air intake ( $RH=60\%$ ,  $P_0=1\text{ atm}$ ,  $T_0=25^\circ\text{C}$ ); and (ii) RER#2 as saturated-air ( $RH=100\%$ ,  $P_0=1\text{ atm}$ ,  $T_0=25^\circ\text{C}$ ) coexisting with infinite body of pure liquid water.

On the one hand, RER#1 overestimates CW exergy flow rates entailing large CW exergy transit crossing the boundaries of PPU sub-systems, thus raising exergy efficiencies and hiding equipment irreversibilities. On the other hand, such aspect is not an issue for overall system analysis owing to internalized CW streams.

RER#2 drastically deflates the exergy flow rate of CW streams inside the processes, showing itself as more adequate for exergy analysis of PPU sub-systems and unveiling process irreversibilities. However, RER#2 does not allow recognizing exergy flows associated to water make-up external streams. Thus, RER#1 is the best choice for overall system analysis. Hereupon, overall exergy efficiencies of FULL-TSA, SS-TSA, and SS-TSA-HI with RER#1 attained 57.9%, 60.0%, and 60.3%, respectively.

Exergy Sankey diagrams evidencing exergy flow rates crossing the boundaries of each sub-system of SS-TSA-HI (and analogously for SS-TSA/FULL-TSA in Appendices W2/W3) clearly demonstrates the above RER#1/RER#2 peculiarities.

The lesson is that exergy assessments must consider RER choices with care, hence analyzing process performance from different perspectives, avoiding misinterpretations, allowing fair evaluation of thermodynamic performances and keeping applicability to real concerns about resources depletion and environmental impacts.

Last but not least, all exergy destruction rates were counter-checked with lost work rates determined from entropy creation rates. Good agreement is demonstrated with discrepancies below 0.25% ensuring consistency of the present exergy analysis. In this regard, compression and air-cooling sub-systems are unveiled as major exergy destructors in all PPU, with SS-TSA-HI being slightly better exergy preserver due to lower temperature differences in MAC

intercooler, since WW outlet temperature has to be sufficiently high for successful TSA regeneration, despite partial offset of such benefit as  $90^{\circ}\text{C}$  CW/WW availability exceeded  $\text{N}_2$  heater demand, forcing the  $90^{\circ}\text{C}$  CW excess to be redirected to cooling-tower increasing CW-System exergy destruction.

#### 4.6. References for Chapter 4

- [1] Higginbotham P, White V, Fogash K, Guvelioglu G. Oxygen supply for oxyfuel  $\text{CO}_2$  capture. *Int J Greenh Gas Con* 2011; 5S:S194–203. <https://doi.org/10.1016/j.ijggc.2011.03.007>
- [2] Acharya DR, Jain R. Recent advances in molecular sieve unit design for air separation plants. *Sep Sci Technol* 1995; 30:3489–07. <https://doi.org/10.1080/01496399508015131>.
- [3] Qasem NAA, Ben-Mansour R. Adsorption breakthrough and cycling stability of carbon dioxide separation from  $\text{CO}_2/\text{N}_2/\text{H}_2\text{O}$  mixture under ambient conditions using 13X and Mg-MOF-74. *Appl Energy* 2018; 230:1093–107. <https://doi.org/10.1016/j.apenergy.2018.09.069>
- [4] Kerry FG. *Industrial gas handbook: gas separation and purification*. Boca Raton, USA: CRC Press; 2006.
- [5] Dawson B, Kalbassi M, Siegmund S, Thayer M. *Optimizing oxygen plant performance: improving production and reliability of existing plants while reducing costs*. ALTA Conference; Perth, Australia; 2010.
- [6] Shi Y, Liu X, Guo Y, Kalbassi MA, Liu YS. Desorption characteristics of  $\text{H}_2\text{O}$  and  $\text{CO}_2$  from alumina F200 under different feed/purge pressure ratios and regeneration temperatures. *Adsorption* 2017; 23:999–1011. <https://doi.org/10.1007/s10450-017-9907-0>
- [7] Van der Ham LV, Kjelstrup S. Exergy analysis of two cryogenic air separation processes. *Energy* 2010; 35:4731–9. <https://doi.org/10.1016/j.energy.2010.09.019>
- [8] Zhou H, Cai Y, Xiao Y, Mkhalel ZA, You B, Shi J, et al. Process configurations and simulations for a novel single-column cryogenic air separation process. *Ind Eng Chem Res* 2012; 51:15431–9. <https://doi.org/10.1021/ie3022225>
- [9] Brigagão GV, Arinelli LO, de Medeiros JL, Araújo OQF. A novel air pre-purification unit for cryogenic separation: low-pressure supersonic separator coupled to finishing adsorption. *Sep Purif Technol* 2019; 215:173–89. <https://doi.org/10.1016/j.seppur.2019.01.015>
- [10] Brigagão GV, Arinelli LO, de Medeiros JL, Araújo, OQF, inventors; Universidade Federal do Rio de Janeiro, applicant. Processo de preparo e purificação do ar para fracionamento criogênico utilizando separador supersônico de baixa pressão. BR patent application 102017027727-5. Filed in December 21st, 2017.
- [11] Machado PB, Monteiro JGM, de Medeiros JL, Epsom HD, Araujo OQF. Supersonic separation in onshore natural gas dew point plant. *J Nat Gas Sci Eng* 2012; 6:43–9. <https://doi.org/10.1016/j.jngse.2012.03.001>
- [12] Arinelli LO, Trotta TAF, Teixeira AM, de Medeiros JL, Araújo OQF. Offshore processing of  $\text{CO}_2$  rich natural gas with supersonic separator versus conventional routes. *J Nat Gas Sci Eng* 2017; 46:199–21. <https://doi.org/10.1016/j.jngse.2017.07.010>
- [13] de Medeiros JL, Arinelli LO, Araújo OQF. Speed of sound of multiphase and multi-reactive equilibrium streams: a numerical approach for natural gas applications. *J Nat Gas Sci Eng* 2017; 46:222–41. <https://doi.org/10.1016/j.jngse.2017.08.006>

- [14] Secchi R, Innocenti G, Fiaschi D. Supersonic swirling separator for natural gas heavy fractions extraction: 1D model with real gas EOS for preliminary design. *J Nat Gas Sci Eng* 2016; 34:197–217. <https://doi.org/10.1016/j.jngse.2016.06.061>
- [15] Kotas TJ. *The exergy method of thermal plant analysis*. 2<sup>nd</sup> ed. Malabar, USA: Krieger Publishing Company; 1995.
- [16] Hepsbali A. A key review on exergetic analysis and assessment of renewable energy resources for a sustainable future. *Renew Sust Energ Rev* 2008; 12:593–61. <https://doi.org/10.1016/j.rser.2006.10.001>
- [17] Gaudreau K, Fraser R, Murphy S. The characteristics of the exergy reference environment and its implications for sustainability-based decision-making. *Energies* 2012; 5(7):2197–213. <https://doi.org/10.3390/en5072197>.
- [18] Gallo WLR, Millanez LF. Choice of a reference state for exergetic analysis. *Energy* 1990; 15(2):113–21. [https://doi.org/10.1016/0360-5442\(90\)90048-7](https://doi.org/10.1016/0360-5442(90)90048-7)
- [19] Teixeira AM, Arinelli LO, de Medeiros JL, Araújo OQF. Exergy Analysis of monoethylene glycol recovery processes for hydrate inhibition in offshore natural gas fields. *J Nat Gas Sci Eng* 2016; 35:798–813. <https://doi.org/10.1016/j.jngse.2016.09.017>
- [20] Ahrendts J. Reference states. *Energy* 1980; 5(8):666–77. [https://doi.org/10.1016/0360-5442\(80\)90087-0](https://doi.org/10.1016/0360-5442(80)90087-0).
- [21] Szargut J, Morris DR, Steward FR. *Exergy analysis of thermal, chemical and metallurgical processes*. New York: Hemisphere Publishing; 1988.
- [22] Ghannadzadeh A, Thery-Hetreux R, Baudouin O, Baudet P, Floquet P, Joulia X. General methodology for exergy balance in ProSimPlus<sup>®</sup> process simulator. *Energy* 2012; 44:38–59. <https://doi.org/10.1016/j.energy.2012.02.017>
- [23] Cornelissen RL, Hirs GG. Exergy analysis of cryogenic air separation. *Energy Convers Manag* 1998; 39(16-18):1821–6. [https://doi.org/10.1016/S0196-8904\(98\)00062-4](https://doi.org/10.1016/S0196-8904(98)00062-4)
- [24] Hinderink AP, Kerkhof FPJM, Lie ABK, Arons JS, Van der Kooi HJ. Exergy analysis with a flowsheeting simulator – I. Theory; calculating exergies of material streams. *Chem Eng Sci* 1996; 51(20):4693–700. [https://doi.org/10.1016/0009-2509\(96\)00220-5](https://doi.org/10.1016/0009-2509(96)00220-5).
- [25] Fu C, Gundersen T. Using exergy analysis to reduce power consumption in air separation units for oxy-combustion processes. *Energy* 2012; 44:60–8. <https://doi.org/10.1016/j.energy.2012.01.065>
- [26] Fu C, Gundersen T. Exergy analysis and heat integration of a coal-based oxycombustion power plant. *Energy Fuels* 2013; 27:7138–49. <https://doi.org/10.1021/ef400867d>
- [27] Van der Ham LV. Improving the exergy efficiency of a cryogenic air separation unit as part of an integrated gasification cycle. *Energy Convers Manag* 2012; 61:31–42. <https://doi.org/10.1016/j.enconman.2012.03.004>
- [28] Querol E, Gonzalez-Regueral B, Ramos A, Perez-Benedito JL. Novel application for exergy and thermoeconomic analysis of processes simulated with Aspen Plus<sup>®</sup>. *Energy* 2011; 36:964–74. <https://doi.org/10.1016/j.energy.2010.12.013>
- [29] Ebrahimi A, Meratizaman M, Reyhani HA, Pourali O, Amidpour M. Energetic, exergetic and economic assessment of oxygen production from two columns cryogenic air separation unit. *Energy* 2015; 90:1298–316. <https://doi.org/10.1016/j.energy.2015.06.083>
- [30] Dillon DJ, White V, Allam RJ, Wall RA, Gibbins J. IEA Greenhouse Gas R&D Programme: Oxy combustion processes for CO<sub>2</sub> capture from power plant. Engineering Investigation Report, 2005.
- [31] Rege SU, Yang RT, Buzanowski MA. Sorbents for air prepurification in air separation. *Chem Eng Sci* 2000; 55:4827–38. [https://doi.org/10.1016/S0009-2509\(00\)00122-6](https://doi.org/10.1016/S0009-2509(00)00122-6)
- [32] Campbell JM. *Gas conditioning and processing, vol. 2: the equipment modules*. 7th ed. Norman, USA: Campbell Petroleum Series; 1992.

## 5. Carbon Capture and Supercritical Fluid Processing with Supersonic Separator: Cleaner Offshore Processing of Natural Gas with Ultra-High CO<sub>2</sub> Content

*This chapter is based on the following publications in Journal of Natural Gas Science and Engineering and Journal of Cleaner Production:*

ARINELLI, L. O.; DE MEDEIROS, J. L.; DE MELO, D. C.; TEIXEIRA, A. M.; **BRIGAGÃO, G. V.**; PASSARELLI, F.; GRAVA, W. M.; ARAÚJO, O. Q. F. Carbon capture and high-capacity supercritical fluid processing with supersonic separator: natural gas with ultra-high CO<sub>2</sub> content. *Journal of Natural Gas Science and Engineering*, 66, 265-283, 2019.

DE MELO, D. C.; ARINELLI, L. O.; DE MEDEIROS, J. L.; TEIXEIRA, A. M.; **BRIGAGÃO, G. V.**; PASSARELLI, F.; GRAVA, W. M.; ARAÚJO, O. Q. F. Supersonic separator for cleaner offshore processing of supercritical fluid with ultra-high carbon dioxide content: economic and environmental evaluation. *Journal of Cleaner Production*, 234, 1385-1398, 2019.

### Abbreviations

C3+ Propane and Heavier; CD Cryogenic Distillation; CPA-EOS Cubic-Plus-Association EOS; CW Cooling-Water; ED Electric-Driver; EOR Enhanced Oil Recovery; EOS Equation-of-State; GT Gas-Turbine; HCDPA Hydrocarbon Dew-Point Adjustment; HPS High-Pressure Separator; HW Hot-Water; JT Joule-Thompson; LLS Liquid-Liquid Separator; LTX Low-Temperature Condensate Catcher; MMSm<sup>3</sup>/d Millions of Standard m<sup>3</sup> per day; MP Membrane-Permeation; MS Molecular-Sieves; NG Natural Gas; NR Not Recycling; PHW Pressurized-Hot-Water; PR-EOS Peng-Robinson EOS; RC Recycling Condensate; SS Supersonic Separator; SW Seawater; TF Thermal-Fluid; TX Turbo-Expander; USD US Dollar; UOE Unit Operation Extension; VLE Vapor-Liquid Equilibrium; WDPA Water Dew-Point Adjustment; WHRU Waste-Heat Recovery Unit; WW Warm-Water.

## Nomenclature

$A(x)$	: SS flow section area ( $m^2$ ) dependent of $x$
$c(T, P, \underline{Z})$	: Sound speed of multiphase fluid at ( $T, P, \underline{Z}$ ) (m/s)
$D_i, D_T, D_O$	: Inlet, throat and outlet SS diameters (m)
$GOR$	: Gas-Oil Ratio ( $sm^3/m^3$ )
$L, L_C, L_D$	: Total, converging and diverging SS lengths (m)
$L^{LAVAL}, L^{Shock}$	: Laval nozzle length and SS axial position at normal shock ( $L^{Shock}=L^{LAVAL}$ ) (m)
$Ma=v/c$	: Mach Number
$Ma^{Shock}$	: Ma just before normal shock and condensate withdrawal
$nc$	: Number of components
$P$	: Absolute pressure (bar)
$REC\%CO_2$	: SS % $CO_2$ recovery
$T$	: Absolute temperature (K)
$x$	: SS axial position (m)
$\underline{Z}$	: Vector ( $nc \times 1$ ) of total species mol fractions in multiphase fluid

### Economy Terms

$AP, GAP, REV$	: Annual profit, gross profit and revenues (USD/y)
$CUT, COM$	: Annual utility and manufacturing costs (USD/y)
$FCI, ITR, NPV$	: Fixed capital investment (USD), income tax rate (%), net present value (USD)

### Greek Terms

$\alpha, \beta$	: SS converging and diverging angles (deg) with linear diameter profiles
$\beta$	: Mole vapor fraction
$\eta^{EXP}\%, \eta^{CMP}\%$	: SS expansion and compression adiabatic efficiencies (%)
$\rho$	: Multiphase fluid density ( $kg/m^3$ )
$\bar{\epsilon}_p \equiv \left( \frac{\partial \rho}{\partial P} \right)_{T, \underline{Z}}$	: Derivative of $\rho$ with $P$ at const. $T, \underline{Z}$ for multiphase fluid ( $kg/Pa.m^3$ )

### Subscripts

$AS, BS$	: Just after shock and just before shock after condensate withdrawal
$C, D, I, O, T$	: Converging, diverging, inlet, outlet, throat
$L, V, W$	: Liquid hydrocarbon, vapor and liquid water at $L^{Shock}$

### Superscripts

$in, out, LAVAL$	: Inlet, outlet, and Laval nozzle
$Diffuser, Diff$	: Diffuser
$Discharge, Feed$	: SS discharge, SS feed
$Shock$	: Just before normal shock and before condensate withdrawal
$Throat, V, L, S$	: Throat, vapor, liquid, solid

## Supplementary Materials

Supplementary Materials for this chapter are found in Appendices X1, X2, X3, and X4.

## 5.1. Introduction

For strategic and environmental reasons, the energy matrix of a country should be diversified and clean as much as possible (Campos et al., 2017). The world claims for less carbon emissions but also demands more energy supply, thus revealing a current dual challenge. This issue is addressed by gradual transition in world energy matrix, foreseeing a future with renewables playing central role in the place of fossil resources. Nevertheless, natural gas (NG) utilization is predicted to increase in the next few decades, acting as a bridge source into a renewable energy future. Furthermore, NG should be the ideal complement to renewable energy supply, presenting  $\approx 50\%$  of CO<sub>2</sub> generation per electric kWh comparatively to coal-based plants, offering cost-effective back-up to typical variability of solar, wind and hydropower stations.

### 5.1.1. Offshore Processing of CO<sub>2</sub>-Rich Natural Gas

Significant fraction of 10% of world proven reserves of NG present high CO<sub>2</sub> content above 15%mol CO<sub>2</sub> (Burgers et al., 2011). In some cases, the NG is featured by ultra-rich CO<sub>2</sub> content in the range of 60-80%mol CO<sub>2</sub>. SE-Brazil, SE-Asia and NW-Australia contain the largest offshore reserves of CO<sub>2</sub>-rich NG. The giant Pre-Salt oil-gas basin of SE-Brazil – illustrated in Fig. 5.1 – comprises reservoirs containing up to 12.6 billion bbl of oil and 400 billion Sm<sup>3</sup> of gas (BP, 2018). Huge amount of CO<sub>2</sub>-rich NG to be processed is tied to oil production in Pre-Salt fields, exhibiting high gas-to-oil ratios  $\approx 400-600 \text{ Sm}^3_{\text{gas}}/\text{m}^3_{\text{oil}}$  and high CO<sub>2</sub> contents (20-80%mol) (Gaffney, Cline & Associates, 2010).

CO<sub>2</sub>-rich raw NG processing in such fields involves the following sequence of operations (Araújo et al., 2017): (i) water dew-point adjustment (WDPA); (ii) hydrocarbon dew-point adjustment (HCDPA); and (iii) CO<sub>2</sub> removal. This latter is naturally the most impactful step, gaining particular importance when dealing with ultra-rich (>60%mol) CO<sub>2</sub> feeds.

#### 5.1.1.1. Conventional Technologies for CO<sub>2</sub> Removal

The most commonly conceived alternatives for CO<sub>2</sub> removal from raw NG are Chemical-Absorption, Physical-Absorption, Membrane-Permeation and Cryogenic-Distillation. CO<sub>2</sub> removal from raw NG with Chemical-Absorption involves an absorption column fed with aqueous alkanolamines and a low-pressure regeneration column producing practically pure CO<sub>2</sub>. Chemical-Absorption is applicable to most CO<sub>2</sub> capture services – performing well for a wide range of CO<sub>2</sub> fugacity – and possesses great advantage of high CO<sub>2</sub>/CH<sub>4</sub> selectivity.

However, high-capacity Chemical-Absorption faces issues of high circulation of solvent ( $10\text{-}18\text{ kg}^{\text{Solvent}}/\text{kg}^{\text{CO}_2}$ ), high heat duty for regeneration ( $2\text{-}4\text{ MJ}/\text{kg}^{\text{CO}_2}$ ) and production of low-pressure  $\text{CO}_2$  entailing high compression ratio for EOR. Physical-Absorption eliminates the heat duty for solvent regeneration, being featured by high-pressure absorption followed by regeneration through liquid depressurization. Physical-Absorption has good performance at high  $\text{CO}_2$  fugacity allowing better capture-ratio ( $1\text{-}10\text{ kg}^{\text{Solvent}}/\text{kg}^{\text{CO}_2}$ ), but still implies in low-pressure  $\text{CO}_2$  being produced and heavy-weight processing plant, with the further disadvantage of poor  $\text{CO}_2/\text{CH}_4$  selectivity entailing high  $\text{CH}_4$  losses.

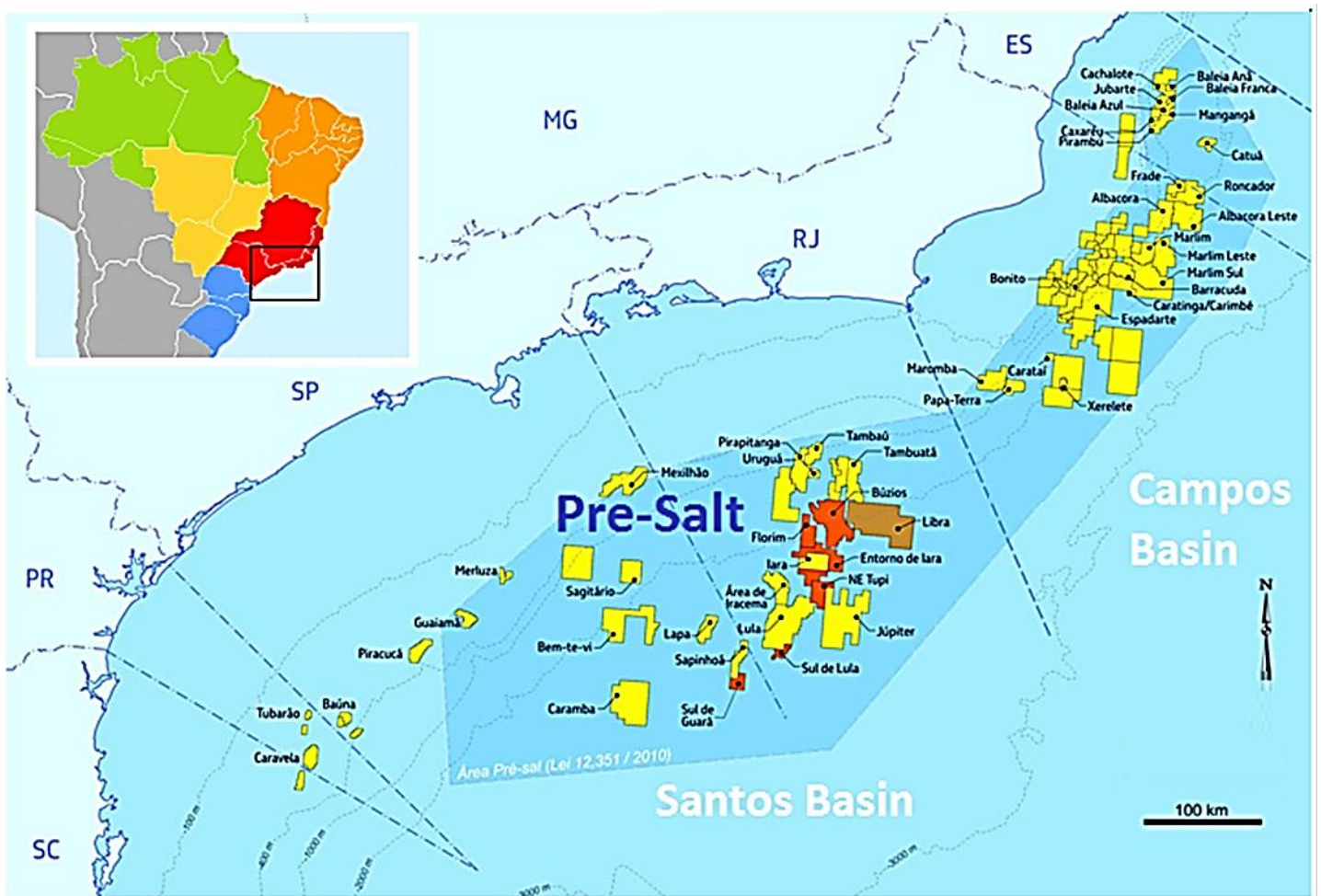


**Fig. 5.1.** Pre-Salt basin in SE-Brazil coast (adapted from ANP 2017).

Membrane-Permeation (MP) is based on distinct molecules permeances and fugacity differences across skin-dense walls (e.g. through cellulose-acetate membranes) arranged in hollow-fiber or spiral-wound module configurations. MP main advantages are modularity and relatively low footprint. Disadvantages are inverse relationship between selectivity and capacity, with high  $\text{CH}_4$  losses for high  $\% \text{CO}_2$  feeds, and low-pressure  $\text{CO}_2$  obtained as permeate entailing high compression power demand for EOR (Araújo et al., 2017).

In relation to CO<sub>2</sub> removal alternatives, Araújo et al. (2017) compared several technologies for offshore processing of 6 MMSm<sup>3</sup>/d of CO<sub>2</sub>-rich raw NG (10%/30%/50%mol CO<sub>2</sub>) – Chemical-Absorption, Physical-Absorption, Membrane-Permeation, and hybrids – and elected as best process alternative a hybrid configuration consisting of one stage of MP followed by finishing purification by Chemical-Absorption treatment, assuming large availability of pressurized-hot-water (PHW) for solvent regeneration from Waste-Heat Recovery Units (WHRU) of gas-turbines (GT).

Cryogenic-Distillation (CD) uses vapor-liquid equilibrium (VLE) to perform CO<sub>2</sub> removal by condensation at high pressures, with advantage of producing liquid CO<sub>2</sub> ready for EOR pumping. In this sense, Langé et al. (2015) pointed superiority of Cryogenic-Distillation over Chemical-Absorption for treating NG with CO<sub>2</sub> contents above 10%mol (as liquid CO<sub>2</sub> is less power-demanding for EOR than low-pressure gaseous CO<sub>2</sub>). However, CD faces issues of complex cryogenic operation involving several fractionation columns, entailing heavy-weight process configurations with prohibitively large footprints for installation in offshore rigs.

#### **5.1.1.2. Conventional Processing for Total Reinjection**

Besides the challenge of CO<sub>2</sub> removal, as remote offshore oil-gas fields may operate without pipeline support for years, difficulties get even worse with impossibility to export the gas. With reinjection being the only alternative, the following steps are generally conceived for CO<sub>2</sub>-rich raw NG processing: (i) dehydration to eliminate chances of hydrate formation in gas processing and transportation; (ii) HCDPA and CO<sub>2</sub> removal from a portion of Dry-Gas to produce Fuel-Gas (FG) that supply rig power demands; and (iii) compression/pumping of Dry-Gas enriched with CO<sub>2</sub>-rich fluid from FG production for dispatch to EOR.

For this scenario, processes with reduced footprints and complexity are firstly taken into consideration, implying in the election of Membrane-Permeation for the service of CO<sub>2</sub> removal. For WDPa and HCDPA, reliability of mature technologies implies the choice of following classical solutions: molecular-sieves (MS) adsorption and Joule-Thompson (JT) expansion. This set of conventional operations applied to offshore processing of CO<sub>2</sub>-rich NG is henceforth named as MS-JT-MP. As conventional technologies present drawbacks at such severe conditions, development of new process solutions with reduced equipment size/weight is needed for improved profitability and reduced carbon emissions of oil-gas upstream activities in this scenario.

### 5.1.2. Supersonic Separators for Natural Gas Processing

A relatively recent operation for raw NG conditioning is the removal of condensable fractions using supersonic separator (SS) (Machado et al., 2012). These operations are featured by a converging-diverging nozzle – the so-called Laval nozzle – that provides expansion of raw NG feeds accelerating the fluid to supersonic velocities, which produces deep  $T$  falls leading to partial condensation. Being most commonly conceived for simultaneous adjustment of water and hydrocarbon dew-points (WDPA+HCDPA), the SS condensate of such application is mainly constituted by water, propane and heavier hydrocarbons (C3+), which are segregated from gas-phase by centrifugal force imposed by a spiralling flow pattern (Schinkelshoek and Epsom, 2008). Fig. 5.3 is the sketch of a SS with rectlinear geometry, showing swirling and collecting vanes, the former being a stationary device at the inlet nozzle impelling the feed to rotational motion, and the latter being openings at the walls (represented as arrows) availed to withdraw centrifuged SS condensate.

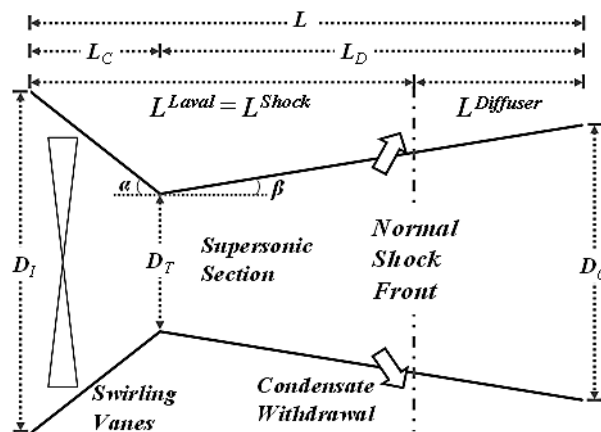


**Fig. 5.3.** SS sketch with linear diameter profiles.

SS correct modeling depends on precise estimation of sound speed ( $c$ ), as Mach Number ( $Ma$ ) is calculated throughout the SS length (Arinelli et al., 2017). The sound speed ( $c$ ) is a thermodynamic property of a material, being highly influenced by density ( $\rho$ ) and isothermal compressibility ( $\mathcal{E}_p \equiv \left( \frac{\partial \rho}{\partial P} \right)_{T,Z}$ ), which are all properties highly sensitive to phase equilibria.

This is exactly the case of any SS application, especially when dealing with raw NG feeds, which are generally characterized by multiphase flow behavior. Both mentioned properties  $\rho$  or  $\mathcal{E}_p$  have inverse influence over  $c$ : the higher the density or isothermal compressibility, the lower the sound speed (de Medeiros et al., 2017). Hence,  $c$  falls when condensation starts.

To evaluate the performance of SS units in Aspen HYSYS, Arinelli et al. (2017) and de Medeiros et al. (2017) created a couple of Unit Operation Extensions (UOE): (i) PEC-UOE, a

rigorous model to estimate phase-equilibrium sound speed (de Medeiros et al., 2017); and (ii) SS-UOE, a rigorous thermodynamic model for SS design and simulation (Arinelli et al., 2017). Arinelli et al. (2017) applied their models SS-UOE and PEC-UOE to evaluate SS performance at WDPA+HCDPA and CO<sub>2</sub> removal in comparison with conventional NG technologies for processing 44%mol CO<sub>2</sub> raw NG: glycol-absorption for dehydration; HCDPA via JT-Expansion; and CO<sub>2</sub> removal through Membrane-Permeation. To evaluate Membrane-Permeation performance, another HYSYS model was developed using permeances estimated from field data: MP-UOE. For WDPA+HCDPA, SS was evinced as the best alternative, attaining leaner NG with reduced Fuel-Gas demand. For CO<sub>2</sub> removal, higher separation was attained via conventional 01-stage Membrane-Permeation: 15%mol CO<sub>2</sub> against 21.85%molCO<sub>2</sub> with SS unit, limited by freeze-out avoidance. On the other hand, SS required 30% less EOR power as it produces high-pressure CO<sub>2</sub>-rich condensate.

Beyond NG WDPA+HCDPA and CO<sub>2</sub> removal applications, other uses for SS involving high-pressure feeds have been proposed. In this sense, using process simulation in Aspen HYSYS with extension models SS-UOE and PEC-UOE via thermodynamic model CPA-EOS, Teixeira et al. (2018) proposed an innovative concept comprising SS utilization to recover thermodynamic hydrate inhibitors from high-pressure raw NG contacted with methanol, ethanol or ethylene-glycol in flowlines, demonstrating striking results.

### **5.1.3. Present Work**

Following the successful applications of Arinelli et al. (2017), de Medeiros et al. (2017) and Teixeira et al. (2018), SS-UOE and PEC-UOE are presently applied to an innovative alternative using only SS operations for offshore processing of CO<sub>2</sub>-rich NG. For the best compactness of gas processing plant, as desirable to a remote floating-hub processing huge gas flow rates, design should discard cumbersome operations entailing large footprints, costs and make-up issues, like glycol and molecular-sieve dehydrations, as well as the majority of conventional CO<sub>2</sub> capture solutions. In this sense, a new process alternative is here proposed conceiving two SS units to perform the services of WDPA+HCDPA and CO<sub>2</sub> removal. Similar conditions of raw NG treatment – with high CO<sub>2</sub> content observing CO<sub>2</sub> freeze-out risks – were never considered before.

The present chapter embraces the contents of two published scientific articles (Appendices M/N) giving emphasis on comparison of process alternatives. Deeper discussion on SS units performances is presented in the reference articles, including thermodynamic diagrams of SS axial profiles, which also configures major originality aspects of the referred publications.

## 5.2. Methods

Technical and economic performances of a plausible large-capacity oil-gas floating-hub are analyzed through the prism of using SS in gas processing whenever possible. Two Case Studies are addressed for comparison of proposed alternatives for this scenario. The gas-hub is centrally positioned on a remote oil-gas offshore field receiving  $\approx 90 \text{ MMSm}^3/\text{d}$  of high-pressure multiphase fluid from risers and exporting  $\approx 50 \text{ MMSm}^3/\text{d}$  of high-pressure EOR-Fluid with  $\leq 270 \text{ ppm } H_2O$  for distributed injection throughout the field. The hub processes  $\approx 1.0 \cdot 10^5 \text{ bbl}/\text{d}$  of oil and  $\approx 50 \text{ MMSm}^3/\text{d}$  of raw NG with  $\approx 68\% \text{ mol } CO_2$ .

Case Study 1 addresses comparison of NG processing through SS-based alternative versus conventional way. The SS-based alternative is named as SS-SS, prescribing a 1<sup>st</sup> SS unit for WDPA+HCDPA and a 2<sup>nd</sup> SS unit for  $CO_2$  removal producing Fuel-Gas. The conventional way is named as MS-JT-MP, prescribing adsorption in Molecular-Sieves (MS) for dehydration, JT-Expansion for HCDPA and Membrane-Permeation for  $CO_2$  capture.

Case Study 2 starts with the SS-SS alternative renamed as Base-Case [RC+JT+SS], addressing the following three structural decisions (maintaining SS use for WDPA+HCDPA):

- (i) should the condensate of 1<sup>st</sup> SS unit be recycled to HPS (RC option) or not (NR option)?
- (ii) should the HPS-Gas be expanded to the working pressure of the 1<sup>st</sup> SS unit in a Joule-Thomson valve (JT option) or in a Turbo-expander for power generation (TX option)?
- (iii) should  $CO_2$  removal be performed by a 2<sup>nd</sup> SS unit (SS option) or by Membrane-Permeation (MP option)?

Among all possible combinations, the following alternatives are selected for comparison: Base-Case [RC+JT+SS], TX-variant [RC+TX+SS], NR-variant [NR+JT+SS] and MP-variant [RC+JT+MP].

### 5.2.1. Modeling of Supersonic Separators

This work applies SS-UOE as rigorous thermodynamic model for SS design and simulation, and PEC-UOE for rigorous estimation of multiphase sound speed in HYSYS 8.8.

### 5.2.2. Process Simulation Assumptions

Table 5.1 summarizes adopted premises for CO<sub>2</sub>-rich NG processing.

### 5.2.3. Heat Inputs, Thermal Utilities, Heat Sinks

In WHRU, two hot utilities are heated by exhaust gas from gas-turbines at  $T \approx 600^\circ\text{C}$ : PHW ( $T^{PHW} \in [110^\circ\text{C}, 210^\circ\text{C}]$ ,  $P^{PHW} = 22 \text{ bar}$ ) and TF ( $T^{TF} \in [220^\circ\text{C}, 380^\circ\text{C}]$ ,  $P^{TF} = 4 \text{ bar}$ ). TF is only used in TX-variant [RC+TX+SS] to heat HPS-Gas up to  $T = 350^\circ\text{C}$ . WHRUs of gas-turbines assume recovery capacity of  $0.75 \text{ MW}_{heat}/\text{MW}_{power}$  (Teixeira et al., 2016). To provide heat integration, water loops are created as hot utilities at different  $T$  recovering heat when cooling fluids down to  $T = 45^\circ\text{C}$ : CW ( $T^{CW} \in [35^\circ\text{C}, 45^\circ\text{C}]$ ), WW ( $T^{WW} \in [35^\circ\text{C}, 80^\circ\text{C}]$ ), and HW ( $T^{HW} \in [35^\circ\text{C}, 110^\circ\text{C}]$ ). Seawater (SW) at  $T = 25^\circ\text{C}$  returning at  $T = 35^\circ\text{C}$  is availed to dissipate residual heat of CW, WW and HW, regenerating them as cold utilities at  $T = 35^\circ\text{C}$ .

### 5.2.4. Refrigeration-Cycle

In cases adopting SS unit for CO<sub>2</sub> capture, a refrigeration-cycle is included to provide partial condensation of Dry-Gas at  $T = -20^\circ\text{C}$  to reduce the CO<sub>2</sub> content of SS feed from  $\approx 69\% \text{ mol}$  to  $\approx 45\% \text{ mol}$ . The refrigeration-cycle uses pure CO<sub>2</sub> as working fluid, which boils at  $T = -25^\circ\text{C}$  with  $5^\circ\text{C}$  of thermal approach (Table 5.1, assumption {F6}). The condenser is installed within the top portion of LTX, being chilled by cold condensate leaving the 1<sup>st</sup> SS unit at  $T = -17^\circ\text{C}$ , which allows heat rejection at  $T = 0^\circ\text{C}$ .

### 5.2.5. Process Economic Evaluation

Economic analysis evaluates the Net Present Value ( $NPV, USD$ ) of alternatives by using the methods of Turton et al. (2009). Formulas and assumptions are detailed in Appendix X1. Revenues ( $REV, USD/y$ ) have contribution from EOR-Fluid, incremental oil production comparatively to the alternative with the lowest production ( $45 \text{ USD}/\text{bbl}$ ), and Fuel-Gas availed to power generation. EOR yield is assumed at  $1 \text{ bbl}/t^{CO_2}$ , resulting in EOR-Fluid valued at  $45 \text{ USD}/t$ . Considering that  $0.6\text{-}2.6 \text{ bbl}/t^{CO_2}$  was reported for injection of pure CO<sub>2</sub> in Texas-US mature fields (McCoy, 2008), the assumed yield is conservative given the oil field is young and higher yield should be obtained with this EOR-Fluid ( $\approx 71\% \text{ mol CO}_2$ ).

**Table 5.1.** Process simulation assumptions: offshore processing of NG with high % CO<sub>2</sub>.

<b>Code</b>	<b>Topic or Unit</b>	<b>Description</b>
{F1}	Simulation	HYSYS 8.8 with unit models: Membrane-Permeation: MP-UOE (Arinelli et al., 2017) Supersonic Separator: SS-UOE (Arinelli et al., 2017) Multiphase Sound Speed: PEC-UOE (de Medeiros et al., 2017)
{F2}	Thermodynamic model	PR-EOS
{F3}	Thermal approach	$\Delta T^{\text{Approach}}=10^\circ\text{C}$ (exception {F6}).
{F4}	Thermal utility loops for heating/cooling under heat recovery with specific T ranges	CW: Cooling-Water, $P=4$ bar, $T\in[35^\circ\text{C},45^\circ\text{C}]$ ; WW: Warm-Water, $P=4$ bar, $T\in[35^\circ\text{C},80^\circ\text{C}]$ ; HW: Hot-Water, $P=4$ bar, $T\in[35^\circ\text{C},110^\circ\text{C}]$ ; PHW: Pressurized-Hot-Water, $P=22$ bar, $T\in[110^\circ\text{C},210^\circ\text{C}]$ ; TF: Thermal-Fluid, $P=4$ bar, $T\in[220^\circ\text{C},380^\circ\text{C}]$ .
{F5}	Heat source	WHRUs fed with exhausts from electric turboshafts and gas-turbines drivers, producing PHW (210°C) or TF (380°C), assuming 75MW-heat per 100MW-power (Teixeira et al., 2016).
{F6}	Refrigeration-cycle for SS CO <sub>2</sub> removal	Working fluid: Pure CO <sub>2</sub> ; $T^{\text{Evaporator}}=-25^\circ\text{C}$ ; $T^{\text{Condenser}}=0^\circ\text{C}$ ; $\Delta T^{\text{Approach}}=5^\circ\text{C}$ .
{F7}	EOR-Fluid	$P=450$ bar
{F8}	1 <sup>st</sup> SS unit WDPA+HCDPA	12 SS nozzles, LTX for L+W condensate, Linear diameter profile (Fig. 5.3) $D_I=100\text{mm}$ , $D_O=80\text{mm}$ , $\alpha=12.67^\circ$ , $\beta=2.66^\circ$ , $\eta^{\text{EXP}\%}=\eta^{\text{CMP}\%}=100\%$ , $P^{\text{in}}=80.5$ bar, $T^{\text{in}}\approx 45^\circ\text{C}$ , $Ma^{\text{Shock}}=1.52$ .
{F9}	2 <sup>nd</sup> SS unit CO <sub>2</sub> removal	Single SS nozzle, no LTX, Linear diameter profile (Fig. 5.3) $D_I=120\text{mm}$ , $D_O=90\text{mm}$ , $\alpha=15^\circ$ , $\beta=2.5^\circ$ , $\eta^{\text{EXP}\%}=\eta^{\text{CMP}\%}=100\%$ , $P^{\text{in}}=84$ bar, $T^{\text{in}}\approx 22^\circ\text{C}$ , $Ma^{\text{Shock}}=1.59$ .
{F10}	Membrane-Permeation CO <sub>2</sub> removal	Counter-current spiral-wound single-stage, $T^{\text{Feed}}=62^\circ\text{C}$ , $P^{\text{Permeate}}=8$ bar, $\Delta P^{\text{Retentate}}\approx 1$ bar,
{F11}	Oil-gas-water process feed	$F=156250$ kmol/h, $P=120$ bar, $T=16^\circ\text{C}$ ; %mol: H <sub>2</sub> O=40.7%, CO <sub>2</sub> =39.7%, N <sub>2</sub> =0.154%, CH <sub>4</sub> =14.6%, C <sub>2</sub> H <sub>6</sub> =1.36%, C <sub>3</sub> H <sub>8</sub> =0.747%, iC <sub>4</sub> H <sub>10</sub> =0.130%, C <sub>4</sub> H <sub>10</sub> =0.291%, iC <sub>3</sub> H <sub>12</sub> =0.094%, C <sub>5</sub> H <sub>12</sub> =0.142%, C <sub>6</sub> H <sub>14</sub> =0.148%, C <sub>7</sub> H <sub>16</sub> =0.208%, C <sub>8</sub> H <sub>18</sub> =0.231%, C <sub>9</sub> H <sub>20</sub> =0.184%, C <sub>10</sub> H <sub>22</sub> =0.148%, C <sub>11</sub> H <sub>24</sub> =0.125%, C <sub>12</sub> H <sub>26</sub> =0.107%, C <sub>13</sub> H <sub>28</sub> =0.113%, C <sub>14</sub> H <sub>30</sub> =0.101%, C <sub>15</sub> H <sub>32</sub> =0.077%, C <sub>16</sub> H <sub>34</sub> =0.053%, C <sub>17</sub> H <sub>36</sub> =0.047%, C <sub>18</sub> H <sub>38</sub> =0.047%, C <sub>19</sub> H <sub>40</sub> =0.042%, C <sub>20+</sub> =0.433% (hypothetical, 409 kg/kmol, 905 kg/m <sup>3</sup> @25°C).
{F12}	Compressors and TX adiabatic efficiency	$\eta=75\%$
{F13}	Intercoolers using CW/WW/HW	$T^{\text{Outlet-Gas}}=45^\circ\text{C}$ , $\Delta P^{\text{Gas}}=0.5$ bar, $T^{\text{Inlet-CW}}=T^{\text{Inlet-WW}}=T^{\text{Inlet-HW}}=35^\circ\text{C}$ .
{F14}	Electric-Driver (ED)	$\text{Power}^{\text{ED}}\in[0,13\text{MW}]$ .
{F15}	Gas-Turbine Driver(GT)	$\text{Power}^{\text{GT}}\in[13\text{MW},28\text{MW}]$ .
{F16}	Molecular-Sieve (MS) Adsorption	Raw-Fluid: 56.16MMSm <sup>3</sup> /d, $P=120$ bar, $T=30.8^\circ\text{C}$ ;2363 ppmH <sub>2</sub> O; Adsorption-Time=20h; Removal <sup>H<sub>2</sub>O</sup> =0.13MMSm <sup>3</sup> /d; Vessels=12 (10 adsorbing, 2 regenerating); $D=4.1$ m; $L=11.2$ m; MS-Inventory=99.9 tons/vessel (1/8" bead). $P=119.9$ bar; $T=32^\circ\text{C}$ ; 1ppmH <sub>2</sub> O;
{F17}	Molecular-Sieve (MS) Regeneration	Total-Regeneration-Time=5h; Heating-Time=3h; Electric heater. $P=119.9$ bar; $T=260^\circ\text{C}$ ; REG-Gas (Dry-Fluid)=5.42MMSm <sup>3</sup> /d;
{F18}	JT HCDPA	Feed: Dry-Fluid, $P=119.9$ bar, $T=32^\circ\text{C}$ ; $\Delta P=64.9$ bar; $P^{\text{Vessel}}=55$ bar; $T^{\text{Vessel}}=-2.29^\circ\text{C}$ .

### 5.3. Case Study 1: Conventional NG Processing vs. SS-SS Alternative

This case study evaluates conventional NG processing against proposed alternative SS-SS. Flowsheets of alternatives MS-JT-MP and SS-SS are depicted in Figs. 5.4 and 5.5.

#### 5.3.1. Process Description

The first part of conventional process MS-JT-MP (Fig. 5.4) coincides with the respective of proposed alternative SS-SS (Fig. 5.5). Process alternatives initiate with multiphase feed from risers being sent to high-pressure separator (HPS) for primary oil-gas-water split ( $120\text{ bar}$ ). HPS-Oil is heated to  $T=90^{\circ}\text{C}$  and then expanded to  $P=20\text{ bar}$  creating a vapor phase, which is removed in the medium-pressure separator (MPS) and sent to compression in the Vapor-Recovery Unit (VRU). The liquid at  $P=20\text{ bar}$  (MPS-Oil) is then further expanded to  $P=1.8\text{ bar}$ , creating more vapor to be removed in the low-pressure separator (LPS) and then sent to VRU. The liquid at  $P=1.8\text{ bar}$  (LPS-Oil) is finally cooled against HPS-Oil heating, thus becoming stabilized oil. After recompression in VRU, LPS-Gas and MPS-Gas are joined to HPS-Gas. The VRU has multiple compression stages with intercoolers and knock-out drums, producing two-phase (water-hydrocarbons) condensates that are pumped back to HPS.

##### 5.3.1.1. Conventional Process: MS-JT-MP

Here, HPS-Gas processing embraces: (i) WDPA via Molecular-Sieve adsorption; (ii) production of Fuel-Gas  $\approx 20\% \text{mol CO}_2$  from Dry-Fluid by Joule-Thompson HCDPA followed by MP for  $\text{CO}_2$  removal; and (iii) EOR-Fluid (Dry-Gas enriched with  $\text{CO}_2$ ) compression/pumping.

VRU-Gas ( $4.15\text{ MMSm}^3/\text{d}$ ) is joined to HPS-Gas ( $\approx 50\text{ MMSm}^3/\text{d}$ ) at  $P=120\text{ bar}$  creating the feed stream of MS adsorption unit for fluid dehydration (Fig. 5.4), which comprises 12 large high-pressure vessels. The MS unit produces Dry-Fluid with only  $1\text{ ppmH}_2\text{O}$ . Further design conditions for MS adsorption and regeneration are presented in Table 5.1 (assumptions {F16} and {F17}). A small portion of the Dry-Fluid is extracted for Fuel-Gas production. Firstly it is sent to JT HCDPA ( $P^{\text{Out}}=55\text{ bar}$ , assumption {F18}), producing condensate to be pumped back to HPS (to improve oil production). The lean gas is heated to  $T=62^{\circ}\text{C}$  and subsequently treated by MP unit for Fuel-Gas production. Low-pressure  $\text{CO}_2$ -rich permeate at  $P=8\text{ bar}$  from MP is sent to  $\text{CO}_2$  compression (03 intercooled stages), from where it is discharged at  $P=119.9\text{ bar}$  to return to the Dry-Fluid Header, thus creating the MC-Gas stream. This stream is processed by Main-Compressor to achieve  $P=240\text{ bar}$  and then its is cooled down to  $T=45^{\circ}\text{C}$  becoming a liquid. Finally, it is pumped to  $P=450\text{ bar}$  for dispatch as EOR-Fluid.

### 5.3.1.2. Proposed Alternative: SS-SS

Here, HPS-Gas processing embraces: (i) WDPA+HCDPA in 1<sup>st</sup> SS unit producing Dry-Gas and water-hydrocarbons condensate (which requires previous expansion of HPS-Gas); (ii) production of Fuel-Gas  $\approx 20\%mol$  CO<sub>2</sub> from Dry-Gas by CO<sub>2</sub> removal in a 2<sup>nd</sup> SS unit; and (iii) EOR-Fluid compression/pumping. Expansion of HPS-Gas to feed 1<sup>st</sup> SS unit is necessary as SS operation has problems with  $\approx 68\%mol$  CO<sub>2</sub> above 85 bar due to high  $\rho$  and  $\bar{\varepsilon}_p$  abating  $c$  (de Medeiros et al., 2017), causing fluid speeds too slow for enough cooling.

The 1<sup>st</sup> SS unit is featured by several SS nozzles (Fig. 5.3) operating in parallel for WDPA+HCDPA. These nozzles are connected to a single LTX receiving L+W condensate, which has its bottoms warmed at  $\approx 20^\circ C$  to avoid hydrate formation. The recovered two-phase (L+W) condensate is pumped back to HPS, increasing flow rates of HPS-Gas, VRU-Gas, and HPS-Oil. The HPS-Gas is heated and expanded to  $P=81$  bar in a JT-valve, and then it is mixed with VRU-Gas creating at  $T=45^\circ C$  a two-phase (water-HCs) condensate that is removed in the pre-flash vessel. This condensate is joined to the condensate of 1<sup>st</sup> SS unit being recycled to the HPS (Fig. 5.5).

A small portion of Dry-Gas from 1<sup>st</sup> SS unit (SS-Gas) is extracted to produce the required flow rate of Fuel-Gas (FG) to the platform. The 2<sup>nd</sup> SS unit is preceded by a pre-decarbonation step with refrigeration-cycle to cool such a portion of SS-Gas to  $T=-20^\circ C$  ( $P\approx 50$  bar), recovering CO<sub>2</sub>-rich liquid. Partial condensation of refrigerated gas with CO<sub>2</sub>-rich liquid removal at  $T=-20^\circ C$  reduces CO<sub>2</sub> content from  $\approx 69\%mol$  to  $45.34\%mol$ , thus preparing the gas to subsequent compression ( $P\approx 84$  bar) and cooling ( $T=-22^\circ C$ ) for CO<sub>2</sub> removal in the 2<sup>nd</sup> SS unit. The 2<sup>nd</sup> SS unit is featured by a single SS nozzle (Fig. 5.3) processing a small fraction of Dry-Gas for CO<sub>2</sub> removal to produce Fuel-Gas and CO<sub>2</sub>-rich condensate to EOR. Both SS products are available for feed cooling: Fuel-Gas at  $T=-28.55^\circ C$  and CO<sub>2</sub>-rich condensate at  $T\approx 61^\circ C$ . This condensate is partially vaporized: the gas-phase (GCO<sub>2</sub>) is recompressed and sent to Main-Compressor after joining SS-Gas header (SSGH), and the liquid (LCO<sub>2</sub>) is directly pumped to EOR-Pump. The CO<sub>2</sub>-rich stream recovered at pre-decarbonation is also available to reduce cooling requirements, being totally vaporized creating the stream GFLS, which is recompressed and sent to Main-Compressor after joining SSGH.

The Main-Compressor feed (stream MC-Gas,  $\approx 50$  MMsm<sup>3</sup>/d,  $P=53.74$  bar,  $\approx 71\%mol$  CO<sub>2</sub>) discharges fluid at  $P=240$  bar to be cooled down to  $T=45^\circ C$ , becoming a liquid. Then it is finally pumped to  $P=450$  bar together with other liquids (e.g. LCO<sub>2</sub>) for dispatch to EOR. More detailed description of SS-SS process flowsheet is provided in Sections 5.4.1 and 5.4.2.

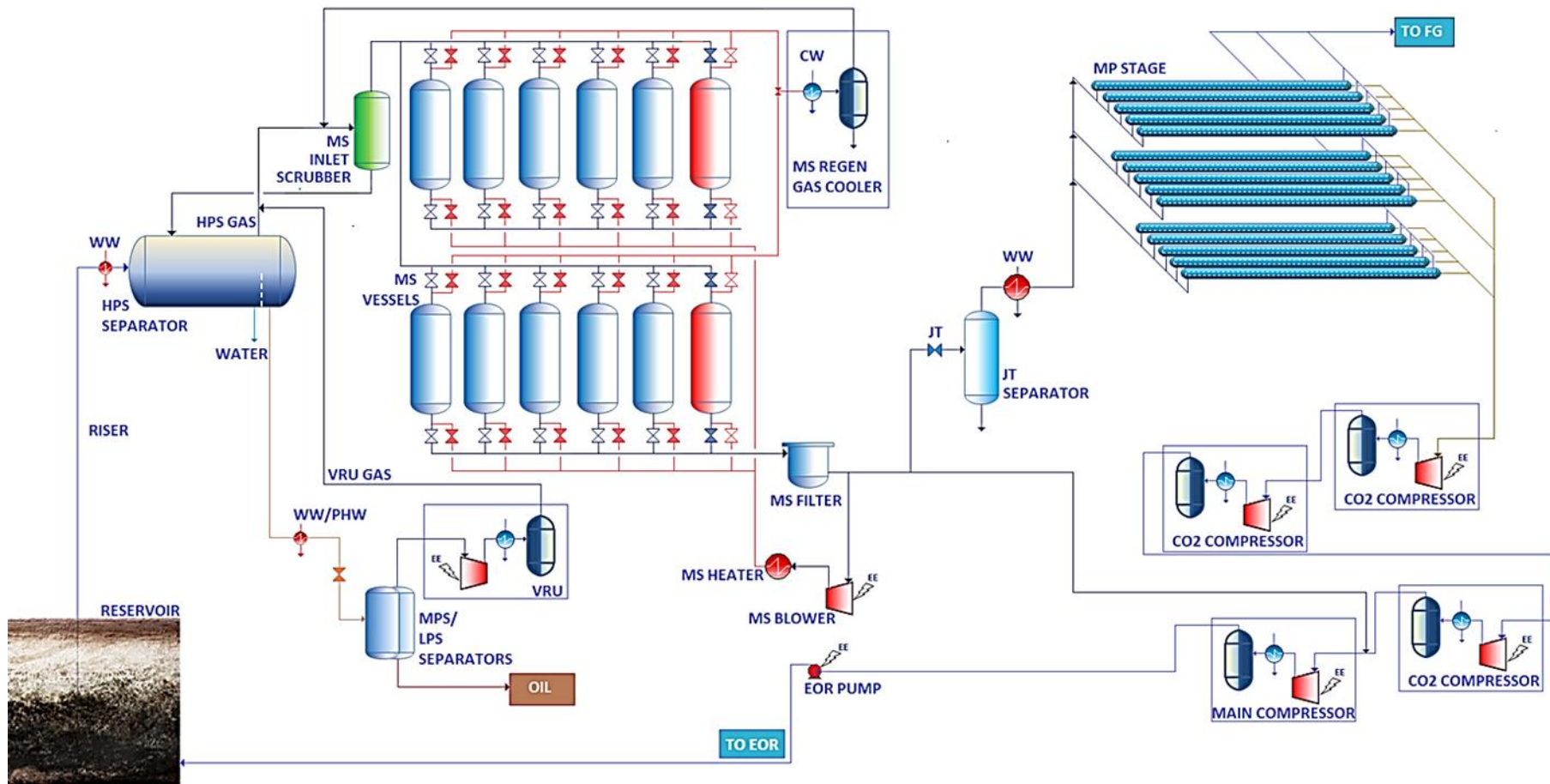


**Fig. 5.4.** Conventional MS-JT-MP supercritical fluid processing: molecular-sieves (MS) WDPA, JT expansion HDPA and Membrane-Permeation (MP) CO<sub>2</sub> removal.

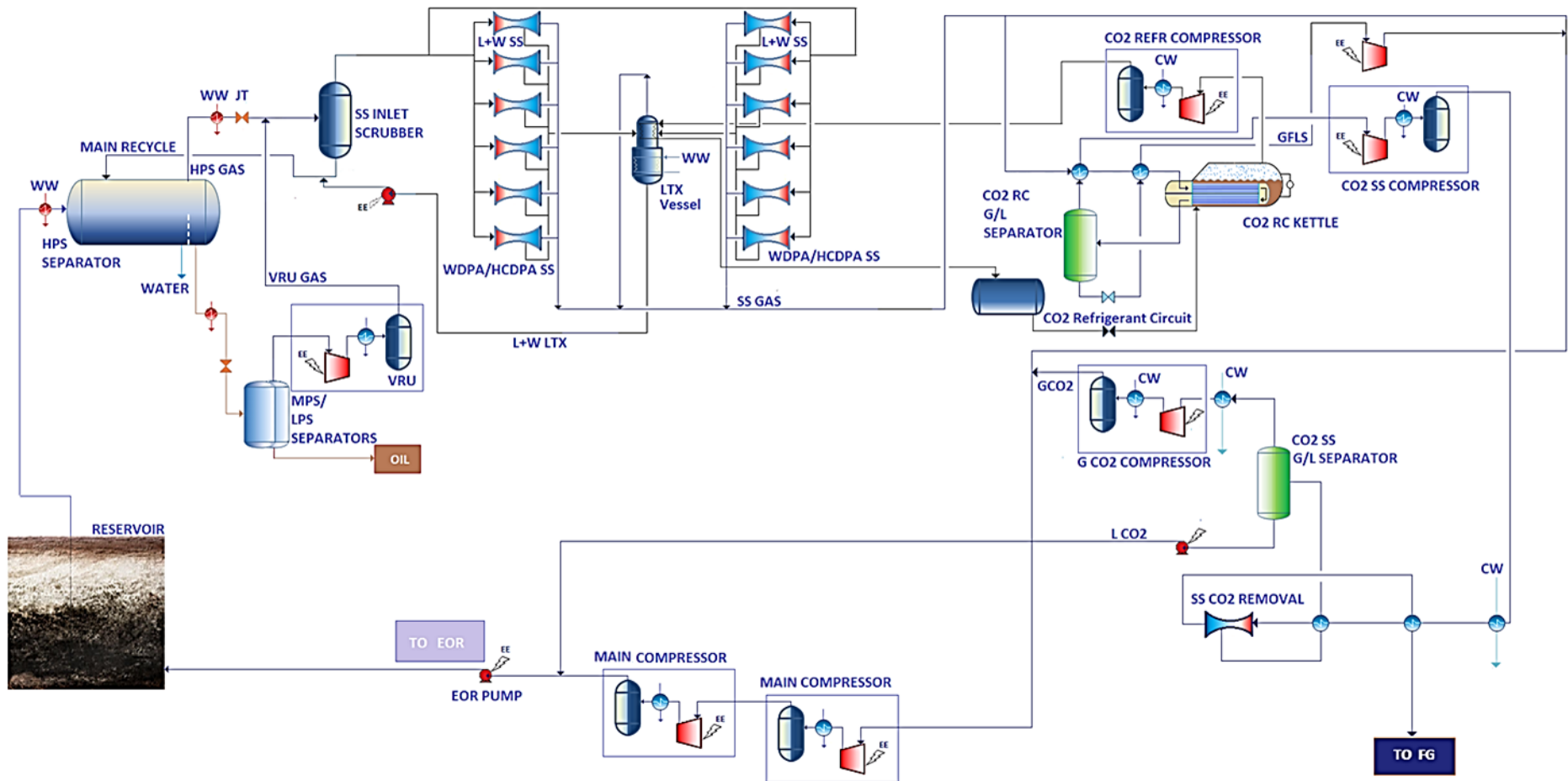


Fig. 5.5. SS-SS supercritical fluid processing: 1<sup>st</sup> SS unit for WDPA-HCDPA, 2<sup>nd</sup> SS unit for CO<sub>2</sub> removal.

### 5.3.2. Results and Discussion

Tables 5.2 and 5.3 unveil simulation results for main streams of alternatives MS-JT-MP and SS-SS. All processes share the same multiphase feed, but each one has its own flow rates of Oil, Fuel-Gas and EOR-Fluid accordingly to their power demand and process performance. Sections 5.3.2.1 and 5.3.2.2 individually address technical results of these alternatives, while comparison of economic and environmental performances is provided in Section 5.3.2.3.

#### 5.3.2.1. Conventional Process MS-JT-MP

MS-JT-MP (Fig. 5.4) produces  $\approx 100,000$  bbl/d of oil ( $15,978$  m<sup>3</sup>/d) with  $34.3^\circ$ API processing  $\approx 50$  MMSm<sup>3</sup>/d of HPS-Gas. The strongest aspects of MS-JT-MP are the extreme degree of dehydration achieved by MS adsorption – as H<sub>2</sub>O content is reduced from  $2363$  ppm to  $1$  ppm-mol (Table 5.2) – and the high MS operating pressure at  $P=120$  bar dispensing the need to expand HPS-Gas, implying in savings in downstream compression demand. However, MS dehydration has drawback of requiring 12 giant high-pressure vessels leading to enormous FCI and high manufacturing costs (which is discussed in Sec. 5.3.2.3) owing to huge flow rate of fluid being processed ( $\approx 54.16$  MMSm<sup>3</sup>/d in the feed, Table 5.2).

Table 5.2 reveals that  $5.00$  MMSm<sup>3</sup>/d of Dry-Fluid leaving the MS at  $T=32^\circ$ C (MS-Gas,  $54.03$  MMSm<sup>3</sup>/d) is extracted for JT HCDPA and CO<sub>2</sub> removal by MP in order to produce Fuel-Gas (FG) to the platform. JT HCDPA inconveniently require intense depressurization – from  $\approx 120$  bar to  $\approx 55$  bar (Table 5.2) – to provide substantial temperature decrease ( $T=-2.29^\circ$ C) to condense C<sub>3</sub>+. This condensate ( $\approx 2.03$  MMSm<sup>3</sup>/d,  $\approx 78\%$ mol CO<sub>2</sub>) is pumped back to HPS (though not shown in Fig. 5.4). About  $\approx 2.97$  MMSm<sup>3</sup>/d of lean gas  $\approx 69\%$ mol CO<sub>2</sub> from JT HCDPA feeds the MP unit for CO<sub>2</sub> removal at  $T=62^\circ$ C and  $P=54$  bar. The MP unit (spiral-wound  $Area^{MP}=4858$  m<sup>2</sup>) produces  $1.04$  MMSm<sup>3</sup>/d of FG with  $19.92\%$ mol CO<sub>2</sub> in retentate side and  $1.93$  MMSm<sup>3</sup>/d of CO<sub>2</sub>-rich fluid at  $P=8$  bar in permeate ( $\approx 86\%$ mol CO<sub>2</sub>). The major disadvantage of MP technology is the need to recompress the permeate from  $P=8$  bar to  $120$  bar to allow its incorporation to Dehydrated-Gas (DHG,  $49.02$  MMSm<sup>3</sup>/d) in Main-Compressor feed (MC-Gas). MS-JT-MP then produces  $\approx 50.96$  MMSm<sup>3</sup>/d of EOR-Fluid at  $P=450$  bar with  $\approx 70\%$ mol CO<sub>2</sub> and  $\approx 1$ ppmH<sub>2</sub>O for dispatch to reinjection (Table 5.2).

**Table 5.2.** Gas-hub main streams for CO<sub>2</sub> ultra-rich NG processing: MS-JT-MP.

System	HPS		Oil	VRU	Molecular-Sieve WDPA			JT HCDPA		Membrane-Permeation			Main Compressor		EOR			
	Riser	Main-Recycle			HPS-Water	HPS-Gas	Final-Oil	VRU-Gas	Feed	MS-Gas	MS-Water	REG-Gas	Feed	C3+		Feed	FG	GCO <sub>2</sub>
T(°C)	30.0	6.18	29.6	29.6	39.6	45.0	30.79	32.0	45.0	32.0	32.0	-2.29	62.0	41.2	38.2	32.0	32.4	78.3
P(bar)	120.0	120.0	120.0	120.0	1.30	120.0	120.0	119.9	118.4	119.9	119.9	55.00	54.00	53.0	8.00	119.9	119.9	450.0
MMsm <sup>3</sup> /d	90.15	2.05	36.63	50.00	1.43	4.15	54.16	54.03	0.13	5.42	5.00	2.03	2.97	1.04	1.93	49.02	50.96	50.96
%Vapor	53.20	0.00	0.00	100	0.00	100	100	100	0.00	0.00	100	0.00	100	100	100	100	100	0.00
%CO <sub>2</sub>	39.72	78.28	0.13	68.81	0.80	71.12	68.97	69.13	0.21	69.13	69.13	78.33	62.84	19.92	85.95	69.13	69.77	69.77
%CH <sub>4</sub>	14.59	12.58	0.00	25.22	0.06	19.41	24.77	24.82	0.00	24.82	24.82	12.58	33.20	69.13	13.85	24.82	24.41	24.41
%C <sub>2</sub> H <sub>6</sub>	1.36	2.47	0.00	2.28	0.11	3.33	2.36	2.37	0.00	2.37	2.37	2.47	2.29	6.49	0.04	2.37	2.28	2.28
%C <sub>3</sub> H <sub>8</sub>	0.75	1.96	0.00	1.21	0.42	2.52	1.31	1.31	0.00	1.31	1.31	1.96	0.86	2.46	0.00	1.31	1.26	1.26
%i-C <sub>4</sub> H <sub>10</sub>	0.13	0.41	0.00	0.21	0.23	0.49	0.23	0.23	0.00	0.23	0.23	0.41	0.10	0.30	0.00	0.23	0.22	0.22
%C <sub>4</sub> H <sub>10</sub>	0.29	0.95	0.00	0.44	0.81	1.16	0.50	0.50	0.00	0.50	0.50	0.95	0.19	0.54	0.00	0.50	0.48	0.48
%i-C <sub>5</sub> H <sub>12</sub>	0.09	0.32	0.00	0.14	0.63	0.35	0.15	0.15	0.00	0.15	0.15	0.32	0.04	0.11	0.00	0.15	0.15	0.15
%C <sub>5</sub> H <sub>12</sub>	0.14	0.48	0.00	0.20	1.19	0.52	0.22	0.22	0.00	0.22	0.22	0.49	0.05	0.13	0.00	0.22	0.22	0.22
%C <sub>6</sub> H <sub>14</sub>	0.15	0.46	0.00	0.19	2.42	0.34	0.20	0.20	0.00	0.20	0.20	0.46	0.02	0.06	0.00	0.20	0.19	0.19
%C <sub>7</sub> H <sub>16</sub>	0.21	0.47	0.00	0.20	6.34	0.18	0.20	0.20	0.00	0.20	0.20	0.47	0.01	0.03	0.00	0.20	0.19	0.19
%C <sub>8</sub> H <sub>18</sub>	0.23	0.44	0.00	0.19	8.30	0.07	0.18	0.18	0.00	0.18	0.18	0.44	0.00	0.01	0.00	0.18	0.18	0.18
%C <sub>9</sub> H <sub>20</sub>	0.18	0.30	0.00	0.13	7.40	0.01	0.12	0.12	0.00	0.12	0.12	0.30	0.00	0.00	0.00	0.12	0.12	0.12
%C <sub>10</sub> H <sub>22</sub>	0.16	0.22	0.00	0.10	7.29	0.00	0.09	0.09	0.00	0.09	0.09	0.22	0.00	0.00	0.00	0.09	0.08	0.08
%C <sub>11</sub> H <sub>24</sub>	0.11	0.14	0.00	0.06	4.86	0.00	0.06	0.06	0.00	0.06	0.06	0.14	0.00	0.00	0.00	0.06	0.06	0.06
%C <sub>12</sub> H <sub>26</sub>	0.13	0.12	0.00	0.05	6.62	0.00	0.05	0.05	0.00	0.05	0.05	0.12	0.00	0.00	0.00	0.05	0.05	0.05
%C <sub>13</sub> H <sub>28</sub>	0.09	0.08	0.00	0.04	4.41	0.00	0.03	0.03	0.00	0.03	0.03	0.08	0.00	0.00	0.00	0.03	0.03	0.03
%C <sub>14</sub> H <sub>30</sub>	0.12	0.06	0.00	0.03	6.45	0.00	0.02	0.02	0.00	0.02	0.02	0.06	0.00	0.00	0.00	0.02	0.02	0.02
%C <sub>15</sub> H <sub>32</sub>	0.07	0.04	0.00	0.02	3.87	0.00	0.01	0.01	0.00	0.01	0.01	0.04	0.00	0.00	0.00	0.01	0.01	0.01
%C <sub>16</sub> H <sub>34</sub>	0.05	0.02	0.00	0.01	2.58	0.00	0.01	0.01	0.00	0.01	0.01	0.02	0.00	0.00	0.00	0.01	0.01	0.01
%C <sub>17</sub> H <sub>36</sub>	0.07	0.02	0.00	0.01	4.07	0.00	0.01	0.01	0.00	0.01	0.01	0.02	0.00	0.00	0.00	0.01	0.01	0.01
%C <sub>18</sub> H <sub>38</sub>	0.04	0.01	0.00	0.00	2.44	0.00	0.00	0.00	0.00	0.00	0.00	0.01	0.00	0.00	0.00	0.00	0.00	0.00
%C <sub>19</sub> H <sub>40</sub>	0.03	0.02	0.00	0.00	1.63	0.00	0.01	0.01	0.00	0.01	0.01	0.02	0.00	0.00	0.00	0.01	0.01	0.01
%C <sub>20+</sub>	0.43	0.00	0.00	0.00	27.08	0.00	0.00	0.00	0.00	0.00	0.00	0.00	0.00	0.00	0.00	0.00	0.00	0.00
%N <sub>2</sub>	0.15	0.08	0.00	0.27	0.00	0.11	0.26	0.26	0.00	0.26	0.26	0.08	0.38	0.80	0.16	0.26	0.26	0.26
ppm H <sub>2</sub> S	29.65	67.29	0.00	48.18	5.28	91.96	51.52	51.64	0.00	51.64	51.64	67.34	40.91	12.97	55.95	51.64	51.81	51.81
ppm H <sub>2</sub> O		676.7		1944	17.77	3802	2363	1.00		1.00	1.00	1.97	0.34	0.11	0.46	1.00	0.98	0.98
%H <sub>2</sub> O	40.70	0.07	99.87	0.194		0.380	0.236		99.78									

**Table 5.3.** Gas-hub main streams for CO<sub>2</sub> ultra-rich NG processing: SS-SS / Base-Case [RC+JT+SS].

System	HPS			Oil	VRU	1 <sup>st</sup> SS unit WDPA+HCDPA					2 <sup>nd</sup> SS unit CO <sub>2</sub> Removal				Main Compressor		EOR
	Stream	Riser	Main-Recycle			HPS-Water	HPS-Gas	Final-Oil	VRU-Gas	Feed	SS-Gas	SS-L+W	LTX-L+W	Feed	FG	GCO2	
T(°C)	30.0	36.4	32.5	32.5	42.5	45.0	46.3	37.7	-17.0	20.0	-22.0	35.0	45.0	16.3	37.7	38.0	80.2
P(bar)	120.0	120.0	120.0	120.0	1.30	80.50	80.50	53.74	53.74	53.74	84.00	36.08	53.74	240.0	53.74	53.74	450.0
MMsm <sup>3</sup> /d	90.15	8.30	36.76	52.24	2.00	7.44	56.68	51.39	5.29	5.29	2.07	1.30	0.63	0.14	42.71	49.96	50.09
%Vapor	53.20	0.00	0.00	100	0.00	100	100	100	0.00	0.00	100	100	100	0.00	100	100	0.00
%CO <sub>2</sub>	39.72	54.39	0.13	67.31	0.64	68.51	68.52	69.57	58.39	58.39	45.34	21.85	83.50	92.90	69.57	70.74	70.80
%CH <sub>4</sub>	14.59	6.91	0.00	23.55	0.05	19.12	23.70	25.60	5.20	5.20	51.02	74.73	12.59	2.62	25.60	24.38	24.32
%C <sub>2</sub> H <sub>6</sub>	1.36	2.76	0.00	2.34	0.09	3.15	2.43	2.39	2.85	2.85	2.18	2.06	2.52	1.74	2.39	2.40	2.40
%C <sub>3</sub> H <sub>8</sub>	0.75	4.81	0.00	1.62	0.46	2.89	1.69	1.29	5.55	5.55	0.59	0.25	1.04	1.67	1.29	1.32	1.32
%i-C <sub>4</sub> H <sub>10</sub>	0.13	1.97	0.00	0.41	0.37	0.80	0.41	0.21	2.32	2.32	0.06	0.01	0.10	0.29	0.21	0.22	0.22
%C <sub>4</sub> H <sub>10</sub>	0.29	6.04	0.00	1.08	1.64	2.25	1.06	0.44	7.07	7.07	0.09	0.01	0.14	0.57	0.44	0.46	0.46
%i-C <sub>5</sub> H <sub>12</sub>	0.09	3.25	0.00	0.47	1.88	0.91	0.42	0.09	3.60	3.60	0.01	0.00	0.01	0.09	0.09	0.09	0.09
%C <sub>5</sub> H <sub>12</sub>	0.14	5.09	0.00	0.72	3.71	1.32	0.60	0.10	5.47	5.47	0.01	0.00	0.01	0.08	0.10	0.10	0.10
%C <sub>6</sub> H <sub>14</sub>	0.15	3.67	0.00	0.53	5.80	0.51	0.32	0.02	3.28	3.28	0.00	0.00	0.00	0.01	0.02	0.02	0.02
%C <sub>7</sub> H <sub>16</sub>	0.21	2.41	0.00	0.37	8.81	0.09	0.16	0.00	1.65	1.65	0.00	0.00	0.00	0.00	0.00	0.00	0.00
%C <sub>8</sub> H <sub>18</sub>	0.23	2.12	0.00	0.33	10.10	0.02	0.10	0.00	1.03	1.03	0.00	0.00	0.00	0.00	0.00	0.00	0.00
%C <sub>9</sub> H <sub>20</sub>	0.18	1.38	0.00	0.22	8.18	0.00	0.04	0.00	0.44	0.44	0.00	0.00	0.00	0.00	0.00	0.00	0.00
%C <sub>10</sub> H <sub>22</sub>	0.16	0.97	0.00	0.15	7.35	0.00	0.02	0.00	0.20	0.20	0.00	0.00	0.00	0.00	0.00	0.00	0.00
%C <sub>11</sub> H <sub>24</sub>	0.11	0.65	0.00	0.10	4.90	0.00	0.01	0.00	0.08	0.08	0.00	0.00	0.00	0.00	0.00	0.00	0.00
%C <sub>12</sub> H <sub>26</sub>	0.13	0.53	0.00	0.08	5.93	0.00	0.00	0.00	0.04	0.04	0.00	0.00	0.00	0.00	0.00	0.00	0.00
%C <sub>13</sub> H <sub>28</sub>	0.09	0.35	0.00	0.06	3.96	0.00	0.00	0.00	0.02	0.02	0.00	0.00	0.00	0.00	0.00	0.00	0.00
%C <sub>14</sub> H <sub>30</sub>	0.12	0.28	0.00	0.04	5.21	0.00	0.00	0.00	0.01	0.01	0.00	0.00	0.00	0.00	0.00	0.00	0.00
%C <sub>15</sub> H <sub>32</sub>	0.07	0.17	0.00	0.03	3.13	0.00	0.00	0.00	0.00	0.00	0.00	0.00	0.00	0.00	0.00	0.00	0.00
%C <sub>16</sub> H <sub>34</sub>	0.05	0.11	0.00	0.02	2.08	0.00	0.00	0.00	0.00	0.00	0.00	0.00	0.00	0.00	0.00	0.00	0.00
%C <sub>17</sub> H <sub>36</sub>	0.07	0.09	0.00	0.01	3.25	0.00	0.00	0.00	0.00	0.00	0.00	0.00	0.00	0.00	0.00	0.00	0.00
%C <sub>18</sub> H <sub>38</sub>	0.04	0.05	0.00	0.01	1.95	0.00	0.00	0.00	0.00	0.00	0.00	0.00	0.00	0.00	0.00	0.00	0.00
%C <sub>19</sub> H <sub>40</sub>	0.03	0.12	0.00	0.02	1.30	0.00	0.00	0.00	0.00	0.00	0.00	0.00	0.00	0.00	0.00	0.00	0.00
%C <sub>20+</sub>	0.43	0.01	0.00	0.00	19.21	0.00	0.00	0.00	0.00	0.00	0.00	0.00	0.00	0.00	0.00	0.00	0.00
%N <sub>2</sub>	0.15	0.03	0.00	0.25	0.00	0.12	0.25	0.27	0.02	0.02	0.71	1.09	0.07	0.01	0.27	0.25	0.25
ppm H <sub>2</sub> S	29.65	81.91	0.00	51.57	4.21	85.63	55.08	51.61	88.83	88.83	28.56	12.57	52.34	70.94	51.61	52.57	52.52
ppm H <sub>2</sub> O		18396		2584	18.93	2972	2666	95.90	27651	27651	7.93	0.06	6.58	88.66	95.90	98.41	98.39
%H <sub>2</sub> O	40.70	1.84	99.87			0.297	0.267		2.765	2.765							

### 5.3.2.2. Proposed Alternative SS-SS / [RC+JT+SS]

SS-SS (Fig. 5.5) produces  $\approx 123,000$  bbl/d of oil ( $19,791$  m<sup>3</sup>/d) with  $37.91^\circ$ API processing  $\approx 52$  MMSm<sup>3</sup>/d of HPS-Gas. The strongest aspect of SS-SS is the increase of oil production capacity in the hub due to great C3+ recovery in L+W condensate of 1<sup>st</sup> SS unit ( $\approx 5.29$  MMSm<sup>3</sup>/d) and its subsequent recycle to HPS jointly with  $\approx 3.00$  MMSm<sup>3</sup>/d of pre-flash condensate, forming Main-Recycle fluid with  $\approx 54\%$ mol CO<sub>2</sub> (Table 5.3). The 1<sup>st</sup> SS unit performs NG WDPA+HCDPA reducing its C3+ content from  $4.83\%$ mol to  $2.15\%$ mol and its water content from  $2666$  ppm to  $95.90$  ppm (a suitable dehydration degree for such working scenario). A further great advantage of SS-SS alternative is that the 2<sup>nd</sup> SS unit produces high-pressure CO<sub>2</sub>-rich fluids for reinjection: GCO<sub>2</sub> ( $100\%$ vapor,  $0.63$  MMSm<sup>3</sup>/d,  $83.50\%$ mol CO<sub>2</sub>) and LCO<sub>2</sub> ( $0\%$ vapor,  $0.14$  MMSm<sup>3</sup>/d,  $92.90\%$ mol CO<sub>2</sub>) (Table 5.3).

About  $\approx 8.7$  MMSm<sup>3</sup>/d of Dry-Gas leaving the 1<sup>st</sup> SS unit (SS-Gas,  $51.39$  MMSm<sup>3</sup>/d,  $69.57\%$ mol CO<sub>2</sub>) is extracted for CO<sub>2</sub> removal to produce Fuel-Gas ( $21.85\%$ mol CO<sub>2</sub>) to the platform. The condensate of pre-decarbonation step is totally vaporized against feed cooling – to minimize refrigeration demand – generating the CO<sub>2</sub>-rich stream GFLS ( $\approx 6.62$  MMSm<sup>3</sup>/d,  $T=16.4^\circ$ C,  $P=41.50$  bar,  $\approx 77\%$ mol CO<sub>2</sub>). Table 5.3 reveals that  $\approx 2.07$  MMSm<sup>3</sup>/d of pre-decarbonated gas with  $45\%$ mol CO<sub>2</sub> is sent to 2<sup>nd</sup> SS unit at  $T=-22^\circ$ C and  $P=84$  bar. The 2<sup>nd</sup> SS unit produces  $1.30$  MMSm<sup>3</sup>/d of FG with  $\approx 22\%$ mol CO<sub>2</sub> and  $0.77$  MMSm<sup>3</sup>/d of CO<sub>2</sub>-rich condensate at  $P=36.6$  bar ( $\approx 85\%$ mol CO<sub>2</sub>). This latter is partially vaporized against feed cooling, then vapor and liquid phases are subsequently compressed/pumped originating GCO<sub>2</sub> and LCO<sub>2</sub> streams. SS-SS produces  $\approx 50.09$  MMSm<sup>3</sup>/d of EOR-Fluid for dispatch at  $P=450$  bar with  $\approx 71\%$ mol CO<sub>2</sub> and  $\approx 98.39$ ppmH<sub>2</sub>O (Table 5.3).

Table 5.4 presents design and operating conditions of 1<sup>st</sup> and 2<sup>nd</sup> SS units. The 1<sup>st</sup> SS unit comprises 12 parallel SS nozzles (Fig. 5.3) with  $L=22.38$ cm of length. Sonic flow is achieved at the SS throat, located at  $x=L_C=7.52$ cm with diameter of  $D_T=6.62$ cm, while maximum supersonic  $Ma$  of design  $Ma^{Shock}=1.52$  is attained at  $x=L^{Shock}=15.96$ cm, where condensate is collected. Right after this position and before normal shock,  $Ma$  falls to  $Ma_{BS}=1.3114$  due to liquid (L+W) withdrawal. After normal shock, the flow becomes subsonic with  $Ma_{AS}=0.8$  and then the fluid decelerates gaining  $P$  and  $T$  through the diffuser designed with  $L^{Diff}=6.42$ cm of length. The fluid enters the nozzle at  $P=80.5$  bar and  $T=45^\circ$ C as  $100\%$  vapor, achieving minimal pressure and minimal temperature of  $P=P_{BS}=25.6$  bar and  $T=T_{BS}=-16.78^\circ$ C at maximum supersonic  $Ma$  ( $Ma^{Shock}=1.52$ ,  $x=15.96$ cm), where it is  $90.67\%$  vapor. The 1<sup>st</sup> SS unit then recovers  $9.33\%$ mol of feed flow rate as two-phase L+W condensate

capturing 96.74% of H<sub>2</sub>O, 11.70% of C<sub>3</sub>+ and 7.95% of CO<sub>2</sub>. The pressure recovery across the SS nozzles of this unit is 66.76% ( $P^{Discharge}=53.74 \text{ bar}$ ).

**Table 5.4.** 1<sup>st</sup> and 2<sup>nd</sup> SS units of SS-SS: SS design and performance

<i>Specified Items</i>	<i>1<sup>st</sup> SS unit WDPA-HCDPA</i>	<i>2<sup>nd</sup> SS unit CO<sub>2</sub> Capture</i>	<i>Calculated by SS-UOE</i>	<i>1<sup>st</sup> SS unit WDPA-HCDPA</i>	<i>2<sup>nd</sup> SS unit CO<sub>2</sub> Capture</i>
<i>No.of SS</i>	12	1	$D_T(m)$	0.0662	0.03573
$D_I(m)$	0.10	0.12	$L_C(m)$	0.0752	0.1573
$D_O(m)$	0.08	0.09	$L_D(m)$	0.1486	0.6219
$\alpha(^{\circ})$	12.67	15	$L(m)$	0.2238	0.7792
$\beta(^{\circ})$	2.66	2.5	$L^{Shock}(m)$	0.1596	0.2560
$Ma^{Shock}$	1.52	1.6	$L^{Diff}(m)$	0.0642	0.5232
$\eta^{EXP}\%$	100	100	$P_{BS}(bar)$	25.60	21.70
$\eta^{CMP}\%$	100	100	$T_{BS}(^{\circ}C)$	-16.78	-61.10
$P^{Feed}(bar)$	80.5	84.0	$Ma_{BS}$	1.3114*	0.9651*+
$T^{Feed}(^{\circ}C)$	45	-22	$P^{Discharge}(bar)$	53.74	36.58
$MMsm^3/d$	56.7	2.07	$T^{Discharge}(^{\circ}C)$	37.73	-28.55
$\%molC_3^{+Feed}$	4.83%	0.75%	$\%P \text{ Recovery}$	66.76%	43.55%
$ppmH_2O^{Feed}$	2666	7.93	$\%mol \text{ Condensate}$	9.33% <sup>#</sup>	37.10% <sup>§</sup>
$\%molCO_2^{Feed}$	68.52%	45.34%	$REC\%molH_2O$	96.74%	99.50%
			$REC\%molC_3^{+}$	11.70%	10.14%
			$REC\%molCO_2$	7.95%	69.69%

\* After condensate withdrawal. <sup>#</sup>Total condensate (39%mol hydrocarbons+3%molH<sub>2</sub>O+58%molCO<sub>2</sub>)

+ No shock. <sup>§</sup>Total condensate (15%mol hydrocarbons+85%molCO<sub>2</sub>)

The 2<sup>nd</sup> SS unit comprises a single SS nozzle (Fig. 5.3) with  $L=77.92cm$  of length. Sonic flow is achieved at the SS throat, located at  $x=L_C=15.73cm$  with diameter of  $D_T=3.57cm$ , while maximum supersonic  $Ma$  of design  $Ma^{Shock}=1.6$  is attained at  $x=L^{Shock}=25.60cm$ , where condensate is collected. Right after this position,  $Ma$  falls to  $Ma_{BS}=0.9651$  due to liquid withdrawal. As this  $Ma_{BS}$  is already subsonic, no normal shock occurs in 2<sup>nd</sup> SS unit, and then the fluid decelerates gaining  $P$  and  $T$  through the diffuser designed with  $L^{Diff}=52.32cm$ . The fluid enters the nozzle at  $P=84.0 \text{ bar}$  and  $T=-22^{\circ}C$  as highly compressible liquid with 20% vapor, showing similar compositions in liquid and vapor phases owing to critical point proximity. As the fluid advances losing  $P$  and  $T$  in SS path, it moves away from critical neighborhood discriminating liquid and vapor compositions, thus allowing CO<sub>2</sub> separation in SS. The fluid achieves minimal pressure and minimal temperature of  $P=P_{BS}=21.7 \text{ bar}$  and  $T=T_{BS}= -61.10^{\circ}C$  (close to CO<sub>2</sub> freeze-out) at maximum supersonic  $Ma$  ( $Ma^{Shock}=1.6$ ,  $x=L^{Shock}=25.60cm$ ), where it is 62.90% vapor. The 2<sup>nd</sup> SS unit then recovers 37.10%mol of feed flow rate as single-phase condensate capturing 69.69% of CO<sub>2</sub> and 10.14% of C<sub>3</sub>+. The CO<sub>2</sub> removal is limited to 21.85%mol CO<sub>2</sub> in FG to avoid freeze-out issues (i.e.  $Ma^{Shock}$  should not be increased). By last, the pressure recovery across the SS nozzle is only 43.55% ( $P^{Discharge}=36.58 \text{ bar}$ ) owing to huge condensate withdrawal (37.10%mol of feed) (Table 5.4).

### 5.3.2.3. Alternatives Comparison

Fig. 5.6 compares alternatives performances concerning oil production, water content in EOR-Fluid, power demand, CO<sub>2</sub> emissions, capital investment (*FCI*) and CH<sub>4</sub> loss in CO<sub>2</sub> removal. *NPV* behavior of alternatives throughout the horizon years is unveiled in Fig. 5.7. Economic results and key streams of MS-JT-MP and SS-SS are respectively shown in Tables 5.5 and 5.6. Table 5.5 unveils SS-SS attaining *NPV* of +8211.7 *MMUSD* after 20 operational years, with capital investment of 925 *MMUSD*, while MS-JT-MP achieves ≈25% lower *NPV* with ≈10% higher *FCI*. Economic superiority of SS-SS is clearly revealed in Figs. 5.6 and 5.7.

**Table 5.5.** Summary of economic results.

<i>Process</i>	<i>FCI</i> ( <i>MMUSD</i> )	<i>COM</i> ( <i>MMUSD/y</i> )	<i>REV</i> ( <i>MMUSD/y</i> )	<i>CUT</i> ( <i>MMUSD/y</i> )	<i>GAP</i> ( <i>MMUSD/y</i> )	<i>NPV</i> ( <i>MMUSD</i> )
<i>SS-SS</i>	936.6	280.3	2363.0	90.3	2083.0	+8211.7
<i>MS-JT-MP</i>	1045.0	292.0	1889.6	83.5	1597.6	+6096.8

Table 5.6 presents flow rates of key streams in *MMSm<sup>3</sup>/d* unit, unveiling higher consumption of Fuel-Gas in SS-SS alternative, implying in higher EOR-Fluid flow rate at MS-JT-MP. This is an outcome of SS-SS higher power demand (Fig. 5.6c) – 167.2 *MW* against 105 *MW* of MS-JT-MP – which also leads to slightly higher CO<sub>2</sub> emissions (Fig. 5.6d). Breakdown of power demands in Fig. 5.6c reveals substantially higher consumption on EOR-Fluid compression at SS-SS, which occurs due to depressurization of HPS-Gas before entering the 1<sup>st</sup> SS unit, entailing one more compression stage to process Dry-Gas, while MS is able to work at the same pressure of HPS-Gas, keeping it as a supercritical fluid at *P*=120 *bar*.

**Table 5.6.** Flow rates in *MMSm<sup>3</sup>/d* of key streams in SS-SS and MS-JT-MP.

<i>MMSm<sup>3</sup>/d</i>	<i>SS-SS</i>	<i>MS-JT-MP</i>
<i>Riser</i>	90.15	90.15
<i>EOR-Fluid</i>	50.09 <sup>*1</sup>	50.96 <sup>#1</sup>
<i>Fuel-Gas</i>	1.30 <sup>*2</sup>	1.04 <sup>#2</sup>
<i>Main Recycle</i>	8.31	2.05
<i>Water-C3+ Condensate</i>	5.29	2.03
<i>HPS-Gas</i>	52.24	50.01
<i>Captured CO<sub>2</sub></i>	0.65611	1.661921
<i>Captured CH<sub>4</sub></i>	0.078585	0.267744
<i>CO<sub>2</sub> Emissions</i>	1.31989	1.1945
<i>Oil</i>	2.0	1.43

<sup>\*1</sup>70.8%mol CO<sub>2</sub>, <sup>#1</sup>69.8%mol CO<sub>2</sub>, <sup>\*2</sup>(%mol) 21.85%CO<sub>2</sub>, 74.73%C1, 2.06%C2, 0.25%C3, 0.02%C4.

<sup>#2</sup>(%mol) 19.92%CO<sub>2</sub>, 69.13%C1, 6.49%C2, 2.46%C3, 0.84%C4, 0.24%C5, 0.06%C6, 0.03%C7.

Emissions of SS-SS and MS-JT-MP are in different proportions to respective power consumptions owing to different Fuel-Gas compositions, as revealed in footnotes of Table 5.6. SS-SS Fuel-Gas has much less heavy hydrocarbons thanks to condensation of heavy components in the 2<sup>nd</sup> SS unit, enriching the Fuel-Gas in CH<sub>4</sub> and CO<sub>2</sub>, while the opposite occurs in Membrane-Permeation at MS-JT-MP alternative, since practically only CH<sub>4</sub> and CO<sub>2</sub> permeate, enriching the Fuel-Gas (retentate) in heavier hydrocarbons. In connection with this, Fig. 5.6f reveals MS-JT-MP with higher CH<sub>4</sub> capture to EOR-Fluid, an outcome of poor CO<sub>2</sub>/CH<sub>4</sub> selectivity of MP unit.

Fig. 5.6a evinces significantly greater oil production of SS-SS alternative, positively affecting gross annual profits (*GAP*) due to increased revenues (*REV*), which mainly explains higher profitability of SS-SS (Table 5.5). This is a consequence of recycling to HPS a high flow rate (5.29 *MMSm*<sup>3</sup>/*d*, Table 5.6) of moderately carbonated L+W condensate from 1<sup>st</sup> SS unit (58.4%*mol* CO<sub>2</sub>, Table 5.3), comparatively to modest flow rate (2.03 *MMSm*<sup>3</sup>/*d*, Table 5.6) of highly-carbonated liquid obtained in JT HCDPA of MS-JT-MP (78.3%*mol* CO<sub>2</sub>, Table 5.2). In addition to the effect of enlarged flows of processed NG, unveiled in Table 5.6, as recycled condensates contain C3+ species, they also increase oil production of respective alternatives. These aspects evinces 1<sup>st</sup> SS unit of SS-SS with higher C3+ recovery than JT at MS-JT-MP.

While SS-SS higher profitability is closely related to its incremental oil production (Fig. 5.6a), SS-SS lower capital investment is mainly connected with water contents in EOR-Fluid. In this regard, Fig. 5.6b unveils strict water content of 1*ppmH*<sub>2</sub>*O* in EOR-Fluid of MS-JT-MP due to much higher dehydration capacity of MS adsorption compared to SS. However, as ≈100*ppmH*<sub>2</sub>*O* in EOR-Fluid of SS-SS is also perfectly acceptable for plant operation, one may guess whether such excessive water removal does appear somewhere as an unnecessary economic charge negatively affecting MS-JT-MP performance. In fact, this charge is found in MS unit *FCI*, shown in Fig. 5.6e, owing to the need for installing 12 large MS vessels (*D*=4.1*m*, *L*=11.24*m*), which indeed constitutes the major share of MS-JT-MP total *FCI*.

Confirming the above discussion suggesting SS-SS as the best process alternative from economic perspective, Fig. 5.7 projects *NPV* of alternatives clearly revealing SS-SS with higher cash flow on all years of analysis.

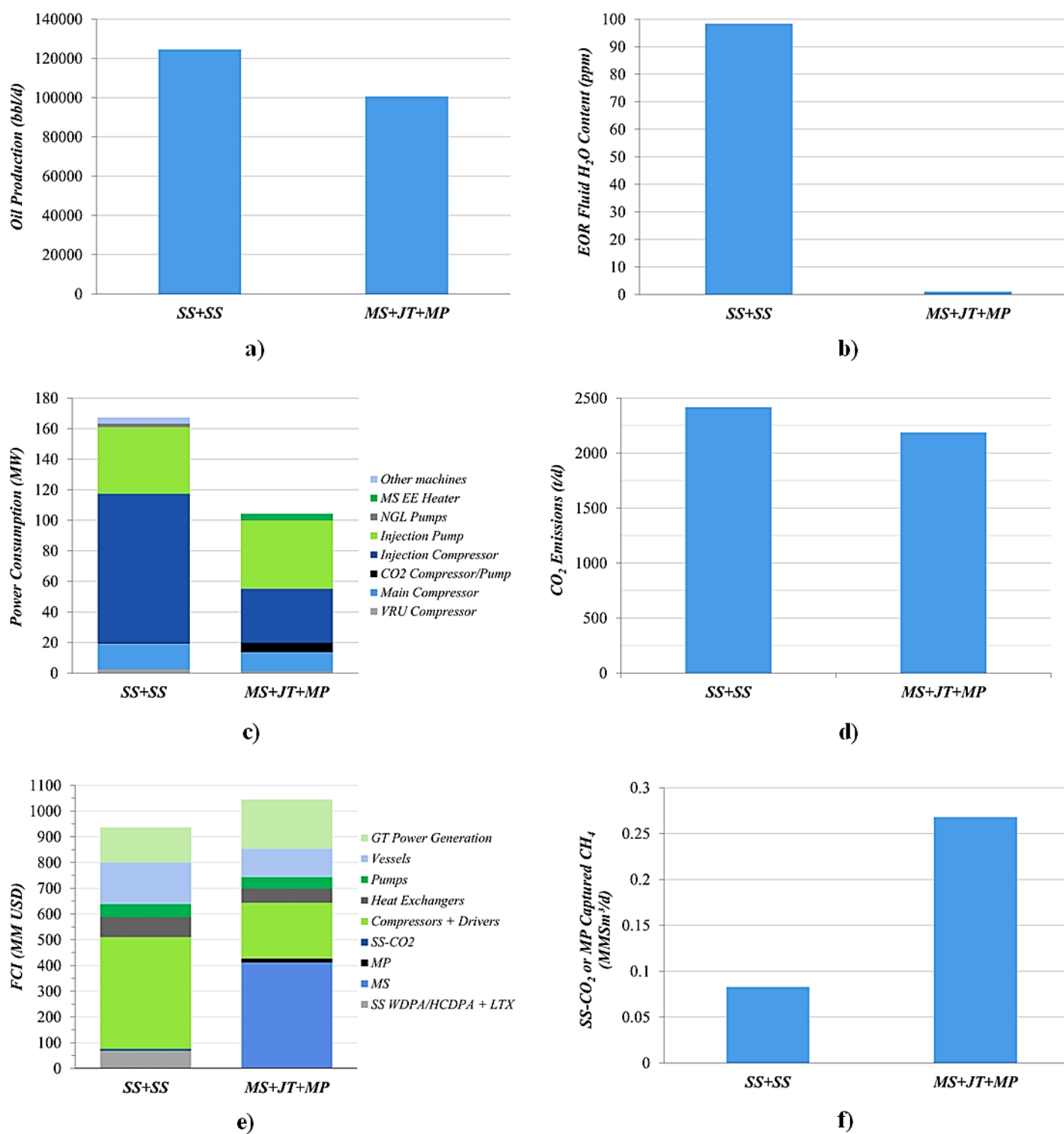


**Fig. 5.6.** SS-SS versus MS-JT-MP: (a) oil production; (b) water content in EOR-Fluid; (c) power consumption; (d) CO<sub>2</sub> emissions; (e) FCI; (f) CH<sub>4</sub> loss in CO<sub>2</sub> removal.

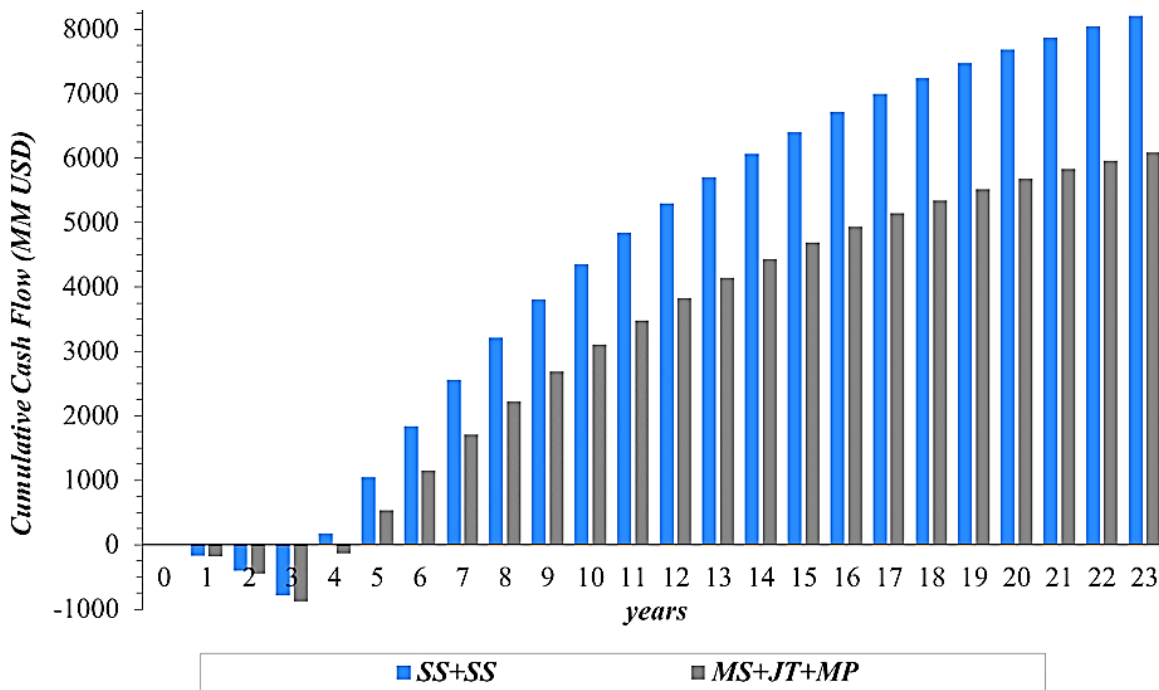


**Fig. 5.7.** Net present value of alternatives.

From the environmental perspective, Fig. 5.6d portrays SS-SS alternative implying little more CO<sub>2</sub> emissions than MS-JT-MP (Table 5.6), reflecting the higher power consumption of SS-SS (Fig. 5.6c), as the 1<sup>st</sup> SS unit requires inlet pressure below 80.5 bar forcing depressurization of HPS-Gas to avoid compressibility shortcomings. However, since SS-SS and MS-JT-SS alternatives have different oil outputs, the SS-SS alternative actually presents lower carbon footprint per barrel of oil, owing to its substantially greater oil production. Moreover, provided the SS-SS process presents very prominent economic advantage over MS-JT-SS, SS-SS also become the best alternative on environmental perspective if this advantage is availed to afford treatment of gas-turbine exhaust-gases by post-combustion CO<sub>2</sub> capture for drastic CO<sub>2</sub> abatement. Therefore, despite presenting slightly higher CO<sub>2</sub> emissions, SS-SS solution can be regarded as a cleaner process alternative.

## 5.4. Case Study 2: SS-SS Alternative Consolidation

### 5.4.1. Gas-Hub Processing Alternatives

Complete process flow diagrams of considered alternatives for this case study ([RC+JT+SS], [RC+TX+SS], [NR+JT+SS], [RC+JT+MP]) are presented in Figs. 5.8a, 5.8b, 5.9a and 5.9c. These processes are here divided in 05 sections: (i) Oil-Gas-Water Separation (Plant A); (ii) HPS-Gas Expansion (Plant B or C); (iii) SS unit for WDPA+HCDPA (Plant D); (iv) Fuel-Gas Production (Plant E or F); and (v) EOR-Fluid compression/pumping (Plant G). Sections (ii) and (iv) have one variant each, defining seven sub-flowsheets for this scenario – Plants A to G – which are represented inside dashed boxes in Figs. 5.8/5.9. Thus, process alternatives (Figs. 5.8/5.9) connect Plants A+B/C+D+E/F+G choosing: (i) recycling (RC) the condensate of WDPA+HCDPA from Plant D to Plant A or not recycling (NR) it for EOR purpose, connecting Plant D to Plant G (intermediated by liquid-liquid phase split); (ii) Plant B (Joule-Thompson valve for expansion) or Plant C (turbo-expander) for HPS-Gas Expansion; and (iii) Plant E (2<sup>nd</sup> SS unit) or Plant F (Membrane-Permeation) for CO<sub>2</sub> removal.

The Base-Case [RC+JT+SS] – equal to SS-SS Alternative of Case Study 1 (Fig. 5.5) – selects Plants A, B, D, E, and G, adopting condensate recycle (Fig. 5.8a). In the TX-variant [RC+TX+SS], Plant B is replaced by Plant C (TX) to convert heat into power for reduction of overall power consumption (Fig. 5.8b). The NR-variant [NR+JT+SS] abandons SS condensate recirculation from Plant D to Plant A, pumping C3+ condensate (LIQ) directly to EOR after water separation (Fig. 5.9a). Eliminating condensate recycle positively reduces processed volumetric flows, shortening equipment and power consumption, but adversely impacts oil production. The MP-variant [RC+JT+MP] replaces SS-based CO<sub>2</sub> capture (Plant E) by Membrane-Permeation (Plant F) (Fig. 5.9b). Despite of Plant F greater simplicity, low-pressure CO<sub>2</sub>-rich stream obtained as permeate implies heavier compressors, as Plant E produces high-pressure – and partially liquefied – CO<sub>2</sub>-rich streams that are also used to EOR.

Flowsheets in Figs. 5.8/5.9 use the following conventions: (i) each compression stage with its respective driver, intercooler and flash-vessel is portrayed as compressor blocks. These blocks are featured by electric-driver (ED) (shaft-power  $\leq 13MW$ ), gas-turbine (GT) (shaft-power  $\in [13MW, 28MW]$ ) or turbo-expander (TX), besides the thermal utility being regenerated in the cooler (CW, WW or HW depending on gas  $T$ ); (ii) thermal utilities are identified in the places where they reach the highest  $T$  of their corresponding ranges (in the outlet stream when availed for cooling, and in the inlet stream when availed for heating).

#### 5.4.2. Sub-Flowsheets Description

Plant A (Figs. 5.8/5.9) separates riser fluid in HPS – after pre-heating to  $T=30^{\circ}\text{C}$  to avoid hydrates – and stabilizes the crude oil. HPS-Oil stabilization occurs in Medium-Pressure Separator ( $P=20\text{ bar}$ ,  $T=90^{\circ}\text{C}$ ) and Low-Pressure Separator ( $P=1.8\text{ bar}$ ,  $T\approx 90^{\circ}\text{C}$ ), with the gas being compressed to  $80.5\text{ bar}$  in a VRU of 04 intercooled stages to join HPS-Gas.

HPS-Gas needs expansion to  $80.5\text{ bar}$  for SS operation. In Plant B (Figs. 5.8a, 5.9a, 5.9b), it is done by JT-Expansion after pre-heating ( $T=65.5^{\circ}\text{C}$ ) for hydrate prevention. Plant C (Fig. 5.8b) is a power-producing (TX) alternative to Plant B where HPS-Gas is pre-heated to  $T=350^{\circ}\text{C}$  in a battery of heat exchangers (HW, PHW, TF) to increase turbo-expander power generation. After TX, the gas is cooled from  $T\approx 323^{\circ}\text{C}$  to  $45^{\circ}\text{C}$  regenerating hot utilities (PHW and HW).

Plant D (Figs. 5.8/5.9) prescribes WDPA+HCDPA of raw NG ( $P=80.5\text{ bar}$ ,  $T=45^{\circ}\text{C}$ ) from Plant B or Plant C in 1<sup>st</sup> SS unit (Sec. 5.3.1.2). Only in the NR-variant [NR+JT+SS], LTX condensate (L+W) is sent to Liquid-Liquid Separation (LLS) for water removal, then humid C3+ condensate (LIQ) is directly sent to EOR-Pump (Plant G), while in all other cases LTX and pre-flash liquid bottoms are mixed and pumped back to HPS (Plant A).

Plant E (Figs. 5.8a, 5.8b, 5.9a) receives a small portion of Dry-Gas ( $\approx 69\% \text{mol CO}_2$ ) leaving Plant D to produce Fuel-Gas through 2<sup>nd</sup> SS unit (Sec. 5.3.1.2). Using heat integration and CO<sub>2</sub>-based refrigeration-cycle (RFG), the feed stream is cooled down to  $-20^{\circ}\text{C}$  for pre-decarbonation. The resulting pre-decarbonated gas ( $P\approx 50\text{ bar}$ ,  $\approx 45\% \text{mol CO}_2$ ) is compressed, cooled with CW, and then chilled with SS products to achieve suitable conditions to feed the 2<sup>nd</sup> SS unit ( $P=84\text{ bar}$ ,  $T=-22^{\circ}\text{C}$ ), where FG ( $\approx 22\% \text{mol CO}_2$ ) is produced.

Membrane-based Plant F (Fig. 5.9b) – as a conventional alternative for offshore rigs – perform CO<sub>2</sub> capture replacing Plant E by expanding Dry-Gas to  $P\approx 44.5\text{ bar}$  and heating it to  $T=62^{\circ}\text{C}$  before feeding Membrane-Permeation modules (spiral-wound  $\text{Area}^{\text{MP}}=11,115\text{ m}^2$ ). Fuel-Gas ( $\approx 20\% \text{mol CO}_2$ ) is produced in retentate side while permeated CO<sub>2</sub>-rich gas at  $P=8\text{ bar}$  goes to double-stage compression to join Main-Compressor feed (MC-Gas).

Plant G (Figs. 5.8/5.9) performs EOR-Fluid compression/pumping, prescribing Main-Compressor with 04 GT-driven shafts in parallel spinning 02 centrifugal stages each to compress MC-Gas. In TX-variant [RC+TX+SS] process, TX is availed to drive one of the shafts, but as TX power exceeds the compression requirements, an electric generator is also connected to TX shaft to avail the excess. As MC-Gas becomes liquid at  $P=240\text{ bar}$  and  $T=45^{\circ}\text{C}$ , other liquids (LCO<sub>2</sub>/LIQ) are joined for final pump to  $P=450\text{ bar}$ .

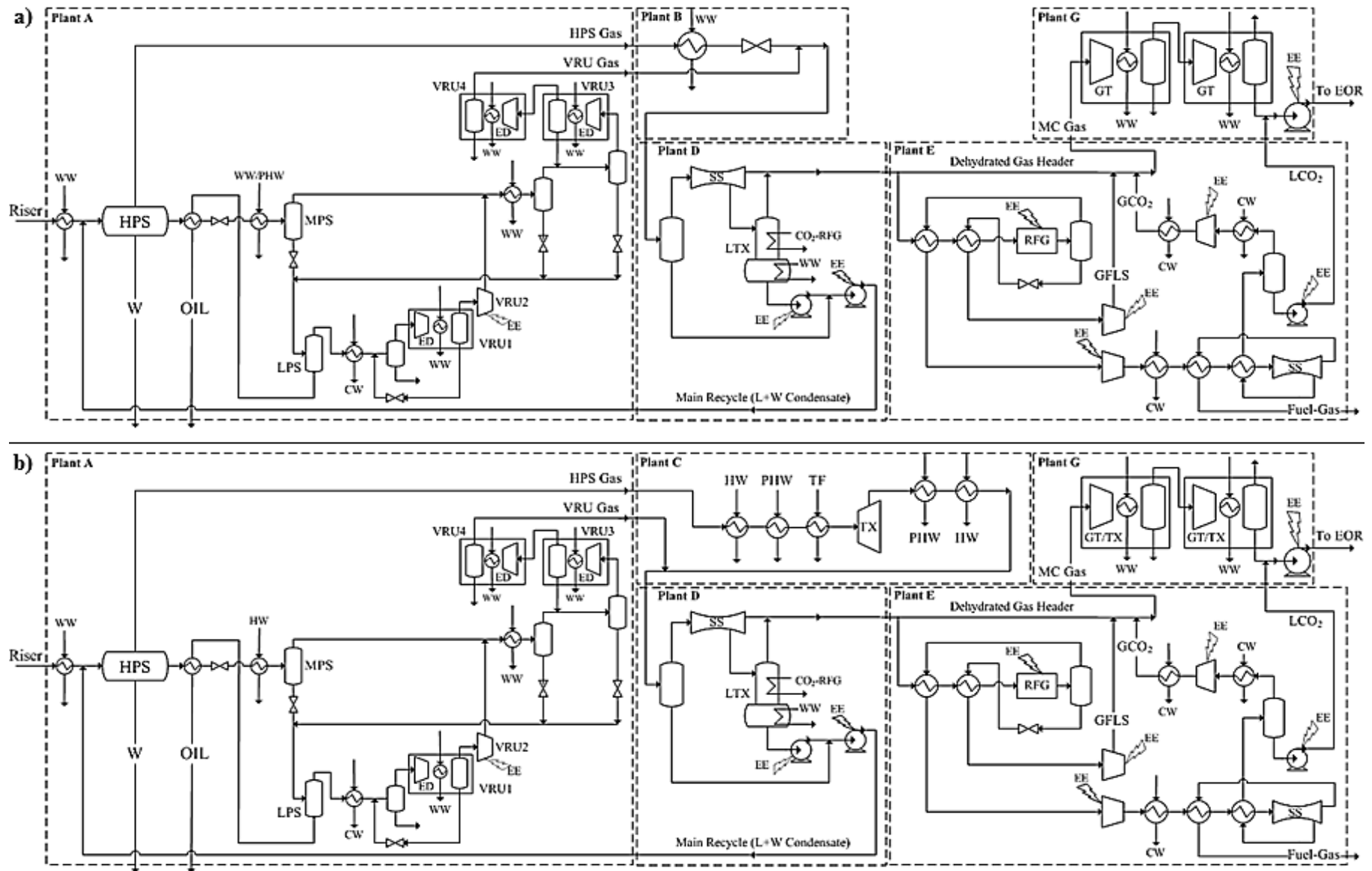


Fig. 5.8. Gas-Hub processing alternatives: a) SS-SS Base-Case [RC+JT+SS], b) TX-variant [RC+TX+SS].

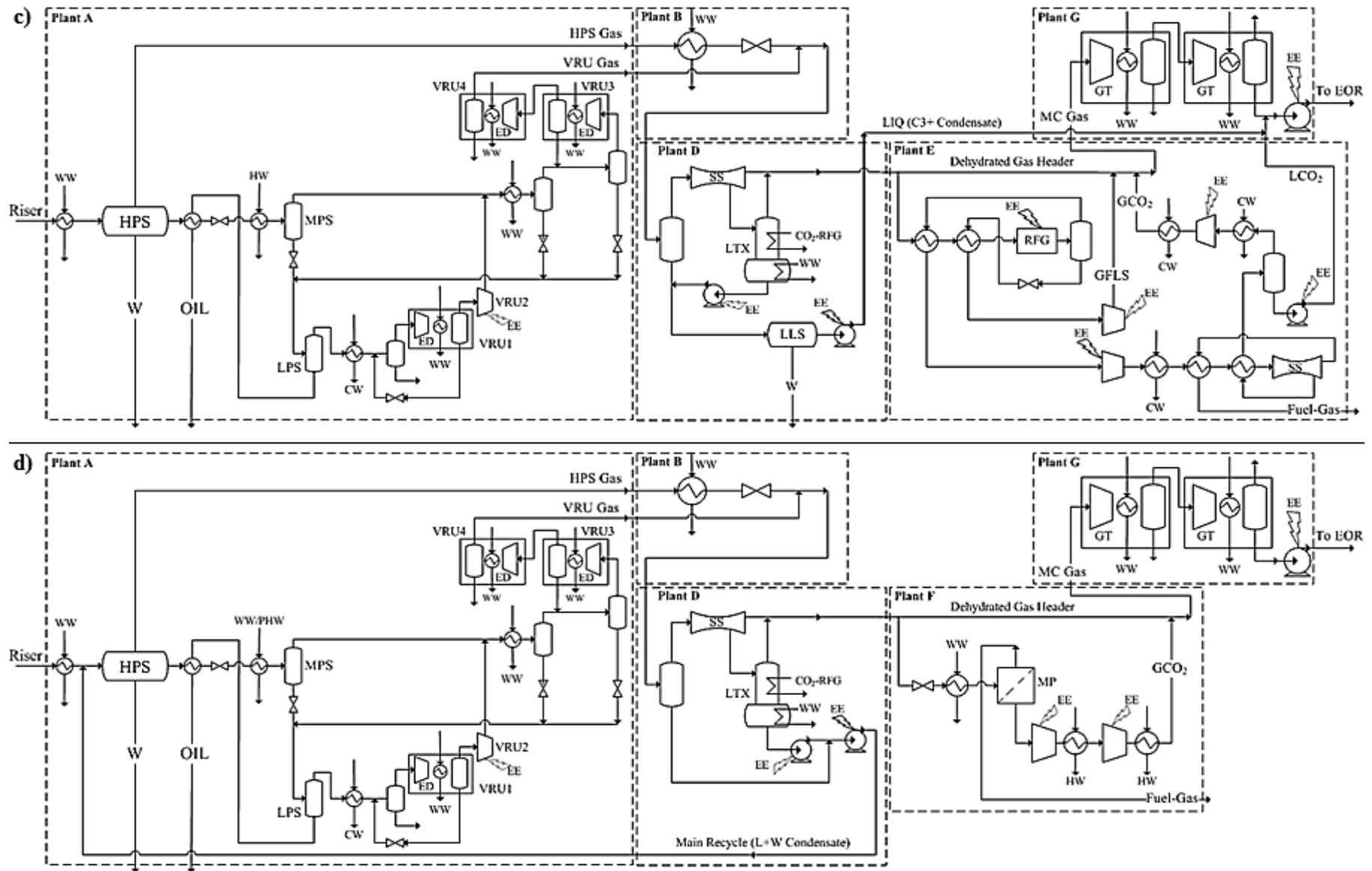
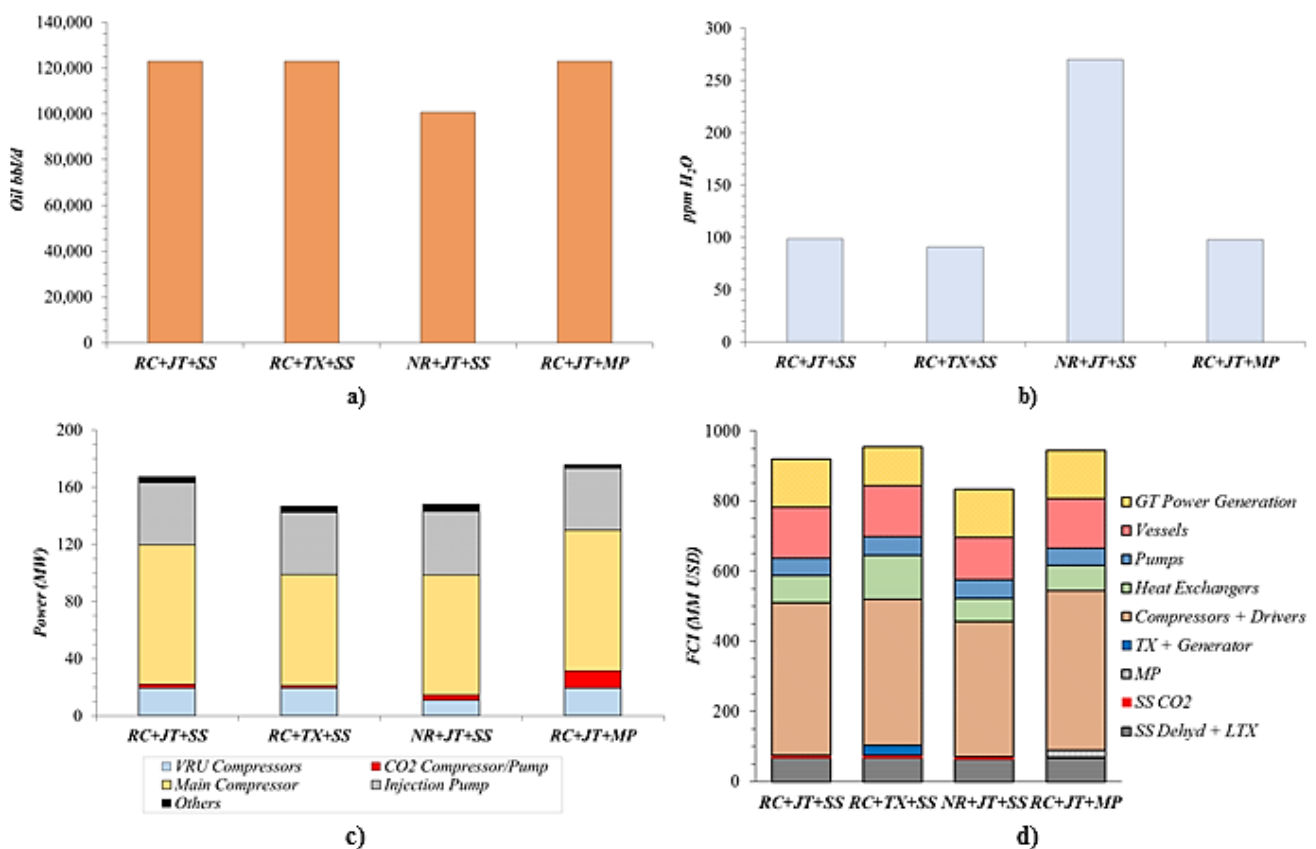


Fig. 5.9. Gas-Hub processing alternatives: a) NR-variant [NR+JT+SS], b) MP-variant [RC+JT+MP].

### 5.4.3. Results and Discussion

SS-SS Base-Case [RC+JT+SS] and other alternatives – TX-variant [RC+TX+SS], NR-variant [NR+JT+SS], and MP-variant [RC+JT+MP] – were implemented in Aspen HYSYS accordingly to process flow diagrams shown in Figs. X2.1, X2.2, X2.3 and X2.4 at Appendix X2. Only the SS-SS Base-Case [RC+JT+SS] have details being presented in this chapter (Sec. 5.3.2): Table 5.3 for conditions of main process streams and Table 5.4 for design and operating conditions of SS units. Operating conditions of main streams in other alternatives (Table 5.3 analogues) are presented in Table X3.1 ([RC+TX+SS]), Table X3.2 ([NR+JT+SS]) and Table X3.3 ([RC+JT+MP]) at Appendix X3. Designs and operating conditions of SS units in other alternatives (Table 5.4 analogues) are presented in Table X4.1 ([RC+TX+SS]), Table X4.2 ([NR+JT+SS]), and Table X4.3 ([RC+JT+MP]) at Appendix X4. These objects are not commented, as results in process variants are analogous to Base-Case [RC+JT+SS] which corresponds to the same process alternative SS-SS of Case Study 1, where discussion in this regard is presented in Sec. 5.3.2.2. Comparisons of process alternatives are made as percent deviations in relation to Base-Case except when stated otherwise. Table 5.7 and Figs. 5.10/5.11 provide the absolute values for comparisons.



**Fig. 5.10.** Gas-hub alternatives: (a) oil (bbl/d); (b) EOR-Fluid  $ppmH_2O$ ; (c) power-consumption (MW); (d) FCI (MMUSD).

### 5.4.3.1. Performance of Gas-Hub Processing Alternatives

Fig. 5.10 depicts the comparison of process alternatives regarding oil production, water content in EOR-Fluid, power demand and Fixed Capital Investment (*FCI*). Fig. 5.10 is supported by simulation results presented in Sec. 5.3.2 and Appendix X3: Tables 5.3 ([RC+JT+SS]), X3.1 ([RC+TX+SS]), X3.2 ([NR+JT+SS]) and X3.3 ([RC+JT+MP]). Table 5.7 unveils flow rates – expressed in  $MMsm^3/d$  – of key-streams in the evaluated process alternatives. Since the  $MMsm^3/d$  of fluids is calculated from molar flows, Table 5.7 does not express oil production in the same proportion of *bbl/d* (Fig. 5.10a) due to different compositions. Fig. 5.11 presents Net Present Values (*NPV*) projections from economic assessments throughout the years of horizon (3 years of construction + 20 years of operation). Fig. 5.11 evinces best cash flows and profitability of Base-Case [RC+JT+SS].

**Table 5.7.** Flow rate of key-streams ( $MMsm^3/d$ ) of alternatives.

$MMsm^3/d$	[RC+JT+SS] Base-Case	[RC+TX+SS]	[NR+JT+SS]	[RC+JT+MP]
Riser (including water)	90.15	90.15	90.15	90.15
EOR-Fluid	50.09 <sup>*1</sup>	50.19 <sup>&amp;1</sup>	50.51 <sup>§1</sup>	50.05 <sup>#1</sup>
Fuel-Gas	1.30 <sup>*2</sup>	1.16 <sup>&amp;2</sup>	1.27 <sup>§2</sup>	1.34 <sup>#2</sup>
Main Recycle	8.31	8.99	---	8.31
Water-C3+ Condensate (1 <sup>st</sup> SS Unit)	5.29	5.65	3.98	5.29
HPS-Gas	52.24	52.85	47.98	52.24
Captured CO <sub>2</sub> (2 <sup>nd</sup> SS or MP)	0.65611	0.712599	0.67056	3.14384
Captured CH <sub>4</sub> (2 <sup>nd</sup> SS or MP)	0.078585	0.079595	0.068	0.326096
CO <sub>2</sub> Emissions (Fuel-Gas)	1.31989	1.1834	1.284839	1.71024
Oil	2.0	2.0	1.43	2.0

<sup>\*1</sup>70.8%CO<sub>2</sub>. <sup>&1</sup>70.68%CO<sub>2</sub>. <sup>§1</sup>70.14%CO<sub>2</sub>. <sup>#1</sup>70.9%CO<sub>2</sub>. <sup>\*2</sup>21.85%CO<sub>2</sub>, 74.73%C1, 2.06%C2, 0.25%C3, 0.02%C4.

<sup>&2</sup>22.08%CO<sub>2</sub>, 74.47%C1, 2.12%C2, 0.25%C3, 0.02%C4. <sup>§2</sup>21.69%CO<sub>2</sub>, 74.95%C1, 2.0%C2, 0.22%C3, 0.02%C4.

<sup>#2</sup>20.0%CO<sub>2</sub>, 62.87%C1, 8.6%C2, 4.71%C3, 2.40%C4, 0.68%C5, 0.06%C6, 0.01%C7.

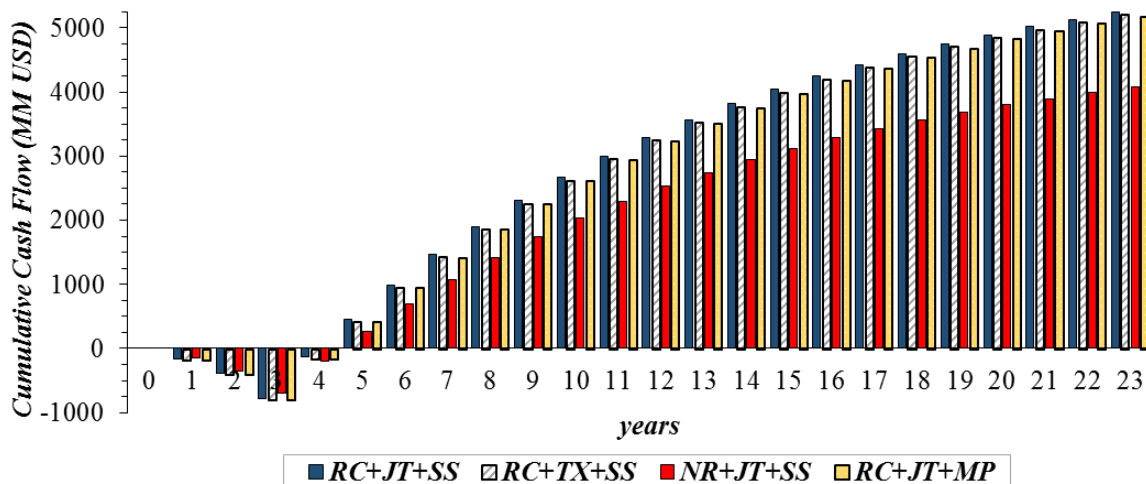


**Fig. 5.11.** NPV (MMUSD) of gas-hub alternatives for 20 operation-years.

#### 5.4.3.2. Comparison of Gas-Hub Alternatives and SS-SS Process Consolidation

Regarding the decision between recycling (RC) or not recycling (NR) condensate from 1<sup>st</sup> SS unit to HPS, economic results in Fig. 5.11 clearly reveals *NPV* advantage of RC option. NR implies in lower flow rates of NG being processed (Table 5.7) saving power demand and equipment sizes, but RC contributes to increase oil production, which is evinced to be economically more significant. Precisely, although the NR-variant [NR+JT+SS] is supposed to have advantages of requiring the lowest *FCI*, as confirmed by Fig. 5.10d (-9.36%), and lower power demand comparatively to RC counterpart (-11.45%) (Fig. 5.10c), it disappoints in profitability potential, with 22% lower *NPV* (the worst profitability) due to reduced revenues, as NR-variant presents the lowest oil production (-18.33%) (Fig. 5.10a). Moreover, Fig. 5.10b unveils a further disadvantage of NR alternative [NR+JT+SS]: the highest water content ( $\approx 270 \text{ ppmH}_2\text{O}$ ) in EOR-Fluid (+174%). Since the C3+ stream (LIQ) sent to injection pump (Fig. 5.9a) is saturated in water, it dramatically increases the water content of EOR-Fluid, potentially raising the risk of hydrate formation in EOR system. Among alternatives with RC option, however, similar oil productions ( $\approx 123,000 \text{ bbl/d}$ ) and EOR-Fluid water contents ( $\approx 95 \text{ ppmH}_2\text{O}$ ) are obtained, as depicted by Figs. 5.10a and 5.10b.

Regarding the decision between choosing JT-valve (Plant B) or TX (Plant C) for HPS-Gas (120 bar) expansion to the working pressure of 1<sup>st</sup> SS unit (80.5 bar), the JT option evinces higher profitability potential despite wasting opportunity to produce power. Among the four process alternatives, economic results in Fig. 5.11 unveils the TX-variant [RC+TX+SS] attaining the second best *NPV*, losing the first place to SS-SS Base-Case [RC+JT+SS] by a narrow margin. In terms of power demands, the TX-variant [RC+TX+SS] naturally outperforms all alternatives (-19.16%) (Fig. 5.10c), but with the drawback of presenting the highest *FCI* (+3.76%), which is mainly explained by higher capital investment on heat exchangers as revealed in *FCI* details shown in Fig. 5.10d. This occurs because large additional exchangers are required to preheat HPS-Gas ( $T=350^\circ\text{C}$ ) – for the best TX power generation efficiency – and also to finish cooling the expanded gas. Nevertheless, the power-saving advantage of TX also implies in the lowest flow rates of Fuel-Gas and CO<sub>2</sub> emission (-10.34%) (Table 5.7), making the TX-variant [RC+TX+SS] the option of best environmental performance.

Adopting TX without high-temperature preheaters and aftercoolers (Fig. 5.8b, Plant C) could save  $\approx 45$  MMUSD of FCI (Fig. 5.10d), but would also reduce TX power from  $\approx 28$  MW to  $\approx 13.7$  MW. TX power generation at  $\approx 28$  MW enables to substitute one of the four gas-turbine drivers of Main-Compressor, which means significant savings in capital investment despite of additional FCI contribution from TX machine. Without this advantage, the capital investment on drivers at TX-variant [RC+TX+SS] ceases to be lower than Base-Case [RC+JT+SS], implying in an intermediary performance in terms of power demand, CO<sub>2</sub> emissions and total FCI, thus intermediary NPV performance would also be obtained.

Regarding the decision between using a 2<sup>nd</sup> SS unit (Plant E) or Membrane-Permeation (Plant F) for CO<sub>2</sub> removal, Fig. 5.11 evinces higher profitability potential of SS-SS alternative. Again, the pragmatic Base-Case [RC+JT+SS] presents better economic results. Among the four process alternatives, the MP-variant [RC+JT+MP] presents the highest power demand (+4.99%) and the second highest capital investment (+2.81%), both aspects explained by higher compression ratio being required to send captured CO<sub>2</sub> (low-pressure permeate) to EOR. Such results express great advantage of 2<sup>nd</sup> SS unit over MP in producing high-pressure CO<sub>2</sub>-rich liquid stream, allowing substantial savings in compression power demand for EOR.

Finally, from economic perspective and by a narrow margin, cumulative cash flows in Fig. 5.11 consolidate the best configuration of proposed innovative SS-SS concept for this scenario as Base-Case [RC+JT+SS]. However, in a practical sense, the choice between Base-Case [RC+JT+SS] and TX-variant [RC+TX+SS] should be done with care. The main issue of the TX-variant [RC+TX+SS] is that its highest capital investment not only impairs cash flows in construction years, but also indirectly raises manufacturing costs (*COM* in Eq. (X1.3a)) reducing annual profits. From the viewpoint of carbon reduction, the TX option is clearly preferred, and the small NPV gap between these alternatives could be overcome if CO<sub>2</sub> taxes were applied to the working scenario. Other alternatives have much weaker performance: (i) the MP-variant [RC+JT+MP] presents the highest CO<sub>2</sub> emissions, placing third in profitability potential; and (ii) the NR-variant [NR+JT+SS] presents the worst annual profits and NPV along the operation years, despite of its lowest capital investment, and second lowest power demand, the latter naturally implying in 2<sup>nd</sup> lowest CO<sub>2</sub> emissions (Table 5.7).

## 5.5. Conclusions for Chapter 5

Large-capacity floating-hub for application in remote offshore oil fields was investigated for processing  $\approx 50 \text{ MMsm}^3/\text{d}$  of  $\text{CO}_2$ -rich raw NG ( $\approx 68\% \text{mol CO}_2$ ) and  $\approx 1.0 \cdot 10^5 \text{ bbl/d}$  of oil. Several process configurations were addressed contemplating oil-gas-water primary separation, NG WDPA, HCDPA,  $\text{CO}_2$  capture for Fuel-Gas production, and EOR-Fluid compression/pumping. Proposed alternative for this scenario – SS-SS – is based on NG treatment by sequential SS steps: a 1<sup>st</sup> SS unit comprising 12 parallel SS nozzles connected to a LTX for WDPA+HCDPA, and a 2<sup>nd</sup> SS unit comprising a single SS nozzle for  $\text{CO}_2$  removal for FG production. Without tiebacks to the coast, almost all processed NG – as supercritical Dry-Gas enriched with  $\text{CO}_2$  captured – is reinjected to the field for EOR. Fuel-Gas is the only fraction of NG being consumed, which is availed to supply the power requirements of the rig, for its self-sufficiency. Two Case Studies were addressed to define the best process configuration for this scenario. Results compare oil productions, power demands,  $\text{CO}_2$  emissions, and economic metrics. Being a relatively recent operation, SS design and simulation in Aspen HYSYS was only possible due to the use of Unit Operation Extensions developed by Arinelli et al. (2017) and de Medeiros et al. (2017).

In Case Study 1, two process alternatives were analyzed: MS-JT-MP and SS-SS. MS-JT-MP is the conventional way, providing dehydration via Molecular-Sieves (MS), HCDPA via JT-Expansion and  $\text{CO}_2$  removal via Membrane-Permeation (MP). Proposed alternative SS-SS presents higher profitability ( $\approx 33\%$  higher *NPV*) with 10% lower capital investment. This higher profitability is mainly an outcome of greater oil production owing to the recycle of WDPA+HCDPA condensate (rich in C3+) – obtained in the 1<sup>st</sup> SS unit – to the primary oil-gas-water separator. SS-SS also presents lower  $\text{CO}_2$  emissions per barrel of oil produced, thus being regarded as a cleaner process alternative.

In Case Study 2, SS-SS process configuration is consolidated by comparison of four alternatives for addressing the following structural decisions: (i) whether the condensate from 1<sup>st</sup> SS unit should be recycled to HPS; (ii) whether Joule-Thompson valve or turbo-expander should be used to expand HPS-Gas to working pressure of 1<sup>st</sup> SS unit; and (iii) whether a 2<sup>nd</sup> SS unit or MP should be used for  $\text{CO}_2$  capture. Results point advantage of recycling condensate due to increased oil production positively influencing net present value (*NPV*). Replacement of JT-Expansion by turbo-expander (TX) for power generation is not justified from economic perspective, with SS-SS pragmatic base-case [RC+JT+SS] showing small

NPV advantage over its TX-variant [RC+TX+SS], unless environmental penalties are taken into consideration. In this sense, TX could become the most profitable option if CO<sub>2</sub> taxes were applied. For CO<sub>2</sub> removal, the use of a 2<sup>nd</sup> SS unit is evinced as more profitable than MP option, though involving more complex flowsheet, including several heat integration exchangers and a refrigeration-machine for pre-decarbonation. It is explained by higher compression power required in MP-variant [RC+JT+MP] to send captured CO<sub>2</sub> to EOR, again pointing superiority of SS-SS Base-Case accounting for its reduced power demand and capital investment.

## 5.6. References for Chapter 5

- ANP, 2017. Bacia de Santos – Sumário geológico e áreas em oferta.  
[http://rodadas.anp.gov.br/arquivos/roundp3/mapas/sumario\\_geologico\\_lp3.pdf](http://rodadas.anp.gov.br/arquivos/roundp3/mapas/sumario_geologico_lp3.pdf)
- Araújo, O.Q.F., Reis, A.C., de Medeiros, J.L., Nascimento, J.F., Grava, W.M., Musse, A.P.S. Comparative analysis of separation Technologies for processing carbon dioxide rich natural gas in ultra-deepwater oil fields. *Journal of Cleaner Production*, 155, 12–22, 2017.  
<https://doi.org/10.1016/j.jclepro.2016.06.073>
- Arinelli, L.O., Trotta, T.A.F., Teixeira, A.M., de Medeiros, J.L., Araújo, O.Q.F. Offshore processing of CO<sub>2</sub> rich natural gas with supersonic separator versus conventional routes. *Journal of Natural Gas Science and Engineering*, 46, 199–221, 2017.  
<https://doi.org/10.1016/j.jngse.2017.07.010>
- BP. Statistical Review of World Energy, UK, 2018.  
<https://www.bp.com/en/global/corporate/energy-economics/statistical-review-of-world-energy.html>
- Burgers, W.F.J, Northrop, P.S., Kheshgi, H.S., Valencia, J.A. Worldwide development potential for sour gas. *Energy Procedia*, 4, 2178-2184, 2011.  
<https://doi.org/10.1016/j.egypro.2011.02.104>
- Campos, A.F. Silva, N.F., Pereira, M.G., Freitas, M.A.V. A review of Brazilian natural gas industry: challenges and strategies. *Renewable and Sustainable Energy Reviews*, 75, 1207-1216, 2017. <https://doi.org/10.1016/j.rser.2016.11.104>
- de Medeiros, J.L., Arinelli, L.O., Araújo, O.Q.F. Speed sound of multiphase and multi-reactive equilibrium streams: a numerical approach for natural gas applications. *Journal of Natural Gas Science and Engineering*. 46, 222-241, 2017.  
<https://doi.org/10.1016/j.jngse.2017.08.006>
- Gaffney, Cline & Associates. Review and evaluation of ten selected discoveries and prospects in the Pre-Salt play of the deepwater Santos Basin, Brazil. CG/JW/RLG/C1820.00/GCABA.1914, ANP, Brazil, 2010.
- Karakatsani, E.K., Kontogeorgis, G.M. Thermodynamic modeling of natural gas systems containing water. *Ind.Eng.Chem.Res.*, 52, 3499–3513, 2013.  
<https://doi.org/10.1021/ie302916h>
- Langé, S., Pellegrini, L.A., Vergani, P., Savio, M. Energy and economic analysis of a new low-temperature distillation process for the upgrading of high-CO<sub>2</sub> content natural gas streams. *Ind. Eng. Chem. Res.*, 54(40), 9770-9782, 2015.  
<https://doi.org/10.1021/acs.iecr.5b02211>

- Machado, P.B., Monteiro, J.G.M., de Medeiros, J.L., Epsom, H.D., Araujo, O.Q.F. Supersonic separation in onshore natural gas dew point plant. *Journal of Natural Gas Science and Engineering*, 6, 43-49, 2012. <https://doi.org/10.1016/j.jngse.2012.03.001>
- McCoy, S.T., The Economics of CO<sub>2</sub> transport by pipeline and storage in saline aquifers and oil reservoirs. PhD Thesis, Carnegie Mellon University, USA, 2008.
- Merkel, T.C., Zhou, M., Baker, R.W., Carbon dioxide capture with membranes at an IGCC power plant. *Journal of Membrane Science*, 389, 441-450, 2012. <https://doi.org/10.1016/j.memsci.2011.11.012>
- Nguyen, T.V., Tock, L., Breuhaus, P., Maréchal, F., Elmegaard, B. CO<sub>2</sub>-mitigation options for the offshore oil and gas sector. *Applied Energy*, 161, 673-694, 2016. <https://doi.org/10.1016/j.apenergy.2015.09.088>
- Schinkelshoek, P., Epsom, H.D., Supersonic gas conditioning - Commercialization of Twister Technology. GPA 87th Annual Conv. Proc., Texas, USA, March 2008, 739-745.
- Teixeira, A.M., Arinelli, L.O., de Medeiros, J.L., Araújo, O.Q.F. Exergy analysis of monoethylene glycol recovery processes for hydrate inhibition in offshore natural gas fields. *J. Nat. Gas Sci. Eng.*, 35, 798-813, 2016. <https://doi.org/10.1016/j.jngse.2016.09.017>.
- Teixeira, A.M., Arinelli, L.O., de Medeiros, J.L., Araújo, O.Q.F. Recovery of thermodynamic hydrate inhibitors methanol, ethanol and MEG with supersonic separators in offshore natural gas processing. *J. Nat. Gas Sci. Eng.*, 52, 166-186, 2018. <https://doi.org/10.1016/j.jngse.2018.01.038>
- Turton, R., Bailie, R.C., Whiting, W.B., Shaeiwitz, J.A. Analysis, synthesis and design of chemical processes. 3<sup>rd</sup> Ed., Prentice Hall International Series, 2009.

## 6. Carbon Dioxide Utilization in a Microalga-Based Biorefinery for Methanol Production: Economic Performance under Carbon Taxation

*This chapter is based on the following publication in Journal of Environmental Management:*

WIESBERG, I. L.; BRIGAGÃO, G. V.; DE MEDEIROS, J. L.; ARAÚJO, O. Q. F. Carbon dioxide utilization in a microalga-based biorefinery: efficiency of carbon removal and economic performance under carbon taxation. *Journal of Environmental Management*, 203, 988-988, 2017.

### Abbreviations

ASU Air Separation Unit; BRY Biorefinery; CCS Carbon Capture and Storage; CCU Carbon Capture and Utilization; CCUS Carbon Capture, Utilization and Storage; EOR Enhanced Oil Recovery; GOX Gaseous Oxygen; GSD Greenhouse Solar Drying; HHV Higher Heating Value; MARR Minimum Acceptable Rate of Return; MEA Monoethanolamine; MeOH Methanol; MMUS\$ Millions of US Dollars; NG Natural Gas; NGCC Natural Gas Combined Cycle; PBR Photobioreactor; PC-SAFT Perturbed-Chain Statistical Association Fluid Theory; PEA Process Economic Analyzer; SRK Soave-Redlich-Kwong; UNIQUAC Universal QuasiChemical.

### Nomenclature

<i>CapEff</i>	: <i>CO<sub>2</sub> capture efficiency (unitless)</i>
<i>CashFlow</i>	: <i>Annual cash flow (MMUS\$/y)</i>
<i>F<sub>CO2</sub></i>	: <i>Mass flow rate of CO<sub>2</sub> (kg/h)</i>
<i>NPV</i>	: <i>Net present value (MMUS\$)</i>
<i>S</i>	: <i>Methanol synthesis coefficient (unitless)</i>
<i>Subscripts</i>	
<i>j</i>	: <i>CO<sub>2</sub> capture/destination route, BRY or CCS</i>
<i>Superscripts</i>	
<i>Avoided</i>	: <i>Avoidance of CO<sub>2</sub> emissions</i>
<i>Consumed</i>	: <i>CO<sub>2</sub> utilization</i>
<i>BAU</i>	: <i>Business-as-usual scenario (conventional technology)</i>
<i>DIF</i>	: <i>Difference between CashFlow<sub>j</sub> and CO<sub>2</sub> taxes payment without capture</i>
<i>Feed</i>	: <i>Biorefinery feed, power plant exhaust gas</i>
<i>Generated</i>	: <i>CO<sub>2</sub> generation</i>
<i>NotProduced</i>	: <i>Avoidance of CO<sub>2</sub> generation comparatively to conventional technology</i>
<i>Tec</i>	: <i>Economic performance of one technological route without CO<sub>2</sub> taxes applied</i>

### Supplementary Materials

Supplementary Materials for this chapter are found in Appendix Y.

## 6.1. Introduction

Technological changes in electricity generation and transportation systems play a central role in response to climate changes, but the majority of these routes face technical challenges and economic barriers, demanding support for their widespread implementation (Kypreos and Turton, 2011). Currently, carbon capture and storage (CCS) and enhanced oil recovery (EOR) are the only pathways including ready-to-implement large-scale solutions: some post-combustion CO<sub>2</sub> capture technologies, CO<sub>2</sub> compression, and pipeline transportation (Araujo et al., 2014). The lack of widespread commercial large-scale CCS initiatives reveals the little appeal of these solutions to investors, as CCS is hampered by diverse obstacles of great relevance, including availability/distance of geological sites for storage (Cuellar-Franca and Azapagic, 2015), installation of pipelines for CO<sub>2</sub> transportation, leakage monitoring (Cheah et al., 2016) and, above all aspects, absence of revenues to the enterprise. As a consequence, severe economic penalties are required for carbon reduction through CCS, entailing both high capital investment and operational costs.

Alternatively, carbon capture and utilization (CCU) is a generally preferred destination for the CO<sub>2</sub>, as it enables to aggregate revenues to the project (Aresta, 2010). However, currently there are few mature chemical pathways employing CO<sub>2</sub> as feedstock in commercial scale (e.g. urea) (Aresta, 2010). In this regard, CO<sub>2</sub> chemical conversion to methanol (MeOH) appears as a promising alternative for widespread large-scale application (Olah et al., 2009; Wiesberg et al., 2016). In this sense, for the methanol synthesis route of CO<sub>2</sub> hydrogenation, Pérez-Fortes et al. (2016) estimated substantial potential for CO<sub>2</sub> emission avoidance ( $2 \text{ kg}^{CO_2}/\text{kg}^{MeOH}$ ).

Comparisons between CCS and CCU routes taking into account economic aspects for working scenarios with incidence of carbon taxation are not commonly found in the literature. In this regard, there is a growing convergence of policy-makers and economists that stablishing a carbon price is an important tool to leverage the reduction of carbon footprints (Kypreos and Turton, 2011). From engineering perspective, CO<sub>2</sub> taxation has the potential to catalyze technological progresses, acting as an operational cost to be minimized with carbon reduction. This is particularly important for the current world scenario, still highly dependent of fossil resources, constituting a driver for CCS and CCU alternatives while renewable sources are not widely and intensively applied. Anyway, the perspective of fossil and renewable resources coexisting in the near future set up a compelling environment for incidence of carbon taxation for governmental control of carbon emissions.

### 6.1.1. Microalgae Cultivation for Carbon Capture and Utilization

In the earliest stages of technological development, microalgae cultivation for CO<sub>2</sub> capture has attracted intense scientific research mainly due to its high growth rates (as microalgae may perform 10x more efficient CO<sub>2</sub> biofixation than terrestrial crops) and also high lipids contents (Skjanes et al., 2007). In this sense, *Chlorella pyrenoidosa*, for example, may present ≤51%w of total lipids per dry biomass (Liu et al., 2011). In relation to microalgae cultivation methods, raceways and photobioreactors (PBRs) are among the most commonly conceived technological alternatives. In a review of biological CO<sub>2</sub> fixation, Goli et al. (2016) pointed superiority of PBRs over raceways. Although PBRs entail higher capital investments to the project, much higher biomass and lipids productivities can be attained (Moheimani, 2016). If successfully developed, CO<sub>2</sub> biofixation by microalgae aiming posterior conversion in a biorefinery generate revenues that could ultimately abate CO<sub>2</sub> mitigation costs in fossil-based power generation.

Thermochemical processing alternatives generally outstand among most conceived options for conception of plausible biofuel-driven biorefineries. Flexibility to biomass feedstocks, for instance, is an important advantage of these routes (Garcia et al., 2016). Biomass gasification, in particular, offers great advantage of allowing a wide range of products due to generation of synthesis gas, a common raw material (comprising mainly H<sub>2</sub>, CO, CO<sub>2</sub>) used in the production of several chemical commodities (e.g. methanol, ammonia) that can also be used as platform chemicals to multifold downstream possibilities. As synthesis gas is usually produced from natural gas (NG) reforming or coal gasification, and chemical commodities normally derives from fossil resources, these biorefineries are able to simultaneously avoid CO<sub>2</sub> emissions and resources depletion for a wide range of products.

When conceived for utilization of CO<sub>2</sub> generated by thermal power stations, biorefineries should concentrate in products with large markets, leveling large-scale CO<sub>2</sub> supply: fuels and chemical commodities (e.g. methanol and ammonia). In this regard, fine chemicals and biomolecules are important for revenues but cannot absorb CO<sub>2</sub> generation rate due to limited demand. Otherwise, excessive production would cause market flooding, with drastic reduction of sales prices. In this sense, for the best economic interest in biorefinery projects, the process scale and portfolio of fuels and commodities have been reported as the most important aspects to be accounted (García et al., 2016). In connection with this, for a biorefinery focusing on CO<sub>2</sub> utilization, the present work applies a single large-scale product complemented by small production of a more expensive chemical for revenues increase.

### 6.1.2. Present Work

Biological CO<sub>2</sub> capture and valorization is challenged by economic aspects, and sustainability analyses of biofuel-driven biorefineries must regard this perspective to improve their attractiveness (Chea et al., 2016). However, studies addressing economic analysis of process alternatives conceiving microalgae cultivation for CCU are rarely found in the literature. This work fills this gap and compares such biorefinery performance with a conventional CCS route prescribing MEA Chemical-Absorption for CO<sub>2</sub> capture. Moreover, this work also applies a relevant and often neglected aspect to be accounted in most economic studies: the incidence of CO<sub>2</sub> taxation leveraging carbon reduction processes. In this sense, while carbon credits application (CO<sub>2</sub> captured as revenue) appears to be the dominant CO<sub>2</sub> management approach in the literature, policy-makers are actually moving towards CO<sub>2</sub> taxation (CO<sub>2</sub> emission as operational cost).

Even considering that technological advancements are needed to allow effective large-scale implementation of microalgae biorefineries for abatement of CO<sub>2</sub> emissions from a power plant, this work approaches a process engineering investigation identifying potential barriers for implementation of such a concept, with its economic performance being evaluated against conventional CCS, both leveraged by an economic scenario with CO<sub>2</sub> taxation policy. Specifically, *Chlorella pyrenoidosa* is availed for biological CO<sub>2</sub> capture in a biorefinery CCU configuration for production of methanol via biomass gasification and microalga oil via extraction with solvent.

The present chapter is a shortened version of a published scientific article (Appendix P) giving emphasis on economic performance of proposed microalga-based biorefinery. Further results are presented in the reference article, including comparison of the two evaluated processes from environmental perspective using the waste reduction algorithm of US-EPA (Young and Cabezas, 1999), which also configures a major originality aspect of the referred publication.

## 6.2. Methods

Two post-combustion CO<sub>2</sub> capture alternatives are investigated: (a) microalga-based biorefinery (BRY), and (b) conventional CCS route adopting MEA Chemical-Absorption. BRY embraces microalga cultivation and harvesting (biomass production), oil extraction with solvent, biomass gasification, methanol production, and co-generation. Besides CO<sub>2</sub> capture with MEA, CO<sub>2</sub> compression and transportation to geological storage is included in conventional CCS route. BRY and CCS flowsheets are implemented in Aspen HYSYS for technical evaluation of alternatives, which results support equipment costing and economic assessment in Aspen Process Economic Analyzer (PEA). A coal-fired power plant is assumed to supply exhaust gas to BRY/CCS and is not included in the analyses. Process boundaries applied to this work are portrayed in Fig. 6.1.

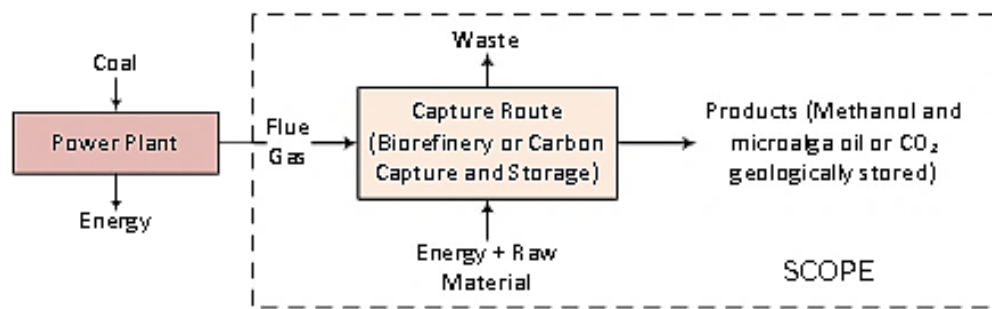


**Fig. 6.1.** Frontiers applied to analyzed processes in this work.

Whole biomass of *Chlorella pyrenoidosa* is modelled in Aspen HYSYS as a combination of biochemical pools – lipids, proteins and carbohydrates – following proportions obtained from literature data for its overall composition (Duan et al., 2013). The implemented pool of lipids is based on fatty acids profile of Tang et al. (2011). Proteins are approached using a single pseudo-component with molecular formula C<sub>10</sub>H<sub>16</sub>N<sub>2</sub>O<sub>8</sub> and carbohydrates are represented by sucrose. The volumetric flow rate of PBR feed is calculated with biomass concentration at approximately  $\approx 4$  g/L (Chisti, 2007), assuming PBR efficiency of CO<sub>2</sub> utilization at 74.5% (Acien et al., 2012), given the stoichiometric proportions of biomass-growth global reaction shown in Eq. (6.1). Further details on simulation assumptions of microalga cultivation and harvesting steps are presented in Appendix Y.



### 6.2.1. CO<sub>2</sub> emissions analysis

BRY route is evaluated against other methanol plants in relation to CO<sub>2</sub> emissions (direct and indirect emissions). Comparison includes emerging chemical routes of CO<sub>2</sub> utilization for methanol production – CO<sub>2</sub> hydrogenation and NG bireforming – besides “business-as-usual” conventional plant. The balance of CO<sub>2</sub> direct emissions supposes combustion of all flammable compounds in residual gaseous streams. Indirect emissions are calculated from process requirements of electricity and heating (low-pressure steam). Adopted metrics of CO<sub>2</sub> emissions are explained in Eqs. (6.2) and (6.3) (Pérez-Fortes et al., 2016). Eq. (6.2) explicits  $F_{CO_2}^{NotProduced}$  as the difference of CO<sub>2</sub> generation rate (direct and indirect generation) between the conventional technology ( $F_{CO_2}^{BAU}$ ) and one CCU route for methanol production ( $F_{CO_2}^{Generated}$ ). Eq. (6.3) then defines the total avoidance of CO<sub>2</sub> emissions of respective CCU route ( $F_{CO_2}^{Avoided}$ ) by adding the CO<sub>2</sub> feed rate ( $F_{CO_2}^{Feed}$ ) to  $F_{CO_2}^{NotProduced}$ .

$$F_{CO_2}^{NotProduced} = F_{CO_2}^{BAU} - F_{CO_2}^{Generated} \quad (6.2)$$

$$F_{CO_2}^{Avoided} = F_{CO_2}^{Feed} + F_{CO_2}^{NotProduced} \quad (6.3)$$

### 6.2.2. Economic assessment

Economic analysis adopts Aspen PEA for estimates of capital investment and operational costs. As the utilized software version gives estimates for plant construction in USA at the 1<sup>st</sup> quarter of 2013, conversion factors are required for the correction of plant location and construction year. These parameters are unveiled in Table 6.1, where the main economic assumptions of this work are presented. The enterprise is projected to a horizon of 20 years of plant operation, with PBR modules being replaced every 5 years, regarding the expected short lifetime of PBR material. In CCS route, 300 km of pipeline is applied to CO<sub>2</sub> transportation to geological storage. The main economic assumptions of CO<sub>2</sub> transportation to storage is summarized in Table 6.2.

Minimum acceptable rate of return (MARR) of 0% is assumed to express solely environmental intentions of the project, for an optimistic sense of economic feasibility, as project goal achievement is associated to gross return of capital investments without profits.

Assuming an economic scenario with incidence of CO<sub>2</sub> taxation, where both direct and indirect emissions are accounted, BRY/CCU and CCS economic feasibilities are linked to the performance of a CO<sub>2</sub> emitting power plant alternative. The cash flow of each capture route  $j$

( $CashFlow_j$ ) is calculated with Eq. (6.4), where  $CapEff_j$  is the CO<sub>2</sub> capture efficiency of  $j$ ,  $F_{CO_2}^{Feed}$  is the flow rate of CO<sub>2</sub> leaving the power plant to feed  $j$  (BRY or CCS), and  $CashFlow_j^{Tec}$  is the cash flow without payment of taxes. Then another metric is created, accordingly to Eq. (6.5), to express the difference between the cash flow of alternative  $j$  and the payment of CO<sub>2</sub> taxes without emissions abatement ( $CashFlow_j^{DIF}$ ). A negative value of  $CashFlow_j^{DIF}$  indicates that paying CO<sub>2</sub> taxes is more economically attractive than investing in CO<sub>2</sub> capture route  $j$ .

$$CashFlow_j = CashFlow_j^{Tec} - F_{CO_2}^{Feed} (1 - CapEff_j) * Tax_{CO_2} \quad (6.4)$$

$$CashFlow_j^{DIF} = CashFlow_j - F_{CO_2}^{Feed} * Tax_{CO_2} \quad (6.5)$$

**Table 6.1.** Summary of main economic assumptions.

Variable	Value
Nationalization Factor <sup>(1)</sup>	Brazil/USA = 1.25
IC Index (Update Factor) <sup>(1)</sup>	2015Q4 = 136.0 2013Q1 = 147.0 2003(avg)= 107.0
Plant start-up year	2015
Project Lifetime (years)	20
PBR Lifetime (years)	5
Annual Operating Hours (h/year)	8000
PBR Price (MMUS\$/ha) <sup>(2)</sup>	0.197
Minimum Acceptable Rate of Return (%)	0
Carbon Taxation (US\$/t CO <sub>2</sub> )	50
GOX Cost (US\$/t O <sub>2</sub> ) <sup>(3)</sup>	31
Nutrients Prices (US\$/t)	NaNO <sub>3</sub> =320 NaH <sub>2</sub> PO <sub>4</sub> =1000 FeCl <sub>3</sub> =350
Utilities Costs	Electricity = 127 US\$/MWh Natural Gas = 19.5 US\$/MMBTU Low-Pressure Steam = 55 US\$/t <sup>(4)</sup>
Products Prices (US\$/t)	Methanol = 400 Microalga oil = 500 <sup>(5)</sup>

<sup>(1)</sup> Intratec, 2016. Useful indexes for the chemical industry. <http://www.intratec.us/free-tools/other-relevant-indexes>

<sup>(2)</sup> Huntley, M.E., Redalje, D.G., 2007. CO<sub>2</sub> mitigation and renewable oil from photosynthetic microbes: a new appraisal. *Mitig. Adapt. Strat. Glob. Change*, 12 (4), 573–608..

<sup>(3)</sup> US Department of Energy, 2013. "Oxygen production". *In: Advanced Carbon Dioxide Capture R&D Program: Technology Update. Appendix B: Carbon dioxide capture technology sheets.*

<sup>(4)</sup> Turton, R., Bailie, R.C., Whiting, W. B., Shaeiwitz, J.A., Bhattacharyya, D., 2012. *Analysis, Synthesis, and Design of Chemical Processes*. Prentice Hall, 4th edition.

<sup>(5)</sup> Soley Biotechnology Institute . <http://www.soleybio.com>

**Table 6.2.** Assumptions for CO<sub>2</sub> transportation via pipeline in CCS route.

Item	Value	Reference
Pipeline length (km)	300 km	-
Nominal diameter (in)	8 in	-
Compression costs (US\$/t CO <sub>2</sub> )	12.58 (0.12 \$/kWh electricity)	McCollum and Ogden (2006)
Maintenance costs (US\$/km/y)	3.100*10 <sup>3</sup> (reference year: 2003) 4.259*10 <sup>3</sup> (updated value)	Wong (2006)
Capital investment (US\$/km/in)	20.989*10 <sup>3</sup> (reference year: 2003) 28.835*10 <sup>3</sup> (updated value)	Wong (2006)

### 6.3. Process Description

Process Flow Diagrams (PFD) of alternatives being compared (BRY, CCS) are briefly described in this section. Further details are provided in Appendix Y1.

#### 6.3.1. Biorefinery – Biomass production, oil extraction and conversion to methanol

Fig. 6.2 depicts the flowsheet of biorefinery first area (BRY-1), comprising microalga cultivation+harvesting and oil extraction (BRY-1). Simplified PFD of biorefinery second area (BRY-2) – comprising biomass gasification, removal of excess CO<sub>2</sub>, and methanol production – is portrayed in Fig. 6.3. Considering market limitations for an abrupt increase of microalgae oil supply, oil extraction receives only 1/4 of biomass production, with the other 3/4 being sent to BRY-2 (after further dewatering stage).

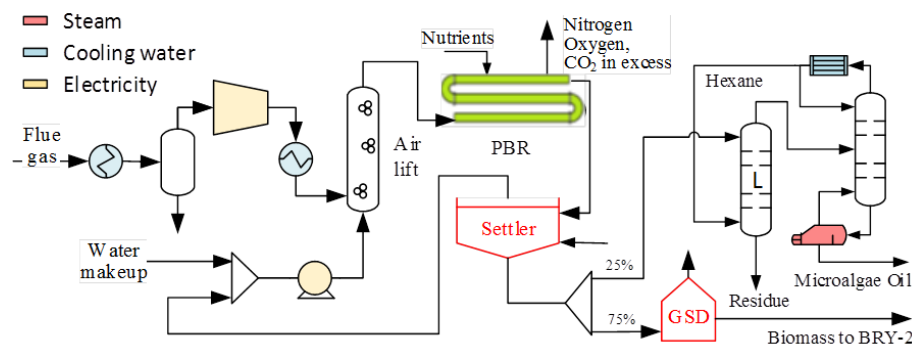


**Fig. 6.2.** Biorefinery flowsheet: biomass production and oil extraction (BRY-1).

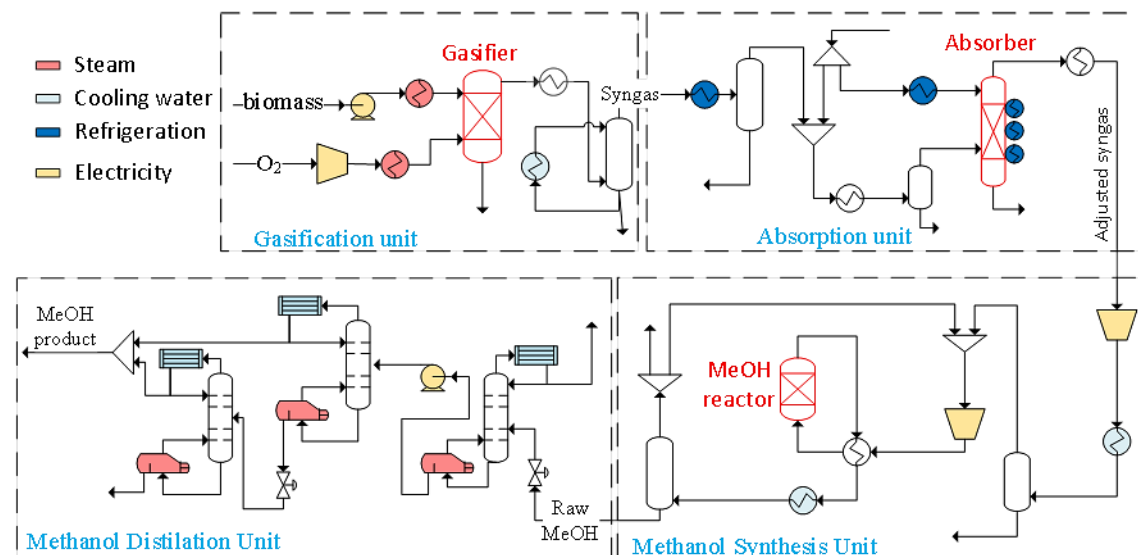


**Fig. 6.3.** Biorefinery flowsheet: biomass gasification and methanol production (BRY-2). Solvent regeneration, CO<sub>2</sub> liquefaction and cogeneration plants are not portrayed.

Flue gas feed is sent to an air lift arrangement, where CO<sub>2</sub> is absorbed in water, contacting inlet gas with clarified liquid from the settler added with water makeup. The air lift is directly connected to the PBR, which consists of several sheet modules of horizontal transparent tubes. Liquid suspension leaving the PBR is sent to dewatering by flocculation/settling.

Concentrated biomass leaves the settler with 7%w of organic matter (Williams and Laurens, 2010) and 75% of this stream is directed to further dewatering to 40%w by Greenhouse Solar Dryer (GSD) (Kurt et al., 2015) for subsequent thermochemical processing by gasification.

In biorefinery second area (BRY-2) (Fig. 6.3), gaseous oxygen at 95%mol – supplied by a low-pressure air separation unit (ASU) and further compressed to 32 bar – is injected in gasifier to oxidate biomass generating heat for gasification. Air injection is not adopted to avoid introduction of N<sub>2</sub> to the system, which dilutes synthesis gas minimizing methanol synthesis yields. Dewatered biomass is preheated and then conveyed to the O<sub>2</sub>-blown gasifier, which produces CO<sub>2</sub>-rich synthesis gas ( $\approx 34\%mol\ CO_2$ ) at 32 bar and 900°C. Gasification reactions are modeled at thermodynamic equilibrium (Gibbs-reactor model), neglecting formation of tars and residual coke/char. The gasifier temperature is controlled at  $\approx 900^\circ C$  by adjustment of oxygen flow rate. The CO<sub>2</sub>-rich synthesis gas is cooled recovering heat to produce high-pressure steam – availed in a cogeneration plant – and is sent to a Physical-Absorption Rectisol unit (absorption with chilled methanol) for CO<sub>2</sub> removal, aiming to adjust the H/C proportion in the syngas. The so-called syngas stoichiometric number  $S = ([H_2] - [CO_2]) / ([CO] + [CO_2])$  of lean syngas to methanol synthesis is 2.15. The captured CO<sub>2</sub> is liquified and exported at 100 bar without adding revenues. The methanol synthesis loop employs the Lurgi process configuration, comprising a tubular fixed-bed reactor, cooled by boiling water, operated at 65 bar and 240-260°C. Raw methanol leaves the synthesis loop to be purified in distillation section accordingly to commercial standard of >99.85%w together with impure methanol from CO<sub>2</sub> absorption unit. Purge gases from methanol plant are availed to increase cogeneration outputs with supplemental fire. HYSYS flowsheets for BRY-2 simulation are found in Figs. Y1.3, Y1.4 and Y1.5 at Appendix Y1.

### 6.3.2 Carbon Capture and Storage

The flowsheet of CO<sub>2</sub> capture by Chemical-Absorption with MEA (representing CCS route) is depicted in Fig. 6.4. Flue gas is sent to the absorber, leaving it as lean gas with  $\approx 4\%mol\ CO_2$  to be discarded to atmosphere. CO<sub>2</sub>-rich solvent is regenerated producing pure CO<sub>2</sub> to be compressed (four-stage intercooled train not shown) and dispatched to geological storage.

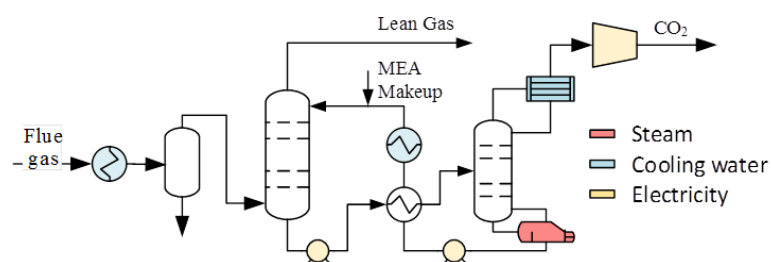


**Fig. 6.4.** Process diagram for the CCS route.

## 6.4. Results and Discussion

Carbon emissions and economic analyses results are presented in this section.

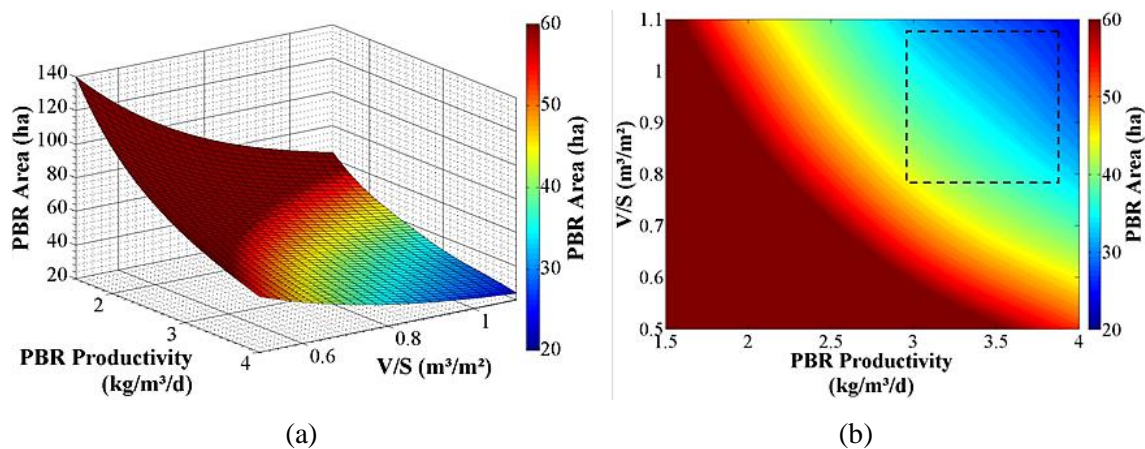
### 6.4.1. Process simulation

Table 6.3 unveils process performances and some typical literature values for comparison.

**Table 6.3.** Process simulation results for biorefinery (BRY) and CCS.

Item	Route	This work	Literature results
<i>Chlorella sp.</i> HHV	BRY	22.2 MJ/kg	22.6 (Duan et al., 2013)
Dilution rate	BRY	0.4046 m <sup>3</sup> /m <sup>3</sup> <sub>reactor</sub> /d	0.384 (Chisti, 2007)
PBR area and investment	BRY	986 ha, 200 MMUS\$	
GSD area and investment	BRY	60 ha, 150 MMUS\$	
Microalga oil production	BRY	2.9 t/h	
Methanol production	BRY	13.87 t/h	
Stripper reboiler duty	CCS	4.36 GJ/tCO <sub>2</sub> <sup>captured</sup>	4.56 (Feron, 2010)

Table 6.3 unveils extremely large area of  $\approx 1000$  ha required for installation of PBR and GSD. With such huge footprint area, this process is most likely to be unattractive. If one specifies drastically lower intended area of  $\approx 50$  ha required for PBR, it would be necessary to have volumetric productivity higher than  $3.0 \text{ kg m}^{-3} \text{ d}^{-1}$  and compactness parameter volume to projected surface ratio ( $V/S$ ) above  $0.8 \text{ m}^3/\text{m}^2$ . Fig. 6.5 presents a sensitivity analysis in this regard, expressing the footprint area as a function of volumetric productivity and  $V/S$  parameters. Although PBR with volumetric productivity  $>3.0 \text{ kg m}^{-3} \text{ d}^{-1}$  remains unrealistic given the current state-of-the-art techniques (Acién et al., 2012), much denser cultures may be prepared (e.g. 2-8 g/L), but at the cost of limited growth due to increased turbidity.



**Fig. 6.5.** PBR footprint area as a function of volumetric productivity and volume/surface ratio ( $V/S$ ): (a) 3D plot; (b) contour levels.

### 6.4.2. CO<sub>2</sub> emissions analysis

Table 6.4 presents total avoidance of CO<sub>2</sub> emissions by methanol production in BRY being compared to competing CCU technologies (NG bi-reforming and CO<sub>2</sub> hydrogenation) and European average data of conventional methanol plants (“business as usual” scenario). All numbers in Table 6.4 are normalized by methanol production rate, so values are expressed in  $t^{CO_2}/t^{MeOH}$  unit. Although direct emissions in BRY are the highest mainly due to incomplete biofixation of CO<sub>2</sub> fed, the amount of CO<sub>2</sub> avoided is twice the value of the CO<sub>2</sub> hydrogenation process (Pérez-Fortes et al., 2016) and 6x the value of NG bi-reforming route (Wiesberg et al., 2016).

**Table 6.4.** Methanol production technologies in terms of CO<sub>2</sub> mitigation ( $t^{CO_2}/t^{MeOH}$ ).

<i>Metrics</i> ( $t^{CO_2}/t^{MeOH}$ )	<i>BRY</i> ( <i>This Work</i> )	<i>Bi-reforming</i> Wiesberg et al. <sup>(1)</sup>	<i>CO<sub>2</sub> Hydrogenation</i> Pérez-Fortes et al. <sup>(2)</sup>	<i>CO<sub>2</sub> Hydrogenation</i> Matzen et al. <sup>(3)</sup>	<i>Business</i> <i>as usual</i> <sup>(4)</sup>
Direct emissions	1.66	0.01	0.09	0.05	0.695
Indirect emissions	0.13	0.40	0.14	0.16	0.073
Total emissions	1.79	0.41	0.23	0.21	0.77
CO <sub>2</sub> feed	5.08 <sup>(5)</sup>	0.28	1.46	1.43	-
CO <sub>2</sub> not produced <sup>(6)</sup>	-1.03	0.36	0.54	0.56	-
CO <sub>2</sub> avoided <sup>(7)</sup>	4.05	0.64	2.00	1.99	-

<sup>(1)</sup> Wiesberg et al. (2016); <sup>(2)</sup> Pérez-Fortes et al. (2016); <sup>(3)</sup> Matzen et al. (2015). <sup>(4)</sup> Average performance of existing methanol plants in Europe (Pérez-Fortes et al., 2016). <sup>(5)</sup> Allocating to MeOH production 3/4 of total CO<sub>2</sub> feed to microalgal cultivation, as 1/4 is allocated to oil production. <sup>(6)</sup> Eq. (6.2); <sup>(7)</sup> Eq. (6.3);

### 6.4.3. Economic assessment

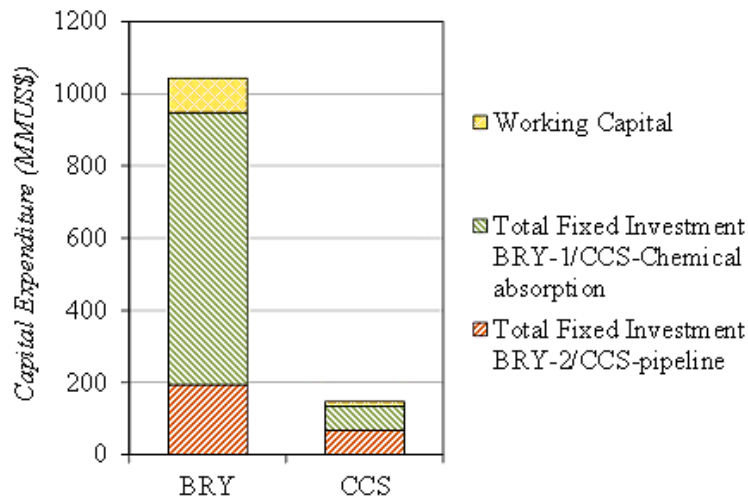
Table 6.5 details operational costs and revenues for BRY and CCS routes. The major share of BRY manufacturing costs is the purchase of gaseous oxygen (39%), while in CCS low-pressure steam utilized in solvent regeneration dominates operational costs (57%). Regarding capital investments, Fig. 6.6 decomposes contributions from BRY-1 and BRY-2 areas, as well as CO<sub>2</sub> capture plant and pipeline in CCS case. The largest share of BRY capital investment is spent in its first area (BRY-1), despite having less complex flowsheet than BRY-2, mainly due to large number of PBR modules required for installation. Hence, enhancing volumetric productivity should be the most significant development to improve the economic performance of BRY. In CCS route, capital investments are evenly distributed between capture plant and pipeline to storage ( $\approx 45\%$  each). Although BRY involves much higher capital investments than CCS (Fig. 6.6), BRY presents lower operational costs and has advantage of adding revenues to cash flows (Table 6.5).

Figs. 6.7a and 6.7b present projections of cumulative cash flow differences ( $CashFlow_j^{DIF}$ , Eq. (6.5)) for plant locations in Brazil and USA, showing periodic falls in BRY performance due to replacement of PBR modules. As both routes demonstrate negative net present values by the end of the project at assumed conditions, merely paying CO<sub>2</sub> taxation of 50 US\$/t without CO<sub>2</sub> capture should be economically more attractive than investing in these technologies for CO<sub>2</sub> abatement, i.e. none of presented alternatives are recommended.

**Table 6.5.** Operational costs and revenues for BRY and CCS.

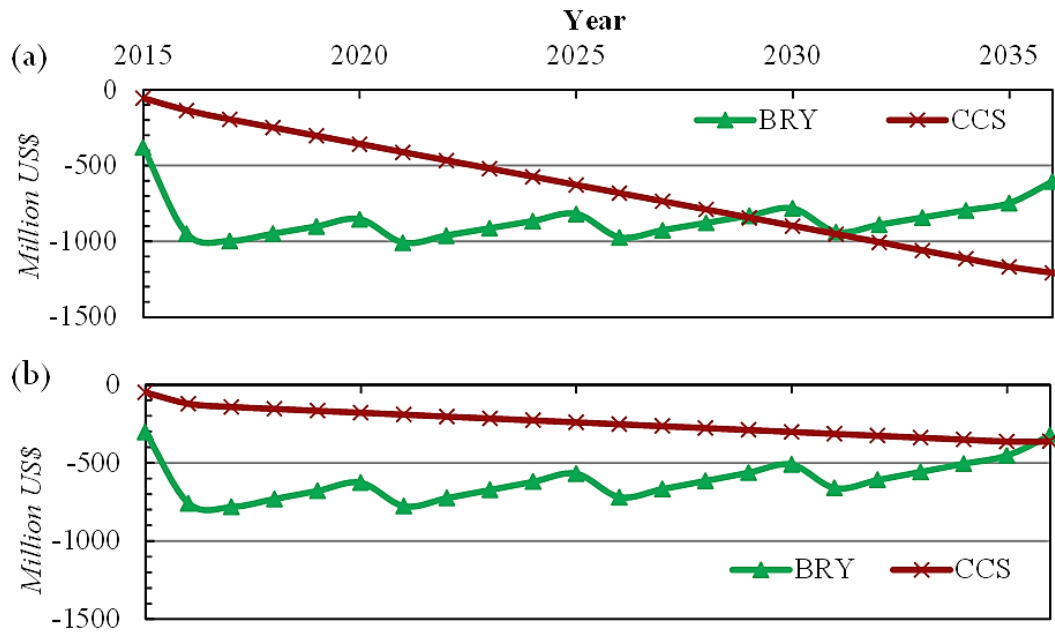
Item	BRY (MMUS\$/y)	CCS (MMUS\$/y)
Microalga Medium + Flocculant	0.7	-
Monoethanolamine (MEA)	-	0.9
Low-Pressure Steam	4.9	45.7
Electricity	1.0	13.2 *
Cooling Water	3.4	5.9
Gaseous Oxygen	6.3	-
Variable Costs	16.3	65.7
Fixed Costs	20.5	15.1
Total Operational Cost	36.8	80.8
Methanol Production	44.4	-
Microalgae Oil Production	14.8	-
Total Revenues	59.2	-

\* Operational expenses with transportation: 6.4 MMUS\$/y



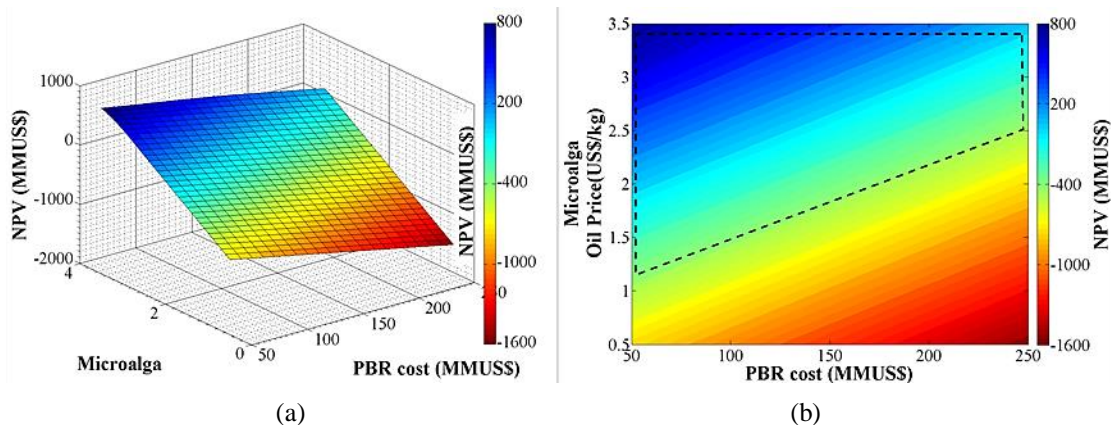
**Fig. 6.6.** Breakdown of capital investments in BRY and CCS.

Fig. 6.7a evinces long-term economic advantage of BRY over CCS for plant location in Brazil, starting from the 14<sup>th</sup> operational year. For an US scenario with low-priced natural gas at 3.0 US\$/MMBTU (EIA, 2016a) and electricity costing 72 US\$/MWh (EIA, 2016b), Fig. 6.7b evinces BRY outperforming CCS only at the last year of project, showing that more favorable economic conditions, with lower costs of fuels and utilities, minimize BRY advantages over conventional CCS route.



**Fig. 6.7.** Projection of cumulative cash flow differences for BRY and CCS routes ( $CashFlow_j^{DIF}$  – Eq. (6.5)) considering plant location in: (a) Brazil; (b) USA.

Sensitivity analyses were performed to evaluate conditions for BRY economic feasibility in Brazilian scenario. In this sense, the chosen variables influencing BRY *NPV* are PBR capital investment and microalga oil price. Fig. 6.8 presents results in this regard, with Fig. 6.8a as a 3D surface and Fig. 6.8b as contour levels expressing *NPV*. Fig. 6.8 unveils economically feasible BRY with microalga oil price above 2500 *US\$/t* (5x the assumed base price) considering PBR base capital investment, which could be just reduced to 1500 *US\$/t* if investments in PBR were below 100 *MM US\$* (less than half of estimated value).



**Fig. 6.8.** Net Present Value (*NPV*) as a function of PBR capital investment and price of microalga oil: (a) 3D plot; (b) contour levels.

Since the price of microalgae oil should be more flexible than PBR capital cost, it is selected to a second sensitivity analysis of BRY *NPV*, where variable  $CO_2$  taxation is applied. With positive *NPV*, Fig. 6.9 shows that BRY can be more economically attractive than merely

paying taxation without carbon abatement if taxes are above  $100 \text{ US}\$/\text{t CO}_2$  (break-even taxation value), assuming base-price of microalgae oil ( $500 \text{ US}\$/\text{t}$ ). With microalga oil price at  $2000 \text{ US}\$/\text{t}$ , just  $\approx 40 \text{ US}\$/\text{t CO}_2$  tax would be sufficient to make BRY economically feasible. While there is a great uncertainty concerning the price of microalga oil, the assumed base value of  $500 \text{ US}\$/\text{t}$  may be regarded as a conservative estimate, as it is in the range of typical chemical commodities (e.g. methanol).

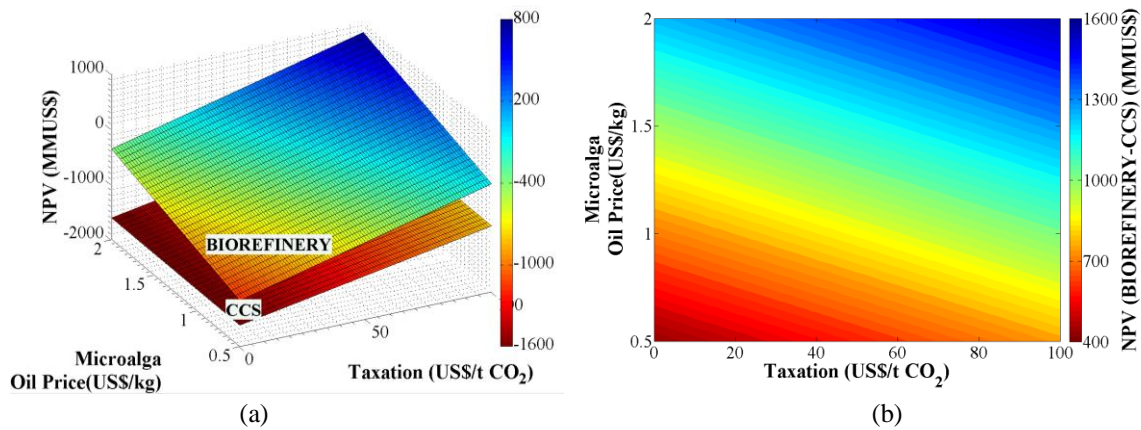


**Fig. 6.9.** Net Present Value ( $NPV$ , MMUS\$) as a function of  $\text{CO}_2$  taxation and microalga oil price: (a) 3D plot; (b) contour levels of the difference (BRY – CCS) between surfaces of (a).

## 6.5. Conclusions for Chapter 6

Although optimistic assumptions were applied to PBR, the BRY was shown to be unfeasible in economic terms. It is most likely to be also unfeasible in practical terms, given the immense required footprint of  $\approx 1000 \text{ ha}$  for capturing  $\text{CO}_2$  from a  $\approx 100 \text{ MW}$  coal power plant, clearly revealing a major technological barrier. As a consequence of such large PBR, the capital investment of BRY is dominated by its first section BRY-1 (comprising microalgae cultivation+harvesting and oil extraction) – about  $\approx 70\%$  – even considering that relatively complex processing plant BRY-2 is applied for biomass thermochemical conversion to methanol. Improvements are needed to increase PBR volumetric productivity and footprint compactness ratio volume/surface ( $V/S$ ). Despite of challenges concerning the high capital investment and availability of immense areas to install PBR modules, and even assuming low-priced microalga oil at  $500 \text{ US}\$/\text{t}$ , BRY can be an economically feasible project to the fossil-fuel power plant owner if very high  $\text{CO}_2$  taxes – above  $100 \text{ US}\$/\text{t}$  – are applied

From  $\text{CO}_2$  emissions perspective, BRY allows much higher  $\text{CO}_2$  emissions avoidance than competing CCU alternatives for methanol production –  $2x$  and  $6x$  higher than  $\text{CO}_2$  hydrogenation and NG bi-reforming/methanol synthesis routes, respectively – pointing clear environmental advantage of BRY technological alternative in this regard.

## 6.6. References for Chapter 6

- Acien, F.G., Fernández, J.M., Magán, J.J., Molina, E., 2012. Production cost of a real microalgae production plant and strategies to reduce it. *Biotechnol. Adv.*, 30, 1344-1353. <https://doi.org/10.1016/j.biotechadv.2012.02.005>
- Araújo, O.Q.F., De Medeiros, J.L., Alves, R.M.B., 2014. CO<sub>2</sub> utilization: A process systems engineering vision, In: Morgado, C.R.V., Esteves, V.P.P. (Eds.), CO<sub>2</sub> Sequestration and Valorization. *InTech*, 35-88. <https://doi.org/10.5772/57560>
- Aresta, M., 2010. Carbon Dioxide as Chemical Feedstock, WILEY-VCH Verlag GmbH & Co.
- Chisti, Y., 2007. Biodiesel from microalgae. *Biotechnol. Adv.*, 25, 3, 294-306. <https://doi.org/10.1016/j.biotechadv.2007.02.001>
- Chisti, Y., 2016. “Large-scale production of algal biomass: raceway ponds”. In: Bux, F., Chisti, Y. (Eds). *Algae biotechnology – products and processes*. Springer.
- Cheah, W.Y., Ling, T.C., Juan, J.C., Lee, D.J., Chang, J.S., Show, P.L., 2016. Biorefineries of carbon dioxide: From carbon capture and storage (CCS) to bioenergies production. *Bioresour. Technol.*, 215, 346–356. <https://doi.org/10.1016/j.biortech.2016.04.019>
- Cuéllar-Franca, R.M., Azapagic, A., 2015. Carbon capture, storage and utilisation technologies: A critical analysis and comparison of their life cycle environmental impacts. *J. CO<sub>2</sub> Util.*, 9, 82–102. <https://doi.org/10.1016/j.jcou.2014.12.001>
- Duan, P., Jin, B., Xu, Y., Yang, Y., Bai, X., Wang, F., 2013. Thermo-chemical conversion of *Chlorella pyrenoidosa* to liquid biofuels. *Bioresour. Technol.*, 133, 197-205. <https://doi.org/10.1016/j.biortech.2013.01.069>
- Feron, P.H.M., 2010. Exploring the potential for improvement of the energy performance of coal fired power plants with post-combustion capture of carbon dioxide. *Int. J. Greenh. Gas Con.*, 4, 152–160. <https://doi.org/10.1016/j.ijggc.2009.10.018>
- García, C.A., Betancourt, R., Cardona, C.A., 2016. Stand-alone and biorefinery pathways to produce hydrogen through gasification and dark fermentation using *Pinus Patula*. *J. Environ. Manage.*, 203(2), 695-703. <https://doi.org/10.1016/j.jenvman.2016.04.001>
- Goli, A., Shamiri, A., Talaiekhosravi, A., Eshtiaghi, N., Aghamohammadi, N., Aroua, M. K., 2016. An overview of biological processes and their potential for CO<sub>2</sub> capture. *J. Environ. Manage.*, 183, 41-58. <https://doi.org/10.1016/j.jenvman.2016.08.054>
- EIA, 2016a. Natural gas spot and futures prices (NYMEX). Accessed in Dec. 22, 2016 [http://www.eia.gov/dnav/ng/ng\\_pri\\_fut\\_s1\\_m.htm](http://www.eia.gov/dnav/ng/ng_pri_fut_s1_m.htm).
- EIA, 2016b. Electricity data. Accessed in Dec. 22, 2016 [https://www.eia.gov/electricity/monthly/epm\\_table\\_grapher.cfm?t=epmt\\_5\\_6\\_a](https://www.eia.gov/electricity/monthly/epm_table_grapher.cfm?t=epmt_5_6_a).
- IPCC, 2011. IPCC special report on renewable energy sources and climate change mitigation. Prepared by Working Group III of the Intergovernmental Panel on Climate Change. Edenhofer, O., Pichs-Madruga, R., Sokona, Y., Seyboth, K., Matschoss, P., Kadner, S. Zwickel, T., Eickemeier, P., Hansen, G., Schlömer, S., Von Stechow, C. (Eds). Cambridge University Press, Cambridge, United Kingdom and New York, NY, USA, 1075 pp.
- Kurt, M., Aksoy, A., Sanin, F., 2015. Evaluation of solar sludge drying alternatives by costs and area requirements. *Water Res.*, 82, 47-57. <https://doi.org/10.1016/j.watres.2015.04.043>
- Kypreos, S., Turton, H., 2011. Climate change scenarios and Technology Transfer Protocols. *Energy Policy*, 39, 844–853, <https://doi.org/10.1016/j.enpol.2010.11.003>
- Letelier-Gordo, C., Holdt, S., De Francisci, D., Karakashev, D., Angelidaki, I., 2014. effective harvesting of the microalgae *Chlorella protothecoides* via bioflocculation with cationic starch. *Bioresour. Technol.*, 167, 214-218. <https://doi.org/10.1016/j.biortech.2014.06.014>

- Liu, A., Chen, W., Zheng, L., Song, L., 2011. Identification of high-lipid producers for biodiesel production from forty-three green algal isolates in China. *Prog. Nat. Sci.-Mater.*, 21, 4, 269-276. [https://doi.org/10.1016/S1002-0071\(12\)60057-4](https://doi.org/10.1016/S1002-0071(12)60057-4)
- Matzen M, Alhajji M, Demirel Y., 2015. Chemical storage of wind energy by renewable methanol production: feasibility analysis using a multi-criteria decision matrix. *Energy*, 93, 343–353. <https://doi.org/10.1016/j.energy.2015.09.043>
- McCollum, D.L., Ogden, J.M., 2006. Techno-economic models for carbon dioxide compression, transport, and storage & correlations for estimating carbon dioxide density and viscosity – Section I. Institute of Transportation Studies.
- Moheimani, N. R., 2016. *Tetraselmis suecica* culture for CO<sub>2</sub> bioremediation of untreated flue gas from a coal-fired power station. *J Appl Phycol*, 28, 2139–2146. <https://doi.org/10.1007/s10811-015-0782-3>
- Olah, G.A., Goepfert, A., Prakash, G.K.S., 2009. Beyond oil and gas: the methanol economy, 2<sup>nd</sup> updated and enlarged edition. WILEY-VCH Verlag GmbH & Co. KGaA, Weinheim.
- Pérez-Fortes, M., Schöneberger, J.C., Boulamanti, A., Tzimas, E., 2016. Methanol synthesis using captured CO<sub>2</sub> as raw material: techno-economic and environmental assessment. *App. Energ.*, 161, 718–732. <https://doi.org/10.1016/j.apenergy.2015.07.067>
- Skjanes, K., Lindblad, P., Muller, J., 2007. BioCO<sub>2</sub> – A multidisciplinary, biological approach using solar energy to capture CO<sub>2</sub> while producing H<sub>2</sub> and high value products. *Biomol. Eng.*, 24, 405–413. <https://doi.org/10.1016/j.bioeng.2007.06.002>
- Tang, D., Han, W., Li, P., Miao, X., Zhong, J., 2011. CO<sub>2</sub> biofixation and fatty acid composition of *Scenedesmus obliquus* and *Chlorella pyrenoidosa* in response to different CO<sub>2</sub> levels. *Bioresour. Technol.* 102(3), 3071–3076. <https://doi.org/10.1016/j.biortech.2010.10.047>
- Turton, R., Bailie, R.C., Whiting, W. B., Shaewitz, J.A., Bhattacharyya, D., 2012. Analysis, synthesis, and design of chemical processes. Prentice Hall, 4th edition. Michigan, USA.
- Wiesberg, I.L., de Medeiros, J.L., Alves, R.M.B., Coutinho, P.L.A., Araújo, O.Q.F., 2016. Carbon dioxide management by chemical conversion to methanol: hydrogenation and bi-reforming. *Energ. Convers. Manage.*, <https://doi.org/10.1016/j.enconman.2016.04.041>
- Williams, P., Laurens, L., 2010. Microalgae as biodiesel & biomass feedstocks: review & analysis of the biochemistry, energetics & economics. *Energy Environ. Sci.* 3, 554–590. <https://doi.org/10.1039/B924978H>
- Wong, S., 2006. CO<sub>2</sub> compression & transportation to storage reservoir, in: APEC Energy Working Group (Ed.), Building Capacity for CO<sub>2</sub> Capture and Storage Project in the APEC Region.
- Young, D.M., Cabezas, H., 1999. Designing sustainable processes with simulation: the waste reduction (WAR) algorithm. *Comput. Chem. Eng.*, 23, 1477–1491. [https://doi.org/10.1016/S0098-1354\(99\)00306-3](https://doi.org/10.1016/S0098-1354(99)00306-3).

## 7. Upstream and Downstream Processing of Microalgal Biogas: Emissions, Energy and Economic Performances under Carbon Taxation

*This chapter is published as an article in Renewable and Sustainable Energy Reviews.*

BRIGAGÃO, G. V.; WIESBERG, I. L.; PINTO, J. L.; ARAÚJO, O. Q. F.; DE MEDEIROS, J. L. Upstream and downstream processing of microalgal biogas: emissions, energy and economic performances under carbon taxation. *Renewable and Sustainable Energy Reviews*, 112, 508-520, 2019.

### Abstract

The study evaluates alternative and innovative arrangements for processing a microalgal biomass (*Nannochloropsis salina*) by anaerobic digestion to produce biogas. Cell wall limits bio-accessibility of microalgal intracellular compounds, demanding pretreatment to improve methane yield. Two pretreatments are evaluated at 75°C using residual heat: thermal (1bar) and thermomechanical (20bar), which increased biogas production in 40% and 159%, respectively. Thermomechanical pretreatment is coupled to the following downstream processing cases: (i) biomethane; (ii) bioelectricity; (iii) biomethane with enhanced oil recovery; (iv) bioelectricity with enhanced oil recovery and (v) pressurized anaerobic digestion (6bar) for biomethane with enhanced oil recovery. Processes are compared in three dimensions: energy, economic and carbon footprint. Such a framework including upstream and downstream processes, besides comparison of atmospheric and pressurized anaerobic digestion, with in-depth economic analysis, configures the main novelties of this work. Resource utilization efficiency metrics point advantage of pressurized anaerobic digestion case, while indicate biomethane production as less efficient than bioelectricity. When carbon dioxide post-combustion capture and enhanced oil recovery are applied to abate bioelectricity emissions, bioelectricity loses competitiveness to biomethane due to high energy penalties. Sensitivity of Net Present Value to varying carbon taxation (increasing costs), Capture & Trade mechanism and enhanced oil recovery (adding revenues) show superior resilience of biomethane with enhanced oil recovery. In base scenario conditions, where 30US\$/GJ electricity is applied, maximum biomass costs to economic feasibility for cases (i) to (v) are 50, 21, 100, 5 and 83US\$/t (dry-basis), respectively. Priced at 50US\$/GJ, the bioelectricity production frontier to feasibility starts at biomass costs  $\approx$ 150US\$/t.

**Keywords:** Biogas; microalga pretreatment; biomethane; bioelectricity; CO<sub>2</sub> capture; anaerobic digestion.

### Supplementary Materials

Supplementary Materials for this chapter are found in Appendices Z1, Z2, Z3 and Z4.

## Abbreviations

AD Anaerobic Digestion; BE Bioelectricity; BM Biomethane; CCU Carbon Capture and Utilization; CW Cooling-Water; EOR Enhanced Oil Recovery; GT Gas Turbine; HRSG Heat-Recovery-Steam-Generation; HRT Hydraulic Retention Time; LHV Lower Heating Value; MEA Monoethanolamine; NOPT No Pretreatment; PAD Pressurized Anaerobic Digestion; PSA Pressure-Swing-Adsorption; ST Steam Turbine; TEG Triethylene Glycol; THPT Thermal Pretreatment; TMPT Thermo-Mechanical Pretreatment; VS Volatile Solids.

## Nomenclature

$\eta_Q, \eta_W$  : Biomethane boiler efficiency, and combined cycle net efficiency  
 $\xi_i, \xi_o$  : Lower heating values of biomass suspension and biomethane (MJ/kg)  
 $F_i, F_o$  : Mass flowrates of biomass suspension and biomethane (kg/s)  
 $nc$  : Number of compressor and pump items  
 $nh$  : Number of heating utility consumer items  
 $nt$  : Number of turbine items  
 $P, T$  : Pressure (bar) and Temperature ( $^{\circ}\text{C}$ )  
 $Q_h$  : Heat duty (MW)  
 $V$  : Volume ( $\text{m}^3$ )  
 $W_c, W_t$  : Electricity consumption and electricity generation (MW)

### Economic terms

$FCI$  : Fixed capital investment (US\$)  
 $CEPCI$  : Chemical engineering plant cost index (unitless)  
 $NPV$  : Net present value (US\$)  
 $COM$  : Cost of manufacturing (US\$/y)  
 $REV$  : Revenues (US\$/y)

### Metrics

$EI$  : Energy Invested, heat and electricity demands in LHV basis (MW)  
 $ER$  : Energy Return, BM or BE production in LHV basis (MW)  
 $EROI$  : Energy Return on Investment (unitless)  
 $\%EnergyOut$  : Percentage of microalgae biomass LHV (unitless)

### Subscripts

$BD$  : Biodigester  
 $c$  : Compressors and pumps  
 $h$  : Heating utilities  
 $i$  : Inputs  
 $o$  : Outputs  
 $t$  : Turbines

## 7.1. Introduction

Bio-based energy is shifting from intensive use of energy crops to diversified substrates, and progressively developing processes using a wide range of raw biomass [1]. Anaerobic digestion (AD) monetizes waste treatment producing a gaseous fuel, being the preferred technology for treating wastes of high moisture contents [2], e.g. microalgae suspensions and food wastes with 74-90% w water [3].

AD produces biogas with reduced Lower Heating Value (LHV) due to its high carbon dioxide (CO<sub>2</sub>) content (30-40%) [4], with methane (CH<sub>4</sub>) ranging 50-65% [2]. To attain high LHV without additional upgrading equipment, Li et al. [2] proposed an *in situ* biogas upgrading consisting of a conventional continuously stirred tank digester (as acidogenesis reactor) followed by a pressurized biofilm AD, evaluated at four pressure levels showing beneficial effects of increasing AD operating pressures. Despite the promising results, the technology is at proof of concept stage.

Besides its low LHV, biogas is generally produced at low pressure, and has other impurities than CO<sub>2</sub> – e.g. ammonia (NH<sub>3</sub>), water (H<sub>2</sub>O) and, depending on substrate composition, hydrogen sulfide (H<sub>2</sub>S) [5]; being off-specified for injection in natural gas distribution grids. Hence, development of biogas upgrading techniques is required [6], demanding energy and capital-intensive downstream processing, and most conventional technologies are economically feasible only for large scale, at biogas flow rates >100 m<sup>3</sup>/h [5].

Depending on the targeted use, different upgrading processes are required. Due to its high content in the biogas, CO<sub>2</sub> removal is the main downstream step, and the separation technology to be adopted depends on specific requirements for biogas utilization, impacting costs [7].

A promising alternative is moving the role of AD from waste treatment to biorefinery arrangements, where a potential application is AD of microalgae feedstocks [8]. These microorganisms are able to perform photosynthesis with particularly high efficiency of solar energy absorption, and has been suggested to be applied in CO<sub>2</sub> capture from thermoelectric plants [9]. Chen et al. [10] reviews “waste biorefineries” which use waste resources, e.g. sludge digestate, to enhance the economic feasibility of microalgae production, challenged by its high costs. Microalgae AD shows low biodegradability due to strong cell walls containing recalcitrant compounds [11]. The variety of cell characteristics and biochemical composition

among species result in different biogas yields being reported for microalgae biomass, in a wide range from 0.05 to 0.8 L CH<sub>4</sub>/g volatile solids (VS) (0.04-0.57 gCH<sub>4</sub>/gVS) [12].

To increase accessibility to microalgal intracellular compounds, pretreatment methods prior to anaerobic digestion are needed [13]. Thermal hydrolysis is often reported as the most efficient pretreatment, with productivity and biodegradability increases over 60% [11]. Other alternatives are mechanical, chemical (acid/alkaline), irradiation and biological pretreatments. The most developed technologies has combined chemical and thermomechanical means of wall disruption, though severe conditions challenges sustainability and cost effectiveness of the process, besides affecting the AD performance [14].

Bravo-Fritz et al. [15] evaluated the economic performance of 11 configurations of microalgae-based biorefinery, including anaerobic digestion as a final processing stage, with almost all the scenarios returning negative economic performance, except for the extraction and commercialization of high added-value product (e.g. concentrated proteins). Few economic analyses are available in the literature [8], despite of the potential role of AD in optimizing biorefinery performance through meeting internal energy demand, employing residual or whole biomass from other biorefinery units. This work assesses the biogas production chain, in the context of a microalgae-based biorefinery, from the upstream pretreatment, the midstream anaerobic digestion and the downstream processing of biogas, using technical and economic indicators obtained through process simulation. Thermal pretreatment is compared to a thermo-mechanical alternative where the biomass suspension is heated and pressurized to disrupt cell wall.

One of the shortcomings of AD technologies is the high capital cost associated with reactors, and large capacity to accommodate long hydraulic residence time (HRT) to hold slowly growing microorganisms [16]. A cost trade-off exists between AD conditions and downstream processing of biogas, explored in the present study, with pressure being the main operational conflict to conciliate, an additional original contribution of the analysis.

To size the relative importance of the compression phase in the biogas processing chain, this work evaluates pressurization of biodigester (1 bar and 6 bar), which reduces compression power (and investment) in the downstream processing of biogas, traded-off by larger digester costs. Two biogas monetization alternatives are evaluated, biomethane production and bioelectricity generation, with and without post-combustion CO<sub>2</sub> capture. These two are selected as biomethane avoids chemical conversion to preserve the biogas heating potential,

while bioelectricity is considered for avoidance of biogas upgrading and pipeline infrastructure, giving place to transmission lines. The obtained CO<sub>2</sub> is compressed and exported to an oil&gas company performing enhanced oil recovery (EOR), integrating renewable energy chain to fossil-based fuel production.

The combination of pretreatment, digestion pressure and downstream options originates a set of seven process systems engineering structures, which are evaluated based on technical and economic indicators, under five economic scenarios involving carbon taxes (cost), CO<sub>2</sub> cap & trade prices (revenue) and CO<sub>2</sub> price for EOR (revenue, derived from oil price), whose uncertainty affect economic performance. The net present value (*NPV*) is calculated also for varying cost of biomass, from null price (a residue) to the threshold of feasibility. To the authors best knowledge, this work is unique in combining deepness of technical approach, including innovative pretreatment and pressurized AD, with rigorous mass and energy balances calculated through process simulation, to the system broadness – from upstream to downstream operations, and economic analysis under diverse scenarios, considering revenues from biogas products and CO<sub>2</sub> sale allied to taxes and cap & trade mechanism.

## 7.2. Upstream Processing

The genus *Nannochloropsis* (Eustigmatophyceae) is one of the most popular groups of microalgae for industrial production of biofuels and synthesis of polyunsaturated fatty acids [17]. Interest in this genus is due to its high capacity of lipid accumulation, biomass production and tolerance to different environmental conditions [18].

The variability of intracellular biochemical composition directly influences the performance of anaerobic digestion of microalgae, with lipids favoring the production of methane (1.0 L CH<sub>4</sub>/gVS), due to its theoretical yield being superior to that of proteins (0.85 L CH<sub>4</sub>/gVS) and carbohydrates (0.42 L CH<sub>4</sub>/gVS) [19]. Proteins present the disadvantage of producing ammonia (NH<sub>3</sub>) during AD, which inhibits methanogenic activity [20]. In this work, microalgal biomass of *Nannochloropsis salina* is selected notably for its high lipid and low protein contents, both aspects favoring methane production by AD [21].

Either whole or residual biomass suspension require a pretreatment stage prior to AD to enhance biodegradability, making organic matter more accessible to anaerobic microorganisms [21]. Because *Nannochloropsis* cells have thick cell wall, the selection of the

rupture method for this genus is a critical factor to intracellular extraction. Hence, techniques that combine high pressure to thermal hydrolysis enhance biodigestion [22].

For low hydraulic retention time (HRT), in continuous systems, enhancements on AD rate may prevail over biogas yield enhancements; thus, the most promising pretreatments are the ones displaying positive effect on degradation rate and biogas yield [1]. Marques et al. [23] reviewed 80 pretreatment experiments applied to 30 microalgae biomasses, concluding that only one thermal pretreatment presented cost-effective enhancement on biomethane production.

Brémont et al. [1] reported that thermal and mechanical pretreatments are already applied at full-scale for a variety of substrates while chemical pretreatment is restricted to laboratory scale due to environmental impacts and costs issues. This work considers two pretreatment alternatives – thermal pretreatment (THPT) and thermo-mechanical pretreatment (TMPT), shown in Fig. 7.1, which are compared to digestion without pretreatment (NOPT). THPT pretreatment (Fig. 7.2) employs low-grade waste heat for increasing biomass temperature to 75°C [24]. TMPT involves further pressurization of the heated suspension to 20 bar prior to entering the pretreatment tank. In both alternatives, HRT of 15 minutes is used [11]. For THPT and TMPT upstream processing routes, a heat integration exchanger (HIE) reduces heat duty in the flue gas cooling heat exchanger (HE), potentializing the use of waste heat. The pretreated biomass feeds the AD process at  $\approx 38^\circ\text{C}$ , while, in NOPT configuration, biomass suspension is directly fed to the digester as received at  $30^\circ\text{C}$ .

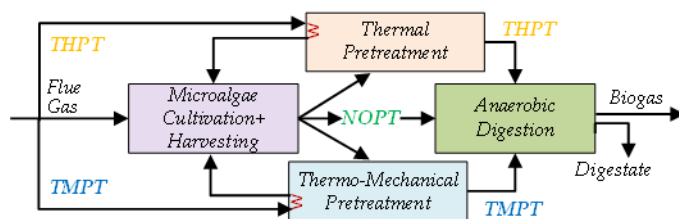


**Fig. 7.1.** Alternatives of biomass pretreatment to anaerobic digestion.

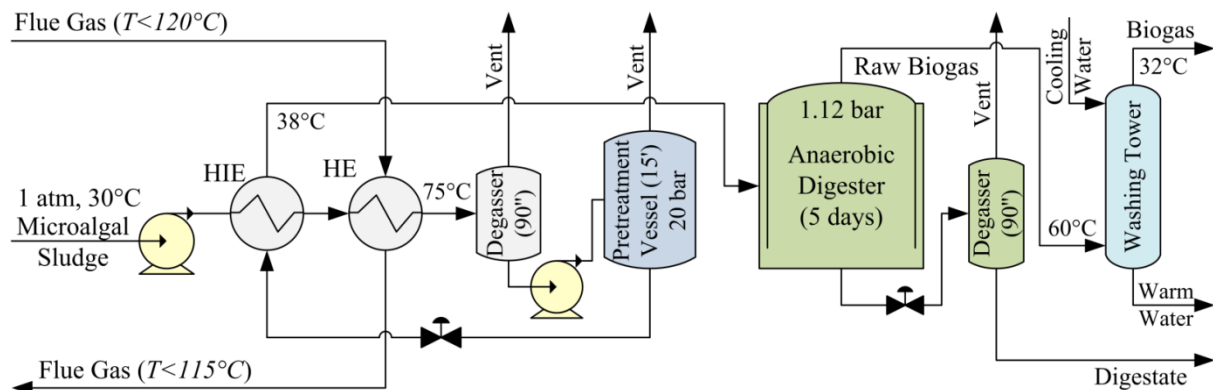


**Fig. 7.2.** Process for biogas production with TMPT of microalgal biomass.

### 7.3. Anaerobic Digestion Process

Although anaerobic digestion can occur at different temperature ranges, thermophilic systems (50-60°C) present higher biogas production per unit of feedstock and digester capacity, besides favoring the destruction of pathogens that act in the range of mesophilic temperature (25-45°C) [25]. The operating temperature depends on the material being digested and the type of system used, to avoid organic overload and subsequent collapse in the biogas production. HRT minimum of 2-4 days is recommended due to growth rate limitations [26]. Biogas yield depends on appropriate functioning of the methanogens in the anaerobic process, correlated to operating temperature, ammonia levels and volatile fatty acids [27]. Biogas production per unit volume of digester capacity is maximum when diameter to depth ratio ranges from 0.66 to 1, with the most active sludge being in the lower half of the digester, which favors aspect ratios close to unit [26]. Table Z1.1 in Appendix Z1 (Supplementary Material) reviews process conditions and performances of microalgae biomass AD.

At laboratory scale, evaluation of AD mainly uses biomethane potential (BMP) tests – a batch method that permits obtaining, from a given substrate, its maximal biogas yield by using high ratio of substrate to inoculum, diluted environment and long incubation time [1]. Brémont et al. [1] points that curves of BMP tests are usually modelled by first order kinetic relations, but, lower dilution and lower ratio of substrate to inoculum are the main differences at industrial scale continuous operation; and it is likely that biogas yield will be lower than results of BMP tests due to shorter degradation time, for both raw and pretreated feedstock.

In this work, biomass suspension is conveyed to multiple parallel ADs and analysis covers two operation pressure alternatives – 1 bar and 6 bar, to size the impact of AD pressure on overall process performance. Increasing AD pressure aims at producing biogas at moderately higher pressure, subtracting two downstream compression stages, significantly reducing costs of biomethane production and costs for conditioning biogas to power generation. Table 7.1 summarizes the adopted process premises.

**Table 7.1.** Process premises for biogas production.

	Pretreatment route			Unit
	Thermal (THPT)	Thermo-mechanical (TMPT)	None (NOPT)	
<i>Pretreatment</i>				
Feed pressure	1.013	20.0	N/A	bar
Feed temperature	75.0	75.0	N/A	°C
<i>Biodigester</i>				
Feed pressure	1.12	1.12	1.12	bar
Feed temperature	38.0	38.0	30.0	°C
Composition (% w)				
Lipids	3.90	7.20	2.80	% w
Proteins	2.14	3.96	1.54	% w
Carbohydrates	3.70	6.84	2.66	% w
Undisrupted cells	10.26	2.00	13.00	% w

In addition to the biogas product stream, mainly CH<sub>4</sub> and CO<sub>2</sub>, digestate is obtained containing non-converted material, intermediate compounds and dissolved gases, mainly NH<sub>3</sub> and CO<sub>2</sub>. The digestate is depressurized in a degasser, with CO<sub>2</sub> being vented to the atmosphere. The resulting digestate mixture may be recycled to the microalgae production, exported as an agricultural fertilizer [28] or used as diluent when concentrated biomass is supplied [16]. In this work, no revenue contribution is assigned to digestate destination but, in counterpart, no environmental impact is associated to this AD product stream.

#### 7.4. Downstream Biogas Processing

In this work, the biogas from the digester is processed through two downstream alternatives to produce bioelectricity (BE process, no heat exportation) or biomethane (BM process). Each alternative evolves to a more complex structure to include CO<sub>2</sub> storage with enhanced oil recovery: BE+EOR and BM+EOR processes. Alternative upstream processes – THPT and NOPT – are evaluated only for the baseline downstream route (BM), with monetization of biogas as biomethane. The best pretreatment option (TMPT) is applied for the remaining downstream alternatives, with BM being the baseline process. Processes shown in Fig. 7.3 are compared in three dimensions: energy, economic and carbon footprint. Process flow diagrams for downstream alternatives are found in Appendix Z3 (Supplementary Material).

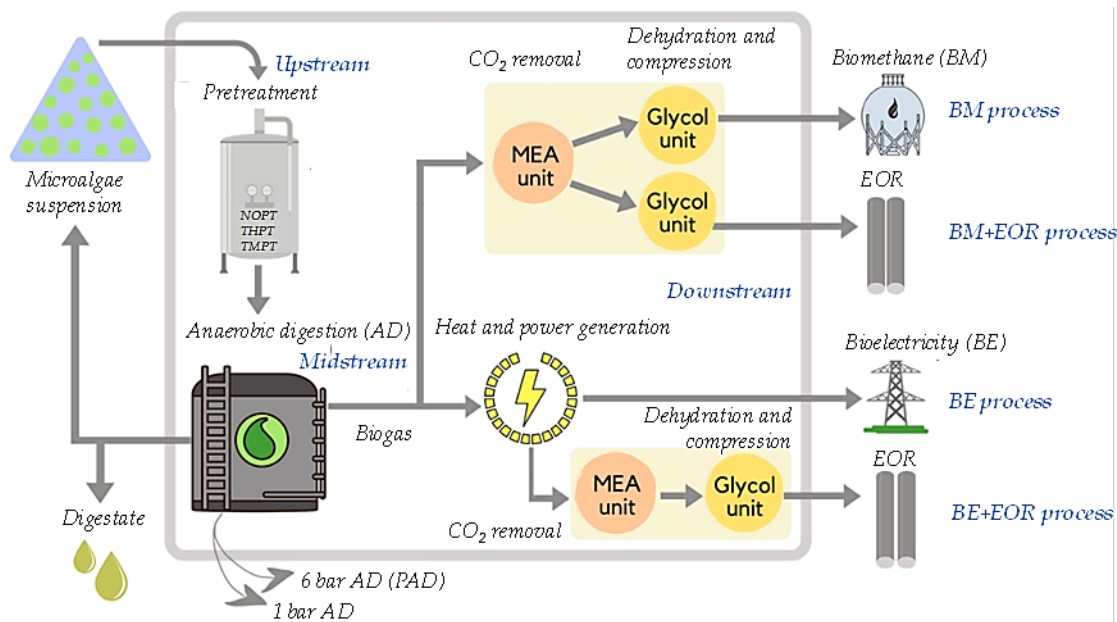


**Fig. 7.3.** Evaluated biogas downstream processes.

#### 7.4.1. Biomethane production process

State-of-the-art biogas upgrading is challenged by efficient low-cost technologies for CO<sub>2</sub> removal, to enhance gas quality, its main economic obstacle. Furthermore, desulfurization, dehydration and compression are also required to meet pipeline specifications [29]. Table Z2.1 of Appendix Z2 presents some specifications imposed to biomethane according to different national grids. This work uses the specification of Brazilian (Southeast region) biomethane from agricultural wastes.

Removal of acid gases (CO<sub>2</sub> and H<sub>2</sub>S) from biogas for biomethane conditioning is performed by chemical absorption with aqueous solution of monoethanolamine (MEA) at 20%w. The choice for MEA absorption regards various advantages of a mature technology enabling simultaneous removal of CO<sub>2</sub> and H<sub>2</sub>S contaminants with particularly high selectivity, producing treated gas with low methane losses (<0.1%) [29] and practically pure CO<sub>2</sub> stream that can be utilized or stored [30]. If simultaneous removal of H<sub>2</sub>S were not applied to biogas upgrading, sulfide scavengers – e.g. zinc-containing chemicals [31] – would be required. Other technologies for CO<sub>2</sub> separation in biogas applications are pressure-swing-adsorption (PSA) [32], membrane separation [29], physical absorption [33], supported amine sorbents [34] and cryogenic distillation [35]. Operation with amines involves handling corrosive and hazardous chemicals [4], so it is generally preferred for large scale applications – which fits the present scenario – on the contrary to most biogas projects, where PSA (e.g. with 13X zeolite) seems to be applied more frequently [36].

Water-saturated biomethane (1.12 bar or 6 bar, depending on the pressure of the AD, respectively with 7.0 and 1.3% mol H<sub>2</sub>O) is obtained at the top of the absorber with 3% mol CO<sub>2</sub> on dry-basis, adjusting solvent load to the targeted purity specification.

Biomethane is sent to a four-stage centrifugal compressor (in pressurized AD case it is three-stage)) to reach 70 bar, from where it is sent to dehydration, which consists in a conventional glycol unit, based on absorption with triethylene glycol (TEG) at 99.3%w [37], to meet the water dew-point gas specification for dispatch (-45°C at 1 atm).

#### 7.4.2. Bioelectricity generation process

For bioelectricity generation, a combined cycle configuration – referred as 2:1 accounting for two gas turbines (GTs) operating in parallel connected to a single steam turbine (ST) – is chosen for best power plant overall efficiency [38]. Biogas-fired boilers are not considered because of their lower efficiency. . Exportation of heating utilities is not applied.

The power plant in this analysis is fueled with raw biogas from the biodigesters (~35% mol CO<sub>2</sub>) – which is compressed and sent to the combustor at nearly 150°C, and is arranged in a single-pressure steam-cycle configuration at 65 bar. Table 7.2 summarizes further assumptions concerning the power plant.

**Table 7.2.** Power plant configuration and operating conditions.

Parameter	Value	Unit
Number of Gas Turbines: Number of Steam Turbines	2:1	-
Number of steam pressure levels	1	-
Combustor inlet pressure	20.0	bar
Turbine inlet pressure	19.6	bar
Turbine inlet temperature	1300	°C
Compression adiabatic efficiency	85	%
Expansion adiabatic efficiency	90	%
Heat Recovery and Steam Generator (HRSG) gas side pressure drop	5	kPa
HRSG minimum temperature difference	15	°C
Steam turbine inlet pressure	65	bar
Steam turbine inlet temperature	560	°C
Steam turbine outlet pressure	0.083	bar
Condenser outlet temperature	40.0	°C

### **7.4.3. Biomethane production process with enhanced oil recovery**

Aiming to mitigate CO<sub>2</sub> emissions, BM+EOR process is proposed, introducing downstream to the BM process a plant for gas compression and dehydration. CO<sub>2</sub> destination is to offshore EOR, determining stringent dew point specifications. CO<sub>2</sub> is compressed, dehydrated and dispatched at 300 bar to oil operators, increasing revenues.

Compressed CO<sub>2</sub> at nearly 50 bar is dehydrated with triethylene glycol (TEG) 99.7%w to attain the required 50 ppmv H<sub>2</sub>O specification for subsea transportation [39]. After dehydration, CO<sub>2</sub> is sent to a last compression stage, reaching 105-120 bar, which is cooled to 40°C, and pumped to the dispatch pressure of 300 bar. Regarding the effect of gravitational compression through subsea course, such dispatch pressure is more advantageous than maintaining pipeline pressure within 80-110 bar, as supercritical conditions ensure stability, releasing the need for recurrent recompression along the way to the offshore reservoir, avoiding shocks by phase change and increased pressure loss due to higher fluid velocities, as CO<sub>2</sub> is close to critical temperature [40].

### **7.4.4. Bioelectricity generation process with enhanced oil recovery**

BE+EOR introduces downstream to the BE process a post-combustion capture plant, based in MEA scrubbing similar to the biogas upgrading cases (BM and BM+EOR), but with increased solvent strength (30%w) due to lower CO<sub>2</sub> fugacity in the gas. The captured CO<sub>2</sub> is sent to compression and dehydration similarly to BM+EOR route.

Table 7.3 summarizes process premises for CO<sub>2</sub> capture, compression and dehydration in both BM+EOR and BE+EOR routes, where reported conditions refer to atmospheric AD of thermo-mechanically pretreated microalgae suspension.

## 7.5. Simulation of Process Alternatives

All process alternatives are simulated in Aspen Hysys v8.8 using Peng-Robinson equation-of-state, except where other thermodynamic packages are recommended: chemical absorption with MEA, Acid Gas Package being preferred; gas dehydration with TEG, where Glycol Package is also most accurate; and free-water/steam systems, where ASME Table is exact.

**Table 7.3.** Process premises and conditions for CO<sub>2</sub> separation and compression.

Item	Value		Unit
	Biogas Upgrading (BM+EOR)	Post-Combustion (BE+EOR)	
CO <sub>2</sub> capture			
Solvent	20	30	%w aq. MEA
Lean MEA	1.46	2.06	%mol CO <sub>2</sub>
Recirculation ratio	21.3	16.7	kg solv./ kgCO <sub>2</sub> in
Absorption stages	20	20	-
Absorption pressure drop	10	10	kPa
Absorption top pressure	1.013	1.013	bar
CO <sub>2</sub> in lean gas (dry-basis)	3.00	0.40	%mol CO <sub>2</sub>
Regeneration stages	10	10	-
Regeneration pressure drop	10	10	kPa
Regeneration top pressure	2.1	2.1	bar
CO <sub>2</sub> compression			
Dehydration pressure	53	48	bar
Pump suction pressure	120	105	bar
Dispatch pressure	300	300	bar
Dispatch temperature	75.5	85.7	°C
H <sub>2</sub> O content (mol)	50.0	50.0	bar

The biomass composition is modelled in Aspen Hysys by representing *Nannochloropsis salina* accordingly to Schwede et al. [21], with chemical formula assigned to the biochemical pools: lipids, proteins and carbohydrates. The same procedure of Picardo et al. [41] is implemented, based on the empirical elemental composition given by Norland et al. [42], shown in Table 7.4 in terms of equivalent reduced chemical formula. The process receives 45.6 kg/s of this biomass suspension with 20%w of organic matter content at 1 atm and 30°C, presenting lower heating value (LHV) of 5,808 kJ/kg (input rate of 265 MW) and 9.8%w (dry-basis) of ash [21]. The ultimate mass composition (dry ash-free) obtained from the model is 59.0%C, 9.4%H, 4.0%N and 27.6%O (C/N=14.8).

**Table 7.4.** Model composition for *Nannochloropsis salina*.

	Reduced Formula <sup>(1)</sup>	Chemical Formula	Mass Fraction <sup>(2)</sup>
Lipids	CH <sub>1.79</sub> O <sub>0.08</sub>	C <sub>16</sub> H <sub>29</sub> O	0.40
Proteins	CH <sub>2.06</sub> N <sub>0.26</sub> O <sub>0.32</sub> S <sub>0.01</sub>	C <sub>10</sub> H <sub>21</sub> N <sub>3</sub> O <sub>3</sub>	0.22
Carbohydrates	CH <sub>2.09</sub> O <sub>0.99</sub>	C <sub>11</sub> H <sub>22</sub> O <sub>11</sub>	0.38

<sup>(1)</sup> Picardo et al. [41]; <sup>(2)</sup> Schwede et al. [21]

This microalgal biomass is assumed to be cultivated abating CO<sub>2</sub> emissions from the flue gas of a 100 MW coal power plant. Steps for biomass cultivation and harvesting are also

simulated in Aspen Hysys v8.8 for tracking the carbon life-cycle from coal flue gas up to the gate of the proposed biogas plant. Biomass production is not included in energy and economic analysis, as they are supposed to be operated by a third-party company. Efficiency of CO<sub>2</sub> biofixation (utilization) is assumed to be ≈75% accordingly to Acien et al. [43]. Further assumptions for simulation of these steps are available in Table Z4.1 of Appendix Z4. The estimated electricity consumption in these steps is 8.65 MW.

AD conversion of biomass is defined in accordance with literature data for different scenarios of biomass upstream processing: 35% without pretreatment [44], 48.7% for thermal pretreatment at 75°C [24] and 90% for thermo-mechanical pretreatment [45]. Simulation of AD in Aspen Hysys v8.8 uses Gibbs reactor model, so that biogas production estimative is the thermodynamic limit (i.e. optimistic estimation).

### 7.5.1. Energy indicators for upstream and downstream processing of microalgal biogas

Internal demand for heat and electricity occurs affecting the overall energy performance, supplied by biomethane energy. In this work, the indicator Energy Return On Investment (*EROI*) is employed, calculated with Eq. (7.1a) in BM and BM+EOR or Eq. (7.1b) in BE and BE+EOR. *EROI* assesses the energy efficiency of a process considering its main products – biomethane in BM and BM+EOR and bioelectricity in BE and BE+EOR routes – expressed as the ratio of the “energy returned to society” (*ER*) – the equivalent output of fuel LHV – to the “energy invested to get that energy” (*EI*) [46], i.e. the input of resources and utilities without including the feedstock (microalgae biomass).

*EROI* is hereafter expressed in terms of biomethane LHV ( $\xi_o$ ) using typical net efficiency coefficients –  $\eta_w=58\%LHV$  for power generation with NG combined cycle and  $\eta_Q=86\%LHV$  for NG-fueled boiler steam generator– allowing to incorporate electricity ( $W_c$ ) and heating ( $Q_h$ ) demands as different types of energy. *EROI* > 1 indicates that the resulting heating value on biomethane production (BM) is higher than the required fuel to produce it [23]. An alternative energy indicator is %*EnergyOut*, Eq. (7.2), the ratio of the net exported energy (*ER*–*EI*) to the LHV of microalgae biomass input ( $F_i \xi_i$ ).

$$EROI_{BM} = ER_{BM} (EI)^{-1} = (F_o \xi_o) * \left( \sum_{c=1}^{nc} W_c / \eta_w + \sum_{h=1}^{nh} Q_h / \eta_Q \right)^{-1} \quad (7.1a)$$

$$EROI_{BE} = ER_{BE} (EI)^{-1} = \left( \sum_{t=1}^{nt} W_t / \eta_w \right) * \left( \sum_{c=1}^{nc} W_c / \eta_w + \sum_{h=1}^{nh} Q_h / \eta_Q \right)^{-1} \quad (7.1b)$$

$$\%EnergyOut = (ER - EI) * (F_i \xi_i)^{-1} \quad (7.2)$$

### 7.5.2. Carbon emissions indicators for processing microalgal biogas

Sankey diagrams are used to track the mass flowrate of equivalent CO<sub>2</sub> along the processing chain, from biomass cultivation, through pretreatment (NOPT, THPT and TMPT) and AD at 1.12 bar, and downstream steps to obtain biomethane. In carbon flows, equivalent CO<sub>2</sub> related to electricity and heating consumption are included. Biomethane (97%CH<sub>4</sub> and 3%CO<sub>2</sub>) is employed to fuel a power plant with efficiencies  $\eta_w=58\%LHV$  (natural gas combined cycle) and  $\eta_Q=86\%LHV$ , and equivalent emission factors of 0.352 and 0.237 t/MWh. Carbon efficiency is then expressed as the feed ratio of equivalent carbon leaving the system as biomethane to the equivalent carbon input from microalgae biomass.

### 7.5.3. Economic Performance

The procedure proposed by Turton et al. is employed in the economic analysis, using CAPCOST spreadsheet [47]. The economic performance of each pretreatment alternative (NOPT, THPT and TMPT) is evaluated for the BM downstream process. The plant is considered to be located in the USA. Calculations are based in the first semester of 2017 and the Chemical Engineering Plant Cost Index (*CEPCI*) is used to update equipment cost accordingly to average values of this period ( $CEPCI_{1H2017}=562.3$ ).

The economic parameters used in the evaluation are listed in Table 7.5. Compressed CO<sub>2</sub> is sold to be used in EOR activity, receiving 50% of the enhanced oil revenue, assuming oil priced at 50 US\$/bbl. The microalgae suspension has its cost estimated based on Wiesberg et al. [48]. This parameter has high uncertainty, thus a sensitivity analysis evaluates its impact in economic performance, where the microalgae price listed in Table 7.5 is used as base scenario. For Carbon Cap & Trade, a mechanism similar to the EU Emissions Trading System is assumed to apply, while for Carbon Taxes, Araújo and de Medeiros [30] supplies practical discussion giving background to selected taxation levels.

An atmospheric biodigester tank of 8328 m<sup>3</sup> with capital cost of 1.25 MMUS\$ (2011-year basis) is used as reference. The  $CEPCI_{2011}=590.1$  is used to update its value to the project year, which is escalated to the required biodigester volume ( $V_{BD}$ ) by the six tenths rule [47] and then multiplied by the Grass Roots Factor and the Total Module Factor [47]. The fixed capital investment of an atmospheric biodigester tank ( $FCI_{BD}$ ) is calculated with Eq. (7.3).

$$FCI_{BD} = 1.25 * 10^6 * (V_{BD} / 8328)^{0.6} * (590.1 / 562.3) * (1.18 + 0.5) \quad (7.3)$$

**Table 7.5.** Economic parameters for capital and operational expenditures (base scenario)

Item	Type	Value	Unit
Biomethane	Product	7.58	US\$/GJ
CO <sub>2</sub> to EOR	Product	25	US\$/t
Microalga 20wt%	Raw Material	234 [48]	US\$/t <sub>dry-basis</sub>
Electricity	Utility/Product	30.00 <sup>(1)</sup>	US\$/GJ
Low pressure steam (6 bar)	Utility	14.10 <sup>(2)</sup>	US\$/GJ
Annual Interest Rate	Parameter	10	%
Project lifetime	Parameter	20	years
Taxation Rate	Parameter	30	%
Carbon Tax	Tax	40	US\$/t
Carbon Cap & Trade	Revenue	40 <sup>(3)</sup>	US\$/t
Biodigester (8,328 m <sup>3</sup> @ 1atm)	Equipment	1.250 <sup>(4)</sup>	MMUS\$ <sub>2011</sub>

<sup>(1)</sup>EIA, U.S. Energy Information Administration, Electric Power Monthly, available on:

[https://www.eia.gov/electricity/monthly/epm\\_table\\_grapher.php?t=epmt\\_5\\_6\\_a](https://www.eia.gov/electricity/monthly/epm_table_grapher.php?t=epmt_5_6_a)

<sup>(2)</sup>Estimated from biomethane cost, using the method of Turton et al. [47]

<sup>(3)</sup>European Parliament and Council of the European Union. Directive 2003/87/EC of the European Parliament and of the Council. Official Journal of the European Union, L 275/32, Oct. 25, 2003. <https://eur-lex.europa.eu/LexUriServ/LexUriServ.do?uri=OJ:L:2003:275:0032:0046:en:PDF>

<sup>(4)</sup>Anaerobic Digestion at Synergy Biogas, LLC: Case Study, Manure Management Program.

## 7.6. Results and Discussion

Results from simulation of the upstream processes, anaerobic digestion and biogas downstream processing allow calculation of performance indicators, presented and discussed in this section.

### 7.6.1. Impacts of biomass pretreatments on biomethane or bioelectricity production

Table 7.6 summarizes performances of process alternatives presenting the differences in pretreatment procedure and results in biomethane production (BM), referring to baseline AD at 1.12 bar. Similarly, Table 7.7 shows results for bioelectricity production (BE). Regardless of the downstream route (BM or BE), AD operation retains at least  $\approx 30.1\%$  of microalgae LHV in biogas, with THPT enhancing retention to  $\approx 42.0\%$  and TMPT to  $\approx 77.9\%$ . All routes have the same input of microalgae biomass suspension, which is outside the frontiers of the analysis – it either is purchased from a nearby plant, or received from an integrated biorefinery.

Biomass conversion can be improved from 35.0 to 48.7% by using cost-effective low-grade thermal pretreatment (THPT), and further to 90.0%, by combining the effects of thermal and mechanical rupture of cell walls (TMPT), enabling to increase biogas production from 4.34 to 11.27 kg/s. CO<sub>2</sub> contents are similar, about 36% mol dry-basis.

**Table 7.6.** BM process performances for the three pretreatment alternatives.

Item	NOPT	THPT	TMPT	Unit
Microalgae biomass feed, LHV basis	265	265	265	MW
Pretreatment temperature	N/A	75	75	°C
Pretreatment pressure	N/A	1.62	20.0	bar
Biogas production, LHV basis	79.7	111.3	206.4	MW
Biogas production, mass basis	4.34	6.06	11.27	kg/s
Biomethane production, mass basis	1.72	2.39	4.42	kg/s
Biomethane production, LHV basis ( <i>ER</i> )	79.3	110.3	203.9	MW
Electricity demand	1.66	2.31	4.38	MW
Heating utility demand (steam)	9.08	12.49	22.82	MW
Energy invested, LHV basis ( <i>EI</i> )	13.4	18.5	34.1	MW
Net energy output, LHV basis ( <i>ER – EI</i> )	65.84	91.82	169.8	MW
Energy Return on Investment ( <i>EROI</i> )	5.90	5.96	5.98	-
Microalgae use efficiency ( <i>%EnergyOut</i> )	24.9	34.7	64.1	%

**Table 7.7.** BE process performances for the three pretreatment alternatives.

Item	NOPT	THPT	TMPT	Unit
Microalgae biomass feed, LHV basis	265	265	265	MW
Pretreatment temperature	N/A	75	75	°C
Pretreatment pressure	N/A	1.62	20.0	bar
Biogas production, mass basis	4.34	6.06	11.27	kg/s
Biogas production, LHV basis	79.7	111.3	206.4	MW
Electricity demand	1.78	2.47	4.65	MW
Heating utility demand (steam)	0.00	0.00	0.00	MW
Total bioelectricity generation	46.2	64.3	118.8	MW
Net bioelectricity generation	44.4	61.8	114.2	MW
Combined cycle efficiency, LHV basis <sup>(1)</sup>	58.0	57.8	57.6	%
Energy Return on Investment ( <i>EROI</i> )	25.9	26.0	25.5	-
Microalgae use efficiency ( <i>%EnergyOut</i> )	28.9	40.2	74.3	%

<sup>(1)</sup> Excluding biogas compression and further auxiliary power demands.

The overall efficiency of microalgae energy conversion (*%EnergyOut*) increases from 24.9 to 34.7% in THPT and further to 64.1% in TMPT through BM downstream route (Table 7.6). Nearly invariant *EROI* is obtained among the upstream alternatives due to low-cost pretreatments – application of low-grade waste heat in THPT and also biomass suspension pumping in TMPT – and dominant energy penalties in downstream biogas processing. These penalties are mainly related to CO<sub>2</sub> removal and biomethane compression, which are proportional to biogas output, considering that minor differences are found in CO<sub>2</sub> contents.

BE route (Table 7.7) presents higher conversion efficiencies (*%EnergyOut*) compared to BM (28.9, 40.2 and 74.3% in NOPT, THPT and TMPT cases) as CO<sub>2</sub> removal is avoided, eliminating the use of solvents and heating utilities, whereas gas compression is still needed to feed the gas turbine. Since biogas compression outstands in overall energy penalty in BE route, *EROI* also remains practically invariant among upstream alternatives, being slightly lower in TMPT case due to electricity consumption in the pretreatment section (Table 7.7).

In terms of microalgae conversion to bioelectricity, overall efficiencies are 16.8, 23.3 and 43.1%LHV for NOPT, THPT and TMPT cases, respectively, showing that AD may produce bioelectricity with similar efficiencies to Biomass-Integrated-Gasification Gas-Turbine technologies [49] as long as cost-effective methods of biomass pretreatment are employed allowing considerably high conversion of the organic content. High-capacity biogas production is also necessary, otherwise less efficient turbines would be applied. With TMPT, the power plant installed capacity for the considered process scale is  $\approx 114$  MW (Table 7.7).

To reduce the penalties of the downstream processing in the BM route, pressurized anaerobic digestion (PAD) of TMPT biomass at 6 bar is compared with baseline AD at 1.12 bar. PAD has the main purpose of saving power in gas compression, also helping to reduce steam demand for MEA regeneration, as CO<sub>2</sub> fugacity in biogas increases significantly, improving the solvent capacity for absorbing CO<sub>2</sub>. The total electricity demand in PAD-TMPT is reduced from 4.38 to 2.51 MW<sub>e</sub> in comparison with baseline TMPT (AD at 1.12 bar), whereas steam demand reduces from 22.8 to 19.4 MW<sub>h</sub>. *EROI* is then improved from 5.98 to 7.58, which is still much lower than BE process performance (*EROI*=25.5). The overall efficiency of microalgae energy conversion (*%EnergyOut*) is also improved with PAD: from 64.1 to 66.7%.

Despite the benefit of improved operational performance favoring downstream processing (with pumps replacing gas compressors for the initial service of pressure elevation), PAD faces technical issues. For large-scale processing capacity, PAD is here suggested to be employed at moderate pressure of 6 bar to avoid extremely high costs of several parallel AD pressure vessels, due to the high HRT needed to achieve significant biomass conversion. At 6 bar, the required shell thickness of digesters fits the usual standard design pressure of 150 psig. Hence, the vessel size constraint is a critical factor for feasibility of PAD systems (diameter < 6m), whereas nearly atmospheric AD systems could be easily scaled to large digester diameters (>20m). Another issue with PAD refers to possible microbial activity inhibition owing to reduced pH from increased CO<sub>2</sub> content in liquid phase or, for instance,

unbearably high concentration of  $\text{NH}_3$ . On the other hand, the higher the pressure, the higher the liquid-phase capacity for dissolved gases, especially  $\text{CO}_2$  and  $\text{NH}_3$ , so that another advantage of PAD is that it invariably produces raw biogas with better quality (higher  $\text{CH}_4$  content, and much less  $\text{NH}_3$ ) as these compounds are partially removed from biogas through the liquid digestate. Simulation results show that PAD at 6 bar increases  $\text{CH}_4$  content from 61.9 to 63%mol and reduces  $\text{NH}_3$  from 1.78 to 0.44%mol, with  $\text{CO}_2$  remaining practically similar within 36–36.5%mol.

Concerning the BM process with AD operation at 1.12 bar, Fig. 7.4A depicts the mass flow rate and proportion of  $\text{CH}_4$  and  $\text{CO}_2$  contained in the biogas from the evaluated pretreatment alternatives. By expressing the same flow rates in relation to the input of volatile solids in biomass suspension, Fig. 7.4B presents biogas yields in normal volumetric basis, enabling comparison with most literature data.

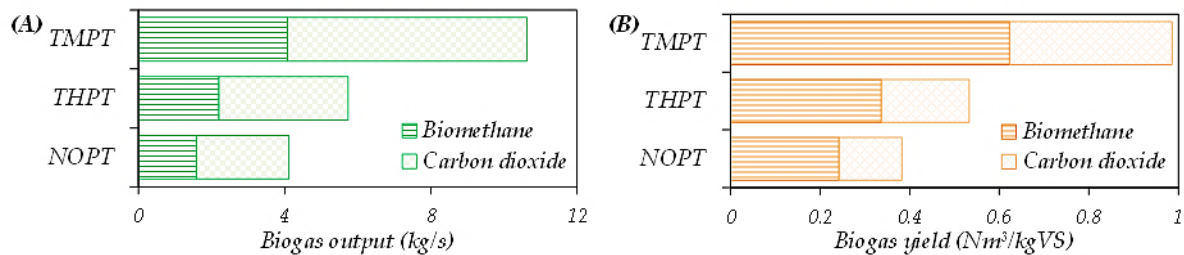


**Fig. 7.4.** Biogas production in each pretreatment alternative in the BM process: (A) biogas output and proportion of  $\text{CH}_4$  and  $\text{CO}_2$ ; (B) Anaerobic digestion yields and proportion of  $\text{CH}_4$  and  $\text{CO}_2$ .

Fig. 7.4B shows that  $\text{CH}_4$  yields in NOPT and THPT, 0.242 and 0.337  $\text{Nm}^3/\text{kgVS}$  (0.17 and 0.24  $\text{kg}/\text{kgVS}$ ), fit the expected range of 0.05-0.80  $\text{Nm}^3/\text{kgVS}$  [12] but are considerably lower than typical experimental AD results, presented in Table Z1.1 (Appendix Z1). It expresses incomplete cell rupture with low-temperature THPT and low HRT, contrasting with some microalgae genera yielding great enhancements, e.g. *Chlorella sp.* [50] and *Scenedesmus sp.* [51]. The actual potential for higher biomethane outputs from *Nannochloropsis salina* – due to more favorable composition with high lipids content – is expected to be exhibited only if TMPT is employed, as purely mechanical rupture methods have been already evinced efficacious [52], allowing relatively high biomethane yield, 0.623  $\text{Nm}^3/\text{kgVS}$  of  $\text{CH}_4$  (0.45  $\text{kg}/\text{kgVS}$ ). By associating the use of low-grade (waste) heat (<120°C) with higher operating pressure ( $\approx 20$  bar) and valve expansion of warm biomass ( $\approx 75^\circ\text{C}$ ), advantageous effects of pressure induced shear stress over the cells are achieved.

### 7.6.2. Technical analysis of downstream processes after thermo-mechanical pretreatment

Table 7.8 reports performances of the considered alternatives for downstream biogas processing – BM, BM + EOR, BE and BE + EOR. It presents technical features, *EROI* and *%EnergyOut* indicators, referring to baseline AD at 1.12 bar, and converting biomass from TMPT, the pretreatment with best performance. The downstream alternatives deriving from BM (Table 7.6) and BE (Table 7.7) – BM+EOR and BE+EOR – assume destination of the captured CO<sub>2</sub> to storage in oil reservoirs, with contribution of EOR to process revenues. For BE+EOR, the compressed CO<sub>2</sub> is obtained from post-combustion capture with MEA absorption, presenting high heating demand for solvent regeneration, while in BM+EOR, practically pure CO<sub>2</sub> is already available from biogas upgrading (necessary step in BM).

It is worth noting that (i) CO<sub>2</sub> exportation rate in BE+EOR is much higher (2.8x) than in BM+EOR (Table 7.8) – which substantially affects electricity consumption – and (ii) CO<sub>2</sub> removal from biogas in BM and BM+EOR have reduced regeneration heat ratio – 3.9 GJ/t CO<sub>2</sub> against 4.9 GJ/t CO<sub>2</sub> for exhaust gas – as a consequence of much higher CO<sub>2</sub> content (high CO<sub>2</sub> fugacity) in raw feed gas. These aspects explain the considerable difference between heating utility demands from BM+EOR (22.9 MW) and BE+EOR (81.2 MW).

Comparing BM and BM+EOR, *EROI* and *%EnergyOut* are slightly reduced from 5.98 and 64.1% to 5.42 and 62.8% (Table 7.8). The main reason is that the higher electricity consumption for CO<sub>2</sub> exportation, from 4.38 to 6.41 MW (Table 7.8), with a minor increase of 0.04 MW on heating demand related to glycol regeneration for CO<sub>2</sub> dehydration, did not significantly affect the energy indicators.

BE and BE+EOR, on the other hand, evinced sharp decline in *EROI* and *%EnergyOut* indicators, from 25.5 and 74.3%, respectively, to 1.77 and 33.6% (Table 7.8). Contrasting with the BE routes, which have electricity demand dominated by biogas compression and no heating utility being consumed, BE+EOR is dominated by high energy requirements from CO<sub>2</sub> capture and conditioning. Although PAD increases performance of the BM route, BE without EOR has exceling performance.

**Table 7.8.** Performances of downstream process alternatives (AD at 1.12 bar, TMPT).

Item	BM	BM+EOR	BE	BE+EOR	Unit
Microalgae biomass feed, LHV basis	265	265	265	265	MW
Biogas production, LHV basis	206.4	206.4	206.4	206.4	MW
Biogas production, mass basis	11.27	11.27	11.27	11.27	kg/s
CO <sub>2</sub> -EOR-fluid exportation, mass basis	N/A	5.89	N/A	16.40	kg/s
Biomethane production, mass basis	4.42	4.42	N/A	N/A	kg/s
Biomethane production, LHV basis	203.9	203.9	N/A	N/A	MW
Electricity demand	4.38	6.41	4.65	12.39	MW
Heating utility demand (steam)	22.82	22.86	0.00	81.23	MW
Total bioelectricity generation	N/A	N/A	118.8	118.8	MW
Net bioelectricity generation	N/A	N/A	114.2	106.4	MW
Energy returned, LHV basis ( <i>ER</i> )	203.9	203.9	204.9	204.9	MW
Energy invested, LHV basis ( <i>EI</i> )	34.1	37.6	8.03	115.8	MW
Net energy output, LHV basis ( <i>ER – EI</i> )	169.8	166.3	196.9	88.98	MW
Energy Return on Investment ( <i>EROI</i> )	5.98	5.42	25.5	1.77	-
Microalgae use efficiency ( <i>%EnergyOut</i> )	64.1	62.8	74.3	33.6	%

### 7.6.3. Tracking of carbon-equivalent flow

Fig. 7.5 shows Sankey diagrams for the three upstream alternatives considering BM as downstream process. CO<sub>2</sub> biofixed in microalgae suspension is the CO<sub>2e</sub> input flow. Figs. 7.5A and 7.5B show that the major share of CO<sub>2</sub> input leaves the process as organic matter in the digestate stream. Differently from the other pretreatment options, Fig. 7.5C shows that TMPT reduces organic content of digestate, and biomethane carries 43.7% of the CO<sub>2</sub> input. NOPT and THPT transform to biomethane only 17.4 and 24.8% of the CO<sub>2</sub> from the flue gas fed to the microalgae cultivation system.

Considering that dissolved CO<sub>2</sub> in digestate is eventually degassed to the atmosphere (0.32 kg/s in TMPT) upon use (e.g. fertigation), total emissions in Carbon Capture and Utilization (CCU) chain for biomethane production from flue gas – not including non-converted organic matter in digestate nor indirect emissions from energy consumption – are approximately 35, 39 and 51% for NOPT, THPT and TMPT. Increase on CO<sub>2</sub> emissions here only expresses higher conversion, as CO<sub>2</sub> is generated in AD and is *a posteriori* removed in biomethane production. When CO<sub>2</sub> captured is utilized or stored, overall emissions becomes similar (25–26.5%), dominated by CO<sub>2</sub> utilization efficiency on microalgae cultivation [53].

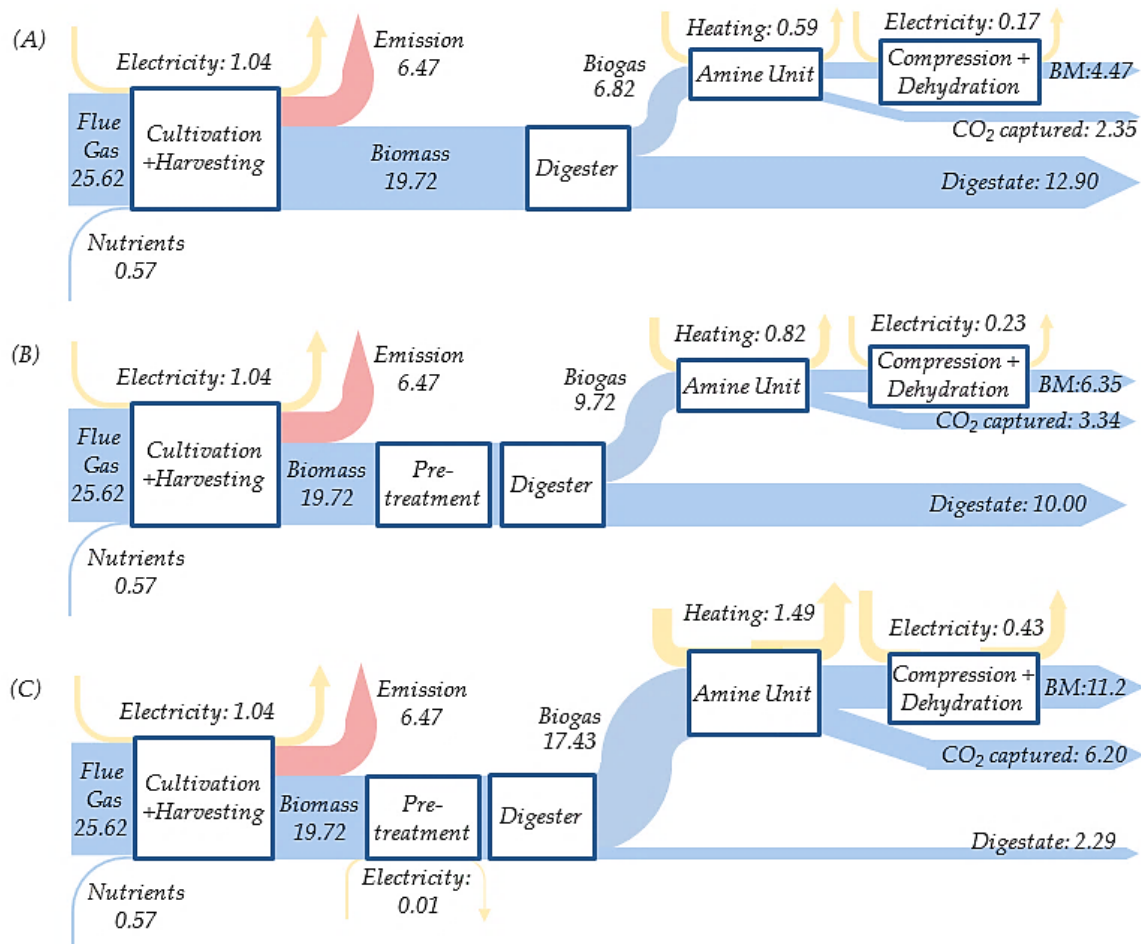


**Fig. 7.5.** Mass flowrate of CO<sub>2</sub>-equivalent (kg/s) along upstream process alternatives: (A) NOPT; (B) THPT; and (C) TMPT.

As an alternative to EOR, CO<sub>2</sub> captured may be recycled to microalgae growth with advantage of not requiring compression to feed the cultivation system, favoring energy performance. However, since this would either reduce the capacity of processing flue gas processing or increase the already large footprint required for microalgae growth [48] (24% less flue gas thus 32% more relative area in TMPT case), CO<sub>2</sub> exportation to EOR is opted.

Since TMPT responds with the best energy performance and carbon efficiency in destination to biomethane, TMPT is the only pretreatment considered for BM+EOR, BE and BE+EOR downstream processes in the economic analysis.

#### 7.6.4. Economic assessments

Fig. 7.6 shows the fixed capital investment (*FCI*) breakdown of the analyzed processes.

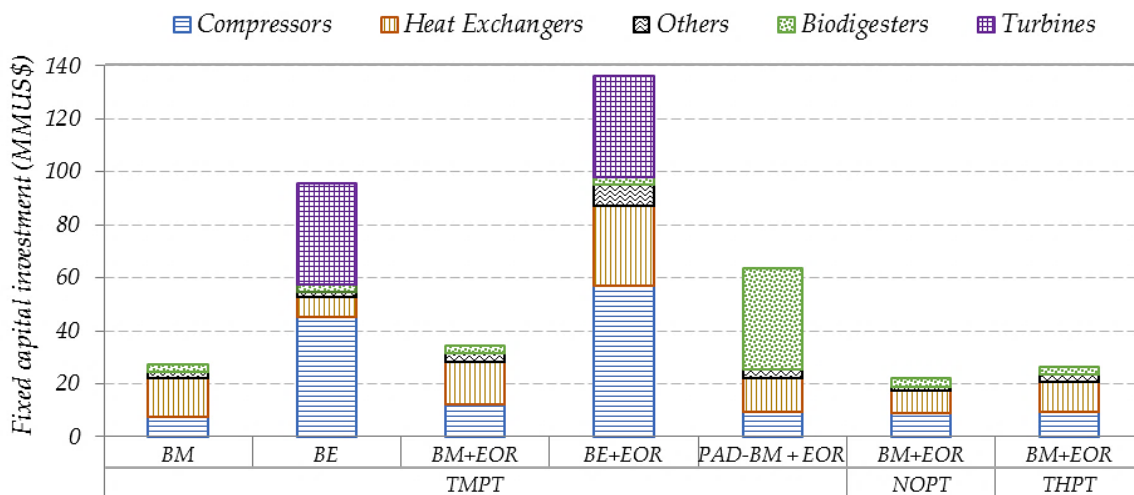


**Fig. 7.6.** FCI breakdown of the analyzed technologies, in MMUS\$.

Bioelectricity routes (BE and BE+EOR) involve larger investments, requiring higher revenues to overcome these costs. Biodigesters do not have a significant weight in the FCI, unless under PAD conditions, with associated economic penalty.

Fig. 7.7 unveils revenues (REV) and cost of manufacturing (COM) breakdown of alternatives in the base scenario. Revenues are plotted as positive values, while COM as negatives, with “CO<sub>2</sub> related” contribution being revenues from EOR and CO<sub>2</sub> Cap & Trade mechanism. Mainly influenced by the high microalga costs, the main bottleneck of most microalgae-based biofuels, none of the alternatives has REV exceeding COM. However, utilities and CO<sub>2</sub> taxes also play an important role in the BE and BE+EOR configurations. Hence, power generation from biomethane has costs associated with CO<sub>2</sub> destination in a taxation scenario: either it pays CO<sub>2</sub> emissions taxes or pays for capturing and conditioning CO<sub>2</sub> to proper destination. It is worth noting that CO<sub>2</sub> biofixed in the microalgae is anthropic (from fuel-fired power plant) and hence adds to global warming potential.

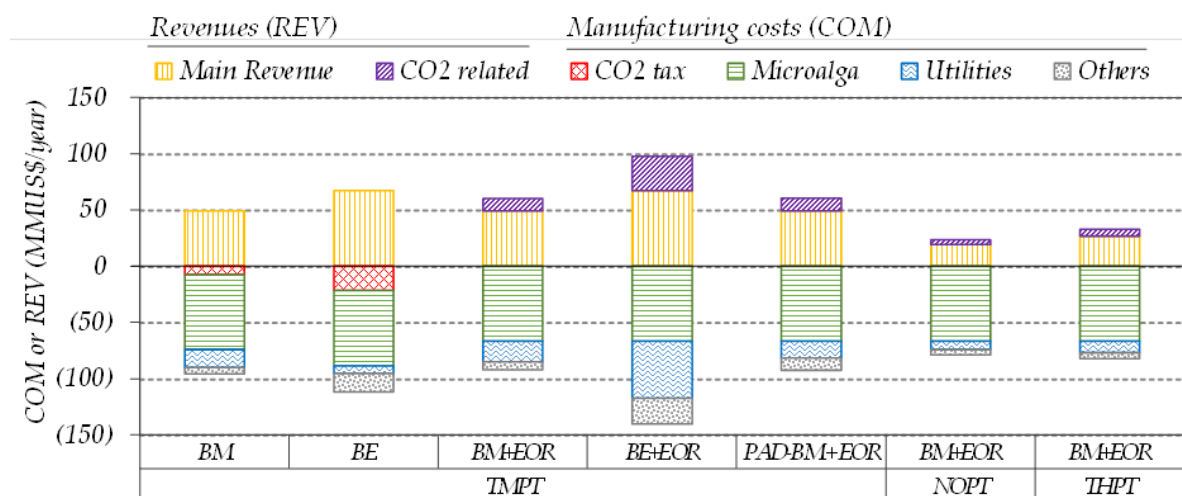


**Fig. 7.7.** Revenues (positive values) and COM breakdown (negative values) of the analyzed technologies in the base scenario, in MMUS\$.

Therefore, a sensitivity analysis is performed varying biomass costs for targeting null final *NPV*, aiming an economic return of the investment of 10%. In this sense, Fig. 7.8 portrays corresponding break-even prices of raw material purchase in each downstream pathway. Processes with high break-even price (maximum biomass cost for feasibility) are more prone to be viable, pointing best economic result to BM+EOR – 100US\$/t – whereas BE (21US\$/t) and BE+EOR (5US\$/t) show worst performance. PAD is not economically advantageous as it is evinced from energy perspective, mainly because of higher *FCI* (Fig. 7.7) overshadowing savings on operational expenses with utilities, which reflects on slightly reduced break-even biomass cost: 83US\$/t (PAD-BM+EOR).

Fig. 7.8 shows that all processes can become feasible depending on biomass cost. For instance, microalgae residues from other processes could be conveniently applied availing the low-cost of material as long as the lipids content is not committed [54].

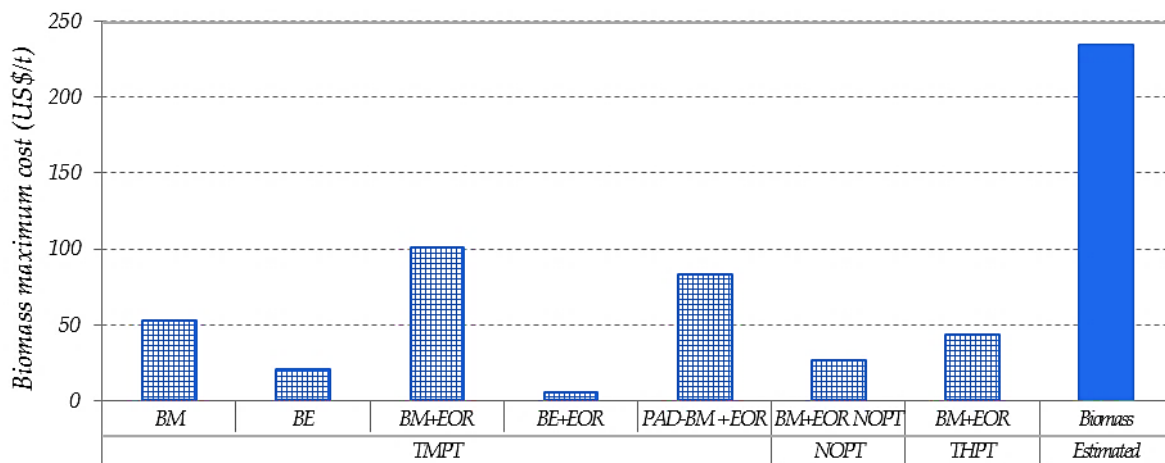


**Fig. 7.8.** Break-even cost of biomass for null *NPV* after 20 years of operation, in MMUS\$. “Biomass Estimated” is the estimated price of biomass based on [48].

Sensitivity analyses on *NPV* are performed varying the prices of biomass purchase and product being sold (biomethane or bioelectricity). The results are presented in Fig. 7.9, with the feasibility regions highlighted. NOPT is not shown because of its worst performance. Depending on the product values and on feedstock costs, the considered alternatives may be viable. For example, BE is feasible with increased electricity price of 50 US\$/GJ for biomass costing <160 US\$/t, remaining feasible at 30 US\$/GJ if costless biomass residue is used. The feasibility region of PAD-BM+EOR is smaller than the BM+EOR, indicating its inferior performance. All other analyzed scenarios have similar area of feasibility.

Another sensitivity analysis evaluates the influence of different CO<sub>2</sub> management policies scenarios on final *NPV*, but adopting costless residual biomass as feedstock. The scenario-

determining factors are associated to the atmospheric carbon budget set by targets to limit global warming: CO<sub>2</sub> taxes (cost) and Cap & Trade (revenue), and on the oil price (revenue through EOR). “Price Scenario 1” represents penalization of CO<sub>2</sub> emissions, intensification of carbon mitigation mechanisms and increase of oil prices; it only differs from “Price Scenario 2” on CO<sub>2</sub> taxation, not present in the latter. “Price Scenario 3” considers increasing carbon taxes and oil prices, while “Price Scenario 4” is similar, but with steady oil prices. A last “Price Scenario 5” evaluates increasing carbon taxes and Cap & Trade, but decreasing price of CO<sub>2</sub> sales to EOR (from decreasing oil price, which determines CO<sub>2</sub> sale price to oil operators). The price scenarios are in the lower set of graphs of Fig. 7.10, while the economic results are shown in the upper set. In all scenarios, BM+EOR is more attractive than BM, since it involves relatively low extra energy consumption to dispatch CO<sub>2</sub> at the required conditions, as pure CO<sub>2</sub> is already available from biogas upgrading. CO<sub>2</sub> exportation to EOR from power generation (BE+EOR) surpasses *FCI* and *COM*, with BM+EOR showing better performance, even with appreciated EOR revenues, despite of reduced CO<sub>2</sub> flowrate.

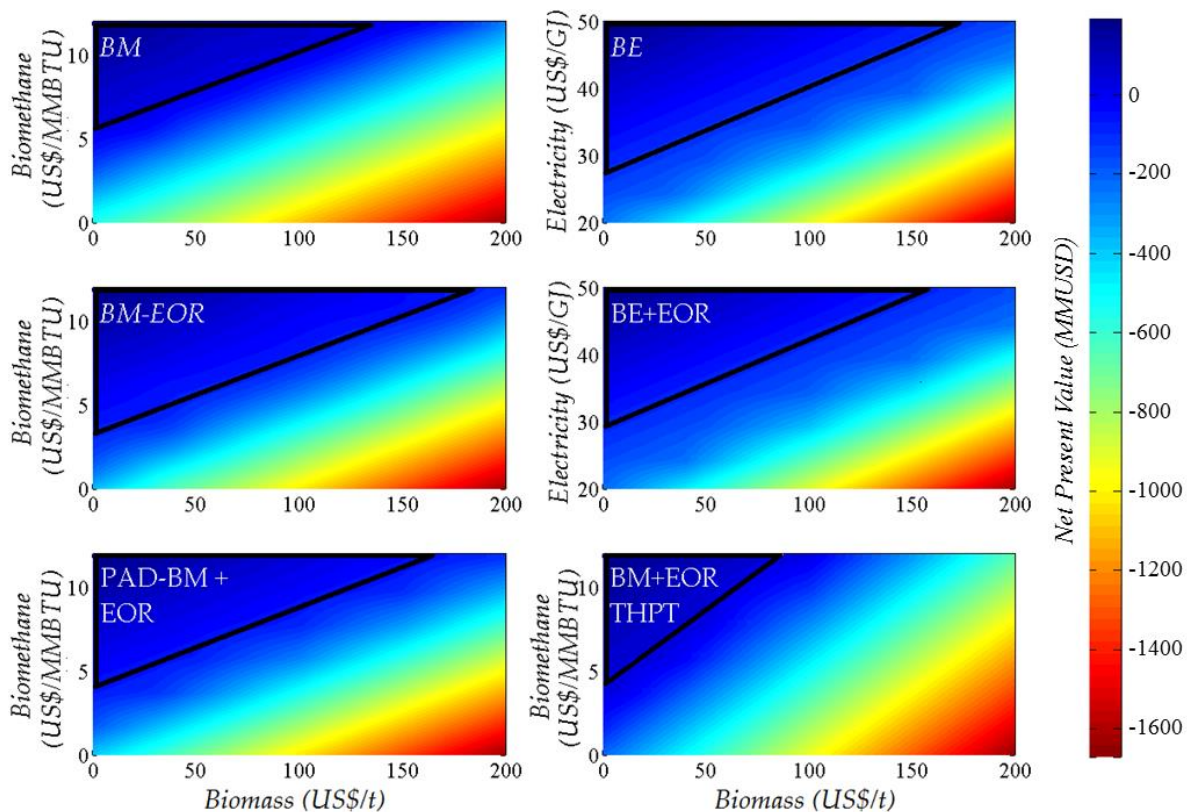


**Fig. 7.9.** Net present values as a function of biomass cost (US\$/t) and biogas price (US\$/MMBTU) or bioelectricity (US\$/GJ) price (triangles are feasibility regions).

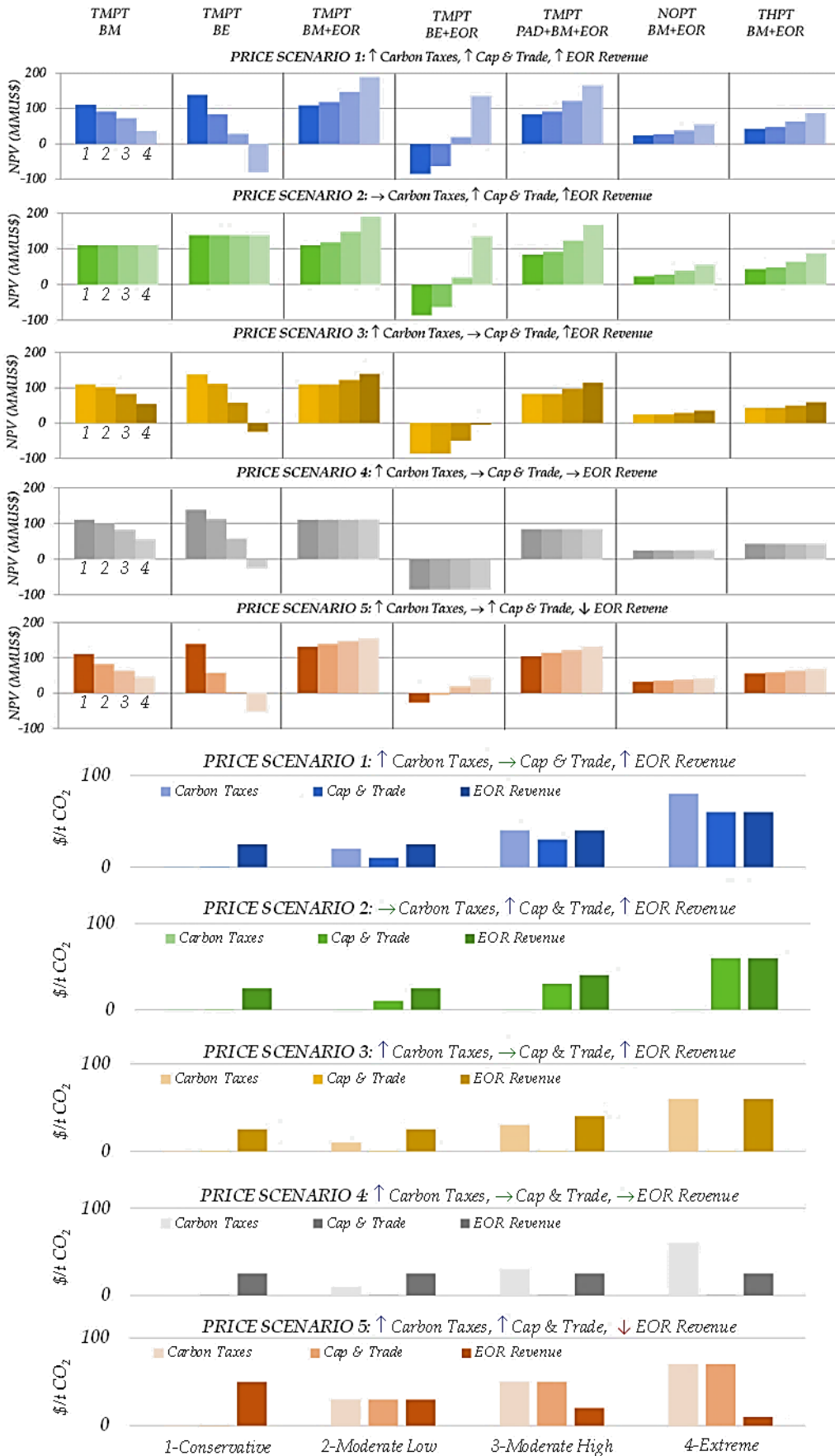


**Fig. 7.10.** Sensitivity analysis of Net Present Value to CO<sub>2</sub> taxation, price of Cap & Trade mechanism and EOR revenue based on 5 price scenario for all the analyzed processes.

Contrarily to base scenario, with very low sustainability incentives (conservative approaches) BE appears as the most attractive alternative regardless of the Price Scenario. Since BE is the most vulnerable route to CO<sub>2</sub> taxes, with accentuated effects in *REV* and *COM* (as all carbon contained in biogas is directed to atmosphere), as long as moderate incentives are applied. BE loses competitiveness and BM+EOR emerges outperforming all alternatives. For instance, in conservative approach of “Price Scenario 1” (Fig. 7.10) – BE yields *NPV*≈140 *MMUS*\$ while BM+EOR presents *NPV*≈110 *MMUS*\$, whereas in most rigorous approach for limiting emissions, BE falls dramatically to *NPV*≈-80 *MMUS*\$ while BM+EOR increases to *NPV*≈190 *MMUS*\$. Moreover, advantage of BM+EOR is confirmed in “Price Scenario 5” even upon low-valued oil prices (Fig. 7.10).

## 7.7. Conclusions for Chapter 7

Several upstream and downstream alternatives for biogas production/utilization from microalgal biomass – covering upstream (THPT, TMPT and NOPT), midstream (AD and PAD) and downstream (BM and BE, with and without CO<sub>2</sub>-EOR) processes – are investigated from a process system engineering perspective, comparing energy and economic performances, and CO<sub>2</sub> emissions. In a CCU chain involving microalgae cultivation (CO<sub>2</sub> biofixation), biomethane production using TMPT route carries ≈44% of CO<sub>2</sub> feed, while BM via NOPT can only retain ≈17% and THPT ≈25%. TMPT allows producing biogas with much higher microalgae conversion, so it is the baseline to downstream processes comparison: (i) BM; (ii) BM+EOR; (iii) bioelectricity (BE); and (iv) BE+EOR. Moreover, pressurized AD (PAD) at 6 bar is also approached aiming to reduce energy requirements and related expenses for gas compression and conditioning for exportation.

Energy Return on Investment (*EROI*) and resource utilization efficiency (*%EnergyOut*) metrics, both defined for the basis of biomethane LHV, are utilized for benchmarking energy efficiency of alternatives, which points significant advantage of PAD (*EROI*=7.58, 66.7%*EnergyOut*) over atmospheric AD for the context of BM production (*EROI*=5.98, 64.1%*EnergyOut*), though still being much less efficient than BE generation without CO<sub>2</sub> capture (*EROI*=25.5, 74.3%*EnergyOut*). It is proven that, as long as cost-effective biomass pretreatment methods are employed, relatively high net efficiency of BE generation can be achieved (43%LHV). However, if carbon capture and storage (with EOR) were applied to abate BE power plant emissions, as considered in BE+EOR (*EROI*=1.77, 33.6%*EnergyOut*), generating bioelectricity would largely lose competitiveness to BM due to high energy

penalties. Biomethane from biogas upgrading already involves capturing CO<sub>2</sub>, explaining similar energy performances of BM and BM+EOR (*EROI=5.42, 62.8%EnergyOut*).

What is of concern, however, is whether the most efficient processes are economically feasible or attractive, compensating the required capital investment and feedstock cost, and in this sense none of the considered processes would be feasible with microalgae priced at 234 US\$/t. BM+EOR, leveraged by extra revenue of CO<sub>2</sub> valuation through EOR, is feasible for biomass costing ≈100 US\$/t, while other configurations would require using low-valued biomass wastes. By assuming different scenarios of CO<sub>2</sub> taxes and cap & trading policies, it would be necessary to have intensification of environmental policies limiting CO<sub>2</sub> emissions to have BM+EOR overcoming BE as most attractive technology. These results evince the importance of CO<sub>2</sub> taxes to increase the interest on biomethane production routes. Finally, EOR throughout the investigated price scenarios attributes resilience to biogas processing.

## 7.8. References for Chapter 7

- [1] Brémond U, de Buyer R, Steyer J-P, Bernet N, Carrere H. Biological pretreatments of biomass for improving biogas production: an overview from lab scale to full-scale. *Renew Sust Energ Rev* 2018; 90:583–604. <https://doi.org/10.1016/j.rser.2018.03.103>
- [2] Li Y, Liu H, Yan F, Su D, Wang Y, Zhou H. High-calorific biogas production from anaerobic digestion of food waste using a two-phase pressurized biofilm (TPPB) system. *Bioresour Technol* 2017; 224:56–62. <https://doi.org/10.1016/j.biortech.2016.10.070>
- [3] Zhang R, Elmashad H, Hartman K, Wang F, Liu G, Choate C, Gamble P. Characterization of food waste as feedstock for anaerobic digestion. *Bioresour Technol* 2007; 98(4):929–35. <https://doi.org/10.1016/j.biortech.2006.02.039>
- [4] Zhou K, Chaemchuen S, Verpoort F. Alternative materials in technologies for biogas upgrading via CO<sub>2</sub> capture. *Renew Sust Energ Rev* 2017; 79:1414–41. <https://doi.org/10.1016/j.rser.2017.05.198>
- [5] Lindeboom REF, Weijma J, van Lier JB. High-calorific biogas production by selective CO<sub>2</sub> retention at autogenerated biogas pressures up to 20 bar. *Environ Sci Technol* 2012; 46(3):1895–902. <https://doi.org/10.1021/es202633u>
- [6] Angelidaki I, Treu L, Tsapekos P, Luo G, Campanaro S, Wenzel H, Kougias PG. Biogas upgrading and utilization: current status and perspectives. *Biotechnol Adv* 2018; 36(2):452–66. <https://doi.org/10.1016/j.biotechadv.2018.01.011>
- [7] Khan IA, Othman MHD, Hashim H, Matsuura T, Ismail AF, Rezaei-DashtArzhandi M, Azelee IW. Biogas as a renewable energy fuel – a review of biogas upgrading, utilisation and storage. *Energ Conver Manage* 2017; 150:277–94. <https://doi.org/10.1016/j.enconman.2017.08.035>
- [8] Uggetti E, Sialve B, Trably E, Steyer J-P. Integrating microalgae production with anaerobic digestion: a biorefinery approach. *Biofuels Bioprod Bioref* 2014; 8:516–29. <https://doi.org/10.1002/bbb.1469>

- [9] Costa JAV, Freitas BCB, Lisboa CR, Santos TD, Brusca LRF, Morais MG. Microalgal biorefinery from CO<sub>2</sub> and the effects under the Blue Economy. *Renew Sust Energ Rev* 2019; 99:58–65. <https://doi.org/10.1016/j.rser.2018.08.009>
- [10] Chen YD, Ho SH, Nagarajan D, Ren NQ, Chang JS. Waste biorefineries – integrating anaerobic digestion and microalgae cultivation for bioenergy production. *Curr Opin Biotechnol* 2018; 50:101–10. <https://doi.org/10.1016/j.copbio.2017.11.017>
- [11] Alzate ME, Muñoz R, Rogalla F, Fdz-Polanco F, Pérez-Elvira SI. Biochemical methane potential of microalgae: influence of substrate to inoculum ratio, biomass concentration and pretreatment. *Bioresour Technol* 2012; 123:488–94. <https://doi.org/10.1016/j.biortech.2012.06.113>
- [12] Córdova O, Santis J, Ruiz-Fillipia G, Zuñiga ME, Feroso FG, Chamy R. Microalgae digestive pretreatment for increasing biogas production. *Renew Sust Energ Rev* 2018; 82:2806–13. <http://dx.doi.org/10.1016/j.rser.2017.10.005>.
- [13] Kendir E, Ugurlu A 2018. A comprehensive review on pretreatment of microalgae for biogas production. *Int J Energ Res* 2018; 42(12):3711–31. <https://doi.org/10.1002/er.4100>
- [14] Zbed HM, Akter S, Yun J, Zhang G, Awad FN, Qi X, Sahu JN. Recent advances in biological pretreatment of microalgae and lignocellulosic biomass for biofuel production. *Renew Sust Energ Rev* 2019; 105:105–28. <https://doi.org/10.1016/j.rser.2019.01.048>
- [15] Bravo-Fritz CP, Sáez-Navarret CA, Herrera-Zepelin LA, Varas-Concha F. Multi-scenario energy-economic evaluation for a biorefinery based on microalgae biomass with application of anaerobic digestion. *Algal Res* 2016; 16:292–307. <https://doi.org/10.1016/j.algal.2016.03.028>
- [16] Budzianowski WM. A review of potential innovations for production, conditioning and utilization of biogas with multiple-criteria assessment. *Renew Sust Energ Rev* 2016; 54:1148–71. <https://doi.org/10.1016/j.rser.2015.10.054>
- [17] Koh HG, Kang NK, Kim EK, Jeon S, Shin S-E, Lee B, Chang YK. Advanced multigene expression system for *Nannochloropsis salina* using 2A self-cleaving peptides. *J Biotechnol* 2018; 278:39–47. <https://doi.org/10.1016/j.jbiotec.2018.04.017>
- [18] Alhattab M, Kermanshahi-Pour A, Brooks MS. Microalgae disruption techniques for product recovery: influence of cell wall composition. *J Appl Phycol* 2018; 1–28. <https://doi.org/10.1007/s10811-018-1560-9>
- [19] Zamalloa C, Vulsteke E, Albrecht J, Verstraete W. The techno-economic potential of renewable energy through the anaerobic digestion of microalgae. *Bioresour Technol* 2011; 102:1149–58. <https://doi.org/10.1016/j.biortech.2010.09.017>
- [20] González-Fernández C, Sialve B, Bernet N, Steyer JP. Impact of microalgae characteristics on their conversion to biofuel. Part II : focus on biomethane production. *Biofuels Bioprod Bioref* 2012; 6:205–18. <https://doi.org/10.1002/bbb.337>
- [21] Schwede S, Rehman ZU, Gerber M, Theiss C, Span R. Effects of thermal pretreatment on anaerobic digestion of *Nannochloropsis salina* biomass. *Bioresour Technol* 2013; 143:505–11. <https://doi.org/10.1016/j.biortech.2013.06.043>
- [22] Liu J, Song Y, Qiu W. Oleaginous microalgae *Nannochloropsis* as a new model for biofuel production: review & analysis. *Renew Sustain Energy Rev* 2017; 72:154–62. <https://doi.org/10.1016/j.rser.2016.12.120>

- [23] Marques AL, Araújo OQF, Cammarota MC. Biogas from microalgae: an overview emphasizing pretreatment methods and their energy return on investment (EROI). *Biotechnol Lett* 2018. <https://doi.org/10.1007/s10529-018-2629-x>
- [24] Passos F, Ferrer I. Microalgae conversion to biogas: thermal pretreatment contribution on net energy production. *Environ Sci Technol* 2014; 48:7171–8. <https://doi.org/10.1021/es500982v>
- [25] Kim JK, Oh BR, Chun YN, Kim SW. Effects of temperature and hydraulic retention time on anaerobic digestion of food waste. *J Biosci Bioeng* 2006; 102(4):328–32. <https://doi.org/10.1263/jbb.102.328>
- [26] Jain S, Jain S, Wolf IT, Lee J, Tong YH. A comprehensive review on operating parameters and different pretreatment methodologies for anaerobic digestion of municipal solid waste. *Renew Sust Energ Rev* 2015; 52:142–54. <http://doi.org/10.1016/j.rser.2015.07.091>
- [27] Lerm S, Kleyböcker A, Miethling-Graff R, Alawi M, Kasina M, Liebrich M, Würdemann H. Archaeal community composition affects the function of anaerobic co-digesters in response to organic overload. *Waste Manage* 2012; 32(3):389–99. <https://doi.org/10.1016/j.wasman.2011.11.013>
- [28] Moller K, Muller T. Effects of anaerobic digestion on digestate nutrient availability and crop growth: a review. *Eng Life Sci* 2012; 12(3):242–57. <https://doi.org/10.1002/elsc.201100085>
- [29] Scholz M, Melin T, Wessling M. Transforming biogas into biomethane using membrane technology. *Renew Sust Energ Rev* 2013, 17:199–212. <https://doi.org/10.1016/j.rser.2012.08.009>
- [30] Araújo OQF, de Medeiros JL. Carbon capture and storage technologies: present scenario and drivers of innovation. *Curr Opin Chem Eng* 2017; 17:22–34. <https://doi.org/10.1016/j.coche.2017.05.004>
- [31] Sun Q, Li H, Yan J, Liu L, Yu Z, Yu X. Selection of appropriate biogas upgrading technology – a review of biogas cleaning, upgrading and utilization. *Renew Sust Energ Rev* 2015; 51:521–32. <https://doi.org/10.1016/j.rser.2015.06.029>
- [32] Riboldi L, Bolland O. Overview on pressure swing adsorption (PSA) as CO<sub>2</sub> capture technology: state-of-the-art, limits and potentials. *Energy Procedia* 2017; 114:2390–400. <https://doi.org/10.1016/j.egypro.2017.03.1385>
- [33] Ryckeboosch E, Drouillon M, Vervaerenc H. Techniques for transformation of biogas to biomethane. *Biomass Bioenerg* 2011; 35(5):1633–45. <https://doi.org/10.1016/j.biombioe.2011.02.033>
- [34] Sutanto S, Dijkstra JW, Pieterse JAZ, Boon J, Hauwert P, Brilman DWF. CO<sub>2</sub> removal from biogas with supported amine sorbents: first technical evaluation based on experimental data. *Sep Purif Technol* 2017; 184:12–25. <https://doi.org/10.1016/j.seppur.2017.04.030>
- [35] Pellegrini L A, De Guido G, Langé S. Biogas to liquefied biomethane via cryogenic upgrading technologies. *Renew Energy* 2017; 124(C):75–83. <https://doi.org/10.1016/j.renene.2017.08.007>
- [36] Kadam R, Panwar NL. Recent advancement in biogas enrichment and its applications. *Renew Sust Energ Rev* 2017; 73:892–903. <https://doi.org/10.1016/j.rser.2017.01.167>

- [37] Machado PB, Monteiro JG, de Medeiros JL, Epsom HD, Araújo OQF. Supersonic separation in onshore natural gas dew point plant. *J Nat Gas Sci Eng* 2012; 6:43–9. <https://doi.org/10.1016/j.jngse.2012.03.001>
- [38] Wood AJ, Wollenberg BF, Sheblé GB. Power generation, operation, and control. 3rd ed. New Jersey: WILEY; 2014.
- [39] IEAGHG. Evaluation and analysis of the performance of dehydration units for CO<sub>2</sub> capture. Technical Report No. 2014/04; April 2014.
- [40] de Medeiros JL, Araújo OQF, Versiani BM. A model for pipeline transportation of supercritical CO<sub>2</sub> for geological storage. *J Pipel Eng* 2008; 7:253–79.
- [41] Picardo MC, de Medeiros JL, Monteiro JGM, Chaloub RM, Giordano M, Araújo OQF. A methodology for screening of microalgae as a decision making tool for energy and green chemical process applications. *Clean Technol Environ Policy* 2013; 15:275–91. <https://doi.org/10.1007/s10098-012-0508-z>
- [42] Norland S, Fagerbakke KM, Heldal M. Light element analysis of individual bacteria by x-ray microanalysis. *Appl Environ Microbiol* 1995; 61(4):1357–62.
- [43] Ación F, Fernández J, Magán J, Molina E. Production cost of a real microalgae production plant and strategies to reduce it. *Biotechnol Adv* 2012; 30(6):1344–53. <https://doi.org/10.1016/j.biotechadv.2012.02.005>
- [44] Bohutskyi P, Chow S, Ketter B, Betenbaugh MJ, Bouwer EJ. Prospects for methane production and nutrient recycling from lipid extracted residues and whole *Nannochloropsis salina* using anaerobic digestion. *Appl Energy* 2015; 154:718–31. <https://doi.org/10.1016/j.apenergy.2015.05.069>
- [45] Abbassi A, Ali M, Watson IA. Temperature dependency of cell wall destruction of microalgae with liquid nitrogen pretreatment and hydraulic pressing. *Algal Res* 2014; 5(1):190–4. <https://doi.org/10.1016/j.algal.2013.12.008>
- [46] Hall CAS, Lambert JG, Balogh SB. EROI of different fuels and the implications for society. *Energy Policy* 2014; 64:141–52. <https://doi.org/10.1016/j.enpol.2013.05.049>.
- [47] Turton R, Bailie RC, Whiting WB, Shaeiwitz JA, Bhattacharyya D. Analysis, synthesis, and design of chemical processes. 4th ed. Prentice Hall, 2012.
- [48] Wiesberg IL, Brigagão GV, de Medeiros JL, Araújo OQF. Carbon dioxide utilization in a microalga-based biorefinery: efficiency of carbon removal and economic performance under carbon taxation. *J Environ Manage* 2017; 203:988–98. <https://doi.org/10.1016/j.jenvman.2017.03.005>
- [49] Aziz M. Integrated supercritical water gasification and a combined cycle for microalgal utilization. *Energy Convers Manage* 2015; 91:140–8. <https://doi.org/10.1016/j.enconman.2014.12.012>
- [50] Wang M, Lee E, Dilbeck MP, Liebelt M, Zhang Q, Ergas SJ. Thermal pretreatment of microalgae for biomethane production: experimental studies, kinetics and energy analysis. *J Chem Technol Biotechnol* 2017; 92(2):399–407. <https://doi.org/10.1002/jctb.5018>
- [51] González-Fernández C, Sialve B, Bernet N, Steyer JP. Thermal pretreatment to improve methane production of *Scenedesmus* biomass. *Biomass Bioenergy* 2012; 40:105–11. <https://doi.org/10.1016/j.biombioe.2012.02.008>
- [52] Zhang R, Parniakov O, Grimi N, Lebovka N, Marchal L, Vorobiev E. Emerging techniques for cell disruption and extraction of valuable bio-molecules of microalgae

*Nannochloropsis* sp. Bioprocess Biosyst Eng 2019; 42(2):173–86.  
<https://doi.org/10.1007/s00449-018-2038-5>

[53] Williams P, Laurens L. Microalgae as biodiesel & biomass feedstocks: review & analysis of the biochemistry, energetics & economics. Energy Environ Sci 2010; 3:554–90.  
<https://doi.org/10.1039/B924978H>

[54] Santos-Bellardo DU, Font-Segura X, Ferrer AS, Barrena R, Rossi S, Valdez-Ortiz A. Valorisation of biodiesel production wastes: anaerobic digestion of residual *Tetraselmis suecica* biomass and co-digestion with glycerol. Waste Manage Res 2015; 33:250–7.  
<https://doi.org/10.1177/0734242X15572182>

## 8. A Techno-Economic Analysis of Thermochemical Pathways for Corncob-to-Energy: Fast Pyrolysis to Bio-Oil, Gasification to Methanol and Combustion to Electricity

*This chapter is published as an article in Fuel Processing Technology.*

BRIGAGÃO, G. V.; ARAÚJO, O. Q. F.; DE MEDEIROS, J. L.; MIKULCIC, H.; DUIC, N. A techno-economic analysis of thermochemical pathways for corncob-toenergy: fast pyrolysis to bio-oil, gasification to methanol and combustion to electricity. *Fuel Processing Technology*, 193, 102-113, 2019.

### Abstract

Global warming concerns have driven developments in carbon neutral energy, pulling initiatives on biofuels production. However, the low bulk density and low specific energy of biomass refrain its widespread use due to logistic costs comprising harvesting and collection, storage, pretreatments and transportation. This work approaches thermochemical conversion of residual biomass to energy products, identifying the best options in terms of energy efficiency and economic indicators. Techno-economic performances of three corncob-to-energy pathways are investigated: gasification to methanol, fast pyrolysis to bio-oil and combustion to electricity. Fast pyrolysis allows higher energy recovery in its products (79%) than biomass gasification to methanol (53%), with biomass densification (volume reduction) of 72.7% and 86.2%, respectively. The combustion route presents net efficiency of 30.2% of biomass lower heating value (LHV). All alternatives are economically feasible provided biomass cost is lower than US\$75.5/t. The minimum allowable product prices for economic attractiveness of gasification, combustion and pyrolysis routes are US\$305/t methanol, US\$80.1/MWh electricity and US\$1.47/gasoline-gallon-equivalent bio-oil. Despite its vulnerability to price volatility, gasification presents the highest net present value, seconded by the combustion route, which has lower medium-term payback and investment than gasification due to its process simplicity.

**Keywords:** corncob; thermochemical conversion; biomass pyrolysis; biomass gasification; methanol synthesis; cogeneration.

### Abbreviations

BECCS Bio-Energy with Carbon Capture and Storage; BTL Biomass-to-Liquids; ¢ US Dollar Cents; COMB Biomass Combustion Route; DCC Direct Contact Column; EOS Equation-of-State; GASIF Biomass Gasification Route; LHV Lower Heating Value; MEA Monoethanolamine; PR Peng-Robinson; PYROL Biomass Fast Pyrolysis Route; ST Steam Turbine; USD US Dollars.

## Nomenclature

<i>%EnergyOut</i>	: Percentage of corncob energy input on LHV basis (unitless);
<i>AP, GAP</i>	: Annual profit and gross profit (USD/y);
<i>CEPCI</i>	: Chemical engineering plant cost index (unitless);
<i>COM</i>	: Annual cost of manufacturing (USD/y);
<i>CRM, CUT</i>	: Annual utility and raw material costs (USD/y);
<i>FCI</i>	: Fixed capital investment (USD);
<i>LHV</i>	: Lower heating value (MJ/kg);
<i>NPV</i>	: Net present value (USD);
<i>NPVREL</i>	: Relative net present value (unitless);
<i>REV</i>	: Revenues (USD/y);
<i>S</i>	: Methanol synthesis coefficient (unitless).

## 8.1. Introduction

Expansion of the world energy demand and global warming concerns have driven developments of carbon neutral energy sources, pushing production of transportation fuels from biomass [1]. Carbon neutrality of biofuels has been challenged, as carbon stock decreases with land use changes. Thus, harvesting for biofuels demands energy conversion efficiency and increased productivity [2].

A promising alternative for increasing energy productivity is the use of agricultural waste to produce electricity, as occur in the sugarcane-based bioethanol industry, where heat and electricity are co-generated from bagasse [3], with significant improvements in energy efficiency [4]. The same applies to corn-ethanol industry, where co-generation has been also suggested to improve its competitiveness over Brazilian sugarcane-ethanol [5]. Among the corn residues (cobs, husks, leaves and stalks), cobs stand out with reduced mineral [6] and nitrogen contents [7], favoring its utilization for combustion applications [6] and biofuels production. Although corncobs are mostly left to decay in the fields after grain harvests [7], energy products from corn residues have received increasing attention, e.g. electricity and products from thermochemical pathways, e.g. pyrolysis to biochar [8] and gasification to dimethyl ether [9] and methanol [10].

Comprising harvesting and collection, storage, pretreatments and transportation, biomass logistics costs refrain its widespread use in electricity and biofuels production [11]. Gallagher et al. [5], for the case of corn-processing regions, considered geographical location as critical for investing in biofuels, not only for the distance but also for the absence of trade barriers. Additional drawbacks in biomass utilization are its variability (chemical composition and physicochemical properties) and low bulk density, which is overcome by biomass

densification [12], allowing higher energy density (i.e. increased volumetric calorific value), thus reducing logistics costs.

Pelleting and briquetting are common densification alternatives being an important issue the ability of the densified biomass to remain intact when handled during storage and transportation. Preheating or steam conditioning of the raw biomass increases durability (i.e. physical strength and mechanical resistance) and can have a significant effect on the calorific value of the pellet and briquet [13]. Briquetting or pelleting corncobs can increase its bulk density to  $\approx 550 \text{ kg/m}^3$  [6], which means halving the grinded corncob volume. Torrefaction, or mild pyrolysis (at 200-300°C), enhances biomass properties (e.g., lower water content and increased heating value), producing a dry carbonaceous solid, where 70% of initial weight and 80-90% of original energy are obtained, reducing logistics costs and can be a pretreatment process prior to pelleting [13].

The recovery of energy from biomass is moving from pelleting and briquetting towards biochemical and thermochemical processes. Besides yielding a wide range of products, replacing their original fossil source, thermochemical processes are flexible with respect to the variety of biomass feedstock [14]. Among thermochemical routes, pyrolysis has higher flexibility as process conditions (temperature, heating rate and residence time) can be optimized to maximize the production of targeted products [15]. It is a promising thermochemical conversion, which decomposes biomass into solid biochar, liquid bio-oil, and combustible gas to meet different process goals [16]. Fast pyrolysis is employed to maximize bio-oil production and occurs at very high heating rates, temperature of  $\approx 500^\circ\text{C}$ , short vapor and char residence times and rapid cooling of pyrolysis vapor [17], while slow pyrolysis applies low heating rate, moderate temperature ( $\approx 400^\circ\text{C}$ ) and high residence time to favor bio-char production [15]. Fast pyrolysis bio-oil has increased energy density,  $\approx 6.5$  fold increase over raw biomass, halving land area requirements for fuel storage and handling, compared to solid fuel handling systems [18].

Bio-oil direct use as fuel presents difficulties due to its high viscosity, poor heating value, corrosiveness, and instability [19]. Hence, bio-oil requires upgrading into naphtha-range transport fuels, which is obtained via two major conventional refinery operations – hydroprocessing and catalytic cracking processes [20], with hydrotreatment under mild conditions (150–450 °C, 50 bar) being one of the main routes [21]. The key to bio-oil upgrading is to remove oxygen with minimal hydrogen consumption, while retaining its

carbon content [22]. A comprehensive review concerning the challenges of bio-oil production and upgrading is provided by Sharifzadeh et al. [23]. A review on the methods used for detailed simulation of fast pyrolysis reactors via computational fluid dynamics is addressed by Xiong et al. [24], which discussed in a later work [25] the trends and major barriers for accurate reactor-scale predictions.

Trippe et al. [26] approached fast pyrolysis for a decentralized fuel production chain, saving in transportation costs due to increased energy density of crude bio-oil mixed with pulverized bio-char (biosyncrude). In fact, the low energy density of raw biomass constrains its transportation to short distances, contrasting with biomass-to-liquids (BTL), which is suitable for large scale facilities. In the business model of Trippe et al. [26], multiple decentralized pyrolysis plants are built to obtain biosyncrude that can be economically transported over long distances to a centralized large scale processing unit [26]. Alternatively, modular and transportable bio-oil plants can be built close to the biomass sources [18].

Experimental work on corncob fast pyrolysis by Zhang et al. [27] employed a bubbling fluidized bed reactor fed with pure nitrogen to investigate performance sensitivity to experimental factors, among which the reaction temperature and particle size. In later work [28], catalytic fast pyrolysis was approached unveiling the existence of a trade-off between bio-oil quantity (yield) and quality (composition or heating value). Zhang et al [29] presented the effects of using different carrier gases on product gas of corncob fast pyrolysis.

Competing with fast pyrolysis, biomass gasification occurs at higher temperatures (700-1000°C) and necessarily with addition of a gasifying agent [30] – generally steam, air or oxygen (O<sub>2</sub>) – yielding product gas containing carbon monoxide (CO), carbon dioxide (CO<sub>2</sub>), hydrogen (H<sub>2</sub>), methane (CH<sub>4</sub>), aliphatic and aromatic light hydrocarbons, tar and water. [31]. Product gas has use in co-generation, thermal cracking or catalytic reforming to yield syngas with reduced hydrocarbon content [32].

Syngas is a versatile building block in the chemical industry, with main use in the synthesis of ammonia (≈55%), H<sub>2</sub> supply to oil refining processes (≈24%), and, to a smaller extent, for methanol production (12%) [32]. Other products derived from syngas are Fischer–Tropsch (FT) fuels, ethanol and synthetic natural gas [1]. FT reaction produces a variety of linear and branched-chain synthetic hydrocarbons [33] while methanol, besides having use as fuel, is a major energy carrier and an important chemical commodity [34].

Anex et al. [35] performed a techno-economic comparison of alternatives for corn stover processing including gasification to FT liquids, fast pyrolysis to bio-oil and biochemical conversion to ethanol (second generation). The authors evaluated the product values for project attractiveness, concluding that pyrolysis has the best economic performance and biochemical conversion the worst. Zhao et al. [36] employed Monte Carlo simulation to compare on economic grounds pathways to produce ethanol and synthetic hydrocarbons, showing that fast pyrolysis of corn stover would be preferred by risk-averse investors.

Regarding the use of corncobs, a literature gap exists in techno-economic comparisons of production routes to bio-oil, methanol and electricity. A review by Brown et al. [37] covering the economic performance of thermochemical pathways to biofuels production included a critical discussion of the major assumptions adopted in the literature. The authors emphasize fixed capital investments and minimum allowable product prices for economic attractiveness.

In this work, gasification of biomass to syngas and its final destination to methanol is compared to fast pyrolysis as biomass energy densification route producing bio-oil. Both alternatives have as competitor the direct combustion of biomass in power plants. The original contribution is to fulfill the identified literature gap on comparative techno-economic analyses of these thermochemical alternatives for conversion of corncob, an agricultural waste abundantly available in the USA. The relevance of the contribution is the context of energy densification of waste biomass for its efficient use and transportation as energy feedstock. Combustion is taken as a reference project, due to its widespread use in biomass-fired steam power plants, and for being supplier of electricity and heat in fast pyrolysis and gasification alternatives. The analysis methods involve process simulation in Aspen HYSYS allowing rigorous thermodynamic models and equipment representation to calculate energy and mass balances for the three processes: fast pyrolysis to bio-oil (PYROL), gasification to methanol (GASIF) and combustion to electricity (COMB). Composition characterization of corncob biomass is presented, with description based on model molecules from experimental results reported in the literature [29]. Simulation results support calculation of energy efficiency, equipment sizing and economic analysis. Sensitivity analysis of economic performance to prices of corncob feedstock and products is presented.

## 8.2. Methods

Techno-economic evaluation of the three investigated process alternatives (GASIF, PYROL and COMB) is performed based on the block diagrams depicted in Fig. 8.1.

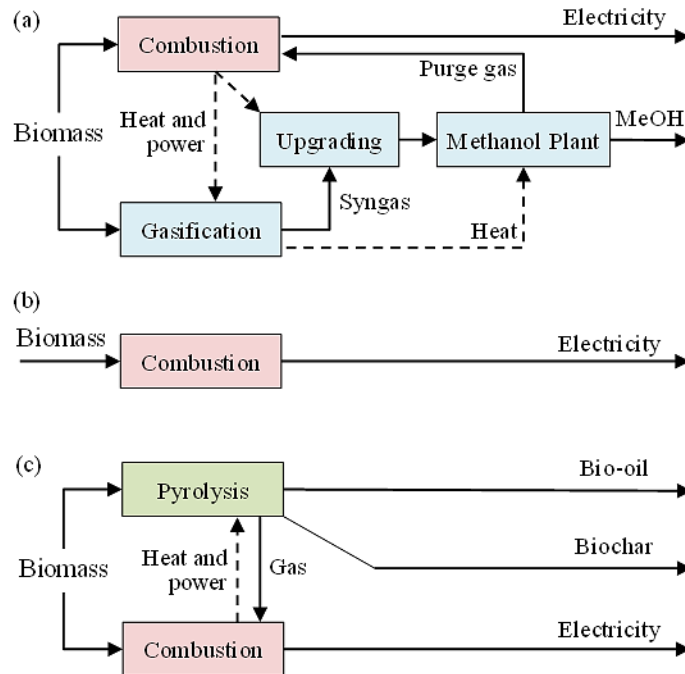


**Fig. 8.1.** Alternatives for energy densification of corncob biomass through thermochemical processes: (a) methanol production through gasification; (b) combustion for power generation (COMB); and (c) pyrolysis for bio-oil. Gasification and pyrolysis employ partial use of biomass in auxiliary combustion process to supply process electricity and heating demands, exporting surplus electricity.

### 8.2.1. Processes Description

The operational conditions and the main aspects of the three thermochemical routes – GASIF (Fig. 8.1a), COMB (Fig. 8.1b) and PYROL (Fig. 8.1c) – are addressed. The process alternatives are equally fed with 96.81 t/h (94.48 t/h on ash-free basis) of corncob biomass grinded with particle size from 1 to 2 mm [27, 29].

### 8.2.1.1. Biomass Gasification

GASIF process flowsheet (Fig. 8.2) uses syngas to produce methanol, with surplus gas used with biomass co-firing for combined heat and power generation. Table 8.1 summarizes process conditions and assumptions for biomass gasification and raw syngas cooling.

**Table 8.1.** Premises and conditions for biomass gasification and raw syngas cooling.

Item	Value	Unit
Biomass feed (ash-free basis)	58.61	t/h
Steam feed rate	58.56	t/h
Steam temperature	250	°C
Syngas temperature	900	°C
Syngas pressure	3.00	bar
HRSG (heat recovery steam generation) boiler pressure	3.25	bar
HRSG gas pressure drop	5.0	kPa
HRSG gas outlet temperature	180	°C
DCC (direct contact column) gas outlet temperature	35.4	°C
DCC pressure drop	10	kPa
DCC theoretical stages	04	-

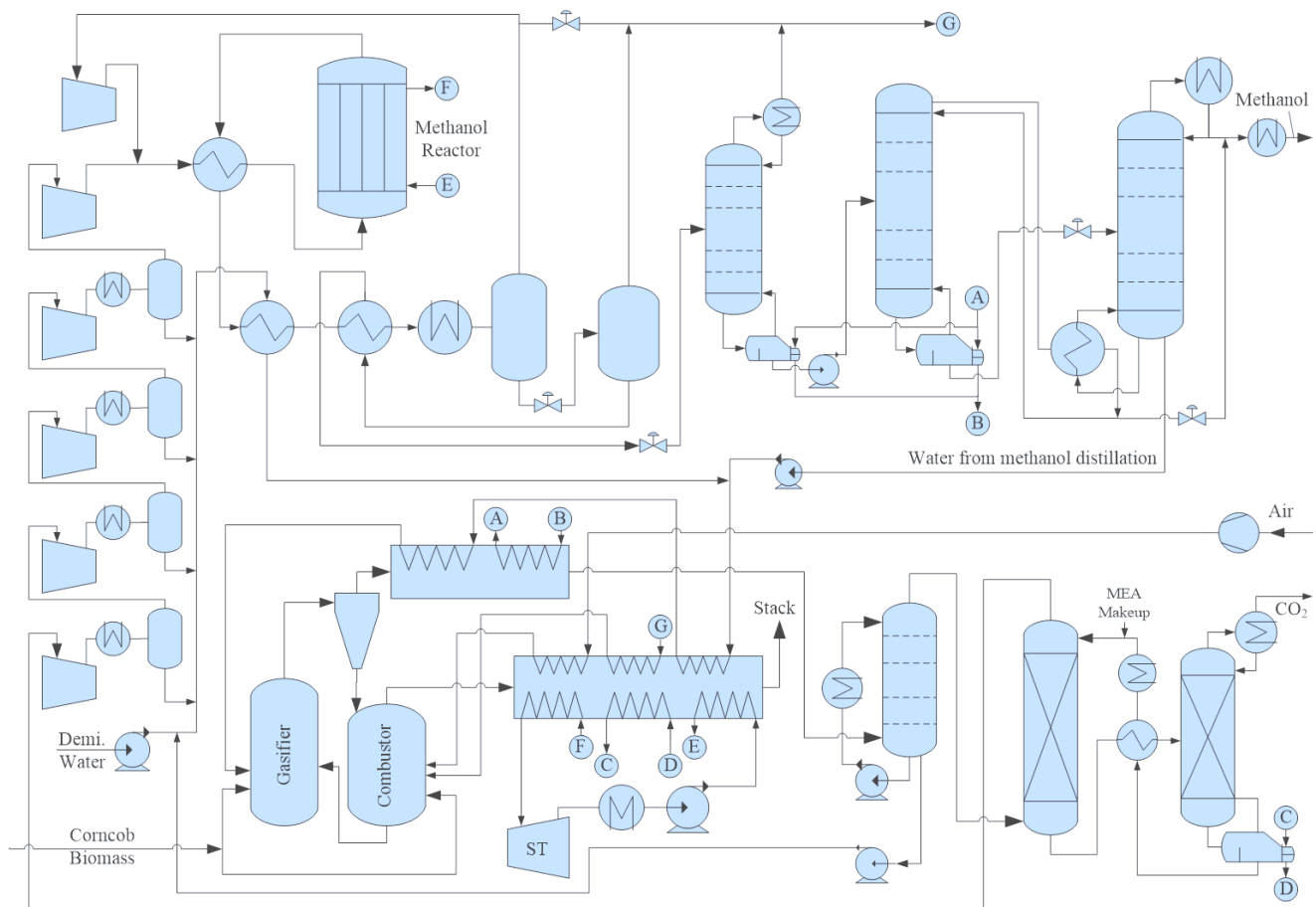


**Fig. 8.2.** Process flowsheet of biomass gasification to produce methanol (GASIF).

A circulating fluidized bed gasifier is employed, with the reaction heat supplied by hot sand provided by biomass combustion. Corncob particles are conveyed to the gasifier with superheated steam at 3 bar and 250°C (1:1 mass ratio) and feed of 58.61 t/h (ash-free basis); the remaining 35.87 t/h is used for combustion to supply internal heat demand. Raw syngas (mainly H<sub>2</sub>, CO and CO<sub>2</sub>) leaves the gasifier at 900°C and goes to a heat recovery steam generator (HRSG), where superheated steam utilized in gasification is produced and saturated water at 3.25 bar is boiled to supply heat demand of the methanol purification section (distillation column reboilers). To minimize condensation of tar compounds in HRSG and associated issues such as corrosion and fouling [38], hot syngas exits HRSG at 180°C, with the finishing cooling being performed in a plate direct contact column (DCC) clad with stainless steel, fed with cold condensate recycled from column bottom. The condensate purge is used to minimize demineralized water consumption, being mixed with other residual aqueous streams in the plant, obtained from condensate drums of the syngas compressor. The condensate mixture is reheated to generate superheated steam to the gasifier.

The cooled raw syngas leaves the DCC at 35.4°C requiring adjustment of the proportion of components H<sub>2</sub>, CO and CO<sub>2</sub> to ideal stoichiometric conditions for methanol synthesis, expressed by *S* coefficient close to 2.0, as defined by Eq. (8.1), where the brackets express the molar contents.

$$S = \frac{[H_2] - [CO_2]}{[CO] + [CO_2]} \quad (8.1)$$

The targeted *S* value is reached via CO<sub>2</sub> removal by chemical absorption with aqueous monoethanolamine (MEA) at 20% w/w. Syngas at 2.5 bar leaves at the top of the absorber with 2.53% mol CO<sub>2</sub> (wet basis). Table 8.2 provides process conditions and premises for simulation of syngas upgrading.

Absorber bottoms (CO<sub>2</sub>-rich MEA) flows to the regeneration column, where CO<sub>2</sub>-rich gas at 1.8 bar (4.17% mol H<sub>2</sub>O) leaves at the top with 99.89% mol CO<sub>2</sub> dry-basis purity. Heat integration of lean and rich solvent streams minimizes heat load to the column's reboiler. It is worth noting that 39.78% of corncob mass flow is carbon and 22% of this amount leaves the MEA regeneration column as practically pure CO<sub>2</sub> (CO<sub>2</sub>-rich gas). It could be monetized after intercooled compression stages, through pipeline dispatch, as a high-pressure liquid or, by truck, as cryogenic liquid (or even as dry-ice). Besides contributing to process revenues from its commercialization, this CO<sub>2</sub>-rich gas could be used as enhanced oil recovery agent. This would characterize the entire process as a negative CO<sub>2</sub> emitter, i.e. a bio-energy with

carbon capture and storage (BECCS) technology. With BECCS, CO<sub>2</sub> storage could contribute to process profitability by considering a cap-and-trade scenario. For the sake of simplicity, destination of this CO<sub>2</sub>-rich gas is not considered in this work.

Table 8.3 summarizes the main premises and conditions related with methanol production.

**Table 8.2.** Premises and conditions for CO<sub>2</sub> removal in syngas upgrading.

Item	Value	Unit
Solvent	20	%w/w aq. MEA
Lean MEA	1.25	%mol CO <sub>2</sub>
Capture-Ratio	17	kg solvent/ kg CO <sub>2</sub>
Absorption stages	15	-
Absorption pressure drop	35	kPa
Absorption top pressure	2.50	bar
CO <sub>2</sub> in lean gas	2.53	%mol CO <sub>2</sub>
Regeneration stages	10	-
Regeneration pressure drop	10	kPa
Regeneration top pressure	1.80	bar

**Table 8.3.** Premises and conditions for methanol production.

Item	Value	Unit
Methanol synthesis (reactor)		
Inlet pressure	60	bar
Inlet temperature	240	°C
Outlet temperature	260	°C
Purification (distillation columns)		
Column#1 condenser temperature	40	°C
Column#2 condenser temperature	119.5	°C
Column#3 reboiler temperature	109.9	°C
Methanol purity	99.85	%w/w

Syngas from MEA absorption presenting  $S=2.018$  is sent to five-stage compression before entering the methanol synthesis loop at  $\approx 60$  bar. The methanol reactor has a steam raising design, configuring a shell and tube heat exchanger, and tubes packed with catalyst (methanol synthesis). It is simulated as an equilibrium reactor, fed with a mixture of fresh syngas and recycled unreacted gas at 240°C. The reaction heat is recovered through steam generation in the shell side at 230°C ( $\approx 28$  bar). The amount of catalyst required is calculated accordingly to typical weight-hourly-space-velocity of  $3\text{h}^{-1}$ . The product outlet at 260°C is firstly cooled down to 107°C in a battery of exchangers to: (i) heat the reactor feed gas; (ii) preheat the water stream for gasifier feed; and (iii) reheat the low-pressure raw methanol sent to purification. Then it is finally cooled down to 40°C for condensation of raw methanol,

leaving substantial amount of tail gas, from which 10% is withdrawn as purge gas, with the other 90% being recycled to reactor feed. Raw methanol is expanded to  $\approx 4$  bar producing a small fraction of gas that is mixed to the purge gas from the synthesis loop. The liquid is then reheated (cooling reactor product) prior to entering the first distillation column to minimize reboiler duty, whereas the purpose of the first distillation column is the removal of light compounds (e.g. dissolved gases). The overhead vapor is mixed to the purge gas and sent to the combustion furnace for co-firing with corncob biomass, supplying 20% of its energy demand. The bottom methanol-water mixture is pumped to the next distillation column at  $\approx 6.5$  bar, where  $\approx 45\%$  of methanol is recovered at the top as commercial grade product (99.85% w/w). The third column finishes the methanol-water fractionation, operating at nearly atmospheric pressure, with the reboiler duty supplied by heat integration with condensation of pressurized methanol vapor from the top of the second column.

Corn cob co-firing (35.87 t/h) with purge gas (6.56 t/h) is performed with 10% excess air producing hot sand for gasification and hot gas at  $1050^\circ\text{C}$  for another HRSG section, where exhaust gas heat is recovered by several process streams and cooled to  $95^\circ\text{C}$ : (i) air feed; (ii) purge gas feed; (iii) non-saturated water that is subsequently heated in other HRSG to produce superheated steam to gasification; (iv) low-pressure saturated water to supply MEA reboiler with steam; (v) water and saturated steam at  $\approx 28$  bar for power generation, with latent heat being supplied by methanol synthesis reaction heat. After pressurized to 28.2 bar, water of Rankine cycle is pre-heated to saturation in exhaust gas HRSG and then sent to boil up in the methanol reactor; produced saturated steam returns for superheating. The steam turbine (ST) is fed with superheated steam at  $560^\circ\text{C}$  and 27.7 bar generating electricity for the plant, mostly to drive the syngas compressor, with the exceeding power (3.7 MW) being exported. The Rankine vacuum condenser operates at 0.096 bar and  $45^\circ\text{C}$ .

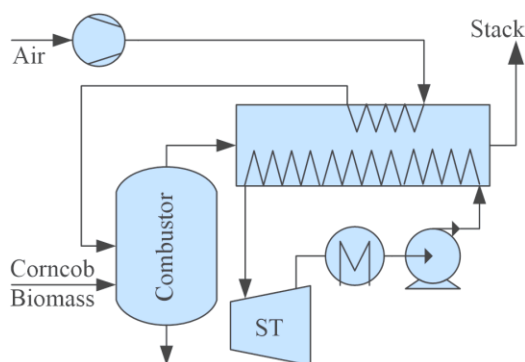
### 8.2.1.2. Biomass Combustion

Fig. 8.3 shows the process flowsheet of the biomass combustion route, which is totally based in electricity generation in a corncob-fired Rankine cycle. Despite not indicated in Fig. 8.3, heat recovery also occurs in the furnace radiation zone to generate superheated steam for the turbine. Able to export 114.10 MW of electricity, the estimated power plant net efficiency is 30.2%LHV. Major assumptions and process conditions are shown in Table 8.4. Contrarily to the biomass gasification route, implementation of BECCS in this case would require CO<sub>2</sub> removal from diluted (N<sub>2</sub>-rich) flue gas, a rather expensive option.

The ST is fed with superheated steam at 560°C and 27.7 bar. The Rankine vacuum condenser also operates at 0.096 bar and 45°C. After being pumped to 28.2 bar, a fraction of pressurized water is sent to the furnace (not shown) and another fraction is sent to exhaust gas HRSG. The exhaust gas is assumed to enter the HRSG at 1050°C, and then released to the atmosphere at 100°C through the stack.

**Table 8.4.** Operating conditions of the power generation process.

Item	Value	Unit
Biomass feed rate	96.81	t/h
Excess air for combustion	10.0	%
ST adiabatic efficiency	90.0	%
ST inlet temperature	560	°C
ST inlet pressure	27.70	bar
ST outlet pressure	0.096	bar
Condenser outlet temperature	45.0	°C



**Fig. 8.3.** Process flowsheet of biomass combustion to produce electricity (COMB).

### 8.2.1.3. Biomass Fast Pyrolysis

Biomass fast pyrolysis route considers exportation of raw bio-oil (i.e., without further treatment or upgrading), with exceeding non-condensable gas available for combined heat and power generation with biomass co-firing. Bio-oil upgrading, stabilization or fractionation for recovery of valuable chemicals is assumed to be performed in a centralized (high capacity) chemical plant or oil refinery, where  $H_2$  is readily available to be utilized for bio-oil hydrotreating. Consequently, the capital investment is drastically minimized. It is worth noting that this alternative involves the lowest capacity machines (turbines, compressors and pumps) in comparison with the other evaluated routes.

The process flowsheet of the biomass pyrolysis route is presented in Fig. 8.4, while process conditions and premises are shown in Table 8.5.

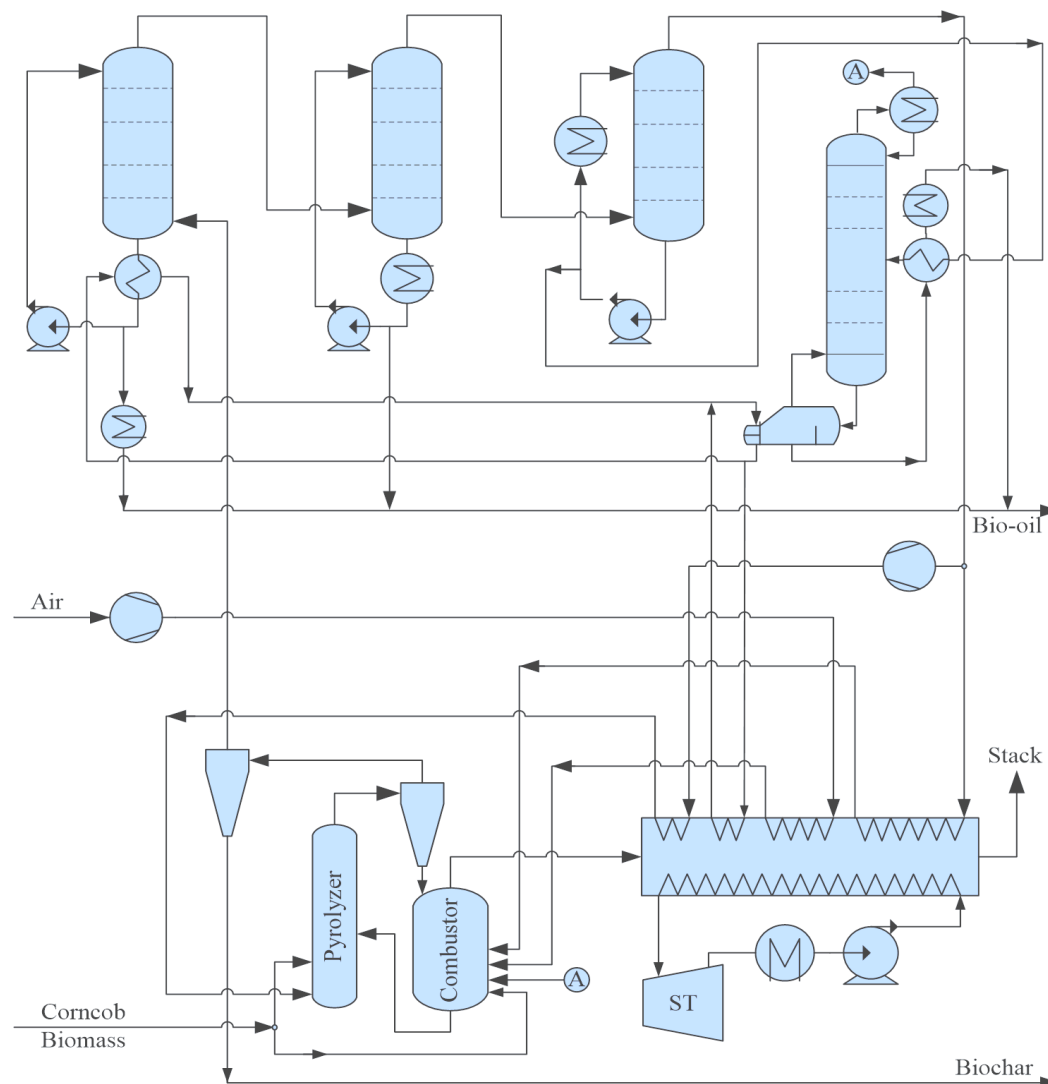


**Fig. 8.4.** Process flowsheet of biomass pyrolysis for bio-oil production (PYROL).

**Table 8.5.** Biomass fast pyrolysis conditions and premises.

Item	Value	Unit
Biomass pyrolysis		
Corncob feed rate (ash-free basis)	82.88	t/h
Operating temperature	550	°C
Outlet pressure	1.46	bar
Pressure drop	20	kPa
Product cooling		
DCC#1 liquid inlet temperature	185	°C
DCC#1 gas outlet temperature	198	°C
DCC#1 pressure drop	10	kPa
DCC#2 liquid inlet temperature	40	°C
DCC#2 gas outlet temperature	103	°C
DCC#2 pressure drop	10	kPa
DCC#3 liquid inlet temperature	40	°C
DCC#3 gas outlet temperature	42	°C
DCC#3 pressure drop	10	kPa
Distillation		
Water content at bottom product	9.62	% w
Water content at top waste vapor	99.3	% w

Fast pyrolysis yields and bio-oil composition are based on experimental results of Zhang et al. [29]. Corncob particles are conveyed to the pyrolysis reactor where they are fluidized with recycled non-condensable gas. The biomass feed rate is 82.88 t/h, while the remaining 11.60 t/h is burnt for supplying the pyrolysis heat demand.

Hot vapor at 550°C and 1.46 bar goes from the fast pyrolysis reactor to solids collection (with assumed 100% efficiency). It is then cooled in a battery of three plate-based DCCs (04 theoretical stages each) quenched with the recycle of cooled bio-oil condensate. Quick cooling after dust removal aims to rapidly cease chemical reactions, besides minimizing fouling and facilitating cleaning [17].

In the first DCC, hot vapor at 550°C is cooled to 198°C by heavy bio-oil at 185°C recycled from column bottoms. This overhead vapor is connected to the bottom of the following DCC, which is fed by the top with a lighter fraction of bio-oil at 40°C, also recycled from column bottoms, that cools the vapor feed down to 103°C. Finally, this vapor enters the third DCC to be cooled down to 42°C. About 57% of the gas leaving the top of DCC#3, consisting mainly of CO<sub>2</sub>, CO, H<sub>2</sub> and CH<sub>4</sub>, is directed to combustion, with the remaining part being recycled to the pyrolysis reactor.

As bio-oil is expected to be highly acidic and corrosive ( $\text{pH}\approx 3$ ), the DCC columns are clad with stainless steel. Hot heavy bio-oil leaves the bottom of DCC#1 at  $237^\circ\text{C}$  and is cooled to  $185^\circ\text{C}$  recovering heat to generate saturated steam, to partially supply a distillation reboiler. In the case of DCC#2, bottom liquid at  $116^\circ\text{C}$  is cooled to  $40^\circ\text{C}$ . Both in DCC#1 and DCC#2, the fraction of bottom liquid that is not recycled is sent to a product header. DCC#3 operates below  $100^\circ\text{C}$  producing condensate at  $82^\circ\text{C}$  with very high water content (71.3% w), which is sent to distillation for recovery of organic compounds. A bio-oil header receives the different fractions produced in DCC#1 and DCC#2, in addition to the light compounds recovered via distillation. The reboiler heat duty is mostly supplied with steam generated from heavy bio-oil cooling at the bottom of DCC#1, which is complemented by saturated steam generated through exhaust gas heat recovery.

Corn cob co-firing (11.60 t/h) with pyrolysis gas (16.42 t/h) employs 10% excess air, producing hot sand for pyrolysis and hot gas at  $1020^\circ\text{C}$  for a HRSG section, where several process streams are heated while the flue-gas cools down to  $100^\circ\text{C}$ : (i) air feed; (ii) pyrolysis gas for combustion; (iii) pyrolysis gas for recycle; (iv) low-pressure saturated water (to supply steam to the distillation reboiler); and (v) Rankine cycle streams. Biomass, air, pyrolysis gas and 15.37 t/h of water vapor (99.3% w/w) from distillation column (avoiding the need of residual water treatment) is sent to the combustor to convert organic compounds. As the pyrolysis plant has low electricity consumption, the ST power is mostly exported (7.85 MW). The ST is also fed with superheated steam at  $560^\circ\text{C}$  and 27.7 bar.

### **8.2.2. Simulation of Process Alternatives**

Process alternatives are simulated in Aspen HYSYS 8.8 using Peng-Robinson Equation-of-State (PR-EOS) with exception of free-water/steam systems that use NBS Steam. For liquid phase containing organic compounds, other thermodynamic models are applied: Cubic Plus Association EOS for high-pressure applications (methanol synthesis loop); UNIQUAC liquid-phase activity coefficient model coupled to PR-EOS vapor-phase for low-pressure systems (biomass pyrolysis and methanol purification), with UNIFAC group contribution method employed to estimate missing binary interaction parameters; and Acid-Gas Package for  $\text{CO}_2$  chemical absorption plant.

Biomass is represented by a mix of model substances to reproduce the empirical elemental composition given by Zhang et al. [29], expressed as reduced chemical formula to  $\text{CH}_{1.554}\text{N}_{0.006}\text{O}_{0.824}$  (excluding  $\text{H}_2\text{O}$ ), with given 8.64% w/w humidity and 2.41% w/w ash

(LHV=16.19 MJ/kg, dry ash-free basis). Several substances available in HYSYS component database were tested for this purpose. The candidate molecules were selected considering their LHV value, allowing representation of biomass, lignite and coal.

The mix is represented by a minimum number of components that satisfies the given reduced chemical formula and meets the following original set of heuristics: {H1} a sugar compound should be the base component, as it presents the closest proportions of chemical elements; {H2} a hydrocarbon of conjugated aromatic rings may be included to increase the element ratios C/H and C/O; {H3} an oxygenated compound of low hydrogen content should be included to balance C/H and C/O ratios; {H4} a nitrogen-containing cyclic molecule should be included and cyclic molecules are desirable to increase the calorific value of the mixture; {H5} molecular weights should be as high as possible to mimic a biomolecule.

For each trial combination of selected model compounds, a set of linear equations were algebraically solved to determine the composition that matches the biomass overall reduced formula. Then, the compositional model of the biomass is validated against the obtained LHV [29]. Following the given guidelines, 20 combinations were tested. Only the mixture showing the best LHV agreement is reported.

Milling power requirement of corncob gridding to produce small particles is not included in the analysis, as it is supposed to be performed by biomass suppliers to improve storage and transportation efficiencies. Additionally, since the three evaluated processes require small sized particles, the gridding operation does not discriminate the alternatives, being excluded from the analysis.

Gasification is simulated with HYSYS Gibbs reactor model, neglecting generation of tar compounds [39], so that syngas production is estimated at its thermodynamic limit. Conversely, since fast pyrolysis products are essentially dependent on kinetic control of chemical reactions, the yields are guided by the experimental results of Zhang et al. [29], which reported different bio-oil compositions for various fluidizing gases, with the assumed product yields presented in Table 8.6. The bio-oil fraction is modelled with composition shown in Table 8.7 using model components for representing each group of substances in accordance with the main compounds obtained by Zhang et al. [29].

**Table 8.6.** Biomass pyrolysis yields (ash-free).

Item	Yield (%), mass-basis
Gas	19.00
H <sub>2</sub>	0.112
CO	6.290
CO <sub>2</sub>	11.834
CH <sub>4</sub>	0.763
Biochar	26.90
Bio-oil	31.60
Water	22.50

**Table 8.7.** Assumed organic composition of bio-oil produced by fast pyrolysis.

Chemical Group	Model Component	Chemical Formula	Mass Fraction
Acids	Acetic acid	C <sub>2</sub> H <sub>4</sub> O <sub>2</sub>	0.152
Alcohols	2-Furanmethanol	C <sub>5</sub> H <sub>6</sub> O <sub>2</sub>	0.034
Aldehydes	Furfural	C <sub>5</sub> H <sub>4</sub> O <sub>2</sub>	0.079
Esters	1,2-Ethanediol diacetate	C <sub>6</sub> H <sub>10</sub> O <sub>4</sub>	0.041
Ethers	Methyl-phenyl ether	C <sub>7</sub> H <sub>8</sub> O	0.025
Ketones	Hydroxyacetone	C <sub>3</sub> H <sub>6</sub> O <sub>2</sub>	0.172
N-containing	2-Pyrrolidone	C <sub>4</sub> H <sub>7</sub> NO	0.033
Phenols	1,2-Benzenediol	C <sub>6</sub> H <sub>6</sub> O <sub>2</sub>	0.285
Sugars	Levoglucosan <sup>a</sup>	C <sub>6</sub> H <sub>10</sub> O <sub>5</sub>	0.089
Others	2,3-Dihydro-benzofuran <sup>b</sup>	C <sub>8</sub> H <sub>8</sub> O	0.040
	Water	H <sub>2</sub> O	0.050

<sup>a</sup> Levoglucosan (C<sub>6</sub>H<sub>10</sub>O<sub>5</sub>) is simulated cloning glucose properties

<sup>b</sup> 2,3-Dihydro-benzofuran (C<sub>8</sub>H<sub>8</sub>O) is simulated cloning acetophenone properties

### 8.2.3. Economic Assumptions

The construction site is assumed to be located in the corn belt of the USA, with centralized units for processing corncobs transported from several suppliers. The method of Turton et al. [40] is employed for economic analysis of alternatives, with Fixed Capital Investment (*FCI*) estimated from equipment sizing accordingly to Campbell [41]. The Chemical Engineering Plant Cost Index (*CEPCI*) is used to update equipment costs, using 2017 as reference year (*CEPCI*=567.5). Premises for economic analysis are summarized in Table 8.8. Project lifetime of 23 years is assumed, considering 20 years of operation (as practiced for most chemical plants) after 03 years of construction, which provides the basis for comparison of the Net Present Value (*NPV*) of alternatives. *NPV* results for a shorter project lifetime of 10 years are also discussed.

**Table 8.8.** Economic premises for estimating capital investment and manufacturing cost (base scenario).

Item	Type	Value	Unit
Biomass	Raw material	50	US\$/t
Electricity	Product	0.1087 <sup>a</sup>	US\$/kWh
Methanol	Product	400	US\$/t
Bio-oil	Product	18	US\$/GJ
Biochar	Product	20	US\$/t
Cooling-water	Utilities	0.016	US\$/t
Demineralized water	Utilities	0.793	US\$/t
Monoethanolamine	Utilities	1500	US\$/t
Methanol catalyst	Utilities	200	US\$/kg
Catalyst lifetime	Parameter	05	years
Construction years	Parameter	03	years
Project lifetime	Parameter	23	years
Annual interest rate	Parameter	10	%
Taxation rate	Parameter	34	%

<sup>a</sup> EIA, U.S. Energy Information Administration, Electric Power Monthly, available on: [https://www.eia.gov/electricity/monthly/epm\\_table\\_grapher.php?t=epmt\\_5\\_6\\_a](https://www.eia.gov/electricity/monthly/epm_table_grapher.php?t=epmt_5_6_a)

The biomass purchase price is based on Maung and Gustafson [42], which report an existent commercial contract with corncob costing ≈US\$50/t. Bio-oil base price is assumed at US\$18/GJ (≈US\$2.16 /gasoline-gallon-equivalent) [43]. Due to high uncertainty of bio-oil price, a sensitivity analysis is performed evaluating its impact on economic performance. Biochar product is priced at US\$20/t in accordance with Brown et al. [44]. All raw materials and product prices are assumed at factory gate.

For comparison of economic performances, this work proposes a metric composed by the *NPV* of alternatives at the end of project lifetime (23 years) – the Relative *NPV* (*NPVREL*) – defined in Eq. (8.2), where superscripts *GASIF*, *PYROL* and *COMB* designate the three evaluated processes.

$$NPVREL = \frac{NPV^{GASIF} - NPV^{PYROL}}{NPV^{COMB}} \quad (8.2)$$

The composite index allows building maps in the space of product prices, depicting regions of dominance of the technologies, where, for positive  $NPV^{COMB}$ , a positive *NPVREL* points to superior performance of *GASIF* over *PYROL*.

### 8.3. Results and Discussion

Sec. 8.3.1 firstly presents results of biomass characterization, while process simulation results comparing the three biomass conversion alternatives are presented and discussed in Sec. 8.3.2; details concerning economic analyses are addressed in Sec. 8.3.3.

#### 8.3.1. Biomass Characterization

One of the main problems when studying biomass feedstock is the requirement of proper characterization, preferably on the basis of few lumped components [34]. In this study, although not shown, several combinations of model components were investigated to reproduce the experimental elemental composition reported by Zhang et al [29]. Validation was performed by comparing the calculated against the experimental biomass LHV [29]. The resulting compositional model with the exact values of the targeted reduced formula ( $\text{CH}_{1.554}\text{N}_{0.006}\text{O}_{0.824}$ ) and best agreement with corncob LHV (15.79 MJ/kg, dry ash-free basis, exhibiting -2.46% deviation) is presented in Table 8.9, and is used to simulate the three alternative routes (GASIF, PYROL and COMB).

**Table 8.9.** Biomass compositional model results (ash-free).

Model Compounds	Chemical Formula	Mass Fraction
Anthracene	$\text{C}_{14}\text{H}_{10}$	0.0264
Maleic anhydride	$\text{C}_4\text{H}_2\text{O}_3$	0.1252
Pyridazine	$\text{C}_4\text{H}_4\text{N}_2$	0.0088
Sucrose	$\text{C}_{12}\text{H}_{22}\text{O}_{11}$	0.7532
Water	$\text{H}_2\text{O}$	0.0864

#### 8.3.2. Energy Analysis

Table 8.10 displays the main simulation results with product flowrates and utilities demands. GASIF shows biomass-to-methanol conversion of 0.3755 kg methanol / kg biomass, corresponding to 53.14% recovery of biomass heating value ( $\%EnergyOut$ , based on LHVs of methanol and biomass), while exporting 3.72 MW of surplus electricity. COMB presents advantage of efficient transportation of biomass energy by transmission lines producing 114.10 MW (Table 8.10) of electricity with net efficiency of 30.2%LHV. Despite of its simplicity, by including the makeup water need to operate a semi-closed cooling-tower system, this alternative has the highest consumption of water (271.0 t/h) due to the high heat duty of the Rankine vacuum condenser.

The bio-oil production from PYROL (28.71 t/h) shows 38.4% for %EnergyOut, based on  $LHV_{\text{Bio-oil}}=18.22$  MJ/kg. Despite having the steam turbine of lowest capacity among the process alternatives, as this process has only pumps and compressors of low power consumption (Table 8.10), it exports more electricity than GASIF (7.85 MW). PYROL is also the process of lowest water consumption (64.3 t/h). Reduced machinery use in PYROL should also imply in increased competitiveness against GASIF and COMB as process scale is reduced, due to typically lower efficiency of small-sized equipment.

In mass ash-free basis, the fast pyrolysis biochar has elemental composition of 65.77%C, 5.03%H, 0.51%N, 28.69%O ( $\text{CH}_{0.911}\text{N}_{0.006}\text{O}_{0.327}$ ), being in the composition range of lignite when plotted in a Van Krevelen (C-H-O) diagram [45], with the ash content being 8.41%w. For the purpose of estimating the biochar LHV, the same model components employed to represent biomass are used, with composition fitted to meet biochar chemical formula, resulting in  $LHV_{\text{Biochar}}=24.75$  MJ/kg (ash-free). Fig. 8.5 presents a comparison of energy densities in volume basis of biomass and products.

**Table 8.10.** Main simulation results.

Item	Type	GASIF	COMB	PYROL	Unit
Biomass feed <sup>a</sup>	Raw material	96.81	96.81	96.81	t/h
Biomass LHV		377.8	377.8	377.8	MW
Methanol production	Product	36.35	-	-	t/h
Methanol purity		99.85	-	-	% w/w
Methanol LHV		200.8	-	-	MW
%EnergyOut		53.14	-	-	%
Bio-oil production	Product	-	-	28.71	t/h
Bio-oil purity		-	-	14.2	% w/w H <sub>2</sub> O
Bio-oil LHV		-	-	145.2	MW
%EnergyOut		-	-	38.4	%
Biochar production <sup>a</sup>	Product	-	-	24.34	t/h
Biochar LHV		-	-	153.3	MW
%EnergyOut		-	-	40.6	%
Electricity exported	Product	3.72	114.10	7.85	MW
Power generation		18.52	116.66	8.35	MW
Power demand		14.80	2.57	0.51	MW
CO <sub>2</sub> -rich gas production	Byproduct	31.54	-	-	t/h
CO <sub>2</sub> purity		98.2	-	-	% w/w
Water consumption <sup>b</sup>	Utility	162.3	271.0	64.3	t/h
MEA consumption	Utility	2.45	-	-	kg/h
Catalyst load <sup>c</sup>	Utility	29.61	-	-	t

<sup>a</sup> Including ash; <sup>b</sup> Both process water and cooling-water make-up; <sup>c</sup> Replacement every 5 years.

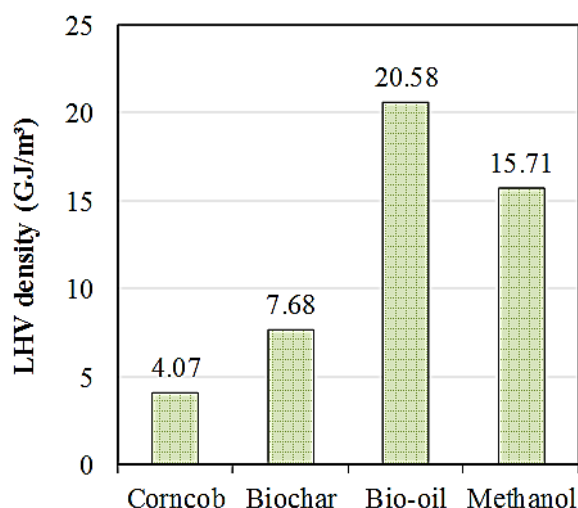


**Fig. 8.5.** Energy densities of grinded biomass and products (LHV basis).

The energy densities signalize possible gains in transportation costs by implementing GASIF and PYROL, where the considered bulk densities are 290 kg/m<sup>3</sup> for grinded corncob [6], 370 kg/m<sup>3</sup> for biochar powder [46], 1130 kg/m<sup>3</sup> for bio-oil and 790 kg/m<sup>3</sup> for methanol (both from simulation, at ≈25°C). Bio-oil presents the highest LHV density (20.58 GJ/m<sup>3</sup>), providing densification of biomass energy (4.07 GJ/m<sup>3</sup>) and biochar production (7.68 GJ/m<sup>3</sup>). With these products, PYROL reduces 72.7% of the original biomass volume. GASIF allows 86.2% of volumetric reduction, with extra advantage of producing a single stable liquid product already in commercial purity, favoring transportation and storage logistics, but with reduced biomass energy recovery (*%EnergyOut*, Table 8.10). On the other hand, COMB eliminates the need for mass transportation but emits to the atmosphere the totality of the corncob carbon as CO<sub>2</sub>. Fig. 8.6 depicts, for each thermochemical alternative, the destination distribution of corncob carbon among products.

While COMB has 100% of corncob carbon being emitted in useless flue gas, GASIF produces 31.54 t/h of CO<sub>2</sub>-rich gas (95.72%CO<sub>2</sub>, 4.17%H<sub>2</sub>O, 0.08%H<sub>2</sub>, 0.03%CO in molar basis) that is emitted to the atmosphere. Should corn agricultural life-cycle impacts be allocated in the use of both grains and cobs [47], CO<sub>2</sub>-rich gas could be sent to BECCS or industrial consumer, after proper conditioning (compression, dehydration and purification, if necessary), rendering GASIF nearly carbon-neutral. In GASIF, CO<sub>2</sub>-rich gas byproduct carries 22.0% of corncob carbon, while methanol recovers 35.4%, with the remaining 42.6% being emitted through flue gas, totaling 90.9 t/h of emitted CO<sub>2</sub> (64.6%).

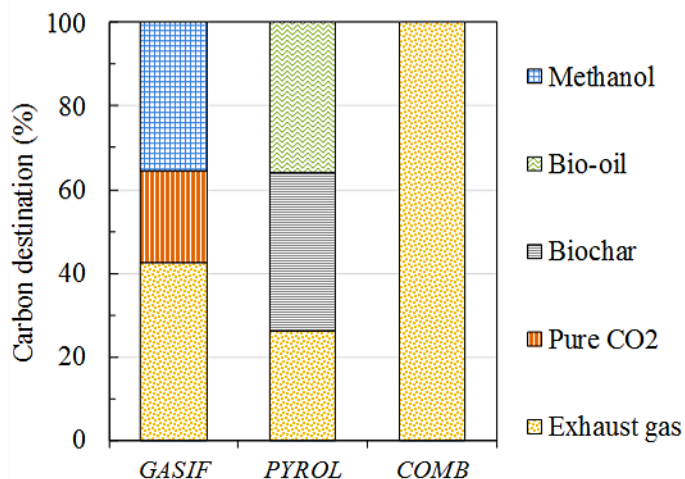


**Fig. 8.6.** Corncob carbon destination among products in each thermochemical process.

The bio-oil exported in PYROL carries 35.7% of corncob carbon, which is very similar to the carbon recovered as methanol in GASIF. In PYROL, biochar takes a larger share of the carbon input (38.0%), with the remaining 26.3% being emitted in flue gas. These aspects indicate that besides presenting higher energy recovery (Table 8.10), PYROL has superior performance concerning the utilization of biomass carbon (Fig. 8.6).

### 8.3.3. Economic Assessment

The detailed comparison of fixed capital investment (*FCI*) of process alternatives is presented in Fig. 8.7, discriminated by equipment types, with biomass converters showing the largest *FCI* share. PYROL has the lowest *FCI*, followed by COMB and GASIF, resulting from employing fewer process machines, with low power consumption, and much smaller reactors for biomass conversion.

GASIF, on the other hand, requires installation of a complex plant with two thermochemical converters of relatively large dimensions including extra expenses with CO<sub>2</sub> separation from syngas, and methanol synthesis and purification. Significant contribution from heat exchangers, compressors and pumps stands out in *FCI* of GASIF (Fig. 8.7) mainly due to the high number of heat exchangers – many of them designed for high pressure application or operation with corrosive fluids (including aqueous MEA).

Additionally, syngas compression requires high pressure ratio and power input (quoted as two motor-driven shafts with five compression stages). In GASIF, biomass thermochemical conversion is  $\approx 1/3$  of  $FCI^{GASIF}$ , while in COMB and PYROL it represents  $\approx 1/2$  of *FCI*.

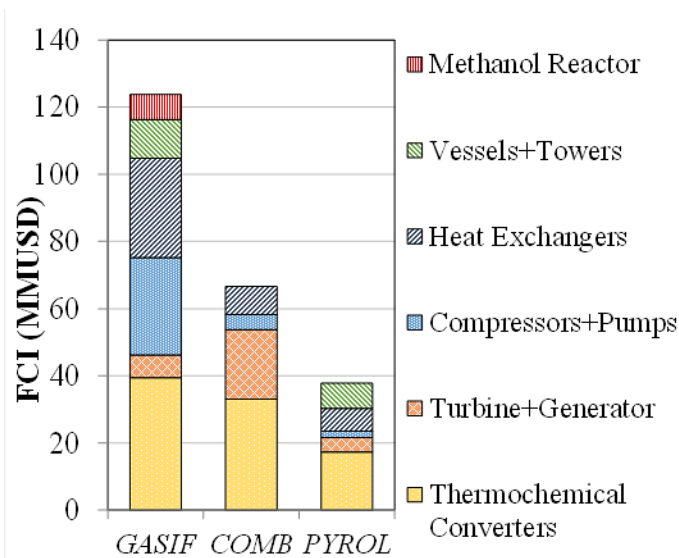


**Fig. 8.7.** Fixed capital investment (*FCI*) of process alternatives.

Table 8.11 displays the economic performance of the process alternatives in the base scenario (refer to Table 8.8). GASIF has best profitability – *NPV* is 118.74 MMUSD in the end of project horizon (20 operational years) – despite presenting the highest *FCI*. COMB is next, with final *NPV* of 110.32 MMUSD. This result is a consequence of GASIF exhibiting the greatest annual profit (*AP*) of 35.29 MMUSD/y against 25.97 MMUSD/y and 21.01 MMUSD/y, of COMB and PYROL, respectively. This is mainly due to its superior revenues (*REV*) from methanol sales, whereas GASIF has *REV* of 119.56 MMUSD/y (20.5% above COMB *REV*) and PYROL has *REV* 13.6% below COMB *REV*.

**Table 8.11.** Economic performance of alternatives in the base scenario.

Item	GASIF	COMB	PYROL	Unit
Fixed Capital Investment ( <i>FCI</i> )	123.76	66.65	37.92	MMUSD
Cost of Manufacturing ( <i>COM</i> )	72.47	63.30	55.81	MMUSD/y
Revenues ( <i>REV</i> )	119.56	99.22	85.69	MMUSD/y
Cost of Raw Material ( <i>CRM</i> )	38.72	38.72	38.72	MMUSD/y
Cost of Utilities ( <i>CUT</i> )	1.61	2.63	0.624	MMUSD/y
Gross Annual Profit ( <i>GAP</i> )	47.09	35.91	29.88	MMUSD/y
Annual Profit ( <i>AP</i> )	35.29	25.97	21.01	MMUSD/y
Payback Time <sup>a</sup>	9	7	6	years
Net Present Value ( <i>NPV</i> )				
10 years of project lifetime	23.08	38.83	44.88	MMUSD
23 years of project lifetime	118.74	110.32	102.62	MMUSD

<sup>a</sup> Including 03 years of construction.

The cost of manufacturing (*COM*) increases from PYROL to COMB and to GASIF. All routes have equal Cost of Raw Material (*CRM*) since the same amount of corncob (the only required raw material) is used for comparison purposes. Cost of Utilities (*CUT*) changes significantly, but with little influence on the final performance, mainly resulting from differences in cooling-water duties and process makeups (MEA and water in GASIF). Expenses with the methanol catalyst are not included in the *CUT* value reported in Table 8.11 but are applied for every 05 years of operation campaign.

In terms of payback time, processes with lowest *FCI* have superior performances, with PYROL being the alternative of best short-term profitability followed by COMB (Table 8.11). This is also shown in Fig. 8.8, which presents *NPV* profiles of GASIF, COMB and PYROL for 23 years of project lifetime, in the base scenario. The initial sequences of bars express the construction years, where GASIF has the lowest *NPVs* due to its higher *FCI*. PYROL starts to present positive *NPV* at the 6<sup>th</sup> year of project (3<sup>rd</sup> year of operation), while COMB payback occurs one year later and GASIF only at the 9<sup>th</sup> year. Supported by the greater annual profits of COMB and GASIF, Fig. 8.8 shows that  $NPV^{COMB}$  first surpass  $NPV^{PYROL}$  at the 14<sup>th</sup> year, with  $NPV^{GASIF}$  overcoming them 3 years later.

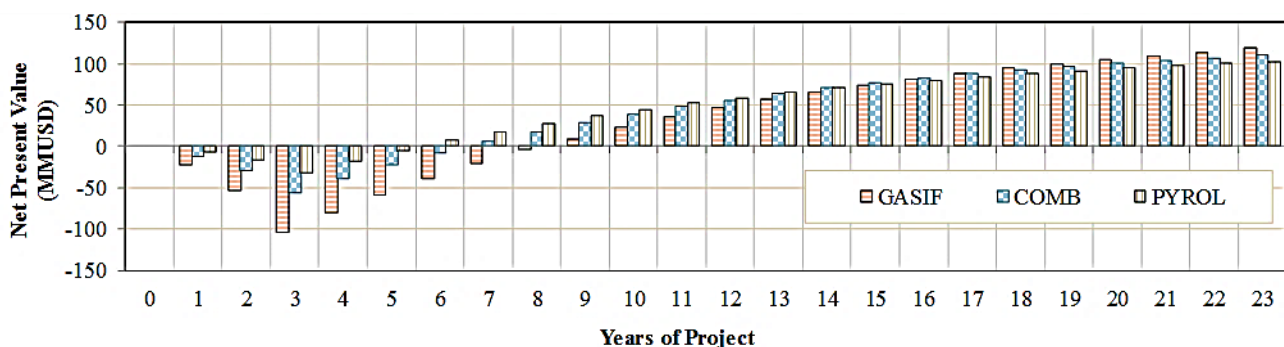


**Fig. 8.8.** Net present value of process alternatives along project lifetime.

In a shorter horizon of 10 years, Table 8.11 and Fig. 8.8 show inversely ranked *NPV* compared to project end, expressing midterm dominance of *FCI* (Fig. 8.7) and indicating the instantly best performance of PYROL, 44.88 MMUSD *NPV* after 10 years, against 38.83 and 23.08 MMUSD in COMB and GASIF, respectively. Differently from process revenues, which grow linearly with process scale, capital costs benefit from enlarging process scale – *FCI* growth factor follows approximately a 0.6 power law with the capacity factor [40]. Consequently, processes exhibiting high *FCI* are favored by large scale, and the observed gradual economic advantage of GASIF and COMB over PYROL (Fig. 8.8) would be considerably lowered by reducing process scales. In addition to longer payback being

expected, *COM* would also be impaired to a little extent at reduced scales in accordance with the applied method [40]. It means that the higher *FCI* of GASIF and COMB alternatives could hamper their economic advantage if profits were not sufficiently high. The assumed scale of processing 96.81 t/h of corncob favors the most capital-intensive routes (Fig. 8.7).

Sensitivity analyses on payback time of alternatives are presented in Fig. 8.9 for variable prices of biomass (Fig. 8.9a) and products (Fig. 8.9b).

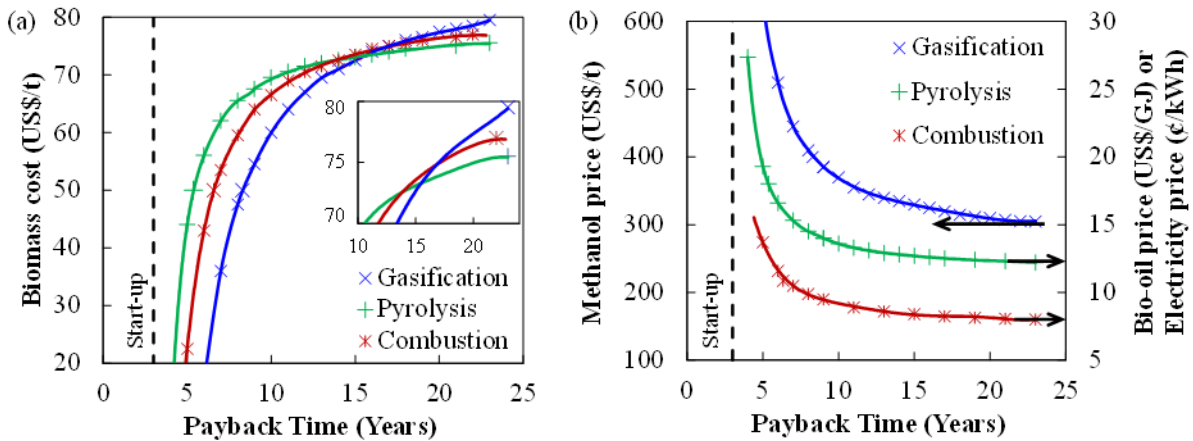


**Fig. 8.9.** Influence of payback time (in years): (a) biomass cost, and (b) product prices.

PYROL (Fig. 8.9a) presents the fastest payback (13 years) as long as biomass cost is lower than  $\approx$  US\$72/t, which may be a plausible value for best profitability and interest of farmers in the US scenario [48]. For higher biomass cost, alternatives with higher revenues (COMB and GASIF) overcome PYROL before reaching a null *NPV* (Fig. 8.9a). Fig. 8.9a shows that the maximum allowable corncob prices yielding positive *NPV* in the end of project lifetime are 79.5, 77.4 and 75.5 US\$/t, respectively for GASIF, COMB and PYROL. Hence, the thermochemical alternatives for corncob processing would be unfeasible in the base scenario if the price of grinded biomass were above US\$80/t. Fig. 8.9b shows that the minimum allowable product prices for attractiveness of GASIF, COMB and PYROL are US\$303/t methanol, US\$80.1/MWh electricity and US\$12.2/GJ bio-oil ( $\approx$ US\$1.47/gasoline-gallon-equivalent).

Table 8.12 shows economic performances and minimum allowable product prices for the investigated routes under three biomass cost scenarios – 30, 50 and US\$70/t, showing that GASIF outperforms the other alternatives, regardless of biomass cost, provided the product prices of the base scenario are constant.

**Table 8.12.** Economic performance of alternatives for different biomass costs.

Item	Low	Base	High	Unit
Biomass Purchase Cost	30	50	70	US\$/t
Net Present Value ( <i>NPV</i> ) <sup>a,b</sup>				
GASIF	199	118	38	MMUS\$
COMB	191	110	30	MMUS\$
PYROL	183	103	22	MMUS\$
Payback Time <sup>b,c</sup>				
GASIF	7	9	14	years
COMB	6	7	12	years
PYROL	5	6	11	years
Minimum Product Price				
GASIF / Methanol	238	303	369	US\$/t
COMB / Electricity	59.2	80.1	101	US\$/MWh
PYROL / Bio-oil	7.63	12.2	16.7	US\$/GJ

<sup>a</sup> *NPV* at the end of 23 years of project; <sup>b</sup> Products at base prices; <sup>c</sup> Including 03 years of construction

Table 8.12 complements Fig. 8.9a with economic analysis results for variable biomass cost. At the high-price of US\$70/t, the final *NPVs* for the evaluated alternatives (*NPV* at the end of the project, including interest rate of 10%) are positive, though lower than *FCI*. Therefore, the mid- to long-term payback of alternatives show that, although the processes are feasible, their attractiveness is low. On the other hand, biomass at US\$30/t renders very attractive the scenario, allowing low minimum product prices and short-term payback of investments. Such low price may be difficult to attain due to handling, grinding and transporting costs.

Fig. 8.10 displays a comparative sensitivity analysis of profitability for the three routes through the Relative *NPV* (*NPVREL*) defined in Eq. (8.2).

The analysis explores sensitivity to variable product prices at three electricity prices – 87.0 (Fig. 8.10a), 108.7 (Fig. 8.10b) and 130.0 US\$/MWh (Fig. 8.10c) – indicating regions of dominant performance of the alternatives in the plane bio-oil versus methanol prices. Positive values mean GASIF outperforming PYROL. The frontiers of COMB dominance region are determined by product prices giving the same final *NPV* (23 years of project). A circle is drawn to indicate performance at methanol and bio-oil base prices (US\$400/t methanol and US\$18/GJ bio-oil), highlighting the movement of the profitability frontier with electricity price. Figs. 8.9b, 8.10a and 8.10c are complementary to each other regarding the economic performance of alternatives.

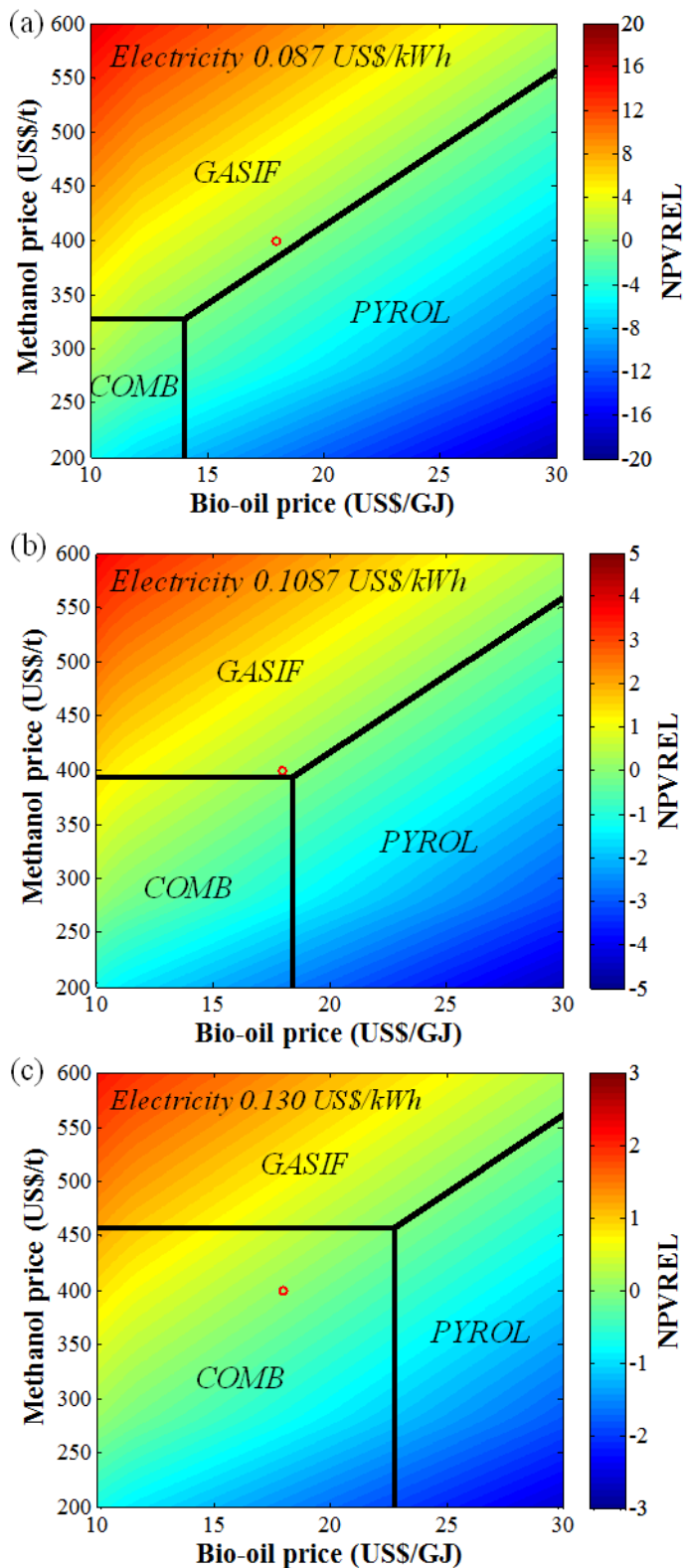


**Fig. 8.10.** Relative net present value ( $NPVREL$ ) for variable product prices and indication of the most profitable process alternative in different energy scenarios: (a) low-priced electricity at US\$87/MWh (-20%); (b) base price of US\$108.7/MWh; and (c) high-priced electricity at US\$130/MWh (+20%). The circle indicates performance with methanol and bio-oil base prices, highlighting the movement of the profitability frontier with electricity price ( $GASIF$ =Gasification;  $COMB$ =Combustion;  $PYROL$ =Pyrolysis).

Fig. 8.10a presents a relatively small region of COMB route, far from the base point circle, with GASIF unveiling best profitability since, in such scenario, equal *NPVs* are achieved with US\$327/t methanol and US\$14.0/GJ bio-oil. In Fig. 8.10b (electricity base price), COMB zone approaches the base scenario circle – also located in GASIF region – indicating proximity of *NPVs*, which equalizes at US\$393/t methanol and US\$18.4/GJ bio-oil. Only in Fig. 8.10c COMB clearly outperforms GASIF and PYROL as their frontiers move to US\$458/t methanol and US\$22.8/GJ bio-oil.

Despite revealing best *NPVs* at the base scenario, GASIF may be vulnerable to product price fluctuation, since methanol price – considered at US\$400/t, 30% above the minimum (Fig. 8.9b) – typically ranges from 200 to 500 US\$/t with high volatility. Besides no longer being the alternative of highest *NPV* for methanol prices below ≈US\$350 (Fig. 8.10), fluctuations below US\$305/t methanol could hamper the investment payback (Fig. 8.9b). However, GASIF profitability can be enhanced through monetization (e.g. BECCS with enhanced oil recovery or CO<sub>2</sub> conversion to chemicals) of the CO<sub>2</sub>-rich gas obtained from syngas upgrading, after appropriate conditioning. For instance, if CO<sub>2</sub>-rich gas is monetized at only US\$10/t, GASIF remains economically feasible even with methanol at US\$288/t.

With less price volatility, as long as the average electricity price remains above US\$87/MWh, COMB is the safest investment, besides the lowest process complexity among the investigated alternatives. Furthermore, COMB avoids transportation and storage costs, while being the most advantageous above 108.7/MWh (Fig. 8.10), presenting mid-term payback and great profitability potential (Table 8.11). Compared to GASIF, COMB has also the advantage of much better flexibility for plant start-up and shutdown, with reduced associated expenses.

PYROL, besides presenting the lowest payback time (Fig. 8.9) due to low *FCI* (Fig. 8.7), reveals good potential of *NPV* competitiveness (Fig. 8.10), but bio-oil price above US\$18/GJ is necessary to overcome GASIF performance. For instance, sale of bio-oil to upgrading refineries in the US scenario makes the end-user price for home heating uncompetitive to replace fuel oil #2, currently priced at about US\$10.5/GJ (≈US\$2/gal) for resellers purchase. Even considering that upgraded bio-oil could be blended with commercial fuel oils, to minimize the impact on wholesale price, PYROL should receive biomass at reduced cost. In this sense, Table 8.12 reveals an attractive minimum allowable bio-oil price of US\$7.6/GJ for biomass costing US\$30/t, but, even in this case, the  $NPV^{GASIF}$  should overcome  $NPV^{PYROL}$ .

Biochar sales would hardly contribute to effectively improve  $AP^{PYROL}$  since it has small participation on  $REV^{PYROL}$ , so that it would be necessary to duplicate the biochar price (US\$40/t) to make  $NPV^{PYROL}$  higher than  $NPV^{COMB}$ , meaning that PYROL would still be less profitable than GASIF. Contrarily, with bio-oil priced at US\$18/GJ and biochar at US\$20/t it would be necessary to increase the considered interest rate from 10% to 16% to make  $NPV^{PYROL}$  overcome the  $NPV$  of other alternatives assisting its rapid payback due to low  $FCI^{PYROL}$ . Therefore, despite of the highest energy recovery and LHV density of its products, and the lowest  $FCI$ , the economic results at the base scenario indicate PYROL as the least attractive route among the considered alternatives.

#### **8.4. Conclusions for Chapter 8**

In this work, three thermochemical pathways – gasification (GASIF), combustion (COMB) and fast pyrolysis (PYROL) – for corncob transformation into energy products – methanol, electricity and bio-oil – are investigated from a process systems engineering perspective comparing their energy and economic performances.

The energy densification potential of GASIF and PYROL are evaluated in terms of biomass volume reductions of 86.2% and 72.7%, respectively. GASIF has the advantage of producing a single stable liquid product already in commercial purity, favoring transportation and storage logistics, but with reduced energy recovery. Expressed as recovery of biomass LHV in products, GASIF shows 53.14% in methanol, while PYROL presents 38.4% in bio-oil and 40.6% in biochar. COMB has the advantage of total volume reduction and the biomass-fueled power plant presents net efficiency of 30.2%LHV.

From the perspective of destination of corncob carbon, GASIF and PYROL avoid  $CO_2$  emissions by 35.4% and 73.7%, respectively, through chemical storage in its corresponding products. Singularly, in the GASIF process,  $CO_2$ -rich gas (nearly pure  $CO_2$ ) could be recovered as byproduct – from syngas upgrading carrying 22% of carbon feed – though this study adopts venting it to the atmosphere. Should it be dispatched for storage (a BECCS application) or for industrial utilization after appropriate conditioning, emission avoidance of 57.4% could be attained. However, even in such scenario, PYROL presents superior performance concerning the utilization of biomass carbon. Further research might explore the entire upstream and downstream chain to determine the carbon footprint though a full Life Cycle Assessment, as transport stage is not considered.

The economic analysis shows that all process alternatives present positive net present value by the end of project lifetime, as long as the biomass cost is below US\$75.5/t. PYROL is the alternative with fastest payback as it requires the lowest fixed capital investment, though exhibiting the lowest long-term profitability. High bio-oil price above US\$18/t would be necessary to have PYROL outperforming other alternatives. In this sense, GASIF is the most profitable route, though presenting the highest vulnerability to product price volatility. Its profitability is followed by the COMB alternative, which advantageously bears operational and construction simplicity.

## 8.5. References for Chapter 8

- [1] W. Zhang, Automotive fuels from biomass via gasification, *Fuel Process. Technol.* 91 (2010) 866–876. <https://doi.org/10.1016/j.fuproc.2009.07.010>
- [2] E. Johnson, Goodbye to carbon neutral: getting biomass footprints right, *Environ. Impact Assess. Rev.* 29 (2009) 165–168. <https://doi.org/10.1016/j.eiar.2008.11.002>.
- [3] R. Contreras-Lisperguer, E. Batuecas, C. Mayo, R. Díaz, F.J. Pérez, C. Springer, Sustainability assessment of electricity cogeneration from sugarcane bagasse in Jamaica, *J. Clean. Prod.* 200 (2018) 390–401. <https://doi.org/10.1016/j.jclepro.2018.07.322>
- [4] M.O.S. Dias, M. Modesto, A.V. Ensinas, S.A. Nebra, R. Maciel Filho, C.E.V. Rossell, Improving bioethanol production from sugarcane: evaluation of distillation, thermal integration and cogeneration systems, *Energy* 36 (2011) 3691–3703. <https://doi.org/10.1016/j.energy.2010.09.024>
- [5] P. Gallagher, G. Schamel, H. Shapouri, H. Brubaker, The international competitiveness of the U.S. corn-ethanol industry: a comparison with sugar-ethanol processing in Brazil. *Agribus.* 22 (2006) 109–134. <https://doi.org/10.1002/agr.20072>.
- [6] N. Kalyian, R.V. Morey, Densification characteristics of corn cobs, *Fuel Process. Technol.* 91 (2010) 559–565. <https://doi.org/10.1016/j.fuproc.2010.01.001>
- [7] C. Jansen, T. Lübberstedt, Turning maize cobs into a valuable feedstock, *Bioenerg. Res.* 5 (2012) 20–31. <https://doi.org/10.1007/s12155-011-9158-y>
- [8] X. Liu, Y. Zhang, Z. Li, R. Feng, Y. Zhang, Characterization of corncob-derived biochar and pyrolysis kinetics in comparison with corn stalk and sawdust, *Bioresour. Technol.* 170 (2014) 76–82. <https://doi.org/10.1016/j.biortech.2014.07.077>.
- [9] Y. Li, T. Wang, X. Yin, C. Wu, L. Ma, H. Li, Y. Lv, L. Sun, 100 t/a-Scale demonstration of direct dimethyl ether synthesis from corncob-derived syngas, *Renew. Energ.* 35 (2010) 583–587. <https://doi.org/10.1016/j.renene.2009.08.002>
- [10] N.S. Shamsul, S.K. Kamarudin, N.A. Rahman, N.T. Kofli, An overview on the production of bio-methanol as potential renewable energy, *Renew. Sustain. Energ. Rev.* 33 (2014) 578–588. <https://doi.org/10.1016/j.rser.2014.02.024>
- [11] K.T. Malladi, T. Sowlati, Biomass logistics: a review of important features, optimization modeling and the new trends, *Renew. Sustain. Energ. Rev.* 94 (2018) 587–599. <https://doi.org/10.1016/j.rser.2018.06.052>.

- [12] J.S. Tumuluru, C.T. Wright, J.R. Hess, K.L. Kenney, A review of biomass densification systems to develop uniform feedstock commodities for bioenergy application, *Biofuels Bioprod. Bioref.* 5 (2011) 683–707. <https://doi.org/10.1002/bbb.324>.
- [13] J.S. Tumuluru, C.T. Wright, K.L. Kenney, J.R. Hess, A review on biomass densification technologies for energy application, INL/EXT-10-18420, Idaho National Laboratory (INL), Biofuels and Renewable Energy Technologies Department, Energy Systems and Technologies Division, Idaho Falls, Idaho 83415, August 2010. <https://doi.org/10.2172/1016196>
- [14] C.A. García, R. Betancourt, C.A. Cardona, Stand-alone and biorefinery pathways to produce hydrogen through gasification and dark fermentation using *Pinus patula*, *J. Environ. Manag.* 203 (2017) 695–703. <https://doi.org/10.1016/j.jenvman.2016.04.001>
- [15] O. Onay, O.M. Kockar, Slow, fast and flash pyrolysis of rapeseed, *Renew. Energ.* 28 (2003) 2417–2433. [https://doi.org/10.1016/S0960-1481\(03\)00137-X](https://doi.org/10.1016/S0960-1481(03)00137-X).
- [16] Z. Chen, M. Wang, E. Jiang, D. Wang, K. Zhang, Y. Ren, Y. Jiang, Pyrolysis of torrefied biomass, *Trends Biotechnol.* 36 (2018) 1287–1298. <https://doi.org/10.1016/j.tibtech.2018.07.005>.
- [17] A.V. Bridgwater, Review of fast pyrolysis of biomass and product upgrading, *Biomass Bioenerg.* 38 (2012) 68–94. <https://doi.org/10.1016/j.biombioe.2011.01.048>
- [18] P.C. Badger, P. Fransham, Use of mobile fast pyrolysis plants to densify biomass and reduce biomass handling costs – a preliminary assessment, *Biomass Bioenerg.* 30 (2006) 321–325. <https://doi.org/10.1016/j.biombioe.2005.07.011>.
- [19] K. Lazdovica, L. Liepina, V. Kampars, Comparative wheat straw catalytic pyrolysis in the presence of zeolites, Pt/C, and Pd/C by using TGA-FTIR method, *Fuel Process. Technol.* 138 (2015) 645–653. <https://doi.org/10.1016/j.fuproc.2015.07.005>
- [20] M.B. Shemfe, S. Gu, P. Ranganathan, Techno-economic performance analysis of biofuel production and miniature electric power generation from biomass fast pyrolysis and bio-oil upgrading, *Fuel* 143 (2015) 361–372. <http://doi.org/10.1016/j.fuel.2014.11.078>
- [21] M. Gholizadeh, R. Gunawan, X. Hu, S. Kadarwati, R. Westerhof, W. Chaiwat, M. Hasan, C.Z. Li, Importance of hydrogen and bio-oil inlet temperature during the hydrotreatment of bio-oil, *Fuel Process. Technol.* 150 (2016) 132–140. <https://doi.org/10.1016/j.fuproc.2016.05.014>
- [22] T. Yang, L. Shi, R. Li, B. Li, X. Kai, Hydrodeoxygenation of crude bio-oil in situ in the bio-oil aqueous phase with addition of zero-valent aluminum, *Fuel Process. Technol.* 184 (2019) 65–72. <https://doi.org/10.1016/j.fuproc.2018.10.025>
- [23] M. Sharifzadeh, M. Sadeqzadeh, M. Guo, T.N. Borhani, N.V.S.N.M. Konda, M.C. Garcia, L. Wang, J. Hallett, N. Shah, The multi-scale challenges of biomass fast pyrolysis and bio-oil upgrading: review of the state of art and future research directions, *Prog. Energ. Combust. Sci.* 71 (2019) 1–80. <https://doi.org/10.1016/j.pecs.2018.10.006>
- [24] Q. Xiong, Y. Yang, F. Xu, Y. Pan, J. Zhang, K. Hong, G. Lorenzini, S. Wang, Overview of computational fluid dynamics simulation of reactor-scale biomass pyrolysis, *ACS Sustain. Chem. Eng.* 5 (2017) 2783–2798. <https://doi.org/10.1021/acssuschemeng.6b02634>
- [25] Q. Xiong, F. Xu, Y. Pan, Y. Yang, Z. Gao, S. Shu, K. Hong, F. Bertrand, J. Chaouki, Major trends and roadblocks in CFD-aided process intensification of biomass pyrolysis, *Chem. Eng. Process.* 127 (2018) 206–212. <https://doi.org/10.1016/j.cep.2018.04.005>

- [26] F. Trippe, M. Fröhling, F. Schultmann, R. Stahl, E. Henrich, Techno-economic analysis of fast pyrolysis as a process step within biomass-to-liquid fuel production, *Waste Biomass Valor.* 1 (2010) 415–430. <https://doi.org/10.1007/s12649-010-9039-1>
- [27] H. Zhang, R. Xiao, H. Huang, G. Xiao, Comparison of non-catalytic and catalytic fast pyrolysis of corncob in a fluidized bed reactor, *Bioresour. Technol.* 100 (2009) 1428–1434. <https://doi.org/10.1016/j.biortech.2008.08.031>
- [28] H. Zhang, R. Xiao, D. Wang, Z. Zhong, M. Song, Q. Pan, G. He, Catalytic fast pyrolysis of biomass in a fluidized bed with fresh and spent fluidized catalytic cracking (FCC) catalysts, *Energ. Fuels* 23 (2009) 6199–6206. <https://doi.org/10.1021/ef900720m>
- [29] H. Zhang, R. Xiao, D. Wang, G. He, S. Shao, J. Zhang, Z. Zhong, Biomass fast pyrolysis in a fluidized bed reactor under N<sub>2</sub>, CO<sub>2</sub>, CO, CH<sub>4</sub> and H<sub>2</sub> atmospheres, *Bioresour. Technol.* 102 (2011) 4258–4264. <https://doi.org/10.1016/j.biortech.2010.12.075>
- [30] P. Basu, *Biomass Gasification, Pyrolysis, and Torrefaction – Practical Design and Theory*, second ed., Elsevier, San Diego, 2013.
- [31] S. Amin, Review on biofuel oil and gas production processes from microalgae, *Energ. Convers. Manag.* 50 (2009) 1834–1840. <https://doi.org/10.1016/j.enconman.2009.03.001>.
- [32] H. Boerrigter, R. Rauch, Review of applications of gases from biomass gasification, *ECN Research*, ECN-RX--06-066 (2006). <https://www.ecn.nl/publicaties/PdfFetch.aspx?nr=ECN-RX--06-066>.
- [33] M.H. Rafiq, H.A. Jakobsen, R. Schmid, J.E. Hustad, Experimental studies and modeling of a fixed bed reactor for Fischer–Tropsch synthesis using biosyngas, *Fuel Process. Technol.* 92 (2011) 893–907. <https://doi.org/10.1016/j.fuproc.2010.12.008>.
- [34] F. Manenti, F. Adani, F. Rossi, G. Bozzano, C. Pirola, First-principles models and sensitivity analysis for the lignocellulosic biomass-to-methanol conversion process, *Comput. Chem. Eng.* 84 (2016) 558–567. <https://doi.org/10.1016/j.compchemeng.2015.05.012>
- [35] R.P. Anex, A. Aden, F.K. Kazi, J. Fortman, R.M. Swanson, M.M. Wright, J.A. Satrio, R.C. Brown, D.E. Daugaard, A. Platon, G. Kothandaraman, D.D. Hsu, A. Dutta, Techno-economic comparison of biomass-to-transportation fuels via pyrolysis, gasification, and biochemical pathways, *Fuel* 89 (2010) S29–S35. <https://doi.org/10.1016/j.fuel.2010.07.015>
- [36] X. Zhao, T.R. Brown, W.E. Tyner, Stochastic techno-economic evaluation of cellulosic biofuel pathways, *Bioresour. Technol.* 198 (2015) 755–763. <https://doi.org/10.1016/j.biortech.2015.09.056>
- [37] T.R. Brown, A techno-economic review of thermochemical cellulosic biofuel pathways, *Bioresour. Technol.* 178 (2015) 166–176. <https://doi.org/10.1016/j.biortech.2014.09.053>
- [38] K. Hakouk, M. Klotz, E. Di Geronimo, V. Ranieri, J.A.Z. Pieterse, G. Aranda-Almansa, A.M. Steele, S. Thorpe, Implementation of novel ice-templated materials for conversion of tars from gasification product gas, *Fuel Process. Technol.* 181 (2018) 340–351. <https://doi.org/10.1016/j.fuproc.2018.10.009>
- [39] M.A. Adnan, Q. Xiong, A. Hidayat, M.M. Hossain, Gasification performance of *Spirulina* microalgae – a thermodynamic study with tar formation, *Fuel* 241 (2019) 372–381. <https://doi.org/10.1016/j.fuel.2018.12.061>
- [40] R. Turton, R.C. Bailie, W.B. Whiting, J.A. Shaeiwitz, D. Bhattacharya, *Analysis, Synthesis, and Design of Chemical Processes*, fourth ed., Prentice Hall, New Jersey, 2012.

- [41] J.M. Campbell, Gas Conditioning and Processing, v. 2: The Equipment Modules, seventh ed., Campbell Petroleum Series, Norman/Oklahoma, 1984.
- [42] T.A. Maung, C.R. Gustafson, The viability of harvesting corn cobs and stover for biofuel production in North Dakota, Proceedings of Agricultural & Applied Economics Association's 2011 AAEA & NAREA Joint Annual Meeting, Pittsburgh, Pennsylvania, July 24-26, 2011.
- [43] M.M. Wright, J.A. Satrio, R.C. Brown, D.E. Daugaard, D.D. Hsu, Techno-economic analysis of biomass fast pyrolysis to transportation fuels, Technical Report, NREL/TP-6A20-46586, November 2010.
- [44] T.R. Brown, Y. Zhang, G. Hu, R.C. Brown, Techno-economic analysis of biobased chemicals production via integrated catalytic processing, *Biofuels Bioprod. Bioref.* 6 (2012) 73–87. <https://doi.org/10.1002/bbb.344>
- [45] J. Poudel, S. Karki, S.C. Oh, Valorization of waste wood as a solid fuel by torrefaction, *Energies* 11 (2018) 1641 <https://doi.org/10.3390/en11071641>
- [46] I.M. Lima, A.A. Boateng, K.T. Klasson, Physicochemical and adsorptive properties of fast-pyrolysis bio-chars and their steam activated counterparts, *J. Chem. Technol. Biotechnol.* 85 (2010) 1515–1521. <https://doi.org/10.1002/jctb.2461>
- [47] R. Frischknecht, Allocation in life cycle inventory analysis for joint production, *Int. J. Life Cycle Assess.* 5 (2000) 85–95. <https://doi.org/10.1007/BF02979729>.
- [48] M.J. Erickson, C. Dobbins, W.E. Tyner, The economics of harvesting corn cobs for energy, *Plant Manag. Netw.* 10 (2011). <https://doi.org/10.1094/CM-2011-0324-02-RS>

## 9. CONCLUSIONS

Technical, economic and environmental assessments were conducted to develop and analyze several new technological alternatives to meet the current challenges associated with carbon reduction in electricity generation and CO<sub>2</sub>-rich NG purification. Three lines of research are addressed: {R1} oxy-combustion CO<sub>2</sub> capture, with emphasis on oxygen production via cryogenic air separation and air pre-purification for oxygen production; {R2} offshore processing of CO<sub>2</sub>-rich NG; and {R3} CO<sub>2</sub> utilization and biorefineries, investigating pathways for carbon reduction using renewable resources: microalgae (due to its high photosynthesis efficiency) and corncobs (a common large-scale agricultural residue). Despite of common objective and several interface topics connecting lines {R1}, {R2} and {R3}, proposed solutions among these research lines are not supposed to be compared as different scopes and working scenarios are applied.

In the research line {R1}, a new cryogenic TVR distillation process was developed as a new ASU concept, the so-called TVR-2REB, which power requirements to produce low-purity (95%mol) and high-purity (99.5%mol) GOX are significantly lower than current state-of-the-art ASUs. The process configuration of TVR-2REB ASU involves a single atmospheric cryogenic top vapor recompression distillation column with two reboilers: the habitual bottom reboiler and an additional intermediate reboiler. This intermediate reboiler is heated with compressed GAN from the column top, while saturated compressed air feed heats the bottom reboiler. The mentioned p-GAN is a fraction of the atmospheric column top vapor, which is pressurized via cryogenic compression. The cryogenic distillation column is fed with LAIR, produced by latent heat exchange boiling O<sub>2</sub> in the column bottom reboiler. It was also demonstrated that compressing GAN cryogenically entails less power consumption than compressing it at ambient temperature, despite increasing efforts for Cold-Box refrigeration.

The new proposed TVR-2REB ASU was coupled to a zero-emission oxyfuel NGCC with CO<sub>2</sub>-EOR – Ox-NGCC-EOR, as a Gas-To-Wire plant – which was investigated considering different economic scenarios of carbon taxation. For a project lifetime of 30 years of operation, any carbon tax above 13.5 USD/tCO<sub>2</sub> would guarantee economic superiority of the proposed Ox-NGCC-EOR with TVR-2REB ASU over conventional CO<sub>2</sub>-emitting air-fed NGCC due to increased oil revenues from EOR and zero taxation costs.

Also in the research line {R1}, a new concept of air pre-purification unit (PPU) for cryogenic fractionation was developed, prescribing the use of a supersonic separator (SS) performing

bulk water removal followed by finishing adsorption to remove CO<sub>2</sub>, residual H<sub>2</sub>O and further minor contaminants. Two embodiments of such invention – SS-TSA and SS-TSA-HI, the latter a SS-TSA variant lowering heating costs via compression heat recovery – were technically and economically compared to conventional TSA-based PPU (FULL-TSA). Insertion of SS significantly reduces utilities consumption, particularly low-pressure steam and N<sub>2</sub> for regeneration. Both new PPUs outperformed FULL-TSA for supplying air to Cold-Box thanks to drastic reduction of air humidity via SS, leaving only a small dehydration load to be executed by smaller finishing TSA units in SS-TSA and SS-TSA-HI. Although this substantial reduction of bed size and regeneration heat consumption is followed by slightly larger air compressor (MAC) to offset small pressure drop in SS, the two new PPUs outperform FULL-TSA in terms of both operational costs and capital investment. The SS produces >98% water removal from raw air with high >98% pressure-recovery, entailing low exergy destruction rate while abates ≈70% of the exergy loss of TSA-System, thus ballasting SS-TSA/SS-TSA-HI superiority also in terms of exergy preservation as shown in Chapter 4, where air pre-purification alternatives SS-TSA and SS-TSA-HI with supersonic separators are proven to have greater exergy efficiency than the conventional FULL-TSA route.

It is worth of mention that it was only possible to explore such new technologies backed by SS utilization because a thermodynamically rigorous, equilibrium-based, SS multiphase simulation model and multiphase (and multi-reactive) sound speed determination tool were developed as reliable and efficient HYSYS Unit Operation Extensions – SS-UOE\* and PEC-UOE† – enabling to compute phase-change effects and multiphase sound speed in SS units for any kind of process with any kind of equation-of-state.

In the research line {R2}, all alternatives comprise a large-scale gas-oil floating-hub contemplating oil/gas/water separation, raw gas dehydration, hydrocarbon dew-point adjustment (HCDPA), CO<sub>2</sub> removal for fuel gas production (availed to meet rig power demands), and EOR fluid compression/pumping. The gas-hub processes a huge flow rate (≈50 MMSm<sup>3</sup>/d) of CO<sub>2</sub>-rich raw NG (≈68% mol CO<sub>2</sub>) that is almost totally exported as EOR fluid (with exception of small portion used as fuel gas) for injection in several wells

---

\* Arinelli, L.O.; Trotta, T.A.F.; Teixeira, A.M.; de Medeiros, J.L.; Araújo, O.Q.F. Offshore processing of CO<sub>2</sub> rich natural gas with supersonic separator versus conventional routes. *Journal of Natural Gas Science and Engineering*, 46, 199–221, 2017. <https://doi.org/10.1016/j.jngse.2017.07.010>

† de Medeiros, J.L.; Arinelli, L.O.; Araújo, O.Q.F. Speed sound of multiphase and multi-reactive equilibrium streams: a numerical approach for natural gas applications. *Journal of Natural Gas Science and Engineering*. 46, 222-241, 2017. <https://doi.org/10.1016/j.jngse.2017.08.006>

throughout the field. Alternatives were evaluated through the prism that main gas processing steps should be conducted by SS whenever possible – in simultaneous adjustment of water and hydrocarbon dew-points (1<sup>st</sup> SS unit), and in CO<sub>2</sub> removal (2<sup>nd</sup> SS unit) – and results were compared in terms of oil productions, power demands, CO<sub>2</sub> emissions, and economic performances.

Firstly, the SS-SS alternative was compared to a fully conventional process MS-JT-MP prescribing molecular sieve (MS) TSA for dehydration, Joule-Thompson expansion for HCDPA, and membrane-permeation for CO<sub>2</sub> removal. SS-SS outperforms MS-JT-MP with ≈33% higher net present value and ≈10% lower capital investment, the latter advantage thanks to outstanding investment of MS TSA units for gas dehydration in the assumed process scale, and the former advantage accounting for much greater oil production in SS-SS case, due to recovery of C3+ condensate in the 1<sup>st</sup> SS unit, which is recycled to the primary oil/gas/water high-pressure separator (HPS).

Secondly, ensuring the use of a 1<sup>st</sup> SS unit for performing WDPA+HCDPA, alternatives were compared in three aspects: (i) recycling or not recycling the condensate of the 1<sup>st</sup> SS unit to the HPS; (ii) HPS gas expansion to 1<sup>st</sup> SS unit working pressure by Joule-Thompson valve or turbo-expander; and (iii) CO<sub>2</sub> removal by 2<sup>nd</sup> SS unit or membrane-permeation. Again, the pragmatic SS-SS base case [RC+JT+SS] achieved the best profitability. Despite causing higher gas circulation rate and equipment sizes, recycling condensate is evinced to improve net present value, due to increased oil revenues, besides lowering the H<sub>2</sub>O content of EOR fluid. For CO<sub>2</sub> removal, despite requiring low-temperature refrigeration and more complex process configuration, the 2<sup>nd</sup> SS unit entails both lower capital investment and power requirement compared to membrane-permeation, accounting for extra compression duty of low-pressure CO<sub>2</sub>-rich permeate. Environmentally, the best scheme is the power-saving variant adopting turbo-expander [RC+TX+SS] – which attained the second best profitability by a narrow margin – as it presented the lowest CO<sub>2</sub> emissions and the lowest consumption of Fuel Gas.

In the research line {R3}, two microalgae conversion pathways were investigated: (a) extraction of microalgae oil and biomass gasification for methanol production; and (b) anaerobic digestion for biogas production to power generation or biomethane production.

In case (a), a CCU process consisting of a biorefinery (BRY) arrangement was investigated prescribing microalgae cultivation for biofixation of CO<sub>2</sub> generated by a power plant, with posterior thermochemical conversion by gasification for methanol production, in addition to

extraction of microalga oil. The CO<sub>2</sub> emissions analysis points BRY superiority over competing CCU alternatives for methanol production. Economic analysis results showed that profitability of proposed alternative BRY may be attained with severe carbon taxation policy above 100 USD/t CO<sub>2</sub>. However, technical drawbacks must be overcome, notably concerning the need for footprint reduction in microalgae cultivation and harvesting: even with optimistic premises being applied to evaluate the photobioreactor (PBR) performance, the BRY route would hardly be feasible for practical implementation as total area needed for these steps accounts ≈1000 ha for the scale of a ≈100 MW coal power plant, suggesting that enhancements are required in footprint compactness and volumetric productivity of PBRs.

In case (b), concerning biogas production from microalgae, several alternatives were investigated, covering upstream (pretreatment procedure), midstream (anaerobic digestion pressure) and downstream variant processes (production of biomethane or electricity, with or without CO<sub>2</sub> exportation to EOR). In this case, microalgal biomass suspension was assumed to be purchased from another company, with economic analysis evincing strong dependence in low purchase prices, challenging practical feasibility of such a concept. Results prove biogas upgrading to biomethane as being economically superior to raw biogas use for power generation at assumed base-conditions, but none of the considered processes are feasible with biomass base-price (234 US\$/t dry-basis). The best process alternative among downstream routes is profitable with ≈100 US\$/t but with the leverage of extra revenue from exportation of excess CO<sub>2</sub> to an oil-gas company performing EOR. For biomethane production without such additional revenue, maximum biomass cost for process feasibility is reduced to ≈50 US\$/t. Pressurized anaerobic digestion is not economically advantageous as it is evinced from the perspective of power and heating demands, mainly because of much higher capital investment on pressurized biodigesters overshadowing savings on operational expenses with utilities, thus reflecting on slightly reduced break-even biomass cost.

Also in the research line {R3}, three process alternatives for thermochemical conversion of corncobs were investigated: combustion to electricity, gasification to methanol, and fast pyrolysis to raw bio-oil. All investigated alternatives are economically feasible provided biomass cost is lower than 75.5 US\$/t. The minimum allowable product prices for economic attractiveness of gasification, combustion and pyrolysis routes are 305 US\$/t methanol, 80.1 US\$/MWh electricity and 12.2 US\$/GJ bio-oil. Neglecting product prices volatilities, gasification to methanol is evinced as the most profitable alternative. The combustion route places second in profitability, but presents faster payback than gasification, due to higher

operational and construction simplicity. Fast pyrolysis is the least profitable alternative but has advantage of presenting the fastest investment payback. From environmental perspective, in terms of corncob elemental carbon destination, while combustion returns all carbon to atmosphere, gasification and pyrolysis routes avoid CO<sub>2</sub> emissions through chemical sequestration in their corresponding products by 35.4% and 73.7%, respectively, thus implying in “negative” CO<sub>2</sub> life-cycle emissions, as biomass is availed as primary resource.

At last, the following main statements can be made as final conclusions of this thesis, aiming to propose implementation of new technological alternatives for carbon reduction:

- TVR-2REB ASU is advantageous to be applied for large-scale oxygen production in any working scenario, especially to supply oxy-combustion systems, for attaining the lowest separation power demand;
- SS-TSA and SS-TSA-HI PPU's should be applied, for the best profitability replacing conventional TSA PPU's, to supply pressurized purified air to large-scale cryogenic fractionation plants, being especially indicated to feed power-saving Cold Boxes conceived for oxy-combustion systems;
- The use of sequential SS steps – WDPA+HCDPA and CO<sub>2</sub> removal – for processing huge flow rates of CO<sub>2</sub>-rich NG in remote offshore oil-gas fields is advantageous for the best overall profitability, increasing oil production and also reducing the weight and footprint of gas processing plant;
- In rural areas with extensive corn crops, corncobs should be availed to feed a centralized power station for large-scale electricity generation, as economic feasibility has been proved with medium-term payback of investment, simultaneously addressing waste management and drastic carbon reduction in power generation sector.

Further ASU configurations for oxygen production using TVR distillation should be explored in future works on research line {R1} to improve the performance of power generation systems with oxy-combustion CO<sub>2</sub> capture. For future works on line {R2}, investigation of novel alternatives considering exportation of conditioned gas from the offshore oil-gas field is suggested. Finally, research line {R3} should be continued with the development of other efficient biorefinery concepts using biomass wastes, for the replacement of conventional industrial processes and thermal power stations based on fossil resources, meeting global demand for a desired transition into a renewable energy future.

## APPENDIX A – Bibliographic production

### A1. Research Products

Table A1.1 presents a summary of all research products from lines {R1}-{R3}, showing the corresponding chapters of this thesis and whether personal contributions led to first authorship of these publications.

**Table A1.1.** Summary of bibliographic production derived from the present research.

Research Line	Appendix/ Front Page	Product Type	Thesis Chapter	First Author	Reference Number
{R1} Oxyfuel CO <sub>2</sub> capture	B	Patent application	–	Yes	[1]
	C	Conference paper	–	Yes	[2]
	D	Scientific article	02	Yes	[3]
	E	Patent application	–	Yes	[4]
	F	Conference paper	–	Yes	[5]
	G	Scientific article	–	Yes	[6]
	H	Scientific article	03	Yes	[7]
	I	Conference paper	–	Yes	[8]
	J	Conference paper	–	Yes	[9]
{R2} Offshore CO <sub>2</sub> - rich NG processing	K	Register of softwares	–		[10-14]
	L	Conference paper	–		[15]
	M	Scientific article	05		[16]
	N	Scientific article	05		[17]
{R3} CO <sub>2</sub> utilization and biorefineries	O	Conference paper	–		[18]
	P	Scientific article	06		[19]
	Q	Conference paper	–	Yes	[20]
	R	Scientific article	07	Yes	[21]
	S	Scientific article	08	Yes	[22]
	T	Scientific article	–		[23]

The following products were derived from the research line {R1} of oxyfuel CO<sub>2</sub> capture:

- Patent application on cryogenic air separation (Appendix B) [1];
- Conference paper on cryogenic air separation – Proceedings of LA-SDEWES2018 (Appendix C) [2];
- Scientific article on cryogenic air separation and Gas-To-Wire electricity generation with oxy-combustion CO<sub>2</sub> capture – Energy Conversion and Management (Appendix D) [3];
- Patent application on air pre-purification for cryogenic separation plants (Appendix E) [4];
- Conference paper on energy assessment of novel air pre-purification units for cryogenic air separation plants – Proceeding of the 4<sup>th</sup> Brazilian Congress on CO<sub>2</sub> in the Oil, Gas and Biofuels Industries (Appendix F) [5];

- Scientific article on energy assessment of novel air pre-purification units for cryogenic air separation plants – Materials Science Forum (Appendix G) [6];
- Scientific article on techno-economic assessment of novel air pre-purification units for cryogenic air separation plants – Separation and Purification Technology (Appendix H) [7];
- Conference paper on exergy analysis of air pre-purification units for cryogenic air separation – Proceedings of SDEWES2018 (Appendix I) [8];
- Conference paper on electricity generation in oxyfuel natural gas combined cycle power plant – Proceedings of Rio Oil & Gas 2016 (Appendix J) [9].

The following products were derived from the research line {R2} of CO<sub>2</sub>-rich NG processing:

- Register of softwares for calculation of multiphase and reactive equilibrium sound speed and simulation of supersonic separators (Appendix K) [10-14];
- Conference paper on offshore CO<sub>2</sub>-rich natural gas processing with supersonic separators – Proceedings of LA-SDEWES2018 (Appendix L) [15];
- Scientific article on offshore CO<sub>2</sub>-rich natural gas processing with supersonic separators – Journal of Natural Gas Science and Engineering (Appendix M) [16];
- Scientific article on offshore CO<sub>2</sub>-rich natural gas processing with supersonic separators – Journal of Cleaner Production (Appendix N) [17].

The following products were derived from the research line {R3} of CO<sub>2</sub> utilization and biorefineries:

- Conference paper on CO<sub>2</sub> utilization in microalga-based biorefinery producing methanol – Proceedings of SDEWES2016 (Appendix O) [18];
- Scientific article on CO<sub>2</sub> utilization in microalga-based biorefinery producing methanol – Journal of Environmental Management (Appendix P) [19];
- Conference paper on sustainability analysis of biogas production from microalgae – Proceedings of LA-SDEWES2018 (Appendix Q) [20];
- Scientific article on techno-economic analysis of biogas production from microalgae – Renewable and Sustainable Energy Reviews (Appendix R) [21];
- Scientific article on techno-economic analysis of thermochemical pathways of corncob conversion – Fuel Processing Technology (Appendix S) [22];
- Scientific article on exergy-based sustainability analysis of CO<sub>2</sub> capture and storage or utilization to methanol production – Renewable and Sustainable Energy Reviews (Appendix T) [23].

## **A2. Contributions on co-authorship works**

### *A2.1. Comments to Chapter 5*

Personal contributions to this work are mostly associated with performing jointly with colleagues all steps of techno-economic analysis of process alternatives, which involves simulation of complete flowsheets in Aspen Hysys v8.8, equipment sizing and economic assessment of all alternatives: SS-SS and MS-JT-MP in Case Study 1, and [RC+JT+SS], [RC+TX+SS], [NR+JT+SS] and [RC+JT+MP] in Case Study 2. Participation in artwork production is a further important contribution. The research of Lara Arinelli is responsible for the integrated modeling of SS and MP unit operations in Aspen Hysys, which configures the major challenge of the work.

### *A2.2. Comments to Chapter 6*

Personal contributions to this work are mostly associated with BRY-2 (microalgae biomass thermochemical processing) large flowsheet conception and simulation in Aspen Hysys. This process is designed to be self-sufficient in electricity, heating utilities, water and chemicals, by availing the supply of microalgal biomass, the final product of downstream processing – methanol, which is used as solvent for CO<sub>2</sub> capture from CO<sub>2</sub>-rich synthesis gas – and the purge gas leaving the synthesis loop, which is a H<sub>2</sub>-enriched non-converted syngas used for power generation. A further important contribution is collaboration in discussing the results.

### A3. Covered topics and chapters connections

**Table A3.1.** Overview of main covered topics and connections of Chapters 02-08.

Research Lines		{R1} Oxy-combustion			{R2} CO <sub>2</sub> -rich NG processing	{R3} CO <sub>2</sub> utilization and biorefineries		
Scientific articles		ASU/NGCC	PPU/Econ.	PPU/Exergy	NG/JNGSE+NG/JCLEPRO	Microalga/MeOH	Microalga/Biogas	Corncobs
References		[3]	[7]	–	[16, 17]	[19]	[21]	[22]
Thesis Chapters/ Appendices	Chapter with Contents	02	03	04	05	06	07	08
	Front Page	D	H	–	M, N	P	R	S
	Suppl.Material	U	V	W	X	Y	Z	-
Subject	Power generation	x	x*	x*		x	x	x
	Raw NG/biogas processing				x		x	
Working scenario	Offshore				x			
	Onshore	x	x	x		x	x	x
	Oil and gas field	x			x			
Capture route	Oxy-combustion	x	x*	x*				
	Post-combustion					x	x	
Carbon destination	CO <sub>2</sub> -EOR	x			x		x	
	CO <sub>2</sub> Storage					x		
	CO <sub>2</sub> Utilization					x	x	
Renewables	Microalgae					x	x	
	Agricultural waste							x
Products	Electricity	x					x	x
	Oxygen	x						
	Purified air		x	x				
	Crude oil				x			
	Biomethane						x	
	Methanol					x		x
	Microalgae oil					x		
Fast pyrolysis bio-oil							x	
Processes	Biomass gasification					x		x
	Combined cycle power gen.	x					x	
	Dehydration w/ TEG	x					x	
	Chemical absorption w/ MEA					x	x	x
	Physical absorption w/ MeOH					x		
Temperature swing adsorption		x	x	x				
Unit ops.	Membrane permeation				x			
	Supersonic separator		x	x	x			

\*Although power generation is not addressed in air pre-purification works, this topic is inserted in the context of cryogenic air separation and oxy-combustion CO<sub>2</sub> capture

#### A4. References for Appendix A

- [1] BRIGAGÃO, G. V., MEDEIROS, J. L., ARAÚJO, O. Q. F., inventors; Universidade Federal do Rio de Janeiro, applicant. Processo de destilação criogênica para separação do ar para produção de oxigênio gasoso. BR Patent Application 102016022807-7. Filed in September 30th, 2016.
- [2] BRIGAGÃO, G. V.; DE MEDEIROS, J. L.; ARAÚJO, O. Q. F. Oxy-combustion CO<sub>2</sub> capture for steam power plants: a novel air separation unit for oxygen supply. 1st Latin-American Conference on Sustainable Development of Energy Water and Environment Systems (LA-SDEWES), Rio de Janeiro, 2018.
- [3] BRIGAGÃO, G. V.; DE MEDEIROS, J. L.; ARAÚJO, O. Q. F. A novel cryogenic vapor-recompression air separation unit integrated to oxyfuel combined-cycle gas-to-wire plant with carbon dioxide enhanced oil recovery: energy and economic assessments. *Energy Conversion and Management*, 189, p. 202-214, 2019.
- [4] BRIGAGÃO, G. V., ARINELLI, L. O., DE MEDEIROS, J. L., ARAÚJO, O. Q. F., inventors; Universidade Federal do Rio de Janeiro, applicant. Purificação do ar para fracionamento criogênico com separador supersônico de baixa pressão. BR Patent Application 102017027727-5. Filed in December 21st, 2017.
- [5] BRIGAGÃO, G. V.; ARINELLI, L. O.; DE MEDEIROS, J. L.; ARAÚJO, O. Q. F. CO<sub>2</sub> emission and energy assessments of a novel pre-purification unit for cryogenic air separation using supersonic separator. 4th Brazilian Congress on CO<sub>2</sub> in the Oil, Gas and Biofuels Industries, Rio de Janeiro, 2018.
- [6] BRIGAGÃO, G. V.; ARINELLI, L. O.; DE MEDEIROS, J. L.; ARAÚJO, O. Q. F. CO<sub>2</sub> emission and energy assessments of a novel pre-purification unit for cryogenic air separation using supersonic separator. *Materials Science Forum*, 965, p. 59–67, 2019.
- [7] BRIGAGÃO, G. V., ARINELLI, L. O., DE MEDEIROS, J. L., ARAÚJO, O. Q. F. A new concept of air pre-purification unit for cryogenic separation: low-pressure supersonic separator coupled to finishing adsorption. *Separation and Purification Technology*, 215, p. 173-189, 2019.
- [8] BRIGAGÃO, G. V.; ARINELLI, L. O.; DE MEDEIROS, J. L.; ARAÚJO, O. Q. F. Exergy analysis of a novel air pre-purification unit for cryogenic fractionation based on low-pressure supersonic separator combined with finishing adsorption step. 13th Conference on Sustainable Development of Energy Water and Environment Systems (SDEWES), Palermo, 2018.
- [9] BRIGAGÃO, G. V.; DE MEDEIROS, J. L.; ARAÚJO, O. Q. F. Performance evaluation of an oxyfuel NGCC process for power generation with organic Rankine cycle for offshore application. Rio Oil & Gas Expo and Conference, Rio de Janeiro, 2016.
- [10] ARINELLI, L. O., DE MEDEIROS, J. L., TEIXEIRA, A. M., BRIGAGÃO, G. V., ARAÚJO, O. Q. F., authors; UNIVERSIDADE FEDERAL DO RIO DE

- JANEIRO, applicant. HEPEC (Hysys Extension Phase Equilibrium Sound Speed). Registered software BR 512017000629-6. Brazilian Patent and Trademark Office. Filed in June 20th, 2017.
- [11] ARINELLI, L. O., DE MEDEIROS, J. L., TEIXEIRA, A. M., BRIGAGÃO, G. V., ARAÚJO, O. Q. F., authors; UNIVERSIDADE FEDERAL DO RIO DE JANEIRO, applicant. HEREC (Hysys Extension Reactive Equilibrium Sound Speed (C)). Registered software BR512017000628-8. Brazilian Patent and Trademark Office. Filed in June 20th, 2017.
- [12] ARINELLI, L. O., DE MEDEIROS, J. L., TEIXEIRA, A. M., BRIGAGÃO, G. V., ARAÚJO, O. Q. F., authors; UNIVERSIDADE FEDERAL DO RIO DE JANEIRO, applicant. HESSO (Hysys Extension Supersonic Separator Operation). Registered software BR512017000627-0. Brazilian Patent and Trademark Office. Filed in June 20th, 2017.
- [13] ARINELLI, L. O., WIESBERG, I. L., DE MEDEIROS, J. L., BRIGAGÃO, G. V., TEIXEIRA, A. M., ARAÚJO, O. Q. F., authors; UNIVERSIDADE FEDERAL DO RIO DE JANEIRO, applicant. AMPEC (Aspen Model of Phase Equilibrium Sound Speed (C)). Registered software BR512018001031-8. Brazilian Patent and Trademark Office. Filed in June 26th, 2018.
- [14] ARINELLI, L. O., WIESBERG, I. L., DE MEDEIROS, J. L., BRIGAGÃO, G. V., TEIXEIRA, A. M., ARAÚJO, O. Q. F., authors; UNIVERSIDADE FEDERAL DO RIO DE JANEIRO, applicant. AMSSO (Aspen Model of Supersonic Separator Operation). Registered software BR512018001032-6. Brazilian Patent and Trademark Office. Filed in June 26th, 2018.
- [15] DE MELO, D. C.; ARINELLI, L. O.; TEIXEIRA, A. M.; VICTOR, G.; PASSARELLI, F.; GRAVA, W. M.; DE MEDEIROS, J. L. Technological alternatives for high CO<sub>2</sub> natural gas processing aiming offshore production of gas associated giant oil fields. 1st Latin-American Conference on Sustainable Development of Energy Water and Environment Systems (LA-SDEWES), Rio de Janeiro, 2018.
- [16] ARINELLI, L. O.; DE MEDEIROS, J. L.; DE MELO, D. C.; TEIXEIRA, A. M.; BRIGAGÃO, G. V.; PASSARELLI, F.; GRAVA, W. M.; ARAÚJO, O. Q. F. Carbon capture and high-capacity supercritical fluid processing with supersonic separator: natural gas with ultra-high CO<sub>2</sub> content. *Journal of Natural Gas Science and Engineering*, 66, p. 265-283, 2019.
- [17] DE MELO, D. C.; ARINELLI, L. O.; DE MEDEIROS, J. L.; TEIXEIRA, A. M.; BRIGAGÃO, G. V.; PASSARELLI, F.; GRAVA, W. M.; ARAÚJO, O. Q. F. Supersonic separator for cleaner offshore processing of supercritical fluid with ultra-high carbon dioxide content: economic and environmental evaluation. *Journal of Cleaner Production*, 234, p. 1385-1398, 2019.
- [18] WIESBERG, I. L.; BRIGAGÃO, G. V.; DE MEDEIROS, J. L.; ARAÚJO, O. Q. F. Economic and environmental analysis of a microalgae-based biorefinery

utilizing CO<sub>2</sub> emitted from coal fired power plant. 11th Conference on Sustainable Development of Energy, Water and Environment Systems (SDEWES), Lisbon, 2016.

- [19] WIESBERG, I. L.; BRIGAGÃO, G. V.; DE MEDEIROS, J. L.; ARAÚJO, O. Q. F. Carbon dioxide utilization in a microalga-based biorefinery: efficiency of carbon removal and economic performance under carbon taxation. *Journal of Environmental Management*, 203, p. 988-988, 2017.
- [20] BRIGAGÃO, G. V.; WIESBERG, I. L.; MORTE, I. B. B.; PINTO, J. L.; ARAÚJO, O. Q. F.; DE MEDEIROS, J. L. Sustainability analysis of biomethane from thermo-mechanically pretreated microalgae. 1st Latin-American Conference on Sustainable Development of Energy Water and Environment Systems (LA-SDEWES), Rio de Janeiro, 2018.
- [21] BRIGAGÃO, G. V.; WIESBERG, I. L.; PINTO, J. L.; ARAÚJO, O. Q. F.; DE MEDEIROS, J. L. Upstream and downstream processing of microalgal biogas: emissions, energy and economic performances under carbon taxation. *Renewable and Sustainable Energy Reviews*, 112, p. 508-520, 2019.
- [22] BRIGAGÃO, G. V.; ARAÚJO, O. Q. F.; DE MEDEIROS, J. L.; MIKULCIC, H.; DUIC, N. A techno-economic analysis of thermochemical pathways for corncob-to-energy: fast pyrolysis to bio-oil, gasification to methanol and combustion to electricity. *Fuel Processing Technology*, 193, p. 102-113, 2019.
- [23] WIESBERG, I. L.; BRIGAGÃO, G. V.; DE MEDEIROS, J. L.; ARAÚJO, O. Q. F. Carbon dioxide management via exergy-based sustainability assessment: carbon capture and storage versus conversion to methanol. *Renewable and Sustainable Energy Reviews*, 112, p. 720-732, 2019.

## APPENDIX B – Patent application on cryogenic air separation

BRIGAGÃO, G. V., DE MEDEIROS, J. L., ARAÚJO, O. Q. F., inventors; Universidade Federal do Rio de Janeiro, applicant. Processo de destilação criogênica para separação do ar para produção de oxigênio gasoso. BR Patent Application 102016022807-7. Filed in September 30th, 2016.



República Federativa do Brasil  
Ministério da Indústria, Comércio Exterior  
e Serviços  
Instituto Nacional da Propriedade Industrial

(21) BR 102016022807-7 A2

(22) Data do Depósito: 30/09/2016

(43) Data da Publicação: 02/05/2018



\* B R 1 0 2 0 1 6 0 2 2 8 0 7 7 A

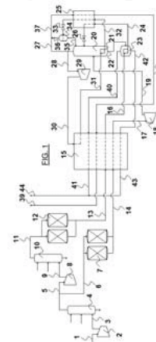
(54) **Título:** PROCESSO DE DESTILAÇÃO CRIOGÊNICA PARA SEPARAÇÃO DO AR PARA PRODUÇÃO DE OXIGÊNIO GASOSO

(51) **Int. Cl.:** F25J 3/04

(73) **Titular(es):** UNIVERSIDADE FEDERAL DO RIO DE JANEIRO

(72) **Inventor(es):** GEORGE VICTOR BRIGAGÃO; OFÉLIA DE QUEIROZ FERNANDES ARAÚJO; JOSÉ LUIZ DE MEDEIROS

(57) **Resumo:** PROCESSO DE DESTILAÇÃO CRIOGÊNICA PARA SEPARAÇÃO DO AR PARA PRODUÇÃO DE OXIGÊNIO GASOSO. A invenção refere-se a um método para produzir oxigênio através da separação criogênica do ar por destilação com recompressão criogênica de parte do vapor de topo da coluna de fracionamento em menor pressão, como forma de produzir o refluxo requerido para operação da própria coluna, eliminando a necessidade haver uma ou mais colunas adicionais em pressão mais elevada para a produção de nitrogênio para refluxo da coluna de menor pressão, que opera em pressão próxima à atmosférica. Como resultado disto, a razão de compressão dos compressores de ar desta invenção é menor do que nos processos convencionais, pois toda a separação é realizada sob baixa pressão. Assim, a presente invenção descreve um processo para produção de oxigênio gasoso em baixa pressão com desempenho energético superior ao de unidades até então consideradas como estado-da-arte. O principal elemento de inovação deste processo consiste em um compressor que opera sob condições criogênicas e que permite a condensação de nitrogênio pela troca térmica com a vaporização de oxigênio líquido(...)



## APPENDIX C – Conference paper on cryogenic air separation – Proceedings of LA-SDEWES2018

BRIGAGÃO, G. V.; DE MEDEIROS, J. L.; ARAÚJO, O. Q. F. Oxy-combustion CO<sub>2</sub> capture for steam power plants: a novel air separation unit for oxygen supply. 1st Latin-American Conference on Sustainable Development of Energy Water and Environment Systems (LA-SDEWES), Rio de Janeiro, 2018.

Conference on Sustainable Development of Energy, Water and Environment Systems, Rio de Janeiro 28.-31.1.2018

**SDEWES.LA2018.0043**

### **Oxy-Combustion CO<sub>2</sub> Capture for Steam Power Plants: a Novel Air Separation Unit for Oxygen Supply**

G. Brigagão\*, J.L. De Medeiros, O. Araujo

Federal University of Rio de Janeiro, Brazil (\*george.victor@poli.ufrj.br)

#### **Abstract**

The development of more efficient air separation units (ASUs) is a major concern in oxyfuel CO<sub>2</sub> capture, which is very energy and capital-intensive, due to the high demand of gaseous oxygen of such processes. In this context, this work proposes an alternative ASU for large scale gaseous oxygen supply by cryogenic fractionation. Instead of using multiple columns at different pressure levels, it is employed top vapor recompression (TVR) distillation in a single atmospheric column as separation principle, where the nitrogen rich column top vapor is compressed and then liquefied within a column reboiler. Several process configurations to produce low-pressure gaseous oxygen were simulated and optimized in Aspen Hysys. The shaft power requirement to produce gaseous oxygen 95%mol at 1 atm in the proposed ASU is 139.0 kWh/t O<sub>2</sub>. A sensitivity analysis varying the specification of oxygen purity was performed showing that, even when oxygen is demanded at higher purities, the proposed new ASU provides the lowest specific power demand, without external heat integration, to produce low-pressure gaseous oxygen. The application of the proposed new ASU to supply low-pressure oxygen to oxyfuel coal-fired power plant can improve net efficiency in about 1.9%LHV, relative to standard ASU, without resorting to compression heat recovery for power generation. Recovery of air compression heat is suggested as a further potential improvement in power plant net efficiency and specific power requirement for oxygen supply. This work contributes to the cutting edge of ASU technology by providing a new process that requires the lowest power demand for large scale gaseous oxygen production.

# APPENDIX D – Scientific article on cryogenic air separation and Gas-To-Wire electricity generation with oxy-combustion CO<sub>2</sub> capture – Energy Conversion and Management

BRIGAGÃO, G. V.; DE MEDEIROS, J. L.; ARAÚJO, O. Q. F. A novel cryogenic vapor-recompression air separation unit integrated to oxyfuel combined-cycle gas-to-wire plant with carbon dioxide enhanced oil recovery: energy and economic assessments. *Energy Conversion and Management*, 189, p. 202-214, 2019.

Energy Conversion and Management 189 (2019) 202–214



Contents lists available at [ScienceDirect](https://www.sciencedirect.com)

## Energy Conversion and Management

journal homepage: [www.elsevier.com/locate/enconman](http://www.elsevier.com/locate/enconman)



---

### A novel cryogenic vapor-recompression air separation unit integrated to oxyfuel combined-cycle gas-to-wire plant with carbon dioxide enhanced oil recovery: Energy and economic assessments

George Victor Brigagão, José Luiz de Medeiros\*, Ofélia de Queiroz F. Araújo

Escola de Química, Federal University of Rio de Janeiro, CT E Ilha do Fundão, Rio de Janeiro, RJ 21941-909, Brazil



---

**ARTICLE INFO**

**Keywords:**  
Air separation  
Vapor-recompression cryogenic distillation  
Oxy-combustion  
CO<sub>2</sub> capture  
Gas-To-Wire  
Natural gas

**ABSTRACT**

Oxyfuel carbon capture is both power and capital intensive due to oxygen demand. Consequently, oxyfuel requires the development of more efficient air separation units. This work proposes an alternative cryogenic distillation process for large-scale gaseous oxygen supply. Instead of using different pressure columns, the new air separation unit couples top vapor recompression to a single atmospheric cryogenic air distillation double-reboiler column, whose nitrogen-rich top vapor is compressed to heat the intermediate column reboiler, while the bottom reboiler is heated with compressed saturated air. Several processes for low-pressure oxygen gas supply were simulated and optimized. The power requirement of the new air separation unit producing atmospheric oxygen at 95%mol attained the best value of 139.0 kWh/t (oxygen basis). A sensitivity analysis for oxygen purity was performed showing that, even for higher purities, the new developed process achieves the lowest specific power for low-pressure gaseous oxygen production. The economic leverage of the new air separation unit is proven via successful supply of low-pressure oxygen to oxyfuel natural gas combined-cycle Gas-To-Wire plant. Assuming carbon dioxide destination to enhanced oil recovery, even with an investment about 100% higher than the counterpart of a conventional air-fed combined-cycle Gas-To-Wire plant and despite net efficiency penalty of 6.88%, the oxyfuel combined-cycle Gas-To-Wire solution coupled to the new air separation unit was capable of achieving comparatively superior profitability under carbon taxation above 13.5 USD/t.

---

### 1. Introduction

The electricity generation sector is a major agent of global carbon dioxide (CO<sub>2</sub>) emissions, where implementation of carbon capture, storage and utilization (CCSU) offers an alternative to limit global warming advance while new energy sources are not widely established. Besides the driving forces of government regulation and international protocols – now converging into charging power companies with carbon taxation – attractiveness of CCSU requires reasonable economic feasibility to assure that CO<sub>2</sub> mitigation would not severely impact the electricity generation cost and sales price. The development of efficient methods to capture CO<sub>2</sub> is then mandatory to reduce the associated mitigation penalty [1].

#### 1.1. Oxy-combustion

Although post-combustion has been the standard solution for CO<sub>2</sub> capture as presents the most well-developed technology, that is easy to

implement in comparison with pre-combustion and oxy-combustion routes, it is not necessarily the most energy efficient choice, nor even possibly the most economical one. Moreover, the oxy-combustion route, i.e. combustion with oxygen (O<sub>2</sub>) replacing air, necessarily offers the best environmental performance, especially when comparing these routes for a fixed power penalty if considering a life-cycle point of view, as it is remarkably the only option enabling zero-emission power generation [2].

The economic competitiveness of oxy-combustion CO<sub>2</sub> capture is heavily dependent on cost-effective large-scale gaseous oxygen (GOX) supply from air separation units (ASU). Such a demand profile is most properly supplied with onsite production from cryogenic air fractionation. Alternatively, ceramic ion transport membranes has recently been suggested as a promising technology for GOX production particularly for this application, due to high selectivity above 800 °C through oxygen-ion (O<sup>2-</sup>) species permeation [3], thus producing high-purity GOX and also enabling integration with power generation processes [2]. However, considering that the maximum demonstrated capacity is

---

\* Corresponding author.  
E-mail address: [jlm@eq.ufRJ.br](mailto:jlm@eq.ufRJ.br) (J.L. de Medeiros).

<https://doi.org/10.1016/j.enconman.2019.03.088>

0196-8904/ © 2019 Elsevier Ltd. All rights reserved.

## APPENDIX E – Patent application on air pre-purification for cryogenic separation plants

BRIGAGÃO, G. V., ARINELLI, L. O., DE MEDEIROS, J. L., ARAÚJO, O. Q. F., inventors; Universidade Federal do Rio de Janeiro, applicant. Purificação do ar para fracionamento criogênico com separador supersônico de baixa pressão. BR Patent Application 102017027727-5. Filed in December 21st, 2017.



República Federativa do Brasil  
Ministério da Economia  
Instituto Nacional da Propriedade Industrial

(21) BR 102017027727-5 A2



(22) Data do Depósito: 21/12/2017

(43) Data da Publicação Nacional: 09/07/2019

(54) Título: PROCESSO DE PREPARO E PURIFICAÇÃO DO AR PARA FRACIONAMENTO CRIOGÊNICO UTILIZANDO SEPARADOR SUPERSÔNICO DE BAIXA PRESSÃO

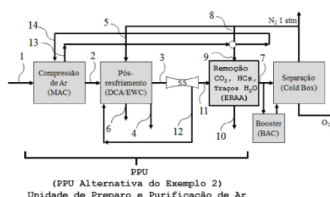
(51) Int. Cl.: B01D 53/00; B01D 53/02; B01D 53/04; B01D 53/047.

(52) CPC: B01D 53/002; B01D 53/02; B01D 53/04; B01D 53/0454; B01D 53/047; (...).

(71) Depositante(es): UNIVERSIDADE FEDERAL DO RIO DE JANEIRO.

(72) Inventor(es): GEORGE VICTOR BRIGAGÃO; JOSÉ LUIZ DE MEDEIROS; LARA DE OLIVEIRA ARINELLI; OFÉLIA DE QUEIROZ FERNANDES ARAÚJO.

(57) Resumo: A presente invenção define um novo conceito de unidade PPU ? Air Preparation and Purification Unit ? para preparo e purificação de ar a ser fracionado criogenicamente na etapa seguinte conhecida como Cold-Box. O conceito PPU Alternativa aqui proposto utiliza separador supersônico em baixa pressão para remover 97,5% da água do ar, seguindo-se etapa de remoção de acabamento por adsorção (ERAA) ou tratamentos similares com meio sólido (por exemplo, adsorção química) para remoção de contaminantes CO<sub>2</sub>, N<sub>2</sub>O e hidrocarbonetos, além de traços residuais de H<sub>2</sub>O, adequando os níveis de contaminantes para posterior processamento na Cold-Box de uma planta criogênica de fracionamento de ar.



(PPU Alternativa do Exemplo 2)  
Unidade de Preparo e Purificação de Ar

## APPENDIX F – Conference paper on energy assessment of novel air pre-purification units for cryogenic air separation plants – Proceeding of the 4th Brazilian Congress on CO<sub>2</sub> in the Oil, Gas and Biofuels Industries

BRIGAGÃO, G. V.; ARINELLI, L. O.; DE MEDEIROS, J. L.; ARAÚJO, O. Q. F. CO<sub>2</sub> emission and energy assessments of a novel pre-purification unit for cryogenic air separation using supersonic separator. 4th Brazilian Congress on CO<sub>2</sub> in the Oil, Gas and Biofuels Industries, Rio de Janeiro, 2018.



### IBP0096\_18 CO<sub>2</sub> EMISSION AND ENERGY ASSESSMENTS OF A NOVEL PRE-PURIFICATION UNIT FOR CRYOGENIC AIR SEPARATION USING SUPERSONIC SEPARATOR

George V. Brigagão<sup>1</sup>, Lara de O. Arinelli<sup>1</sup>,  
José L. de Medeiros<sup>2</sup>, Ofélia Q. F. Araújo<sup>3</sup>

Copyright 2018, Brazilian Petroleum, Gas and Biofuels Institute - IBP

This Technical Paper was prepared for presentation at the *4<sup>th</sup> Brazilian Congress on CO<sub>2</sub> in the Oil, Gas and Biofuels Industries*, held between June 28-29, 2018, in Rio de Janeiro. This Technical Paper was selected for presentation by the Technical Committee of the event according to the information contained in the final paper submitted by the author(s). The organizers are not supposed to translate or correct the submitted papers. The material as it is presented, does not necessarily represent Brazilian Petroleum, Gas and Biofuels Institute' opinion, or that of its Members or Representatives. Authors consent to the publication of this Technical Paper in the *4<sup>th</sup> Brazilian Congress on CO<sub>2</sub> in the Oil, Gas and Biofuels Industries Proceedings*.

#### Abstract

Thermal power plants with oxy-combustion CO<sub>2</sub> capture are featured by large scale oxygen demand, where cryogenic air separation is most suitable. In such context, a Pre-Purification Unit (PPU) is required, prior to air fractionation, to remove hazardous air contaminants – H<sub>2</sub>O, CO<sub>2</sub> and several trace-species – preventing ingress into the Cold Box. The conventional PPU – named FULL-TSA – remove those contaminants by means of Temperature Swing Adsorption (TSA), ordinarily using double-layered bed with activated alumina for adsorbing H<sub>2</sub>O and zeolitic molecular sieve for adsorbing CO<sub>2</sub> and further trace-species, which implicates in relatively high demand of low-pressure steam for impurities desorption. A novel pre-purification concept (SS-TSA) embraces a Supersonic Separator (SS) performing the bulk of separation service, abating nearly 98.5% of H<sub>2</sub>O, followed by a finishing single-bed molecular sieve (MS) TSA step, which is featured by its relatively small size, for removing CO<sub>2</sub> and remaining impurities. This work presents the energy analysis, as well as the related indirect CO<sub>2</sub> emissions, of such a novel concept (SS-TSA) comprising air compression, cooling, SS dehydration and finishing MS-TSA against the conventional method fully based in TSA purification (FULL-TSA). Process simulation in HYSYS 8.8 assisted technical evaluation and comparison of alternatives, which included the use of two Hysys Unit Operation Extensions – SS-UOE and PEC-UOE – for rigorous thermodynamic SS modeling with phase-equilibrium sound speed. SS was designed to impose only 1.4% of head loss, while shrinking TSA service to about 10% of FULL-TSA counterpart, also recovering super-cooled aqueous condensate that reduces water make-up and N<sub>2</sub> consumption for cooling. Changing from FULL-TSA to SS-TSA the average demand of low-pressure steam reduced from 1.37 to 0.16 MW. In terms of electricity demand the difference was quite small, referring to a tiny increase of 0.07 MW in SS-TSA comparatively to total power demand of 14.97 MW in FULL-TSA. Assuming a natural gas combined cycle cogeneration plant matching requirements to air compression and pre-purification process, equivalent reduction in CO<sub>2</sub> indirect emission was 20 kg/h for SS-TSA. These results point superiority of SS-TSA.

#### 1. Introduction

Concerning the dominance of fossil fuel based power plants in the world abroad, allied to increased electricity demand, the electric sector has been the in head of global CO<sub>2</sub> emissions since the half of 20<sup>th</sup> century. Despite of some factual progresses in developed countries in moving towards renewable energy sources, considerable worldwide adhesion will take a long-term horizon of several decades, meanwhile fossil fuel will still be dominant. However, even in those greener countries thermal power plants have a relevant function of base supply assurance amortizing dynamic behavior of wind and solar power plants. As long as new energy sources have not been widely established, Carbon Capture and Storage or Utilization (CCSU) is a leading alternative for drastic abatement of CO<sub>2</sub> emissions to restrain global warming advance. In this context, oxy-combustion is one plausible route for CO<sub>2</sub> capture, based on power generation from combustion with practically pure oxygen replacing air, mixed with recycled CO<sub>2</sub> or H<sub>2</sub>O for flame temperature reduction, to produce a flue gas constituted mainly by CO<sub>2</sub> and H<sub>2</sub>O, so CO<sub>2</sub> is easily recovered with water condensation. Mainly because of technological barriers and competition with easy-to-implement post-combustion alternatives, oxy-combustion power plants still did not cross the readiness technological level of industrial demonstration. However, a known key feature of those plants is

# APPENDIX G – Scientific article on energy assessment of novel air pre-purification units for cryogenic air separation plants – Materials Science Forum

BRIGAGÃO, G. V.; ARINELLI, L. O.; DE MEDEIROS, J. L.; ARAÚJO, O. Q. F. CO<sub>2</sub> emission and energy assessments of a novel pre-purification unit for cryogenic air separation using supersonic separator. *Materials Science Forum*, 965, p. 59–67, 2019.

*Materials Science Forum*  
ISSN: 1662-9752, Vol. 965, pp 59-67  
doi:10.4028/www.scientific.net/MSF.965.59  
© 2019 Trans Tech Publications Ltd, Switzerland

Submitted: 2018-12-15  
Accepted: 2019-04-26  
Online: 2019-08-08

## CO<sub>2</sub> Emission and Energy Assessments of a Novel Pre-Purification Unit for Cryogenic Air Separation Using Supersonic Separator

George Victor Brigagão<sup>1,a\*</sup>, Lara de Oliveira Arinelli<sup>1,b</sup>,  
José Luiz de Medeiros<sup>1,c\*</sup> and Ofélia de Queiroz Fernandes Araújo<sup>1,d</sup>

<sup>1</sup>Escola de Química, Federal University of Rio de Janeiro, CT, E, Ilha do Fundão, Rio de Janeiro, RJ, 21941-909, Brazil

<sup>a</sup>george.victor@poli.ufrj.br, <sup>b</sup>lara.arinelli@gmail.com, <sup>c</sup>jlmed@eq.ufrj.br, <sup>d</sup>ofelia@eq.ufrj.br

\*corresponding author: george.victor@poli.ufrj.br

**Keywords:** air pre-purification; air dehydration; supersonic separator; cryogenic air separation.

**Abstract.** Thermal power plants with oxy-combustion CO<sub>2</sub> capture are featured by large scale oxygen demand, where cryogenic air separation is most suitable. In such context, a Pre-Purification Unit (PPU) is required, prior to air fractionation, to remove hazardous air contaminants – H<sub>2</sub>O, CO<sub>2</sub> and several trace-species – preventing ingress into the Cold Box. The conventional PPU – named FULL-TSA – remove those contaminants by means of Temperature Swing Adsorption (TSA), ordinarily using double-layered bed with activated alumina for adsorbing H<sub>2</sub>O and zeolitic molecular sieve for adsorbing CO<sub>2</sub> and further trace-species, which implicates in relatively high demand of low-pressure steam for impurities desorption. A novel pre-purification concept (SS-TSA) embraces a Supersonic Separator (SS) performing the bulk of separation service, abating nearly 98.5% of H<sub>2</sub>O, followed by a finishing single-bed molecular sieve (MS) TSA step, which is featured by its relatively small size, for removing CO<sub>2</sub> and remaining impurities. This work presents the energy analysis, as well as the related indirect CO<sub>2</sub> emissions, of such a novel concept (SS-TSA) comprising air compression, cooling, SS dehydration and finishing MS-TSA against the conventional method fully based in TSA purification (FULL-TSA). Process simulation in HYSYS 8.8 assisted technical evaluation and comparison of alternatives, which included the use of two Hysys Unit Operation Extensions – SS-UOE and PEC-UOE – for rigorous thermodynamic SS modeling with phase-equilibrium sound speed. SS was designed to impose only 1.4% of head loss, while shrinking TSA service to about 10% of FULL-TSA counterpart, also recovering super-cooled aqueous condensate that reduces water make-up and N<sub>2</sub> consumption for cooling. Changing from FULL-TSA to SS-TSA the average demand of low-pressure steam reduced from 1.37 to 0.16 MW. In terms of electricity demand the difference was quite small, referring to a tiny increase of 0.07 MW in SS-TSA comparatively to total power demand of 14.97 MW in FULL-TSA. Assuming a natural gas combined cycle cogeneration plant matching requirements to air compression and pre-purification process, equivalent reduction in CO<sub>2</sub> indirect emission was 20 kg/h for SS-TSA. These results point superiority of SS-TSA.

### Introduction

Concerning the dominance of fossil fuel based power plants in the world abroad, allied to increased electricity demand, the electric sector has been the in head of global CO<sub>2</sub> emissions since the half of 20<sup>th</sup> century. Despite of some factual progresses in developed countries in moving towards renewable energy sources, considerable worldwide adhesion will take a long-term horizon of several decades, meanwhile fossil fuel will still be dominant. However, even in those greener countries thermal power plants have a relevant function of base supply assurance amortizing dynamic behavior of wind and solar power plants. As long as new energy sources have not been widely established, Carbon Capture and Storage or Utilization (CCSU) is a leading alternative for drastic abatement of CO<sub>2</sub> emissions to restrain global warming advance. In this context, oxy-combustion is one plausible route for CO<sub>2</sub> capture, based on power generation from combustion

# APPENDIX H - Scientific article on techno-economic assessment of novel air pre-purification units for cryogenic air separation plants – Separation and Purification Technology

BRIGAGÃO, G. V., ARINELLI, L. O., DE MEDEIROS, J. L., ARAÚJO, O. Q. F. A new concept of air pre-purification unit for cryogenic separation: low-pressure supersonic separator coupled to finishing adsorption. *Separation and Purification Technology*, 215, p. 173-189, 2019.

Separation and Purification Technology 215 (2019) 173–189



Contents lists available at [ScienceDirect](#)

## Separation and Purification Technology

journal homepage: [www.elsevier.com/locate/seppur](http://www.elsevier.com/locate/seppur)



---

### A new concept of air pre-purification unit for cryogenic separation: Low-pressure supersonic separator coupled to finishing adsorption



George Victor Brigagão, Lara de Oliveira Arinelli, José Luiz de Medeiros\*, Ofélia de Queiroz F. Araújo

*Escola de Química, Federal University of Rio de Janeiro, CT, E, Ilha do Fundão, Rio de Janeiro, RJ 21941-909, Brazil*

---

**ARTICLE INFO**

**Keywords:**  
Air pre-purification  
Air dehydration  
Supersonic separator  
Multiphase supersonic flow  
Multiphase sound speed

**ABSTRACT**

In commercial cryogenic manufacturing of oxygen, air to the Cold-Box must pass through a Pre-Purification Unit (PPU) to remove water, CO<sub>2</sub> and other impurities. The conventional PPU – FULL-TSA – comprises compression, cooling pre-dehydration and temperature-swing adsorption (TSA) for dehydration and CO<sub>2</sub> removal, supplying treated air at 3.1 bar. This work discloses a new PPU concept – SS-TSA – prescribing a supersonic separator (SS) upstream to TSA handling 98.5% of dehydration, greatly lowering TSA costs. SS-TSA comprises compression, cooling pre-dehydration, SS dehydration and a smaller TSA for finishing dehydration and CO<sub>2</sub> removal. A SS-TSA variant – TSA-HI – additionally recovers compression heat lowering heating costs. SS-TSA, FULL-TSA and SS-SS-TSA-HI were analyzed. Flowsheets were simulated in HYSYS with full thermodynamic SS modeling via a new HYSYS Unit Operation Extension – SS-UOE – rigorously calculating the multiphase sound speed. SS was designed for only 3.5% of head-loss, recovering 98.5% of water as super-cooled liquid, lowering make-up and chilled-water costs, while shrinking the TSA service to 10% of the FULL-TSA counterpart. For commercial-scale PPU considering 20 years of operation at 10% interest rate, the purified 3.1 bar air breakeven prices reached 5.28, 5.19, and 5.18 US\$/kNm<sup>3</sup>, respectively for FULL-TSA, SS-TSA and SS-TSA-HI, establishing superiority of SS alternatives over the conventional FULL-TSA.

---

### 1. Introduction

Cryogenic air separation units (ASU) configure the most suitable technology for large-scale air fractionation, currently widespread applied for oxygen supply to steelworks and coal gasification [1]. The uprising of oxy-combustion CO<sub>2</sub> capture in thermoelectric plants signalizes a probable increase of the global demand for oxygen gas in next decades requiring large-scale efficient ASUs. Large-scale ASU comprises two processes with very distinct characteristics, namely: (i) air compression, pre-cooling and purification hereinafter referred to as Pre-Purification Unit (PPU); and (ii) cryogenic fractionation or Cold-Box. PPU supplies purified pressurized air to Cold-Box, both owned by the same company according to current practices. However, it is conceivable, particularly in large-scale ASUs, to have outsourced PPU for best overall profitability. As the Cold-Box is highly capital intensive, the development of more efficient large-scale PPU is interest of oxy-combustion.

PPU compresses and treats air preventing entrance of ice-forming contaminants (H<sub>2</sub>O and CO<sub>2</sub>) and traces of flammable hydrocarbons (HCs) in the Cold-Box. Freezing-out components plug the main Cold-Box heat exchanger, representing operational and safety hazards, besides economic loss associated to defrosting shut-downs, while HCs concentrate in the oxygen sump of the main column thanks to higher boiling points than oxygen, leading to dangerous auto-ignition mixtures [2].

Currently, the most common PPU concept – so-called FULL-TSA PPU

---

Abbreviations: 1D, one-dimensional; AA, activated alumina; ASU, air separation unit; BAC, booster air compressor; C3+, propane and heavier HCs; ChW, chilled water; CW, cooling water; DCA, direct contact aftercooler; EOS, equation of state; EWC, evaporative water cooler; FULL-TSA, conventional TSA PPU; HC, hydrocarbon; HCDPA, hydrocarbon dew-point adjustment; LP, low-pressure; MAC, main air compressor; MMSm<sup>3</sup>/d, millions standard m<sup>3</sup> per Day; MS, molecular Sieve; MS-TSA, smaller TSA of SS PPU; MMUSD/y, millions USD/y; NG, natural gas; PPU, pre-purification unit; PR-EOS, Peng-Robinson EOS; PSA, pressure-swing adsorption; REVEX, reversing heat exchanger; RH, relative humidity; SS, supersonic separator; SS-TSA, New SS + TSA PPU; SS-TSA-HI, New SS + TSA heat-integrated PPU; TSA, temperature-swing adsorption; VLE, vapor-liquid equilibrium; VLWE, vapor-liquid-water equilibrium; UOE, unit operation extension; USD, US dollar; WDP, water dew-point; WDPA, water dew-point adjustment; WW, warm water

\* Corresponding author.  
E-mail addresses: [jlm@eq.ufrj.br](mailto:jlm@eq.ufrj.br) (J.L. de Medeiros), [ofelia@eq.ufrj.br](mailto:ofelia@eq.ufrj.br) (O.d.Q.F. Araújo).

<https://doi.org/10.1016/j.seppur.2019.01.015>  
Received 19 August 2018; Received in revised form 15 December 2018; Accepted 5 January 2019  
Available online 08 January 2019  
1383-5866/ © 2019 Elsevier B.V. All rights reserved.

## APPENDIX I – Conference paper on exergy analysis of air pre-purification units for cryogenic air separation – Proceedings of SDEWES2018

BRIGAGÃO, G. V.; ARINELLI, L. O.; DE MEDEIROS, J. L.; ARAÚJO, O. Q. F. Exergy analysis of a novel air pre-purification unit for cryogenic fractionation based on low-pressure supersonic separator combined with finishing adsorption step. 13th Conference on Sustainable Development of Energy Water and Environment Systems (SDEWES), Palermo, 2018.

Conference on Sustainable Development of Energy, Water and Environment Systems, Palermo, 30.9.-4.10.2018

**SDEWES2018.0068**

### **Exergy Analysis of a Novel Air Pre-Purification Unit for Cryogenic Fractionation Based on Low-Pressure Supersonic Separator Combined with Finishing Adsorption Step**

G. Brigagão\*, L. De Oliveira Arinelli, J.L. De Medeiros, O. Araujo

Federal University of Rio de Janeiro, Brazil (\*george.victor@poli.ufrj.br)

#### **Abstract**

Cryogenic air fractionation requires raw air compression and pre-purification, and the conventional process – FULL-TSA – uses Temperature-Swing-Adsorption (TSA) with large activated-alumina beds for removing H<sub>2</sub>O and small molecular-sieve beds for CO<sub>2</sub> and trace-species. A novel alternative – SS-TSA – prescribes a Supersonic Separator (SS) abating 98.65% H<sub>2</sub>O followed by molecular-sieve TSA for finishing purification. A new variant deriving from SS-TSA – SS-TSA-HI – uses compression heat to regenerate TSA beds. Exergy analysis of FULL-TSA, SS-TSA and SS-TSA-HI was executed to investigate thermodynamic performances also locating where improvements can better reduce utilities consumption. Air compression and cooling steps were unveiled as major exergy destructors, with SS-TSA-HI being slightly superior at this point due to lower temperature approach in intercoolers. Utilization of SS reduced exergy loss of pre-purification by 61% for savings on steam and nitrogen demand in TSA system. Overall exergy efficiencies of FULL-TSA, SS-TSA and SS-TSA-HI were found as 57.9%, 60.0%, and 60.3%, respectively.

## APPENDIX J – Conference paper on electricity generation in oxyfuel natural gas combined cycle power plant – Proceedings of Rio Oil & Gas 2016

BRIGAGÃO, G. V.; DE MEDEIROS, J. L.; ARAÚJO, O. Q. F. Performance evaluation of an oxyfuel NGCC process for power generation with organic Rankine cycle for offshore application. Rio Oil & Gas Expo and Conference, Rio de Janeiro, 2016.



**IBP1579\_16**  
**PERFORMANCE EVALUATION OF AN OXYFUEL NGCC PROCESS FOR POWER GENERATION WITH ORGANIC RANKINE CYCLE FOR OFFSHORE APPLICATION**  
George V. Brigagão<sup>1</sup>, José Luiz de Medeiros<sup>2</sup>,  
Ofélia Q. F. Araújo<sup>3</sup>

### Copyright 2016, Brazilian Petroleum, Gas and Biofuels Institute - IBP

This Technical Paper was prepared for presentation at the *Rio Oil & Gas Expo and Conference 2016*, held between October, 24-27, 2016, in Rio de Janeiro. This Technical Paper was selected for presentation by the Technical Committee of the event according to the information contained in the final paper submitted by the author(s). The organizers are not supposed to translate or correct the submitted papers. The material as it is presented, does not necessarily represent Brazilian Petroleum, Gas and Biofuels Institute's opinion, or that of its Members or Representatives. Authors consent to the publication of this Technical Paper in the *Rio Oil & Gas Expo and Conference 2016 Proceedings*.

### Abstract

Carbon Capture and Storage (CCS) technology represents the leading alternative to reduce CO<sub>2</sub> global emission from burning fossil fuels. In the CCS context, the oxyfuel (oxy-combustion) route emerges as an alternative that enables expressive reductions on power requirement for CO<sub>2</sub> removal from flue gas. This work focuses on the performance evaluation of an oxyfuel NGCC process with water recycle for flame temperature abatement through process simulation. Water recycle oxyfuel processes has H<sub>2</sub>O as the dominant component in its flue gas, so much low-grade heat is commonly lost at water condensation. The implementation of an Organic Rankine Cycle (ORC) to such a process is presented in this work in order to transform such low-grade heat into electricity. Deeply extracted seawater at nearly 4°C is proposed as the cooling medium to dissipate waste heat from the ORC. A heat integration analysis was also performed by pinch design to evaluate the maximum benefit from recovering compression heat to pre-heat recycled water. Without compression heat recovery, saturated water with small percentage of vapor would be injected into the combustor, corresponding to an overall efficiency of 44.71%LHV. The corresponding overall efficiency for the heat integrated case without ORC is 46.47%LHV, where almost half of the H<sub>2</sub>O injected into the combustor is in vapor phase. Considering pure propane as the ORC working fluid, the net efficiency would be equivalent to 50.03%LHV, while the optimal hydrocarbon composition for this process would result in 50.20%LHV. Through implementing the proposed ORC, with optimum recovery of compression heat, the water recycle concept exceeds the Graz oxyfuel cycle efficiency by nearly 1%LHV. Consequently, the power penalty for CO<sub>2</sub> capture in the considered oxyfuel NGCC process with ORC is in the range of 7-8%LHV. This work aims to contribute to improve energy efficiency in offshore power generation.

### 1. Introduction

Carbon Capture and Storage (CCS) technology represents the leading alternative to reduce CO<sub>2</sub> global emission from burning fossil fuels. In the CCS context, the oxyfuel (oxy-combustion) route emerges as an alternative that enables expressive reductions on power requirement for CO<sub>2</sub> removal from flue gas. The oxyfuel combustion preferably employs stoichiometric gaseous oxygen (GOX) to burn the fuel completely, with the consequence that the flue gas is mainly constituted by CO<sub>2</sub> and steam, meaning that CO<sub>2</sub> can be directly captured after water condensation. Also, since near zero N<sub>2</sub> is introduced in the combustor, the oxy-combustion drastically cuts NO<sub>x</sub> emissions (AL-ABBAS et al, 2012). On the other hand, the oxyfuel route demands the operation of an exclusive Air Separation Unit (ASU), which is highly intensive in energy and capital. Conventional gas-fired and coal-fired power plants are the major source of global anthropogenic CO<sub>2</sub> emissions, so a gradual transition for CO<sub>2</sub> capture process schemes is expected for the near future, where oxy-combustion is a promising option.

Natural gas (NG) thermoelectric plants typically use a combination of two cycles for power generation – the gas turbine (GT) cycle (Brayton cycle) and the steam turbine (ST) cycle (Rankine cycle) – which is called Natural Gas Combined Cycle (NGCC). In this case, the Rankine steam cycle recovers heat from the GT exhaust gas to run a steam turbine. The waste heat (low-grade heat) is then dissipated to the atmosphere usually through heat exchange against

## **APPENDIX K – Register of softwares for calculation of multiphase and reactive equilibrium sound speed and simulation of supersonic separators**

### **K1. Hysys Extension Phase Equilibrium Sound Speed**

ARINELLI, L. O., DE MEDEIROS, J. L., TEIXEIRA, A. M., BRIGAGÃO, G. V., ARAÚJO, O. Q. F., authors; UNIVERSIDADE FEDERAL DO RIO DE JANEIRO, applicant. HEPEC (Hysys Extension Phase Equilibrium Sound Speed). Registered software BR512017000629-6. Brazilian Patent and Trademark Office. Filed in June 20th, 2017.

### **K2. Hysys Extension Reactive Equilibrium Sound Speed**

ARINELLI, L. O., DE MEDEIROS, J. L., TEIXEIRA, A. M., BRIGAGÃO, G. V., ARAÚJO, O. Q. F., authors; UNIVERSIDADE FEDERAL DO RIO DE JANEIRO, applicant. HEREC (Hysys Extension Reactive Equilibrium Sound Speed (C)). Registered software BR512017000628-8. Brazilian Patent and Trademark Office. Filed in June 20th, 2017.

### **K3. Hysys Extension Supersonic Separator Operation**

ARINELLI, L. O., DE MEDEIROS, J. L., TEIXEIRA, A. M., BRIGAGÃO, G. V., ARAÚJO, O. Q. F., authors; UNIVERSIDADE FEDERAL DO RIO DE JANEIRO, applicant. HESSO (Hysys Extension Supersonic Separator Operation). Registered software BR512017000627-0. Brazilian Patent and Trademark Office. Filed in June 20th, 2017.

### **K4. Aspen Model of Phase Equilibrium Sound Speed**

ARINELLI, L. O., WIESBERG, I. L., DE MEDEIROS, J. L., BRIGAGÃO, G. V., TEIXEIRA, A. M., ARAÚJO, O. Q. F., authors; UNIVERSIDADE FEDERAL DO RIO DE JANEIRO, applicant. AMPEC (Aspen Model of Phase Equilibrium Sound Speed (C)). Registered software BR512018001031-8. Brazilian Patent and Trademark Office. Filed in June 26th, 2018.

### **K5. Aspen Model of Supersonic Separator Operation**

ARINELLI, L. O., WIESBERG, I. L., DE MEDEIROS, J. L., BRIGAGÃO, G. V., TEIXEIRA, A. M., ARAÚJO, O. Q. F., authors; UNIVERSIDADE FEDERAL DO RIO DE JANEIRO, applicant. AMSSO (Aspen Model of Supersonic Separator Operation). Registered software BR512018001032-6. Brazilian Patent and Trademark Office. Filed in June 26th, 2018.

## APPENDIX L – Conference paper on offshore CO<sub>2</sub>-rich natural gas processing with supersonic separators – Proceedings of LA-SDEWES2018

DE MELO, D. C.; ARINELLI, L. O.; TEIXEIRA, A. M.; VICTOR, G.; PASSARELLI, F.; GRAVA, W. M.; DE MEDEIROS, J. L. Technological alternatives for high CO<sub>2</sub> natural gas processing aiming offshore production of gas associated giant oil fields. 1st Latin-American Conference on Sustainable Development of Energy Water and Environment Systems (LA-SDEWES), Rio de Janeiro, 2018.

Conference on Sustainable Development of Energy, Water and Environment Systems, Rio de Janeiro 28.-31.1.2018

**SDEWES.LA2018.0067**

### **Technological Alternatives for High CO<sub>2</sub> Natural Gas Processing Aiming Offshore Production of Gas Associated Giant Oil Fields**

D. C. De Melo<sup>\*1</sup>, L. De O. Arinelli<sup>2</sup>, A. M. Teixeira<sup>2</sup>, G. Victor<sup>2</sup>, F. M. Passarelli<sup>1</sup>, J. Ferreira Do Nascimento<sup>1</sup>, W. M. Grava<sup>1</sup>, J.L. De Medeiros<sup>3</sup>

<sup>1</sup>PETROBRAS, Brazil; <sup>2</sup>Universidade Federal do Rio de Janeiro, Brazil; <sup>3</sup>Federal University of Rio de Janeiro, Brazil (\*darley@petrobras.com.br)

#### **Abstract**

The population growth followed by economy activity intensification is the driver of a growing demand for energy, among its various forms, for oil and natural gas (NG). The importance of the energy sector for socio-economic development is undeniable. Today in the world one can not imagine a developed country that does not have adequate access to energy sources. In addition, it is notable that a country's energy matrix should be diversified and cleaned as much as possible, for strategic, environmental and supply security reasons. In the Americas, some countries such as Brazil, Canada, Colombia, the United States and Peru have growing and robust energy sectors with technological and operational practice advances. These innovations allow the production development, for example, of tight oil and shale gas in the United States, oil sands in Canada, and of ultra deepwater offshore hydrocarbon sources, with both oil and gas, in Brazil, located in a very promising area known as Pre-Salt.

The oil-associated gas produced contain water and in some cases, relatively high content of acid components, which may present problems to its final utilization, like hydrates build up and corrosion in flowlines. Therefore, offshore process units, with a desirable simpler scheme, have to be designed to process this gas. In this case, the main purposes of the process are to remove acid components, dehydrate and adjust the hydrocarbon dew point of the gas. Other equipment, such as gas compressors, may also be necessary, and generally are, by the need to deliver the gas at a minimum pressure in order to be reinjected into the reservoir or to be injected into the pipe to reach the final gas processing unit on earth.

In the present work, it is evaluated the innovative implementation of full offshore large-scale processing of a CO<sub>2</sub> high (67%mol) NG exclusively with Super Sonic (SS) operations. In spite of higher complexity in terms of number of equipment, heat integration and use of refrigeration cycle, SS Process Flow Diagram (PFD) has lower investment and demands less power when compared to MP (membrane permeation) PFD, both aspects explained by huge CO<sub>2</sub> compressors for the low pressure CO<sub>2</sub> permeate produced by MP. Therefore, the best alternative for the studied scenario is the case that comprises recycle of condensate, SS dehydration, CO<sub>2</sub> removal for FG production via SS, and compression/pumping for EOR, with NPV of 5234 million USD after 20 years of operation.

# APPENDIX M- Scientific article on offshore CO<sub>2</sub>-rich natural gas processing with supersonic separators - Journal of Natural Gas Science and Engineering

ARINELLI, L. O.; DE MEDEIROS, J. L.; DE MELO, D. C.; TEIXEIRA, A. M.; BRIGAGÃO, G. V.; PASSARELLI, F.; GRAVA, W. M.; ARAÚJO, O. Q. F. Carbon capture and high-capacity supercritical fluid processing with supersonic separator: natural gas with ultra-high CO<sub>2</sub> content. Journal of Natural Gas Science and Engineering, 66, p. 265-283, 2019.

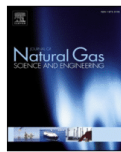
Journal of Natural Gas Science and Engineering 66 (2019) 265–283



Contents lists available at [ScienceDirect](#)

## Journal of Natural Gas Science and Engineering

journal homepage: [www.elsevier.com/locate/jngse](http://www.elsevier.com/locate/jngse)



---

### Carbon capture and high-capacity supercritical fluid processing with supersonic separator: Natural gas with ultra-high CO<sub>2</sub> content



Lara de Oliveira Arinelli<sup>a</sup>, José Luiz de Medeiros<sup>a,\*</sup>, Darley Carrijo de Melo<sup>b</sup>, Alexandre Mendonça Teixeira<sup>a</sup>, George Victor Brigagão<sup>a</sup>, Fabio Menezes Passarelli<sup>b</sup>, Wilson Mantovani Grava<sup>b</sup>, Ofélia de Queiroz F. Araújo<sup>a</sup>

<sup>a</sup> Escola de Química, Federal University of Rio de Janeiro, CT, E, Ilha do Fundão, Rio de Janeiro, RJ, 21941-909, Brazil  
<sup>b</sup> CENPES, PETROBRAS S.A., Ilha do Fundão, Rio de Janeiro, RJ, 21941-970, Brazil

---

#### ARTICLE INFO

**Keywords:**  
Supersonic separator  
Supercritical fluid processing  
Ultra-high CO<sub>2</sub> content  
Natural gas conditioning  
CO<sub>2</sub> removal  
CO<sub>2</sub> freeze-out

#### ABSTRACT

Some deep-water offshore fields produce oil with high gas/oil ratios and ultra-high %CO<sub>2</sub> (> 60%mol) with the onus of processing low-grade gas simultaneously handling huge CO<sub>2</sub> dispatch goals. Thus, processing solutions are needed to make feasible such high-capacity gas rigs hundreds of kilometers offshore. Feasibility relies on the choices for CO<sub>2</sub> capture and adjustment of water and hydrocarbon dew-points of such high flow rate gas. This problem was approached adopting supersonic separators for dew-point adjustments and for CO<sub>2</sub> capture on a floating-hub processing 50 MMsm<sup>3</sup>/d of CO<sub>2</sub> ultra-rich gas, reinjecting 96% of treated CO<sub>2</sub>-rich gas for enhanced oil recovery, while reserving 4% as fuel-gas after CO<sub>2</sub> abatement to 20%mol for power production. Process alternatives were assessed in terms of power demand and profitability comparing supersonic separator with membrane-permeation for CO<sub>2</sub> removal. Results show that 1st supersonic separator for dew-point adjustments of raw gas recycling condensate to the oil-gas-water separator and 2nd supersonic separator for CO<sub>2</sub> removal avoiding CO<sub>2</sub> freeze-out, give optimum net present value and minimum CO<sub>2</sub> emissions. On one hand, these facts are consequences of less compressor investment as 2nd supersonic separator ejects pressurized CO<sub>2</sub> condensate requiring 5% less compression power for enhanced oil recovery relatively to the power required by the low-pressure CO<sub>2</sub>-rich permeate from the membrane-permeation alternative. On the other hand, the best net value of supersonic separator alternative also reflects its highest revenues derived from recycling condensate from 1st supersonic separator entailing 18% higher oil production.

---

#### 1. Introduction

The processing of raw natural gas (NG) to fuel-gas comprises well-known operations normally in the following order: (i) H<sub>2</sub>S removal; (ii) water dew-point adjustment (WDPA) via dehydration; (iii) hydrocarbon dew-point adjustment (HCDPA) via hydrocarbon removal (i.e., propane and heavier or C<sub>3</sub>+); and (iv) CO<sub>2</sub> removal. Over 10% of world NG reserves contain 15–80%mol CO<sub>2</sub> classified as medium (15–30%mol), rich (30–60%mol) and ultra-rich (> 60%mol) CO<sub>2</sub> NG (Burgers et al., 2011). CO<sub>2</sub> removal is not only important to reach specifications, but

also to reduce CO<sub>2</sub> emissions with economic benefits if CO<sub>2</sub> is injected in oil fields for enhanced oil recovery (EOR) (Araújo and de Medeiros, 2017). EOR is economically positive as shown by tests of CO<sub>2</sub> injection and depletion for heavy oil recovery after cold production with oil-sands in Canada (Shokri and Babadagli, 2017). In non-associated NG fields, CO<sub>2</sub> can be pipeline-dispatched to EOR, or can be stored in depleted fields or aquifers (Indonesia, Norway) (Burgers et al., 2011). Some examples of huge NG reserves with high CO<sub>2</sub> contents are: Brazil offshore fields with high gas-oil ratio (GOR) such as Libra (Oil ≈ 15 × 10<sup>9</sup> bbl, GOR ≈ 500 sm<sup>3</sup>/m<sup>3</sup>, CO<sub>2</sub> ≈ 45%mol); US LaBarge gas field (CO<sub>2</sub> ≈

---

**Abbreviations:** C<sub>3</sub>+, Propane and Heavier; CFD, Computational Fluid Dynamics; CPA-EOS, Cubic-Plus-Association EOS; CW, Cooling-Water; ED, Electric-Drive; EOR, Enhanced Oil Recovery; EOS, Equation-of-State; GT, Gas-Turbine; HCDP, Hydrocarbon Dew-Point; HCDPA, Hydrocarbon Dew-Point Adjustment; HPS, High-Pressure Separator; HW, Hot-Water; JT, Joule-Thomson; LLS, Liquid-Liquid Separator; LTX, Low-Temperature Condensate Catcher; MMsm<sup>3</sup>/d, Millions of standard m<sup>3</sup> per day; NG, Natural Gas; PHW, Pressurized-Hot-Water; PR-EOS, Peng-Robinson EOS; SS, Supersonic Separator; SVLE, Solid-Vapor-Liquid Equilibrium; SW, Seawater; TF, Thermal-Fluid; TX, Turbo-Expander; USD, US Dollar; UOE, Unit Operation Extension; VLE, Vapor-Liquid Equilibrium; VLWE, Vapor-Liquid-Water Equilibrium; WDP, Water Dew-Point; WDPA, Water Dew-Point Adjustment; WHRU, Waste-Heat Recovery Unit; WW, Warm-Water

\* Corresponding author.  
E-mail address: [jlm@eq.ufjr.br](mailto:jlm@eq.ufjr.br) (J.L. de Medeiros).

<https://doi.org/10.1016/j.jngse.2019.04.004>  
Received 19 November 2018; Received in revised form 21 March 2019; Accepted 5 April 2019  
Available online 12 April 2019  
1875-5100/ © 2019 Elsevier B.V. All rights reserved.

# APPENDIX N – Scientific article on offshore CO<sub>2</sub>-rich natural gas processing with supersonic separators – Journal of Cleaner Production

DE MELO, D. C.; ARINELLI, L. O.; DE MEDEIROS, J. L.; TEIXEIRA, A. M.; BRIGAGÃO, G. V.; PASSARELLI, F.; GRAVA, W. M.; ARAÚJO, O. Q. F. Supersonic separator for cleaner offshore processing of supercritical fluid with ultra-high carbon dioxide content: economic and environmental evaluation. *Journal of Cleaner Production*, 234, p. 1385-1398, 2019.

Journal of Cleaner Production 234 (2019) 1385–1398

Contents lists available at ScienceDirect

**Journal of Cleaner Production**

journal homepage: [www.elsevier.com/locate/jclepro](http://www.elsevier.com/locate/jclepro)

---

## Supersonic separator for cleaner offshore processing of supercritical fluid with ultra-high carbon dioxide content: Economic and environmental evaluation



Darley C. de Melo<sup>b</sup>, Lara de O. Arinelli<sup>a</sup>, José Luiz de Medeiros<sup>a,\*</sup>, Alexandre M. Teixeira<sup>a</sup>, George Victor Brigagão<sup>a</sup>, Fabio M. Passarelli<sup>b</sup>, Wilson M. Grava<sup>b</sup>, Ofélia de Q.F. Araujo<sup>a</sup>

<sup>a</sup> Escola de Química, Federal University of Rio de Janeiro, CT, E. Ilha do Fundão, Rio de Janeiro, RJ, 21941-909, Brazil  
<sup>b</sup> CENPES, PETROBRAS S.A., Ilha do Fundão, Rio de Janeiro, RJ, 21941-970, Brazil

---

**ARTICLE INFO**

**Article history:**  
Received 2 March 2019  
Received in revised form 29 May 2019  
Accepted 27 June 2019  
Available online 28 June 2019

Handling editor: Prof. Jiri Jaromir Klemes

**Keywords:**  
Natural gas  
Supercritical fluid  
CO<sub>2</sub>  
Supersonic separator  
Offshore processing  
Environmental analysis

**ABSTRACT**

Offshore gas processing presents challenges, especially when high flow rates, high-pressure and high carbon dioxide contents are involved. The present scenario comprehends offshore processing of high flow rate of high-pressure natural gas with 68%mol carbon dioxide, which results from oil production and behaves as a dense supercritical fluid. The processing goals with this fluid comprise: [A] water dew-point adjustment; [B] hydrocarbon dew-point adjustment; [C] decarbonation of a small part to 20%mol carbon dioxide fuel-gas for power production; and [D] compression/pumping of the remaining fluid enriched with carbon dioxide from decarbonation for enhanced oil recovery. For these tasks the industry considers traditional well established processes such as molecular-sieves adsorption for water dew-point adjustment, Joule-Thompson expansion for hydrocarbon dew-point adjustment and membrane-permeation for carbon dioxide removal. However, conventional technologies can become cumbersome in such awkward conditions. Thus, unconventional solutions are sought for reliability, lower equipment size/weight, and better power consumption, emissions and environmental sustainability. Recently, supersonic separators have been analyzed in proof-of-concept researches for natural gas processing. In this regard, this work quantitatively proves that goals [A],[B],[C] are achievable using only supersonic separators, attaining 33% higher net value, 40% greater oil production, 10% lower investment and economic leverage to reach lower carbon emission relatively to conventional counterparts.

© 2019 Elsevier Ltd. All rights reserved.

---

### 1. Introduction

Population growth and economy intensification drive increasing demand for oil and natural gas (NG). Faster increase of natural resources consumption motivated by economy intensification can be identified clearly (Wu et al., 2017). It is notable that a country's energy matrix should be diversified and clean as much as possible, for strategic and environmental reasons (Campos et al., 2017). In this context, NG is considered an important energy source among fossil-fuels as it emits ≈ 50% of coal carbon dioxide (CO<sub>2</sub>) emissions per MW. Moreover, NG is the ideal complement to renewables, being a cost-effective back-up to the variability of hydropower, solar and wind generation. NG and renewable energy are pointed as effective alternatives to other fossil-fuels (e.g., coal and oil) that are currently responsible for the greatest share of CO<sub>2</sub> emissions in certain big countries such as Brazil and China (Dong et al., 2017).

Fig. 1 projects NG and renewable energy sources responding for at least 40% of 2040 world demand (26% NG, 14% renewables) in scenario-1 that foresees moderate changes in technology policies and social preference (BP, 2018), where the growing world economy requires more energy but consumption increases slower than in the past. In 2040 scenario-2, carbon price rises faster and policies favor energy efficiency gains and fuel switching, resulting that NG

---

Abbreviations: C3+, Propane and Heavier; CW, Cooling-Water; EOR, Enhanced Oil Recovery; HCDPA, Hydrocarbon Dew-Point Adjustment; HPS, High-Pressure Separator; HW, Hot-Water; JT, Joule-Thomson; LTX, Low-Temperature Separator; MMSm<sup>3</sup>/d, Millions of Standard m<sup>3</sup> per day; MS, Molecular-Sieves; NG, Natural Gas; PHW, Pressurized-Hot-Water; PR-EOS, Peng-Robinson Equation-of-State; SS, Supersonic Separator; SVLE, Solid-Vapor-Liquid Equilibrium; USD, US Dollar; VLE, Vapor-Liquid Equilibrium; WDPA, Water Dew-Point Adjustment; WHRU, Waste Heat Recovery Unit; WW, Warm-Water.

\* Corresponding author.  
E-mail address: [jlm@eq.ufrj.br](mailto:jlm@eq.ufrj.br) (J.L. de Medeiros).

<https://doi.org/10.1016/j.jclepro.2019.06.304>  
0959-6526/© 2019 Elsevier Ltd. All rights reserved.

## APPENDIX O – Conference paper on CO<sub>2</sub> utilization in microalga-based biorefinery producing methanol – Proceedings of SDEWES2016

WIESBERG, I. L.; BRIGAGÃO, G. V.; DE MEDEIROS, J. L.; ARAÚJO, O. Q. F. Economic and environmental analysis of a microalgae-based biorefinery utilizing CO<sub>2</sub> emitted from coal fired power plant. 11th Conference on Sustainable Development of Energy, Water and Environment Systems (SDEWES), Lisbon, 2016.

### Economic and environmental analysis of a microalgae-based biorefinery utilizing CO<sub>2</sub> emitted from coal fired power plant

Igor L. Wiesberg, George V. Brigagão, Jose Luiz de Medeiros, Ofélia Q. F. Araújo<sup>1</sup>  
School of Chemistry  
Federal University of Rio de Janeiro, Rio de Janeiro, Brazil  
e-mail: ofelia@eq.ufrj.br

#### ABSTRACT

Coal fired power plants are major stationary sources of CO<sub>2</sub> and environmental constraints demand technologies for abatement. Carbon Capture and Storage is the most mature route for this purpose but it imposes severe economic penalty for power generation. Chemical or biochemical conversion of CO<sub>2</sub> to valuable products, which is known as Carbon Capture and Utilization, monetizes CO<sub>2</sub>, potentially mitigating the penalty associated to emissions reduction. This work evaluates the economic feasibility of CO<sub>2</sub> bio-capture by *Chlorella pyrenoidosa* and use of the resulting biomass as a feedstock to a biorefinery. The proposed mainstream arrangement is composed by: CO<sub>2</sub> biocapture at photobioreactor, microalgae oil extraction with part of the obtained biomass and gasification with the rest for biosyngas production, and finally methanol synthesis via biosyngas and purification. The photobioreactor is responsible for nearly one fifth of the total CAPEX and occupies an area of 986 ha, posing the most significant barrier to the implementation and economic feasibility of the biorefinery. Considering the net CO<sub>2</sub> capture, microalgae has a cost of 162 \$/t while CCS has 225\$/t.

#### KEYWORDS

Carbon capture and storage; carbon capture and utilization; microalgae; biorefinery; biomass gasification; methanol synthesis.

#### INTRODUCTION

The world economy is heavily dependent on fossil fuels, generating emissions with high concentrations of CO<sub>2</sub>. [1] investigates the post-combustion capture of CO<sub>2</sub> exhaust gases and its utilization in approaches that employ different technological routes. There are few applications on a commercial scale for CO<sub>2</sub>, both in the energy sector and in other industrial activities, resulting in emissions to the atmosphere due to lack of competitive technology to capture and allocate it.

Coal fired power plants are intensive stationary sources of carbon dioxide emissions. The atmospheric concentration of CO<sub>2</sub> has increased in the last decades due to the growth of industrial activity, which has impacted the natural balance of CO<sub>2</sub> in the atmosphere. Thus, environmental concerns promote a global research to develop technologies to reduce emissions and stabilize its concentration. One important way to reduce the global emission of greenhouse gases (GHG) is the practice of Carbon Capture, Utilization, and Storage (CCUS), which represents a group of technologies to capture CO<sub>2</sub> from industrial sources, e.g., flue gas, and then utilizing it physically (e.g., EOR), chemically (e.g., as a feedstock to the

# APPENDIX P – Scientific article on CO<sub>2</sub> utilization in microalga-based biorefinery producing methanol – Journal of Environmental Management

WIESBERG, I. L.; BRIGAGÃO, G. V.; DE MEDEIROS, J. L.; ARAÚJO, O. Q. F. Carbon dioxide utilization in a microalga-based biorefinery: efficiency of carbon removal and economic performance under carbon taxation. *Journal of Environmental Management*, 203, p. 988-988, 2017.

Journal of Environmental Management 203 (2017) 988–998

---



Contents lists available at [ScienceDirect](#)

## Journal of Environmental Management

journal homepage: [www.elsevier.com/locate/jenvman](http://www.elsevier.com/locate/jenvman)



---

Research article

### Carbon dioxide utilization in a microalga-based biorefinery: Efficiency of carbon removal and economic performance under carbon taxation

 CrossMark

Igor Lapenda Wiesberg, George Victor Brigagão, José Luiz de Medeiros, Ofélia de Queiroz Fernandes Araújo\*

Federal University of Rio de Janeiro, Rio de Janeiro, Brazil

---

**ARTICLE INFO**

*Article history:*  
Received 11 January 2017  
Received in revised form 25 February 2017  
Accepted 2 March 2017  
Available online 8 March 2017

*Keywords:*  
Carbon capture and storage  
Carbon dioxide utilization  
Microalgae  
Biorefinery  
Biomass gasification  
Methanol synthesis

**ABSTRACT**

Coal-fired power plants are major stationary sources of carbon dioxide and environmental constraints demand technologies for abatement. Although Carbon Capture and Storage is the most mature route, it poses severe economic penalty to power generation. Alternatively, this penalty is potentially reduced by Carbon Capture and Utilization, which converts carbon dioxide to valuable products, monetizing it. This work evaluates a route consisting of carbon dioxide bio-capture by *Chlorella pyrenoidosa* and use of the resulting biomass as feedstock to a microalgae-based biorefinery; Carbon Capture and Storage route is evaluated as a reference technology. The integrated arrangement comprises: (a) carbon dioxide bio-capture in a photobioreactor, (b) oil extraction from part of the produced biomass, (b) gasification of remaining biomass to obtain bio-syngas, and (c) conversion of bio-syngas to methanol. Calculation of capital and operational expenditures are estimated based on mass and energy balances obtained by process simulation for both routes (Carbon Capture and Storage and the biorefinery). Capital expenditure for the biorefinery is higher by a factor of 6.7, while operational expenditure is lower by a factor of 0.45 and revenues occur only for this route, with a ratio revenue/operational expenditure of 1.6. The photobioreactor is responsible for one fifth of the biorefinery capital expenditure, with footprint of about 1000 ha, posing the most significant barrier for technical and economic feasibility of the proposed biorefinery. The Biorefinery and Carbon Capture and Storage routes show carbon dioxide capture efficiency of 73% and 48%, respectively, with capture cost of 139\$/t and 304\$/t. Additionally, the biorefinery has superior performance in all evaluated metrics of environmental impacts.

© 2017 Elsevier Ltd. All rights reserved.

---

#### 1. Introduction

The world economy is heavily dependent on fossil fuels, generating massive emissions of carbon dioxide (CO<sub>2</sub>). Coal fired power plants are among the major stationary sources of CO<sub>2</sub> emissions, where Carbon Capture and Storage (CCS) is the leading technology for CO<sub>2</sub> management. Besides recognized technical barriers – e.g., existence of geological sites (Cuéllar-Franca and Azapagic, 2015), CO<sub>2</sub> monitoring for leakage (Cheah et al., 2016) – the absence of revenues imposes relevant economic penalty to the CO<sub>2</sub> source processes due to the significant capital investment required.

Alternatively, utilization of CO<sub>2</sub> aims to add value to the captured CO<sub>2</sub> (Carbon Capture and Utilization, CCU), through its chemical conversion (Aresta, 2010). The ensemble of technologies for CO<sub>2</sub> management is referred to CCUS (i.e., CCS + CCU), spanning from storage to physical, chemical and biochemical utilization (e.g., Enhanced Oil Recovery – EOR, methanol production). It is worth noting that a few chemical syntheses employ CO<sub>2</sub> as feedstock at a commercial scale (e.g., urea) (Aresta, 2010), where most alternatives are at the earlier stages of technology readiness level (most of them are still at laboratory or bench scale). Conversion of CO<sub>2</sub> to methanol (MeOH) outstands as a promising alternative, accordingly to technical and economic studies evaluating capital and operational expenditures, and environmental performance. Kourkoumpas et al. (2016) investigated the methanol production based on CO<sub>2</sub> capture from lignite power plants, estimating MeOH production cost of 421€/t in case of a power plant owner investment. Pérez-Fortes et al. (2016) investigated the direct CO<sub>2</sub>

---

\* Corresponding author.  
E-mail addresses: [igorwg@ufRJ.br](mailto:igorwg@ufRJ.br) (I.L. Wiesberg), [george.victor@poli.ufRJ.br](mailto:george.victor@poli.ufRJ.br) (G.V. Brigagão), [jlm@eq.ufRJ.br](mailto:jlm@eq.ufRJ.br) (J.L. de Medeiros), [ofelia@eq.ufRJ.br](mailto:ofelia@eq.ufRJ.br) (O. de Queiroz Fernandes Araújo).

## APPENDIX Q – Conference paper on sustainability analysis of biogas production from microalgae – Proceedings of LA-SDEWES2018

BRIGAGÃO, G. V.; WIESBERG, I. L.; MORTE, I. B. B.; PINTO, J. L.; ARAÚJO, O. Q. F.; DE MEDEIROS, J. L. Sustainability analysis of biomethane from thermo-mechanically pretreated microalgae. 1st Latin-American Conference on Sustainable Development of Energy Water and Environment Systems (LA-SDEWES), Rio de Janeiro, 2018.

Conference on Sustainable Development of Energy, Water and Environment Systems, Rio de Janeiro 28.-31.1.2018

**SDEWES.LA2018.0046**

### **Sustainability Analysis of Biomethane from Thermo-Mechanically Pretreated Microalgae**

G. Brigagão<sup>\*1</sup>, I. Lapenda Wiesberg<sup>2</sup>, I. Barboza Boa Morte<sup>3</sup>, J. Pinto<sup>3</sup>, O. Araujo<sup>1</sup>, J.L. De Medeiros<sup>1</sup>

<sup>1</sup>Federal University of Rio de Janeiro, Brazil; <sup>2</sup>Federal University of Rio de Janeiro, Escola de Química/ Escola Politécnica, Brazil; <sup>3</sup>Federal University of Rio de Janeiro, Escola de Química, Brazil (\*george.victor@poli.ufrj.br)

#### **Abstract**

Biodigestion of microalgae is a potentially sustainable strategy to recycling carbon dioxide via biofixation, substituting fossil fuels. This study compares technical and economic performance of three alternative microalgae-based biorefinery arrangements, consisting of a photobioreactor growing *Nannochloropsis salina*, alternative preheating strategies, biodigestion of the biomass and biogas processing to produce biomethane. The alternatives differ in the biomass pretreatment stage: (i) no pretreatment; (ii) thermal pretreatment (75 °C); and (iii) thermo-mechanical pretreatment (20 bar). Flue gas waste heat is used to supply heating demand. Process simulation is employed to support technical and economic analyses. Biogas production from thermo-mechanically pretreated microalgae is twice larger than biogas obtaining with thermal pretreatment. Assuming a carbon tax of 75 US\$ per ton of emitted CO<sub>2</sub>, the thermo-mechanical pretreatment is the only configuration among the investigated alternatives that shows Net Present Value more attractive than merely paying the tax.

# APPENDIX R – Scientific article on techno-economic analysis of biogas production from microalgae – Renewable and Sustainable Energy Reviews

BRIGAGÃO, G. V.; WIESBERG, I. L.; PINTO, J. L.; ARAÚJO, O. Q. F.; DE MEDEIROS, J. L. Upstream and downstream processing of microalgal biogas: emissions, energy and economic performances under carbon taxation. *Renewable and Sustainable Energy Reviews*, 112, p. 508-520, 2019.

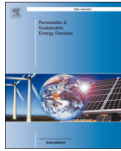
Renewable and Sustainable Energy Reviews 112 (2019) 508–520



Contents lists available at [ScienceDirect](#)

## Renewable and Sustainable Energy Reviews

journal homepage: [www.elsevier.com/locate/rser](http://www.elsevier.com/locate/rser)



---

### Upstream and downstream processing of microalgal biogas: Emissions, energy and economic performances under carbon taxation

George Victor Brigagão, Igor Lapenda Wiesberg, Juliana Leite Pinto, Ofélia de Queiroz Fernandes Araújo\*, José Luiz de Medeiros

Escola de Química, Federal University of Rio de Janeiro, CT, E, Ilha do Fundão, Rio de Janeiro, RJ, 21941-909, Brazil



---

**ARTICLE INFO**

**Keywords:**  
Biogas  
Microalga pretreatment  
Biomethane  
Bioelectricity  
CO<sub>2</sub> capture  
Anaerobic digestion

**ABSTRACT**

The study evaluates alternative and innovative arrangements for processing a microalgae biomass by anaerobic digestion to produce biogas. Cell wall limits bio-accessibility of microalgal intracellular compounds, demanding pretreatment to improve methane yield. Two pretreatments are evaluated at 75 °C using residual heat: thermal (1 bar) and thermomechanical (20 bar), which increased biogas production in 40% and 159%, respectively. Thermomechanical pretreatment is coupled to the following downstream processing cases: (i) biomethane; (ii) bioelectricity; (iii) biomethane with enhanced oil recovery; (iv) bioelectricity with enhanced oil recovery and (v) pressurized anaerobic digestion (6 bar) for biomethane with enhanced oil recovery. Processes are compared in three dimensions: energy, economic and carbon footprint. Such a framework including upstream and downstream processes, besides comparison of atmospheric and pressurized anaerobic digestion, with in-depth economic analysis, configures the main novelties of this work. Resource utilization efficiency metrics point advantage of pressurized anaerobic digestion case, while indicate biomethane production as less efficient than bioelectricity. When carbon dioxide post-combustion capture and enhanced oil recovery are applied to abate bioelectricity emissions, bioelectricity loses competitiveness to biomethane due to high energy penalties. Sensitivity of Net Present Value to varying carbon taxation (increasing costs), Capture & Trade mechanism and enhanced oil recovery (adding revenues) show superior resilience of biomethane with enhanced oil recovery. In base scenario conditions, where 30US\$/GJ electricity is applied, maximum biomass costs to economic feasibility for cases (i) to (v) are 50, 21, 100, 5 and 83US\$/t (dry-basis), respectively. Priced at 50US\$/GJ, the bioelectricity production frontier to feasibility starts at biomass costs ≈ 150US\$/t.

---

### 1. Introduction

Bio-based energy is shifting from intensive use of energy crops to diversified substrates, and progressively developing processes using a wide range of raw biomass [1]. Anaerobic digestion (AD) monetizes waste treatment producing a gaseous fuel, being the preferred technology for treating wastes of high moisture contents [2], e.g. microalgae suspensions and food wastes with 74–90%w water [3].

AD produces biogas with reduced Lower Heating Value (LHV) due to its high carbon dioxide (CO<sub>2</sub>) content (30–40%) [4], with methane (CH<sub>4</sub>) ranging 50–65% [2]. To attain high LHV without additional

upgrading equipment, Li et al. [2] proposed an *in situ* biogas upgrading consisting of a conventional continuously stirred tank digester (as acidogenesis reactor) followed by a pressurized biofilm AD, evaluated at four pressure levels showing beneficial effects of increasing AD operating pressures. Despite the promising results, the technology is at proof of concept stage.

Besides its low LHV, biogas is generally produced at low pressure, and has other impurities than CO<sub>2</sub> – e.g. ammonia (NH<sub>3</sub>), water (H<sub>2</sub>O) and, depending on substrate composition, hydrogen sulfide (H<sub>2</sub>S) [5]; being off-specified for injection in natural gas distribution grids. Hence, development of biogas upgrading techniques is required [6],

---

Abbreviations: AD, Anaerobic Digestion; BE, Bioelectricity; BM, Biomethane; CCU, Carbon Capture and Utilization; CW, Cooling-Water; EOR, Enhanced Oil Recovery; GT, Gas Turbine; HRSG, Heat-Recovery-Steam-Generation; HRT, Hydraulic Retention Time; LHV, Lower Heating Value; MEA, Monoethanolamine; NOPT, No Pretreatment; PAD, Pressurized Anaerobic Digestion; PSA, Pressure-Swing-Adsorption; ST, Steam Turbine; TEG, Triethylene Glycol; THPT, Thermal Pretreatment; TMPT, Thermo-Mechanical Pretreatment; VS, Volatile Solids

\* Corresponding author.

E-mail addresses: [george.victor@poli.ufrj.br](mailto:george.victor@poli.ufrj.br) (G.V. Brigagão), [igorwg@ufrj.br](mailto:igorwg@ufrj.br) (I.L. Wiesberg), [juliana.pinto@eq.ufrj.br](mailto:juliana.pinto@eq.ufrj.br) (J.L. Pinto), [ofelia@eq.ufrj.br](mailto:ofelia@eq.ufrj.br) (O.d.Q.F. Araújo), [jlm@eq.ufrj.br](mailto:jlm@eq.ufrj.br) (J.L. de Medeiros).

<https://doi.org/10.1016/j.rser.2019.06.009>  
Received 19 December 2018; Received in revised form 4 June 2019; Accepted 6 June 2019  
1364-0321/ © 2019 Elsevier Ltd. All rights reserved.

# APPENDIX S – Scientific article on techno-economic analysis of thermochemical pathways of corncob conversion – Fuel Processing Technology

BRIGAGÃO, G. V.; ARAÚJO, O. Q. F.; DE MEDEIROS, J. L.; MIKULCIC, H.; DUIC, N. A techno-economic analysis of thermochemical pathways for corncob-to-energy: fast pyrolysis to bio-oil, gasification to methanol and combustion to electricity. *Fuel Processing Technology*, 193, p. 102-113, 2019.

Fuel Processing Technology 193 (2019) 102–113

Contents lists available at [ScienceDirect](#)

## Fuel Processing Technology

journal homepage: [www.elsevier.com/locate/fuproc](http://www.elsevier.com/locate/fuproc)



---

Research article

### A techno-economic analysis of thermochemical pathways for corncob-to-energy: Fast pyrolysis to bio-oil, gasification to methanol and combustion to electricity

George Victor Brigagão<sup>a</sup>, Ofélia de Queiroz Fernandes Araújo<sup>a</sup>, José Luiz de Medeiros<sup>a</sup>, Hrvoje Mikulcic<sup>b,\*</sup>, Neven Duic<sup>b</sup>

<sup>a</sup> Escola de Química, Federal University of Rio de Janeiro, CT, E, Ilha do Fundão, Rio de Janeiro, RJ 21941-909, Brazil  
<sup>b</sup> Department of Energy, Power Engineering and Environment, Faculty of Mechanical Engineering and Naval Architecture, University of Zagreb, Luciceva 5, HR-10000 Zagreb, Croatia

---

**ARTICLE INFO**

**Keywords:**  
Corncob  
Thermochemical conversion  
Biomass pyrolysis  
Biomass gasification  
Methanol synthesis  
Cogeneration

**ABSTRACT**

Global warming concerns have driven developments in carbon neutral energy, pulling initiatives on biofuels production. However, the low bulk density and low specific energy of biomass refrain its widespread use due to logistic costs comprising harvesting and collection, storage, pretreatments and transportation. This work approaches increasing land energy productivity by thermochemical conversion of residual biomass to energy products, identifying the best options in terms of energy efficiency and economic indicators. Techno-economic performance of three corncob-to-energy pathways is investigated: gasification to methanol, fast pyrolysis to bio-oil and combustion to electricity. Fast pyrolysis allows higher energy recovery in its products (79%) than biomass gasification to methanol (53%), with biomass densification (volume reduction) of 72.7% and 86.2%, respectively. The combustion route presents net efficiency of 30.2% of biomass low heating value (LHV). All alternatives are economically feasible provided biomass cost is lower than US\$75.5/t. The minimum allowable product prices for economic attractiveness of gasification, combustion and pyrolysis routes are US\$305/t methanol, US\$80.1/MWh electricity and US\$1.47/gasoline-gallon-equivalent bio-oil. Despite its vulnerability to price volatility, gasification presents the highest net present value, seconded by the combustion route, which has lower medium-term payback and investment than gasification due to its process simplicity.

---

### 1. Introduction

Expansion of the world energy demand and global warming concerns have driven developments of carbon neutral energy sources, pushing production of transportation fuels from biomass [1]. Carbon neutrality of biofuels has been challenged, as carbon stock decreases with land use changes. Thus, harvesting for biofuels demands energy conversion efficiency and increased productivity [2].

A promising alternative for increasing energy productivity is the use of agricultural waste to produce electricity, as occur in the sugarcane-based bioethanol industry, where heat and electricity are co-generated from bagasse [3], with significant improvements in energy efficiency [4]. The same applies to corn-ethanol industry, where co-generation has been also suggested to improve its competitiveness over Brazilian sugarcane-ethanol [5]. Among the corn residues (cobs, husks, leaves and stalks), cobs stand out with reduced mineral [6] and nitrogen contents [7], favoring its utilization for combustion applications [6] and biofuels production. Although corncobs are mostly left to decay in the fields after grain harvests [7], energy products from corn residues have received increasing attention, e.g. electricity and products from thermochemical pathways, e.g. pyrolysis to biochar [8] and gasification to dimethyl ether [9] and methanol [10].

Comprising harvesting and collection, storage, pretreatments and transportation, biomass logistics costs refrain its widespread use in electricity and biofuels production [11]. Gallagher et al. [5], for the case of corn-processing regions, considered geographical location as critical for investing in biofuels, not only for the distance but also for the absence of trade barriers. Additional drawbacks in biomass utilization are its variability (chemical composition and physicochemical properties) and low bulk density, which is overcome by biomass

---

\* Corresponding author.  
E-mail addresses: [george.victor@poli.ufrj.br](mailto:george.victor@poli.ufrj.br) (G.V. Brigagão), [ofelia@eq.ufrj.br](mailto:ofelia@eq.ufrj.br) (O. de Queiroz Fernandes Araújo), [jlm@eq.ufrj.br](mailto:jlm@eq.ufrj.br) (J.L. de Medeiros), [hrvoje.mikulcic@fsb.hr](mailto:hrvoje.mikulcic@fsb.hr) (H. Mikulcic), [neven.duic@fsb.hr](mailto:neven.duic@fsb.hr) (N. Duic).

<https://doi.org/10.1016/j.fuproc.2019.05.011>  
Received 28 February 2019; Received in revised form 18 April 2019; Accepted 9 May 2019  
0378-3820/ © 2019 Elsevier B.V. All rights reserved.

# APPENDIX T – Scientific article on exergy-based sustainability analysis of CO<sub>2</sub> capture and storage or utilization to methanol production – Renewable and Sustainable Energy Reviews

WIESBERG, I. L.; BRIGAGÃO, G. V.; DE MEDEIROS, J. L.; ARAÚJO, O. Q. F. Carbon dioxide management via exergy-based sustainability assessment: carbon capture and storage versus conversion to methanol. *Renewable and Sustainable Energy Reviews*, 112, p. 720-732, 2019.

Renewable and Sustainable Energy Reviews 112 (2019) 720–732



Contents lists available at [ScienceDirect](#)

## Renewable and Sustainable Energy Reviews

journal homepage: [www.elsevier.com/locate/rser](http://www.elsevier.com/locate/rser)



---

### Carbon dioxide management via exergy-based sustainability assessment: Carbon Capture and Storage versus conversion to methanol



Igor Lapenda Wiesberg, George Victor Brigagão, Ofélia de Queiroz F. Araújo,  
José Luiz de Medeiros\*

*Escola de Química, Federal University of Rio de Janeiro, CT, E, Ilha do Fundão, Rio de Janeiro, RJ, 21941-909, Brazil*

---

**ARTICLE INFO**

**Keywords:**  
Exergy analysis  
Methanol production  
CO<sub>2</sub> hydrogenation  
CO<sub>2</sub> Bi-Reform  
Natural gas  
CO<sub>2</sub> capture

**ABSTRACT**

Carbon Capture and Storage and Carbon Capture and Utilization refer to carbon dioxide management technologies for its removal from flue-gases, followed by carbon recycling or storage, aiming at limiting global warming. For large-scale deployment, geological storage is the most promising alternative but imposes an economic penalty to the emitting process, while the utilization monetizes carbon dioxide contributing to compensate for the large capture costs. The exergy concept builds a suitable framework to measure useful power according to the Second Law of Thermodynamics, such that maximizing exergy efficiency necessarily promotes sustainability. This work applies a novel framework for exergy assessment of processes with chemical reactions, which is employed to evaluate the performance of two methanol production routes from carbon dioxide from power plant flue-gas: the direct hydrogenation and the indirect conversion through natural gas bi-reforming for synthesis gas production. Exergy efficiency of the direct route is about 66.3%, against 55.8% for the indirect one, indicating the lower sustainability of the latter. Carbon capture and storage had the worst Exergy efficiency, even lower than the emission scenario, accounting for 44.8% against 53.5%. Exergy metrics pinpoint low scalability as the main drawback of the utilization technologies, despite high exergy and capture efficiency.

---

### 1. Introduction

Carbon Capture and Utilization (CCU) technologies have potential to considerably contribute for improved sustainability of industrial and power generation activities while adding revenues to carbon dioxide (CO<sub>2</sub>) destination from chemical conversion to marketed products. Thus, CCU stands as an important solution to limit global warming while potentially enabling economically feasible replacement of fossil feedstocks to the chemical and energy industries. In this sense, methanol synthesis has been considered as one of the most promising routes for large-scale CCU [1], accounting for its widespread use and potential for a rapid growing demand, not only as a bulk commodity but also for its direct use as vehicle [2] and shipping fuel [3], as renewable energy carrier [4]. Moreover, methanol-to-olefins technology is of great importance because it replaces oil-derived products [5]. However, due to its chemical stability [6], CO<sub>2</sub> conversion requires severe reaction conditions [1], resulting in compression and heating

operations. A review of Life Cycle Assessments (LCA) of various CCU routes showed that the efficiency of the carbon removal and the environmental impacts varies greatly and are not always exciting when compared to CCS [7]. Unfortunately, as far as the authors are aware, there is no LCA study in the literature comparing CCS and CCU with methanol production.

Carbon Capture and Storage (CCS) alternatives, on the other hand, have the economic obstacle of being unprofitable activities that require large capital investment [8] and may only be economically attractive if the storage site is an oil reservoir, for Enhanced Oil Recovery (EOR), or a stringent carbon taxation policy is applied [9]. Indeed, the majority of the early CCS projects are for EOR purposes [10]. However, CCS is a promising technology for CO<sub>2</sub> mitigation from power plants emissions in a long term [8]. In order to increase its techno-economic feasibility, Calderon et al. [11] analyzed the recirculation of exhaust gases to rise the CO<sub>2</sub> partial pressure in the flue-gas of a NG power plant, simultaneously lowering the regeneration duty, its flow rate and its O<sub>2</sub>

---

**Abbreviations:** CCU, Carbon Capture and Utilization; CCS, Carbon Capture and Storage; DIRECT, Direct methanol production route through CO<sub>2</sub> hydrogenation; EOR, Enhanced Oil Recovery; INDIRECT, Indirect methanol production route through NG bi-reforming; LCA, Life Cycle Assessment; LPS, Low-pressure steam; MEA, Monoethanolamine; NG, Natural Gas; PFD, Process Flow Diagram; RER, Reference Environmental Reservoir

\* Corresponding author.  
E-mail addresses: [igorwg@ufRJ.br](mailto:igorwg@ufRJ.br) (I.L. Wiesberg), [george.victor@poli.ufRJ.br](mailto:george.victor@poli.ufRJ.br) (G.V. Brigagão), [ofelia@eq.ufRJ.br](mailto:ofelia@eq.ufRJ.br) (O.d.Q.F. Araújo), [jlm@eq.ufRJ.br](mailto:jlm@eq.ufRJ.br) (J.L. de Medeiros).

<https://doi.org/10.1016/j.rser.2019.06.032>  
Received 21 December 2018; Received in revised form 5 June 2019; Accepted 12 June 2019  
1364-0321/ © 2019 Elsevier Ltd. All rights reserved.

## APPENDIX U – Supplementary Material for Chapter 02

### U1. Detailed Process Conditions of Novel ASU TVR-2REB

Fig. 2.3 presents the flowsheet of the new proposed TVR-2REB ASU for low-pressure GOX supply. Air is split in a single TVR atmospheric cryogenic distillation column (structured packing for 72 theoretical stages) with an intermediate reboiler and a bottom reboiler. The column has two air feeds: saturated air vapor (37<sup>th</sup> stage) and liquefied air (7<sup>th</sup> stage). The reboilers are located under 45<sup>th</sup> and 72<sup>nd</sup> (bottom) stages. The main TVR-2REB innovation consists in the cryogenic recompression of top vapor nitrogen followed by its condensation in the intermediate reboiler, while a part of the fed air is liquefied by heating the bottom reboiler. About 17% of column top vapor goes to a cryogenic compressor, discharging superheated vapor cooled in the MHX to its dew-point. The saturated N<sub>2</sub> vapor is then condensed, sub-cooled, expanded to the column pressure and returned as top liquid reflux.

Air is compressed by MAC and cooled by direct-contact with cooling-water. A good fraction of the air feed goes to a pre-purification unit, and the rest goes to the booster air compressor (BAC) discharging high-pressure air to another pre-purification unit. Cryogenic refrigeration is promoted by expanding ≈64% of the high-pressure air after-cooled in MHX. TVR-2REB prescribes a compander fed with ≈2% of the air feed, in order to reduce power demand by reducing MAC discharge pressure. Thus, the Cold-Box is supplied with air at three pressures: 2.04 bar (MAC), 3.87 bar (BAC), and 5.87 bar (compander).

Liquid oxygen (LOX) is withdrawn from the column bottom and is vaporized in MHX, liquefying a small portion of medium-pressure air (MP-AIR) from BAC. GOX can also be alternatively withdrawn from the column above the liquid sump, while the medium-pressure air feed is condensed in the bottom reboiler. The majority of the impure N<sub>2</sub> top product sub-cools the liquefied nitrogen (LIN) and the liquefied air (LAIR) streams. After heat transfer in MHX, atmospheric GOX and waste nitrogen are obtained as products.

**Table U1.1.** Streams of TVR-2REB ASU.

<i>Stream</i>	<i>Air Intake</i>	<i>LP-PPU Feed</i>	<i>LP-AIR to MHX</i>	<i>MP-PPU Feed</i>	<i>MP-AIR to MHX</i>	<i>HP-AIR to Coolers</i>	<i>HP-AIR to MHX</i>	<i>HP-TX Inlet</i>	<i>HP-TX Outlet</i>	<i>LP-TX Inlet</i>	<i>LP-TX Outlet</i>	<i>MP-AIR to Cond.</i>	<i>p-LAIR to Subcool.</i>	<i>Subcooled p-LAIR</i>
%Vapor	100	100	100	100	100	100	100	100	100	100	100	43.0	0.00	0.00
T(°C)	15.0	12.0	20.0	15.1	20.0	62.2	20.0	-90.0	-135	-180	-190	-180	-181	-189
P(bar)	1.013	2.04	1.94	3.87	3.77	5.62	5.47	5.41	1.86	1.84	1.22	3.67	3.67	3.66
F(tmol/h)	32.13	19.71	19.57	12.29	11.50	0.73	0.73	0.73	0.73	20.30	20.30	11.50	11.50	11.50
%N <sub>2</sub>	77.30	77.54	78.11	77.73	78.11	78.11	78.11	78.11	78.11	78.11	78.11	78.11	78.11	78.11
%O <sub>2</sub>	20.74	20.80	20.95	20.85	20.95	20.95	20.95	20.95	20.95	20.95	20.95	20.95	20.95	20.95
%Ar	0.92	0.93	0.93	0.93	0.93	0.93	0.93	0.93	0.93	0.93	0.93	0.93	0.93	0.93
ppmCO <sub>2</sub>	356	358	-	358	-	-	-	-	-	-	-	-	-	-
ppmH <sub>2</sub> O	10,070	6907	-	4591	-	-	-	-	-	-	-	-	-	-

<i>Stream</i>	<i>LAIR to COL</i>	<i>LP-AIR to COL</i>	<i>COL Top Vapor</i>	<i>GAN to Compr.</i>	<i>p-GAN to MHX</i>	<i>p-GAN to Subcool.</i>	<i>p-GAN to Cond.</i>	<i>p-LIN to Subcool.</i>	<i>Subcooled p-LIN</i>	<i>LIN to COL</i>	<i>GAN to MHX</i>	<i>GAN Prod.</i>	<i>LOX to MHX</i>	<i>GOX Prod.</i>
%Vapor	3.46	100	100	100	100	100	100	0.00	0.00	0.00	100	100	0.00	100
T(°C)	-193	-190	-193	-193	-166	-181	-185	-186	-191	-194	-183	17.2	-182	17.2
P(bar)	1.22	1.22	1.20	1.20	2.79	2.78	2.77	2.77	2.76	1.20	1.19	1.09	1.25	1.15
F(tmol/h)	11.50	20.30	31.24	5.40	5.40	5.40	5.40	5.40	5.40	5.25	25.99	25.99	5.81	5.81
%N <sub>2</sub>	78.11	78.11	94.97	94.97	94.97	94.97	94.97	94.97	94.97	94.87	94.99	94.99	2.61	2.61
%O <sub>2</sub>	20.95	20.95	4.42	4.42	4.42	4.42	4.42	4.42	4.42	4.50	4.40	4.40	95.00	95.00
%Ar	0.93	0.93	0.61	0.61	0.61	0.61	0.61	0.61	0.61	0.62	0.61	0.61	2.39	2.39
ppmCO <sub>2</sub>	-	-	-	-	-	-	-	-	-	-	-	-	-	-
ppmH <sub>2</sub> O	-	-	-	-	-	-	-	-	-	-	-	-	-	-

## U2. Detailed Process Conditions of Ox-NGCC-EOR.

**Table U2.1.** Streams of Ox-NGCC-EOR (composition in molar basis).

<i>System</i>	<i>GOX Compression</i>			<i>Gas Turbine</i>				<i>Rankine Cycle</i>				<i>Direct Contact Cooler</i>			
<i>Stream</i>	<i>GOX Feed</i>	<i>Compressor Discharge</i>	<i>Recycle to Compress.</i>	<i>Compressor Discharge</i>	<i>NG Feed</i>	<i>GT Inlet</i>	<i>GT Outlet</i>	<i>ST Inlet</i>	<i>ST Outlet</i>	<i>Cond. Outlet</i>	<i>Feed Water</i>	<i>HRSG Outlet</i>	<i>DCC Outlet</i>	<i>Bottom Water</i>	<i>Water Purge</i>
%Vapor	100	100	100	100	100	100	100	100	90.1	0.00	0.00	100	100	0.00	0.00
T(°C)	15.0	140	30.0	430	25.0	1300	680	560	38.0	35.0	35.6	89.4	30.0	49.5	25.0
P(bar)	1.013	40.0	1.013	40.0	40.0	39.5	1.053	56.0	0.066	0.056	56.5	1.033	1.013	1.033	1.10
F(tmol/h)	5.81	5.81	38.44	38.44	2.65	47.02	47.02	19.96	19.96	19.96	19.96	47.02	41.76	177.6	5.26
%CO <sub>2</sub>	-	-	86.78	86.78	2.50	77.08	77.08	-	-	-	-	77.08	86.78	-	-
%H <sub>2</sub> O	-	-	4.18	4.18	0.01	14.89	14.89	100	100	100	100	14.89	4.18	100	100
%O <sub>2</sub>	95.00	95.00	0.00	0.00	-	0.00	0.00	-	-	-	-	0.00	0.00	-	-
%Ar	2.39	2.39	4.17	4.17	-	3.71	3.71	-	-	-	-	3.71	4.17	-	-
%N <sub>2</sub>	2.61	2.61	4.87	4.87	0.38	4.32	4.32	-	-	-	-	4.32	4.87	-	-
%CH <sub>4</sub>	-	-	-	-	89.00	-	-	-	-	-	-	-	-	-	-
%C <sub>2</sub> H <sub>6</sub>	-	-	-	-	7.00	-	-	-	-	-	-	-	-	-	-
%C <sub>3</sub> H <sub>8</sub>	-	-	-	-	1.00	-	-	-	-	-	-	-	-	-	-
%nC <sub>4</sub> H <sub>10</sub>	-	-	-	-	0.10	-	-	-	-	-	-	-	-	-	-
%nC <sub>5</sub> H <sub>12</sub>	-	-	-	-	0.01	-	-	-	-	-	-	-	-	-	-
%TEG	-	-	-	-	-	-	-	-	-	-	-	-	-	-	-
<i>System</i>	<i>CO<sub>2</sub> Compression</i>				<i>Glycol Dehydration</i>				<i>Liquefaction of EOR Fluid</i>						
<i>Stream</i>	<i>CO<sub>2</sub> Feed</i>	<i>CO<sub>2</sub> to ABS</i>	<i>CO<sub>2</sub> from ABS</i>	<i>Compressor Discharge</i>	<i>Lean TEG to ABS</i>	<i>Rich TEG to REG</i>	<i>Lean TEG from REG</i>	<i>TEG Makeup</i>	<i>Vapor Purge</i>	<i>Condenser Outlet</i>	<i>Flash Gas</i>	<i>EOR Fluid</i>			
%Vapor	100	100	100	100	0.00	0.00	0.00	0.00	100	0.00	100	100			
T(°C)	30.0	30.0	32.5	122	30.0	160	187	25.0	95	30.0	30.0	72.8			
P(bar)	1.013	50.5	50.0	130.5	50.0	1.05	1.05	1.05	1.013	130	130	350			
F(tmol/h)	3.33	3.19	3.15	3.15	0.12	0.13	0.12	2e-6	7e-3	3.15	0.00	3.15			
%CO <sub>2</sub>	86.78	90.38	90.45	90.45	-	0.97	-	-	17.31	90.45	90.45	90.45			
%H <sub>2</sub> O	4.18	4.18	138 ppm	138 ppm	11.27	15.3	11.27	11.27	82.69	138 ppm	138 ppm	138 ppm			
%O <sub>2</sub>	0.00	0.00	0.00	0.00	-	-	-	-	-	0.00	0.00	0.00			
%Ar	4.17	4.17	4.40	4.40	-	-	-	-	-	4.40	4.40	4.40			
%N <sub>2</sub>	4.87	4.87	5.13	5.13	-	-	-	-	-	5.13	5.13	5.13			
%CH <sub>4</sub>	-	-	-	-	-	-	-	-	-	-	-	-			
%C <sub>2</sub> H <sub>6</sub>	-	-	-	-	-	-	-	-	-	-	-	-			
%C <sub>3</sub> H <sub>8</sub>	-	-	-	-	-	-	-	-	-	-	-	-			
%nC <sub>4</sub> H <sub>10</sub>	-	-	-	-	-	-	-	-	-	-	-	-			
%nC <sub>5</sub> H <sub>12</sub>	-	-	-	-	-	-	-	-	-	-	-	-			
%TEG	-	-	-	-	88.73	65.49	88.73	88.73	-	-	-	-			

### U3. Relationships for Economic Analysis

Here the Fixed Capital Investment ( $FCI$ ) of the Air Separation Unit is calculated extrapolating a reference cost – quoted for the year of 2007 – of  $FCI_{2007}=141$  MMUSD for producing 52 kg/s GOX [38], which is corrected with inflationary factor Chemical Engineering Plant Cost Index (CEPCI) of 567.5 for the reference of 2017 (Chem. Eng. Magazine, Mar-2018), in accordance with Eq. (U3.1a), where the exponent for ASU extrapolation is 0.5 [38].

$$FCI_{2017}^{ASU} = FCI_{2007}^{ASU} (CEPCI_{2017} / CEPCI_{2007}) * (CF / CF^{REF})^{0.5} \quad (U3.1a)$$

Following the methods of Turton et al. [35], except for the Air Separation Unit, the Fixed Capital Investment ( $FCI$ ) is calculated using a base bare-module cost ( $C_{BM}^0$ ) in a reference capacity and condition, corrected with same inflationary factor CEPCI of 567.5 for 2017, which is then multiplied by the design pressure and material factor ( $F_{BM}$ ) to give the total bare-module installed cost ( $C_{BM}=C_{BM}^0 * F_{BM}$ ). Contingency ( $C_{BM} * 0.18$ ) – for unexpected expenses and uncertainties – and auxiliary facility costs ( $C_{BM}^0 * 0.50$ ) – related to land purchase, off-sites and utility systems – are then included to  $FCI$  (USD), so that it is obtained using Eq. (U3.1b), where  $N_{EQ}$  represents the number of equipment items.

$$FCI = 1.18 * \sum_{i=1}^{N_{EQ}} C_{BM\ i} + 0.5 * \sum_{i=1}^{N_{EQ}} C_{BM\ i}^0 \quad (U3.1b)$$

When the required capacity is out of the range of cost predictors ( $C_{BM}^0$ ),  $FCIs$  are extrapolated from limiting bound of capacity using the *Six-Tenth Rule* in Eq. (U3.2), where  $CF$  is the capacity factor – power for machines, area for exchangers and flow rate for separators. The annual Cost of Manufacturing ( $COM$ ) is calculated using Eq. (U3.3), where  $CRM$ ,  $CUT$ ,  $COL$ ,  $CWT$  are, respectively, annual costs (USD/y) of raw materials, utilities, labor and waste treatment [35]. Formulae of Gross Annual Profit ( $GAP$ , USD/y), Annual Profit ( $AP$ , USD/y) and Net Present Value ( $NPV$ , USD) are given in Eqs. (U3.4) to (U3.6), where  $REV$  (USD/y),  $DEPR$  (USD/y),  $N$ ,  $i$  (%) and  $ITR$  (%), refer, respectively, to revenues, annual depreciation (10% annual rate), operational years of analysis ( $N=30$  with invariant feed and conditions), annual interest rate ( $i=10\%$ ) and income tax rate ( $ITR=34\%$ ).

$$FCI = FCI^{LIMIT} * (CF / CF^{LIMIT})^{6/10} \quad (U3.2)$$

$$COM = 0.18 * FCI + 2.73 * COL + 1.23 * (CRM + CUT + CWT) \quad (U3.3)$$

$$GAP = REV - COM \quad (U3.4)$$

$$AP = GAP - (ITR / 100) * (GAP - DEPR) \quad (GAP > DEPR) \quad \text{or} \quad AP = GAP \quad (U3.5)$$

$$NPV = -(0.2 + 0.3 * q^{-1} + 0.5 * q^{-1}) FCI + AP \left\{ \sum_{i=3}^{N+3} q^{-i} \right\}, \quad q = (1 + i / 100) \quad (U3.6)$$

## APPENDIX V – Supplementary Material for Chapter 03

### V1. Supersonic Separator Thermodynamic Modeling

A rigorous thermodynamic modeling of a supersonic separator (SS) was implemented in HYSYS 8.8 as a Unit Operation Extension (UOE) – SS-UOE – whose algorithm is disclosed (Arinelli et al., 2017, [19]). SS-UOE executes rigorous multiphase supersonic flow on a converging-diverging nozzle and can work with any thermodynamic package available in HYSYS (e.g. PR-EOS, CPA-EOS) for solving multiphase equilibrium (VLE or VLWE). SS-UOE uses another UOE – PEC-UOE – for calculating the phase-equilibrium (VLE or VLWE) sound speed property ( $c$ ) which is not detailed here (de Medeiros et al., 2017, [20]). The main premise in SS-UOE and PEC-UOE is that thermodynamic equilibrium exists everywhere in the SS, excepting across the irreversible normal shock transition.

#### V1.1. SS-UOE Algorithm

Properties are expressed in molar basis and strict SI units (see Nomenclature). All thermodynamic properties (1<sup>st</sup> and 2<sup>nd</sup> order) are multiphase VLWE properties, except after normal shock. When multiphase states are unfeasible, HYSYS flashes automatically converge to single-phase states. This version assumes linear diameter profiles as in Fig. 3.1, but other geometries can be installed as in the example of Appendix B. Also the SS adiabatic efficiencies are supposed as  $\eta^{EXP\%} = \eta^{CMP\%} = 100\%$ . Cases with  $\eta^{EXP\%} < 100\%$  and/or  $\eta^{CMP\%} < 100\%$  are discussed in [19]. In SS-UOE the throat diameter  $D_T$  is sought to match  $Ma=1$ . Mach and length tolerances are  $\delta_M \approx 10^{-3}$  and  $\delta_L \approx 10^{-3}$  m. SS-UOE algorithm has eight steps: [Step 1] Input Information; [Step 2] Subsonic Acceleration; [Step 3] SS Sizing; [Step 4] Supersonic Acceleration; [Step 5] Pre-Shock Fractionation; [Step 6] Normal Shock Front; [Step 7] Subsonic Deceleration; [Step 8] Finishing Calculations.

**[Step 1] Input Information.**  $F_E, T_E, P_E$  and  $\underline{Z}_E$  are retrieved from SS feed in the flowsheet.  $D_I, D_O, \alpha, \beta, Ma^{Shock}$  are entered via SS-UOE user-interface. Calculate  $M_{ME}$  and  $q_E = F_E \cdot M_{ME}$ . Eqs. (V1.1a) to (V1.1d) calculate entrance flow properties.

$$\text{Flash} ( P_E, T_E, \underline{Z}_E ) \xrightarrow{\text{Multiphase Property}} \bar{H}_E, \bar{S}_E, \rho_E \quad (\text{V1.1a})$$

$$\text{PEC-UOE} ( P_E, T_E, \underline{Z}_E ) \xrightarrow{\text{Multiphase Sound Speed}} c_E \quad (\text{V1.1b})$$

$$v_E = 4q_E / (\pi \cdot D_I^2 \cdot \rho_E), \bar{K}_E = M_{ME} \cdot v_E^2 / 2 \quad (\text{V1.1c})$$

$$\bar{E}_E = \bar{H}_E + \bar{K}_E, Ma_E = v_E / c_E \quad (\text{V1.1d})$$

**[Step 2] Subsonic Acceleration.** Subsonic acceleration in the converging section is solved by small isentropic expansions (index  $n$ ) from entrance until  $Ma=1$  obtaining throat diameter  $D_T$ . Expansion step  $\delta_p$  ( $\leq 10^4 Pa$ ) is handled. Eqs. (V1.2a) to (V1.2c) are initializations. Eqs. (V1.2d) to (V1.2j) are iterated.

$$n = 0, \quad x^{(0)} = 0, \quad P^{(0)} = P_E, \quad T^{(0)} = T_E \quad (\text{V1.2a})$$

$$D^{(0)} = D_I, \quad v^{(0)} = v_E, \quad \delta_p = 10^4 Pa \quad (\text{V1.2b})$$

$$\bar{K}^{(0)} = \bar{K}_E, \quad \bar{H}^{(0)} = \bar{H}_E, \quad c^{(0)} = c_E, \quad Ma^{(0)} = Ma_E \quad (\text{V1.2c})$$

----- Do-Loop -----

$$n \equiv n + 1, \quad P^{(n)} \equiv P^{(n-1)} - \delta_p \quad (\text{V1.2d})$$

$$\text{Flash} ( P^{(n)}, \bar{S}_E, \underline{Z}_E ) \xrightarrow{\text{Multiphase Prop.}} T^{(n)}, \bar{H}^{(n)}, \rho^{(n)} \quad (\text{V1.2e})$$

$$\text{PEC-UOE} ( P^{(n)}, T^{(n)}, \underline{Z}_E ) \xrightarrow{\text{Multiphase Sound Speed}} c^{(n)} \quad (\text{V1.2f})$$

$$\bar{K}^{(n)} = \bar{E}_E - \bar{H}^{(n)}, \quad v^{(n)} = \sqrt{2 \cdot \bar{K}^{(n)} / M_{ME}} \quad (\text{V1.2g})$$

$$Ma^{(n)} = v^{(n)} / c^{(n)}, \quad D^{(n)} = \sqrt{4q_E / (\pi \cdot v^{(n)} \cdot \rho^{(n)})} \quad (\text{V1.2h})$$

$$\text{if } Ma^{(n)} < 1 - \delta_M \rightarrow \text{Handle } \delta_p \text{ with } Ma^{(n)} \text{ \& Do Eqs. (V1.2d) to (V1.2i)} \quad (\text{V1.2i})$$

$$\text{if } Ma^{(n)} > 1 + \delta_M \rightarrow \text{Reduce } \delta_p, n \equiv n - 1 \text{ \& Do Eqs. (V1.2d) to (V1.2i)} \quad (\text{V1.2j})$$

----- End-of-Loop -----

$$D_T = D^{(n)} \quad (\text{V1.2k})$$

$$\text{if } 1 - \delta_M \leq Ma^{(n)} \leq 1 + \delta_M \longrightarrow \text{Stop} \quad (\text{V1.2m})$$

**[Step 3] SS Sizing.** Eqs. (V1.3a) and (V1.3b) give SS lengths and axial locations of all diameters with  $D_T$ .

$$L_C = \frac{D_I - D_T}{2 \cdot \tan \alpha}, \quad L_D = \frac{D_O - D_T}{2 \cdot \tan \beta}, \quad L = L_C + L_D \quad (\text{V1.3a})$$

$$\text{For all } D^{(k)} \text{ (} k = 1 \rightarrow n \text{) obtain } x^{(k)} = L_C - \frac{D^{(k)} - D_T}{2 \cdot \tan \alpha} \quad (\text{V1.3b})$$

**[Step 4] Supersonic Acceleration.** Supersonic acceleration in the diverging section is handled via small isentropic expansions (index  $n$ ) from the throat until  $Ma = Ma^{Shock}$ . Step  $\delta_p$  ( $\leq 10^4 Pa$ ) is handled. Eq. (V1.4a) is initialization. Eqs. (V1.4b) to (V1.4i) are iterated.

$$\delta_p = 10^4 Pa$$

(V1.4a)

----- Do-Loop -----

$$n \equiv n + 1, \quad P^{(n)} \equiv P^{(n-1)} - \delta_p \quad (\text{V1.4b})$$

$$\text{Flash } (P^{(n)}, \bar{S}_E, \underline{Z}_E) \xrightarrow{\text{Multiphase Property}} T^{(n)}, \bar{H}^{(n)}, \rho^{(n)} \quad (\text{V1.4c})$$

$$\text{PEC-UOE } (P^{(n)}, T^{(n)}, \underline{Z}_E) \xrightarrow{\text{Multiphase Sound Speed}} c^{(n)} \quad (\text{V1.4d})$$

$$\bar{K}^{(n)} = \bar{E}_E - \bar{H}^{(n)}, \quad v^{(n)} = \sqrt{2 \cdot \bar{K}^{(n)} / M_{ME}} \quad (\text{V1.4e})$$

$$Ma^{(n)} = v^{(n)} / c^{(n)}, \quad D^{(n)} = \sqrt{4q_E / (\pi \cdot v^{(n)} \cdot \rho^{(n)})} \quad (\text{V1.4f})$$

$$x^{(n)} = L_C + \frac{D^{(n)} - D_T}{2 \cdot \tan \beta} \quad (\text{V1.4g})$$

$$\text{if } Ma^{(n)} < Ma^{Shock} - \delta_M \rightarrow \text{Handle } \delta_p \text{ with } Ma^{(n)} \text{ \& Do Eqs. (V1.4b) to (V1.4h)} \quad (\text{V1.4h})$$

$$\text{if } Ma^{(n)} > Ma^{Shock} + \delta_M \rightarrow \text{Reduce } \delta_p, n \equiv n - 1 \text{ \& Do Eqs. (V1.4b) to (V1.4h)} \quad (\text{V1.4i})$$

----- End-of-Loop -----

$$T^{Shock} = T^{(n)}, \quad P^{Shock} = P^{(n)} \quad (\text{V1.4j})$$

$$L^{Shock} = x^{(n)}, \quad D^{Shock} = D^{(n)}, \quad v^{Shock} = v^{(n)} \quad (\text{V1.4k})$$

$$\text{if } Ma^{Shock} - \delta_M \leq Ma^{(n)} \leq Ma^{Shock} + \delta_M \rightarrow \text{Stop} \quad (\text{V1.4m})$$

**[Step 5] Pre-Shock Fractionation.**  $Flash(P^{Shock}, T^{Shock}, \underline{Z}_E)$  solved at  $x=L^{Shock}$  in Eq. (V1.5a). Liquid phases “L” and “W” are collected as two-phase “L+W” condensate, while the vapor is kept as working fluid. Stagnation  $(T, P)$  of L+W condensate is adjusted later at the discharge pressure. Eqs. (V1.5b) and (V1.5c) give velocities of L+W condensate and of vapor ( $v_{L+W}$ ,  $v_V$ ) after fractionation under constant flow section. Properties just before shock are retrieved from segregated vapor via Eqs. (V1.5d) to (V1.5g). Eqs. (V1.5h) to (V1.5i) finish pre-shock properties.

$$Flash ( P^{Shock}, T^{Shock}, \underline{Z}_E ) \rightarrow \left\{ \begin{array}{l} F_V, \underline{Y}, \rho_V, \bar{H}_V, \bar{S}_V, M_{MV} \\ F_L, \underline{X}_L, \rho_L, \bar{H}_L, \bar{S}_L, M_{ML} \\ F_W, \underline{X}_W, \rho_W, \bar{H}_W, \bar{S}_W, M_{MW} \end{array} \right\} \quad (V1.5a)$$

$$v_V = \frac{(F_V \cdot M_{MV} / \rho_V) \cdot v^{Shock}}{F_V \cdot M_{MV} / \rho_V + F_L \cdot M_{ML} / \rho_L + F_W \cdot M_{MW} / \rho_W} \quad (V1.5b)$$

$$v_{L+W} = \frac{(F_L \cdot M_{ML} / \rho_L + F_W \cdot M_{MW} / \rho_W) \cdot v^{Shock}}{F_V \cdot M_{MV} / \rho_V + F_L \cdot M_{ML} / \rho_L + F_W \cdot M_{MW} / \rho_W} \quad (V1.5c)$$

$$P_{BS} \equiv P^{Shock}, \quad T_{BS} \equiv T^{Shock}, \quad D_{BS} = D^{Shock} \quad (V1.5d)$$

$$M_{MBS} = M_{MV}, \quad \bar{H}_{BS} = \bar{H}_V, \quad \bar{S}_{BS} = \bar{S}_V \quad (V1.5e)$$

$$\underline{Z}_{BS} = \underline{Y}, \quad v_{BS} = v_V, \quad \rho_{BS} = \rho_V \quad (V1.5f)$$

$$F_{BS} = F_V, \quad q_{BS} = F_{BS} \cdot M_{MBS} \quad (V1.5g)$$

$$PEC - UOE ( P_{BS}, T_{BS}, \underline{Z}_{BS} ) \xrightarrow{\text{Multiphase Sound Speed}} c_{BS} \quad (V1.5h)$$

$$Ma_{BS} = v_{BS} / c_{BS}, \quad \bar{K}_{BS} = M_{MBS} \cdot v_{BS}^2 / 2, \quad \bar{E}_{BS} = \bar{K}_{BS} + \bar{H}_{BS} \quad (V1.5i)$$

**[Step 6] Normal Shock Front.** If flow is supersonic after condensate withdrawal (checked by Eq. (V1.6a) with  $Ma_{BS}$ ), cross-shock energy, momentum and mass balances are solved – Eqs. (V1.6b), (V1.6c) and (V1.6e) – for temperature ( $T_{AS}$ ), pressure ( $P_{AS}$ ) and velocity ( $v_{AS}$ ) after shock. An embedded  $Flash(P_{AS}, T_{AS})$  gives single-phase properties  $\bar{H}$ ,  $\rho$  after shock.  $v_{AS}$  is eliminated in terms of  $T_{AS}$  and  $P_{AS}$  by Eq. (V1.6e), giving Eqs. (V1.6b) and (V1.6c) for  $T_{AS}$  and  $P_{AS}$  which are numerically solved via Newton-Raphson Method. Eqs. (V1.6f) to (V1.6h) calculate single-phase after shock flow properties (with/without an actual shock).

$$\text{if } Ma_{BS} \leq 1 \longrightarrow T_{AS} = T_{BS}, P_{AS} = P_{BS}, v_{AS} = v_{BS}, \text{ Go to Eq. (V1.6f)} \quad (\text{V1.6a})$$

----- Newton-Raphson Method -----

$$\bar{H}(T_{AS}, P_{AS}, \underline{Z}_{BS}) + M_{MBS} \frac{(v_{AS}(T_{AS}, P_{AS}))^2}{2} - \bar{H}_{BS} - \bar{K}_{BS} = 0 \quad (\text{V1.6b})$$

$$\rho(T_{AS}, P_{AS}, \underline{Z}_{BS})(v_{AS}(T_{AS}, P_{AS}))^2 + P_{AS} - \rho_{BS}v_{BS}^2 - P_{BS} = 0 \quad (\text{V1.6c})$$

$$Flash(P_{AS}, T_{AS}, \underline{Z}_{BS}) \xrightarrow{\text{Single/Multi Phase Property}} \bar{H}(P_{AS}, T_{AS}, \underline{Z}_{BS}), \rho(P_{AS}, T_{AS}, \underline{Z}_{BS}) \quad (\text{V1.6d})$$

$$v_{AS}(T_{AS}, P_{AS}) = \frac{4q_{BS}}{\pi D_{BS}^2 \rho(T_{AS}, P_{AS}, \underline{Z}_{BS})} \quad (\text{V1.6e})$$

----- End of Newton-Raphson Method -----

$$M_{MAS} = M_{MBS}, \underline{Z}_{AS} = \underline{Z}_{BS}, \rho_{AS} = \rho(T_{AS}, P_{AS}, \underline{Z}_{AS}) \quad (\text{V1.6f})$$

$$\bar{H}_{AS} = \bar{H}(T_{AS}, P_{AS}, \underline{Z}_{AS}), \bar{S}_{AS} = \bar{S}(T_{AS}, P_{AS}, \underline{Z}_{AS}) \quad (\text{V1.6g})$$

$$PEC - UOE(P_{AS}, T_{AS}, \underline{Z}_{AS}) \xrightarrow{\text{Single-Phase Sound Speed}} c_{AS} \quad (\text{V1.6h})$$

$$q_{AS} = q_{BS}, F_{AS} = F_{BS}, D_{AS} = D_{BS}, v_{AS} = \frac{4q_{AS}}{\pi D_{AS}^2 \rho_{AS}} \quad (\text{V1.6i})$$

$$\bar{K}_{AS} = M_{MAS} \frac{v_{AS}^2}{2}, \bar{E}_{AS} = \bar{H}_{AS} + \bar{K}_{AS}, Ma_{AS} = v_{AS} / c_{AS}, \Delta \bar{S}^{Shock} = \bar{S}_{AS} - \bar{S}_{BS} \quad (\text{V1.6j})$$

**[Step 7] Subsonic Deceleration.** Diffuser subsonic compression is handled by small isentropic compressions (index  $n$ ) from  $x=L^{Shock}$  to  $x=L$ . Step  $\delta_p$  ( $\leq 10^4 Pa$ ) is handled. Eqs. (V1.7a) to (V1.7c) are initializations. Eqs. (V1.7d) to (V1.7o) are iterated.

$$n = n + 1, \quad x^{(n)} = L^{Shock}, \quad P^{(n)} = P_{AS}, \quad T^{(n)} = T_{AS} \quad (V1.7a)$$

$$D^{(n)} = D_{AS}, \quad v^{(n)} = v_{AS}, \quad \delta_p = 10^4 Pa \quad (V1.7b)$$

$$\bar{K}^{(n)} = \bar{K}_{AS}, \quad \bar{H}^{(n)} = \bar{H}_{AS}, \quad c^{(n)} = c_{AS}, \quad Ma^{(n)} = Ma_{AS} \quad (V1.7c)$$

----- Do-Loop -----

$$n \equiv n + 1, \quad P^{(n)} \equiv P^{(n-1)} + \delta_p \quad (V1.7d)$$

$$Flash ( P^{(n)}, \bar{S}_{AS}, \underline{Z}_{AS} ) \xrightarrow{Single-Phase Property} T^{(n)}, \bar{H}^{(n)}, \rho^{(n)} \quad (V1.7e)$$

$$PEC-UOE ( P^{(n)}, T^{(n)}, \underline{Z}_{AS} ) \xrightarrow{Single-Phase Sound Speed} c^{(n)} \quad (V1.7f)$$

$$\bar{K}^{(n)} = \bar{E}_{AS} - \bar{H}^{(n)}, \quad v^{(n)} = \sqrt{2 \cdot \bar{K}^{(n)} / M_{MAS}} \quad (V1.7g)$$

$$Ma^{(n)} = v^{(n)} / c^{(n)}, \quad D^{(n)} = \sqrt{4q_{AS} / (\pi \cdot v^{(n)} \cdot \rho^{(n)})}, \quad x^{(n)} = L_C + \frac{D^{(n)} - D_T}{2 \cdot \tan \beta} \quad (V1.7h)$$

$$\text{if } x^{(n)} < L - \delta_L \rightarrow \text{Handle } \delta_p \text{ with } x^{(n)} \text{ \& Do Eqs. (V1.7d) to (V1.7i)} \quad (V1.7i)$$

$$\text{if } x^{(n)} > L + \delta_L \rightarrow \text{Reduce } \delta_p, n \equiv n - 1 \text{ \& Do Eqs. (V1.7d) to (V1.7i)} \quad (V1.7j)$$

----- End-of-Loop -----

$$P^{Discharge} = P^{(n)}, \quad T^{Discharge} = T^{(n)}, \quad \underline{Z}^{Discharge} = \underline{Z}_{AS}, \quad F^{Discharge} = F_{AS} \quad (V1.7k)$$

$$\bar{H}^{Discharge} = \bar{H}^{(n)}, \quad \bar{S}^{Discharge} = \bar{S}( P^{(n)}, T^{(n)}, \underline{Z}_{AS} ) \quad (V1.7m)$$

$$v^{Discharge} = v^{(n)}, \quad Ma^{Discharge} = Ma^{(n)}, \quad \rho^{Discharge} = \rho^{(n)} \quad (V1.7n)$$

$$\text{if } L - \delta_L \leq x^{(n)} \leq L + \delta_L \longrightarrow \text{Stop} \quad (V1.7o)$$

**[Step 8] Finishing Calculations.** Eqs. (V1.8a) and (V1.8b) collate data of  $L+W$  condensate ejected from SS. Eq. (V1.8c) adjusts  $L+W$  condensate to stagnation at  $P^{Discharge}$ . Discharge gas and stagnant condensate data are inserted in the flowsheet products (Eqs. (V1.8d) and (V1.8e)).

$$F_{L+W} = F_L + F_W, \quad P_{L+W} = P^{Discharge}, \quad \underline{Z}_{L+W} = \frac{F_L \underline{Z}_L + F_W \underline{Z}_W}{F_L + F_W} \quad (V1.8a)$$

$$\bar{H}_{L+W} = \left( \frac{F_L \bar{H}_L + F_W \bar{H}_W}{F_L + F_W} \right) + \left( \frac{F_L M_{ML} + F_W M_{MW}}{F_L + F_W} \right) \frac{v_{L+W}^2}{2} \quad (V1.8b)$$

$$Flash (P_{L+W}, \bar{H}_{L+W}, \underline{Z}_{L+W}) \xrightarrow{\text{Multiphase Property}} T_{L+W}, \rho_{L+W}, \bar{S}_{L+W} \quad (V1.8c)$$

$$L+W \text{ Condensate: } F_{L+W}, T_{L+W}, P_{L+W}, \underline{Z}_{L+W}, \bar{H}_{L+W}, \rho_{L+W}, \bar{S}_{L+W} \quad (V1.8d)$$

$$Lean Gas: F^{Discharge}, T^{Discharge}, P^{Discharge}, \underline{Z}^{Discharge}, \bar{H}^{Discharge}, \rho^{Discharge}, \bar{S}^{Discharge} \quad (V1.8e)$$

## V2. Throat Signatures of SS Axial Profiles and Validation of SS-UOE

Let the flow section area of converging-diverging nozzles,  $A(x)$ , where  $x$  is nozzle axial position. SS axial profiles of several variables in converging-diverging nozzles with  $(dA/dx)^{Throat} \neq 0$  must present certain characteristic features proved in [20].

### V2.1. Throat Signatures in SS Profiles

Any compressible isentropic supersonic 1D flow through a converging-diverging nozzle with  $(dA/dx)^{Throat} \neq 0$  (e.g. Fig. 3.1), with either single-phase real gas or two-phase vapor-liquid equilibrium or any multiphase equilibrium compressible fluid or even any multiphase and multi-reactive equilibrated compressible fluid (i.e. undertaking chemical reactions at equilibrium) must exhibit spatial gradient  $\pm\infty$  singularities at the throat under  $Ma^{Throat} \rightarrow I^-$ , the throat sonic limit in Eq. (V2.1), where  $Ma=v/c$ ,  $v$  is the axial flow velocity and  $c$  the thermodynamic sound speed property. Eq. (V2.1) is a very general relationship as single-phase or multiphase and/or multi-reactive flows apply [20], being the necessary and sufficient condition compressible 1D isentropic equilibrium flow with  $(dA/dx)^{Throat} \neq 0$ .

$$\frac{dT}{dx} = -\infty, \quad \frac{dP}{dx} = -\infty, \quad \frac{dv}{dx} = +\infty \quad (Ma^{Throat} \rightarrow I^-, \quad \left(\frac{dA}{dx}\right)^{Throat} \neq 0) \quad (V2.1)$$

It can be shown [20] that Eq. (V2.1) leads to Eqs. (3.2a) and (3.2b) whether the multiphase and/or multi-reactive 1D compressible isentropic flow is, respectively, *vapor-dominated* ( $\psi \approx 1$ ) or *liquid-dominated* ( $\psi < \approx 0.5$ ). It is seen that the only difference between Eqs. (3.2a) and (3.2b) is the  $dc/dx$  sign at the throat. These limit throat gradients are true SS “signatures” which only occur at the throat in regular SS operation under throat sonic limit ( $Ma^{Throat} \rightarrow I^-$ ) and  $(dA/dx)^{Throat} \neq 0$ .

## V2.2. Inexistent SS Signatures at Throat Sonic Flow: SS-UOE Validation

In SS nozzles designed with  $(dA/dx)^{Throat} = 0$  SS profiles does not show SS “signatures” in the sense of Sec. V2.1. This was the case when Yang et al. [26] validated their SS CFD framework with an old work of Arina [26]. Arina studied SS with  $3.071 \text{ kmol/h}$  of dry air ( $21\%O_2, 79\%N_2$ ) with  $P^{Inlet} = 100000 \text{ Pa}$ ,  $T^{Inlet} = 288 \text{ K}$ ,  $P^{Outlet} = 83049 \text{ Pa}$ . This is a SS at low-pressure without phase-change as air is dry and supercritical. Arina’s nozzle in Fig. V2.1a, has non-linear diameter profiles given in Eqs. (V2.2) with  $(dA/dx)^{Throat} = 0$ , where inlet, throat and outlet diameters were, respectively,  $D_I = 17.84 \text{ mm}$ ,  $D_T = 11.28 \text{ mm}$  and  $D_O = 13.82 \text{ mm}$ , with converging, diverging and total lengths respectively  $L_C = 50 \text{ mm}$ ,  $L_D = 50 \text{ mm}$ ,  $L = 100 \text{ mm}$ .

$$D(\text{mm}) = \sqrt{400 * (2.5 + (Z - 1.5) * 3Z^2) / \pi} \quad , \quad Z = x / L_C \quad , \quad 0 \leq x \leq L_C \quad (\text{V2.2a})$$

$$D(\text{mm}) = \sqrt{400 * (3.5 - (6 - 4.5Z + Z^2) * Z) / \pi} \quad , \quad Z = x / L_C \quad , \quad L_C \leq x \leq L \quad (\text{V2.2b})$$

Yang et al.[26] validated their CFD modeling by plotting their SS pressure profile against Arina’s (also obtained via CFD) in their Fig. 2 with good agreement. Both profiles, as expected, did not have the  $dP/dx = -\infty$  singularity at sonic throat, a consequence of  $(dA/dx)^{Throat} = 0$ . As phase-change is ruled out, also there is no reason for discrepancies between Arina’s data and the SS model of present work – SS-UOE – which handles phase-changes and multiphase compressible flow rigorously. This, if true, validates the present thermodynamic SS framework. To do this, Arina’s diameter profiles where installed in SS-UOE as shown in Fig. V2.1a (throat at  $x = L_C = 0.05 \text{ m}$ ). Arina’s nozzle was simulated by SS-UOE using PR-EOS, with results in Figs. V2.1b and V2.1c. Fig. V2.1b shows SS-UOE pressure profile against Arina’s counterpart, with everywhere perfect concordance, except at normal shock, where Arina’s CFD profile exhibits a discreet, but perceptible, inclined shock jump, which should be a truly vertical discontinuity as obtained by SS-UOE. Fig. V2.1c depicts only SS-UOE profiles for  $T$  and  $c$  as there are no Arina’s counterparts.

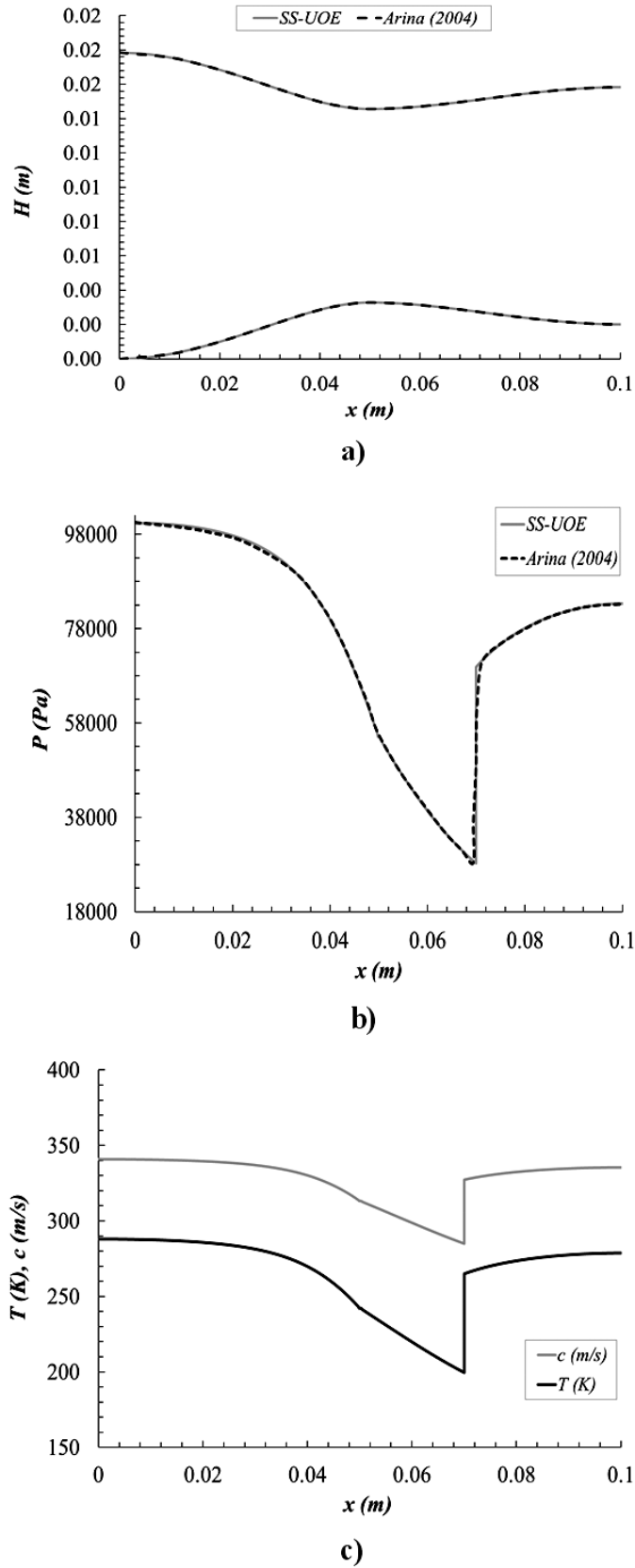


**Fig. V2.1.** SS with dry air: (a) Diameter of Arina's nozzle vs  $x(m)$  and as installed in SS-UOE; (b) SS-UOE  $P(Pa)$  vs  $x(m)$  vs Arina's data; (c) SS-UOE  $T(K)$ ,  $c(m/s)$  vs  $x(m)$ .

## APPENDIX W – Supplementary Material for Chapter 04

### W1. Description of Air Pre-Purification Units

All PPU's start with atmospheric air at  $1\text{ atm}$ ,  $25^\circ\text{C}$  and  $60\%\text{RH}$  (stream #1) passing by a particulate filter (not shown in Figs. 4.2 and 4.3) and being compressed from  $\approx 1\text{ bar}$  to  $\approx 2\text{ bar}$  in the first MAC stage. Air at  $\approx 100^\circ\text{C}$  then goes to the intercooler, achieving  $40^\circ\text{C}$  and  $\Delta P=10\text{ kPa}$  in the outlet. A vessel for condensate withdrawal (stream #19) follows the intercooler, but at such conditions ( $40^\circ\text{C}$  and  $1.9\text{ bar}$ ) no liquid phase is formed. The MAC second stage then discharges air (stream #2) at  $3.180\text{ bar}$  in FULL-TSA (Fig. 4.2a) but at somewhat higher pressure in both SS-TSA and SS-TSA-HI (Figs. 4.2b-4.2c) –  $3.225\text{ bar}$  from simulation results – to accommodate SS head-loss targeting the same purified air pressure ( $3.10\text{ bar}$ ) at TSA-System. Air Compression sub-system (Figs. 4.3a-4.3c) comprises these steps also including CW Supply to intercooler (stream #17) and CW Return to CW-System (stream #18). In FULL-TSA and SS-TSA (Figs. 4.2a-4.2b) stream #18 is CW at  $45^\circ\text{C}$ , while in SS-TSA-HI (Fig. 4.2c) it is WW at  $90^\circ\text{C}$ . SS-TSA-HI has 02 further water streams crossing the boundaries – #13 (WW at  $90^\circ\text{C}$ ) and #23 (CW at  $30^\circ\text{C}$ ) – integrating MAC intercooler with  $\text{N}_2$  heater at TSA-System (Figs. 4.2c and 4.3c).

The compressed air (stream #2) is then sent to the DCA/EWC (Figs. 4.3a-4.3c) to be cooled to  $10^\circ\text{C}$  (stream #3) before pre-purification. Stream #2 enters the bottom of the Direct-Contact Aftercooler (DCA) against descendent CW in the bottom warmer packing, producing a CW stream, including air condensate, sent to CW-System (stream #4), while in the DCA top cold section it is contacted with Chilled-Water (ChW) produced in the Evaporative Water-Cooler (EWC) fed with  $\text{N}_2$  (stream #5) (Figs. 4.2a-4.2c). ChW streams are not crossing any boundaries as they are confined to DCA/EWC System (Figs. 4.3a-4.3c) requiring just water make-up at ambient conditions (stream #15) in EWC feed to compensate evaporative losses (wet nitrogen release) at the top (stream #6). SS-TSA and SS-TSA-HI have the peculiar feature of SS condensate injection into the ChW loop (stream #12). Process alternatives were similar in this sub-system except for a small difference in air pressure and SS condensate injection, but contrasts became more significant from this point onwards.

In SS-TSA and SS-TSA-HI cold compressed air at  $10^\circ\text{C}$  (stream #3) is firstly sent to SS, unlike FULL-TSA where it is directly sent to TSA-System. The SS is isolated in an exclusive sub-system (Figs. 4.3b-4.3c) for better comprehension about its thermodynamic performance,

instead of lumping air pre-purification steps (SS+TSA). In the new pre-purification concept (SS-TSA and SS-TSA-HI), SS plays a central role abating most H<sub>2</sub>O contained in cold compressed air at 10 °C (stream #3) – 98.65% at 3.165 bar from simulation results – leaving less than 500 ppm of contaminants to be removed by TSA in a MS bed (stream #11). The SS cold condensate (stream #12) is sent to DCA/EWC to be mixed with ChW (Figs. 4.2b and 4.2c).

Besides cold pressurized air – saturated-air (stream #3) in FULL-TSA and dehydrated air (stream #11) in SS-TSA and SS-TSA-HI – the TSA-System also receives N<sub>2</sub> to regenerate adsorbents (stream #8) and a heating utility (stream #13) to increase the N<sub>2</sub> temperature to desorb retained impurities – WW in SS-TSA-HI and LPS in FULL-TSA and SS-TSA. The new finishing TSA step of SS-TSA and SS-TSA-HI, hereinafter called MS-TSA, differs considerably from conventional TSA of FULL-TSA PPU mainly because H<sub>2</sub>O removal bed (AA) is eliminated considerably reducing TSA inventory and equipment size. Purified air then leaves TSA and passes through a particulate filter (not shown in Figs. 4.2-4.3) before being exported at appropriate conditions to cryogenic fractionation in the Cold-Box (stream #7), while N<sub>2</sub> carrying impurities from TSA is released to the atmosphere (stream #10).

CW to DCA and MAC intercooler (streams #16 and #17) is produced by CW-System, which regenerates streams #4 and #18 in an atmospheric cooling-tower with water make-up at 25°C / 1 atm (stream #22). An exhaust fan installed at the top of the cooling-tower forces atmospheric air to flow counter-currently against CW, releasing wet air through stream #21. In SS-TSA-HI (Fig. 4.2c), CW-System also pumps WW at 30°C returning from TSA-System (stream #14) sending it to Air Compression sub-system (Fig. 4.3c), where WW (stream #23) is mixed with CW to MAC intercooler (stream #17).

### **W1.1. Systems Definition for Exergy Analysis**

Besides Overall System analyses – full flowsheets from Figs. 4.2a-4.2c – sub-flowsheets are created to investigate local exergy efficiencies and losses. Table W1.1 presents general definition of input and output material and power (shaft-power) streams of each system as disclosed in the contours of gray boxes in Figs. 4.3a-4.3c. Process alternatives peculiarities are indicated as overwritten numbers in parenthesis. For better comprehension of Table W1.1 and Figs. 4.3a-4.3c, a brief description of stream numbers (#) in accordance with Figs. 4.2a-4.2c is shown in Table W1.2, besides disclosing the origin and destination of each stream relatively to the concerned systems.

**Table W1.1.** Material and energy streams crossing boundaries of each system.

<b>System</b>	<b>Power Inputs (Equipment)</b>	<b>Material Inputs (Stream #)</b>	<b>Products (Stream #)</b>	<b>Residues (Stream #)</b>
<b>Air Compression</b>	MAC	1, 17, 23 <sup>(3)</sup>	2, 18, 19, 13 <sup>(3)</sup>	–
<b>DCA/EWC</b>	ChW Pumps	2, 5, 12 <sup>(2,3)</sup> , 15, 16	3, 4	6
<b>SS</b> <sup>(2,3)</sup>	–	3 <sup>(2,3)</sup>	11 <sup>(2,3)</sup> , 12 <sup>(2,3)</sup>	–
<b>TSA-System</b>	N <sub>2</sub> Blower	3 <sup>(1)</sup> , 11 <sup>(2,3)</sup> , 8, 13	7, 14	10
<b>CW-System</b>	Air Fan	4, 18, 19, 20, 22,	16, 17, 23 <sup>(3)</sup>	21
	CW Pumps	14 <sup>(3)</sup>		
<b>Overall System</b>	MAC Blower Pumps Air Fan	1, 13 <sup>(1,2)</sup> , 15, 20, 22	7, 14 <sup>(1,2)</sup>	6, 10, 21

<sup>(1)</sup> FULL-TSA; <sup>(2)</sup> SS-TSA; <sup>(3)</sup> SS-TSA-HI.

**Table W1.2.** Origin, destination and description of material streams in Figs. 4.2a-4.2c and 4.3a-4.3c.

Stream #	Description	FULL-TSA (Fig. 4.3a)		SS-TSA (Fig. 4.3b)		SS-TSA-HI (Fig. 4.3c)	
		Origin	Destination	Origin	Destination	Origin	Destination
1	Process air intake	External <sup>†</sup>	Air Compression	External <sup>†</sup>	Air Compression	External <sup>†</sup>	Air Compression
2	Pressurized air from MAC	Air Compression	DCA/EWC	Air Compression	DCA/EWC	Air Compression	DCA/EWC
3	Cold air from DCA	DCA/EWC	TSA-System	DCA/EWC	SS	DCA/EWC	SS
4	CW return from DCA	DCA/EWC	CW-System	DCA/EWC	CW-System	DCA/EWC	CW-System
5	N <sub>2</sub> injection to EWC	External <sup>†</sup>	DCA/EWC	External <sup>†</sup>	DCA/EWC	External <sup>†</sup>	DCA/EWC
6	Wet N <sub>2</sub> release to ATM	DCA/EWC	ATM <sup>†</sup>	DCA/EWC	ATM <sup>†</sup>	DCA/EWC	ATM <sup>†</sup>
7	Purified air to Cold Box	TSA-System	External <sup>†</sup>	TSA-System	External <sup>†</sup>	TSA-System	External <sup>†</sup>
8	N <sub>2</sub> to TSA-System	External <sup>†</sup>	TSA-System	External <sup>†</sup>	TSA-System	External <sup>†</sup>	TSA-System
9*	Heated N <sub>2</sub> to TSA*	(Internal stream)					
10	TSA purge gas to ATM	TSA-System	ATM <sup>†</sup>	TSA-System	ATM <sup>†</sup>	TSA-System	ATM <sup>†</sup>
11	Dehydrated air from SS	–	–	SS	TSA-System	SS	TSA-System
12	Cold condensate from SS	–	–	SS	DCA/EWC	SS	DCA/EWC
13	Heating utility supply to TSA	External <sup>†</sup>	TSA-System	External <sup>†</sup>	TSA-System	Air Compression	TSA-System
14	Heating utility return from TSA	TSA-System	External <sup>†</sup>	TSA-System	External <sup>†</sup>	TSA-System	CW-System
15	Water makeup to EWC	External <sup>†</sup>	DCA/EWC	External <sup>†</sup>	DCA/EWC	External <sup>†</sup>	DCA/EWC
16	CW supply to DCA	CW-System	DCA/EWC	CW-System	DCA/EWC	CW-System	DCA/EWC
17	CW supply to intercooler	CW-System	Air Compression	CW-System	Air Compression	CW-System	Air Compression
18	CW return from intercooler	Air Compression	CW-System	Air Compression	CW-System	Air Compression	CW-System
19	Condensate from intercooler	Air Compression	CW-System	Air Compression	CW-System	Air Compression	CW-System
20	CW tower air intake	External <sup>†</sup>	CW-System	External <sup>†</sup>	CW-System	External <sup>†</sup>	CW-System
21	CW tower air release to ATM	CW-System	ATM <sup>†</sup>	CW-System	ATM <sup>†</sup>	CW-System	ATM <sup>†</sup>
22	Water makeup to CW tower	External <sup>†</sup>	CW-System	External <sup>†</sup>	CW-System	External <sup>†</sup>	CW-System
23	Water for heat integration	–	–	–	–	CW-System	Air Compression

\*Internal stream not crossing any boundaries; <sup>†</sup>External streams crossing outer boundaries of Overall System. ATM = Atmosphere (waste streams).

## W2. FULL-TSA Exergy Sankey Diagrams

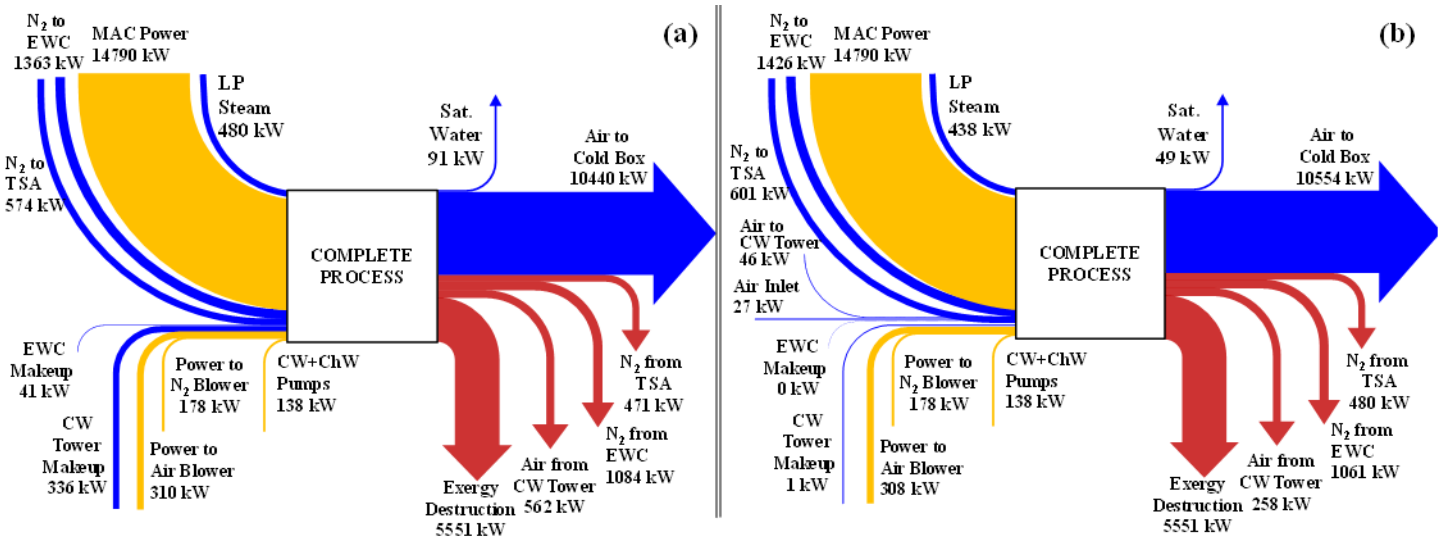


**Fig. W2.1.** FULL-TSA overall exergy Sankey diagram: (a) RER#1; (b) RER#2.

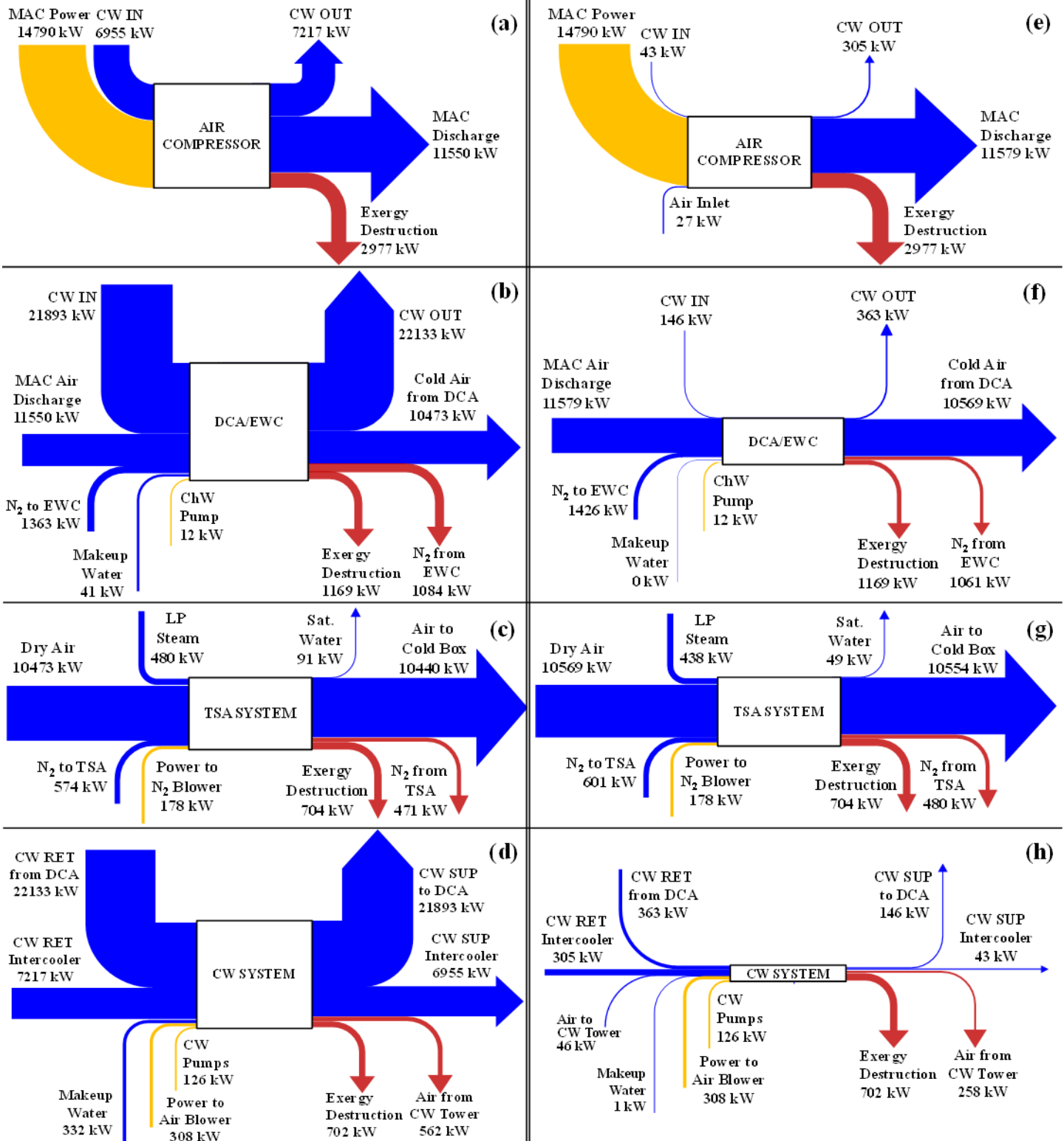


**Fig. W2.2.** FULL-TSA exergy Sankey diagrams: (a)-(d) RER#1, (e)-(h) RER#2 (RET=return, SUP=supply, REG=regeneration).

### W3. SS-TSA Exergy Sankey Diagrams

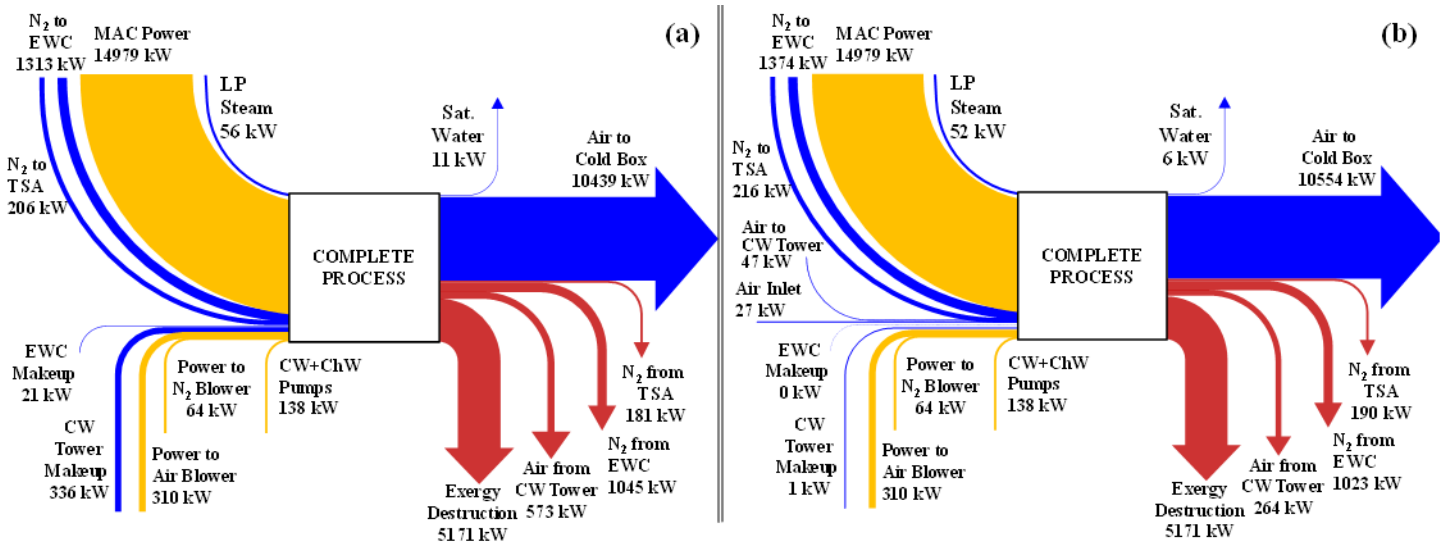
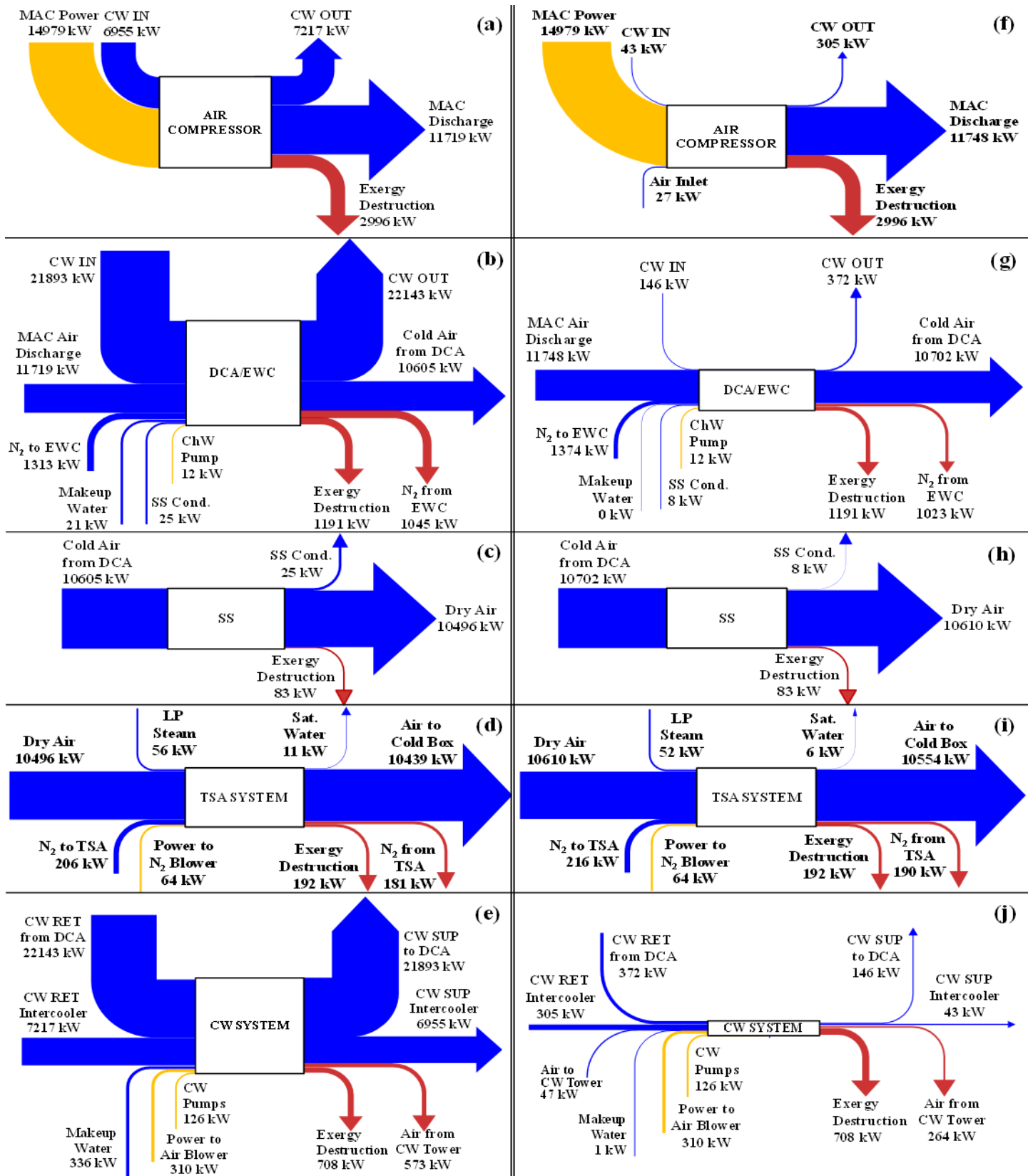


Fig. W3.1. SS-TSA overall exergy Sankey diagram: (a) RER#1; (b) RER#2.



**Fig. W3.2.** SS-TSA exergy Sankey diagrams: (a)-(e) RER#1, (f)-(j) RER#2 (RET=return, SUP=supply, REG=regeneration).

## APPENDIX X – Supplementary Material for Chapter 05

### X1. Economic Analysis: Relationships and Assumptions

Fixed Capital Investment ( $FCI, USD$ ) is estimated via base bare-module cost ( $C_{BM}^0$ ) corrected with design/pressure/material factors (Turton et al., 2009) giving bare-module installed-cost ( $C_{BM} = C_{BM}^0 * F_D * F_P * F_M$ ). Contingency costs are added to  $FCI$  as  $0.5 * C_{BM}^0$ . Thus, for onshore processes,  $FCI$  follows Eq. (X1.1) for  $N_{EQ}$  equipment items with updated  $C_{BM}^0$  using  $CEPCI=550.3$ , Sept-2015 Chemical Engineering Plant Cost Index (Chem.Eng., Jan-2016).

$$FCI^{ONSHORE} = 1.18 * \sum_{i=1}^{N_{EQ}} C_{BMi} + 0.5 * \sum_{i=1}^{N_{EQ}} C_{BMi}^0 \quad (X1.1)$$

When required capacities exceed cost correlations capacity limits, costs were extrapolated via Eq. (X1.2a), “Six-Tenth Rule”, where  $C$  is capacity – power (machines), area (exchangers), flow rate (separators). Eq. (X1.2b) adopts a 2.2 factor as offshore systems have costlier installation than onshore counterparts. Eq. (X1.3a) estimates Cost of Manufacturing ( $COM, USD/y$ ), where  $COL$ ,  $CRM$ ,  $CUT$ ,  $CWT$  are, respectively, costs ( $USD/y$ ) of labor, raw materials, utilities and waste treatment. Gross Annual Profit ( $GAP, USD/y$ ), Annual Profit ( $AP, USD/y$ ) and Net Present Value ( $NPV, USD$ ) follow in Eqs. (X1.3b) to (X1.3d), where  $REV(USD/y)$ ,  $ITR(\%)$ ,  $DEPR(USD/y)$ ,  $N(years)$ , represent, respectively, revenues, income tax rate ( $ITR=34\%$ ), depreciation ( $0.1 * FCI$ ), horizon ( $N=20$ ) and annual interest rate ( $i=10\%$ ). The remaining economic assumptions follow in Table X1.1.

$$FCI^{ONSHORE} = FCI^{ONSHORE^{LIMIT}} * (C / C^{LIMIT})^{6/10} \quad (X1.2a)$$

$$FCI^{OFFSHORE} = 2.2 * FCI^{ONSHORE} \quad (X1.2b)$$

$$COM = 0.18 * FCI^{OFFSHORE} + 2.73 * COL + 1.23 * (CRM + CUT + CWT) \quad (X1.3a)$$

$$GAP = REV - COM \quad (X1.3b)$$

$$AP = \begin{cases} GAP - (ITR / 100) * (GAP - DEPR) & \{GAP > DEPR \\ GAP & \{GAP \leq DEPR \end{cases} \quad (X1.3c)$$

$$NPV = -(0.2 + 0.3 * q^{-1} + 0.5 * q^{-2}) FCI^{OFFSHORE} + AP \left\{ \sum_{k=3}^{N+3} q^{-k} \right\}, q \equiv (1 + i / 100) \quad (X1.3d)$$

**Table X1.1.** Complementary economic assumptions for process evaluation.

<i>Code</i>	<i>Topic or Equipment</i>	<i>Description</i>
{E1}	Vessels	$P^{DESIGN} = 1.15 * P^{OPERATION}$
{E2}	Membrane-Permeation	$FCI^{ONSHORE}(USD) = 500 * area(m^2)^{\#}$ ; $CRM(USD/y) = 40 * area(m^2)^{\#}$ .
{E3}	Turboshafts/GTs	28MW at 161.4MW/MMsm <sup>3</sup> /d for 20%molCO <sub>2</sub> Fuel-Gas.
{E4}	Fuel-Gas flow rate	$MMsm^3/d = POWER^{RIG}(MW) / 161.4$ ; $POWER^{RIG}(MW) = 1.1 * POWER^{Gas-Plant}(MW) + 28MW$ .
{E5}	Power-Plant $FCI^{ONSHORE}$	From number of 28MW turboshafts for electricity peak-demand plus one.
{E6}	SS $FCI^{ONSHORE}$	Eq. (X1.2a) using $FCI^{ONSHORE}$ for 6MMsm <sup>3</sup> /d <sup>&amp;</sup> .
{E7}	Prices	Raw-NG=0; Oil=45USD/bbl; Fuel-Gas=3.2 USD/MMBTU; EOR-Fluid=45USD/t.
{E8}	Thermal utilities	Costless SW/CW/WW/HW/PHW/TF.
{E9}	CUT (USD/y)	Fuel-Gas
{E10}	Construction	Three years allocating 20%/30%/50% capital
{E11}	Operation	8000 h/y

<sup>#</sup>Merkel et al. (2012). <sup>&</sup>Machado et al. (2012).

**X2. HYSYS PFDs of Alternatives [RC+JT+SS], [RC+TX+SS], [NR+JT+SS] and [RC+JT+MP]**

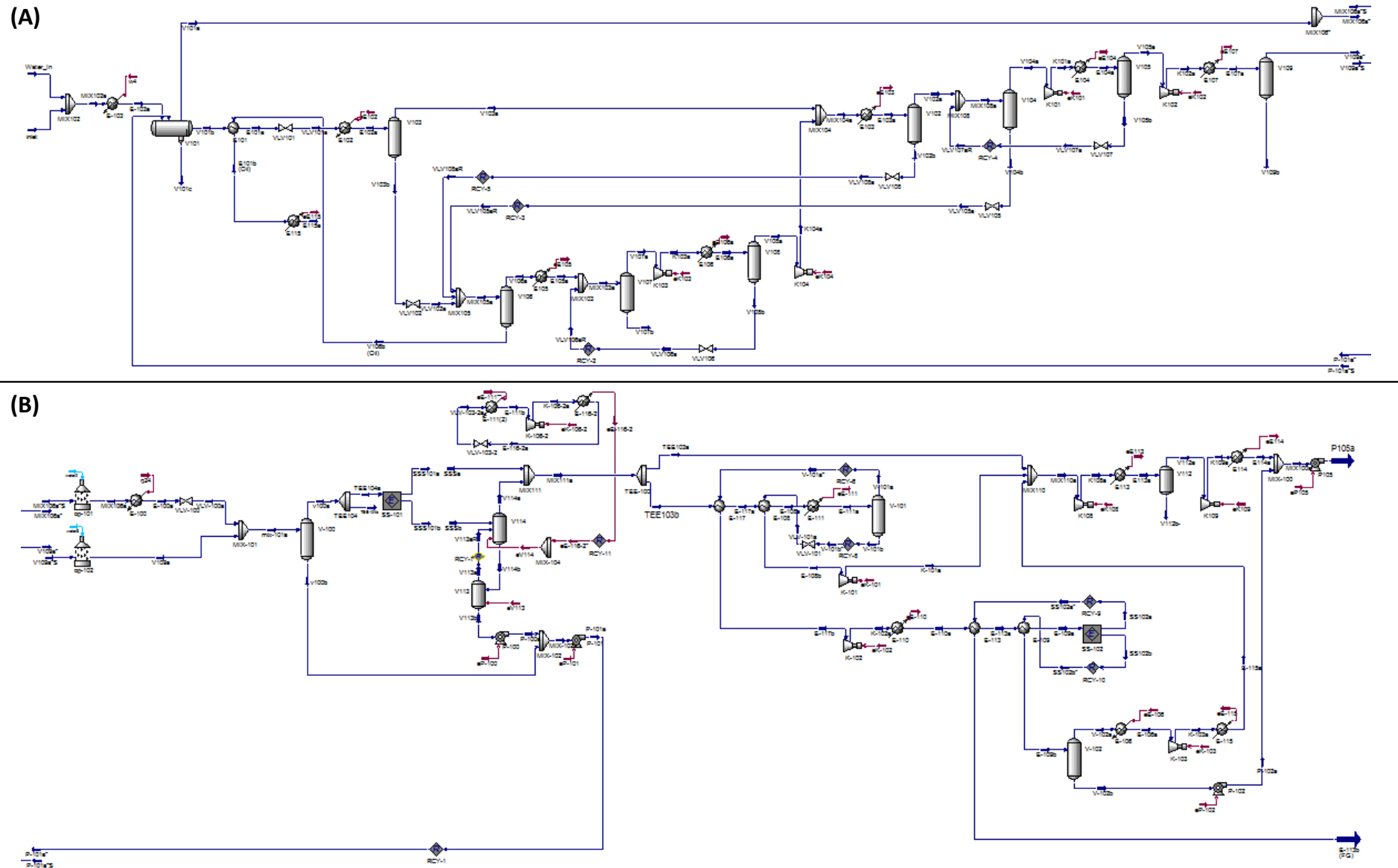


**Fig. X2.1. HYSYS PFD for Base-Case Process [RC+JT+SS]**





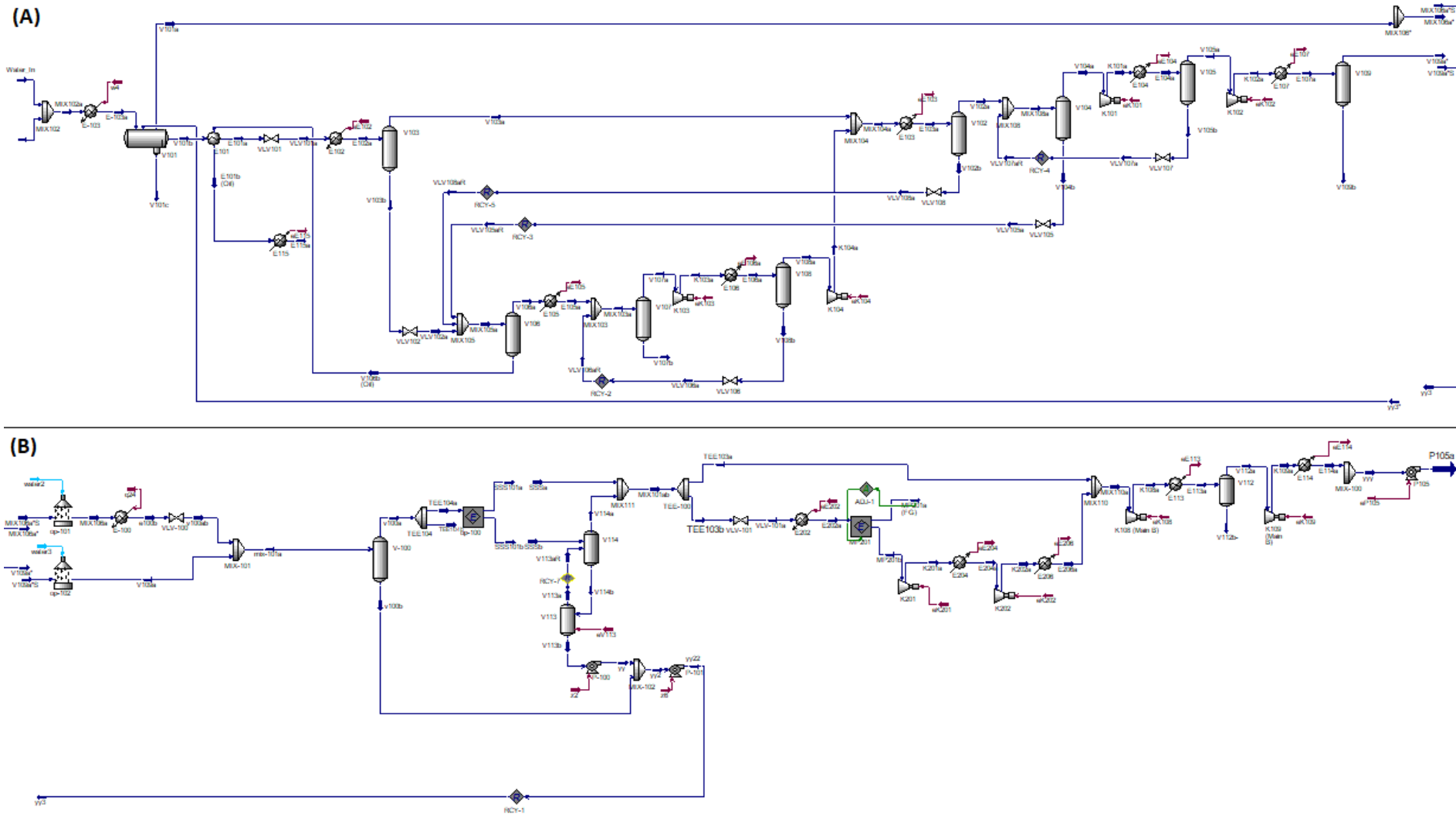


Fig. X2.4. HYSYS PFD for Process Alternative [RC+JT+MP]

**X3. Analogues of Table 5.3 for Cases [RC+TX+SS], [NR+JT+SS], [RC+JT+MP]**

**Table X3.1.** Streams of gas-hub for CO<sub>2</sub> ultra-rich NG: Case [RC+TX+SS]

System	HPS			Oil	VRU	SS					SS			Main		EOR	
	Riser	Main-Recycle	HPS-Water	HPS-Gas	Final-Oil	VRU-Gas	Feed	SS-Gas	SS-L+W	LTX-L+W	Feed	FG	GCO2	LCO2	SSGH	MC-Gas	EOR-Fluid
<i>T</i> (°C)	30.0	36.5	32.5	32.5	42.6	45.0	45.1	34.2	-18.1	20.0	-22.0	35.0	45.0	15.2	34.2	34.0	80.3
<i>P</i> (bar)	120.0	120.0	120.0	120.0	1.30	80.50	80.50	50.96	50.96	50.96	84.00	35.10	50.96	240.0	50.96	50.96	450.0
<i>MMsm</i> <sup>3</sup> / <i>d</i>	90.15	8.99	36.76	52.85	2.00	7.52	56.99	51.34	5.65	5.65	1.91	1.16	0.62	0.13	44.72	50.07	50.19
%Vapor	53.20	0.00	0.00	100	0.00	100	100	100	0.00	0.00	100	100	100	0.00	100	100	0.00
%CO <sub>2</sub>	39.72	55.16	0.13	67.39	0.64	68.40	68.57	69.57	59.43	59.43	45.59	22.08	83.66	92.99	69.58	70.62	70.68
%CH <sub>4</sub>	14.59	6.91	0.00	23.36	0.04	19.05	23.58	25.61	5.12	5.12	49.53	74.47	12.37	2.49	25.61	24.53	24.48
%C <sub>2</sub> H <sub>6</sub>	1.36	2.75	0.00	2.34	0.09	3.15	2.43	2.39	2.84	2.84	2.25	2.12	2.58	1.76	2.39	2.40	2.40
%C <sub>3</sub> H <sub>8</sub>	0.75	4.83	0.00	1.66	0.46	2.93	1.72	1.29	5.57	5.57	0.61	0.25	1.06	1.70	1.29	1.32	1.32
%i-C <sub>4</sub> H <sub>10</sub>	0.13	1.99	0.00	0.43	0.39	0.82	0.42	0.21	2.34	2.34	0.06	0.01	0.10	0.29	0.21	0.22	0.22
%C <sub>4</sub> H <sub>10</sub>	0.29	6.10	0.00	1.13	1.70	2.34	1.10	0.44	7.11	7.11	0.09	0.01	0.14	0.57	0.44	0.45	0.45
%i-C <sub>5</sub> H <sub>12</sub>	0.09	3.22	0.00	0.50	1.95	0.94	0.43	0.09	3.53	3.53	0.01	0.00	0.01	0.09	0.09	0.09	0.09
%C <sub>5</sub> H <sub>12</sub>	0.14	4.97	0.00	0.74	3.81	1.34	0.60	0.09	5.26	5.26	0.01	0.00	0.01	0.08	0.09	0.09	0.09
%C <sub>6</sub> H <sub>14</sub>	0.15	3.44	0.00	0.53	5.76	0.50	0.31	0.02	3.00	3.00	0.00	0.00	0.00	0.01	0.02	0.02	0.02
%C <sub>7</sub> H <sub>16</sub>	0.21	2.27	0.00	0.38	8.74	0.08	0.15	0.00	1.50	1.50	0.00	0.00	0.00	0.00	0.00	0.00	0.00
%C <sub>8</sub> H <sub>18</sub>	0.23	2.02	0.00	0.34	10.04	0.02	0.09	0.00	0.93	0.93	0.00	0.00	0.00	0.00	0.00	0.00	0.00
%C <sub>9</sub> H <sub>20</sub>	0.18	1.32	0.00	0.22	8.15	0.00	0.04	0.00	0.40	0.40	0.00	0.00	0.00	0.00	0.00	0.00	0.00
%C <sub>10</sub> H <sub>22</sub>	0.16	0.94	0.00	0.16	7.33	0.00	0.02	0.00	0.18	0.18	0.00	0.00	0.00	0.00	0.00	0.00	0.00
%C <sub>11</sub> H <sub>24</sub>	0.11	0.63	0.00	0.11	4.89	0.00	0.01	0.00	0.07	0.07	0.00	0.00	0.00	0.00	0.00	0.00	0.00
%C <sub>12</sub> H <sub>26</sub>	0.13	0.52	0.00	0.09	5.93	0.00	0.00	0.00	0.04	0.04	0.00	0.00	0.00	0.00	0.00	0.00	0.00
%C <sub>13</sub> H <sub>28</sub>	0.09	0.35	0.00	0.06	3.95	0.00	0.00	0.00	0.01	0.01	0.00	0.00	0.00	0.00	0.00	0.00	0.00
%C <sub>14</sub> H <sub>30</sub>	0.12	0.27	0.00	0.05	5.21	0.00	0.00	0.00	0.01	0.01	0.00	0.00	0.00	0.00	0.00	0.00	0.00
%C <sub>15</sub> H <sub>32</sub>	0.07	0.16	0.00	0.03	3.13	0.00	0.00	0.00	0.00	0.00	0.00	0.00	0.00	0.00	0.00	0.00	0.00
%C <sub>16</sub> H <sub>34</sub>	0.05	0.11	0.00	0.02	2.09	0.00	0.00	0.00	0.00	0.00	0.00	0.00	0.00	0.00	0.00	0.00	0.00
%C <sub>17</sub> H <sub>36</sub>	0.07	0.09	0.00	0.02	3.27	0.00	0.00	0.00	0.00	0.00	0.00	0.00	0.00	0.00	0.00	0.00	0.00
%C <sub>18</sub> H <sub>38</sub>	0.04	0.06	0.00	0.01	1.96	0.00	0.00	0.00	0.00	0.00	0.00	0.00	0.00	0.00	0.00	0.00	0.00
%C <sub>19</sub> H <sub>40</sub>	0.03	0.12	0.00	0.02	1.31	0.00	0.00	0.00	0.00	0.00	0.00	0.00	0.00	0.00	0.00	0.00	0.00
%C <sub>20+</sub>	0.43	0.01	0.00	0.00	19.16	0.00	0.00	0.00	0.00	0.00	0.00	0.00	0.00	0.00	0.00	0.00	0.00
%N <sub>2</sub>	0.15	0.03	0.00	0.25	0.00	0.12	0.25	0.27	0.02	0.02	0.66	1.05	0.06	0.01	0.27	0.25	0.25
ppm H <sub>2</sub> S	29.65	82.48	0.00	51.99	4.19	85.75	55.35	51.59	89.53	89.53	29.54	12.70	52.86	71.32	52.44	52.47	52.49
ppm H <sub>2</sub> O				2606	18.90	2974	2687	88.48	26295	26295	7.15	0.06	5.69	79.95	88.62	90.70	90.68
%H <sub>2</sub> O	40.70	1.73	99.87	0.261		0.297	0.269		2.630	2.630							

**Table X3.2.** Streams of gas-hub for CO<sub>2</sub> ultra-rich NG: Case [NR+JT+SS]

System	HPS			Oil	VRU	SS					SS				Main	EOR	
	Riser	Main-Recycle	HPS-Water	HPS-Gas	Final-Oil	VRU-Gas	Feed	SS-Gas	SS-L+W	LTX-L+W	Feed	FG	GCO2	LCO2	SSGH	MC-Gas	EOR-Fluid
T(°C)	30.0	N.A.	30.0	30.0	40.0	45.0	45.3	40.5	-20.1	20.0	-22.0	35	45.0	18.3	40.5	41.3	78.6
P(bar)	120.0	N.A.	120.0	120.0	1.30	80.50	80.50	59.33	59.33	59.33	84.00	37.90	59.33	240.0	59.33	59.33	450.0
MMsm <sup>3</sup> /d	90.15	N.A.	36.64	47.98	1.43	4.12	51.38	47.40	3.98	3.98	1.92	1.27	0.53	0.13	37.77	46.01	50.72
%Vapor	53.20	N.A.	0.00	100	0.00	100	100	100	0.00	0.00	100	100	100	0.00	100	100	0.00
%CO <sub>2</sub>	39.72	N.A.	0.13	68.41	0.80	71.11	68.93	68.70	71.69	71.69	43.48	21.69	83.95	93.67	68.70	69.93	69.94
%CH <sub>4</sub>	14.59	N.A.	0.00	25.74	0.06	19.54	25.46	27.15	5.36	5.36	53.10	74.95	12.53	2.70	27.15	25.90	24.06
%C <sub>2</sub> H <sub>6</sub>	1.36	N.A.	0.00	2.27	0.11	3.34	2.35	2.34	2.55	2.55	2.08	2.00	2.39	1.64	2.34	2.35	2.37
%C <sub>3</sub> H <sub>8</sub>	0.75	N.A.	0.00	1.18	0.42	2.50	1.26	1.04	3.87	3.87	0.48	0.22	0.89	1.36	1.04	1.06	1.31
%i-C <sub>4</sub> H <sub>10</sub>	0.13	N.A.	0.00	0.20	0.22	0.48	0.21	0.13	1.18	1.18	0.04	0.01	0.07	0.19	0.13	0.13	0.23
%C <sub>4</sub> H <sub>10</sub>	0.29	N.A.	0.00	0.42	0.79	1.15	0.46	0.24	3.13	3.13	0.05	0.01	0.09	0.33	0.24	0.24	0.49
%i-C <sub>5</sub> H <sub>12</sub>	0.09	N.A.	0.00	0.13	0.61	0.35	0.14	0.04	1.28	1.28	0.00	0.00	0.01	0.04	0.04	0.04	0.15
%C <sub>5</sub> H <sub>12</sub>	0.14	N.A.	0.00	0.19	1.15	0.51	0.19	0.04	1.99	1.99	0.00	0.00	0.01	0.04	0.04	0.04	0.22
%C <sub>6</sub> H <sub>14</sub>	0.15	N.A.	0.00	0.18	2.34	0.34	0.16	0.01	1.88	1.88	0.00	0.00	0.00	0.01	0.01	0.01	0.20
%C <sub>7</sub> H <sub>16</sub>	0.21	N.A.	0.00	0.18	6.14	0.18	0.13	0.00	1.67	1.67	0.00	0.00	0.00	0.00	0.00	0.00	0.19
%C <sub>8</sub> H <sub>18</sub>	0.23	N.A.	0.00	0.18	8.15	0.07	0.10	0.00	1.27	1.27	0.00	0.00	0.00	0.00	0.00	0.00	0.18
%C <sub>9</sub> H <sub>20</sub>	0.18	N.A.	0.00	0.12	7.38	0.01	0.05	0.00	0.63	0.63	0.00	0.00	0.00	0.00	0.00	0.00	0.12
%C <sub>10</sub> H <sub>22</sub>	0.16	N.A.	0.00	0.09	7.35	0.00	0.02	0.00	0.32	0.32	0.00	0.00	0.00	0.00	0.00	0.00	0.08
%C <sub>11</sub> H <sub>24</sub>	0.11	N.A.	0.00	0.06	4.90	0.00	0.01	0.00	0.14	0.14	0.00	0.00	0.00	0.00	0.00	0.00	0.06
%C <sub>12</sub> H <sub>26</sub>	0.13	N.A.	0.00	0.05	6.71	0.00	0.01	0.00	0.07	0.07	0.00	0.00	0.00	0.00	0.00	0.00	0.04
%C <sub>13</sub> H <sub>28</sub>	0.09	N.A.	0.00	0.03	4.47	0.00	0.00	0.00	0.03	0.03	0.00	0.00	0.00	0.00	0.00	0.00	0.03
%C <sub>14</sub> H <sub>30</sub>	0.12	N.A.	0.00	0.02	6.52	0.00	0.00	0.00	0.01	0.01	0.00	0.00	0.00	0.00	0.00	0.00	0.02
%C <sub>15</sub> H <sub>32</sub>	0.07	N.A.	0.00	0.01	3.91	0.00	0.00	0.00	0.00	0.00	0.00	0.00	0.00	0.00	0.00	0.00	0.01
%C <sub>16</sub> H <sub>34</sub>	0.05	N.A.	0.00	0.01	2.61	0.00	0.00	0.00	0.00	0.00	0.00	0.00	0.00	0.00	0.00	0.00	0.01
%C <sub>17</sub> H <sub>36</sub>	0.07	N.A.	0.00	0.01	4.09	0.00	0.00	0.00	0.00	0.00	0.00	0.00	0.00	0.00	0.00	0.00	0.01
%C <sub>18</sub> H <sub>38</sub>	0.04	N.A.	0.00	0.00	2.46	0.00	0.00	0.00	0.00	0.00	0.00	0.00	0.00	0.00	0.00	0.00	0.00
%C <sub>19</sub> H <sub>40</sub>	0.03	N.A.	0.00	0.01	1.64	0.00	0.00	0.00	0.00	0.00	0.00	0.00	0.00	0.00	0.00	0.00	0.01
%C <sub>20+</sub>	0.43	N.A.	0.00	0.00	27.17	0.00	0.00	0.00	0.00	0.00	0.00	0.00	0.00	0.00	0.00	0.00	0.00
%N <sub>2</sub>	0.15	N.A.	0.00	0.28	0.00	0.11	0.23	0.29	0.02	0.02	0.77	1.13	0.07	0.01	0.29	0.27	0.25
ppm H <sub>2</sub> S	29.65	N.A.	0.00	47.43	5.25	91.62	50.71	47.73	86.23	86.23	26.08	12.04	50.07	67.05	47.73	48.66	52.00
ppm H <sub>2</sub> O		N.A.		2241	18.06	2960	2308	71.75	28939	28939	6.37	0.05	5.53	73.38	71.75	73.72	269.76
%H <sub>2</sub> O	40.70	N.A.	99.87	0.224		0.296	0.231		2.894	2.894							

**Table X3.3.** Streams of gas-hub for CO<sub>2</sub> ultra-rich NG: Case [RC+JT+MP]

System	HPS			Oil	VRU	SS					MP				Main Compressor		EOR
	Stream	Riser	Main-Recycle	HPS-Water	HPS-Gas	Final-Oil	VRU-Gas	Feed	SS-Gas	SS-L+W	LTX-L+W	Feed	FG	GCO <sub>2</sub>	LCO <sub>2</sub>	SSGH	MC-Gas
T(°C)	30.0	36.4	32.5	32.5	42.5	45.0	46.3	37.7	-17.0	20.0	62.0	44.4	45.0	N.A.	37.7	38.2	80.5
P(bar)	120.0	120.0	120.0	120.0	1.30	80.50	80.50	53.74	53.74	53.74	43.13	42.13	53.74	N.A.	53.74	53.74	450.00
MMsm <sup>3</sup> /d	90.15	8.31	36.76	52.24	2.00	7.44	56.68	51.39	5.29	5.29	4.90	1.34	3.56	N.A.	46.49	50.05	50.05
%Vapor	53.20	0.00	0.00	100	0.00	100	100	100	0.00	0.00	100	100	100	N.A.	100	100	0.00
%CO <sub>2</sub>	39.72	54.39	0.13	67.31	0.64	68.51	68.52	69.57	58.39	58.39	69.57	20.00	88.31	N.A.	69.57	70.90	70.90
%CH <sub>4</sub>	14.59	6.91	0.00	23.55	0.05	19.12	23.70	25.60	5.20	5.20	25.60	62.87	11.50	N.A.	25.60	24.60	24.60
%C <sub>2</sub> H <sub>6</sub>	1.36	2.76	0.00	2.34	0.09	3.15	2.43	2.39	2.85	2.85	2.39	8.60	0.04	N.A.	2.39	2.22	2.22
%C <sub>3</sub> H <sub>8</sub>	0.75	4.81	0.00	1.62	0.46	2.89	1.69	1.29	5.55	5.55	1.29	4.71	0.00	N.A.	1.29	1.20	1.20
%i-C <sub>4</sub> H <sub>10</sub>	0.13	1.97	0.00	0.41	0.37	0.80	0.41	0.21	2.32	2.32	0.21	0.78	0.00	N.A.	0.21	0.20	0.20
%C <sub>4</sub> H <sub>10</sub>	0.29	6.04	0.00	1.08	1.64	2.25	1.06	0.44	7.07	7.07	0.44	1.62	0.00	N.A.	0.44	0.41	0.41
%i-C <sub>5</sub> H <sub>12</sub>	0.09	3.25	0.00	0.47	1.88	0.91	0.42	0.09	3.60	3.60	0.09	0.33	0.00	N.A.	0.09	0.08	0.08
%C <sub>5</sub> H <sub>12</sub>	0.14	5.09	0.00	0.72	3.71	1.32	0.60	0.10	5.47	5.47	0.10	0.35	0.00	N.A.	0.10	0.09	0.09
%C <sub>6</sub> H <sub>14</sub>	0.15	3.67	0.00	0.53	5.80	0.51	0.32	0.02	3.28	3.28	0.02	0.06	0.00	N.A.	0.02	0.02	0.02
%C <sub>7</sub> H <sub>16</sub>	0.21	2.41	0.00	0.37	8.81	0.09	0.16	0.00	1.65	1.65	0.00	0.01	0.00	N.A.	0.00	0.00	0.00
%C <sub>8</sub> H <sub>18</sub>	0.23	2.12	0.00	0.33	10.10	0.02	0.10	0.00	1.03	1.03	0.00	0.00	0.00	N.A.	0.00	0.00	0.00
%C <sub>9</sub> H <sub>20</sub>	0.18	1.38	0.00	0.22	8.18	0.00	0.04	0.00	0.44	0.44	0.00	0.00	0.00	N.A.	0.00	0.00	0.00
%C <sub>10</sub> H <sub>22</sub>	0.16	0.97	0.00	0.15	7.35	0.00	0.02	0.00	0.20	0.20	0.00	0.00	0.00	N.A.	0.00	0.00	0.00
%C <sub>11</sub> H <sub>24</sub>	0.11	0.65	0.00	0.10	4.90	0.00	0.01	0.00	0.08	0.08	0.00	0.00	0.00	N.A.	0.00	0.00	0.00
%C <sub>12</sub> H <sub>26</sub>	0.13	0.53	0.00	0.08	5.93	0.00	0.00	0.00	0.04	0.04	0.00	0.00	0.00	N.A.	0.00	0.00	0.00
%C <sub>13</sub> H <sub>28</sub>	0.09	0.35	0.00	0.06	3.96	0.00	0.00	0.00	0.02	0.02	0.00	0.00	0.00	N.A.	0.00	0.00	0.00
%C <sub>14</sub> H <sub>30</sub>	0.12	0.28	0.00	0.04	5.21	0.00	0.00	0.00	0.01	0.01	0.00	0.00	0.00	N.A.	0.00	0.00	0.00
%C <sub>15</sub> H <sub>32</sub>	0.07	0.17	0.00	0.03	3.13	0.00	0.00	0.00	0.00	0.00	0.00	0.00	0.00	N.A.	0.00	0.00	0.00
%C <sub>16</sub> H <sub>34</sub>	0.05	0.11	0.00	0.02	2.08	0.00	0.00	0.00	0.00	0.00	0.00	0.00	0.00	N.A.	0.00	0.00	0.00
%C <sub>17</sub> H <sub>36</sub>	0.07	0.09	0.00	0.01	3.25	0.00	0.00	0.00	0.00	0.00	0.00	0.00	0.00	N.A.	0.00	0.00	0.00
%C <sub>18</sub> H <sub>38</sub>	0.04	0.05	0.00	0.01	1.95	0.00	0.00	0.00	0.00	0.00	0.00	0.00	0.00	N.A.	0.00	0.00	0.00
%C <sub>19</sub> H <sub>40</sub>	0.03	0.12	0.00	0.02	1.30	0.00	0.00	0.00	0.00	0.00	0.00	0.00	0.00	N.A.	0.00	0.00	0.00
%C <sub>20+</sub>	0.43	0.01	0.00	0.00	19.21	0.00	0.00	0.00	0.00	0.00	0.00	0.00	0.00	N.A.	0.00	0.00	0.00
%N <sub>2</sub>	0.15	0.03	0.00	0.25	0.00	0.12	0.25	0.27	0.02	0.02	0.27	0.66	0.12	N.A.	0.27	0.26	0.26
ppm H <sub>2</sub> S	29.65	81.91	0.00	51.57	4.21	85.63	55.08	51.61	88.83	88.83	51.61	14.84	65.52	N.A.	51.61	52.60	52.60
ppm H <sub>2</sub> O		18396		2584	18.93	2972	2666	95.90	27651	27651	95.90	27.57	121.7	N.A.	95.90	97.74	97.74
%H <sub>2</sub> O	40.70	1.84	99.87			0.297	0.267		2.765	2.765				N.A.			

#### X4. Analogues of Table 5.4 for Cases [RC+TX+SS], [NR+JT+SS], [RC+JT+MP]

**Table X4.1.** Design parameters and results of 1<sup>st</sup> (WDPA+HCDPA) and 2<sup>nd</sup> (CO<sub>2</sub> removal) SS units: Case [RC+TX+SS]

<i>Specified Items</i>	<i>WDPA HCDPA</i>	<i>CO<sub>2</sub> Capture</i>	<i>Calculated by SS-UOE</i>	<i>WDPA HCDPA</i>	<i>CO<sub>2</sub> Capture</i>
No.of SS	12	1	$D_T(m)$	0.0666	0.03421
$D_I(m)$	0.10	0.12	$L_C(m)$	0.0744	0.1601
$D_O(m)$	0.08	0.09	$L_D(m)$	0.1445	0.6749
$\alpha(^{\circ})$	12.67	15	$L(m)$	0.2188	0.8350
$\beta(^{\circ})$	2.66	2.5	$L^{Shock}(m)$	0.1664	0.2570
$Ma^{Shock}$	1.52	1.6	$L^{Diff}(m)$	0.0524	0.5780
$\eta^{EXP}\%$	100	100	$P_{BS}(bar)$	24.95	21.60
$\eta^{CMP}\%$	100	100	$T_{BS}(^{\circ}C)$	-17.95	-60.92
$P^{Feed}(bar)$	80.5	84.0	$Ma_{BS}$	1.3055*	0.9384* <sup>+</sup>
$T^{Feed}(^{\circ}C)$	45	-22	$P^{Discharge}(bar)$	50.96	35.60
$MMsm^3/d$	56.99	1.91	$T^{Discharge}(^{\circ}C)$	34.19	-29.85
$\%C3^{+Feed}$	4.90%	0.78%	$\%Condensate$	9.91%	39.11%
$ppmH_2O^{Feed}$	2687	7.15	$REC\%CO_2$	8.59%	71.26%
$\%CO_2^{Feed}$	68.57%	46.78%	$\%P Recovery$	63.31%	42.38%

\* After condensate withdrawal      <sup>+</sup> Normal shock does not occur

**Table X4.2.** Design parameters and results of 1<sup>st</sup> (WDPA+HCDPA) and 2<sup>nd</sup> (CO<sub>2</sub> removal) SS units: Case [NR+JT+SS]

<i>Specified Items</i>	<i>WDPA HCDPA</i>	<i>CO<sub>2</sub> Capture</i>	<i>Calculated by SS-UOE</i>	<i>WDPA HCDPA</i>	<i>CO<sub>2</sub> Capture</i>
No.of SS	12	1	$D_T(m)$	0.0627	0.0347
$D_I(m)$	0.10	0.12	$L_C(m)$	0.0830	0.1592
$D_O(m)$	0.08	0.09	$L_D(m)$	0.1867	0.6346
$\alpha(^{\circ})$	12.67	15	$L(m)$	0.2697	0.7938
$\beta(^{\circ})$	2.66	2.5	$L^{Shock}(m)$	0.1549	0.2517
$Ma^{Shock}$	1.52	1.6	$L^{Diff}(m)$	0.1148	0.5421
$\eta^{EXP}\%$	100	100	$P_{BS}(bar)$	26.15	21.80
$\eta^{CMP}\%$	100	100	$T_{BS}(^{\circ}C)$	-20.21	-61.28
$P^{Feed}(bar)$	80.5	84.0	$Ma_{BS}$	1.3217*	1.0062*
$T^{Feed}(^{\circ}C)$	45	-22	$P^{Discharge}(bar)$	59.33	38.40
$MMsm^3/d$	51.38	1.92	$T^{Discharge}(^{\circ}C)$	36.45	-25.79
$\%C3^{+Feed}$	2.75%	0.57%	$\%Condensate$	7.75%	33.97%
$ppmH_2O^{Feed}$	2308	6.37	$REC\%CO_2$	8.06%	67.06%
$\%CO_2^{Feed}$	68.93%	43.48%	$\%P Recovery$	73.71%	45.71%

\* After condensate withdrawal

**Table X4.3.** Design parameters and results of 1<sup>st</sup> (WDPA+HCDPA) SS unit: MP-variant alternative [RC+JT+MP] (No 2<sup>nd</sup> SS unit)

<i>Specified Items</i>	<i>WDPA HCDPA</i>	<i>CO<sub>2</sub> Capture</i>	<i>Calculated by SS-UOE</i>	<i>WDPA HCDPA</i>	<i>CO<sub>2</sub> Capture</i>
<i>No.of SS</i>	12	-	<i>D<sub>T</sub>(m)</i>	0.0662	-
<i>D<sub>f</sub>(m)</i>	0.10	-	<i>L<sub>C</sub>(m)</i>	0.0752	-
<i>D<sub>O</sub>(m)</i>	0.08	-	<i>L<sub>D</sub>(m)</i>	0.1486	-
<i>α(°)</i>	12.67	-	<i>L(m)</i>	0.2238	-
<i>β(°)</i>	2.66	-	<i>L<sup>Shock</sup>(m)</i>	0.1596	-
<i>Ma<sup>Shock</sup></i>	1.52	-	<i>L<sup>Diff</sup>(m)</i>	0.0642	-
<i>η<sup>EXP</sup>%</i>	100	-	<i>P<sub>BS</sub>(bar)</i>	25.60	-
<i>η<sup>CMP</sup>%</i>	100	-	<i>T<sub>BS</sub>(°C)</i>	-16.78	-
<i>P<sup>Feed</sup>(bar)</i>	80.5	-	<i>Ma<sub>BS</sub></i>	1.3114*	-
<i>T<sup>Feed</sup>(°C)</i>	45	-	<i>P<sup>Discharge</sup>(bar)</i>	53.74	-
<i>MMsm<sup>3</sup>/d</i>	56.7	-	<i>T<sup>Discharge</sup>(°C)</i>	37.73	-
<i>%C<sub>3</sub><sup>+Feed</sup></i>	4.83%	-	<i>%Condensate</i>	9.33%	-
<i>ppmH<sub>2</sub>O<sup>Feed</sup></i>	2666	-	<i>REC%CO<sub>2</sub></i>	7.95%	-
<i>%CO<sub>2</sub><sup>Feed</sup></i>	68.52%	-	<i>%P Recovery</i>	66.76%	-

\*After condensate withdrawal



At BRY-1 (Fig. Y1.1), CO<sub>2</sub> in flue gas is absorbed into water in an air lift arrangement. Carbonated water is fed to the PBR, consisting of horizontal transparent tubes in a vertical arrangement. The bioreactor product (microalga suspension at  $\approx 4$  g/L) is sent to dewatering, which accounts for 20-30% of the overall biomass production cost (Molina-Grima et al., 2003). Dewatering operations are: flocculation+settling (E7) and, for the biomass fraction sent to BRY-2, evaporation in Greenhouse Solar Dryer (GSD) (E10), producing biomass with 60%*w* water content (Kurt et al., 2015). At BRY-2 (Fig. Y1.2), the gasifier is fed with preheated biomass and gaseous oxygen (GOX) at high-pressure of 32 bar. The formation of tars and residual coke/char is neglected as chemical reactions are modeled via thermodynamic equilibrium approach (Gibbs reactor), minimizing Gibbs free energy for the given system of compounds: H<sub>2</sub>, CO, CO<sub>2</sub>, CH<sub>4</sub>, H<sub>2</sub>O, O<sub>2</sub>, Ar, N<sub>2</sub>, NH<sub>3</sub> and biomass model constituents, with minor S-containing components being not simulated. GOX 95%*mol* – supplied by a state-of-the-art low-pressure Air Separation Unit (ASU) consuming 158 kWh/t O<sub>2</sub> (Higginbotham et al., 2011) – is compressed to 32 bar at BRY-2. Raw syngas temperature at gasifier outlet is maintained at  $\approx 900^\circ\text{C}$  controlling GOX flow rate, which corresponds to the of GOX/Biomass (humid) mass feed ratio of 0.334. Hot CO<sub>2</sub>-rich syngas flows through a heat recovery steam generation section, supplying the combined heat and power generation system, where it is cooled down to  $\approx 100^\circ\text{C}$ . The majority of this heat is availed by a Rankine cycle that is equipped with supplemental fire driven by purge (fuel) gas from the upcoming methanol (MeOH) synthesis and distillation unit. Syngas low-grade heat is dissipated by direct contact with cooling water achieving  $\approx 40^\circ\text{C}$ . HYSYS process flow diagram of Biorefinery Area 02 (BRY-2) simulation is unveiled in Fig. Y1.3.

The CO<sub>2</sub>-rich syngas is then directed to a Rectisol unit (Physical-Absorption with refrigerated MeOH) for CO<sub>2</sub> removal, adjusting the proportion of H/C elements to achieve a syngas stoichiometric number  $S = ([H_2] - [CO_2]) / ([CO] + [CO_2])$  of 2.15, being slightly above 2.00 as recommended for MeOH synthesis. After entering the absorption unit, the CO<sub>2</sub>-rich syngas is cooled down to  $\approx 10^\circ\text{C}$ . Raw syngas is then mixed with cold MeOH and the mixture is cooled by heat exchange with product streams. The resulting gas is sent to the absorber – which is equipped with three intermediary coolers – operating at sub-ambient temperatures of  $-50 \leq T(^{\circ}\text{C}) \leq -20$ . Treated syngas leaving the top of the absorber has  $\approx 2\%$  CO<sub>2</sub>. The CO<sub>2</sub>-rich solvent obtained at column bottoms is expanded in three stages to release most of the absorbed light gases, and is sent to the main stripping column, where pure MeOH is recovered at the bottom. Pure MeOH is then chilled to  $-50^\circ\text{C}$  and recycled to the top of the

main absorber as lean solvent. The HYSYS subflowsheet of CO<sub>2</sub> absorption unit simulation is portrayed in Fig. Y1.4.

The CO<sub>2</sub> liquefaction unit processes CO<sub>2</sub> captured by absorption, basically consisting of multistage intercooled compression to  $\approx 80$  bar followed by total condensation by cooling to  $\approx 30^\circ\text{C}$  and final dispatch by pumping to 100 bar (no revenues are applied).

The considered MeOH synthesis unit is based on the Lurgi MeOH reactor and process scheme. It consists of a fixed bed reactor operated at 65 bar where the reaction temperature is maintained in the range of 240-260°C by heat recovery for steam generation. The unreacted gas – the gas phase obtained after raw MeOH condensation – is partially recycled and mixed with syngas feed in order to increase the H<sub>2</sub> content of reactant mixture, favoring the conversion of CO and CO<sub>2</sub> into MeOH. The carbon efficiency of this plant – i.e. the conversion of CO+CO<sub>2</sub> – is  $\approx 87\%$ . The remaining part of the H<sub>2</sub>-rich gas (MeOH synthesis purge gas) is utilized as fuel gas for supplemental firing at the steam-cycle. The raw MeOH stream is expanded to near atmospheric pressure, mixed with impure MeOH from the absorption unit, and sent to the distillation section, consisting of a 3-column process scheme. The first column removes light contaminants, e.g. dissolved gases and dimethyl-ether, and the following two columns perform methanol/water fractionation in a heat integrated process scheme, with pure MeOH 99.9%w being recovered at the top of both columns. A small portion of this MeOH is taken for solvent make-up at the absorption unit. Released light gas of raw MeOH expansion and the top vapor of the first distillation column are mixed with the purge gas of synthesis loop and utilized as fuel gas in a boiler for supplemental fire. The HYSYS subflowsheet of methanol plant simulation is portrayed in Fig. Y1.5.

The cogeneration unit is based on a Rankine steam-cycle without reheat adopting two pressure levels of superheated steam. The largest part of heat supply is obtained at raw syngas cooling. Significant portion of low-pressure steam is extracted from the power-cycle in order to supply BRY heating demands (e.g. reboilers). The vacuum condenser operates at 0.11 bar processing inlet stream with  $\approx 0.88$  of vapor fraction.

**Table Y1.1.** Assumptions for biorefinery simulation (BRY).

Process unit	Item	Specification
(Any)	Adiabatic efficiency for compressors	85%
	Adiabatic efficiency for pumps	75%
	Electric drivers efficiency (pumps / compressors)	98%
	Thermal approach at steam generation	15 °C
	Thermal approach for shell and tube heat exchangers	10 °C
	Thermal approach for plate heat exchangers	5.0 °C
ASU	Thermodynamic model	Peng-Robinson
	GOX pressure	1.013 bar
	GOX mass fractions	N <sub>2</sub> : 0.0173
		Ar: 0.0377 O <sub>2</sub> : 0.9451 (Dillon et al., 2005)
Gasification unit	Thermodynamic model	Peng-Robinson
	Gasifier pressure	32.0 bar
	Gasifier outlet temperature	900 °C
	Reaction model	Gibbs reactor
Absorption unit	Thermodynamic model	PC-SAFT with parameters from Gatti et al. (2014)
	Solvent	Pure MeOH
	Solvent load	3.30 molMeOH/ molCO <sub>2</sub>
	Syngas stoichiometric number	2.15
Methanol unit	Thermodynamic model	SRK for MeOH synthesis and UNIQUAC / SRK for MeOH distillation
	Reactor type	Fixed bed tubular reactor, cooled by steam generation
	Reactor pressure	64.7 bar
	Reactor temperature	240-260 °C
	Reaction modeling	Kinetic model of Vanden Bussche and Froment (1996)
CO <sub>2</sub> liquefaction	Thermodynamic model	Peng-Robinson
	Compressor suction/discharge pressure	6.30 / 76.0 bar
	Liquid CO <sub>2</sub> export pressure	100 bar
Cogeneration	Thermodynamic model for combustion	Peng-Robinson
	Thermodynamic model for the steam cycle	NBS Steam
	Steam turbine inlet pressure	98.5 / 4.10 bar
	Steam turbine outlet pressure	4.10 / 0.11 bar
	Steam turbine inlet temperature	570 / 173 °C
	Steam turbine adiabatic efficiency	90%
	Condensate content at turbine outlet (vacuum)	12%
	Generator electrical efficiency	98%

Table Y1.2 summarizes the main streams of BRY-1, while Table Y1.3 shows specific premises for its simulation.

**Table Y1.2.** Description of streams from biorefinery first area (BRY-1) – Fig. Y1.1.

Stream (BRY-1)	Description (PFD of Fig. Y1.2)
1	Mass flow: 706.5 t/h (CO <sub>2</sub> =92.2 t/h); $P=1$ atm; $T=70$ °C; Mass fractions: N <sub>2</sub> =0.7631, CO <sub>2</sub> =0.1305, O <sub>2</sub> =0.0442, H <sub>2</sub> O=0.0622.
7	Nitrogen, oxygen and non-converted CO <sub>2</sub>
9	Microalga growth medium: NaNO <sub>3</sub> =500 mg/L; NaH <sub>2</sub> PO <sub>4</sub> ·2H <sub>2</sub> O=7.7 mg/L; FeCl <sub>3</sub> ·6H <sub>2</sub> O=6.3 mg/L (Wang et al., 2014).
11	Biomass of pure <i>Chlorella pyrenoidosa</i> . Mass composition (ash-free basis): Carbohydrates=21.94%; Proteins=48.85%; Lipids=29.2 % (Duan et al., 2013) Fatty acids profile (% w/w): 16:0=27.94%, 16:3=20.85%, 17:0=3.35%, 18:1=2.46%, 18:2=6.49%, 18:3=38.91% (based on Tang et al., 2011). Empirical formula: CO <sub>0.473</sub> H <sub>1.934</sub> N <sub>0.230</sub> P <sub>0.017</sub> S <sub>0.005</sub> (Picardo et al., 2013).
13	Cationic starch as bioflocculation agent (Letelier-Gordo et al., 2014).
15	Water makeup to PBR
20	Evaporated water at Greenhouse Solar Dryer (GSD).
21	Biomass to gasification (organic matter ≈40%w)
22	Biomass to oil extraction (organic matter ≈7%w)
24	Residual biomass from extraction
29	Microalga oil (product)

**Table Y1.3.** Operational data for simulation of biorefinery first area (BRY-1).

Item (BRY-1)	Simulation inputs
Compressor (E3)	Discharge pressure: 2 bar
Chemical-Pretreatment	H <sub>2</sub> SO <sub>4</sub> : mass flow is 1% of the water in feed (Davis et al., 2014).
PBR (E6)	Biomass concentration: 3.974 g/L (Chisti, 2007); Biomass productivity: 1.535 g/L/d (Chisti, 2007); Volume/surface: 0.07 m <sup>3</sup> /m <sup>2</sup> (Acién et al., 2012); Efficiency of CO <sub>2</sub> utilization: 74.5% (Acién et al., 2012); Daily uptime 24 h (daily average productivity);
Settler (E7)	Flocculant concentration: 0.040 g/L (Letelier-Gordo et al., 2014); Flocculant efficiency: 95 % (Letelier-Gordo et al., 2014); Organic matter in the product: 7.0 % w (Williams and Laurens, 2010)
GSD (E10)	Solar irradiation: 215 W/m <sup>2</sup> ; Organic matter content of product: 40 % (Kurt et al., 2015).
Oil Extraction (E11)	Chemical pretreatment with H <sub>2</sub> SO <sub>4</sub> : 1% of water in liquor; Hexane load: 5 kg hexane: 1 kg dry biomass (Davis et al., 2014);

Table Y1.4 summarizes the main streams of BRY-2, while Table Y1.5 shows specific premises for its simulation.

**Table Y1.4.** Description of streams from biorefinery second area (BRY-2) – Fig. Y1.2.

<b>Stream (BRY-2)</b>	<b>Description (PFD of Fig. Y1.2)</b>
1	Biomass for gasification. Stream #21 in BRY-1 (Fig. Y1.1)
4	Gaseous oxygen 95% mol produced by the Air Separation Unit: 26.7 t/h, 30°C, 1 atm, 94.5% O <sub>2</sub> , 3.77% Ar, 1.73% N <sub>2</sub> (% w/w).
7	Hot raw syngas – heat supply for cogeneration (steam generation at E6)
9	Raw syngas – feed stream for absorption unit: 56.4 t/h; 39°C; 30 bar; Composition: 4.00% H <sub>2</sub> , 23.35% CO, 67.20% CO <sub>2</sub> , 3.47% N <sub>2</sub> , 1.54% Ar (% w/w).
16	Adjusted syngas for MeOH synthesis. 19.6 t/h, 20°C, 28 bar, 11.4% H <sub>2</sub> , 65.5% CO, 8.65% CO <sub>2</sub> , 9.69% N <sub>2</sub> , 4.20% Ar (% w/w)
36	Pure MeOH product stream. 13.9 t/h, 40°C, 1 atm, 99.90% w MeOH.
37	Wastewater from MeOH distillation: 0.27 t/h, 40°C, 1 atm, 100% w/w H <sub>2</sub> O, less than 1 ppm MeOH (w/w)
38	Light contaminants in methanol+water mixture (e.g. dissolved gases).
42	Purge gas from MeOH synthesis – fuel for cogeneration; Composition: 8.17% H <sub>2</sub> , 19.6% CO, 17.7% CO <sub>2</sub> , 35.4% N <sub>2</sub> , 15.4% Ar (% w/w).
54	Ashes

**Table Y1.5.** Equipment input of biorefinery second area (BRY-2).

<b>Item (BRY-2)</b>	<b>Simulation inputs</b>
Air Separation Unit	Three-column process demanding 158 kWh/t O <sub>2</sub> (Higginbotham et al., 2011).
Gasification unit	Thermodynamic model: Peng-Robinson; Gasifier conditions: 900°C / 32 bar. Gibbs reactor is utilized for reaction modelling. Formation of tars and residual coke/char is neglected.
Absorption unit	Thermodynamic model: PC-SAFT, with model parameters from Gatti et al. (2014); Solvent: MeOH at -50°C; load: 3.30 molMeOH/molCO <sub>2</sub> ; The absorber has three intermediate coolers (-30°C); Syngas H/C target ratio: 2.15.
MeOH unit	Thermodynamic model: SRK for MeOH synthesis section and UNIQUAC / SRK for distillation section; Reactor conditions: 240-260°C / 64.7 bar; Kinetic model from Vanden Bussche and Froment (1996).
CO <sub>2</sub> liquefaction	Thermodynamic model: Peng-Robinson; Compressor suction/discharge pressure: 6.30 / 76.0 bar; Liquefaction at 30°C; CO <sub>2</sub> exportation at 100 bar.
Cogeneration unit	Thermodynamic model: NBS Steam for the steam cycle and Peng-Robinson for the other process streams; Steam turbine inlet conditions: 570°C / 98.5 bar and 173°C / 4.10 bar (intermediate inlet stream); Steam turbine outlet conditions: 0.11 bar / 0.88 vapor fraction.

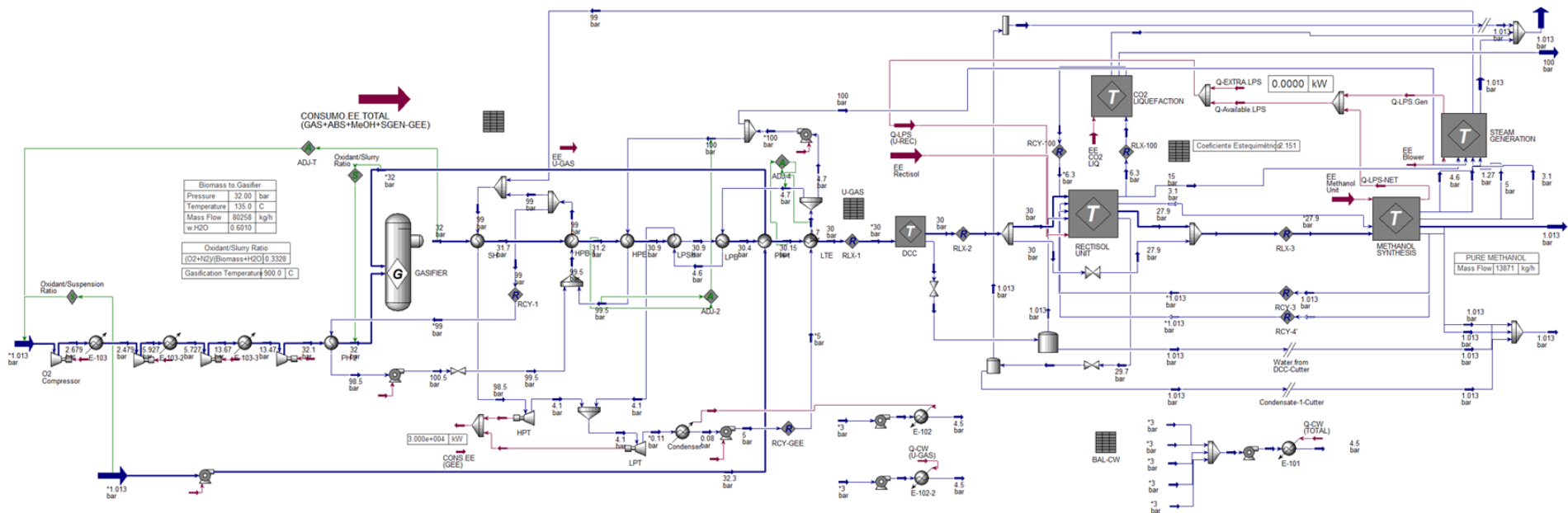
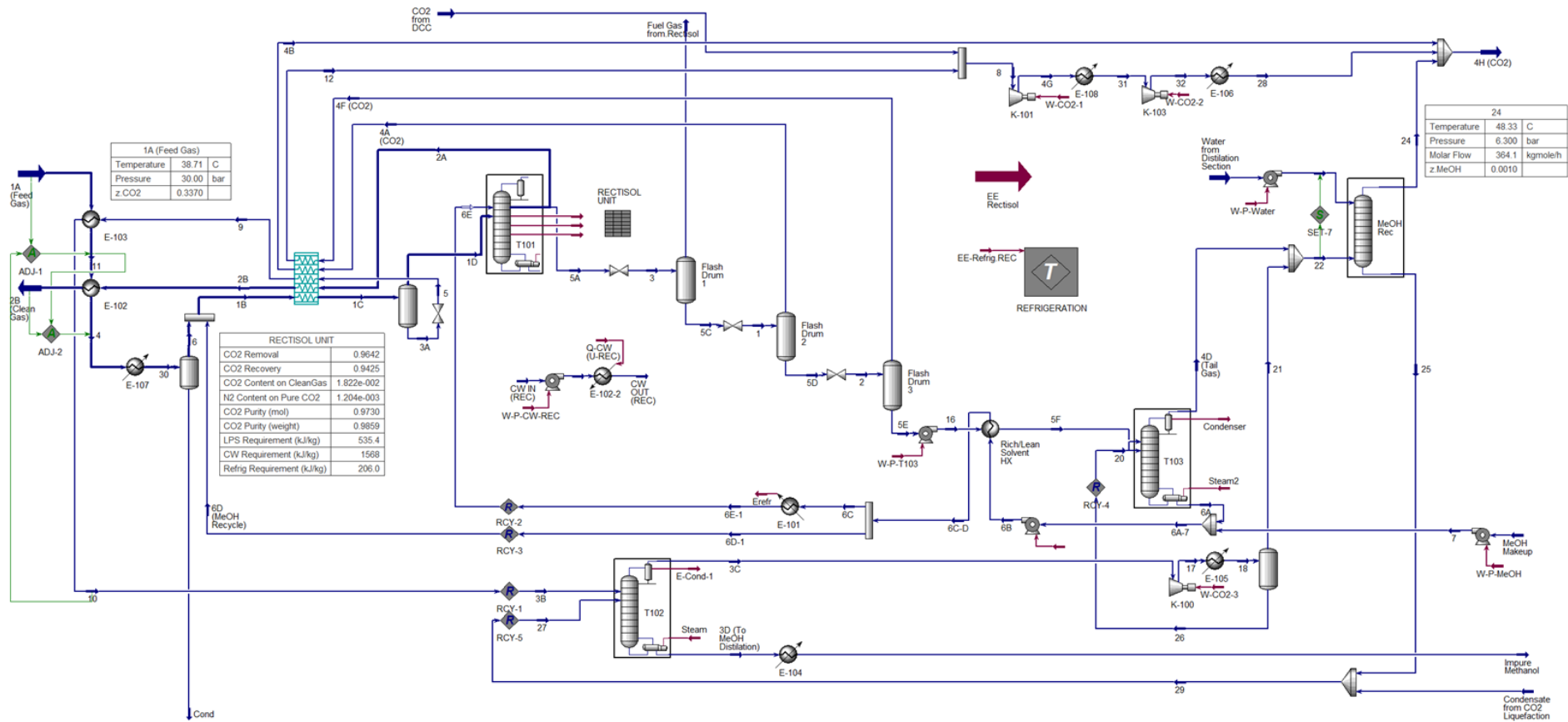


Fig. Y1.3. HYSYS PFD of BRY-2 simulation: overview of microalgal biomass termochemical processing for conversion to methanol.



**Fig. Y1.4.** HYSYS PFD of BRY-2 simulation: subflowsheet of CO<sub>2</sub> physical absorption unit.

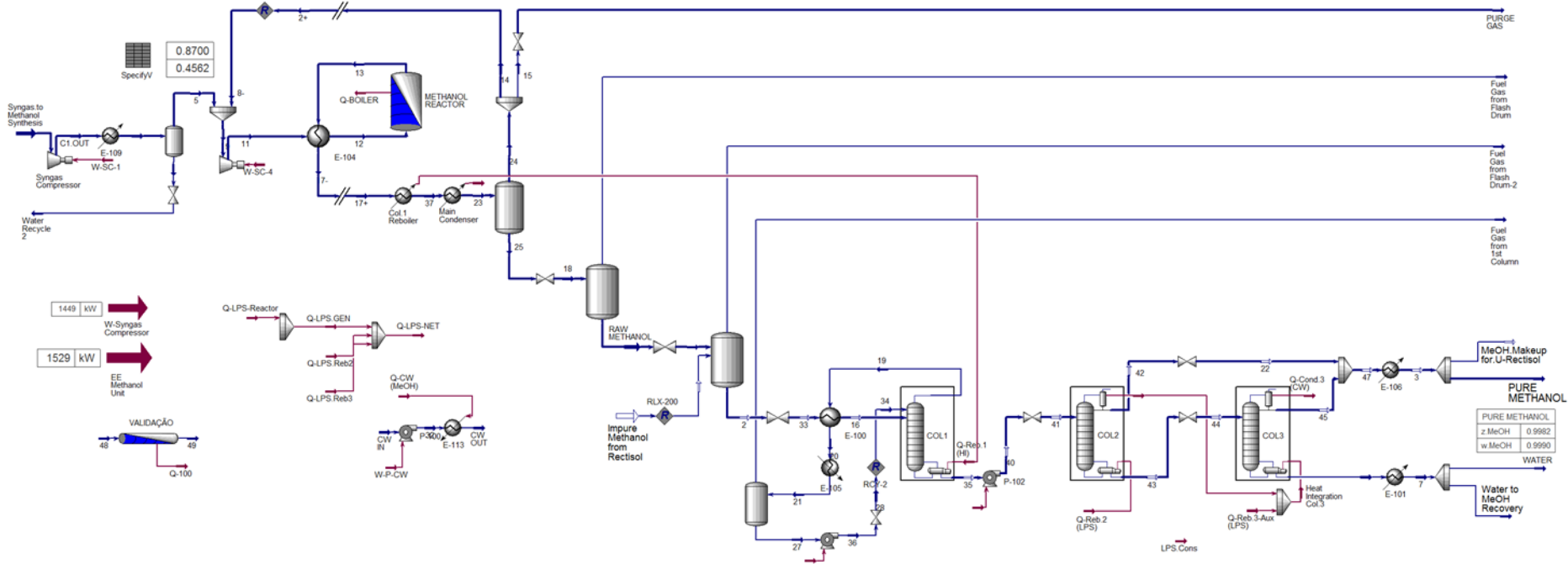


Fig. Y1.5. HYSYS PFD of BRY-2 simulation: subflowsheet of methanol synthesis and distillation.

## Y2. References for Appendix Y

- Acién, F.G., Fernández, J.M., Magán, J.J., Molina, E., 2012. Production cost of a real microalgae production plant and strategies to reduce it. *Biotechnol. Adv.* 30 (6), 1344–1353. <https://doi.org/10.1016/j.biotechadv.2012.02.005>
- Chisti, Y., 2007. Biodiesel from microalgae. *Biotechnol. Adv.* 25 (3), 294e306. <https://doi.org/10.1016/j.biotechadv.2007.02.001>
- Davis, R., Kinchin, C., Markham, J., Tan, E., Laurens, L., Sexton, D., Knorr, D., Schoen, P., Lukas, J., 2014. Process design and economics for the conversion of algal biomass to biofuels: algal biomass fractionation to lipid- and carbohydrate-derived fuel products. Technical Report. National Renewable Energy Laboratory (NREL).
- Dillon, D.J., White, V., Allam, R.J., Wall, R.A., Gibbins, J., 2005. IEA Greenhouse Gas R&D Programme: Oxy-combustion processes for CO<sub>2</sub> capture from power plant. Engineering Investigation Report.
- Duan, P., Jin, B., Xu, Y., Yang, Y., Bai, X., Wang, F., 2013. Thermo-chemical conversion of *Chlorella pyrenoidosa* to liquid biofuels. *Bioresour. Technol.* 133, 197–205. <https://doi.org/10.1016/j.biortech.2013.01.069>
- Gatti, M., Martelli, E., Marechal, F., Consonni, S., 2014. Review, modeling, Heat Integration, and improved schemes of Rectisol<sup>®</sup>-based processes for CO<sub>2</sub> capture. *Appl. Therm. Eng.* 70, 1123–1140. <https://doi.org/10.1016/j.applthermaleng.2014.05.001>
- Higginbotham, P., White, V., Fogash, K., Guvelioglu, G., 2011. Oxygen supply for oxycoal CO<sub>2</sub> capture. *Energy Proced.* 4, 884–891. <https://doi.org/10.1016/j.egypro.2011.01.133>.
- Kurt, M., Aksoy, A., Sanin, F., 2015. Evaluation of solar sludge drying alternatives by costs and area requirements. *Water Res.*, 82, 47-57. <https://doi.org/10.1016/j.watres.2015.04.043>
- Letelier-Gordo, C., Holdt, S., De Francisci, D., Karakashev, D., Angelidaki, I., 2014. Effective harvesting of the microalgae *Chlorella protothecoides* via bioflocculation with cationic starch. *Bioresour. Technol.* 167, 214–218. <https://doi.org/10.1016/j.biortech.2014.06.014>
- Molina Grima, E., Belarbi, E.-H., Acién Fernández, F.G., Robles Medina, A., Chisti, Y., 2003. Recovery of microalgal biomass and metabolites: process options and economics. *Biotechnol. Adv.* 20 (7-8), 491–515. [https://doi.org/10.1016/S0734-9750\(02\)00050-2](https://doi.org/10.1016/S0734-9750(02)00050-2)
- Picardo, M.C., de Medeiros, J.L., Monteiro, J.G.M., Chaloub, R.M., Giordano, M., Araújo, O.Q.F., 2013. A methodology for screening of microalgae as a decision making tool for energy and green chemical process applications. *Clean Technol. Environ. Policy* 15, 275–291. <https://doi.org/10.1007/s10098-012-0508-z>
- Tang, D., Han, W., Li, P., Miao, X., Zhong, J., 2011. CO<sub>2</sub> biofixation and fatty acid composition of *Scenedesmus obliquus* and *Chlorella pyrenoidosa* in response to different CO<sub>2</sub> levels. *Bioresour. Technol.* 102(3), 3071–3076. <https://doi.org/10.1016/j.biortech.2010.10.047>

Uduman, N., Qi, Y., Danquah, M. K., Forde, G. M., Hoadley, A., 2010. Dewatering of microalgal cultures: a major bottleneck to algae-based fuels. *J. Renew. Sust. Energy* 2, 012701. <https://doi.org/10.1063/1.3294480>

Vanden Bussche, K.M., Froment, G.F., 1996. A steady-state kinetic model for methanol synthesis and the water gas shift reaction on a commercial Cu/ZnO/Al<sub>2</sub>O<sub>3</sub> catalyst. *J. Catal.*, 161(1), 1–10. <https://doi.org/10.1006/jcat.1996.0156>

Wang, W., Han, F., Li, Y., Wu, Y., Wang, J., Pan, R., 2014. Medium screening and optimization for photoautotrophic culture of *Chlorella pyrenoidosa* with high lipid productivity indoors and outdoors, *Bioresour. Technol.* 170, 395-403. <https://doi.org/10.1016/j.biortech.2014.08.030>

Williams, P., Laurens, L., 2010. Microalgae as biodiesel & biomass feedstocks: review & analysis of the biochemistry, energetics & economics. *Energy Environ. Sci.* 3, 554–590. <https://doi.org/10.1039/B924978H>

## APPENDIX Z – Supplementary Material for Chapter 07

### Z1. Review on experimental results of microalgae biomass anaerobic digestion

Table Z1.1 collects process conditions and performances of microalgae biomass anaerobic digestion (AD) in accordance with experimental results reported in recent literature.

**Table Z1.1.** AD of microalgae biomass: process conditions and performance.

<i>Reactor Type</i>	<i>Substrate</i>	<i>HRT*</i> (days)	<i>OLR†</i> (g <sup>VS</sup> /L/d)	<i>T</i> (°C)	<i>Scale</i>	<i>Yield</i> (L/g <sup>VS</sup> )	<i>Ref.</i>
Batch	<i>Nannochloropsis salina</i>	30	-	35	-	0.557 (CH <sub>4</sub> )	<sup>(1)</sup>
Batch	<i>Nannochloropsis salina</i>	19	-	35	-	0.43 (CH <sub>4</sub> ) 0.70 (Biogas)	<sup>(2)</sup>
CSTR	Microalgae wastewater (mainly <i>Nannochloropsis limnetica</i> )	15	1.4	53±1	1 L	0.313±0.013 (CH <sub>4</sub> )	<sup>(3)</sup>
CSTR semi continuous	3:1 (mass) co-digestion of <i>Opuntia maxima</i> with <i>Scenedesmus sp.</i>	15	5.33	37	3 L	0.308±0.022 (CH <sub>4</sub> )	<sup>(4)</sup>
Batch	<i>Nannochloropsis oculata</i>	12	-	37	-	0.33 (CH <sub>4</sub> ) 0.44 (Biogas)	<sup>(5)</sup>
CSTR 2-stage	<i>Arthrospira platensis</i> with macroalgae <i>Laminaria digitata</i>	12	2.0	37±1	5 L	0.245 (CH <sub>4</sub> )	<sup>(6)</sup>
CSTR semi continuous	Algal sludge mainly comprising <i>Scenedesmus</i> + <i>Chlorella spp.</i>	10	4.0	35±1	4 L	0.143±0.007 (CH <sub>4</sub> )	<sup>(7)</sup>
Batch	2:1:2 (mass) mixture of <i>Chlamydomonas</i> , <i>Scenedesmus</i> and <i>Nannochloropsis, spp.</i>	5	2.0	35	-	0.304 (CH <sub>4</sub> )	<sup>(8)</sup>
Tubular	<i>Phaeodactylum tricornutum</i>	2.3 ±0.6	2.0 ±0.7	54±2	2 L	0.29±0.11 (CH <sub>4</sub> )	<sup>(9)</sup>

<sup>(1)</sup> Zhao and Su (2014); <sup>(2)</sup> Quinn et al. (2014); <sup>(3)</sup> Tsapekos et al. (2018); <sup>(4)</sup> Ramos-Suárez et al. (2014);

<sup>(5)</sup> Marsolek et al. (2014); <sup>(6)</sup> Ding et al. (2018); <sup>(7)</sup> Yen and Brune (2007); <sup>(8)</sup> Alzate et al. (2012);

<sup>(9)</sup> Zamalloa et al. (2012).

\* HRT = Hydraulic Retention Time

† OLR = Organic Loading Rate

## Z2. Pipeline specifications for biomethane commercialization (review)

Pipeline specifications are imposed to biomethane, differing according to the national grids, and regions, shown in Table Z2.1.

**Table Z2.1.** Pipeline specifications for biomethane.

<i>Spec.</i>	<i>Unit</i>	<i>USA<sup>(1)</sup></i>	<i>Brazil, from agricultural and forestry residues<sup>(2)</sup></i>	<i>Brazil, from landfills/wastewater treatment, for residential/vehicular use<sup>(3)</sup></i>	<i>Germany<sup>(1)</sup></i>
HHV	kWh/m <sup>3</sup>	-	9.72-11.94	9.72-11.94 <sup>(4)</sup>	8.4-13.1
LHV	kWh/m <sup>3</sup>	9.8-11.4	-	-	8.4-13.1
WI*	kWh/m <sup>3</sup>	-	12.9-14.9	12.9-14.9 <sup>(4)</sup>	12.8-15.7
CH <sub>4</sub>	mol%	-	>90	>90	-
CO <sub>2</sub>	mol%	<2-4	< 3	< 3	-
CO <sub>2</sub> +O <sub>2</sub> +N <sub>2</sub>	mol%	-	-	<10	-
O <sub>2</sub>	mol%	0.2-1	< 0.8	< 0.8	< 3
H <sub>2</sub> S	mg /m <sup>3</sup>	-	< 1	< 10	-
Siloxanes	mg Si/m <sup>3</sup>	-	-	<0.3	-
Chlorides	mg Cl/m <sup>3</sup>	-	-	<5	-
Fluorides	mg F/m <sup>3</sup>	-	-	<5	-
H <sub>2</sub> O	-	<120 ppm	< -45°C <sup>(4, 5)</sup> WDP <sup>†</sup> @ 1atm	< -45°C <sup>(4, 5)</sup> WDP@ 1atm	-

<sup>(1)</sup>Scholz et al.(2013); <sup>(2)</sup>ANP (2015); <sup>(3)</sup>ANP (2017); <sup>(4)</sup>Except North/Brazil; <sup>(5)</sup>Except Northeast/Brazil

\* WI = Wobbe Index

† WDP = Water Dew Point

### Z3. Process flow diagrams for downstream alternatives

Downstream process alternatives – BM, BM+EOR, BE and BE+EOR – with thermo-mechanical pretreatment of microalgal sludge are respectively depicted in Figs. Z3.1-Z3.4.

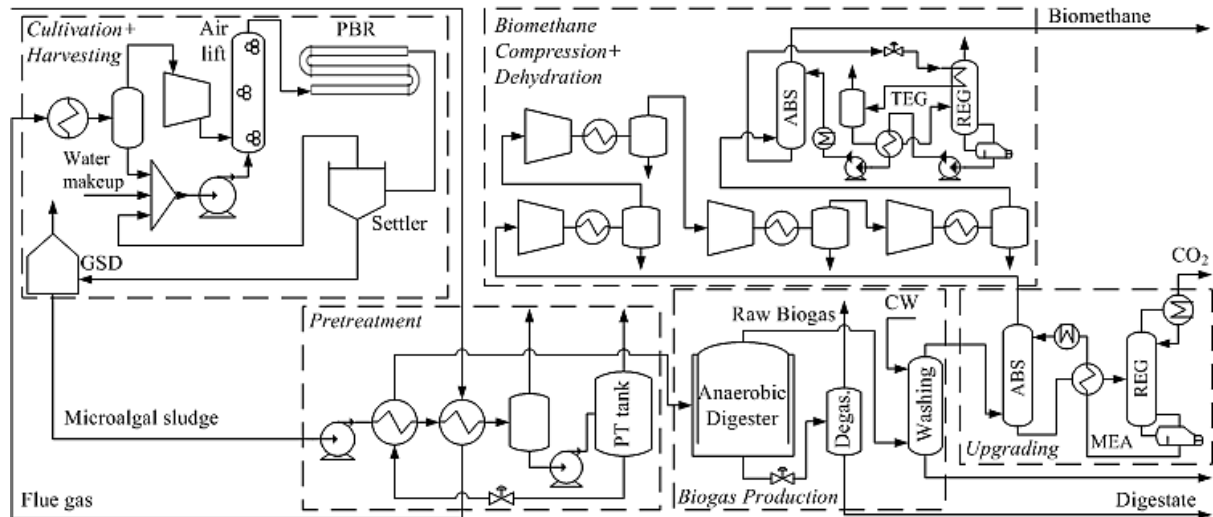


**Fig. Z3.1.** Process flow diagram for biomethane production (BM).

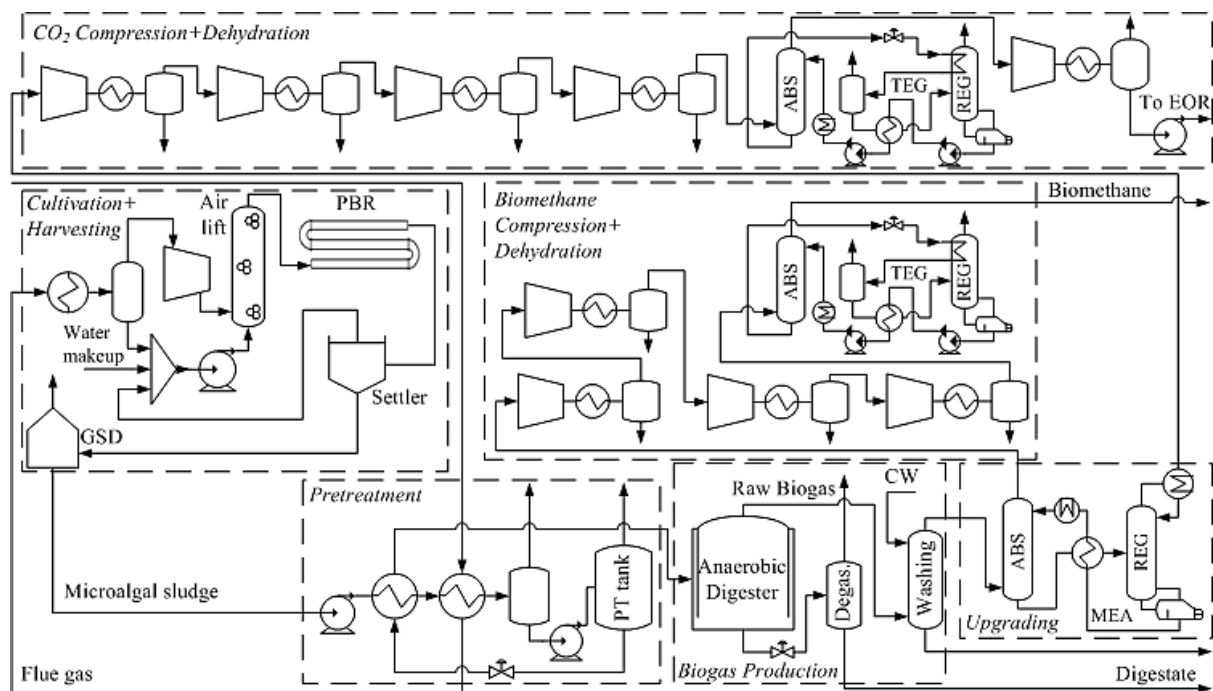


**Fig. Z3.2.** Process flow diagram of biomethane production with CO<sub>2</sub> conditioning for enhanced oil recovery (BM+EOR).

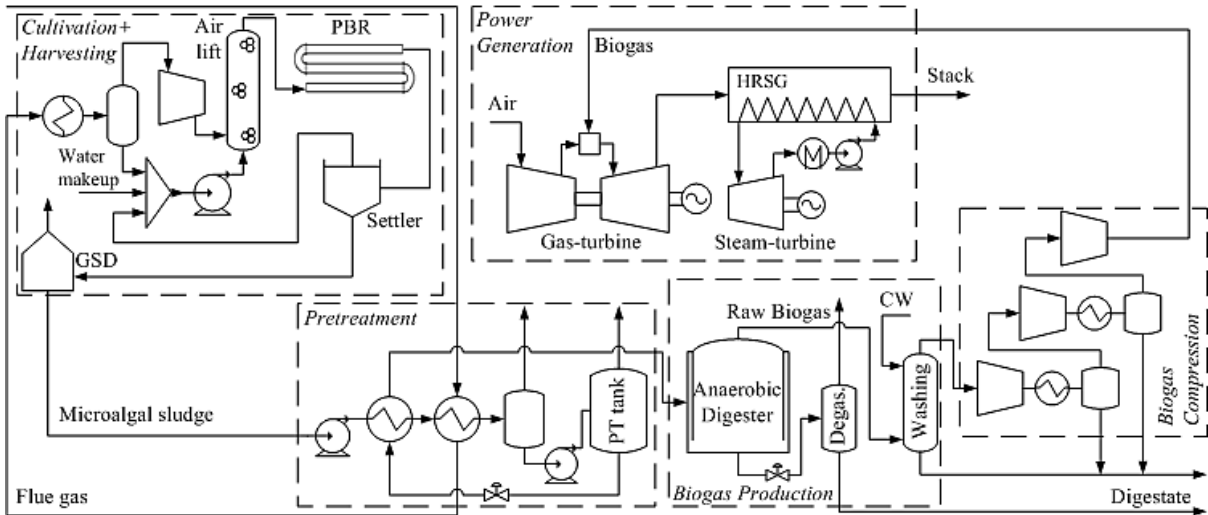


**Fig. Z3.3.** Process flow diagram for bioelectricity production (BE).

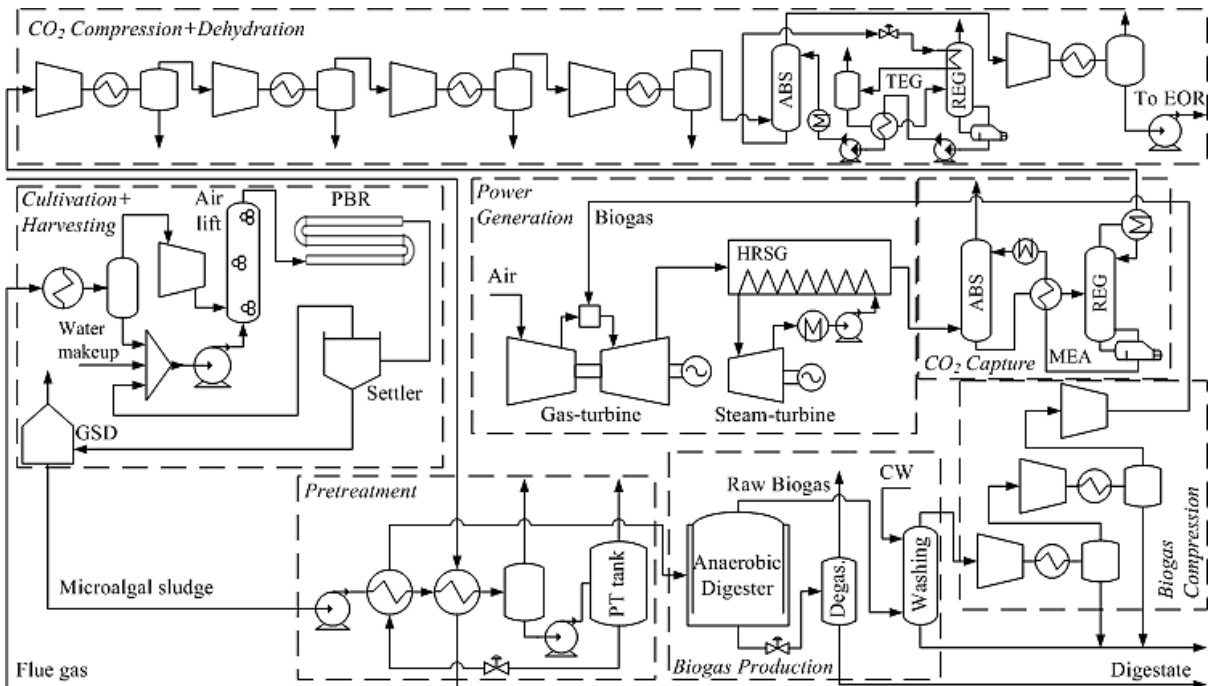


**Fig. Z3.4.** Process flow diagram of bioelectricity production with CO<sub>2</sub> conditioning for enhanced oil recovery (BE+EOR).

## Z4. Production of microalgal suspension

Flue gas from any source can be utilized to feed microalgae cultivation in this process. In this case the composition of the flue gas from a natural gas-fired boiler was assumed. Changing the source would practically influence only the power required to feed the air lift, since the level of contaminants can be suited to meet microalga tolerance, avoiding growth inhibition. Electricity consumption for microalgae cultivation and harvesting is estimated as 8.65 MW, with photosynthesis consuming 75% of total CO<sub>2</sub> feed from flue gas and ≈267 MW of solar energy, producing microalgal biomass with 265 MW of available energy (LHV).

**Table Z4.1.** Key assumptions for process simulation and analysis.

<i>Object</i>	<i>Variable</i>	<i>Value</i>	<i>Unit</i>	<i>Ref.</i>
Flue Gas	Mass flow	196.25 (CO <sub>2</sub> : 25.6)	kg/s	(1)
	Temperature	107	°C	(1)
	Pressure	1.00	atm	(1)
	Composition (mass fractions)	N <sub>2</sub> : 0.7631 O <sub>2</sub> : 0.0442 CO <sub>2</sub> : 0.1305 H <sub>2</sub> O: 0.0622	-	(1)
Air Lift	Inlet pressure	2.00	bar	(2)
	Air lift CO <sub>2</sub> efficiency	100	%	–
PBR*	Biomass concentration	4.00	g/L	(3)
	Biomass productivity	1.535	kg/m <sup>3</sup> /d	(3)
	Volume/Surface	0.07	m <sup>3</sup> /m <sup>2</sup>	(4)
	Efficiency of CO <sub>2</sub> utilization	75	%	(4)
	Daily uptime	24 (average productivity)	h	–
Settler	Efficiency	95	%	(5)
	Flocculant (cationic starch) conc.	0.04	g/L	(5)
	Organic matter content in product	7.0	% w	(6)
GSD†	Organic matter content in product	20	% w	–

(1) Wiesberg et al. (2017); (2) Stephenson et al. (2010); (3) Chisti et al. (2007); (4) Acien et al. (2012);

(5) Letelier-Gordo et al. (2014); (6) Williams et al. (2010)

\* PBR = Photobioreactor

† GSD = Greenhouse Solar Dryer

## Z5. References for Appendix Z

Acién F, Fernández J, Magán J, Molina E. Production cost of a real microalgae production plant and strategies to reduce it. *Biotechnol Adv* 2012; 30(6):1344–53.

<https://doi.org/10.1016/j.biotechadv.2012.02.005>

Alzate ME, Muñoz R, Rogalla F, Fdz-Polanco F, Pérez-Elvira SI. Biochemical methane potential of microalgae: Influence of substrate to inoculum ratio, biomass concentration and pretreatment. *Bioresour Technol* 2012; 123:488–94.

<https://doi.org/10.1016/j.biortech.2012.06.113>

ANP (The Brazilian National Agency of Petroleum, Natural Gas and Biofuels). Resolution No. 5/2015. Establish Biomethane Specification. Brazilian National Press, Daily Official Journal, June 6<sup>th</sup> 2017 (in Portuguese).

<http://legislacao.anp.gov.br/?path=legislacao-anp/resol-anp/2015/janeiro&item=ramp-8--2015>

ANP (The Brazilian National Agency of Petroleum, Natural Gas and Biofuels). Resolution No. 685/2017. Establish Biomethane Specification. Brazilian National Press, Daily Official Journal, No. 22, Section 1, pp 100-101, February 2nd 2015 (in Portuguese).

<http://legislacao.anp.gov.br/?path=legislacao-anp/resol-anp/2017/junho&item=ramp-685--2017>

Chisti Y. Biodiesel from microalgae. *Biotechnol Adv* 2007; 25(3):294–306.

<https://doi.org/10.1016/j.biotechadv.2007.02.001>

Ding L, Gutierrez EC, Cheng J, Xia A, O'Shea R, Guneratnam AJ, Murphy JD. Assessment of continuous fermentative hydrogen and methane co-production using macro- and micro-algae with increasing organic loading rate. *Energy* 2018; 151:760–70.

<https://doi.org/10.1016/j.energy.2018.03.103>

Letelier-Gordo CO, Holdt SL, de Francisci D, Karakashev DB, Angelidaki I. Effective harvesting of the microalgae *Chlorella protothecoides* via bioflocculation with cationic starch. *Bioresour Technol* 2014; 167:214–8.

<https://doi.org/10.1016/j.biortech.2014.06.014>

Ma, J., Techno-Economic Analysis and Engineering Design Consideration of Algal Biofuel in Southern Nevada, Final Report for Subtask 1.3 of Project of Nevada Renewable Energy Consortium, 2011.

Marsolek MD, Kendall E, Thompson PL, Shuman TR. Thermal pretreatment of algae for anaerobic digestion. *Bioresour Technol* 2014; 151:373–7.

<https://doi.org/10.1016/j.biortech.2013.09.121>

Quinn JC, Hanif A, Sharvelle S, Bradley TH. Microalgae to biofuels: life cycle impacts of methane production of anaerobically digested lipid extracted algae. *Bioresour Technol* 2014; 171:37–43.

<https://doi.org/10.1016/j.biortech.2014.08.037>

Ramos-Suárez JL, Martínez A, Carreras N. Optimization of the digestion process of *Scenedesmus sp.* and *Opuntia maxima* for biogas production. *Energy Convers Manage* 2014; 88:1263–70. <https://doi.org/10.1016/j.enconman.2014.02.064>

Scholz M, Melin T, Wessling M. Transforming biogas into biomethane using membrane technology. *Renew Sust Energ Rev* 2013, 17:199–212. <https://doi.org/10.1016/j.rser.2012.08.009>

Stephenson AL, Kazamia E, Dennis JS, Howe CJ, Scott SA, Smith AG. Life-cycle assessment of potential algal biodiesel production in the United Kingdom: a comparison of raceways and air-lift tubular bioreactors. *Energy Fuels* 2010; 24(7):4062–77. <https://doi.org/10.1021/ef1003123>

Tsapekos P, Kougias PG, Alvarado-Morales M, Kovalovszki A, Corbière M, Angelidaki I. Energy recovery from wastewater microalgae through anaerobic digestion process: methane potential, continuous reactor operation and modelling aspects. *Biochem Eng J* 2018; 139:1–7. <https://doi.org/10.1016/j.bej.2018.08.004>

Wiesberg IL, Brigagão GV, de Medeiros JL, Araújo OQF. Carbon dioxide utilization in a microalga-based biorefinery: efficiency of carbon removal and economic performance under carbon taxation. *J Environ Manage* 2017; 203:988–98. <https://doi.org/10.1016/j.jenvman.2017.03.005>

Williams P, Laurens L. Microalgae as biodiesel & biomass feedstocks: review & analysis of the biochemistry, energetics & economics. *Energy Environ Sci* 2010; 3:554–90. <https://doi.org/10.1039/B924978H>

Yen H, Brune DE. Anaerobic co-digestion of algal sludge and waste paper to produce methane. *Bioresour Technol* 2007; 98:130–4. <https://doi.org/10.1016/j.biortech.2005.11.010>

Zamalloa C, Boon N, Verstraete W. Anaerobic digestibility of *Scenedesmus obliquus* and *Phaeodactylum tricornutum* under mesophilic and thermophilic conditions. *Appl Energy* 2012; 92:733–8. <https://doi.org/10.1016/j.apenergy.2011.08.017>

Zhao B, Su Y. Process effect of microalgal-carbon dioxide fixation and biomass production: a review. *Renew Sust Energ Rev* 2014; 31:121–32. <https://doi.org/10.1016/j.rser.2013.11.054>